NOTE TO USERS

The diskette is not included in this original manuscript. It is available for consultation at the author's graduate school library.

This reproduction is the best copy available.

UMI

Ultra-high Pressure Composite Vessels with Efficient Stress Distributions

Greg Rohrauer

A thesis

in

The Department

of

Mechanical Engineering

Presented in Partial Fulfillment of the Requirements
for the Degree of Doctor of Philosophy at
Concordia University
Montreal, Quebec, Canada.

June 1999

Volume I
Theoretical and Experimental

Canada

Abstract

Ultra-high Pressure Composite Vessels with Efficient Stress Distributions

Greg Rohrauer, Ph.D.
Concordia University, 1999

The techniques for the design, analysis and the construction of composite pressure vessels have been established since the 1960's. Their development has become refined and the composite materials employed for their construction have seen major improvement. The one area where only marginal advancement has been achieved is with the ultra-high pressure applications.

Vessels designed and constructed to operate in the 20,000 - 25,000 psi (140 - 170 MPa) range have been few in number and poor in efficiency. Applications for such high pressure containment vessels are varied but one potentially marketable idea is to develop these vessels with the capacity to hold hydrogen and methane (natural gas) at liquid densities yet ambient temperature. These could be used as fuel tanks in both combustion and fuel cell powered vehicles, filled at service stations with cryogenic liquid in a manner identical to the filling of conventional propane bottles. Safety requirements demand burst pressures from twice to three times operating conditions and this leads to the realm of thick-walled design. For the anisotropic composite materials the stresses through the wall thickness tend to fall much more rapidly than with their isotropic metallic counterparts. This effect leads to a greatly reduced vessel efficiency quotient PV/W. To date, little is

understood about the phenomena underlying this rapid decay in load bearing or how it can be counteracted.

The work performed analyses the corresponding anisotropic elasticity problem to determine the exact nature of the challenge and then addresses a solution based on variable elasticity to counter this intrinsic behaviour. The method employed seeks to elicit appropriate through-thickness material property variation rates to attain a more level stress distribution (or incipient failure throughout the wall) while restricting property changes to values attainable in commercially available composites. A computer code based on closed form elasticity solutions complete with damage / failure modeling and graphic interactive editing was written to carry out the computations. This tool enables the development of application specific designs. A prototype vessel is constructed and data from this and other vessels are checked to see how well the computations correlate to the theory advanced.

Acknowledgements

Table of Contents

Volume I: Theory and Experimental

Chapter 1 Introduction and Objectives

Chapter 2 Development History and Current State of the Art

Chapter 6 Numerical Solution Method for Variable Properties

Chapter 7 Micromechanics, Damage and Post FPF Design

Chapter 8 Description of Software with Examples

Chapter 9 Design Considerations, Validation and Contributions to Knowledge

References

Volume II: Appendices and Computer Code

A) Pressure vessels manufactured by Lincoln Composites

B) Source Code Listing

List of Figures

Chapter 4

Chapter 5

Chapter 7

AS4/3501-6 under biaxial loading.

List of Tables

Chapter 2

Chapter 4

Chapter 7

List of Symbols

Default notation, unless defined otherwise for local purposes.

V = volume

W = weight

TLEV = abreviation: transitional low emission vehicle

LEV = abreviation: low emission vehicle

ULEV = abreviation: ultra low emission vehicle

ZLEV = abreviation: zero emission vehicle

Z = compressibility factor

R = universal gas constant

T = tempertature (absolute)

T_c = critical temperature

P_c = critical pressure

υ = specific volume

t = cylinder wall thickness

d = cylinder diameter

l = length along cylinder axis

e = fiber band thickness

n = orthotropy exponent (spherical or cylindrical)

K = orthotropy exponent (fixed material properties)

k = slippage tendency constant

a = inside radius of cylinder

b = outside radius of cylinder

c = relative thickness (a/b)

P = Internal pressure

Q = external pressure

F = axial load resultant

ρ = arbitrary radius

α = winding angle referenced to cylinder axis or meridian

r = radial direction

θ = circumferential direction; angular position of meridian wrt. coordinate system

z = axial direction

u, v, w = displacements along coordinate directions

x, y, z = principal directions (rectangular)

$_{ij}$ = index for directional notation $(1,2,3...6)$, (r,θ,z), (ρ,φ,θ)
depending on coordinate system convention

$_i$ = index for direction $(1,2,3... n)$ or (m) to denote various constants or layers

$_m$ = index to denote arbitrary layer

$_n$ = index to denote outermost layer

$_0$ = index to denote initial quantity

E_{ij} = engineering tensile modulus

G_{ij} = engineering shear modulus

a_{ij} = compliance matrix term

β_{ij} = reduced compliance terms (generalized plane strain cylindrical system)

A_{ij} = stiffness matrix term

σ_{ij} = normal stress

τ_{ij} = shear stress

ε_{ij} = normal strain

γ_{ij} = shear strain

S_{ij} = strength

F_{ij} = strength parameter for failure envelope

C = axial constant (strain)

D = general axial displacement function

A, B = integration constants for bending deflections

ϑ = twist per unit axial length

F, Ψ = stress functions

ϕ, φ = derivatives of the stress functions F and Ψ respectively

C_i = integration constants

$f(\ ), g(\ )$ = function of

y_i = particular solution

λ_i = characteristic root

s, t = roots for the case of a common property variation rate "n"

$W_i, Y_i, \chi_m, \delta_m, \Delta, L, \mu_i, \wedge_i, \Gamma_i$ = mathematical grouping of terms

L'_i = grouping of partial derivatives

ϖ = Wronskian

M_i = resultant moments

ω_i = small rotations (radians)

U, V, W, U_1, V_1, W_1 = displacement functions

RHS, LHS = abreviation: right hand side, left hand side

α_{ij}, γ_{ij} = base compliance quantity

$l, m, d, s, p, q, h, k, i, j, e, u, v$ = exponents to property variation rate functions

x_i, w_i = numerical solution meshpoints

h = numerical solution interval

M, M_f, M_m = composite modulus and corresponding fiber and matrix moduli

η = stress partitioning parameter

ξ = empirical measure of fiber reinforcement

$_T$ = subscript indicating transverse

$_A$ = subscript indicating axial

ν_T, ν_A = transverse Poisson's ratio, axial Poisson's ratio

n = axial modulus

l = Poisson related modulus

G_A, G_T = engineering shear moduli

E_A, E_T = engineering tensile moduli

k_T = plane strain bulk modulus, alternatively K_{23}

λ^* = Lamé's constant

I_i = Cauchy strain invariant

J_i = invariants for infinitesimal strains

X, X', Y, Y', S = uniaxial strengths, axial, transverse, shear; (' = compressive)

R = safety factor

G_{IC} = mode I fracture toughness

ζ = geometry parameter for fracture

a, a_{min}, a_{max}, a_c = pertaining to flaw or crack size

a_{eq} = equivalent crack length

ε = arbitrary loading

ε_{eq} = equivalent loading

ε_{CI} = equivalent loading at crack initiation

ε_{CS} = equivalent loading at crack saturation state

D_{eq} = equivalent crack density

D_{CS} = saturation crack density

L_{CS} = saturated crack spacing

D_ε = empirical crack saturation density parameter

RS_{eq} = residual equivalent stiffness

$\varepsilon_{eq}^{CW}, \varepsilon_{eq}^{C}, CK, \alpha_R, \alpha_W$ = curve fitting parameters

U = strain energy

W = work per unit volume

t_0, t_{90} = thickness of $0°$, $90°$ plies respectively

K_t = shear lag parameter for tensile loading

K_s = shear lag parameter for shear loading

Chapter 1

Introduction and Objectives

1.0 Origin of Filament Wound Structures

The filament winding of composite glass-fiber based pressure vessels evolved from a demonstration project at Hercules Powder Corp. in 1948. These first filament wound items, solid rocket motor nozzles for the X248 missile, were a follow-on to the experimental and pioneering *World War II* work of Theodore Von Kármán. After a 7-year lapse, in 1955, North American Aviation (Rocketdyne) engaged Hercules in another demonstration project, wrapping the MATADOR motorcase with fiberglass. By 1963, the first filament wound motor case (a strap-on booster for the TITAN missile and launch vehicle) was in production [1].

Meanwhile, from the mid 1950's to the early 1960's, research was underway at Air Force, Navy, Military and private laboratories funded by weapons research. Material development and testing was carried out in conjunction with the design and construction of filament wound pressure vessels, rocket motor cases, nozzles and launch tubes [2]. Development was carried out by the major industrial subcontractors. Among them were Walter Kidde & Co., Brunswick Corp., Aerojet General Corp. , Rocketdyne, Thiokol, Owens-Corning and many others. Techniques still considered advanced today, such as computer controlled pre impregnated winding were being employed as early as 1961 [3].

Insight to the breadth and depth of development efforts prior to 1962 can be

appreciated by considering the 169 contracts reviewed in a Military commissioned survey [4], both classified and non-classified. This report covered developments since the MATADOR program. Many other successful missiles projects such as POLARIS, MINUTEMAN II, REDEYE and SPRINT followed.

1.1 Development of Pressure Vessels

By the mid 1960's there was a broadening in the design of smaller vessels destined for containment of oxidizer / fuel mixtures such as aerozine-50 (H_2O_2) and nitrogen tetroxide (N_2O_4) [5][6][7]. These corrosive fuels required resistant and non-permeable liners of polymeric or metallic materials. Interest soon shifted to the cryogenic fuel and oxidizer containment needed for extended manned space flights. This topic became the principal focus of development during the mid to late 1960's [6][8][9][10-13]. The thin metal shell lined, full composite overwrapped, pressure vessels that were conceived during this period have evolved to become the mainstay of today's commercial composite pressure vessel market [14]. Research and development work that progressed these designs to those of today are reviewed in Chapter 2.

In the late 1960's composite vessels with ultra-high burst pressures 30,000-60,000 psi or (200 - 400 MPa) were first investigated. Work taking this direction has continued to the present but success is still limited [15][16][17][18][19]. Despite 30 years of effort, the highest rated operating pressures of vessels in aerospace service today remain in the 10,000 to 15,000 psi (70 - 100 MPa) range [20]. Only a minuscule fraction of composite

2

pressure vessels built operate at such high pressures.

Invariably the forefront of pressure vessel development has focused on greater containment *efficiency*. Namely to contain the most fluid at the greatest pressure within the smallest volume and at the lowest weight. A performance factor, based on burst pressure P, volume V and weight W, (PV/W) is defined to express efficiency. Burst pressure is divided by a design factor (generally ranging 1.5 - 3.5) to arrive at an operating pressure. This factor is dependent on the number of pressure cycles, materials, environment and subjective safety considerations.

1.2 Markets for Composite Pressure Vessels

Commercial applications of these vessels have found many markets and there were already over 200,000 composite pressure vessels in service by 1984 [21]. By 1997 this figure exceeded 1 million vessels from the production of one company alone, Structural Composite Industries (SCI) [22]. Some mainstream applications are, in-flight aircraft engine starters, firefighter's and aviator's breathing apparatus, cockpit ejection systems, mountaineering expedition equipment, medical oxygen supplies and diving tanks. Composite vessels are used in inflation devices for aircraft emergency chutes, flotation bags for downed helicopters and life rafts. Fire extinguishing systems and compressed natural gas fuel cylinders are now standard [23].

Potentially the largest market yet is automotive. Currently there are over 700,000 compressed natural gas (CNG) fueled vehicles worldwide, more than 30,000 in the USA

and a large number in Canada [24][25]. Due to a renewed emphasis on reducing emissions, the three major domestic auto manufacturers along with their overseas counterparts have steadily produced alternate fueled vehicles commencing with the 1995 model year being sold into fleet service. New legislation driven pollution requirements (TLEV, LEV, ULEV, ZLEV) tightening on a yearly basis till year 2003, have already taken effect for heavy vehicles and are being phased in for commercial fleets. In North America, for the 1997 model year and onwards, new passengers vehicles must comply with these more stringent regulations and there are special quotas relating to major metropolitan areas. The mandated objective is to have 1 million alternative fueled vehicles by year 2004 [26]. There are many ongoing and far reaching initiatives driven by recent success in fuel cell technology (Ballard Power Systems and other competitors) which presently show about 20 - 30% better overall energy conversion efficiency than thermal combustion engine vehicles and have no direct CO_2 emissions. Currently fuel cells exhibit over 60% thermal efficiency. These require hydrogen to operate or may use methane (natural gas) in conjunction with a reformer to extract the hydrogen. Much of this technology has already been demonstrated but the major obstacle is storing a sufficient quantity of fuel onboard [27].

The combined threats imposed by air quality, global heating, imported and finite supplies of available oil are forcing alternate fuels. Among the limited options available, natural gas (methane) is one of the strongest contender. It is low cost, renewable, and there are vast proven natural reserves. In combustion engines, only hydrogen burns cleaner and produces, for all practical intents, no greenhouse gases. Methane can be blended with a small fraction of hydrogen to speed combustion and eliminate nearly all pollutants

4

[21][26][28]. One of the current limitations to natural gas is the lack of vehicle range between refueling stops. The problem amounts to insufficient compressed density of the fuel. Currently only large vehicles as trucks and buses have sufficient storage space available to make this alternative fuel reasonably practical [24][27][30][31]. Weight and cost of the containment vessel are also a crucial consideration.

Present commercial composite pressure vessel technology is restricted to thin-walled vessels. The construction of commercial composite pressure vessels is governed by certification procedures. These, developed initially for the Military's internal use, were later adapted to civilian purposes [32][33][34][35]. Under such guidelines the transport of any vessel operating above 5000 psi (34.5 MPa), is not approved on public roads or commercial airspace. A pressure of 4350 psi (30 MPa) is the maximum recommended for vehicular use and 3600 psi (21 MPa) is a standard refueling system's maximum output pressure. Tanks are nominally charged to 3000 psi. Clearly there is need for advancement in the pressure vessel technology within this arena.

1.3 Thick-Walled Vessels and their Commercial Potential

Considering the decades engineers have sought to explore the domain of thick-walled composite vessels, advancement appears at a virtual standstill. The problems of winding thick vessels are quite considerable, yet still possible when restricted to a reasonable wall thickness. Vessels with burst pressures in the 50,000 - 60,000 psi (345 - 414 MPa) range were achieved in the late 1970's through mid 1980's. Given the typical

2.25 design factor used on the latest vehicular gaseous fuel tanks, a 25,000 psi (172 MPa) operating pressure appears within reach. Such a vehicular fuel tank would hold the compressed natural gas (CNG) or hydrogen (H_2) within near its cryogenic liquid density, but at ambient temperature. Achieving efficient and reliable design of such vessels would make the driving range with CNG and H_2 comparable to liquid fueled vehicles. To arrive at such pressures only liquefied gas cylinder filling is practical. Pressure then rises as heat transfer takes effect. The required loss-less cryogenic filling techniques have been studied since the 1960's and are practiced in rocketry and the cryogenics transport industry [36].

1.4 Thick-Walled Vessel Design Problems

One of the biggest concerns in the design of ultra-high pressure isotropic metallic vessels is their rapid decline in stress through the wall thickness. Measures for pre-stressing the material favorably during construction have been developed so as to result with a more even stress distributions while under load. For composite vessels this natural decline in stress is much more pronounced since it is dependent upon the material's anisotropy ratio and generally worsens with increases in the composite's stiffness. Fiber pretensioning and cure schedules have been studied and applied but shown to have limited influences in effecting a desired residual stress distribution. The rapid decline of stresses through the wall of a thick composite vessel translates into a low efficiency for the entire structure since the material in the outer portions of the vessel wall contributes much less to carrying the load than the inner material.

Among drawbacks attributed to the current ultra-high pressure vessels are their low efficiency but also a fundamental lack of confidence and ability to understand and predict their behavior. The dilemma to successful ultra-high pressure vessel design lies at a very rudimentary level, namely understanding the requirements for controlling stress distributions within a body under fixed loading. Conventionally, engineers vary the geometry of a design to optimize stress distributions. However when the geometry is fixed or already optimal then the material itself is the only remaining variable.

Clear comprehension in designing composite pressure vessels entails not only a rigorous enough stress analysis, but further treating the independent material properties as variables to the solution and thereupon designing the *variable* material. This latter approach has as yet only been touched in theoretical mechanics through description of anisotropic bodies and vaguely broached via experimental efforts directed at improving operating pressures in vessels. To date nobody has approached the problem in the practical sense while having both clear analytical methods and fundamental insight.

1.5 Thesis Objectives and Organization

The work of this thesis focuses on determining how to obtain a more effective utilization of available material strength. The question posed is: How can one design a thick-walled vessel such that the stress distributions within can be controlled at will, and further how can this information be used to entail designs that create a more even incipient failure distribution throughout the wall, thereby maximizing material use efficiency. These

challenges are broached by first examining the geometry and construction then by exploring anisotropic elements constituting the general thick pressure vessel. The wall construction is idealized as a constituting of a *variable property monolithic material* whose range of properties are restricted. The property limits imposed are dictated by commercially available composites as used in discrete layered approximations of the variable elastic properties wall. Two parallel design methods are used, one based on the monolithic continuum, the other on a discrete layered approximation thereof.

A thick-walled vessel is built and tested to verify the theory, and also some past experimental results emanating from others are re-examined. The aim is to generate some fundamental understanding as to how stress distributions within thick-walled vessel are governed and how they can be shaped. The complementary objective is to put together a computer design tool founded on these insights which can then be used as a basis for designing and building prototype vessels. These can be destined for future vehicular or complementary commercial applications requiring ultra-high pressure containment.

The manuscript is subdivided into 9 chapters, each dealing with specific concerns: Chapter 2 reviews the literature commencing with composite vessels designed from the mid 1960's to present. Sub-topics include liners and cryogenics, CNG / H_2 in vehicles, regulations, testing, certification and other specifics on the problem. Chapter 3 covers certain analytical aspects of winding geometry, dome profiles and the associated filament stresses and stability of the windings on these surfaces. Chapter 4 pertains to the orthotropic multi-layered solution for thick-walled cylinders. Chapter 5 deals with the generalized plane strain solution and examines various cases, including a general variable

property approximation to a monolithic thick cylinder. Chapter 6 extends the Chapter 5 derivations to encompass individual elastic property variation rates representative of real materials, and sets up the problem for numerical solution. Chapter 7 expands on micromechanics, failure criteria and the elastic property changes that accompany damage development in the laminate. Chapter 8 demonstrates features and operation of the software following example cases. Chapter 9 discusses current limitations, analyses data from tests, reviews contributions and indicates the areas and direction of future work. References follow the last chapter and the appendix holds the computer code.

Chapter 2

Development History and Current State of the Art

2.0 Topics Considered for Review

The scope of this chapter is intentionally broad. The aim is to present some developments other researchers in the field have covered with the hope that this background can serve to place the present efforts into a better context. The topic of composite pressure vessel analysis and design has seen over 50 years of development, few ideas if any are wholly unique, only their improved implementation can substantiate such a claim. In reviewing the literature previous researcher's successes and failures must be taken in context with the era in which the work was performed. Fibers and resin systems are continually evolving and the same is true of winding equipment, computing power and theoretical approaches. In many cases a conclusion drawn before a technology matured no longer carries validity. As examples, the characteristics of carbon fibers, or early versions of Kevlar® (then referred to as PRD-I / PRD-III) were not nearly as impressive as they are today.

Approximately 350 papers, defense reports, computer listings, books, products literature, conference proceedings, thesis, standards and web pages were consulted or studied in the process of carrying out the present review. These are referenced throughout the text.

Chapter 1 briefly described the rocket ancestry of filament winding, outlined some

basics of composite pressure vessels and their utility, establishing the aim of the thesis work and its organization.

This chapter is specific to pressure vessels and deals mainly with past works supportive of their design. The subject can be grouped into three main areas. First are reviews of experimental work and practical findings, this also covers safety and regulatory issues. Second, analytical approaches, applicable design theories and failure predictions are broached. Lastly, a short summary of the various considerations described is interpreted in a sense to indicate which factors or techniques are most appropriate for the design and construction of ultra-high pressure composite vessels.

2.1 Definition of Pressure Vessel Efficiency

For constant material technology, the parametric performance of a pressure vessel can be evaluated as a constant determined by PV/W (pressure times volume divided by total weight). Units are "inches" in the imperial system and "Km" in metric with an equivalence of 39,370 in. = 1 Km. The structural efficiency of the best all metal pressure vessels (titanium spheres) is around 0.6 million inches. The better composite vessels with a metallic liner and connection bosses are capable of performance factors around 1.2 million inches [29]. When the composite alone is considered, over 2 million inches can be found quoted in the literature. Considering the composite independently is appropriate when comparing on the basis of efficient use of the fiber thus separating its performance from that of the liner. However because liner, connection boss and composite must co-exist in

11

practice, the overall performance factors will be referred to throughout for consistency.

2.2 Vessels Classification by Liner

Terminology referring to various types of composite pressure vessels can lead to confusion. Aside from homogenous metal vessels four distinct classes of high pressure composite vessels exist. Unlike low pressure tanks and pipes, composite vessel require liners to overcome leakage and hence are easily distinguished by this feature. In the first category are tanks rarely considered to be true composite vessels. They consist of hoop windings reinforcing a conventional thick metal shell, usually referred to as either "circumferentially reinforced", "thick-liner" or "hoop-wound". This primitive category is omitted from all further discussion. Second are thin metal lined full composite overwrap vessels. Equivalent names are "metal-lined", "thin-walled liner", "load-sharing", "fully overwrapped" among others. In the third category are bonded-metal foil-lined fully-overwrapped vessels. Most authors refer to these as "bonded liner" or "foil-lined". The fourth class of vessel is distinguished by a polymeric liner. Elastomers, drawn thin films and molded thermoplastics can be used. Terms such as "all plastic" and "fully composite" or "plastic-lined" are often used to describe them.

The feature differentiating "load-sharing" and "foil-lined" vessels is that foils depend on bonding with the composite to avoid buckling or wrinkling of the liner during depressurization. In contrast, load-sharing liners are sufficiently thick to maintain elastic stability under the compressive loads experienced after depressurization subsequent to a

12

prescribed amount of yielding on first pressurization or "sizing". The actual thicknesses involved are a function of liner material, vessel geometry, strain range, cyclic life and other parameters related to manufacturing. Load-sharing liners are normally not bonded to the composite.

2.2.1 Foil-Lined Vessels

The foil-lined vessel is a concept which has evolved and is suitable for low cyclic applications. This construction has inherent high efficiency, and uses the thinnest possible liner consistent with manufacturing techniques. The liner serves only as a permeation barrier whilst the composite overwrap is the primary load carrying element. Because no metal has an elastic strain range as great as that of the composite, the liner cycles through its plastic range on every pressurization. It must be well bonded to the overwrap to prevent the formation of wrinkles on depressurization as it is being forced into its plastic compressive region.

In operation, as the vessel is pressurized it strains 1% - 2%. The liner yields at ¼ - ½ percent strain and deforms plastically thereon. On depressurization, the liner can only recover elastically about ½ % , the rest of the strain is plastic compressive and relies on adhesion to the composite. If the bond fails, the liner buckles and crimps locally which leads to failure on subsequent cycles. This design is feasible only for a very limited number of pressurizations.

The concept was extensively evaluated by NASA and best results were achieved

using the higher modulus materials for overwinding, limiting strain range and thereby extending life. Initially this concept was successful for the storage of nitrogen tetroxide propellant where a 30 day life and 25 cycles of pressurization were the extent of the requirements. The filaments used were S-glass with liners of 0.006" (0.15 mm) thickness in type 347 stainless steel. Burst pressures required were only 750 psi. Liner debonding was well noted by Sanger, Mulho and Morris [5] who reported on this work in 1966.

Later, in 1974, Hoggat [37] achieved *PV/W* values around 0.9 million inches on aramid fiber vessels with thin liners fabricated from type 321 stainless steel. The vessels failed within 20 cycles at 50% - 75% of the predicted burst pressure of 2500 psi. Rupture was as the result of localized wrinkling of the liner either during cure or by subsequent debonding. The same vessels survived, in the range of 100 - 900 cycles subject to similar conditions with an elastomeric liner. One exceptional vessel saw 2493 cycles to 75% of predicted burst pressure prior to failing in the composite of the dome region. Variability in the results was notably extensive and cyclic testing inevitably ended up testing the liner rather than the overwrap. Most investigators resorted to using identical rubber lined vessels to ascertain the longevity of the composite with respect to cyclic loads.

Development carried out at a later period for the Space Shuttle program continued with titanium (Ti-6AL-4V) and 5086 alloy aluminum liners 0.020" thick using high strength, intermediate modulus carbon fiber. Experiments showed that the titanium yielded at about 56% of the burst pressure while the aluminum yielded at about 20%. As expected, cyclic tests at 50% burst endured about 550 cycles for the aluminum but 2200 cycles for the titanium lined vessels. The liner life was entirely consistent with life data

taken from handbook values for these metals [38]. Later NASA programs for the Space Shuttle studied strain intensity ranges on load-sharing liners and employed low cycle fatigue approximations to predict failures [39].

Cyclic life with thin bonded liners is dependent on material and the level of plastic deformation seen during each cycle. Integrity of the bond is paramount and assuming the bond does not fail, representative cycles to failure using current technologies might be as follows: Titanium liner - carbon overwrap, cyclic load 50% of 6900 psi (48 MPa) burst, 2000 - 3000 cycles. Aluminum liner - Kevlar 49® overwrap, cyclic load 67% of 4200 psi (29 MPa) burst, 550 cycles [40].

In summary, although efficient weight-wise and non-permeable, a foil liner is usually responsible for a vessel's failure under cyclic loading. The liner debonds locally and buckles. Plastic deformations result in the foil's fracture causing the vessel to leak. Subsequent vessel leakage due to matrix cracking is normal and expected.

Clearly thin liners, even after long and thorough development have limitations considering their cyclic life. The advent of higher modulus carbon fibers and a maturing of liner designs have helped bring this method to a point where vessels can sustain a few thousand cycles. It should be noted also that because these efficient (light liner) designs are generally reserved for space applications they tend to be much more highly stressed and operate at safety factors ranging 1.5 and 2 times. Most testing is carried out at cyclic stress levels exceeding 50% rupture loads. This high loading biases survival results in a negative way relative to the load-sharing liner concept discussed below where lower cyclic levels are generally seen in testing.

2.2.2 Load-Sharing Liners

Composite vessels with a thin load-sharing liner were originated by Johns and Kaufman in 1966. The concept gained acceptance because of its greatly superior fatigue performance at the expense of a weight increase. The technique, almost universal today, uses a moderately thick liner (typically 0.040" - 0.080") which carries a fraction of the load. The actual percentage of the load carried varies greatly and in fact can be as low as 5% when a very thick-walled composite overwrap is considered.

Mulho and Landes [19] also concluded (1968) that a load-bearing non-buckling metal liner would be best if it could be plastically deformed initially and then work in the tensile and compressive elastic regions. Advantages would be elimination of a supporting mandrel (expendable tooling), no need for bonding between liner and composite, elimination of specialized fabrication and handling techniques (electron beam welding), greatly extended cyclic life and faster production. The drawback is a lower performance factor due to increased liner weight.

In operation, during the initial or "proof" pressurization cycle of a vessel, the metal liner is plastically strained while the composite overwrap is elastically strained. On depressurization the liner, having been subjected to a permanent set, is put into compression by the overwrap which is trying to return to its unstrained condition. Hence the liner is "sized" or "autofrettaged" into the composite during this proof cycle. Subsequent cycles at operating pressure (lower than the sizing cycle pressure) result in loads that can be carried within the elastic strain capability of both the composite

16

overwrap and the liner material [40].

Effectively the technique nearly doubles the available elastic strain range of the

metal liner. Figures 2.1 and 2.2 show strains in the liner and overwrap during the sizing

cycle and operating cycles for both foil-lined and load-sharing liner concepts. The

minimum liner thickness is dictated by its stability against buckling. Representative weight

savings are perhaps 40% over an optimized all metal titanium vessel when using Kevlar

49® on a load sharing stainless steel liner. For similar vessels constructed of carbon fiber

with a 6900 psi (48 MPa) design burst, a 15% gain in performance might be expected in

moving from a load-sharing liner to a foil-lined vessel [40].
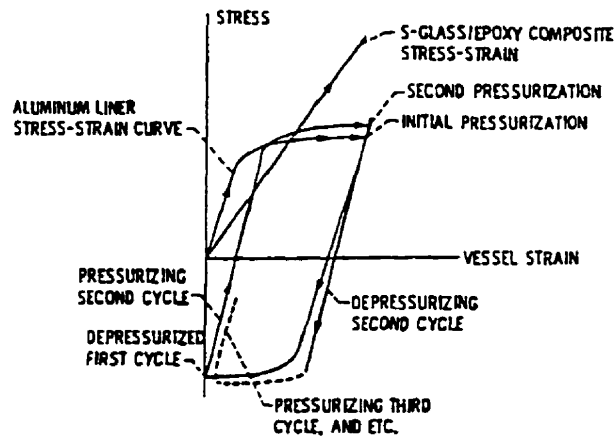
Figure 2.1 Typical stress-strain plot for an adhesively
bonded foil-lined composite vessel [40].
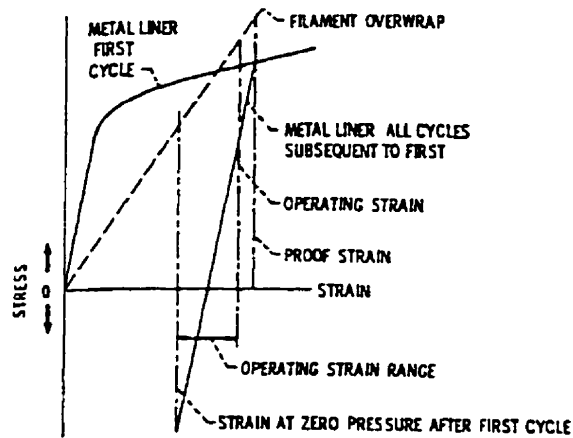
Figure 2.2 Typical stress-strain plot for composite vessel
with a metallic load-sharing liner [40].

Unless the overwrap is very stiff and low straining (as with HM type carbon fiber)

the liner's total elastic strain range can be as low as 30% of the fiber's permissible

elongation. In load-sharing liners the cyclic operating pressures are limited by low-cycle

fatigue as with the foil-lined vessels. Under identical cyclic stain, the lower weight foil-

lined vessels should provide the same life provided they maintain a perfect bond with the

composite. Such bonding is rarely if ever achieved.

The lower limit of liner thickness is dictated by the buckling criteria. This effect is

proportional to liner thickness to diameter ratio cubed $(t/d)^3$ for a cylinder and modified by

restraint conditions at the boundary. Axial length determines the number of lobes in the

buckled state. For a fixed (t/d) ratio the number of lobes decreases along with the critical

pressure for collapse as the cylinder is made longer [41]. In this respect it is evident that

shapes close to spherical are superior. For liner design the conditions of compressive

yielding or *inelastic* buckling are sought. Conventionally the criteria assumes a uniform

18

exterior pressure. In the case of a vessel liner the pressure loading on a potential lobe diminishes rapidly as the liner begins to deform hence adding complexity to the phenomena.

2.3 Development and Manufacture of Liners and Bosses

Fibers in the composite overwrap are taken to high stress levels, from 60% to 70% of their ultimate strength. These stress levels result in significant elongation of the composite (0.5% to over 2.0% depending on material) and extensive crazing or cracking of the resin matrix between the fibers results. Crazing becomes significant at composite stresses in the range of 10% to 40% of fiber ultimate strength. Eckold [42] maintains that at 0.3% strain micromechanical damage such as resin cracking and debonding between fibers appears. Because the craze paths join to form a leak path, an internal liner must be provided to contain the fluid or gas. Necessary characteristics are chemical compatibility, impermeability, elongation during pressurization and the ability to return to a stable and non-buckled position after the pressure is reduced.

Conventional low pressure filament wound structures such as tanks and pipes for the chemical processing industry operate at less than 10% of ultimate fiber stress levels and a resin rich gel coat or surface veil provides adequate sealing. Elastomers such as butyl rubber can be used as liners for moderate temperatures and pressures but are inadequate at cryogenic conditions in combination with high pressures. Elastomers exhibit brittle behavior at temperatures below their second glass transition and most cannot strain

19

with the composite overwrap lest they crack. The mismatch in thermal contraction with the composite leads to debonding. At high pressures, permeability to the gas causes blistering of the liners when absorbed gas is released during depressurization.

In answer to the permeation problems and resistance to cryogenic temperatures, metal liners have long been the basis for achieving fluid containment at high pressures. A liner must be capable of being formed into thin sections and amenable to assembly by welding. The fragile nature of such foil liners (thickness 0.006" - 0.030") requires that the liner be supported during winding, generally by plaster or inorganic salt mandrels fitted with a shaft to position it on the winder. The mandrel is removed by flushing with hot water or weak acids after curing the overwind.

In the program reported on by Mulho and Landes in 1968 [19], metal foil (0.006") liners were used. In Aerojet General's experience, the complexities related to hydroforming the thin stainless-steel liners and welding the various sections together with the end bosses were manageable. Maintaining liner integrity during the winding posed a bigger challenge due to the difficulty of finding a wash-out mandrel support that did not shrink.

Mandrels for supporting the liners are necessary in cases where the liner is not rigid enough to act as the support or form upon which the winding is placed. The criteria are: (a) dimensional stability, (i.e.: no shrinkage on curing), (b) a matching coefficient of thermal expansion, (c) castability, (d) ease of removal, (e) sufficient compressive strength and modulus.

Mulho and Landes [19] attempted many methods to support their metal foil liners.

One was to pressurize the liner but rippling resulted at the roving cross-over points. This was attributed to the shape of the liner being substantially different than the neutral axis configuration of the complete wound tank. Low melting alloys were tried (tin-bismuth) but the density of the material is so high that it is difficult to cast and the liner can distort from its weight. Different types of specialty plasters were experimented with. Shrinkage, despite manufacturers claims, was a big problem especially at elevated curing temperatures (300 °F). The material finally used was a sand-PVA mix even though it has the drawback of low compressive strength.

Traditionally, all foil metal liners succumb to failure and are especially prone to do so at the welds, either at the equator or dome-to-boss junction. In addition, this is often preceded by debonding which leads to microbuckling. The debonding generally occurs first at junctions and discontinuities. One approach much researched was the "hinged boss" design, Figure 2.3.

(a) CONVENTIONAL THIN-LINER-TO-BOSS ATTACHMENT.

(b) "HINGE-BOSS" THIN-LINER-TO-BOSS ATTACHMENT.
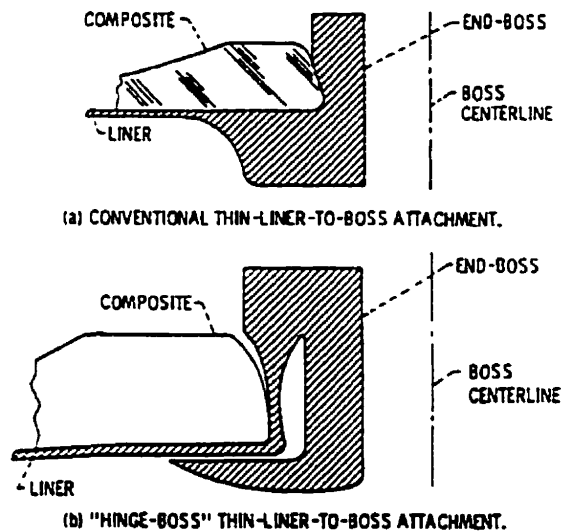
Figure 2.3 Hinge-boss design for thin metal liner to fill stem attachment [43].

Even in cases where liner rupture at the boss could be avoided failure at other weld points would inevitably follow [43][37].

Single-piece liner construction has advantages and electroforming is one such method. Guess [16] used this technique and plated copper over an aluminum sphere incorporating a stainless-steel fill stem. After etching away the aluminum, the copper remained with a metallurgically bonded fill stem. Because the fill stem was very small and appropriately designed, the calculated stress intensity factor at the junction was only 1.11. Gerstle and Kunz [44] made similar size liners for thin-walled vessels using hydroformed 1100-0 aluminum hemi-shells, electron beam welded at the equator. Fill stem and south pole bosses were machined from 5086-0 alloy and welded in place. An overall stress concentration factor near 1.25 was estimated, due in part to the difference in yield strength between the two alloys. Figures 2.4 and 2.5 show some details of electro-formed liners and electron-beam welded ones from the above mentioned authors respectively.

Geometry	Liner ϵ_θ) Max/ϵ_θ) Nom	Composite Shell σ_θ) Max / σ_θ) Nom
1	8.90	1.37
2	3.36	1.11
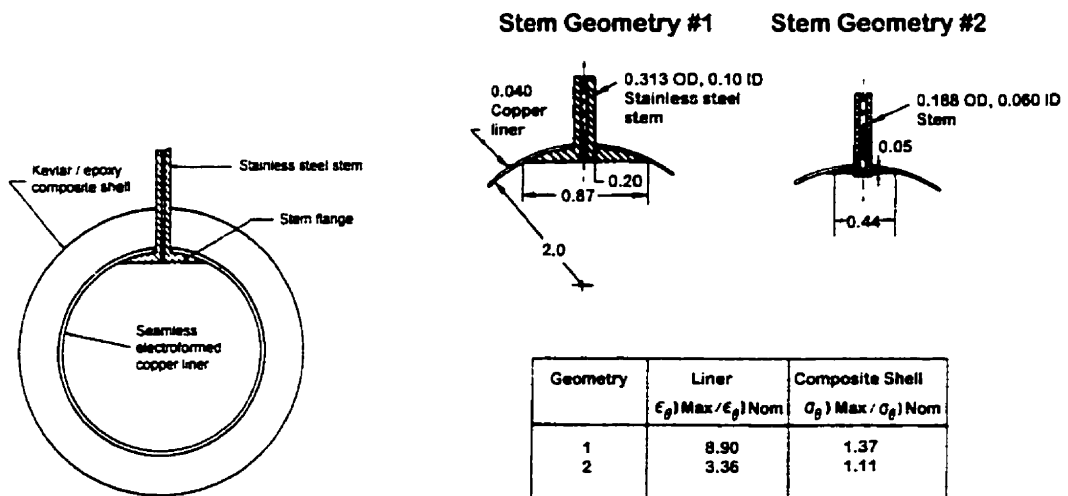
Figure 2.4 Dimensions pertaining to different stem geometries and values of stress concentrations associated with each design [18].
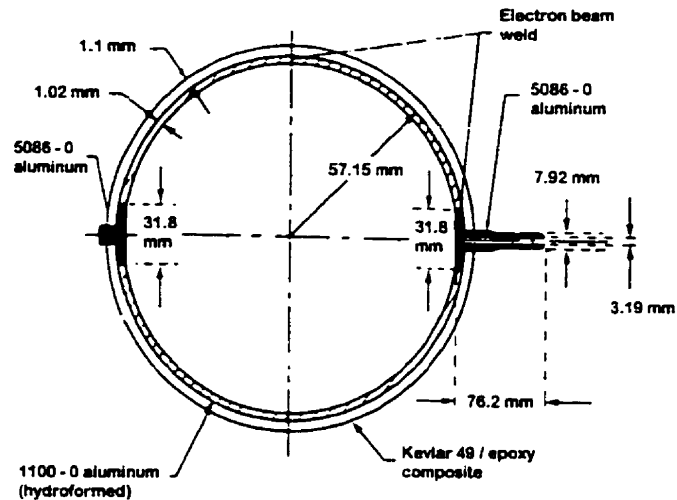
Figure 2.5 Geometry of aluminum lined Kevlar-49® epoxy vessel.
Failure point in composite was next to the weld between
the 1100 and 5086 aluminum [44].

Thin cylindrical aluminum 6061-T6 liners were formed by impact extrusion in the

program reported by Grover and Alyer [45]. A three step boss was used to minimize the

wind build-up at the vessel ends. Two such extrusions were welded together to form a self

supported liner. The wind angle was chosen in order that each helical layer lay adjacent to

the largest unwound step diameter. When the composite reached the top of the step, the

winding pattern was changed in order that the band lay adjacent to the next smaller boss

step diameter. This procedure prevents excessive fiber build-ups and bridging. Liner

thickness at the polar opening is dictated by the local shear strength requirement to

prevent blowout of the boss. The steps reduce both composite and liner weight while

lowering the stress concentration at the tangent line between dome and boss. Also it

appears that the stepped boss, acting as a rigid body, distributes load to the intermediate

23

layers at each step interface.

With current production methods, thin aluminum liners are commonly fabricated by deep-drawing and spin-closing a round sheet. This forms a single boss liner. Alternatively, drawn aluminum tubing can be spun closed at both ends to obtain a vessel with two openings. In each case, the spinning process limits the minimum thickness. Chemical milling has been used to reduce the thickness from 0.080" down to 0.023" and lower for specialized applications [14].

Most commercial production thin metal-lined (load sharing) vessels today use 6061-T6 aluminum alloy because of its availability however it is known that 6351-T6 has superior corrosion resistance and strength [46].

Development work on Skylab and the Space Shuttle focused on vessels of the load sharing liner design [39]. Inconel 718 and Ti-6Al-4V liners were examined. Inconel remains inert with oxygen (life-support) while titanium liners were slated for use with helium for expulsion of the fuels to the rocket nozzles.

In commercial applications, especially vehicular, the liner cost and its weight are significant considerations. The price ratio between a conventional gasoline fuel tank and the equivalent fuel containment in glass composite gas cylinders has been estimated at 25 times [31]. This is rapidly changing. The cost of the metal liner and its contribution to the total weight is significant. Vessels incorporating blow-molded HDPE plastic liners using encapsulated aluminum bosses overwrapped with either E-glass or glass / carbon hybrids have recently been introduced for vehicular application [24]. The manufacturer states that the plastic liner can be produced for 50% of the cost relative to a metallic one. For plastic

liners, data on permeation resistance to the methane molecule at 3000-4000 psi is very difficult to find [31]. Hydrogen is known to permeate more than methane, but not very significantly more. Cylinder manufacturers have had to perform their own testing.

Authors Hamstad and Chiao [38] had successfully used fatigue resistant plastic liners in 1974 to contain nitrogen. Helium however was too permeable.

Brunswick states that permeation rates for its plastic-lined pressure vessels are under 0.1% of the allowable under the ANSI/AGA NGV2 standard. Surface treatments are also under examination to further reduce permeation if so required. In production, the plastic is extruded into a tube by a die that can vary the resulting wall thickness along the parison's (pre-form) length. The plastic is blown against the closed mold halves and the wall in the parison is designed to result in a liner with gradual transitions in wall thickness. This minimizes strain concentrations, weight, and elevates cyclic life capability [47].

Approaches using integral foils or electro-deposited metal on the plastic liners were long ago tried for containment of hydrogen at cryogenic temperatures. These experiments were not successful. It was concluded that polymeric films will always be permeable to the rare gases. [11]

Presently there is no known effort to re-evaluate the capability of polymeric liners for use with low reactivity gases such as methane or hydrogen at cryogenic temperatures.

2.4 Liner Fracture

A different aspect of materials technology is liner fracture toughness. In a program reported on by Gleich [48], testing on Kevlar® spherical vessels with a thin cryoformed 301 stainless steel liner showed virgin fracture toughness of over 180 ksi $\sqrt{in}$ (200 MPa$\sqrt{m}$) and better than 100 ksi $\sqrt{in}$ (110 MPa$\sqrt{m}$) in the heat affected zone of the weld. Critical flaw length was 4 times liner thickness in this 200-260 ksi strength material. A leak before burst (LBB) condition was theoretically assured and tested to be so. Severe hydrogen embrittlement around the girth was instigated artificially and lead to complete and instantaneous failure (10^{-4} to 10^{-6} sec.) throughout the liner with negligible affect upon the fibers. Even at a 50% reduced fiber overwrap thickness there was never any form of catastrophic materials release while the liner fractured at the operating pressure. There are on-going studies examining the safety of designs in current and future aerospace composite pressure vessels, specifically impact / damage tolerance related [60].

Schmidt [49] published a fracture mechanics design method used at Brunswick Corp. to predict dynamic loadings imposed by liner failures and showed that potential problems can arise when the liner is very thick relative to the overwrap.

In certain cases it has been debated if the liner itself affects the failure mode of the composite. Grover and co-authors [17] substituted their aluminum liner with a rubber bladder and found no evidence of any change.

During a Space Shuttle development program, titanium liners were found to be quite flaw sensitive around the welds. Examinations also showed that titanium is

susceptible to cracks initiated at brittle oxide layers as a result of inadequate furnace control during liner annealing. Dye penetrant testing and X-ray inspection were performed prior to winding. The X-ray inspection was repeated after the sizing cycle when cracks grow and open under pressure. Subsequently fracture mechanics was applied to predict service life [39]. With titanium the critical flaw size can be less than the liner thickness hence extensive quality control is requisite.

2.5 Composite Material Property Requirements

Estimation of the safe working life of a composite vessel requires an assumption about the controlling failure mode. Some applications require storage at high pressure with only slight cyclic variations in pressure. When considering only the time at pressure, correlation can be drawn to creep-rupture tests. Extensive work was carried out with Kevlar 49$^{®}$ and S-glass / epoxy using both impregnated strands (Chiao and co-authors [50]) and actual pressure vessels (Gerstle and Kunz [44]). Although strand-based and vessel quasi-static strength data showed little variation, creep-rupture data presented considerable scatter. Based on a "one in a million" failure rate, the investigators concluded that a safety factor between 1.8 to 2.7 would be suitable for vessels needing to remain in service for 10 years. This variability was attributed to inconsistencies in the Kevlar 49$^{®}$'s characteristics from spool to spool. Within a particular spool, failure was entirely consistent. (One might assume that consistency problems today are less likely). It was noted that extreme sensitivity of pressure on failure times in creep rupture experiments

27

requires very tight limits on pressure or stress. A 20 ksi (138 MPa) increase in the applied stress can reduce life by a factor of 10.

Impregnated strand tests indicated that S-glass / epoxy degraded near twice the rate of the Kevlar 49[®] / epoxy and that for equal time to failure the Kevlar[®] system could sustain a slightly higher percentage of its ultimate stress than S-glass. Unlike Kevlar[®] and glass, carbon fiber is almost insensitive to sustained loads and tolerant in fatigue. As early as 1969, cyclic testing on Thornel 50 carbon fiber vessels at up to 90% of static burst showed one unit that survived over 1000 cycles. Performance in this respect is an order of magnitude above what could be expected of glass or Kevlar[®] [43]. Babel and Vickers [51] experimented with carbon fiber vessels loaded to 97% of their expected rupture and used this data in conjunction with strand tests. The purpose of the study was to provide assurance of a 30 year life with 50% sustained load combined with periodic cycling for use aboard Space Station Freedom. The probability of survival under 50% sustained load was estimated to be better than 99.9999%.

It should be noted that many of the works reported on were performed whilst Kevlar 49[®] (Dupont's trade name for their aromatic polyamide or aramid fiber) was in the development phases, designated PRD-III. To be accurate, the PRD and early references to "Kevlar" were based on poly-p-benzamide (patent 1967 & 1972), and only later did Kevlar 29[®], Kevlar 49[®] and Kevlar T950/956[®], based on p-phenylene terephthalamide (patent 1974), come to replace these. Similarly, glass and especially carbon fibers have seen a great deal of technological evolution [52]. The manufacturers of these have continually made advances and over the years many of the smaller companies have seen

their product lines and trade-names merged with the multinationals. Divisions are bought and sold so the geneology of particular fibers is often difficult to follow. Among the major manufacturers in existence today are Toray, AMOCO, Hexcel, Zoltek, Akzo, Mitsubishi, DuPont, Owens-Corning and Vetrotex-Certin-Teed [53].

Experience has shown that impregnated strand test data can be translated to an allowable vessel layer stress given that an appropriate correction factor (translation factor) is applied. As far back as 1964 it was realized that hoop windings on vessels can achieve very near laboratory strand tensile results, whereas for the helical layers 85% was a reasonable expectation. Table 2.1, taken from Shibley [54] on stress correction factors, relates to glass fibers and shows the reduction factors used over laboratory uniaxial tests as a function of overall vessel size.

Table 2.1 Correction factors for allowable stress [54].

Diameter, in. (cm)	Hoop Filament	Longitudinal Filament
4 (10)	0.99	0.95
18 (46)	0.96	0.89
36 (91)	0.94	0.87
44 (112)	0.93	0.87
54 (137)	0.92	0.86
300* (762)	0.87	0.83

* extrapolated

In a cylindrical pressure vessel, translation efficiencies are lower for helical fibers than for hoop fibers. This is because the helical fibers suffer from the overlaps and cross-overs, as well as the discontinuities at the dome cylinder junction and the polar boss region. For these reasons, the helical to hoop fiber stress ratio may range 0.75 to 1.0

depending on the severity of these factors.

Peters, Humphrey and Foral [55] discuss Kevlar 49[®]. In a biaxial tension field like a pressure vessel, Kevlar 49[®] exhibits lower translation efficiencies than glass or graphite, typically 70 - 80% of the strand tensile value. Translation efficiency is affected by fiber damage during winding, voids, complex stress states, etc., which are present in the laminate but not in the strand tensile specimen. Kevlar[®] with its fibrous micro-structure, is easily split longitudinally by matrix cracks, given the matrix is tightly bonded to the fiber. When the fiber is coated with a release agent (silicone oil) prior to winding, matrix cracking by-passes the fiber thereby improving efficiency.

Where interlaminar shear strength is important, fibers would not be "released" from the matrix. Reflecting this, in a cylindrical pressure vessel, the hoop fibers can be coated in oil while the helically wound fibers, with discontinuities at the dome cylinder junction and polar boss, would not be released. Translation efficiencies in the hoop fibers would typically increase from 70% to 85% by releasing. Releasing glass and graphite fibers has not been found effective at improving their translation efficiencies.

Micromechanical modeling of the time dependent properties of Kevlar[®] suggests that if the fiber is well bonded to the matrix it may be subject to longitudinal cracking because of its inherent weakness in this direction. Statistical studies and models for Kevlar[®] fiber's strength and stress-rupture behavior are well documented in a publication by Phoenix and Wu [56]. Failure modes in Kevlar[®] fiber and their origin are also discussed by Morgan et al. [57].

Low velocity impacts on pressure vessels have been assessed by Knight [58]

experimentally and computer modeled by Yener and Wolcott [59]. There is an ongoing study presently (COPV) at the NASA JSC White Sands facility to evaluate damage development and advanced non-destructive testing techniques. These include IR thermography, ultrasound, eddy current and acoustic emission for vessels subject to impact and / or chemical attack of the liner [60].

DuPont produces many forms of Kevlar® and has developed a variation with higher modulus (Type 149), or variants that have doubled impact and improved strength translation by 40% in hoop windings (Type 49-981) [37][61].

Studies on environmental effects have shown Kevlar®'s sensitivity to UV radiation. Its fabric degrades to half the original strength in only 5 weeks of exposure to strong sunlight. Humidity effects on Kevlar® are for the most part reversible and dependent on resin properties. Glass based composites suffer to a greater degree. The temperature limitations for Kevlar® are 200 °C, beyond which significant property degradations over time can be expected [62]. Carbon fiber are comparatively stable but not the resin systems.

2.6 Cryogenic Properties

Nickel base alloys, stainless steel, aluminum and titanium, of differing compositions were evaluated as load sharing liners at cryogenic conditions along with glass composite overwraps [8]. The composite showed an increase in strength of approximately 25% at -320 °F (77 °K). Titanium, followed by aluminum liners, promised the lightest structure while stainless steel, titanium and the nickel base alloys show

31

enhanced properties at cryogenic temperatures. Titanium has the highest liner elastic range (0.6%), aluminum (0.4% - 0.5%) while stainless steel is non-linear and subject to work-hardening. Stainless-steel liners are therefore habitually cryoformed in liquid nitrogen as this allows strain hardening by a factor up to 7 times. Even sizing can be performed in a liquid nitrogen bath [46].

Electro-deposited nickel and metallized Mylar® films among many candidate materials were tested by Toth back in 1964 [10][11]. He determined both permeation rates and elongation characteristics at 20 °K (liquid hydrogen temperature). The electro-deposited nickel 0.005" thick performed best, surviving +/- 0.83% strain for 250 cycles. This takes the nickel well into plastic deformation on every cycle. Also for single cycle burst tests the electro-deposited liner remained intact at the 2.5% - 3% strain experienced. At 20 °K, electroformed nickel exhibits 20% elongation and a 110 ksi (758 MPa) yield strength.

The high differential contraction rates of polymeric films relative to the composite and their low elongation rendered them unsuitable at these temperatures. Reactivity of the liquid oxygen (LOX) with hydrocarbon-based polymers can lead to small detonations when subject to severe impact [11][63].

The above work by Toth, Caren [13], Pope [12] and others was part of a NASA sponsored exploratory program to evaluate polymeric films as liners for cryogenic containment of fuel / oxidizers. Candidate elastomeric materials including Teflon, PVDF, polyimide and polyamide films, TFE, FEP, CTFE and many others were examined in the mid to late 1960's.

Space flight requires the containment under pressure of propellants: Liquid hydrogen, liquid oxygen, and fuels pentaborane, chlorine trifluoride, 50% / 50% dimethylhydrazine-hydrazine mixtures and nitrogen tetroxide. Kapton® film (polyimide) was eventually selected as the best candidate material in these early studies. It exhibited about 10% strain at 20 °K but further evaluation showed it fractured quickly under cyclic conditions. Only 6 cycles were survived at 1.2% strain [9]. Previous studies at 77 °K by Boeing had indicated that this film might be suitable. In general the limitations encountered with polymeric liners included permeability, erosion under rapid flow, low elasticity at cryogenic temperatures, short fatigue life and manufacturing problems. Such complications, given the materials, requirements imposed and technology available, led to an abandonment of the idea [6][40][63].

Evaluation of materials for a proposed British reusable orbital launch vehicle authored by Walmsley and Wilson [64] sees APC-2 (PEEK thermoplastic / carbon fiber) showing good promise for a thin-walled vessel storing liquid hydrogen at 20 °K. APC-2 appears to have low susceptibility to microcracking as opposed to other composites. In the past, numerous epoxy resin matrix composite vessels of glass, Kevlar® or carbon have seen service at cryogenic temperatures. Thermal conductivity values and contraction coefficients as temperature functions are known and standards for outgassing under vacuum have been established for service in space [65]. The National Bureau of Standards (NBS) in the U.S. has established parameters when using elastomeric O-rings as static seals at 77 °K. The confined rings are compressed as much as 80% before subjecting them to low temperature. On the whole, 30% strength and 10% modulus increases are expected

for most fibers as one approaches absolute zero. The ultimate strains of the fluoropolymers vary significantly within the cryogenic range, and some are useable at under -200 °C (-328 °F).

Kasen [63][66] reviews properties of both resins and fibers at cryogenic temperature. This work, although dated, is comprehensive and reviews all available data through 1975. Some facts evident are that Kevlar® expands greatly when cooled whereas carbon fibers show a minimal positive coefficient of thermal expansion and glass contracts. The modulus of Kevlar® increases about 40% at 77 °K while strength is about 90% of room temperature values. Carbon fiber's modulus is stable but the low temperature strength degrades somewhat although fatigue performance remains superior to all other fiber types. Variability resulting from the broad base of the test data reviewed remains an obscuring factor.

2.7 Safety Standards

There exist so many different applications, materials and methods of construction, service life and exposures to environmental hazards that every design and application needs to have its safety examined. Standards and test methods evolve, progress and get revised with accumulation of experience and the evolution of newer designs. Surveying the literature has shown the upper range of safety factors in the neighborhood of 3.5 while the lowest are around 1.5 times the burst pressure. Different regulations exist for military and civilian use. Illustration and example over the spectrum in various applications can

serve to condense and clarify. The commonly known ASME pressure vessel code (Section-X) restricts itself to a maximum of 200 psi (1.4 MPa) for composite vessels hence other guidelines are presently being followed [32].

2.7.1 Military Standards

Military Specifications (MIL-R-8573 for steel tanks and MIL-T-25363 for all composite tanks) were originally written in the 1950's. These MIL-STD's later became the basis for civilian Department of Transport (DOT) exemptions and later DOT specifications for composite pressure vessels.

Representative of one extreme, Charpentier and Reuille [67] report on implementation of MIL-STD-1522A (USAF) [33] for thin-walled titanium lined carbon or Kevlar$^{\circledR}$ vessels intended for service on satellites designed by Aerospatial. The standard proposes two routes for qualification testing. For safety factors (SF) equal or above 2.0, a conventional route is chosen. This comprises a stress analysis and a fatigue analysis. Then the vessels are proof tested to 1.5 times operating pressure, cycle tested and finally burst. The standard however is really geared to permit construction of vessels with safety factors as low as 1.5 minimum. Typically such vessels would see service in unmanned devices launched into space where the design requirements are to withstand perhaps 20 pressurization cycles before burst. In such a case more extensive analysis is carried forth including a fracture analysis to establish if a "leak before burst" situation will result. Proof pressure is established at (SF + 1)/2 times operating pressure for a fail-safe mode and 1.25

35

times maximum expected operating pressure (MEOP) if analysis or tests show catastrophic failure modes. Both situations reduce to applying a proof pressure 1.25 times MEOP when designing to the lowest permissible safety factor of 1.5.

2.7.2 Civilian Standards

Until the event of composite pressure vessels, regulations for compressed gas cylinders were based on ASME rules. The basis of such mechanical engineering practices date back to the 1930's. ASME regulations are conservative and adequate for welding bottles and bulk storage facilities for the commercial gas storage and transport industries.

The US Department of Transport (DOT) has the authority under Title 49 of the Code of Federal Regulations - Transportation, by means of container specification, to govern pressure vessel use and to mandate their periodic re-testing.

Commonly, development in technology precedes regulations and standards set forth by rule makers. Proponents of composite pressure vessels succeeded in swaying acceptance from the DOT with the help of NASA technology transfer programs, commitment from aerospace giants like Boeing and pressure vessel specialists Structural Composites Industries (SCI), a primary aerospace subcontractor in this field today. DOT's first exemptions for load sharing metal lined vessels were granted in 1976 for a fireman's breathing air supply and the Boeing 747 escape shutes [46].

DOT specifications have evolved over the years in response to manufacturers requests for exemptions. Specifications include DOT 3-AA, 3-AL, 3-F (proposed for high

36

alloy steel), FRP-1, FRP-2. When development precedes available specifications, DOT issues transport exemptions. In Canada, the Canadian Transportation Commission (CTC) has likewise issued exemptions [35]. For Example CTC 1465 / DOT E-8725 applies to metal lined full-wrapped glass composite cylinders, DOT E-8162 for Kevlar® composite vessels and CTC 1880 / DOT E-8965 pertains to steel lined hoop wrapped vessels [24]. Other exemptions exist for composite vessels used in breathing apparatus, inflation devices, etc. One of the latest is E-10945 issued to SCI in late 1996 for their carbon fiber overwrapped self-contained breathing apparatus, also applicable to a host of other vessels designed to similar specifications [22].

2.7.3 Vehicular Fuel Cylinder Standards

The National Highway and Traffic Safety Administration (NHTSA), a department within the DOT was handed responsibility for NGV containers from the Hazardous Materials Branch. In 1990 NHTSA gave advanced notice of a proposed rule-making but did not act (President Bush had at that time imposed a moratorium on new rulemaking). Their inaction lead the vessel manufacturers, gas associations and related equipment manufacturers to implement ANSI/AGA NGV2-1992, a standard that permits 4 classes of cylinders [34]. This standard is geared specifically for automotive requirements and is similar but not identical to older DOT FRP-1, FRP-2 guidelines. It should be noted that the DOT regulations and exemptions do not presently address the use of vehicular fuel containers but are rather intended as approvals for common carriers (truck, rail, air) to

allow for a filled composite vessel's interstate transport.

The specter of product liability is an important concern for the big three U.S. car

manufacturers. These OEMs favor the latest plastic lined full-wrapped technology but they

lack a fully adopted and accepted NTHSA standard to back them. The newest

technologies are attractive due to greatly decreased weight and slightly greater contained

volume, Figure 2.6 and Table 2.2. However as late as the 1995 model year production
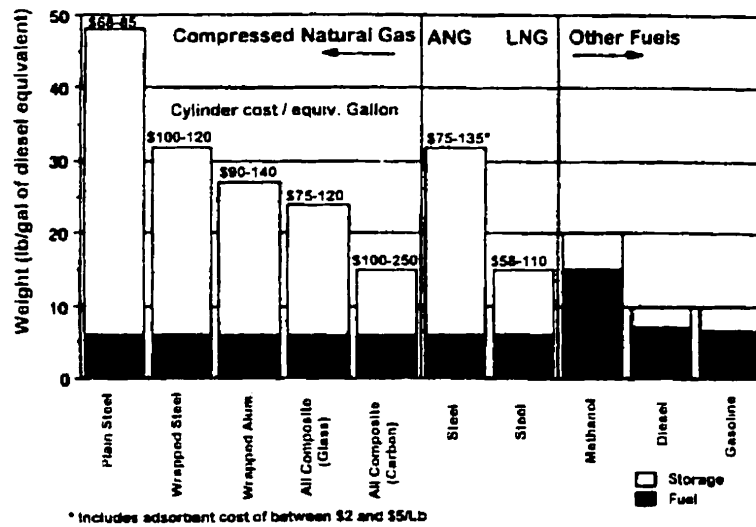
Figure 2.6 Comparison of storage systems
            weights for various alternate fuels [30].

light and medium duty trucks still used hoop-wound steel cylinder technology. Emphasis is

steadily shifting towards the more advanced technologies. Part of this is due to increasing

cost benefits as the price of carbon fiber falls and the estimated 30% reduction in vessel

Table 2.2 Attractiveness index of competing vehicular fuel cylinders [30].

Technology 3000 psi containment (circa 1993)	P Pressure Psi	V Volume Scf***	1/W Weight Lb^{-1}	1/C Cost $^{-1}$	PV/WC	PV/C
Hoop Wound Steel	1.00	1.00	1.00	1.00	1.00	1.00
Hoop Wound Aluminum	1.00	0.93	1.35	0.85	1.07	0.79
Fully Overwrapped Alum.	1.00	0.95	1.51	0.95	1.37	0.90
All Composite E-glass	1.00	0.95	1.79	1.15	1.95	1.09
All Composite Carbon*	1.00	1.14	3.57	1.10	4.48	1.25
All Composite Carbon**	1.00	1.14	3.57	0.90	3.66	1.03

*** Standard cubic foot
** assumes $13/lb carbon
* assumes $8/lb carbon

cost as a result of using blown thermoplastic liners. Presently the lowest cost carbon fibers

are $6.50 /lb. and optimistic expectations are in the $5.00 /lb. range for the year 2000.

Meanwhile retrofitters are using the latest technology. While Brunswick

Corporation was the first to market a plastic lined cylinder, EDO of Canada, Comdyne,

Atlantic Research, ABB of Sweden and Ullit of France each have their versions [30].

Newer regulations and standards are forthcoming. In Canada there exists a (draft)

"Appendix G" to the Canadian Boiler and Pressure Vessel Code and a standard (CAN

B51) for vehicular fuel cylinders. The International Standards Organization (ISO) is

looking at standards by the International Association for Natural Gas Vehicles (IANGV).

A draft standard (ISO DIS 11439) was published in 1997 and reviewed twice in 1998,

now to be redrafted by Powertech of Canada into 4 separate documents and submitted to

the ISO for approval [258]. The American Gas Association (AGA) has developed

recommendation for a standard on fuel dispensing and bulk storage facilities [68].

2.7.4 ANSI / AGA NGV2-1992 Specifications

Under the ANSI / AGA standard there are 4 classes. The first two of these concern metal and hoop reinforced metal cylinders. The third, NGV2-3, pertains to metal lined full wrapped cylinders. The fourth, NGV2-4, relates to plastic-lined full wrapped cylinders.

The standard applies to vessels up to 4350 psi (300 bar ≅ 29.6 MPa) maximum and applicable safety factors (SF) are defined as a function of the fiber type: Glass; SF = 3.5, aramid; SF = 3.0 and carbon; SF = 2.25. Service temperature limits are placed between -40 °C to 82 °C. Gas temperature at 57 °C defines maximum operating pressure.

Service life is 15 years, and for non-metallic liners maximum permeation is limited to 0.25 normal cc/hr per liter water capacity of the vessel while at service pressure.

Generally, for a 6061-T6 aluminum liner, the tensile stresses in the wall are 95% (compressive) and 60% tensile, relative to the yield strength at zero and operating pressures respectively [46].

Autofrettage pressure must be at least 105% of proof pressure (nominally 110%) and proof must be 1.5 times service pressure. Vessels are to be tested in maximum lots of 200 units or one shift of production, with destructive testing carried out on at least one such vessel.

5000 cycles from 10% to 125% operating pressure must be survived prior to burst testing on the test vessel taken from each production lot.

Minimum burst is defined by the safety factor multiplied by operating pressure.

Each individual vessel in the lot is proof tested to 1.5 times operating.

Aside from not leaking, the requirement is that permanent volumetric expansion must not exceed 5% of the total volume expansion seen under proof testing.

Additionally tensile and impact tests must be performed on a virgin liner.

The above represents the basics for lot acceptance and lot testing. Design qualification testing (essential for new designs) is more rigorous and includes the following:

a) Pressure cyclic testing: A new vessel is subjected from 10% to 100% pressurization for 13,000 cycles followed by 10% to 125% for 5000 cycles (max. rate 10 cycles / min).

b) Environmental cyclic testing: After having preconditioned a new vessel for 45 days at various temperatures and 67% service pressure with natural gas, compressor oils, water, hydrogen sulfide, and carbon dioxide (contaminants) according to a specified schedule, the vessel is subjected to the following:

5000 cycles 10% to 125% pressurization at 60 °C and 95% relative humidity followed by 10% to 100% pressurization at -40 °C for another 5000 cycles.

c) Burst tests: Three vessels are brought to the minimum required burst pressure (determined by the safety factor assigned to the material of construction), held for 10 seconds, then pressurized further till burst.

d) Damage Tolerance: A flaw tolerance test using a 1 inch (25 mm) long by 0.030" (0.75 mm) deep cut, an impact test at various points with a prescribed pendulum of 30 Nm energy and a drop test from a 10' (3 m) height to a concrete floor must be

performed. In each of the above tests the vessel must subsequently survive 1500 cycles from 10% to 100% pressure and be followed by a burst test.

e)   Fire: A bonfire test must be performed in different positions with 20 minutes exposure or stopped once the vessel vents through the safety valve. (Vessel must not burst).

f)   Creep: Testing is mandatory for vessels with non-metallic liners or with low glass transition resins. The test involves 125% pressure for 200 hrs at 20 °C above the maximum design material temperature. Afterwards the vessel is checked for conformance by a hydrostatic expansion test, leak test and burst test.

g)   Gunfire: Tests using a 30 caliber armor-piercing projectile (tungsten carbide) at 2800 ft/s ($\cong$ 850 m/s) are used to ensure the vessel does not experience fragmentation failures. Should pieces be released that have sufficient energy to pierce through automobile sheet metal, the vessel would not be considered acceptable.

h)   Gas permeation: This test is required for non-metallic lined vessels.

Severe abuse tests were extensively carried out at the request of the DOT in the early 1980's when composite vessels where first put into vehicles [69]. These tests included attempted destruction of filled vessels with dynamite, dropping NGV fueled cars from cranes 90 feet high, repeated blasts at point blank range from police issue 357 magnum "hot" charges, 50,000 cycles pressurization ambient and 25,000 cycles both cold and hot, and so forth. For example, in the drop test the vehicle's rear bumper ends up in a position originally occupied by the back seat. The vehicle collapses around the cylinders to

approximately half its initial length. In each such test the vessels survived. ANSI / NGV2 specifications are designed on the basis of utilizing the composite to a stress level commensurate with a 0.999999 reliability (1/million) for a period of 15 years [47]. Manufacturers tend to exceed the ANSI / AGA and DOT specifications by a small margin (example: SF = 2.35 is used rather than 2.25 as mandated for carbon fiber by Brunswick). Estimates exceeding 1 million fill cycles under normal pressurization have been made. Carbon is generally hybrid with a small amount of glass to increase damage tolerance. Some manufacturers use a tumbling 50 caliber gunfire test (specified by the military for gunfire tolerance) rather than 30 caliber [47]. This slight over design is likely to eradicate costly lot rejections, lessens a manufacturer's legal liability and helps cater to a broader market.

2.8 Thick-walled Vessels

Thick-walled composite pressure vessels were defined by authors Mulho and Landes in 1968 as vessels operating at 30,000 psi (200 MPa) or higher [19]. Guess [16] has indicated 22,000 psi (150 MPa) as the cut-off point while Grover, Foral and Humphrey and Ayler [17][45] infer that 25,000 psi (172 MPa) operating, 50,000 psi (345 MPa) burst are considered "ultra-high". On the whole, "thick-walled" and "ultra-high" are synonymous in this context.

Thin wall theory assumes that stresses through the wall thickness remain constant. Conventionally it is viewed that for radius to thickness ratios above 10 ($r/t > 10$) thin-wall

vessel theory is adequate. For thick-walled vessel design the nomenclature used is more

commonly the outer to inner radius ratio (b/a). The 10:1 rule of thumb does not extend

well to composite designs. The above assumption translates to a load drop of about 9.9%

at the outer wall for a pressurized sphere ($r/t = 10$, or $b/a = 1.1$) if the material is

isotropic. In spherical vessels, load drop is related to a material's orthotropy exponent

defined as $n = \dfrac{1}{2}\sqrt{1 + 8\dfrac{A_{\theta\theta} + A_{\theta\phi} - A_{\theta\rho}}{A_{\rho\rho}}}$, where the A's refer to the stiffness matrix terms

in the radial (ρ), hoop (ϕ) and meridional (θ) directions [15][16]. For isotropic materials n

$= 1.5$, but will range from 3-6 for composites. Kevlar at 70% volume fraction has $n =$

3.065. In the example above it would sustain a 12.9% load drop. Thornel 75S carbon fiber

at 51% volume fraction has $n = 6.13$. It would experience a 23% stress reduction with the

equivalent geometry. Clearly the thickness ratio chosen to define "thick" is a strong

function of material properties. For cylindrical vessels a similar factor is designated

$K = \sqrt{\dfrac{\beta_{11}}{\beta_{22}}}$, and the definitions for these terms can be found in Chapter 4 (equation 4.13).

K is a function of the winding angle (whereas n is defined in terms of axisymmetric

properties requisite for a sphere). For isotropic materials $K = 1$ but ranges $\cong 3$ for

composite laminates at typical winding angles near 55°. The implications for diminished

stress at the outer surface are parallel to those for spherical vessels.

The report authored by Mulho and Landes in 1968 is probably the earliest

work specifically related to the design and construction of high pressure thick-walled

vessels. Their vessel's thickness ratio are barely considered "thick" today with $r/t = 11$ (b/a

$= 1.09$). Owens-Corning 901-S1 glass was the material of construction. The program

established was not successful in arriving at relatively modest goals. Applications for the work were not specified but a design target was set at 15 cycles to 15,000 psi (103 MPa) and a 33,000 psi (227 MPa) burst pressure. The best vessel survived 13 cycles to 15,000 psi (103 MPa) and the highest burst pressure achieved was 23,800 psi (164 MPa). 16 vessels were built.

The investigators did correctly identify the essence of the problem facing them and this assessment has some validity today. To summarize, the following is excerpted:

"The thick-wall composite shell required to react high internal pressures introduces discontinuity stresses that must be minimized to achieve a uniform stress field throughout. These stresses result principally from the head-contour difference between inner and outer layers, and from uncontrolled filament tension during winding. The stress distribution in a pressurized thick-walled structure, calculated by the equations developed by Lamé are such that the outer surface is subjected to low stresses and is therefore inefficient. Several methods have been recommended for the construction of thick-walled, filament wound, high pressure vessels that will elastically resist relatively high internal pressures and will make effective use of the material near the outer surface. Basically they create pre-stresses of different magnitudes throughout the vessel wall, so that the resultant stress distribution will approach a constant value for each structural element when internal pressure is applied. The more practicable methods to accomplish this condition include the following:

* Varying winding tension of discrete layers of glass filaments during fabrication.

* Application of discrete layers of pre-stressed glass filaments with different

elastic moduli.

* Addition of an outer overwrap of a pre-stressed metal filament layer in

    order to achieve greater elastic restraint.

* A combination of the above methods."

Only the first method involving variable tension in the filaments was tried. At the

time, only glass filaments were readily available, precluding the variable moduli approach.

In the study by Mulho and Landes, an oblate spheroid, which constitutes two

geodesic or planar heads back to back without a cylindrical section, was chosen. This

configuration was based on one of their previous reports which indicated that the sphere

which represents the optimum configuration for homogeneous metal pressure vessels, is

theoretically no more efficient for filament-wound structures than is a vessel of any other

shape. Their test results indicated that the non-uniformities and stress concentrations

caused by the filament cross-overs of the multiple wrap patterns required to react a 1:1

biaxial force field relegate the filament-wound sphere to an efficiency below that of oblate

spheroids and cylindrical pressure vessels. Their studies indicated that the oblate spheroid

as the most efficient filament wound pressure vessel structure, followed by cylindrical and

torroidal shapes.

The method of increasing the winding tension of the filaments with each successive

layer was employed in the above study. For this design, the 330 ksi (2275 MPa) filament

stress was calculated to reduce to 280 ksi (1930 MPa) at the outer surface using the Lamé

equations. In the experiments winding tension was begun at 9.5 ksi (65 MPa) and

increased with each layer to the winder's maximum of 48 ksi (331 MPa) . Pre-impregnated

rovings were used, an intermediate cure was performed after half the wind thickness was complete. For some of these vessels the outer half was wet-wound.

Alternately, it was computed that a 3% increase in stiffness per layer would provide an equivalent effect (constant design stress).

The authors could offer little evidence that the fiber pre-stress was maintained after the curing.

Knight [70] and Leavesley [71] performed finite element studies about 20 years later which modelled the winding tension. Their studies were performed on wound spheres with the winding pattern reproduced concisely in the element generation scheme. They found that for thicker windings as much as half the wall thickness can end up in a state of compression. First there will be the effect of tension loss due to mandrel deflection. As each successive layer is applied its tension must be resisted by the mandrel. Any deflection will relieve fiber tension. Second there is the bulk motion of resin flowing outwards allowing the fibers to migrate inwards. Resin shrinkage and the thermal cycle during cure also contribute to the state of residual stress. Vessel strength degradation due to relaxed, wrinkled or locally buckled fibers resulting from a state of compression is a serious detrimental effect and can outweigh gains anticipated by pre-stressing.

In the 1980's a new application was found that required containment of helium at 25 ksi (172 MPa) operating, 50 ksi (345 MPa) burst, pressure as a power source for the pneumatic actuator systems aboard air-launched tactical missiles. A few researchers worked on the topic.

Grover and Ayler [45] used S-2 glass, Kevlar 49[R] and carbon fiber with increasing

stiffness towards the vessel exterior. A major difficulty arose when trying to surpass 35,000 psi (241 MPa). Development efforts showed that radial stiffness of the laminates is crucial. At 20 ksi (138 MPa), unidirectional Kevlar[®] fails under compression in a radial (transverse) direction. For small angle ± helical windings, the radial strength is higher but when the matrix fails, adjacent constraining layers rotate in opposite directions resulting in an abrupt loss of stiffness. A minimum weight and thickness design dictates that all helical and hoop layers are consolidated, with the hoop layers on the outside. The rotation effects can best be kept in check by having many thin and interspersed constraining layers. In Grover and Ayler's work helical layers with a ± 75° wind were interspersed with a ± 37° wind for this reason. Low radial stiffness also results from high void content, delamination and / or a high resin content.

In winding spherical vessels, Grover, Foral and Humphery [17] employed quasi-isotropic annular doilies with decreasing radius as interplies around the fill boss. In this region the rovings are all oriented tangent to the boss and susceptible to compressive failure due to radial loads. Also the fiber path can be concave due to fiber build-up at the beginning of each pattern causing fiber bridging, voids or weak resin filled areas.

Ericson and Yorgason [72] used finite element methods to study parameters affecting stress concentrations near the bosses. They evaluated and tested configurations for different wafers of reinforcement within the composite in this area and achieved a 17% stress reduction with a two step hoop wound dome wafer. Their work on graphite epoxy vessels lists a summary of techniques, identifying those detrimental and others which are beneficial over standard thin-walled vessel construction techniques.

Grover and co-authors [17] investigated spherical Kevlar pressure vessels for 25 ksi (172 MPa) operating, 50 ksi (345 MPa) burst pressure. Nine polar wind patterns from 11.7 to 90 degrees (planar) were used to build up the wall. Vessels with outer to inner diameter ratios up to 1.5 ($r/t = 3$) were constructed. Ductile 5086-0 aluminum 0.050" (1.25 mm) thick was hydroformed into hemispheres and welded at the equator. Prior to welding, polar fittings were machined from 17-4 PH stainless steel and bonded under temperature and pressure to the liner halves with chlorobutyl rubber. Their investigation showed that radial compaction effects may be taking place which lead to a delay in the onset of strain within the outer layers. Thermal curing stresses were found to be the major source of delamination. A 140 °F (60 °C) cure resin system was used to alleviate the situation allowing the design objectives to be met. The best PV/W was 0.361 million inches with b/a at 1.5.

Guess [16][18] published experiments related to the development of spherical and cylindrical pressure vessels in 1984. 62.5 ksi (430 MPa) containment was achieved in a spherical vessel consisting of Kevlar® over an electroformed copper liner with integral stainless steel fitting. The vessel sizes tested were very small (about 4" or 100 mm dia.) but scale effects were investigated over a 2:1 range; no changes resulted. The copper liners, when free of defects, would survive 20 pressurization cycles (maximum tested). The best cylindrical vessel burst at 58.1 ksi (400 MPa) . Guess used non-linear finite elements to refine the fill stem connection and arrived at a very small fitting that limited stress concentration to 11%. PV/W was calculated as 0.639 million inches with b/a at 1.35.

Recently Lal [73] presented an overview on a 28 ksi (193 MPa) burst pressure

containment vessel designed for helium. The author employed Torayca T-1000 fibers (1

million psi or $\cong$ 7000 MPa tensile strength) and used aluminum liners designed for a

previous 18 ksi (124 MPa) series of vessels. These liners were formed from a single piece

cold drawn shell. They were subject to a spinning process that built up the neck region and

chem-milled to reduce thickness elsewhere. The burst pressure target was met and 1367

cycles were survived at 0 - 10 ksi (70 MPa) cyclic loading. A fiber design stress of 700 ksi

(4900 MPa) was used. Vessel efficiency was stated as 1.16 million inches.

In the above study, basic engineering calculations showed that the liner design

employed had a safety factor below unity based on yielding, for the boss hoop stress, neck

shear stress and flange bending stress. A finite element analysis (COSMOSM) on the

composite revealed a severe stress spike near the dome to boss junction which was

reduced by the addition of a doily.

Efficiency in thick-walled design remains low, with PV/W values roughly half what

appears possible for lower pressure designs. Ultra high strength fibers such as T-1000

(first introduced at approximately USD $1000/ lb.) appear to be capable of extending

good efficiency values to higher pressures since they permit a reduction in wall thickness.

The last decade has seen fewer experimental programs with ultra high pressure

vessels but there has been work in an ongoing study evaluating mostly low velocity impact

(< 15 ft-lbs) upon vessels operating the 4,000 - 10,000 psi (28 - 70 MPa) range for space

flight applications. Naval efforts have centered on designing submarine inner hulls capable

of diving to the deepest ocean bottom. Also U.S. Army Armament Research has studied

lengthening their cannons with thick composite overwraps while retaining the inertial

characteristics of the metal ones[74].

2.9 Thermodynamics

A fundamental for the design of any pressure vessel is that all gases follow

approximately the same compressible behavior when normalized to their critical pressure

P_c and critical temperature T_c ratio. This is known as the *principle of corresponding*

states [75]. Generalized compressibility charts can be used to estimate the state or

thermodynamic tables can be referenced [76]. Figure 2.7 depicts the features of such a

chart [77].

Below a critical temperature T_c and pressure P_c, a liquid state can exist. Above T_c

the fluid is commonly termed "superheated vapor", below T_c "compressed liquid".

At high pressures these fluids become increasingly difficult to compress hence

pressures rises quickly with little gain in density. The point of diminishing returns is a

function of both the fluid's critical temperature and pressure. At low pressures one can

calculate on the basis of the ideal gas law $\dfrac{P\upsilon}{RT} = Z$. The compressibility factor Z remains

near or below unity (unity equals ideal gas behavior) for pressure ratios $P_r = \dfrac{P}{P_c}$ below 7 -

8. For methane, at room temperature, this translates to about 5200 psi ($\cong$ 36 MPa).

Hydrogen by comparison would show lowered compressibility (higher compressibility

factor Z) beginning at 1500 psi (10 MPa). A feature of this chart is that although the onset

51

.

of higher compressibility factors begins earlier for low boiling point gases like hydrogen

(lower critical temperature), the rate of increase of Z as a function of pressure is also less.

Methane's relatively high boiling point puts its $T_r = \dfrac{T}{T_c}$ at a low value of around 1.6. This

causes it to exhibit a severe increase in the compressibility factor for pressure ratios above

ten times P_c (near the saturated liquid line).

Citing values from thermodynamic tables [76] rather than interpolating on the

chart, the following is illustrative: Methane, in doubling the pressure from 500 bars (7,250

psi) to 1000 bars (14,500 psi) experiences a density increase of 25% whereas the same

pressure change upon hydrogen increases its density by 60%.

Reflected upon pressure vessel design for natural gas containment, the ratio of fuel

/ vessel mass is penalized by the increase in the compressibility factor Z multiplied by the

reduction in wall efficiency commensurate with higher pressure. The gas's compressibility

is thermodynamically imposed. For methane at 1000 bar (14.5 ksi) and room temperature,

the gaseous fluid is at 80% of liquid density relative to the atmospheric pressure boiling

point (111 °K). Extrapolation of the thermodynamic charts to 1700 bar (25 ksi) puts this

value about equal to 90% liquid density. The compressibility factor at this pressure is

about 2.6 whereas at 1000 bar (14.5 ksi) it is 1.9. Further compression of the fluid would

tend towards the slope of the "saturated liquid" compressive line. This constant slope

effectively represents a bulk modulus. Naturally it is pointless to seek the compression of

a "liquid". It must be noted that the conventional measure of vessel efficiency PV/W loses

its applicability at these extreme pressure since the implicit assumption that PV is a

constant is being violated. The compressibility factor Z may range as high as 2.8 at 40,000

psi (276 MPa). A pressure representing the best compromise between decreasing exterior
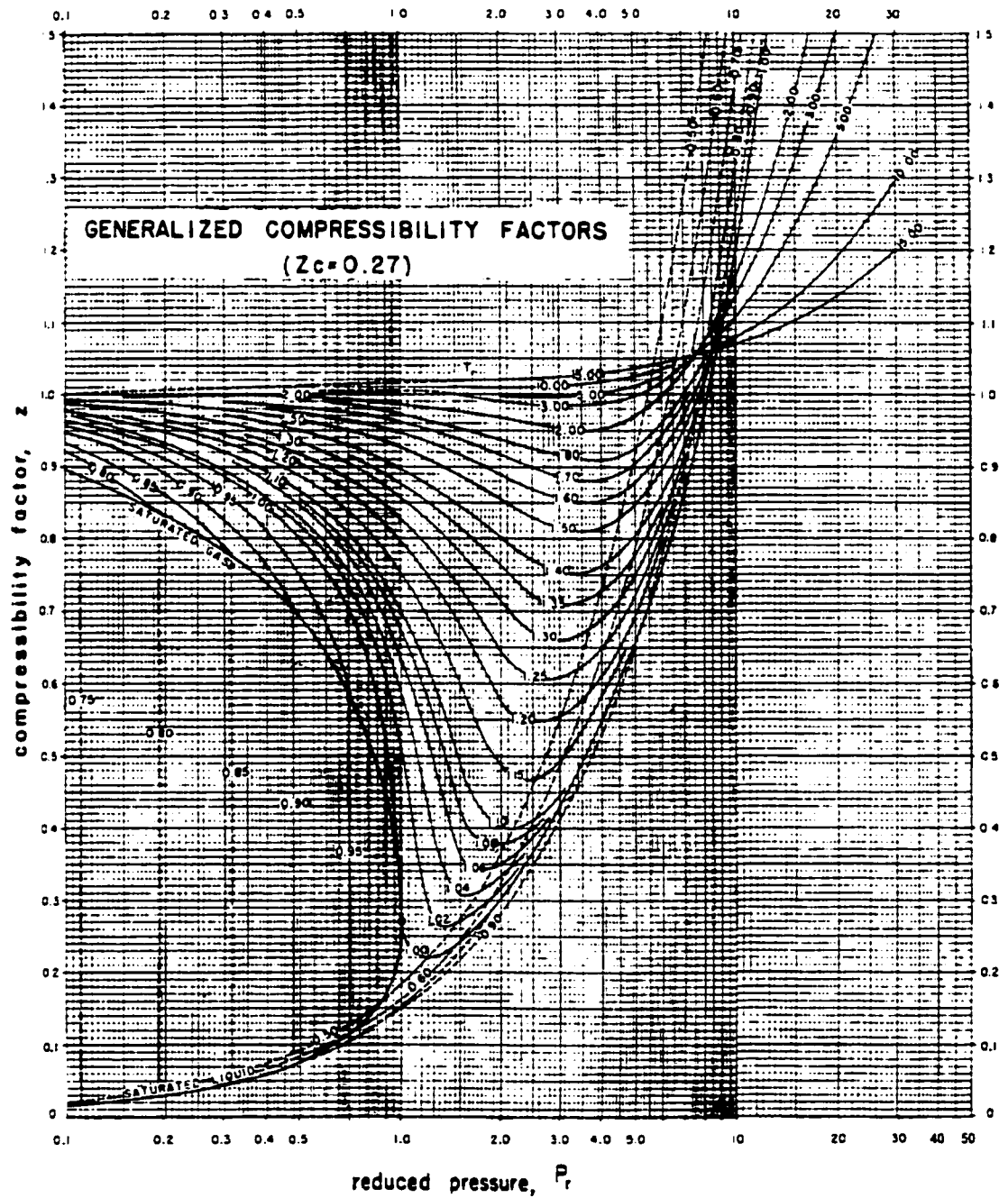
Figure 2.7 Generalized compressibility chart [77].

vessel volume per unit mass fuel and total weight is modified by considerations of cost, wall efficiency attained and manufacturing complexity. Clearly this point will lie below 1700 bars (25 ksi), probably in the 1000 - 1400 bar (15 - 20 ksi) range for methane. Mass of fuel contained for such a pressure would increase by a factor of approximately 2 - 2.5 compared to vessels in use today. The implications for hydrogen storage are different and commonly one would be tempted to seek the highest containment pressures achievable since vehicle range is rather short due to the low density of this fuel, even when in a quasi liquid state. A 20,000 - 25,000 psi (138 - 172 MPa) operating pressure would bring a 3.5 - 4.5 fold increase over conventional vessels in mass of fuel contained, a worthwhile benefit considering that present hydrogen fueled vehicles have about 100 mile (160 Km) range (about 200 mile or 320 Km for natural gas). With commercialization of Ballard's proton exchange membrane (PEM) fuel cell , and other competitor's derivatives, the possibility of making hydrogen powered vehicles into a commercial reality is further enhanced by the fact that the electrochemical conversion process inside such a fuel cell is already 20 - 30% more efficient than the thermodynamic process in today's best gasoline and diesel engines [78], and there is potential for far greater conversion efficiencies. The efficiencies realizable today would render the alternate fueled vehicle range comparable to conventional gasoline and diesel when using ultra-high pressure tanks. It is difficult to find tabulated values for gases above 1000 bars (14.5 ksi) so rather than attempt extrapolation from tables it is best to turn directly to the equations used to generate them. Figure 2.8 is a plot calculated from the 8 constant Benedict-Webb-Rubin equation of state for methane [75]. The 6 constant Beattie-Bridgeman equation of state with constants modified by

Deming and Shupe (which are listed in a text by Dodge [79]), making it more applicable in

the very high pressure range, was used for hydrogen. For comparison the more convienent

2 constant Redlich-Kwong prediction for hydrogen is also shown. Dodge [79] notes that

the simpler equations of state tend to overestimate the compressibility factor at very high

pressures and warns against their use.
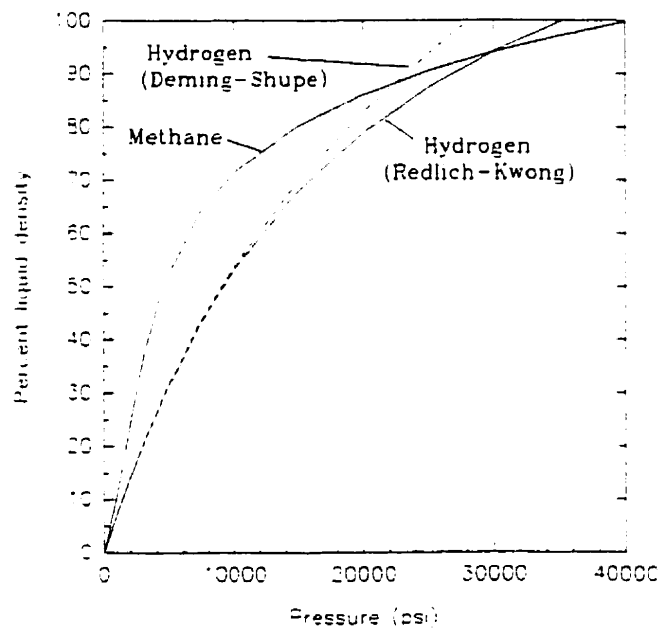
Figure 2.8 Relative density of compressed gas compared to its cryogenic
liquid state as a function of containment pressure at 27 °C.

An interesting fact derived from these curves is that there exists at ambient

temperature an effective limit pressure for hydrogen and methane: Approximately 28,000

and 40,000 psi (193 and 276 MPa) respectively, when one uses a liquid (cryogenic)

cylinder filling technique. Simply, at this pressure the cryogenic liquid density is maintained and the vessel can be filled to 100% of its volume and capped. In practice as the pressure builds the vessel expands volumetrically, typically about 3 - 4%, therefore even the calculated limit pressure is not reached. The shortfall is $\cong$ 2000 - 5000 psi (14 - 35 MPa) depending on ambient temperature, vessel expansion and type of gas contained. Even at the stated 57 °C maximum service conditions for NGV application the maximum expected pressure would be under 38,000 psi (260 MPa) for methane and about 29,000 psi (200 MPa) for hydrogen.

The questions pertaining to what containment pressures are practical remain unresolved. Answers on this point entail considerations broader than strict engineering. However we can say that in designing a hypothetical vessel with a nominal 25,000 psi (172 MPa) operating pressure and considering the safety factor needed, it would be unlikely to fail from being accidentally overfilled. The engineering focus is to achieve the most stress efficient vessel walls, the balance is reducible to an economics problem.

2.10 Permeation

Toth [11] indicates that for metal systems the permeation rate varies as the square root of the metal thickness and directly as the differential pressure for the polymers. Intact metal films 0.002" (0.05 mm) or thicker exhibit insignificant diffusion. For polymers Fick's law describes the system provided that no pin-holes exist.

$q = KAt(\Delta p)/d$ or $K = \rho A \, \Delta p/d$

Permeability ρ is a temperature function [13] described by

$$\rho = \rho_0 \rho^{-E/kT}$$ where: k = Boltzman's constant
E = characteristic activation energy
K = permeation rate
A = film area
T = absolute temperature
d = membrane thickness
Δp = pressure differential
t = time
q = total amount of material

In the presence of pinholes, capillary flow equations govern. For non-reactive gases permeability ratios among different gases remain close to one another over the wide range of permeabilities (greater than 2 million : 1) being exhibited by the different polymers they permeate across [80]. Methane has approximately 1/3 the permeability of nitrogen. Helium, the smallest molecule, is on the order of 100 times as permeable as nitrogen [81]. Among the polymers exhibiting the greatest resistance to permeation are: (in descending order) Saran, PVDF, PET (Mylar), P-CTFE (Aclar), E-CTFE (Halar), PVF, ETFE.

At ambient pressure methane liquefies at 111 °K (-162 °C). P-CTFE (poly chloro-trifluoro-ethelyene copolymer) is a candidate liner material combining a very low permeation rate and a lower service temperature limit around 20 °K (-253 °C), the temperature of liquid hydrogen. For tests performed in liquid nitrogen at 77 °K (-196 °C), P-CTFE elongates 5 - 7% and ECTFE exhibits 3 - 6% strain. The permeation rate of HDPE, as used in current plastic lined cylinders for natural gas, is at least 20 times greater than P-CTFE in nitrogen [61]. Similar improved performance can be anticipated with methane or hydrogen.

The possibility of arriving at a successful thermoplastic liner to contain liquid methane at -162 °C (111°K) should not be discounted. Today's HDPE liners become rigid at -50 °C. Boeing had some success with Kapton (polyimide) at -196 °C (77 °K) using glass fiber vessels that strained near 3%. P-CTFE has the lowest thermal coefficient of any fluorocarbon. If a fluoroplastic liner such as P-CTFE can survive repeated thermal shock, the actual mechanical strain required of the liner is negligible given one employs a cryogenic liquid filling technique. Pressure only builds in the vessel as temperature increases thus the strain demanded of the liner grows in conjunction with ambient temperature. Today's primary construction material (carbon) has high modulus, and ultimate strain. Even at burst, strain usually remains below 1.5%.

ANSI/AGA NGV2 stipulates a 0.25 cc/hr/liter-vessel figure as the maximum permeation allowed. This translates to about 300 cc/day assuming a modest 50 liter vessel. One can consider the feasibility of meeting these permeation requirements with a thermoplastic lined ultra-high pressure vessel operating at a maximum of 1800 atmospheres (182 MPa) . Assuming the diffusion laws can be taken to this level of pressure and using some typical vessel geometry allows the maximum diffusion rate for the liner to be estimated. For the hypothetical case of an 8" ($\cong$ 200 mm) inside diameter by 5' (1.5 m) long cylindrical vessel of 50 liter capacity (approximately 1550 in.^{2} or $\cong$ 1 m^2 internal surface) with a 1/4" (6.4 mm) liner, the permeation rate needs to be at or lower than 2.7 cc-mil/day-atm-100 in. sq. The fluoropolymer E-CTFE can meet this requirement for nitrogen [81][82]. The larger methane molecule poses a much lesser problem and hydrogen is very similar.

The permeabilities at room and cryogenic temperatures of glass composites to hydrogen, helium and air were investigated by Evans and Morgan [83]. They determined that porosity (causing capillary flow) is a factor contributing to great variability in the permeation measurement of the laminates. Only high quality laminates (by vacuum resin impregnation or other means) were measurable whereas a commercial filament wound tube had a permeability over 5 million times that which can be expected from neat resin films.

A compilation of properties for fluoropolymers by Schramm et al. [84] indicates that at very high hydrostatic pressures the stress-strain curves change remarkably. For instance, P-CTFE's ultimate strain of 95% with a UTS of 4300 psi (28 MPa) under atmospheric conditions becomes 16% with a UTS of 25,000 psi (172 MPa) as the hydrostatic pressure is raised to 113 ksi (779 MPa). Figure 2.9 shows such a series of curves. The similarity of these plots to conventional stress - strain curves where the test temperature is progressively lowered is remarkable. Such behavior (likely reflected in all polymers and perhaps metals) may become a factor for vessels with burst pressures in the 50 - 70 ksi (350 - 480 MPa) range.
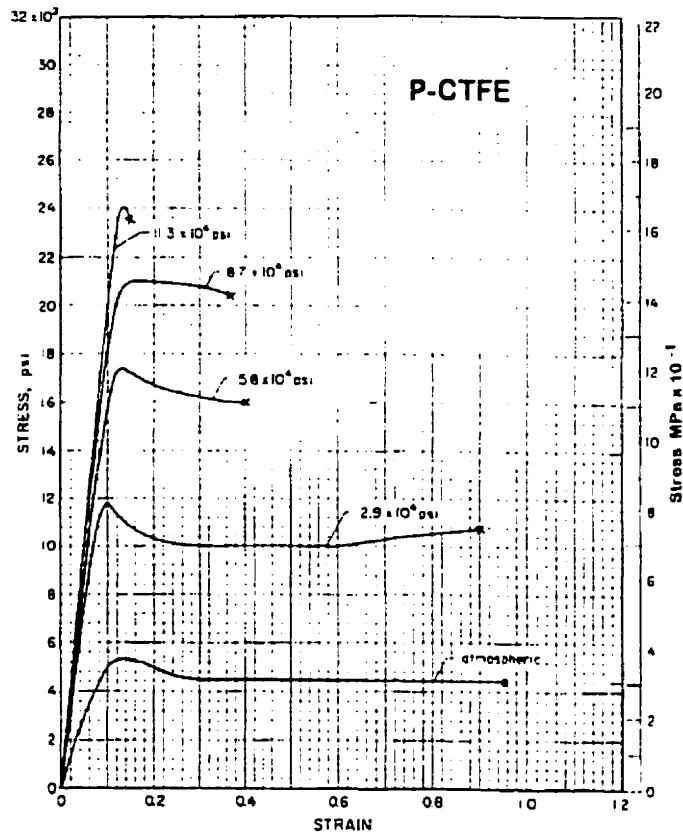
Figure 2.9 Stress-strain curves for P-CTFE liner material
as a function of hydrostatic pressure [84].

2.11 Matrix Properties and Processing

Filament wound vessels impose specific demands on the resin matrix. High

strength, modulus and elongation are desirable attributes. These properties control

transverse and shear strength. Inevitably the desirables are somewhat mutually exclusive

and suitable compromises must be sought.

Epoxy systems are used almost universally. The basic resin is most often of type

diglycidylether-bisphenol-A (DGEBA). This is suitable for use to 120 °C. Epoxydized

novolacs are important for temperature resistant resin formulations. In the aerospace

industry polyfunctional epoxies as tetra-gylcidyl-methylene-dianiline (TGMDA) and

triglycidyl-p-aminophenol see application since they are best cured at or above 180 °C

[85]. Curing temperature virtually determines glass transition points hence establishes the

upper limit of service temperature. Cycloaliphatic epoxies are important for electrical

properties and weathering resistance. Sometimes two or more resins are blended to lower

viscosity or to arrive at some other combination of properties. A great variety of curing

agents and catalysts are used with the epoxies. Nadic methyl anhydride (NMA) and

metaphenylene diamine (MPDA) are two of the most popular. Hundreds of varieties of

anyhdrides and amines exist. Curing agents are frequently modified by the addition of

accelerators to increase the cure rate, conversely by partial reaction with a small amount

of resin to slow the cure rate. Compounds can be added to improve solubility in the resin

and to prevent crystallization of the of the curing agent. At times reactive tougheners (ex:

dibutylphthalate) and diluents are specified. For filament winding, latent curatives or

accelerators (activated by heat) can be added to the formulation.

The selection of a resin system for a specific application is dependent on its

processing characteristics, its curing temperature, and its effect on composite properties.

The viscosity and pot life of the catalyzed system, that is the initial viscosity and the

change of viscosity with time are the major processing considerations. Gel time and resin

flow during winding / cure are other rheological factors. A low viscosity is essential for

complete wetting of the reinforcement and for removal of bubbles, it helps any solvent to

evaporate. For winding the best working viscosities fall in the range of 350 - 1500

centipoise. If the system is too fluid, fibers (especially carbon) will not pick up enough resin. In other instances, the winding tension will force resin to the outer surface leaving dry inner layers. When the resin is too viscous, fibers will fuzz in the resin bath and feed eye, coating fibers unevenly [54]. The increased friction due to the obstructed bath can further increase tension promoting fiber breakage and entrapped air. High modulus yarns tend to fuzz heavily and can be near impossible to wind with.

Variables that must be met concurrently for wet winding include viscosity of 2000 cps or lower (2 Pa.S), low toxicity, low exotherm and long pot life (preferably 6 hrs or more). At the risk of ending up with too much resin drainage and dry spots, it is desirable to wind with the lowest viscosity possible. Low viscosity promotes fiber wetting, band spreading and low friction over the guides (reduced fiber damage). When resin viscosity is too high, pot life can be traded for lower viscosity by heating the resin. A system with a room temperature pot life of a several days might, for example, at 38 °C be of half the viscosity and retain an 8 hour pot life. In many cases such trade-offs are good ones.

Table 2.3 lists representative curing agents and Tables 2.4 - 2.6 group fibers and their property ranges by class. Table 2.7 is a compilation of fiber properties based on the manufacturer's data grouped by strain capability. There are essentially two varieties of curing agents in use, amines and anhydrides. The anhydrides are noted for their long pot life, elevated cures and high heat distortion temperatures. Viscosities of the amines are somewhat lower and may not require heating. Aromatic amines are cured at an intermediate temperature and are faster setting while aliphatic amines have been formulated with an extended pot life and a low temperature cure. Amines are easily "B-

Table 2.3 Typical filament winding resin formulations [55]

Component	Equivalent Weight	1	2	3	4	5	6	7	8	9	10	11	12	13	14	
		Long Pot Life				Toughened				High Temperature		Anhydride		Vinylester and Polyester		
RESINS																
DER 332	174	100	100	100	100	100	100	100	100							Dow
EPON 826	178										100	100				Shell
CIBA 0510	100									100						Ciba Geigy
EPON 828	188												100			Shell
DERAKANE 411-45														100		Dow
STYPOL 40-2508															100	Freeman
DILUENTS, ADDITIVES																
KELPOXY 272	340						50.6		25.1							Spencer Kellog
KELPOXY 293	340					29	50.6	50.1	25.1							Spencer Kellog
EPIREZ 5022	130										25					Interez
HELOXY 68	75					84	123.5									Wilmington
CURING AGENTS, CATALYSTS, ACCEL.																
JEFFAMINE D230	8.3				34.6											Texaco
JEFFAMINE T403	6.1	36						51.5	51.1							Texaco
TONOX 60-40	37					45	61			49.8	30					Uniroyal
DMHDA	72		21.8													Pacific Anchor
MNDA	82			24.8												Rohm & Haas
NMA (CIBA 906)	180											90	90			Ciba Geigy
BDMA													1			Ciba Geigy (DY062)
EMI-24	55											1				Fike
MEK PEROXIDE														1	2.5	US Peroxygen
CO NAPTHENATE														0.3	0.6	Witco
DIMETHYLANILINE														0.5	0.6	DuPont
REFERENCES		3	4,5	4,6	7	8	8	8	8	9	10,11	12	13	14	15	

Table 2.4 Glass fibers for filament winding [55]

Type	Nominal Tensile Modulus GPa (psi x 10⁶) Strand	Nominal Tensile Strength MPa (psi x 10³) Strand	Ultimate Strain (%)	Maximum Number of Filaments Per Strand	Fiber Density kg/m³ (lb - in.³)	Suppliers
"E"	72.4 (10.5)	3447 (500)	4.8	4000 (single end roving)	2600 (0.093)	Pittsburg Plate Glass, Manville Co. Owens Corning Fiberglas
"R"	86.2 (12.5)	2068 (300)	5.1	60	2491 (0.089)	Vetrotex St. Gobain
"S-2"®	86.9 (12.6)	4585 (665)	5.4	~ 12,000	2550 (0.092)	Owens Corning

staged" and form a stable glass at room temperature which will then flow and cure at
elevated temperatures.

63

Table 2.5 Organic fibers for filament winding [55]

Type	Nominal Tensile Modulus GPa (psi x 10^6) Strand	Nominal Tensile Strength MPa (psi x 10^3) Strand	Ultimate Strain (%)	Maximum Number of Filaments Per Strand	Fiber Density kg/m^3 (lb - in.^3)	Suppliers/Products
Aramid (Medium Modulus)	62 (9.0)	3617 (525)	4.0	1000	1440 (0.052)	DuPont, Kevlar 29
Oriented Polyethylene	117 (17)	2585 (375)	3.5	118	968 (0.035)	Allied Fibers, Spectra 900
Aramid (Intermediate Modulus)	124 (18)	3792 (550)	2.9	5000	1440 (0.052)	DuPont, Kevlar 49
Oriented Polyethylene	172 (25)	3274 (471)	2.7	120	968 (0.035)	Allied Fibers, Spectra 1000
Aramid (High Modulus)	186 (27)	3445 (500)	1.8	5000	1440 (0.052)	DuPont, Kevlar 149

Table 2.6 Carbon and graphite fiber for filament winding [55]

Class of Fiber	Nominal Tensile Modulus GPa (psi x 10^6) Strand	Nominal Tensile Strength MPa (psi x 10^3) Strand	Ultimate Strain (%)	Maximum Number of Filaments Per Strand	Fiber Density kg/m^3 (lb - in.^3)	Suppliers/Typical Products
High Tensile Strength	227 (33)	3996 (580)	1.60	12,000	1750 (0.063)	Amoco, T-300 Hercules, AS-4
High Strain	234 (34)	4100 (594)	1.95	6,000	1790 (0.064)	Courtaulds Grafil, 33-600
Intermediate Modulus	275 (40)	5133 (745)	1.75	12,000	1740 (0.062)	Hercules IM-6 Amoco, T-40 Courtaulds Grafil, 42-500
Very High Strength	289 (42)	7027 (1020)	1.82	12,000	1820 (0.066)	Toray, T-1000
High Modulus	358 (52)	2482 (360)	0.70	3,000	1810 (0.065)	Amoco, T-50 Celanese, G-50
High Modulus (Pitch)	379 (55)	2068 (300)	0.50	4,000	2000 (0.072)	Amoco, P-55
Ultra High Modulus (Pitch)	517 (75)	1816 (270)	0.36	384	1960 (0.070)	Celanese, GY-70
Ultra High Modulus (Pitch)	517 (75)	2068 (300)	0.40	2,000	2000 (0.072)	Amoco, P-75
Extreme High Modulus (Pitch)	689 (100)	2240 (325)	0.31	2,000	2150 (0.077)	Amoco, P-100

As an approximation, general purpose systems are cured at 120 - 135 °C, heat resistant systems fall in the range 175 - 200 °C, flexibilized systems often can see only 80 °C. Higher temperature curing increases resin shrinkage and thermal contraction stresses. Shrinkage on the order of 2 - 8% is normal [54]. To illustrate, Grover and co-authors succeeded in producing 50,000 psi vessels only after having switched from an intermediate / high temperature curing system (160 °C) to a flexibilized system with a 60 °C curing temperature. This resin system used a polyoxopropylene amine hardener. X-rays had

Table 2.7 Tensile properties of specific carbon fibers grouped by type [83]

Manufacturer	Fiber	E (GPa)	σ (MPa)	ε (%)
PAN-based High Modulus (Low strain to Failure)				
Celanese	Celion GY-70	517	1860	0.4
Hercules	HM-S Magnamite	345	2210	0.6
Hysol Grafil	Grapfil HM	370	2750	0.7
Toray	M40	390	2700	0.7
Toray	M50	500	2500	0.5
Toray	M50J	490	4000	0.8
Toray	M55J	540	3630	0.7
PAN-based Int. Modulus (Int. strain to failure)				
Celanese	Celion 1000	234	3240	1.4
Hercules	IM-6	276	4400	1.4
Hysol Grafil	Apollo IM 43-600	300	4000	1.3
Toho Belson	Sta-grade Besfight	240	3730	1.6
Union Carbide	Thornel 300	230	3100	1.3
Toray	M30	294	3920	1.3
PAN-based HS (High strain to failure)				
Celanese	Celion ST	235	4340	1.8
Hercules	AS-6	241	4140	1.7
Hysol Grafil	Apollo HS 38-750	260	5000	1.9
Toray	T 800	300	5700	1.9
Toray	T 1000	294	7060	2.4
Mesophase-Pitch based				
Union Carbide	Thornel P-25	140	1400	1.0
Union Carbide	Thornel P-55	380	2100	0.5
Union Carbide	Thornel P-75	500	2000	0.4
Union Carbide	Thornel P-100	690	2200	0.3
Union Carbide	Thornel P-120	820	2200	0.2
Osaka Gas	Donacarbo F-140	140	1800	1.3
Osaka Gas	Donacarbo F-600	600	3000	0.5

shown severe delamination during cooling after curing, even though they had employed multiple intermediate vacuum bagged cures in an autoclave to compact the laminate [17]. Such defects became minimal afterwards.

With amine hardeners, epoxy equivalent weight (EEW) must be matched to the amine hydrogen equivalent weight (AHEW) to get a stoichiometric mix of the components. Similarly with anhydride based curatives, anhydride groups must be matched to epoxy groups. Within a limited scale it is possible to accelerate or retard cure rate by adjusting the exact stoichiometry without significantly affecting the curing mechanism and basic properties of the resin. Many formulations with a long history of "success" have been varied off stoichiometric to achieve specific end results. A key consideration is deciding between wet or pre-preg winding. One limitation of pre-preg winding is the constrained choice of resin-fiber systems commercially available. The exact compositions of pre-preg resins are for the most part proprietary. The process often entails the use of solvents such as ketones (ex: Propan-2-one, or Butan-2-one). 1.5 - 2.5% volatile content in rovings for winding after B-staging can be expected if a high tack is to be maintained [87]. In contrast pre-preg laminas for panel lay-ups usually have 0.5 - 1% volatiles. Flow properties are of great significance with pre-pregs. Sufficient tack and flow are needed to ensure bonding of successive layers. These properties are resin functions, the degree of B-staging and the level of residual volatiles. Initial flow properties can usually be maintained for 6 months under refrigeration. The latest generation of pre-pregs (available through Thiokol) have a 1 year storage life under ambient conditions [53]. On the whole, pre-pregs maintain closely controlled properties and assure a level of performance. With pre-pregs winding

path restrictions are fewer since the material's tackiness creates enough friction to permit a significant deviation from geodesic (the shortest path between points on a surface) and largely prevents filament slippage. Higher material cost with this process is a concern. Wet winding facilitates experimenting with a wider array of resin / fiber combinations but requires accurate control of the vessel geometry in order to permit lay-down without fiber slippage. Mathematical restraints on vessel geometry and fiber lay-down paths are further discussed in Chapter 3.

Of the many epoxy resin systems existing, few are well suited to filament winding. Some systems in current use were originally developed for applications that were quite different. Filament winding is often not specified in product applications literature. The higher operating temperature systems generally require higher curing temperature and exhibit lower strains to failure. Resin systems can be toughened to lessen the severity of impacts from foreign objects. Possible methods include:

* Introducing elastomer particles.

* Blending to form an interpenetrating network (IPN)

* Adding thermoplastic particles

* Interleaving with thermoplastic film

* Decreasing cross-link density

* Using special fiber orientations and weaves (including 3-D)

* Using a thermoplastic matrix

* Using a thermoplastic fiber

There are no commercial hetrophase (elastomer containing) pre-pregs for filament

winding. Presently the most used formulations depend on the addition of a pre-reacted epoxy resin (CTBN rubber polymer) to achieve toughness without shortening pot life. Formulations 5-8 in Table 2.3 are representative. The drawback is a lowered heat distortion temperature. Polyblends incorporating polyurathane resin (Adiprene L-100) with epoxy and methylenedianiline hardener exhibited outstanding thermal shock and impact properties at cryogenic temperatures in one investigation although room temperature properties were low. After extensive evaluations, a NASA sponsored cryogenic program selected a modified epoxy system using Dodecenyl succinic anhydride (DSA) and Benzyldimethylamine (BDMA) hardeners as the optimal for service at 20 and 77 °K [66].

Fiber hybridization is another toughening mechanism. For example, a viscoelastic fiber like Spectra (polyethylene) can be combined with carbon. Brunswick Corp. uses some glass fibers in their carbon fiber cylinders to this end [47]. Thermoplastic composites have G_{IC} values nearly an order of magnitude above thermosets and impact energies 2 or 3 times greater. Processing techniques are different and not fully explored.

Polyurathane based resins appear to have an advantage especially as adhesives under cryogenic conditions and are known to be most resistant to thermal shock. Room temperature vulcanizing (RTV) silicones have relatively low (approximately 500 psi) lap shear strength but this value remains near constant down to -253 °C yet the same silicones survive at over 300 °C. Better cryogenic adhesives such as epoxy-nylons can give of the order of 5000 psi shear strength cold but are not useful in hot environments above 150 °C [63].

Reference [85] and specifically manufacturer's literature covers many aspects of the chemistry, physical properties and applications of available resin systems.

2.12 Design Analysis Methods

Three basic approaches have been used in the analysis of composite material vessels, namely netting analysis, linear anisotropic elasticity theory (continuum) and finite element analysis.

Netting analysis treats the vessel as a netted structure of fibers, ignoring matrix effects. Netting is valuable because it helps define fiber paths that are stable without restraint from the matrix hence is the basis for winding on a geodesic path over end domes. As a failure model, netting would entail that the matrix has totally disintegrated before fiber failure occurs. This is not true. Netting was used in the early days of rocket booster design and has since been superseded by anisotropic elasticity methods and finite elements.

The continuum analyses assume linear elastic material properties. Wound layers of a particular orientation or material are treated as a monolith with orthotropic properties. These layers can be combined when coupled with appropriate boundary conditions.

The simplest type of vessel construction involves the use of one material layer. Lamé's solution (published 1852) is sufficient to characterize the state of stress in the cylindrical wall of a monolayered isotropic material. S.G. Lekhnitskii [88] presents a more general stress solution for a monolayered anisotropic cylinder and shows how it is

extensible to multilayered design in the case of a plane stress formulation in [89].

Lekhnitskii's original book (1950) is a compilation, work on anisotropic cylinders and

spheres dates back to W. Voigt (1886) and Saint-Venant (1865) respectively. Many

authors over the century have since expanded or presented simplifications for special cases

and uses [74][90][91]. For cylindrical vessels, Grover and Ayler [45] model the vessel as a

long layered orthotropic cylinder following classic plane stress formulations. By contrast,

Witherell [74] in a more recent report has presented a refined solution method for multi-

layered orthotropic open ended cylinders (gun barrels) which equilibrates for plain strain

axial deformations ($\varepsilon_z = 0$) and solves the problem via a 3-step superposition procedure

to correct for the resulting additional radial stresses emanating from the non-zero axial

strain. Accounting for such second order effects changes the classical results. but even in

worst cases. by under 10%. Hoa and Mannarino [92] investigated twisting effects due to

stacking sequence using a numerical solution and noted that the effects were on the order

of a few hundred microstrain, disappearing with any appreciable thickness.

The literature assembled by Lekhnitskii is quite generalized and covers cases of

pressures, bending, twisting, and deals with different levels of anisotropy and symmetry.

Solutions specific to pressure vessels descendant from this body of work are presented by

Roy, Sherrer, Grover. Chen, Foral, Guess, Rogers [93][94][91][95][45][43][16][96]

among many other authors. Chapter 4 expands on this topic and corrects errors of

omission in Roy and Tsai's definitive work. The beginning of Chapter 5 looks at an even

more general formulation (the careful reader will pick out typographical errors that were

corrected from Likhniskii's manuscript) and then moves on to variable elastic property

formulations.

Other methods of solution exist. One approach is to extend shell theory. Whitney [97], Widera and Logan [98], Reuter [99] followed this method. Lingstrom [100] used a power series approximation for thick shells and developed the method further. Kamal and Chaudhuri [101] also attempt to extend shell theory to thicker cylinders using constant shear angle theory. Bryon and Vinson [102] employ a 1-dimensional finite element technique using anisotropic thick-walled cylindrical shell elements. Vasilev [103] presents an extensive development on composite shells including cases of local loadings. With these methods certain theoretical advantages exist like series approximations for point or line loading conditions but the methods appear difficult to justify in view of the fact that continuum solutions exist for many of these cases.

Horgan [104] relates Saint-Venant end effects for anisotropic cylinders and shows that discontinuity stresses have an exponential characteristic decay length (l) that can be approximated by $(radius/3.83)(E_{11}/G_{12})^{1/2}$. This translates to about ¼ the decay rate in carbon fiber composites relative to isotropic materials.

Finite element analysis and finite difference techniques have long been employed to calculate strains and to model attachments and bosses. They are invaluable where the geometries are not reducible to simple coordinate systems such as spherical or cylindrical. The FEM method is often used as a tool to refine on analytically based designs [105] but there are now far fewer reasons preventing use of the technique for the design of entire vessels. This is increasingly the method of choice [60].

As an example, Ericson and Yorgason [72] used finite element methods to study parameters affecting stress concentrations near the bosses. They evaluated and tested

configurations for different wafers of reinforcement within the composite in this area and achieved a 17% stress reduction with a two step hoop wound dome wafer. Their paper on graphite epoxy vessels gives a summary of techniques both detrimental and beneficial with regard to standard thin-wall vessel design practices.

As expected, the computational methods tend to match closely with continuum solutions away from discontinuities. Rogers and co-authors [106] describe higher order finite elements to model filament wound composite spheres. Gleich [107] relates that finite difference techniques have been implemented to model fracture propagation in vessels with artificially induced cracks in brittle liners.

Shortcoming of the finite element techniques are that they provide answers without revealing *why* stresses distribute as they do. Fundamental mechanisms that govern stress distribution remain obscured.

2.13 Failure Criteria and Optimization

A design technique for spherical vessels using two distinct materials was presented by Roy and Massard [94] that makes use of the quadratic interaction failure criteria in 3 dimensions. Seven terms are needed, rather than 6 for 2-D analysis. The additional F_{yz} interaction term is back-calculated from coupon tests in the through-thickness direction. For carbon fiber / epoxy in a $\pm 45°$ or $\pm 90°$ layup (typical of quasi-isotropic constituent plies) the interaction term averages -0.84. By using either maximum strain or maximum stress failure criteria one would predict that the compressive strength of the laminate

equals the compressive strength of the unidirectional lamina. This predicted strength is about 3 times lower than the value for the laminate estimated by the quadratic criterion because of the interaction terms [93]. The study by Roy and Massard was to assess the possibility of designing for a 200 MPa operating pressure with a 1.5 safety factor. These authors used IM6 and T300 carbon fiber properties, the quadratic failure envelope and the classic equations for a layered thick orthotropic sphere. Limiting wall thickness to a practical $b/a = 1.25$, the full range of two-layer designs was studied. By maintaining the thickness of the inner T300 layer between 20 to 80% of the total thickness, a burst pressure of 240 MPa would result. A similar earlier study by Foral [43] using S-glass and Kevlar-49[®] presented the range of achievable burst pressures for a two-layer hybrid sphere. Foral used maximum strain criteria and presented his results in the form of a 3 dimensional graphic depicting PV/W, layer thickness percentage and inner to outer thickness ratio. The ridge on his graphic surface represents simultaneous failure of inner and outer layer. The results predict that up to 280 MPa Kevlar[®] alone presents a superior vessel, thereon up to 850 MPa, Kevlar[®] over S-glass is more efficient. 950 MPa is the S-glass limit pressure. Figure 2.10 shows some of these predictions.

Gerstle's [108] comprehensive analysis of metal liner behavior also investigates the ramifications of assuming 3 different failure criteria. Maximum strain, maximum stress and the less known Norris-Ashkenasi $\{(S_\theta/F_\theta)^2 - 2S_\theta S_r/F_\theta F_r + (S_r/F_r)^2 > 1\}$. Gerstle noted that the penalty for using a (single) highly anisotropic composite is the negligible increase in burst pressure with greater wall thickness. Further he concludes the radial compressive strength of the laminate must be substantially higher than the design pressure and that the

failure pressure approaches the radial compressive strength asymptotically. (The point on radial compressive strength is not correct - see Kallas and Hahn below). Also a high fiber volume fraction increases laminate strength more rapidly than does the corresponding stress gradient due to laminate anisotropy.
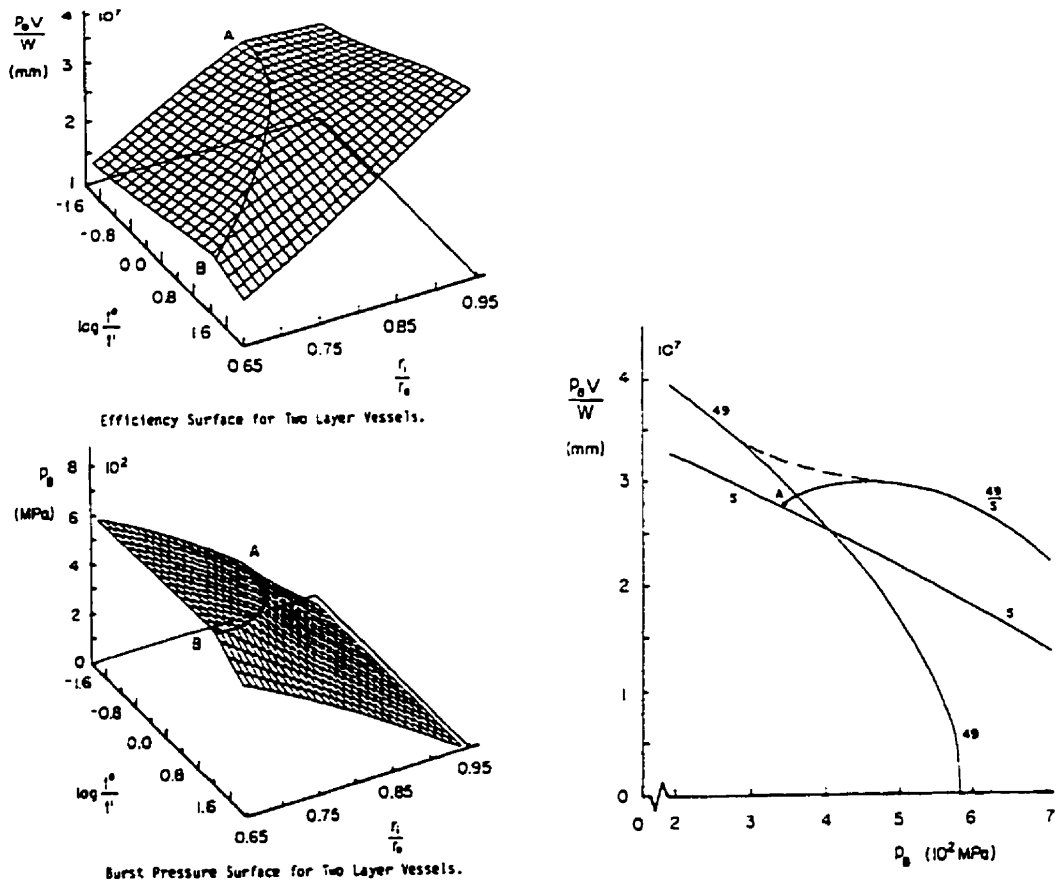
Figure 2.10 Efficiency plots for a two layer spherical vessel constructed from S-glass and Kevlar [43].

Roy and Tsai [91] investigate 2 and 3 layer wall combinations for cylinders with different +/- winding angles on each layer using a single fiber type. They found an

increase in ultimate pressure capacity results at the expense of vessel efficiency by putting

the stiffer (closer to hoop direction) windings nearer the outside on high pressure thick

walled cylinders. These authors analyzed vessel efficiency in terms of the material's

strength utilization and defined a strength ratio R. They described laminate failure using a

3-dimensional quadratic interaction failure criterion. Failure is followed ply by ply with

degradation factors assigned to failed plies until last ply failure occurs. The R ratio

describes the material's actual stress to its ultimate breaking stress at any point in the

vessel wall. Ideally the ratio is unity. On surfaces where failure occurs the material needs

to be "softened" by winding at angles more in the axial direction while the opposite

surface would need "stiffening" using angles closer to hoop. In general this implies a shift

towards higher angle winds on the outside of thicker vessels. More over it was discovered

that certain materials, T300/5208 for example, see a reversal of this situation prior to the

point where a certain thickness ratio is reached. This implies that T300/5208 material

fractures on the *exterior* prior to reaching a wind thickness ratio of $b/a = 1.15$ at the

optimum efficiency $55°$ wind angle. Thereafter material use efficiency reverses and

fracture initiates on the *inside* for thicker vessels. IM6 material does not show this effect.

(Some analysis in Chapter 7 comparing various failure criteria has lead this author to

conclude that the discovered "phenomena" is simply a product of the quadratic criterion,

not actual). The number of +/- winding angle layers needed to level out the strength ratio

R can be as low as 2 or 3. Additional layers bring about diminishing returns.

Tauchert [109] introduced a method based on the minimization of elastic strain

energy for single material vessel walls. He shows optimized fiber volume fraction

distributions for different average levels of volume fraction throughout. Results were presented for relative wall thicknesses (b/a) and matrix to fiber stiffness ratios. Failure pressure estimates increased about 5-30% depending on the degree of anisotropy.

Christensen and Swanson [110], have presented a new model that separates the criteria for fiber and matrix interphase failure. Although it might at first glance appear too simple, experimental evidence appears to support that ultimate fiber strain is the overwhelming factor dictating last ply failure in biaxial stress fields and is insensitive to the exact state of the applied stresses.

Christensen expands upon his work in [111-113][115][116] and shows how for 3-D analysis certain stiffnesses remain almost invariant with fiber orientation. Separate explicit criteria are developed for fiber and matrix-interface failure. The effects of dilational as opposed to deviatoric strains are examined. Micromechanics models by the same author are discussed in [113][115][116] and used in Chapter 7.

Feng [117] presented a 2 failure envelope theory based on the concept of strain invariants. Efforts were made to validate this theory among others using tubular specimens [118]. The results of these tests available in [119] give little indication that either Feng's theory, quadratic interaction or simple uniaxial stress failure surfaces show any merit under biaxial loading, especially in relation to ultimate failure predictions. Maximum strain theory was shown to be non-conservative in some cases but came closest to fitting the data.

Tennyson and co-authors [120][121] advocate the use of a cubic tensor polynomial form. Their work shows that in biaxial loading cases, particularly pressure in

cylinders, quadratic criteria underestimate ultimate failure loads by 30 - 40%. The failure

envelopes are tested for plane stress cases, their suitability for plane strain is not broached.

Obtaining all the interaction terms involves specialized biaxial and shear experiments, thus

limiting practical applications of this criterion.

Wei-Xun [122] discusses polynomial stress tensor failure criteria in general,

showing interrelations and special cases. He indicates the limits of applicability its many

variants have (Von Mises, Tsai-Wu, etc.) as a function of the material's strength and the

relative stress ratios the material is capable of being subject to.

Kallas and Hahn [123] present concisely the three-dimensional failure criterion

used by Roy and Tsai. The criterion indicates that under hydrostatic conditions axial

compressive strength will be greatly increased. The effect has been verified independently

both for polymers and in composites where it causes bi-linear behavior. This failure

envelope has direct consequences for deep submersible vessel design and presents a

refinement for both internally and externally pressurized vessels.

Guess [124] tried to match bi-axial test data from tubes to failure envelopes but

was not successful due to scatter. He did however present a simple concept he named the

"laminate interaction diagram" based on the maximum stress criteria. This appears to be

capable of describing the lamina failure(s) in the correct sequence.

Uemura and Fukunaga [125] apply Weibull distributions to constituent laminae

comprising a cylinder. They then compute 50% probability of failure using Tsai-Wu and

maximum stress theories and assign degraded ply properties thereafter. Also they take into

account the non-linear shear stress-strain curve, approximating it by a cubic spline. Their

method appears to predict correctly the strain curves to failure and the ultimate pressure.

Knight [126] used a two parameter Weibull criteria on ultimate stress for individual elements of his finite element model of the wound sphere. The burst predictions (400 MPa) correspond well to the failure pressures attained in such spheres through related programs by authors Gerstle and Guess who worked on the manufacture and testing of such vessels.

2.14 Liner Behavior

Foral [127] presents a complete model for a liner's plastic behavior including assumed linear strain hardening in conjunction with a single material continuum equation based on Love's analysis for the composite sphere. Guess [18][16], who published results for 430 MPa burst pressure sphere (the highest known), used a classic layered analysis for his spheres, essentially an equation set similar to that presented for cylindrical vessels in Chapter 4. He includes a term to describe the contribution of a fully plastic liner. Maximum strain criteria is used in his work, both on spherical and cylindrical configurations. Guess refined his boss geometry with SASL, a finite element program to reduce the stress concentrations from an original 1.37 to a factor of 1.11 near the fill stem. The finite elements showed that stresses predicted by the analytical methods matched at all locations except at the fill stem region.

The US Army more recently investigated lengthening their guns and cannons (while maintaining current inertia characteristics) by machining down the outer wall of the

barrel and overwinding with carbon fiber / bismalemide resin composite. In reference to this work Chen [128][129] presents solutions for the metal liner's elastic and plastic strain and also for the compressive elastic stress state after unloading with the Bauschinger (hardening) effect omitted. Solutions presented by the same author exist incorporating the Bauschinger non-linearities for other similar autofrettaged designs. Moss [130] presents equations for liner yielding and the radius of the elastic-plastic boundary. Gerstle [108] develops equivalent equations and applies failure criteria to the liners.

Roy [131] also derived a thermal analysis based on the strain equations for the multilayered orthotropic cylinder. The formulations could be useful to estimate liner pressures resulting from cure temperature changes, chemical shrinkage and contributions from initial winding tension. The effect of temperature differences between the inside and outside of the vessel, as in cryogenic filling, could also be studied.

2.15 Process Modeling

Hjellming and Walker [132] consider the curing cycles necessary to prevent thermal run-away due to exotherm while maintaining low enough surface viscosity to allow proper resin flow and degassing on very thick cylindrical sections.

Tarnopol'skii et al. [133] presents an extensive analysis of tensioning effects using pre-preg materials on wound cylinders. The anisotropy ratio $b = \sqrt{\dfrac{E_1}{E_3}}$ of the pre-preg material is a governing variable that changes with curing. Methods such as fiber compaction, ply-by-ply curing and programmed tension winding are analyzed with the

goal of effecting the greatest tension in all the winding layers. A thermo-elastic analysis is also presented. It is concluded that winding tension can combat cracking which results from thermal cool-down stresses on thick-wall windings.

Process models have been developed at length and constitute a most valuable optimization tool for the manufacturing processes involving composites.

Complete process models for the filament winding of thick cylinders have been proposed and tested. These models each constitute a number of submodels determining the instantaneous material or other time dependent properties, processed iteratively in time steps. The accuracy depends on the completeness of the submodels and each of these must be verified. Lee and Springer [134] incorporate temperature in the cylinder and mandrel, degree of cure and viscosity, fiber tensions and positions, stresses and strains in the materials. Olofsson et al. [135] extend the above model to include a micromechanics model and reaction kinetics for the epoxy and compaction data on the fibers with variable initial tension and generalize the thermal boundary conditions. Spencer's [136] process model shows that B-stage duration needs to be complete to limit residual stresses. Steam curing techniques are also detrimental because they induce rapid exotherm. He notes that pre-tension schemes have little effect on either layer position or residual stress, the effects diminishing with part thickness.

Prater and Hackett [137] present a method of calculating the viscoelastic response of pressure vessels under proof testing conditions. The model uses the method of Laplace transforms and predicts noticeable differences in the stress-strain curves between virgin vessels and ones with a damaged matrix.

2.16 Filament Winding Parameters and Models

Filament winding and the study of fiber trajectories during the winding process can be traced to the textiles industry. Analytical models for the motion of the winding point and the fiber delivery point, to wrap cylinders, cones and arbitrary surfaces of rotation have existed since the 1950's. Efremov [138-140] has published such analytical methods. Geodesic path deviations, given frictional restraints, were the issue of his later publications [141][142]. Optimal dynamics during reversal of the fiber delivery point in textile systems is discussed by Vulfson [143].

The mathematics of winding textile bobbins were not immediately adapted to the construction of rocket motor cases and pressure vessels. Early literature, for example Shibley's 1962 review [4] and Hofeditz [144], describe descriptive geometry construction techniques to arrive at a dome shape. Shibley also discussed a few entirely experimental methods to arrive at stable fiber paths across vessel domes. Skipping to the present, computer modeling and multi-axis equipment control has become quite standardized.

Traditionally vessels were constructed on mechanical winders with fixed ratios governing the motion between each axis. The path described by the filament lay in a plane close to the polar axis, hence the term *planar* (sometimes termed polar) winding. A *geodesic* path is one that describes the shortest distance over a surface and stable winding requires the filament follows this path. Computer controlled machinery can achieve this. Any sideways displacement of the filament would require it to stretch.

Another important criterion for a wound vessel is that once pressurized, the

filaments everywhere should be stressed equally (isotensoid). This makes the most economic use of material and results in the lightest weight design.

Planar winding over the poles of a sphere meets the stability and constant fiber stress conditions as computed by netting analysis. If one arrives at a scheme for distributing the fiber uniformly across the surface is all directions (quasi-isotropic properties), the winding problem is solved. The "delta axisymetric" buildup consisting of increasing angle polar patterns is one such approximate method [17] and is patented.

For planar wound cylindrical vessels, end-domes can be designed with a shape such that the profile causes constant fiber stress [105]. The fiber paths however are not stable and usually displace themselves after they are laid down. This causes loss of tension, waviness and an associated degradation of composite properties. Alternately, to maintain a geodesic path, a different dome profile can be designed. In this case the winding path deviates significantly from the simple planar and computer controlled equipment becomes necessary both to cut the mandrel shape and to control the fiber pay-out eye during winding. The combination of head profile and fiber path is termed *geodesic intensoid.*

A shortcoming of the geodesic profile is that it only describes a vessel with equal polar openings at each end. Controlled deviation from the geodesic path leads to the method of constant slippage tendency. Fiber stability is ensured by determining that the friction forces exceed the transverse forces. In effect the ratio of the filament's transverse force to normal force must remain below the friction coefficient between the fiber / mandrel surface. This permits the design of cylindrical vessels with unequal polar openings but at the price of slightly increased filament stress. Deviations from the isotensoid

82

condition are proportional to the perturbations from geodesic. Applications of this technique have become widespread.

For spherical vessels the need to fit fill stem bosses complicates the winding situation and has prompted may constructors to build oblate spheroids. These have the shape of back to back heads or end-domes (without a cylindrical section) either of planar or geodesic design.

Denost [145] describes Aerospatial's implementation of constant slippage tendency winding for cases requiring unequal polar openings. In one example with planar winding, the necessary friction coefficient was 0.28 on the forward dome and 0.25 on the aft dome. The same vessel optimized for constant slippage throughout, including the cylindrical section, reduced the necessary friction coefficient to 0.11.

Wells and McAnulty [146] performed tests on a smooth ellipsoidal mandrel to determine friction coefficients using both resin wetted and dry fiber. Speed showed no effect and tension remained a constant 15 N (3.3 lbs). Friction coefficients determined were: $\mu = 0.24 - 0.25$ dry and $\mu = 0.29 - 0.37$ wet. The range indicates the beginning of slip up to instability. With dry fibers slippage is sudden and catastrophic. Friction coefficients obtained by winding atop wet filaments may be substantially lower.

Barbalat and co-authors [147] study a construction technique using a series of stepped back windings over very shallow end domes. Each set of windings follows a geodesic path calculated from the filament wound profile of the precedent set. Depth to diameter ratios were cut from the habitual 0.6 down to 0.2 in the domes. Weight savings of 10% overall are estimated since this technique lessens material usage in the less efficient

dome region. The authors point out that a star shaped wind (4 - 6 circuits per pattern) gives a more homogeneous material distribution.

Tezak [148] describes a special winder designed to lay down only tapered spiral wound annular doilies. The computer controlled machine uses prepreg and film adhesive with heating and cooling of the mandrel. The resulting tapered doilies were wrinkle free and minimized stress concentrations.

Hady et al. [149] relate a method to describe geodesic domes by an elliptical approximation. Error between the two profiles is typically negligible, and even for conical shapes the winding angle remains within 1.6% from true geodesic. The authors concentrate on 3 and 4-axis winding equipment. They relate feed eye positions for winding on a geodesic dome profile calculated from the differential geometry of the surface. Constant winding length is employed in their software and the basis of their feed eye rotation criteria is presented.

Hamouda [150] derives equations for the movement of the winding point for arbitrary rotationally symmetric shapes. Xian and Lin [151] present calculations and curves showing winding angles on surfaces as a function of different slippage factors and for a number of starting angles. They cover cylinders, cones, spheres, ellipsoids and paraboloids. Marchetti et al. [152] suggest a method to approximate both axis and non axi-symmetric shapes by a matched series of truncated cones. Slippage factors over each conical section can be varied to give non-geodesic trajectories.

Wells and McAnulty [146] report on an integrated CAD approach for winding where the geometry of the mandrel is taken directly from the surface modeller and the

curvatures are differentiated. Fiber paths can be projected with a controlled level of incipient slip.

CAD software developed and used at Morton Thiokol is described by Vogt [153]. Although faceted surfaces are an easy approach, they lack second derivatives thus anything that depends on curvature is undefined. This leads to error in estimating important parameters such as the slippage tendency. Thiokol's software relies on B-splines to model surfaces, though it is noted that user intervention is required to get the surface representations just right.

Bunakov and Radovinskii [154] consider the contribution of the matrix, rather than using the netting approximation. They invent a factor (k) to relate the ratio of matrix to fiber stress desired. Higher vessel efficiency can be obtained because the technique relies on a matrix contribution. However the matrix's intactness up to fiber breakage must be assured. The profiles generated are more voluminous (closer to spherical) and different from geodesic-isotensoid over a significant region. There is thus more reliance on friction to maintain stability. Bunakov and Protasov [155] have compiled a large body of concise analytical approaches for winding composite pressure vessel domes and analyzing shells thus created. They treat constant slippage, stepped back winding, and cover design methods for spherical polar bosses, winding on geodesic, polar, and combined profiles. Shell stiffnesses, failure theory and deformations including those at the cylinder to dome junctions are treated.

An interesting concept developed jointly by Brookhaven National Laboratory and Thiokol concerns packaging a set of 3 pressure vessels by squashing them together and

making the central one assume a quasi-elliptical shape. The contacting face of the outer

vessels are also distorted to closely match this shape. The entire assembly is then

overwound to bind it together. Packages constituting 2 vessels in such an arrangement

also exist. The idea is to fill a quasi-rectangular volume (as occupied by a conventional

vehicular fuel tank) with a space efficient pressure vessel assembly. With this concept 50%

more fuel can be stored in the same space [53].

2.17 Carbon Fibers

Carbon fibers are close to realizing their theoretical tensile modulus of 1060 GPa.

It must be noted that organic polymers have a theoretical potential of about 300 GPa [86].

The term "graphite fiber" is a misnomer presently for all but fibers originating from a

mesophase pitch (MP) precursor or gas-phase grown types which are heat treated above

2800 °K. All other fiber types, namely the polyacrylonitrile (PAN) variety in common use

might better be referred to as "carbon". Commercially available HT type fibers have layer

spacing in the 0.350 - 0.360 nm range. An average interlayer distance of 0.344 nm or

lower is the accepted threshold to correctly employ the terminology "graphite" [156]. An

interlayer distance of 0.336 nm corresponds to a perfect crystalline graphite structure.

The corresponding theoretical transverse modulus of graphite is 36.5 GPa and the shear

modulus between layers is only 4.5 GPa. Figure 2.11 shows some structural detail.

It is known that the highest modulus requires maximizing the preferred orientation

of the polycarbon layers in the direction of the fiber axis. High strength necessitates the

highest degree of defects in the ultrastructure in order to hinder the formation of

crystalline graphite with 3-dimensional order and thus low shear modulus.
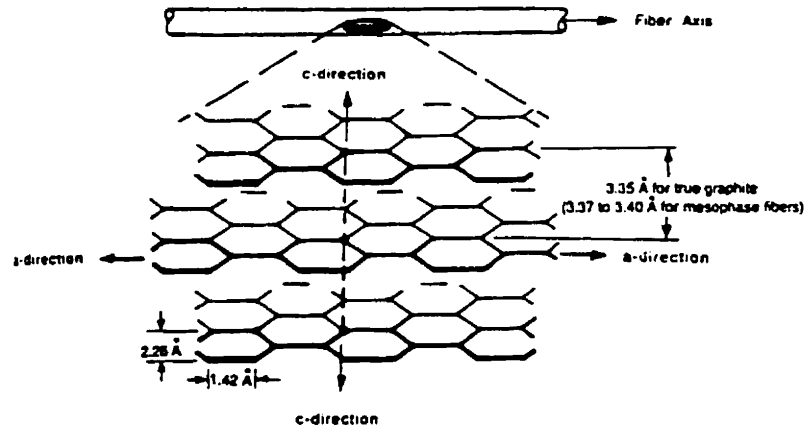
Figure 2.11 Carbon / graphite fiber structure [156].

The best commercial mesophase (pitch) fibers reach 85% of their tensile stiffness.

Theoretical strength should be near 10% of the modulus, or 106 GPa. Only a small

fraction of this value has been attained. The current objective is to attain 20 GPa. The

highest strength fibers today (PAN based) can strain 2.4% and have a strength of 7 GPa,

although the modulus attained is only 294 GPa. The higher strain resins are more effective

in translating this fiber strength to composite properties. Over 550 ksi (3.85 GPa)

composite tensile strength has been shown [157].

Ideally for a pressure vessel, assuming it were constructed of a monolith of carbon

or graphite, one would continuously vary the material properties from inside to outside in

a manner to best react the stresses. Other materials and combinations of materials would

87

constitute an equally valid example provided their properties could be varied in a smooth manner. A broad range of carbon fibers exist spanning the range high strength / low modulus to high modulus / low strength. In practice the ideal monolith would be approximated by a series of discrete fiber types laminated in graded fashion.

A pressure vessel's strain is naturally highest on the inside diminishing towards the outside. A stiffer more graphitic structure on the outside will provide more restraint. The radial orthotropy ratio "K" can be viewed as a global parameter describing the rate of strain decay through the wall thickness of a vessel. It is lower when using macroscopically defect free HT type carbon fiber. Higher modulus graphite fiber has an intrinsic high anisotropy ratio (result of crystallite properties) and will suffer more through-thickness deformation from radial stresses than carbon fiber. Hence it is less effective at transmitting the strain in the through-thickness direction. Mitigating this effect in pressure vessel design requires an increase in the rate of change of anisotropy ratio through the thickness. The key factor condenses to determining the appropriate local rate of change in anisotropy ratio corresponding to the sequence of materials building up the wall and their respective strengths. The bounds imposed are the composite's realizable anisotropic properties such as those descendant from graphite crystals, glass fibers, or organic polymers. These can be estimated through suitable micromechanics models. This topic is explored further in Chapter 7. One goal is to expose the basic relations that influence the elasticity constants in a lamina and also show why single stiffness variation rates, as assumed by earlier researchers, are not admissible.

2.18 Summary and Assessment

The design of a high pressure containment vessel needs consideration from a very broad range of viewpoints. It is apparent that for repeated cyclic applications, and in view of the scope of commercial standards, that conventional foil lined vessels cannot meet the requirements. Thin metal lined vessel are in the process of being superseded by plastic lined equivalents. Recently reemerged are laminated metallized polymeric bladders used both as inflatable mandrels and integral liners for the low cost production of experimental natural gas and hydrogen cylinders for automotive use [256]. Fundamentally there is little evidence showing that plastic liners would not perform at much higher pressures. Suitability of plastic liners for mild cryogenic temperatures (111 °K), as would be experienced with liquid cylinder filling techniques for methane, are more in doubt. Such liners may fail due to repeated thermal shock and this certainly is a point worthy of study. The mitigating factor in the above is that relatively little tensile strain would be demanded of the liner and composite until the vessel warms up.

Gas permeation through plastic liners does not seem to be an insurmountable problem for current designs and it is likely that greatly increased operating pressure could be handled. In terms of safety qualification tests there is no evident criteria that could not be met. It is probable that thicker walled vessels will fare substantially better in mechanical abuse tests (drop damage, bullets, fire). This could eventually lead to acceptance of somewhat lower safety factor requirements. The design of valving for pressure release due to fire or other heat sources may need to be held at a smaller tolerance because pressure

dependence on temperature is directly proportional to the compressibility factor *(Z)*. The enormous physical strength of such vessels makes them practically impervious to destruction from vehicle accidents.

Traditionally the high elastic strain of the composite has far exceeded elastic limits of the metal liners, even after liner elastic limits have effectively been doubled during proofing. Two methods around this are to use the stiffer carbon fibers or resort to a plastic liner. Unfortunately, stiff carbon fibers lack strength and possess a high orthotropy exponent *"K"* making them less effective in thick layers. Glass fiber properties are technically obsolete, only their low price gives them credence. Kevlar® has been overtaken by the carbon fibers in performance as well as cost. Kevlar®'s toughness still makes it important. Carbon fiber is now available in a wide range of properties. It is about the only composite that can have its properties tailored to demand. Prices of the extremely high strength or high modulus carbon fibers are still so prohibitive as to render them non-viable in the commercial market. Boron fibers which possess excellent transverse stiffness also fall into this price range. They however are not in production and effectively obsolete. Their diameter and flexural stiffness would not be very suitable for winding in any case.

Fiber prices are habitually quoted on a weight basis. This is confusing for economic design considerations. A proper unit of measurement is cost per unit achieved strength of cross-section. This implies a *volume* basis and incorporates the matrix's cost.

2.19 Perspective on Research and Development

In terms of vessels slated for research and testing of more efficient wall constructions, excessive detail spent on liner design is not warranted since cyclic testing, the cause of most liner failures, will not be performed until the basic thick-wall construction theories are confirmed. One of the simplest methods is to use existing liners from commercial vessels and attempt to deal with their limitations. A specific problem is insufficient material thickness around the boss connections. Other factors are probable non-optimal dome contours and generally a lack of freedom to specify any design parameters. The choice of metal liner can be quite limited unless one has the manufacturing capability. Essentially one does not know exactly what is on hand until it is cut apart and measured. Vessel manufacturers keep such details proprietary and will not openly sell their liners. However it has been discovered that a majority of the thin metallic liners for both commercial and aerospace applications originate from a single 3rd party supplier [158]. The other choice is to attempt to mold one's own thermoplastic liners or find a commercial source.

The selection of epoxy is important with preference given towards a lower temperature curing system in order to lessen thermal stress buildup. For thick walls, separate curing of the intermediate layers is likely the easiest way of eliminating fiber buckling, exotherm problems, and avoiding use of high winding tensions. In commercial production, a process model would be valuable in minimizing time requirements without jeopardizing the structure. Good elongation characteristics and a high matrix modulus are

needed. A stiff matrix and high fiber volume fraction lowers the orthotropy exponent, while good elongation allows high strain fibers to develop their best strength. To an extent these properties are exclusive from one another and must be balanced by design compromises. Micromechanics can in part estimate the sensitivity of such parameters.

For thick vessels, accurate fiber placement is important to maintain geodesic fiber paths. Fiber buildup causing a change in vessel shape is a real concern especially for cylindrical vessels. Techniques of stepping back the winding at the polar bosses to reduce buildup and incorporation of circumferential doilies to lessen bridging are known to help. Use of a pre-pregged tow is the easiest remedy for most of the above concerns but an alternative not available when using many different materials on a small scale unless one is prepared to do one's own pre-preging.

For practical purposes, a 3-4 axis computer controlled winder along with good fiber placement simulation and machine motion control software is essential [164].

The choice of vessel shape in experiments is dictated both by winding equipment and liner / mandrel considerations. For test purposes cylinders are most practical although spherical vessels could also be considered if the winding equipment and software were adapted. Cylindrical vessel end domes can be somewhat overdesigned in order to ascertain the validity of theoretical predictions in the wall portions of the central section. Finite elements are a good tool, well suited to design refinements at later stages of investigation. Continuum theory based on the compilations presented in Lekhnitskii's work and followed in some form by a majority of researchers is concise and powerful. The failure theories are numerous. A popular method is the quadratic interaction criterion in 3-D. Cubic tensors

have greater flexibility to model bi-axial and tri-axial stress states but the many constants requiring evaluation make them practically impossible to apply. Christensen's micromechanics models render good insight upon the power of constituent characteristics over composite properties. The failure theories extended from them lend credibility to the maximum strain fiber failure criteria, or something that is close. This maximum strain theory has for decades been verified independently by nearly every experimentalist in the field and found to be reasonably accurate.

Winding paths and dome geometries for constant fiber stress are determinable analytically and are presented in Chapter 3. Computer incremental methods based on determining the appropriate differentials directly off surface modelers using B-splines to describe surface geometry as in the high end CAD software using solid models are an alternative solution. A limited number of off-line winding simulation packages are available but their output (if they are able to generate machine motion code) must still be adapted to the individual winder since there are no standard machine interface languages akin to ANSI G-code as used in CNC machine tools.

Virgin material properties and the general effects of environment, long term loads, fatigue, impacts, temperature and practically any variable one may be concerned about can be found in the literature. For analysis purposes, most of these can be taken as known or predictable quantities.

2.20 Scope of Work

In the following chapters, derivations and research are presented on key parameters necessary for the analytical design of thick cylinder walls. The aim is two-fold: First, to extend these analytical methods into the arena of efficient thick-wall vessel construction. Second, to present them as complete derivations rather than the abstracted forms, brushed over in virtually all literature. The methods and work presented are an expansion drawn from many sources combined with the author's own contributions. Chapter 3, expands on netting analysis and presents formulations requisite for designing dome shapes and some factors that yield influence over the programming of winder motions. Thereon, closed form solutions to the stress distributions in thick cylindrical walls are developed. These analytical formulations are meant to shed some light and understanding on a dark area. The methods described are blended into a computer program that allows modeling and prediction of failures. The on-screen presentation is real-time and graphically oriented yet the numbers generated at any loading can be output to file or printer at a keystroke. In the final two chapters program results are interpreted with the help of hypothetical examples and also test vessels built are examined and compared to program predictions.

Chapter 3

Filament Winding - Netting Analysis

3.0 Analytical Methods for Fiber Path and Dome Profile

The complete analysis of a filament wound structure requires a fundamental understanding of parameters that will affect the stress distributions around the end closures of the vessel. Any optimization achieved in the wall construction as described in subsequent chapters will fall short of realization if end closures are neglected since a pressure vessel cannot be complete without them. Closed form solutions pertaining to through thickness stress distributions employing a full material description have so far been obtained only for very simple geometries that have surfaces defined along the principal axis of a coordinate system. Geometries any more complex would be exceedingly difficult to calculate. Since the surface geometries required to sustain the position of filaments during winding are very involved they can at best be approximated.

Fiber paths for arbitrary shapes can be calculated by numerical techniques and the software is commercially available from each major winding equipment manufacturer and also from 3rd party vendors. Nevertheless, leading equipment manufacturers such as *McClean Anderson* are defining the dome shapes for pressure vessels using computer algorithms that generate simple ellipses. Such geometrical simplifications may be theoretically questionable, but considering tolerances that can be held during manufacture and the expediency needed in design and production, these simplifications are an every-day reality.

This chapter presents a detailed analysis of fiber paths both without and with incipient slip. By this method the physical limits of what dome shapes can (or cannot) be wound are explored. The entire chapter is based on a netting analysis. This entails that the matrix contribution is wholly neglected. The advantage of the approach is that the mathematical simplification due to the simple description of the material (fibers only) allows a complete description of the surface geometry needed to load the filaments evenly and optimally. The final equations lead to important interpretations concerning the magnitude and sense in which the fiber stresses vary when non-ideal conditions of surface geometry are encountered. The equations also indicate clearly where to anticipate the location of the maximum stress in the profile and thus define the limiting design parameters.

From the historical standpoint, many authors since the 1950's have presented design methods encompassing both cylindrical and spherical filament wound pressure vessels. Computations based on netting analysis for the cylindrical section on thin-walled vessels is now widely known but head design, due to its complexity, is not. Equations describing optimum filament wound shells of revolution have been available since the 1960's. Possibly the most complete works, translated from Russian and published mid 1970's and onwards, have been complied by V.A. Bunakov, and co-authors V.D. Protasov, S.B. Cherevatskii and A.L. Radovinskii [154]. Interpreting their work requires significant mathematical abilities.

By the 1970's government agencies / contractors and winding equipment manufacturers were working on the creation of optimized wound pressure vessel domes.

Gradually the equipment and methods being used shifted from mechanical planar winding to computer controlled equipment capable of laying geodesic fiber paths. Head profiles and fiber paths were the result of proprietary computer algorithms. The basis for many advanced designs can be traced to the equations and a computer code published by Aerojet General in 1966 under a NASA contract [158]. During the 1970's and 1980's, these equations were extended to include fiber slippage considerations. More recently (1988), the principal design equations in use at Aerospatial were presented by J.P. Denost to NATO members [105].

Today, most designs are complemented and refined using the FEM. A designer's comprehension of interactions among the governing variables makes the analytical model indispensable. From an engineering standpoint, the geometric significance given to terms that comprise the fundamental equations in Denost's presentation, in contrast to the work of Bunakov et al., makes the former more comprehensible to engineers.

The following derivations (expanded from Denost's paper) are for a thin-walled cylindrical pressure vessel design. The main features to be extracted for a thick-wall design are the relations concerning the winding geometry and head profile, rather than the stress analysis. One must note that thick-wall vessels undergo a continual change in dome profile as the fiber builds which in turn requires modified winding angles to compensate.

Below, the cylindrical portion is designed according to a (very simplified) netting analysis. The basic assumptions are:

1) Fibers carry all the load.

97

2) Matrix serves only to hold the fibers to the vessel shape and transmits secondary loads.

3) There is no interaction between layers.

4) Stress distribution through the wall is constant.

5) All layers carry the same load.

It is clear that for thick-walled cylinders all the above assumptions are to some degree violated. However the basics remain valid and some elements of simple netting theory are requisite to the derivation of dome geometry and fiber path.

A combination of circumferential and helical (satellite) windings comprise the cylinder wall. With reference to Figure 3.1 and 3.2, a balance of forces in the principal directions gives:
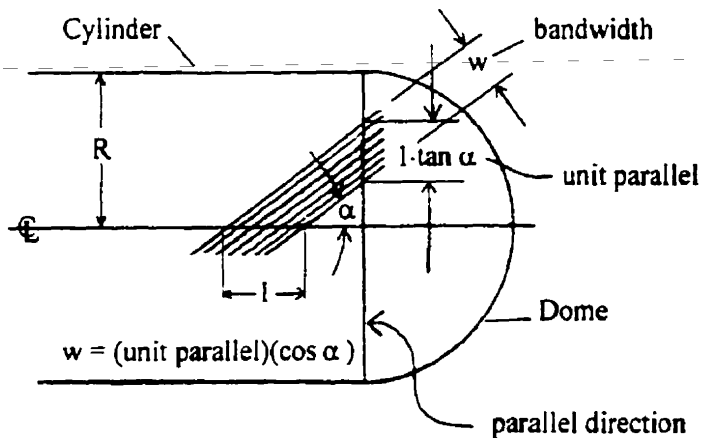
Figure 3.1 Fiber-band on cylinder.
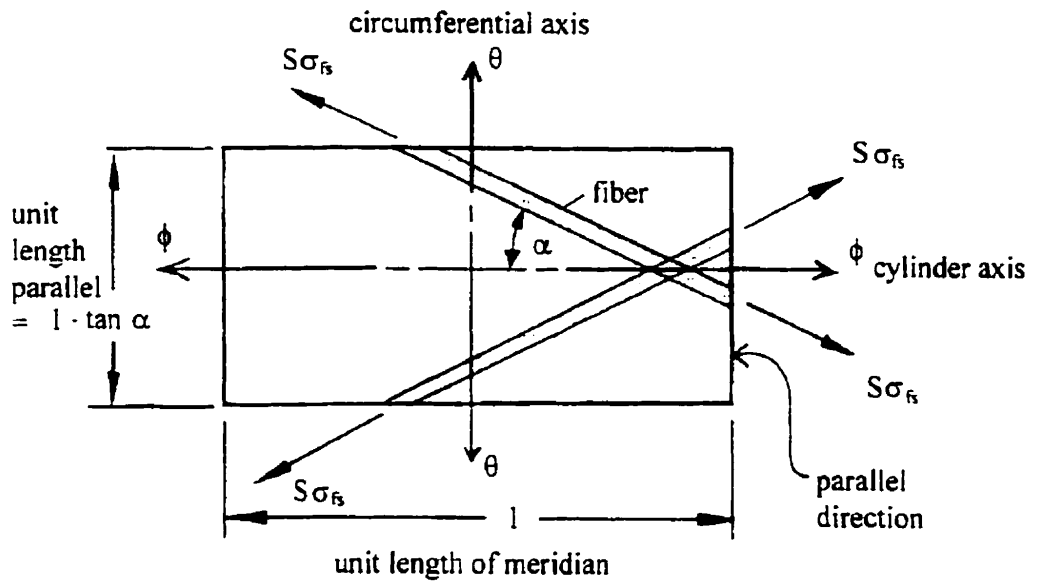
Figure 3.2 Element within the winding.

Notation for preceding figures:

ρ = radius at any point

ρ_c = inside radius of cylinder ($\rho_c = R$)

α = winding angle

N_ϕ, N_θ = membrane load / unit length

$N_{\phi r}, N_{\theta r}$ = Force in ϕ or θ direction per unit length parallel / meridian

$1 \cdot \tan \alpha$ = length of parallel in element

$\cos \alpha$ = component in ϕ

$\sin \alpha$ = component in θ

P = internal pressure

N = number of fibers per unit length of parallel

99

S = cross-sectional area of one fiber

σ = stress

e = thickness

υ_f = fiber volume fraction (constant)

Subscripts:

$_\phi$ = along meridian direction

$_\theta$ = along circumferential direction

$_s$ = satellite (helical) direction

$_c$ = circumferential (hoop) direction

$_f$ = referring to fiber

$_0$ = condition at cylinder-dome junction

Axial direction $\qquad\qquad\qquad\qquad$ $N_{\phi\phi} = N_{\phi s} + N_{\phi c}$ $\qquad\qquad$ (3.1)

Circumferential direction $\qquad\qquad$ $N_{\theta\theta} = N_{\theta s} + N_{\theta c}$ $\qquad\qquad$ (3.2)

$\qquad\qquad\qquad\qquad\qquad\qquad\qquad\qquad$ ↑ $\qquad$ ↑

$\qquad\qquad\qquad\qquad\qquad\qquad\qquad$ helical $\quad$ circumferential
$\qquad\qquad\qquad\qquad\qquad\qquad\qquad$ fibers $\quad$ fibers

Where: $\qquad$ $N_{\phi\phi} = PR/2$ $\qquad$ (axial load)

$\qquad\qquad\quad$ $N_{\theta\theta} = PR$ $\qquad\quad$ (hoop load)

The circumferential layer contribution towards resisting

forces in the axial direction is nonexistent.

$N_{\phi c} = 0$ $\qquad\qquad\qquad\qquad\qquad\qquad\qquad\qquad\qquad\qquad\qquad$ (3.3)

The circumferential load / unit parallel can be expressed as:

$$N_{\theta c} = \upsilon_f e_c \sigma_{fc} \qquad\qquad (3.4)$$

The helical winding portion supports loads in two directions. A balance of forces yields:

$$N_{\phi r}\tan\alpha = N\tan\alpha\ S\sigma_{fs}\cos\alpha \qquad \text{(axial)} \qquad (3.5)$$

$$1\cdot N_{\theta r} = N\tan\alpha\ S\sigma_{fs}\sin\alpha \qquad \text{(circumferential)} \qquad (3.6)$$

Since (width)(thickness) = area, the composite layer thickness can be expressed as:

$$\text{layer thickness} = \frac{X - \text{sectional area of layer}}{\text{bandwidth of layer}}$$

Using the terminology of Figure 3.1, on the basis of a length defined along the parallel, the helical thickness of a composite layer at any point can be expressed in terms of the unit parallel length. First, defining the numerator above:

$$X\text{-sectional area of layer} = \frac{\text{area of fibers}}{\text{fiber volume fraction}}$$

area of fibers = (# fibers in a bandwidth)·(area of a fiber)

Therefore:

$$\text{layer thickness} = \frac{(\#\ \text{fibers in a bandwidth})\cdot(\text{area of a fiber})}{(\text{fiber volume fraction})\cdot(\text{bandwidth})}$$

where: bandwidth = (unit length parallel)(cos α)

and   N = (# fibers in a bandwidth) / (unit length parallel)

hence:

$$e_s = NS\,/\,(\upsilon_f \cos\alpha) \qquad\qquad (3.7)$$

Solving for N in (3.7) and substituting into (3.5) & (3.6):

$$N_{\phi s} \tan\alpha = (e_s \upsilon_f \cos\alpha \, S\sigma_{fs} \cos\alpha \tan\alpha)/S$$

$$N_{\phi s} = \upsilon_f e_s \sigma_{fs} \cos^2\alpha \tag{3.8}$$

Similarly

$$N_{\theta s} = (e_s \upsilon_f \cos\alpha \tan\alpha \, S\sigma_{fs} \sin\alpha)/S$$

$$N_{\theta s} = \upsilon_f e_s \sigma_{fs} \sin^2\alpha \tag{3.9}$$

substituting (3.8) & (3.9) into (3.1) & (3.2) gives:

$$\frac{PR}{2} = \upsilon_f e_s \sigma_{fs} \cos^2\alpha \tag{3.10}$$

$$PR = \upsilon_f e_s \sigma_{fs} \sin^2\alpha + \upsilon_f e_c \sigma_{fc} \tag{3.11}$$

By re-arranging the above equations, filament stress is:

$$\sigma_{fs} = \frac{PR}{(2\upsilon_f e_s \cos^2\alpha)} \tag{3.12}$$

$$PR = \upsilon_f e_s \frac{PR}{2\upsilon_f e_s \cos^2\alpha} \sin^2\alpha + \upsilon_f e_c \sigma_{fc}$$

$$PR\left(1 - \frac{\tan^2\alpha}{2}\right) = \upsilon_f e_c \sigma_{fc}$$

$$\sigma_{fc} = \frac{PR}{\upsilon_f e_c}\left(1 - \frac{\tan^2\alpha}{2}\right) \tag{3.13}$$

If circumferential winding is to be eliminated, combining (3.10) & (3.11):

$$2\upsilon_f e_s \sigma_{fs} \cos^2 \alpha = PR = \upsilon_f e_s \sigma_{fs} \sin^2 \alpha$$

hence:
$$\tan^2 \alpha = 2 \qquad (3.14)$$

If the fibers in the circumferential and helical windings are equally stressed

($\sigma_{fc} = \sigma_{fs}$) and having equal fiber volume fractions, then (3.12) & (3.13) combine:

$$\frac{PR}{(2\upsilon_f e_s \cos^2 \alpha)} = \left(\frac{PR}{\upsilon_f e_c}\right)\left(1 - \frac{\tan^2 \alpha}{2}\right)$$

$$\frac{e_c}{e_s} = 2\cos^2 \alpha\left(1 - \frac{\tan^2 \alpha}{2}\right) = 2\cos^2 \alpha - \sin^2 \alpha$$

$$\frac{e_c}{e_s} = 3\cos^2 \alpha - 1 \qquad (3.15)$$

Cylinder wall thickness equations have been defined above.

The heads contain only helical winding; hoop layers are confined to the cylindrical section.

The shape of the heads and the lay-up line of the filaments must be defined next. Two

conditions must be met:

1) The filaments must counterbalance the stresses from the internal pressure.

2) Stresses in the filaments must remain constant along their length.

The above two conditions constitute "intensoid" design. The head geometry must be

defined mathematically. Equations of equilibrium for membrane shells are well known and

can be referenced in any suitable text. For example in [161] section 18.10, the notation of

Figure 3.3 is followed.
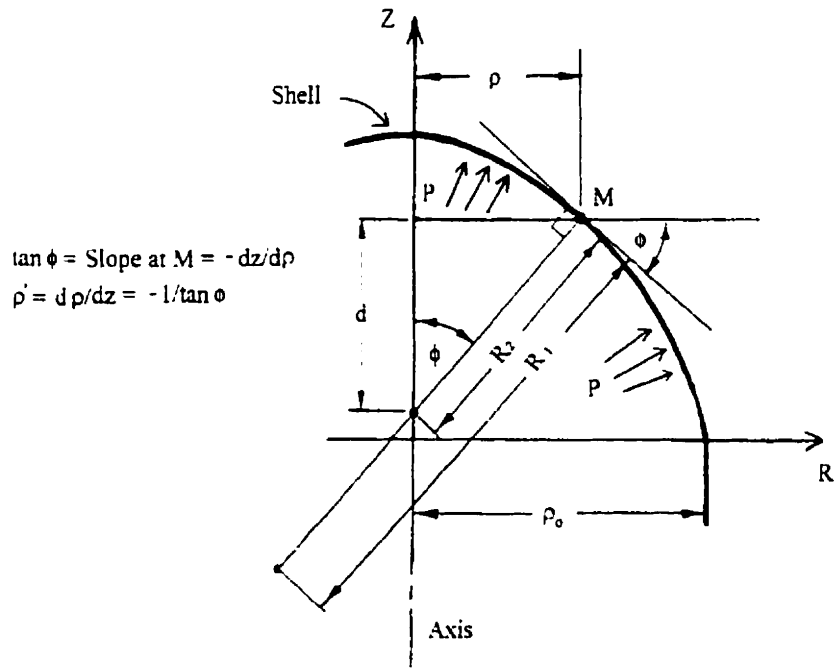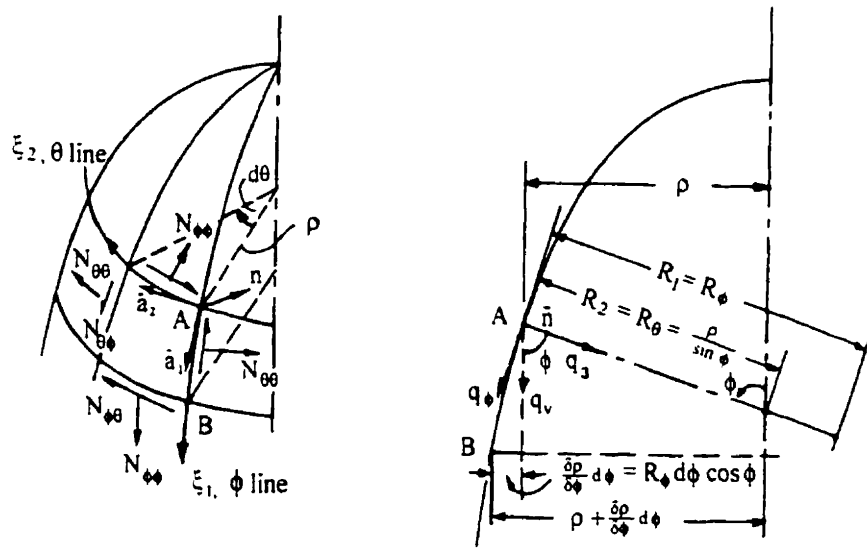
Figure 3.3 Head geometry parameters. Adapted from [161].

Generalized equilibrium equations for membrane shells (no stress couples and no shear) are stated in terms of the fundamental magnitudes in (3.16) below [161].

$$V_{23} = V_{13} = 0$$

$$N_{12} = N_{21}$$

$$\frac{\partial}{\partial \xi_1}\left(\sqrt{G}N_{11}\right) + \frac{\partial}{\partial \xi_2}\left(\sqrt{E}N_{21}\right) + N_{12}\frac{\partial \sqrt{E}}{\partial \xi_2} - N_{22}\frac{\partial \sqrt{G}}{\partial \xi_1} + q_1\sqrt{EG} = 0 \tag{3.16}$$

$$\frac{\partial}{\partial \xi_1}\left(\sqrt{G}N_{12}\right) + \frac{\partial}{\partial \xi_2}\left(\sqrt{E}N_{22}\right) + N_{21}\frac{\partial \sqrt{G}}{\partial \xi_1} - N_{11}\frac{\partial \sqrt{E}}{\partial \xi_2} + q_2\sqrt{EG} = 0$$

$$\frac{N_{11}}{R_1} + \frac{N_{22}}{R_2} + q_3 = 0$$

where: N_{ij} = membrane force per unit length

$_{i,j}$ = subscripts denote principal directions

E, G = first fundamental magnitudes

ξ_1, ξ_2 = Gaussian (surface) coordinates

R_1, R_2 = principal radii of curvature

q_i = surface traction (per unit area)

V_{ij} = shear forces

Switching from subscripts 1,2 to ϕ, θ the generalized equations in (3.16) above

can be expressed in more familiar notation. In any shell of revolution the first fundamental

magnitudes E, G are respectively R_ϕ^2, ρ^2. (Note; equivalences in notation are: $R_1 = R_\phi$).

(Figure 3.3) In this case ξ_1 is identified with ϕ, and ξ_2 with θ directions. Because we are

looking at a body with rotational symmetry (θ direction), the fundamental magnitudes E

and G are independent of θ. Thus the terms containing $\partial/\partial \xi_2$ cease to exist when they

105

differentiate a radius. Also from Figure 3.3 the relation $\partial\rho/\partial\phi = R_1\cos\phi$ can be applied.

The last three equations of (3.16) can thus be restated more specifically as:

$$\frac{\partial}{\partial\phi}\left(\rho N_{\phi\phi}\right) + R_1\frac{\partial N_{\phi\theta}}{\partial\theta} - N_{\theta\theta}R_1\cos\phi + q_\phi R_1\rho = 0 \tag{3.16a}$$

$$\frac{\partial}{\partial\phi}\left(\rho N_{\theta\phi}\right) + R_1\frac{\partial N_{\theta\theta}}{\partial\theta} + N_{\phi\theta}R_1\cos\phi + q_\theta R_1\rho = 0 \tag{3.16b}$$

$$\frac{N_{\phi\phi}}{R_1} + \frac{N_{\theta\theta}}{R_2} + q_3 = 0 \tag{3.16c}$$

For symmetrical loading of the shell (as with uniform internal pressure) the

equations do not depend on θ, hence both $N_{\theta\phi}$ and q_θ must equal zero and (3.16b) is

identically satisfied. Replacing $\rho = R_2\sin\phi$, from (3.16c), $N_{\theta\theta}$ is expressed as:

$$N_{\theta\theta} = -\frac{N_{\phi\phi}\rho}{R_1\sin\phi} - \frac{\rho q_3}{\sin\phi} \tag{3.17}$$

Substituting (3.17) into (3.16a) and multiplying the result by $\sin\theta$ we find that the

following re-arrangement is possible:

$$\frac{d}{d\phi}\left(\rho N_{\phi\phi}\sin\phi\right) + \rho R_1\left(q_\phi\sin\phi + q_3\cos\phi\right) = 0 \tag{3.18}$$

Integrating with respect to ϕ, we solve for $N_{\phi\phi}$ by writing (3.18) in the following form:

$$N_{\phi\phi} = -\frac{1}{2\pi\rho\sin\phi}\left[\int_o^\phi 2\pi\rho R_1\left(q_\phi\sin\phi + q_3\cos\phi\right)d\phi\right] \tag{3.19}$$

106

With reference to Figure 3.3 and 3.4, the term $\left(q_\phi \sin\phi + q_3 \cos\phi\right)$ has a vertical resultant

(q_V in Figure 3.3) that acts on an annular area $2\pi\rho R_1 d\phi$.
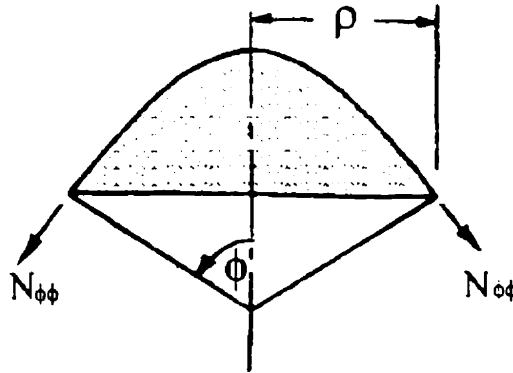
Figure 3.4 Force resultant. Adapted from [161].

The integral on the *RHS* of (3.19) can be replaced by the resultant of the total load

acting on that part of the shell corresponding to the angle ϕ. We set:

$$F = \int_o^\phi 2\pi\rho R_1\left(q_\phi \sin\phi + q_3 \cos\phi\right)d\phi$$

This gives:

$$N_{\phi\phi} = \frac{-F}{2\pi\rho \sin\phi} \tag{3.20}$$

For the case in study, that of a circular shell under internal pressure, the global force

resultant F is simply $\pi\rho^2 P$.

Where: P = internal pressure = $-q_3$

Hence we have:

$$N_{\phi\phi} = \frac{\pi\rho^2 P}{2\pi\rho\sin\phi} = \frac{P\rho}{2\sin\phi} = \frac{PR_2}{2}$$

(3.21)

where: $R_2\sin\phi = \rho$ (Figure 3.3)

from (3.17)

$$N_{\theta\theta} = -\frac{P\rho\rho}{2\sin\phi R_1\sin\phi} - \frac{\rho q_3}{\sin\phi}$$

or

$$N_{\theta\theta} = -\frac{PR_2^2\sin^2\phi}{2R_1\sin^2\phi} + \frac{PR_2\sin\phi}{\sin\phi}$$

$$N_{\theta\theta} = \frac{PR_2}{2}\left(2 - \frac{R_2}{R_1}\right)$$

(3.22)

Also the principal radii R_1 & R_2 can be expressed in terms of the slope and curvature at a point. By mathematical definition, for example see [160], the meridional radius of curvature at M (in the plane of the paper) for a generating curve $\rho_{(z)}$ is:

$$R_1 = \frac{-[1+(\rho')^2]^{3/2}}{\rho''}$$

(3.23)

A second radius of curvature R_2 exists in the R-Z plane describing the circumferential radius at M about the Z-axis via its surface normal.

With reference to Figure 3.3:

$$R_2^2 = \rho^2 + d^2 = \rho^2 + (\rho/\tan\phi)^2 = \rho^2 + (\rho\rho')^2$$

$$R_2^2 = \rho^2(1 + \rho'^2)$$

$$R_2 = \rho[1 + \rho'^2]^{\frac{1}{2}} \tag{3.24}$$

since from (3.8) & (3.9) we have

$$\frac{N_{\theta\theta}}{N_{\phi\phi}} = \tan^2\alpha$$

introducing (3.21) & (3.22)

$$\frac{N_{\theta\theta}}{N_{\phi\phi}} = \frac{(PR_2/2)(2 - R_2/R_1)}{(PR_2/2)}$$

from (3.23) & (3.24) the first condition of intensoid design reduces to:

$$\tan^2\alpha = 2 - \frac{R_2}{R_1} = 2 - \frac{\rho(1 + \rho'^2)^{\frac{1}{2}}\rho''}{-(1 + \rho'^2)^{\frac{1}{2}}} = 2 + \frac{\rho\rho''}{1 + \rho'^2} \tag{3.25}$$

The second condition requires that the stress in the

filament remains constant. From (3.8)

$$\sigma_{fs} = \frac{N_{\phi\phi}}{\upsilon_f e_s \cos^2\alpha} \tag{3.26}$$

Relation (3.7) which expresses the local thickness can be written for the junction

of the head and cylinder as:

$$e_{0s} = \frac{N_0 S}{\upsilon_f \cos\alpha_0}$$

(3.27)

where: α_0 fiber angle at cylinder to dome junction.

Also, since all the filaments cutting the parallel at the junction of the head and cylinder will cut the parallel at any arbitrary point on the head being considered, the following is true:

$$2\pi\rho N = 2\pi\rho_0 N_0 \quad ; \quad \frac{N}{N_0} = \frac{\rho_0}{\rho}$$

and (3.27) becomes

$$\frac{e_s \cos\alpha}{N} = \frac{e_{0s} \cos\alpha_0}{N_0}$$

(3.28)

hence local thickness is:

$$e_s = \frac{e_{0s} N \cos\alpha_0}{N_0 \cos\alpha} = \frac{e_{0s}\rho_0 \cos\alpha_0}{\rho \cos\alpha}$$

(3.29)

from (3.26)

$$\sigma_{fs} = \frac{N_{\phi}\rho \cos\alpha}{\upsilon_f e_{0s} \rho_0 \cos\alpha_0 \cos^2\alpha} = \frac{PR_2 \rho}{2\upsilon_f e_{0s} \rho_0 \cos\alpha \cos\alpha_0}$$

$$\sigma_{fs} = \frac{P\rho^2 (1+\rho'^2)^{\frac{1}{2}}}{2\upsilon_f e_{0s} \rho_0 \cos\alpha \cos\alpha_0}$$

(3.30)

Factoring out constant terms, the requirement for constant stress in the filaments (second condition) can be stated as:

110

$$\rho^2(1+\rho'^2)^{\frac{1}{2}} / \cos\alpha = k \tag{3.31}$$

The shape of the head $\rho_{(z)}$ and fiber path $\alpha_{(z)}$ can now be determined by solution of the system

$$2 + \frac{\rho\rho''}{1+\rho'^2} = \tan^2\alpha \quad ; \quad \frac{\rho^2(1+\rho'^2)^{\frac{1}{2}}}{\cos\alpha} = k = \text{constant} \tag{3.32}$$

The relation between α and ρ can be found as follows.

Differentiation of (3.31) wrt. z gives:

$$\frac{dk}{dz} = 0$$

$$0 = \frac{\cos\alpha[2\rho\rho'(1+\rho'^2)^{\frac{1}{2}} + \frac{1}{2}\rho^2(1+\rho'^2)^{-\frac{1}{2}}2\rho'\rho''] + \sin\alpha \cdot \alpha'[\rho^2(1+\rho'^2)^{\frac{1}{2}}]}{\cos^2\alpha}$$

$$0 = \cos\alpha\, 2\rho\rho'(1+\rho'^2)^{\frac{1}{2}} + \frac{1}{2}\rho^2(1+\rho'^2)^{-\frac{1}{2}}2\rho'\rho''\cos\alpha + \alpha'\sin\alpha[\rho^2(1+\rho'^2)^{\frac{1}{2}}]$$

$$0 = \cos\alpha\, 2\rho'\rho + \rho^2(1+\rho'^2)^{-1}\rho'\rho''\cos\alpha + \alpha'\sin\alpha(\rho)^2$$

$$0 = 2\rho' + \frac{\rho\rho'\rho''}{(1+\rho'^2)} + \rho\alpha'\tan\alpha \tag{3.33}$$

substituting the first relation of (3.32) gives

$$2\rho' + \rho'(\tan^2\alpha - 2) + \rho\alpha'\tan\alpha = 0$$

$$\rho'\tan^2\alpha + \rho\alpha'\tan\alpha = 0$$

$$\rho'\tan\alpha = -\rho\alpha'$$

$$\frac{\rho'}{\rho} = \frac{-\alpha'}{\tan \alpha} \qquad (3.34)$$

integrating yields:

$$\ln \rho + C_1 = -\ln \sin \alpha + C_2$$

$$\ln \rho + \ln \sin \alpha = C_3$$

$$\ln (\rho \sin \alpha) = C_3$$

$$\rho \sin \alpha = e^{C_3} = \text{constant} \qquad (3.35)$$

The above condition (Clairaut's equation) relates the winding angle to the local radius. It will be shown more definitively later that relation (3.35) is a characteristic property of geodesic lines belonging to any surface of revolution. In the particular case of "intensoid" design, (3.35) makes it possible to obtain the winding law once the head is geometrically defined. In other words, laying filaments along geodesic lines for the "intensoid" shape ensures that they will be subject to constant stress.

An equation linking the coordinates ρ and z is required to specify the function describing the shape of the "intensoid" head. (3.32) can be written as:

$$2 + \frac{\rho \rho''}{(1+\rho'^2)} = \tan^2 \alpha \quad ; \quad \frac{\rho^4(1+\rho'^2)}{k^2} = \cos^2 \alpha \qquad (3.36)$$

using identity: $\tan^2 \alpha + 1 = \dfrac{1}{\cos^2 \alpha}$

$$3 + \frac{\rho \rho''}{(1+\rho'^2)} = \frac{k^2}{\rho^4(1+\rho'^2)} \qquad (3.37)$$

Another form can be derived: (multiplying by $2\rho^5\rho'$)

112

$$6\rho^5\rho' + \frac{\rho^5(2\rho\rho'\rho'')}{(1+\rho'^2)} = \frac{k^2(2\rho^5\rho')}{\rho^4(1+\rho'^2)}$$

$$6\rho^5\rho' + \frac{\rho^6(2\rho'\rho'')}{(1+\rho'^2)} = \frac{k^2(2\rho\rho')}{(1+\rho'^2)}$$

or

$$6\rho^5\rho'(1+\rho'^2) + \rho^6(2\rho'\rho'') = k^2(2\rho\rho')$$

this can be expressed as a differential:

$$\left[\rho^6(1+\rho'^2)\right]' = k^2(\rho^2)'$$

integration yields

$$\rho^6(1+\rho'^2) = k^2\rho^2 + C \tag{3.38}$$

At ρ_0, $\rho_0' = 0$, thus the integration constant C is evaluated as:

$$C = \rho_0^6 - k^2\rho_0^2$$

(3.38) becomes

$$\rho^6(1+\rho'^2) = k^2\rho^2 + \rho_0^6 - k^2\rho_0^2$$

dividing by ρ_0^6

$$(\rho/\rho_0)^6(1+\rho'^2) = (k^2/\rho_0^4)(\rho/\rho_0)^2 + 1 - (k^2/\rho_0^4)$$

$$(\rho/\rho_0)^6(1+\rho'^2) = -(k^2/\rho_0^4)[1 - (\rho/\rho_0)^2] + 1$$

but at ρ_0, $\rho_0' = 0$ and $\alpha = \alpha_0$

so the second condition of (3.32) can be stated as:

113

$$\frac{k^2}{\rho_0^4} = \frac{1}{\cos^2 \alpha_0}$$

$$(\rho/\rho_0)^6 (1+\rho'^2) = -\left(1/\cos^2 \alpha_0\right)\left[1-(\rho/\rho_0)^2\right]+1$$

$$\cos^2 \alpha_0 (\rho/\rho_0)^6 (1+\rho'^2) = \cos^2 \alpha_0 - [1-(\rho/\rho_0)^2]$$

$$1+\rho'^2 = \frac{\cos^2 \alpha_0 - [1-(\rho/\rho_0)^2]}{\cos^2 \alpha_0 (\rho/\rho_0)^6}$$

$$\rho'^2 = \frac{\cos^2 \alpha_0 - \cos^2 \alpha_0 (\rho/\rho_0)^6 - [1-(\rho/\rho_0)^2]}{\cos^2 \alpha_0 (\rho/\rho_0)^6}$$

$$\frac{1}{\rho'^2} = \frac{\cos^2 \alpha_0 (\rho/\rho_0)^6}{\cos^2 \alpha_0 - \cos^2 \alpha_0 (\rho/\rho_0)^6 - [1-(\rho/\rho_0)^2]}$$

rewriting with the introduction of new terms as:

$$\frac{1}{\rho'^2} = \frac{\cos^2 \alpha_0 (\rho/\rho_0)^6}{-[1-(\rho/\rho_0)^2]+\cos^2 \alpha_0 [1-(\rho/\rho_0)^2][(\rho/\rho_0)^2+(\rho/\rho_0)^4]+\cos^2 \alpha_0 [1-(\rho/\rho_0)^2]}$$

$$\frac{1}{\rho'^2} = \frac{\cos^2 \alpha_0 (\rho/\rho_0)^6}{[1-(\rho/\rho_0)^2]\left[\cos^2 \alpha_0 + \cos^2 \alpha_0 [(\rho/\rho_0)^2+(\rho/\rho_0)^4]-1\right]}$$

$$\frac{1}{\rho'^2} = \frac{\cos^2 \alpha_0 (\rho/\rho_0)^6}{[1-(\rho/\rho_0)^2]\left[\cos^2 \alpha_0 (\rho/\rho_0)^2[1+(\rho/\rho_0)^2]-\sin^2 \alpha_0\right]}$$

$$\frac{1}{\rho'} = \frac{(\rho/\rho_0)^3 \cos \alpha_o}{\left\{[1-(\rho/\rho_0)^2]\left[\cos^2 \alpha_0 (\rho/\rho_0)^2[1+(\rho/\rho_0)^2]-\sin^2 \alpha_0\right]\right\}^{\frac{1}{2}}}$$

introducing the variables:

$$t = \frac{\rho}{\rho_0}, \quad \gamma = \frac{z}{\rho_0}, \quad \text{then} \quad \frac{\gamma}{t} = \frac{(z/\rho_0)}{(\rho/\rho_0)} = \frac{z}{\rho}$$

so $\dfrac{dy}{dt} = \dfrac{dz}{d\rho}$

$$\rho' = \frac{d\rho}{dz}, \quad t' = \frac{\rho'}{\rho_0}, \quad \frac{1}{t'} = \rho_0\left(\frac{1}{\rho'}\right) = \frac{\rho_0 dz}{d\rho} = \rho_0\left(\frac{dy}{dt}\right)$$

hence $\dfrac{1}{\rho_0 t'} = \dfrac{dy}{dt}$

$$\frac{1}{\rho_0 t'} = \frac{t^3 \cos\alpha_0}{\left\{(1-t^2)[t^2(1+t^2)\cos^2\alpha_0 - \sin^2\alpha_0]\right\}^{\frac{1}{2}}}$$

$$\frac{dy}{dt} = \frac{t^3 \cos\alpha_0}{\left\{(1-t^2)[t^2(1+t^2)\cos^2\alpha_0 - \sin^2\alpha_0]\right\}^{\frac{1}{2}}}$$

$$z = \gamma\rho_0 = \rho_0 \int_0^t \frac{t^3 \cos\alpha_0\, dt}{\left\{(1-t^2)[t^2(1+t^2)\cos^2\alpha_0 - \sin^2\alpha_0]\right\}^{\frac{1}{2}}} \qquad (3.39)$$

$$\text{where: } t = \frac{\rho}{\rho_0}$$

(3.39) allows computation of a non-dimensionalized head shape in terms of axial

coordinate z and radial coordinate ρ. The integral is evaluated numerically.

A cylindrical tank has two heads and therefore two planes of junction between the

cylinder and head. The geodesic line on the cylinder is a helix. The winding angle α is

constant and the same at these two junctions.

$$\alpha_{01} = \alpha_{02} = \alpha_0$$

At the opening (fiber turn-around point) $\alpha = 90°$

Relation (3.35) leads to the conclusion that:

$$\rho_{F_1} = \rho_{F_2} = \rho_0 \sin\alpha_0$$

where: ρ_{F_1} and ρ_{F_2} are radii of the polar opening flanges.

115

1) The "intensoid" design only allows fabrication of vessels with identical polar openings.

2) At $\alpha = 54.75°$, $\tan^2\alpha = 2$ and by the first condition of (3.32) ρ'' must equal 0.

In this case the meridians present an inflection point. Current practice is to extend the head profile in the region of $55° < \alpha < 90°$ by the construction of a spherical cap of radius R_2 in this region. Generally internal metal bosses extend from this point to the opening providing secondary reinforcement. More complex head profiles in this region are derived in [155].

3.1 Balanced winding with controlled stability

To overcome the limitations governing the size of the polar openings and to avoid fiber slippage which adversely affects the performance of the product, the stability of the winding must be detailed. Current design methods incorporate an enhancement to the second condition of (3.32) which take into account the friction available to hold a fiber on a path deviating from the geodesic line. The ability to deviate off the geodesic line is required to maintain a margin of geometric freedom in the size of the openings. Many pressure vessels require only one opening, or different size openings.

During the winding phase, the filament is laid on the mandrel with a tension $\bar{T}$. Figure 3.5 illustrates some parameters of what follows:
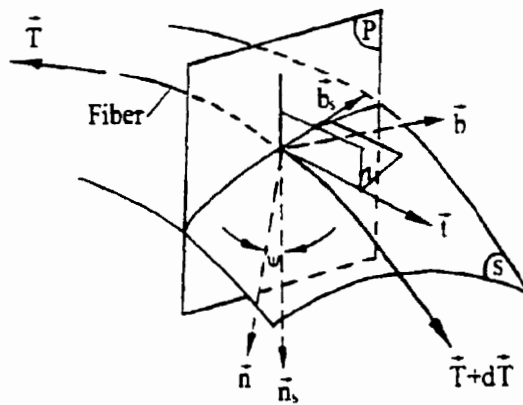
Notation:

ψ = rotation about $\bar{t}$

$\bar{n}_s$ = surface normal

$\bar{n}$ = fiber path normal

$\bar{b}_s$ = binormal vector

$\bar{T}$ = tension in filament

ς = curvature

λ = lengthwise

υ = sideways

μ = downwards

S = mandrel surface

P = plane of parallel

Figure 3.5 Force vectors acting on fiber.

The mandrel exerts a force $\bar{F}$ per unit length filament.

$$\bar{F} = \lambda \bar{t} + \mu \bar{n}_s + \upsilon \bar{b}_s$$

For a small element in equilibrium, the values of λ, μ, υ have the following expressions:

$$\lambda = \frac{-d\bar{T}}{d\bar{S}} \text{ (change in tension along length of fiber)}$$

$$\mu = -\bar{T}\varsigma \cos \psi \text{ (tension component downwards)}$$

$$\upsilon = -\bar{T}\varsigma \sin \psi \text{ (tension component sideways)}$$

Under the effects of tension, the filament tends to slip in the direction of vector $\bar{b}$. The slippage tendency can be characterized by:

$$k = \left| \frac{\upsilon}{\mu} \right| = |\tan \psi| \tag{3.40}$$

117

Relation (3.40) shows that the angle ψ is the value characterizing the stability of the winding. (In effect it is the friction coefficient). Consequently the angle will be taken into account in the second condition of (3.32) leading to modified expressions for $\alpha_{(z)}$. The determination of such follows. With reference to Figure 3.6, the components of the unit normal vector $(\vec{n}_s)$ in the x, y, z coordinate system are determined:
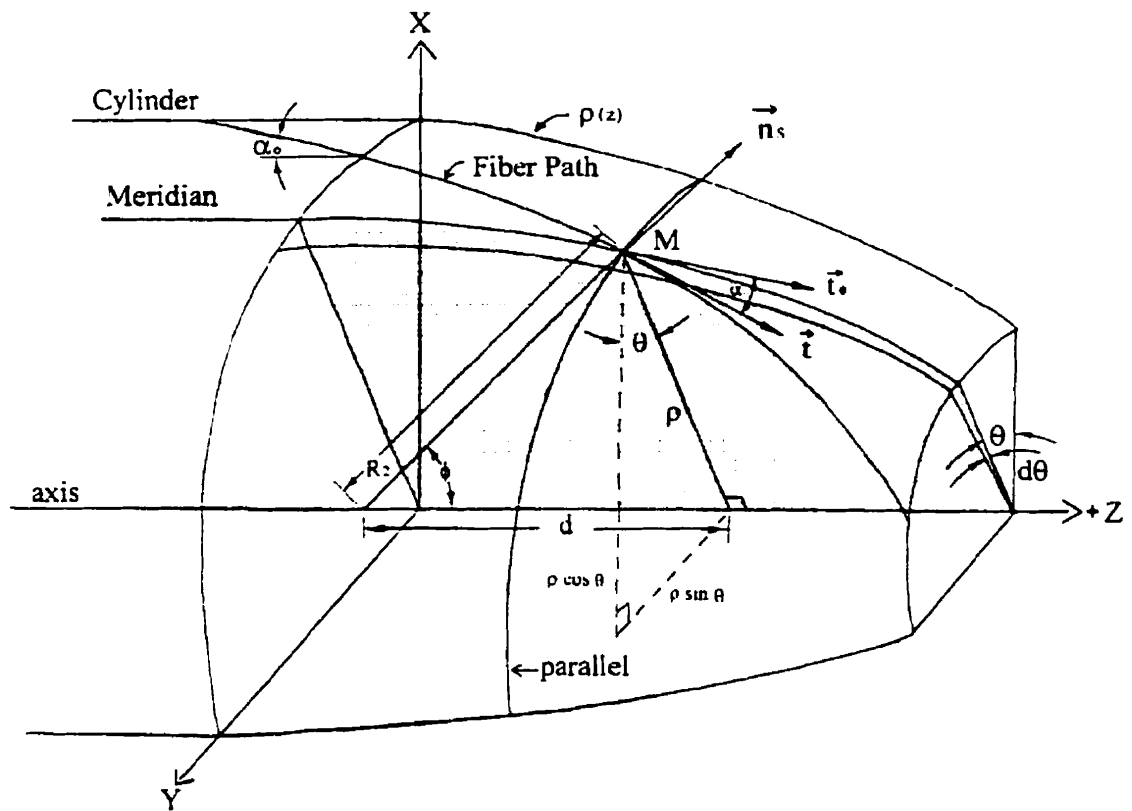
Notation:

$\vec{t}$ = tangent to fiber path at M
α = angle between meridian
      plane and fiber
θ = angle of meridian wrt. coordinate
      system
$\vec{n}_s$ = outward normal

Figure 3.6 Fiber orientation on head surface.

Letting R_2 represent the radius along the outward normal to the surface, its magnitude can be expressed as:

$$R_2 = \left| \rho(1+\rho'^2)^{\frac{1}{2}} \right|$$
(from equation (3.24))

its component in $(x) = \rho\cos\theta$

its component in $(y) = \rho\sin\theta$

its component in $(z) = d = \dfrac{\rho}{\tan\phi} = -\rho\rho'$
(from Figure 3.3)

where: slope ρ' is negative

The normalized components are:

$$\bar{n}_s = \frac{\rho\cos\theta}{\rho(1+\rho'^2)^{\frac{1}{2}}}, \frac{\rho\sin\theta}{\rho(1+\rho'^2)^{\frac{1}{2}}}, \frac{-\rho\rho'}{\rho(1+\rho'^2)^{\frac{1}{2}}}$$

The unit outward normal $(\bar{n}_s)$ is

$$\bar{n}_s = \frac{\cos\theta}{D}, \frac{\sin\theta}{D}, -\frac{\rho'}{D}$$
(3.41)

Where: $D = (1+\rho'^2)^{\frac{1}{2}}$

Components of the tangent (to fiber path) vector ($\bar{t}$) can be computed by examining the geometry of Figure 3.7 and supplementary details of Figure 3.8.
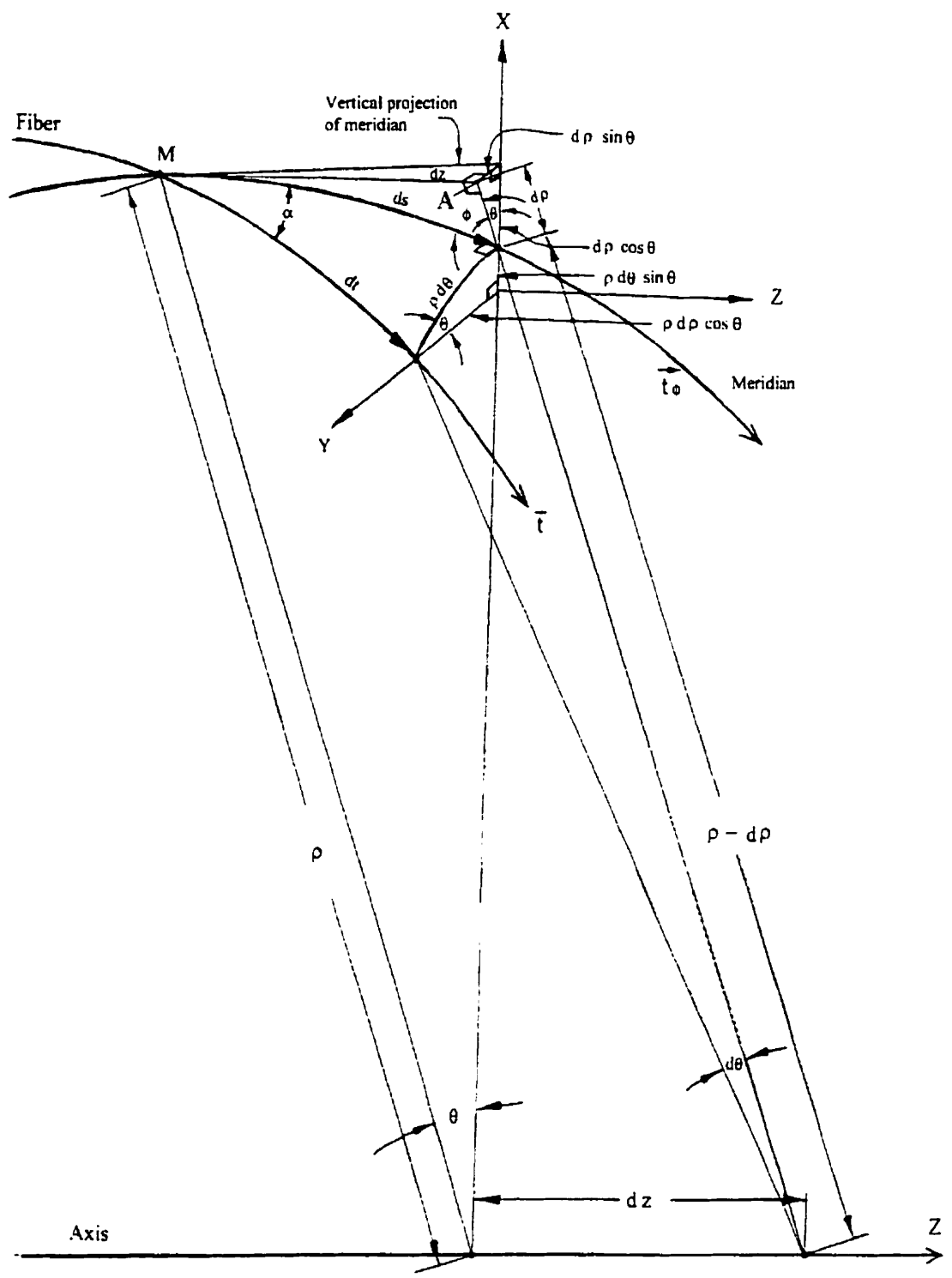
Figure 3.7 Vector components along fiber path.
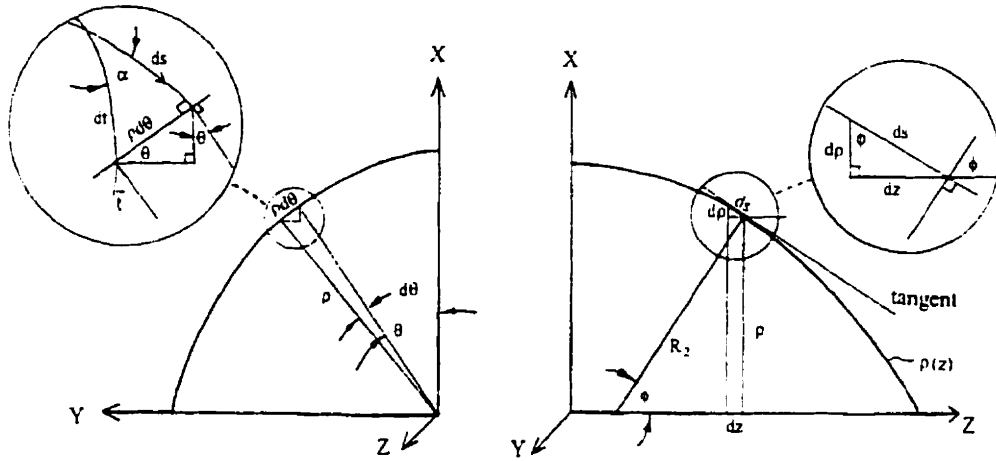
Relations

$$\frac{\rho d\theta}{ds} = \tan\alpha$$

$$\frac{dz}{-d\rho} = \tan\phi = -\frac{1}{\rho'}$$

$$\frac{\rho d\theta}{dz(1+\rho'^2)^{\frac{1}{2}}} = \tan\alpha$$

$$ds^2 = dz^2 + d\rho^2 = dz^2 + (\rho' dz)^2$$

$$\frac{d\theta}{dz} = \frac{(1+\rho'^2)^{\frac{1}{2}} \tan\alpha}{\rho}$$

$$ds^2 = dz^2(1+\rho'^2)$$

$$\frac{d\theta}{dz} = \frac{D\tan\alpha}{\rho}; \quad D = (1+\rho'^2)^{\frac{1}{2}}$$

$$ds = dz(1+\rho'^2)^{\frac{1}{2}}$$

Figure 3.8 Details of fiber path geometry.

Letting (dt) represent the unit vector $(\bar{t})$ in the figures, the components constituting (dt) in the x, y, z directions, divided by (dt), will comprise the required unit vector $(\bar{t})$. Length M-A in Figure 3.7 equals (dz), the (z) component. Taking 'A' as the reference point the other components are derived:

$(\vec{t}\,)$ components in (x): $\dfrac{-dt\cos\alpha\cos\phi\cos\theta}{dt}-\dfrac{dt\sin\alpha\sin\theta}{dt}$

but

$$\frac{d\rho}{ds}=\cos\phi=\frac{-\rho'dz}{dz(1+\rho'^2)^{1/2}} \quad ; \quad D=(1+\rho'^2)^{1/2}$$

therefore:

$$(\vec{t}\,),(x)\,\text{component}=\frac{\rho'\cos\theta\cos\alpha}{D}-\sin\alpha\sin\theta$$

$(\vec{t}\,)$ components in (y): $\dfrac{-dt\cos\alpha\cos\phi\sin\theta}{dt}+\dfrac{dt\sin\alpha\cos\theta}{dt}$

$$(\vec{t}\,),(y)\,\text{component}=\frac{\rho'\cos\alpha\sin\theta}{D}+\sin\alpha\cos\theta$$

$(\vec{t}\,)$ components in (z): $dz=ds/(1+\rho'^2)^{1/2}$ $\qquad$ (see Figure 3.8)

$$(\vec{t}\,),(z)\,\text{component}=\frac{dt\cos\alpha}{dt(1+\rho'^2)^{1/2}}=\frac{\cos\alpha}{D}$$

in summary:

$$(\vec{t}\,)=\frac{\rho'\cos\theta\cos\alpha}{D}-\sin\alpha\sin\theta,\;\frac{\rho'\cos\alpha\sin\theta}{D}+\sin\alpha\cos\theta,\;\frac{\cos\alpha}{D}$$

$$(3.42)$$

From Figure 3.8 the following relation is evident:

$$\theta'=\frac{d\theta}{dz}=\frac{D\tan\alpha}{\rho} \qquad\qquad (3.43)$$

Subsequently a vector in the *direction* of $(\vec{n})$ must be found. From differential

geometry, a vector in the direction of $(\vec{n})$ can be found by taking the derivative of vector

($\bar{t}$) with respect to the fundamental variable, which in this case is z. The new vector will be normal to the tangent vector ($\bar{t}$). The components of this new vector are derived from the constituents of ($\bar{t}$) as expressed in equations (3.44):

$\dfrac{d\bar{t}}{dz}$, (x) component =

$$\frac{\left\{1+\rho'^2\right\}^{\frac{1}{2}}\left[\rho''\cos\alpha\cos\theta - \rho'\alpha'\sin\alpha\cos\theta - \rho'\theta'\cos\alpha\sin\theta\right]}{(1+\rho'^2)} -$$

$$\frac{\left[\rho'\cos\alpha\cos\theta\left[\frac{1}{2}(1+\rho'^2)^{-\frac{1}{2}}\right]2\rho'\rho''\right]}{(1+\rho'^2)} - (\alpha'\cos\alpha\sin\theta + \theta'\cos\theta\sin\alpha)$$

but; $\quad \theta' = \dfrac{d\theta}{dz} = \dfrac{D\sin\alpha}{\rho\cos\alpha} \quad$ and; $\quad D = (1+\rho'^2)^{\frac{1}{2}}$

the (x) component is rewritten as:

$$\frac{\rho''\cos\alpha\cos\theta}{D} - \frac{\rho'\alpha'\sin\alpha\cos\theta}{D} - \frac{\rho'\sin\alpha\sin\theta}{\rho} - \frac{\rho'^2\rho''\cos\alpha\cos\theta}{D^3} - \alpha'\cos\alpha\sin\theta - \frac{D\sin^2\alpha\cos\theta}{\rho\cos\alpha}$$

$$(3.44\text{-}x)$$

$\dfrac{d\bar{t}}{dz}$, (y) component =

$$\frac{\left\{1+\rho'^2\right\}^{\frac{1}{2}}\left[\rho''\cos\alpha\sin\theta - \alpha'\rho'\sin\alpha\sin\theta + \rho'\theta'\cos\alpha\cos\theta\right]}{(1+\rho'^2)} -$$

$$\frac{\left[\rho'\cos\alpha\sin\theta\left[\frac{1}{2}(1+\rho'^2)^{-\frac{1}{2}}\right]2\rho'\rho''\right]}{(1+\rho'^2)} + \alpha'\cos\alpha\cos\theta - \theta'\sin\theta\sin\alpha$$

The (y) component can be written as:

123

$$\frac{\rho''\cos\alpha\sin\theta}{D}-\frac{\rho'\alpha'\sin\alpha\sin\theta}{D}+\frac{\rho'\sin\alpha\cos\theta}{\rho}-\frac{\rho'^2\rho''\cos\alpha\sin\theta}{D^3}+\alpha'\cos\alpha\cos\theta-\frac{D\sin^2\alpha\sin\theta}{\rho\cos\alpha}$$

<div align="right">(3.44-y)</div>

$\dfrac{d\vec{t}}{dz}$, (z) component =

$$\frac{-(1+\rho'^2)^{\frac{1}{2}}\alpha'\sin\alpha-\cos\alpha\,2\rho'\rho''\,\frac{1}{2}(1+\rho'^2)^{-\frac{1}{2}}}{(1+\rho'^2)}=\frac{-\alpha'\sin\alpha}{D}-\frac{\rho'\rho''\cos\alpha}{D^3}$$

<div align="right">(3.44-z)</div>

The quantity $\tan\psi$, taken between vectors $\vec{n}$ (3.44) and $\vec{n}_s$ (3.41) can

be defined by the following vector properties:

$$\tan\psi=\frac{\|\vec{n}\times\vec{n}_s\|}{\vec{n}\cdot\vec{n}_s}=\frac{\|\vec{n}\|\|\vec{n}_s\|\sin\psi}{\|\vec{n}\|\|\vec{n}_s\|\cos\psi}$$

From equations (3.41) and (3.44), the dot product $\vec{n}\cdot\vec{n}_s$ is:

$$\frac{\rho''\cos\alpha\cos^2\theta}{D^2}-\frac{\rho'\alpha'\sin\alpha\cos^2\theta}{D^2}-\frac{\rho'\sin\alpha\sin\theta\cos\theta}{\rho D}-\frac{\alpha'\cos\alpha\sin\theta\cos\theta}{D}-$$

$$\frac{D\sin^2\alpha\cos^2\theta}{\rho D\cos\alpha}-\frac{\rho'^2\rho''\cos\alpha\cos^2\theta}{D^4}+\frac{\rho''\cos\alpha\sin^2\theta}{D^2}-\frac{\rho'\alpha'\sin\alpha\sin^2\theta}{D^2}+$$

$$\frac{\rho'\sin\alpha\cos\theta\sin\theta}{\rho D}+\frac{\alpha'\cos\alpha\cos\theta\sin\theta}{D}-\frac{D\sin^2\alpha\sin^2\theta}{\rho D\cos\alpha}-$$

$$\frac{\rho'^2\rho''\cos\alpha\sin^2\theta}{D^4}+\frac{\rho'\alpha'\sin\alpha}{D^2}+\frac{\rho'^2\rho''\cos\alpha}{D^4}$$

using: $\cos^2\theta+\sin^2\theta=1$

$$\vec{n}\cdot\vec{n}_s=\frac{\rho''\cos\alpha}{D^2}-\frac{\rho'\alpha'\sin\alpha}{D^2}-\frac{\sin^2\alpha}{\rho\cos\alpha}-\frac{\rho'^2\rho''\cos\alpha}{D^4}+\frac{\rho'\alpha'\sin\alpha}{D^2}+\frac{\rho'^2\rho''\cos\alpha}{D^4}$$

<div align="center">124</div>

$$\vec{n}\cdot\vec{n}_s = \frac{\rho''\cos\alpha}{D^2} - \frac{\sin^2\alpha}{\rho\cos\alpha}$$ (3.45)

The cross product magnitude $\|\vec{n}\times\vec{n}_s\|$ is:

$$\left\{ \left\| n_y n_{sz} - n_z n_{sy} \right\|^2 + \left\| n_z n_{sx} - n_x n_{sz} \right\|^2 + \left\| n_x n_{sy} - n_y n_{sx} \right\|^2 \right\}^{\frac{1}{2}}$$

first term, $(n_y n_{sz} - n_z n_{sy})$ is:

$$\frac{\rho''\rho'\cos\alpha\sin\theta}{D^2} - \frac{\rho'^2\alpha'\sin\alpha\sin\theta}{D^2} + \frac{\rho'^2\sin\alpha\cos\theta}{\rho D} + \frac{\rho'\alpha'\cos\alpha\cos\theta}{D} - \frac{D\rho'\sin^2\alpha\sin\theta}{\rho D\cos\alpha} -$$

$$\frac{\rho'^3\rho''\cos\alpha\sin\theta}{D^4} - \frac{\alpha'\sin\alpha\sin\theta}{D^2} - \frac{\rho'\rho''\cos\alpha\sin\theta}{D^4}$$

which simplifies to:

$$\frac{-(1+\rho'^2)\alpha'\sin\alpha\sin\theta}{D^2} - \frac{(1+\rho'^2)\rho'\rho''\cos\alpha\sin\theta}{D^4} + \frac{\rho'\rho''\cos\alpha\sin\theta}{D^2} +$$

$$\frac{\rho'^2\sin\alpha\cos\theta}{\rho D} + \frac{\rho'\alpha'\cos\alpha\cos\theta}{D} - \frac{\rho'\sin^2\alpha\sin\theta}{\rho\cos\alpha}$$

and reduces to:

$$-\alpha'\sin\alpha\sin\theta + \frac{\rho'^2\sin\alpha\cos\theta}{\rho D} + \frac{\alpha'\rho'\cos\alpha\cos\theta}{D} - \frac{\rho'\sin^2\alpha\sin\theta}{\rho\cos\alpha}$$

Second term, $(n_z n_{sx} - n_x n_{sz})$ is:

$$\frac{\alpha'\sin\alpha\cos\theta}{D^2} + \frac{\rho'^2\rho''\cos\alpha\cos\theta}{D^4} - \frac{\rho'\rho''\cos\alpha\cos\theta}{D^2} + \frac{\rho'^2\alpha'\sin\alpha\cos\theta}{D^2} + \frac{\rho'^2\sin\alpha\sin\theta}{\rho D} +$$

$$\frac{\rho'\alpha'\cos\alpha\sin\theta}{D} + \frac{D\rho'\sin^2\alpha\cos\theta}{\rho D\cos\alpha} + \frac{\rho'^3\rho''\cos\alpha\cos\theta}{D^4}$$

125

and reduces to:

$$\alpha' \sin\alpha \cos\theta + \frac{\rho'^2 \sin\alpha \sin\theta}{\rho D} + \frac{\rho'\alpha' \cos\alpha \sin\theta}{D} + \frac{\rho' \sin^2\alpha \cos\theta}{\rho \cos\alpha}$$

Third term, $(n_x n_{sy} - n_y n_{sx})$ is:

$$\frac{-\rho'' \cos\alpha \cos\theta \sin\theta}{D^2} + \frac{\rho'\alpha' \sin\alpha \cos\theta \sin\theta}{D^2} + \frac{\rho' \sin\alpha \sin^2\theta}{\rho D} + \frac{\alpha' \cos\alpha \sin^2\theta}{D} +$$

$$\frac{D \sin^2\alpha \cos\theta \sin\theta}{\rho D \cos\alpha} + \frac{\rho'^2 \rho'' \cos\alpha \cos\theta \sin\theta}{D^4} + \frac{\rho'' \cos\alpha \sin\theta \cos\theta}{D^2} - \frac{\rho'\alpha' \sin\alpha \sin\theta \cos\theta}{D^2} +$$

$$\frac{\rho' \sin\alpha \cos^2\theta}{\rho D} + \frac{\alpha' \cos\alpha \cos^2\theta}{D} - \frac{D \sin^2\alpha \sin\theta \cos\theta}{\rho D \cos\alpha} - \frac{\rho'^2 \rho'' \cos\alpha \sin\theta \cos\theta}{D^4}$$

Canceling terms gives:

$$\frac{\rho' \sin\alpha}{\rho D}(\sin^2\theta + \cos^2\theta) + \frac{\alpha' \cos\alpha}{D}(\sin^2\theta + \cos^2\theta) = \frac{\rho' \sin\alpha}{\rho D} + \frac{\alpha' \cos\alpha}{D}$$

The first term squared $(n_y n_{sz} - n_z n_{sy})^2$ equals:

$$\alpha'^2 \sin^2\alpha \sin^2\theta + \frac{\rho'^4 \sin^2\alpha \cos^2\theta}{\rho^2 D^2} + \frac{\rho'^2\alpha'^2 \cos^2\alpha \cos^2\theta}{D^2} +$$

$$\frac{\rho'^2 \sin^4\alpha \sin^2\theta}{\rho^2 \cos^2\alpha} - \frac{2\alpha'\rho'^2 \sin^2\alpha \sin\theta \cos\theta}{\rho D} - \frac{2\rho'\alpha'^2 \sin\alpha \sin\theta \cos\alpha \cos\theta}{D} + \frac{2\rho'\alpha' \sin^3\alpha \sin^2\theta}{\rho \cos\alpha} +$$

$$\frac{2\rho'^3\alpha' \cos\alpha \sin\alpha \cos^2\theta}{\rho D^2} - \frac{2\rho'^3 \sin^3\alpha \sin\theta \cos\theta}{\rho^2 D \cos\alpha} - \frac{2\rho'^2\alpha' \cos\alpha \cos\theta \sin^2\alpha \sin\theta}{D\rho \cos\alpha}$$

The second term squared $(n_z n_{sx} - n_x n_{sz})^2$ equals:

$$\alpha'^2 \sin^2\alpha \cos^2\theta + \frac{\rho'^4 \sin^2\alpha \sin^2\theta}{\rho^2 D^2} + \frac{\rho'^2\alpha'^2 \cos^2\alpha \sin^2\theta}{D^2} \frac{\rho'^2 \sin^4\alpha \cos^2\theta}{\rho^2 \cos^2\alpha} +$$

126

$$\frac{2\alpha'\rho'^2\sin^2\alpha\cos\theta\sin\theta}{\rho D} + \frac{2\alpha'^2\rho'\sin\alpha\cos\theta\cos\alpha\sin\theta}{D} + \frac{2\rho'\alpha'\sin^3\alpha\cos^2\theta}{\rho\cos\alpha} +$$

$$\frac{2\rho'^3\alpha'\sin\alpha\cos\alpha\sin^2\theta}{\rho D^2} + \frac{2\rho'^3\sin^3\alpha\sin\theta\cos\theta}{\rho^2 D\cos\alpha} + \frac{2\rho'^2\alpha'\cos\alpha\sin\theta\sin^2\alpha\cos\theta}{D\rho\cos\alpha}$$

Canceling terms and using $\sin^2\theta + \cos^2\theta = 1$ reduces the above two terms to:

$$\alpha'^2\sin^2\alpha + \frac{\rho'^4\sin^2\alpha}{\rho^2 D^2} + \frac{\rho'^2\alpha'^2\cos^2\alpha}{D^2} + \frac{\rho'^2\sin^4\alpha}{\rho^2\cos^2\alpha} + \frac{2\rho'\alpha'\sin^3\alpha}{\rho\cos\alpha} + \frac{2\rho'^3\alpha'\sin\alpha\cos\alpha}{\rho D^2}$$

The third term squared equals: $(n_x n_{sy} - n_y n_{sx})^2$

$$\frac{\rho'^2\sin^2\alpha}{\rho^2 D^2} + \frac{\alpha'^2\cos^2\alpha}{D^2} + \frac{2\rho'\alpha'\sin\alpha\cos\alpha}{\rho D^2}$$

Combining the above two quantities allows simplification to:

$$\frac{(1+\rho'^2)\rho'^2\sin^2\alpha}{\rho^2 D^2} + \frac{(1+\rho'^2)\alpha'^2\cos^2\alpha}{D^2} + \frac{2(1+\rho'^2)\alpha'\rho'(\sin\alpha\cos\alpha)}{\rho D^2} +$$

$$\alpha'^2\sin^2\alpha + \frac{\rho'^2\sin^4\alpha}{\rho^2\cos^2\alpha} + \frac{2\rho'\alpha'\sin^3\alpha}{\rho\cos\alpha}$$

and can be compressed further

$$\|\vec{n}\,X\vec{n}_s\|^2 = \alpha'^2 + \frac{\rho'^2\sin^2\alpha}{\rho^2} + \frac{2\alpha'\rho'\sin\alpha\cos\alpha}{\rho} + \frac{\rho'^2\sin^4\alpha}{\rho^2\cos^2\alpha} + \frac{2\rho'\alpha'\sin^3\alpha}{\rho\cos\alpha}$$

$$(3.46)$$

(3.45) can be expressed as:

$$D^2\rho\cos\alpha(\vec{n}\cdot\vec{n}_s) = -\rho''\rho\cos^2\alpha + D^2\sin^2\alpha \qquad (3.47)$$

multiplying (3.46) by $(D^2\rho\cos\alpha)^2$:

$$\alpha'^2\rho^2 D^4\cos^2\alpha + D^4\rho'^2\sin^2\alpha\cos^2\alpha + 2\alpha'\rho'\rho D^4\cos^3\alpha\sin\alpha + \rho'^2 D^4\sin^4\alpha + 2\rho'\rho\alpha'D^4\cos\alpha\sin^3\alpha$$

regrouping as:

$$D^4 [\alpha'^2 \rho^2 \cos^2 \alpha + \rho'^2 \sin^2 \alpha \cos^2 \alpha + 2\alpha' \rho' \rho(\cos^3 \alpha \sin \alpha + \cos \alpha \sin^3 \alpha) + \rho'^2 \sin^4 \alpha]$$

expanding to:

$$D^4 [(\alpha'^2 \rho^2 \cos^2 \alpha + \rho'^2 \sin^2 \alpha(1 - \sin^2 \alpha) + 2\alpha' \rho' \rho(\cos \alpha \sin \alpha)(\cos^2 \alpha + \sin^2 \alpha) + \rho'^2 \sin^4 \alpha]$$

allows cancellation to:

$$D^4 (\alpha'^2 \rho^2 \cos^2 \alpha + \rho'^2 \sin^2 \alpha + 2\alpha' \rho' \rho \cos \alpha \sin \alpha) = D^4 (\alpha' \rho \cos \alpha + \rho' \sin \alpha)^2$$

therefore $D^2 \rho \cos \alpha \| \vec{n} \times \vec{n}_s \|$ has been condensed to:

$$D^2 (\alpha' \rho \cos \alpha + \rho' \sin \alpha) \qquad (3.48)$$

Finally the quantity $\tan \psi$ can be obtained from (3.47) and (3.48).

$$\tan \psi = \frac{\| \vec{n} \times \vec{n}_s \|}{\vec{n} \cdot \vec{n}_s} = \frac{D^2 (\alpha' \rho \cos \alpha + \rho' \sin \alpha)}{\rho \rho'' \cos^2 \alpha - D^2 \sin^2 \alpha} \qquad (3.49)$$

A characteristic property of a geodesic curve on a surface of revolution is that the normal to the surface and the normal to the curve are coincident. From (3.49) and Figure 3.5, it is evident that this condition is met when $\tan \psi = 0$. Thus the numerator of (3.49) equals zero for the geodesic fiber path. Referring back to (3.34) & (3.35) it is clear that

$$\rho' \tan \alpha = -\rho \alpha'$$

is the same as:

$$\alpha' \rho \cos \alpha + \rho' \sin \alpha = 0$$

Integrating the above equation yields:

$$\rho \sin \alpha = \text{constant}$$

128

The above is again Clairaut's equation.

With the first condition unchanged, which is filaments only counterbalance stress, the system to be solved now is: [refer back to equations (3.32) and (3.49)]

$$2 + \frac{\rho\rho''}{(1+\rho'^2)} = \tan^2\alpha \qquad \text{and;}$$

$$\frac{(\alpha'\rho\cos\alpha + \rho'\sin\alpha)(1+\rho'^2)}{\rho\rho''\cos^2\alpha - (1+\rho'^2)\sin^2\alpha} = k \tag{3.50}$$

In what follows, designs will be sought such that the slippage tendency of the filaments remains constant $(\tan\psi = k)$ along their length. This allows one to explore the geometric limits of the vessel openings at either end.

Unfortunately equations (3.50) are not easily integrated and are thus solved numerically. A standard method of resolution is the Runge-Kutta method, order 4. The system is reduced to first order. Using the first equation of (3.50) we let:

$$\rho' = u \tag{3.51-1}$$

so: $\quad u' = \dfrac{1+u^2}{\rho}(\tan^2\alpha - 2) \tag{3.51-2}$

for α', the second condition is rearranged:

$$(1+\rho'^2)(\alpha'\rho\cos\alpha + \rho'\sin\alpha) = k[\rho\rho''\cos^2\alpha - (1+\rho'^2)\sin^2\alpha]$$

$$\alpha' = \left\{\frac{1}{\rho\cos\alpha}\right\}\left\{\frac{k[\rho(1+u^2)/\rho](\tan^2\alpha-2)\cos^2\alpha-(1+u^2)\sin^2\alpha]}{(1+u^2)} - u\sin\alpha\right\}$$

$$\alpha' = \left\{\frac{1}{\rho\cos\alpha}\right\}\left\{\frac{k[(1+u^2)(\sin^2\alpha - 2\cos^2\alpha) - (1+u^2)\sin^2\alpha]}{(1+u^2)} - u\sin\alpha\right\}$$

$$\alpha' = -(1/\rho\cos\alpha)(2k\cos^2\alpha + u\sin\alpha) \tag{3.51-3}$$

The system (3.51) can be expressed as 3 functions:

$f_1(u,\alpha,\rho)$, $f_2(u,\alpha,\rho)$ and $f_3(u,\alpha,\rho)$.

Knowing that at the cylinder-dome junction; $\alpha = \alpha_0$, $u' = 0$, $\rho = \rho_0$, the Runge-Kutta calculations, presented below, can be started and subsequently determine a series of discrete values tabulating α, u, ρ.

If the functions (3.51) for α and u have values α_i, u_i for $\rho = \rho_i$, the values of α_{i+1}, u_{i+1} for $\rho = \rho_i + \Delta\rho$ are determined by performing stepwise the following series of calculations [161]:

$$\alpha_i'^0 = f_1(\alpha_i, u_i, \rho_i)$$

$$u_i'^0 = f_2(\alpha_i, u_i, \rho_i)$$

$$\rho_i'^0 = f_3(\alpha_i, u_i, \rho_i)$$

$$\alpha_i'^1 = f_1(\alpha_i + \tfrac{1}{2}\alpha_i'^0\Delta\rho, u_i + \tfrac{1}{2}u_i'^0\Delta\rho, \rho_i + \Delta\rho/2)$$

$$u_i'^1 = f_2(\alpha_i + \tfrac{1}{2}\alpha_i'^0\Delta\rho, u_i + \tfrac{1}{2}u_i'^0\Delta\rho, \rho_i + \Delta\rho/2)$$

$$\rho_i'^1 = f_3(\alpha_i + \tfrac{1}{2}\alpha_i'^0\Delta\rho, u_i + \tfrac{1}{2}u_i'^0\Delta\rho, \rho_i + \Delta\rho/2)$$

$$\alpha_i'^2 = f_1(\alpha_i + \tfrac{1}{2}\alpha_i'^1\Delta\rho, u_i + \tfrac{1}{2}u_i'^1\Delta\rho, \rho_i + \Delta\rho/2)$$

$$u_i'^2 = f_2(\alpha_i + \tfrac{1}{2}\alpha_i'^1\Delta\rho, u_i + \tfrac{1}{2}u_i'^1\Delta\rho, \rho_i + \Delta\rho/2)$$

$$\rho_i'^2 = f_3(\alpha_i + \tfrac{1}{2}\alpha_i'^1\Delta\rho, u_i + \tfrac{1}{2}u_i'^1\Delta\rho, \rho_i + \Delta\rho/2)$$

$$\alpha_i'^3 = f_1(\alpha_i + \alpha_i'^2\Delta\rho, u_i + u_i'^2\Delta\rho, \rho_i + \Delta\rho)$$

$$u_i'^3 = f_2(\alpha_i + \alpha_i'^2\Delta\rho, u_i + u_i'^2\Delta\rho, \rho_i + \Delta\rho)$$

$$\rho_i'^3 = f_3(\alpha_i + \alpha_i'^2\Delta\rho, u_i + u_i'^2\Delta\rho, \rho_i + \Delta\rho)$$

$$\alpha_{i+1} = \alpha_i + (\Delta\rho/6)(\alpha_i'^0 + 2\alpha_i'^1 + 2\alpha_i'^2 + \alpha_i'^3)$$

$$u_{i+1} = u_i + (\Delta\rho/6)(u_i'^0 + 2u_i'^1 + 2u_i'^2 + u_i'^3)$$

$$\rho_{i-1} = \rho_i + (\Delta\rho/6)(\rho_i'^0 + 2\rho_i'^1 + 2\rho_i'^2 + \rho_i'^3)$$ (3.52)

The solution of equations (3.52) can be used as a basis for comparing the constant slip profiles (as determined above) to elliptical dome shapes and / or other approximate profiles one wishes to wind over.

3.2 Design of the Cylindrical Part:

The technique of winding on the cylindrical part with constant slippage tendency can be exploited to reduce the overall slippage required on the end domes for vessels with different sized openings. Equation (3.49) can be reduced to the following form using the conditions that $r = r_0$, $r' = 0$. On the cylindrical surface (3.50) becomes:

$$\frac{-\alpha' \rho_0 \cos\alpha}{\sin^2\alpha} = \tan\psi = k$$

At two points separated by length ℓ (along the z-direction), the winding angles

α_1, α_2 are related as follows:

$$\alpha' = \frac{d\alpha}{dz} = \frac{d\alpha}{d\ell}$$

$$\frac{-d\alpha}{d\ell}\frac{(\rho_0 \cos\alpha)}{\sin^2\alpha} = k$$

$$-\int_{\alpha_1}^{\alpha_2} \frac{\cos\alpha}{\sin^2\alpha}d\alpha = \int_{\ell_1}^{\ell_2} \frac{k}{\rho_0}d\ell$$

$$-\left[-\left(\sin^{-1}\alpha\right)\Big|_{\alpha_1}^{\alpha_2}\right] = \frac{k(\ell_2 - \ell_1)}{\rho_0} = \frac{k\ell}{\rho_0}$$

131

or; $1/\sin\alpha_2 - 1/\sin\alpha_1 = \dfrac{k\ell}{\rho_0}$ (3.53)

Similarly the change in the angle α can be quantified in relation to the rotation angle θ by the following manipulations, from (3.43):

$$\frac{d\theta}{dz} = \frac{D\tan\alpha}{\rho_0}$$

integrating;

$$\int d\theta = \int \frac{(1+\rho'^2)^{\frac{1}{2}}\tan\alpha\,dz}{\rho_0} \qquad \text{where;} \quad r' = 0$$

but; $\dfrac{d\alpha}{dz} = \dfrac{-k\sin^2\alpha}{\rho_0\cos\alpha}$; $dz = \dfrac{-\rho_0\cos\alpha\,d\alpha}{k\sin^2\alpha}$

$$\int_{\theta_1}^{\theta_2} d\theta = -\int_{\alpha_1}^{\alpha_2} \frac{\tan\alpha\,\rho_0\cos\alpha}{k\rho_0\sin^2\alpha}\,d\alpha$$

$$\theta_2 - \theta_1 = -(1/k)\int_{\alpha_1}^{\alpha_2} \csc\alpha\,d\alpha$$

$$\theta_2 - \theta_1 = -(1/k)\ln(\csc\alpha - \cot\alpha)\Big|_{\alpha_1}^{\alpha_2}$$

From (3.53)

$$\frac{1}{\sin\alpha_2} = \left(\frac{k\ell}{\rho_0}\right) + \frac{1}{\sin\alpha_1} \qquad \text{also;} \quad \csc^2\alpha - 1 = \cot^2\alpha$$

$$\theta_2 - \theta_1 = -\left(\frac{1}{k}\right)\ln\left\{\left[\left(\frac{k\ell}{\rho_0}\right)+\left(\frac{1}{\sin\alpha_1}\right)\right]-\left\{\left[\left(\frac{k\ell}{\rho_0}\right)\right]+\left(\frac{1}{\sin\alpha_1}\right)^2-1\right\}^{\frac{1}{2}}-\ln\left[\left(\frac{1}{\sin\alpha_1}\right)-\left(\frac{1}{\tan\alpha_1}\right)\right]\right\}$$

(3.54)

The sizes of the openings on the end domes are described by the factors F_1, F_2.

These represent a fraction of the cylindrical radius r_0. When designing a vessel, the

parameters $\rho_0 F_1$, $\rho_0 F_2$ (size of openings) are imposed by the application. An estimate of the

friction coefficient allowable for the winding method being considered (wet winding vs.

pre-preg tow) brackets $\tan \psi$. Solution of the system (3.52) for a range of $\tan \psi$ values

using fixed sets of initial conditions α_0, ρ_0 allows point by point generation of the

diagram depicted in Figure 3.9 [105]. The points m_1, m_2 represent the combination of

conditions existing at the two heads.
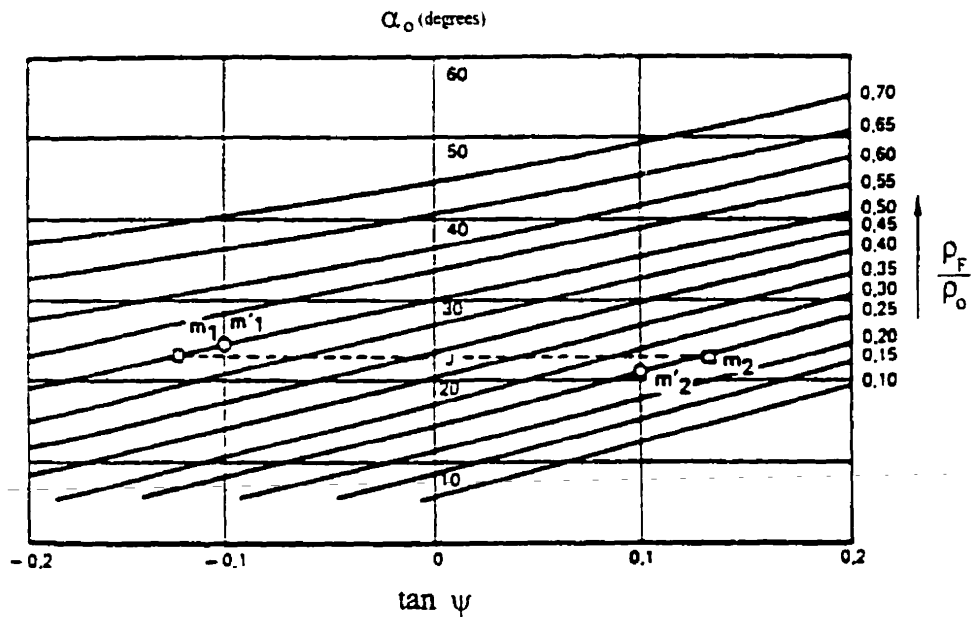
Figure 3.9 Friction requirements as a function of head opening sizes and wind angle.
Adapted from reference [105].

The essential parameters are illustrated by example. For a vessel with two different

openings:

$\rho_{F_1} / \rho_0 = 0.50$ (aft dome opening)

$\rho_{F_2} / \rho_0 = 0.25$ (forward dome opening)

For a non-slip (helicoidal or geodesic) trajectory on the cylinder, α_c must be the same at both head to cylinder junctions. The most stable winding in this situation is obtained by equalizing slippage on each dome. This case is represented by m_1 and m_2 on the diagram.

The parameters are: $\qquad \alpha_0 = 23°$

$$\|\tan \psi\| = 0.13 \; ; \; \psi = 7.4°$$

A lesser overall friction coefficient can result when the cylindrical section is also permitted a degree of incipient slip. Again equalizing the slippage tendency at each head, an alternative solution, m_1' and m_2' can be found. In this case:

$$\tan \psi = 0.10 \; ; \; \psi = 5.7°$$

This solution shows that $\alpha_2 = 21°$ and $\alpha_1 = 24.5°$

Equation (3.53) will determine if the slippage factor k is acceptable on the cylindrical section. If the cylindrical portion l is long enough and factor k is high, large differences between α_1 and α_2 can be tolerated.

3.3 Stress in the Filaments:

When winding with constant slippage tendency, the stress in the filaments will be changing. This results because the constant stress condition of equation (3.31) is not adhered to when solving the system (3.50). However changes in the filament stress can be determined by (3.30).

$$\sigma_{fs} = \frac{H\rho^2(1+\rho'^2)^{\frac{1}{2}}}{\cos\alpha} \quad ; \quad H = \frac{P}{2\upsilon_f e_{0s}\rho_0 \cos\alpha_0}$$

$$\frac{d\sigma_{fs}}{dz} = H\left\{\frac{\cos\alpha[(2\rho\rho')(1+\rho'^2)^{\frac{1}{2}} + \frac{1}{2}\rho^2(1+\rho'^2)^{-\frac{1}{2}}2\rho'\rho''] + \alpha'\sin\alpha\rho^2(1+\rho'^2)^{\frac{1}{2}}}{\cos^2\alpha}\right\}$$

$$\frac{d\sigma_{fs}}{dz} = H\left\{\frac{2\rho\rho'D}{\cos\alpha} + \frac{\rho^2\rho'\rho''}{D\cos\alpha} + \frac{\alpha'\rho^2 D\sin\alpha}{\cos^2\alpha}\right\} \qquad (3.55)$$

It is instructive to note the rate at which the stresses are changing and what factors are responsible. (3.55) is reduced as follows using (3.25) to eliminate ρ'' :

$$\frac{d\sigma_{fs}}{dz} = H\left\{\frac{2\rho\rho'D\cos\alpha}{\cos^2\alpha} + \frac{\rho^2\rho'(\tan^2\alpha - 2)(1+\rho')^2}{\rho D\cos\alpha} + \frac{\alpha'\rho^2 D\sin\alpha}{\cos^2\alpha}\right\}$$

$$\frac{d\sigma_{fs}}{dz} = HD\left\{\frac{2\rho\rho'\cos\alpha + \rho\rho'\cos\alpha(\tan^2\alpha - 2) + \alpha'\rho^2\sin\alpha}{\cos^2\alpha}\right\}$$

$$\frac{d\sigma_{fs}}{dz} = HD\left\{\frac{2\rho\rho'\cos\alpha + \rho\rho'\sin\alpha\tan\alpha - 2\rho\rho'\cos\alpha + \alpha'\rho^2\sin\alpha}{\cos^2\alpha}\right\}$$

$$\frac{d\sigma_{fs}}{dz} = HD\left\{\frac{\rho\rho'\sin\alpha\tan\alpha + \alpha'\rho^2\sin\alpha}{\cos^2\alpha}\right\}$$

$$\frac{d\sigma_{fs}}{dz} = \rho HD\tan\alpha\left\{\frac{\rho'\sin\alpha}{\cos^2\alpha} + \frac{\alpha'\rho}{\cos\alpha}\right\}$$

$$\frac{d\sigma_{fs}}{dz} = \rho HD\tan\alpha\left\{\frac{\rho'\sin\alpha}{\cos^2\alpha} + \frac{\alpha'\rho\cos\alpha}{\cos^2\alpha}\right\} \qquad (3.56)$$

Equation (3.49) can also be written in a different form.

$$\tan \psi = \frac{D^2 \alpha' \rho \cos \alpha + D^2 \rho' \sin \alpha}{\rho \rho'' \cos^2 \alpha - D^2 \sin^2 \alpha}$$

$$\tan \psi = \frac{\alpha' \rho \cos \alpha + \rho' \sin \alpha}{\left(\frac{\rho \rho''}{D^2}\right) \cos^2 \alpha - \left(\frac{D^2}{D^2}\right) \sin^2 \alpha}$$

again, using (3.25)

$$\tan \psi = \frac{\alpha' \rho \cos \alpha + \rho' \sin \alpha}{-(2 - \tan^2 \alpha) \cos^2 \alpha - \sin^2 \alpha}$$

$$\tan \psi = \frac{\alpha' \rho \cos \alpha + \rho' \sin \alpha}{-2 \cos^2 \alpha + \sin^2 \alpha - \sin^2 \alpha}$$

hence:

$$2 \tan \psi = \frac{\alpha' \rho \cos \alpha + \rho' \sin \alpha}{-\cos^2 \alpha} \tag{3.57}$$

thus (3.56) reduces to:

$$\frac{d\sigma_{fs}}{dz} = -2\rho HD \tan \alpha \tan \psi \tag{3.58}$$

Given that one is designing a vessel on the principle of minimizing the slip, where equal and opposite quantities are sought for (tan ψ) to minimize the overall slippage tendency, then from Figure 3.9 and equation (3.58), the following observations can be made:

1) Manufacturing constraints will likely impose that (tan ψ) be negative for the

head with the larger opening and positive for the head with the smaller opening.

136

2) One can see from equation (3.58) that $\dfrac{d\sigma_{fs}}{dz}$ is positive when $(\tan \psi)$ is

negative. Since all other quantities are known to be positive, stress in the

filaments increases for the dome with negative $(\tan \psi)$.

3) Equation (3.55) states the filament stresses on the dome in terms of the fixed

quantities at the cylinder to dome juncture. Thus from the juncture to the point

of inflection (where $\alpha = 54.7°$ and the geodesic profile becomes undefined) the

head with the larger opening will see a rise in stress from the nominal amount

and the dome with the smaller opening will see a proportional reduction in

filament stress. The inflection point indicates the position where the iso-tensoid

conditions can no longer be maintained, and in practice a spherical dome of

radius R_2 is used to define the shape up to the opening.

The head with the larger opening will dictate the limiting design factor establishing

wind thickness. The advantages of using small and near equal size openings should be

evident.

The utility of the foregoing equations in designing head profiles for thick vessels is

in practice limited by a number of factors. First it must be recognized that the fiber band

overlaps itself (unlike on the cylindrical surface) as it traces multiple circuits over the

dome enclosure to complete one full pattern. This has the effect of thickening the lay-up

locally and causing a coarse overlapping step-pattern (prone to void formation) most

notably adjacent to the polar opening. The thickening effect changes the profile of the

head upon which subsequent layers are overwound. This new surface is not geodesic-

isotensoid. Band overlapping is a source of stress concentration. The abrupt band drop-off

step can at best result in resin-rich pockets unless it is filled in by manually placed fabric or random mat doilies. Here the fiber band is forced to kink at every drop-off point, an area of weakness. Also because low compressive radial moduli results from voids and resin rich areas it leads a poor capacity in transmitting radial stress outward. This magnifies the stress gradient and serves to overload the innermost layers

Refined designs employ finite element models in an attempt to minimize stress concentrations due to such factors in the region of the end closures. The better winding software permits calculation (by numerical methods) of winding paths around arbitrary shapes. However an optimum starting point for the inner filaments (which carry the highest stress) is based upon the foregoing equations, lending justification to their development.

In winding a typical vessel with one small opening it is evident that incipient slip can be spread out across the length of the cylindrical portion, and $\tan \psi$ will be very small. In this case equation (3.58) indicates that stress in the filaments will remain virtually constant, or can even be designed to decrease around the dome enclosure especially if we compensate by winding with higher incipient slip elsewhere.

For the cylindrical portion of a thick-walled vessel, equation (3.15) is not adequate because the assumption of equal through-thickness stresses fails to hold up. With this netting based design of filament wound vessels as background, we now turn to a detailed analysis concerning the cylindrical portion of a thick-walled pressure vessel. This constitutes the focus of the present work. In contrast with the above simplified analysis, the approach employed in subsequent chapters is founded on 3-dimensional anisotropic elasticity equations.

Chapter 4

Analytical Methods for Discrete Layer Design

4.0 Elasticity Solutions using Fixed Material Properties

The analysis of cylindrical structures by elasticity solutions can be subdivided into "thin wall" and "thick wall". The division point is often arbitrarily chosen as a radius to thickness (r/t) ratio of 10. This ratio is not appropriate for composite structures, especially when designing with highly anisotropic advanced materials. The underlying assumption in thin-wall vessel design is that the strains are uniform through the thickness. Geometry alone fixes strain distributions for isotropic structures. Higher degrees of anisotropy in a composite material result in strain distributions governed by the material's internal mechanics as well as by geometry.

Closed form solutions are possible whenever the geometry of the item being analyzed can be represented by a standard coordinate system (rectangular, polar, cylindrical, spherical). Items of more arbitrary geometry must be reduced to a finite number of elementary shapes before analysis techniques can be applied. This, the finite element approach, is especially powerful yet still limited to the assumptions implicit within the formulation of the elements. When the geometry is relatively simple, as in a cylindrical vessel, the problem is already reduced to that of one large element. The attractiveness of an encompassing elasticity solution is that it sheds light on the action of parameters governing internal stress distributions. Although finite elements do predict an outcome for

139

more complex structures the precise internal mechanisms at work can still remain obscured.

In the following work, a plain strain analysis with specified end conditions is used to study the behavior of thick cylindrical constructions subject to pressure loading.

4.1 Elasticity Foundations

Within each lamina 3 mutually perpendicular planes (orthotropic planes) are modeled. The material properties are taken to be symmetric about these planes. Namely for each lamina there exists symmetry through the thickness, along the fiber direction and across the fiber direction.

The theory of elasticity requires ideal elastic behavior and hence yields results which are approximately equal to the stresses in the physical body because the physical body will deviate from the ideal elastic material assumed. Furthermore, elastic homogeneity in the lamina is assumed thus solutions derived are only applicable on a scale which is large in relation to the microstructure of the material.

Stress-strain equations without any form of material symmetry (triclinic symmetry or fully anisotropic) are written as:

$$\varepsilon_x = a_{11}\sigma_x + a_{12}\sigma_y + a_{13}\sigma_z + a_{14}\tau_{yz} + a_{15}\tau_{xz} + a_{16}\tau_{xy}$$
$$\varepsilon_y = a_{21}\sigma_x + a_{22}\sigma_y + a_{23}\sigma_z + a_{24}\tau_{yz} + a_{25}\tau_{xz} + a_{26}\tau_{xy}$$
$$\varepsilon_z = a_{31}\sigma_x + a_{32}\sigma_y + a_{33}\sigma_z + a_{34}\tau_{yz} + a_{35}\tau_{xz} + a_{36}\tau_{xy}$$
$$\gamma_{yz} = a_{41}\sigma_x + a_{42}\sigma_y + a_{43}\sigma_z + a_{44}\tau_{yz} + a_{45}\tau_{xz} + a_{46}\tau_{xy} \qquad (4.0)$$
$$\gamma_{xz} = a_{51}\sigma_x + a_{52}\sigma_y + a_{53}\sigma_z + a_{54}\tau_{yz} + a_{55}\tau_{xz} + a_{56}\tau_{xy}$$
$$\gamma_{xy} = a_{61}\sigma_x + a_{62}\sigma_y + a_{63}\sigma_z + a_{64}\tau_{yz} + a_{65}\tau_{xz} + a_{66}\tau_{xy}$$

The contracted tensor notation for the above form is

$$\varepsilon_i = a_{ij}\sigma_j \qquad i,j = 1,2,\dots 6$$

Similarly the inverse of relation (4.1) can be expressed as

$$
\begin{aligned}
\sigma_x &= A_{11}\varepsilon_x + A_{12}\varepsilon_y + A_{13}\varepsilon_z + A_{14}\gamma_{yz} + A_{15}\gamma_{xz} + A_{16}\gamma_{xy}\\
\sigma_y &= A_{21}\varepsilon_x + A_{22}\varepsilon_y + A_{23}\varepsilon_z + A_{24}\gamma_{yz} + A_{25}\gamma_{xz} + A_{26}\gamma_{xy}\\
\sigma_z &= A_{31}\varepsilon_x + A_{32}\varepsilon_y + A_{33}\varepsilon_z + A_{34}\gamma_{yz} + A_{35}\gamma_{xz} + A_{36}\gamma_{xy}\\
\tau_{yz} &= A_{41}\varepsilon_x + A_{42}\varepsilon_y + A_{43}\varepsilon_z + A_{44}\gamma_{yz} + A_{45}\gamma_{xz} + A_{46}\gamma_{xy}\\
\tau_{xz} &= A_{51}\varepsilon_x + A_{52}\varepsilon_y + A_{53}\varepsilon_z + A_{54}\gamma_{yz} + A_{55}\gamma_{xz} + A_{56}\gamma_{xy}\\
\tau_{xy} &= A_{61}\varepsilon_x + A_{62}\varepsilon_y + A_{63}\varepsilon_z + A_{64}\gamma_{yz} + A_{65}\gamma_{xz} + A_{66}\gamma_{xy}
\end{aligned}
$$

$$(4.1)$$

In tensor notation

$$\sigma_i = A_{ij}\varepsilon_j$$

There are 36 constants to describe each of these systems, but not all are independent. Materials for which an elastic potential or strain energy density function exists exhibit an incremental work per unit volume of

$$dW = \sigma_i\, d\varepsilon_i$$

when the stresses σ_i act through strains $d\varepsilon_i$. However because of the stress-strain relations (4.1) the incremental work becomes

$$dW = A_{ij}\varepsilon_j\, d\varepsilon_i .$$

Upon integration for all strains, the work per unit volume is

$$W = \tfrac{1}{2} A_{ij}\varepsilon_i\varepsilon_j$$

However Hooke's law, equation (4.1), can be derived from the above via

141

$$\frac{\partial W}{\partial \varepsilon_j} = A_{ij}\varepsilon_j$$

whereupon

$$\frac{\partial^2 W}{\partial \varepsilon_i \partial \varepsilon_j} = A_{ij}$$

Similarily

$$\frac{\partial^2 W}{\partial \varepsilon_j \partial \varepsilon_i} = A_{ji}$$

but the order of differentiation on W must be immaterial (otherwise the the work would

assume a non-conservative character) and hence we conclude that

$$A_{ij} = A_{ji}$$

Reasoning similar to the above paragraph leads to the correlative conclusion that

$$a_{ij} = a_{ji}$$

hence 21 constants can be used to describe elastic behavior [173].

In many situations it is clarifying to describe the compliances in terms of their

physical meaning. Aside from the well known engineering properties constituting 3

Young's moduli, 3 shear moduli, and 6 Poisson's ratios, a general material has additional

influence coefficients. These can be divided into 3 groups. The 6 *Chentsov's coefficients*,

characterize shears in planes parallel to the co-ordinate planes produced by shearing

stresses acting in other planes parallel to the co-ordinate planes $(a_{45}, a_{46}, a_{56}, a_{54}, a_{64}, a_{65})$.

Another group of 9, termed mutual influence coefficients *of the first kind*, characterize

extensions in the direction of the co-ordinate axis as a result of shearing stresses acting in

the coordinate axis $(a_{14}, a_{15}, a_{16}, a_{24}, a_{25}, a_{26}, a_{34}, a_{35}, a_{36})$. Finally, a group of 9 mutual

influence coefficients *of the second kind* express shears in the co-ordinate planes due to normal stresses acting in the directions of the co-ordinate axis. These are

$$(a_{41}, a_{42}, a_{43}, a_{51}, a_{52}, a_{53}, a_{61}, a_{62}, a_{63}).$$

A type of symmetry is expressed by the statement that the coefficients A_{ij} (or a_{ij}) remain invariant under a transformation of coordinates which describe this symmetry. We shall consider the cases: {1} Symmetry with respect to a plane, {2} symmetry with respect to two mutually perpendicular planes, {3} symmetry of rotation with respect to one axis, {4} symmetry of rotation with respect to two mutually perpendicular axes.

A monoclinic symmetry defines case {1}, a situation where one plane of elastic symmetry exists. On either side of this cutting plane the constants associated with the axis of symmetry must be the same, and Hooke's law gets simplified. If the symmetry plane lies in the 1-2 (*x-y*) plane, or z = 0, the components $a_{14}, a_{24}, a_{34}, a_{15}, a_{25}, a_{35}, a_{46}, a_{56}$ and their symmetric counterparts disappear. Thirteen constants remain to describe the system shown below. Together the equations hold 20 non-zero terms. Should the plane of symmetry be rotated at some angle to a principal plane, 36 terms will again be necessary to describe the system.

$$
\begin{aligned}
\varepsilon_x &= a_{11}\sigma_x &+ a_{12}\sigma_y &+ a_{13}\sigma_z &+ 0 &+ 0 &+ a_{16}\tau_{xy} \\
\varepsilon_y &= a_{21}\sigma_x &+ a_{22}\sigma_y &+ a_{23}\sigma_z &+ 0 &+ 0 &+ a_{26}\tau_{xy} \\
\varepsilon_z &= a_{31}\sigma_x &+ a_{32}\sigma_y &+ a_{33}\sigma_z &+ 0 &+ 0 &+ a_{36}\tau_{xy} \\
\gamma_{yz} &= 0 &+ 0 &+ 0 &+ a_{44}\tau_{yz} &+ a_{45}\tau_{xz} &+ 0 \\
\gamma_{xz} &= 0 &+ 0 &+ 0 &+ a_{54}\tau_{yz} &+ a_{55}\tau_{xz} &+ 0 \\
\gamma_{xy} &= a_{61}\sigma_x &+ a_{62}\sigma_y &+ a_{63}\sigma_z &+ 0 &+ 0 &+ a_{66}\tau_{xy}
\end{aligned}
$$

$$(4.2)$$

For case {2}, material symmetry with respect to two mutually perpendicular planes, the substance is said to have *orthotropic* properties (equation 4.3). In this case 9 constants are sufficient to describe behavior and a total of 12 non-zero terms remain in the elasticity equations. If the symmetry planes are not coincident with the reference coordinates, the non-zero components can increase to those of equation (4.1). Should one of the symmetry planes coincide with the 3 or "z" axis the non-zero components will be those shown in equation (4.2) The number of (independent) constants necessary to describe any "rotated" system however depends only on the material's symmetry conditions, not on its degree of alignment with the principal axis.

$$
\begin{aligned}
\varepsilon_x &= a_{11}\sigma_x + a_{12}\sigma_y + a_{13}\sigma_z + 0 + 0 + 0 \\
\varepsilon_y &= a_{21}\sigma_x + a_{22}\sigma_y + a_{23}\sigma_z + 0 + 0 + 0 \\
\varepsilon_z &= a_{31}\sigma_x + a_{32}\sigma_y + a_{33}\sigma_z + 0 + 0 + 0 \\
\gamma_{yz} &= 0 + 0 + 0 + a_{44}\tau_{yz} + 0 + 0 \\
\gamma_{zx} &= 0 + 0 + 0 + 0 + a_{55}\tau_{zx} + 0 \\
\gamma_{xy} &= 0 + 0 + 0 + 0 + 0 + a_{66}\tau_{xy}
\end{aligned}
$$

$$(4.3)$$

The next higher level of material symmetry, case {3}, defines a transversely isotropic material. A material which possesses an axis of symmetry, in the sense that all rays at right angles to this axis are equivalent, meets the criteria. Five constants define the system. When the isotropic plane lies coincident with one of the coordinate planes there are 12 non-zero terms. For the case of isotropy in the 2-3 or "y-z" plane, equation (4.4) below describes the system. Should none of the symmetry axis be aligned with the principal directions, 36 terms as in (4.1) will be necessary. In a case where the 3 or "z" axis is a plane of symmetry 20 non-zero terms as in (4.2) will describe the behavior.

144

Independent constants however remain fixed at 5. This is an important case since it is used to describe the elastic properties of fibers and their constituent unidirectional laminas.

$$
\begin{aligned}
\varepsilon_x &= a_{11}\sigma_x + a_{12}\sigma_y + a_{13}\sigma_z + 0 + 0 + 0 \\
\varepsilon_y &= a_{12}\sigma_x + a_{11}\sigma_y + a_{13}\sigma_z + 0 + 0 + 0 \\
\varepsilon_z &= a_{13}\sigma_x + a_{13}\sigma_y + a_{33}\sigma_z + 0 + 0 + 0 \\
\gamma_{yz} &= 0 + 0 + 0 + \tfrac{1}{2}(a_{22}-a_{23})\tau_{yz} + 0 + 0 \\
\gamma_{xz} &= 0 + 0 + 0 + 0 + a_{66}\tau_{xz} + 0 \\
\gamma_{xy} &= 0 + 0 + 0 + 0 + 0 + a_{66}\tau_{xy}
\end{aligned}
$$

(4.4)

For fiber reinforced composites 3-dimensional material models are derived using the above (transversely isotropic) idealization. To restate, in such a situation there exists one principal direction and an infinite number of principal directions normal to the first. In essence, rotational symmetry about the fiber direction.

The highest level of symmetry, case{4}, defines isotropy where only 2 independent material constants remain: Poisson's ratio and the normal (Young's) modulus. The 3 dimensional elasticity equations require 12 non-zero terms regardless of orientation.

$$
\begin{aligned}
\varepsilon_x &= a_{11}\sigma_x + a_{12}\sigma_y + a_{12}\sigma_z + 0 + 0 + 0 \\
\varepsilon_y &= a_{12}\sigma_x + a_{11}\sigma_y + a_{12}\sigma_z + 0 + 0 + 0 \\
\varepsilon_z &= a_{12}\sigma_x + a_{12}\sigma_y + a_{11}\sigma_z + 0 + 0 + 0 \\
\gamma_{yz} &= 0 + 0 + 0 + \tfrac{1}{2}(a_{11}-a_{12})\tau_{yz} + 0 + 0 \\
\gamma_{xz} &= 0 + 0 + 0 + 0 + \tfrac{1}{2}(a_{11}-a_{12})\tau_{xz} + 0 \\
\gamma_{xy} &= 0 + 0 + 0 + 0 + 0 + \tfrac{1}{2}(a_{11}-a_{12})\tau_{xy}
\end{aligned}
$$

(4.5)

More explicit details describing the tensor mathematics which lead to the elimination of the various compliance (or stiffness) coefficients for the 4 cases of

145

symmetry described above can be followed in A.S. Saada's text, chapter 8, reference [161].

Rectilinear anisotropy exists where planes of elastic equivalence follow parallel directions, similarly curvilinear anisotropy is characterized by having elastic equivalence following a defined curve. When a coordinate system can be chosen in a manner where the principal directions coincide with equivalent elastic directions at different points of the body, then any element delineated by 3 pairs of coordinate planes will possess identical elastic properties.

Laminate properties along the 3 principle directions (x,y,z) or (r,θ,z) in the case of a cylinder can be written based on equations (4.1) along with appropriate transformation equations for coordinate system rotation. Lekhnitskii [88], pages 40-50, gives a concise description of such transformations under fully anisotropic conditions for the compliance terms a_{ij}. Equation (4.6) along with Table 4.1 defines the transformed compliances $\{a_{ij}'\}$ in a rectilinear system given rotation about one coordinate axis (z-axis in this case). Equations defining rotation about any other coordinate axis can be derived by using a permutation of the indexes in Table 4.1. The rotation is described by the following equation.

$$a_{ij}' = \sum_{m=1}^{6} \sum_{n=1}^{6} a_{mn} \, q_{im} \, q_{jn}$$

(4.6)

146

Table 4.1 Coefficients for rotation about "3" axis

i\j	1	2	3	4	5	6
1	$\cos^2 \alpha$	$\sin^2 \alpha$	0	0	0	$\sin \alpha \cos \alpha$
2	$\sin^2 \alpha$	$\cos^2 \alpha$	0	0	0	$-\sin \alpha \cos \alpha$
3	0	0	1	0	0	
4	0	0	0	0	0	
5	0	0	0	$\sin \alpha$	$\cos \alpha$	
6	$-2 \sin \alpha \cos \alpha$	$-2 \sin \alpha \cos \alpha$	0	0	0	$\cos^2 \alpha - \sin^2 \alpha$

In (4.6) the first subscript in the symbols q_{ij} indicates a row number in Table 4.1, the second a column number. The transformed compliances $\{a'_{ij}\}$ condensed to a single equation in (4.6) expand to the following:

$$a'_{11} = a_{11}\cos^4\phi + a_{22}\sin^4\phi + (2a_{12} + a_{66})\sin^2\phi\cos^2\phi + 2(a_{16}\cos^2\phi + a_{26}\sin^2\phi)\sin\phi\cos\phi$$

$$a'_{22} = a_{11}\sin^4\phi + a_{22}\cos^4\phi + (2a_{12} + a_{66})\sin^2\phi\cos^2\phi + 2(a_{16}\sin^2\phi + a_{26}\cos^2\phi)\sin\phi\cos\phi$$

$$a'_{33} = a_{33}$$

$$a'_{44} = a_{44}\cos^2\phi - 2a_{45}\sin\phi\cos\phi + a_{55}\sin^2\phi$$

$$a'_{55} = a_{55}\cos^2\phi + 2a_{45}\sin\phi\cos\phi + a_{44}\sin^2\phi$$

$$a'_{13} = a_{13}\cos^2\phi + a_{36}\sin\phi\cos\phi + a_{23}\sin^2\phi$$

$$a'_{23} = a_{23}\cos^2\phi - a_{36}\sin\phi\cos\phi + a_{13}\sin^2\phi$$

$$a'_{66} = 4(a_{11} + a_{22} - 2a_{12} - a_{66})\sin^2\cos^2\phi + a_{66} - 4(a_{16} - a_{26})(\cos^2\phi - \sin^2\phi)\sin\phi\cos\phi$$

$$a'_{12} = (a_{11} + a_{22} - 2a_{12} - a_{66})\sin^2\phi\cos^2\phi + a_{12} - (a_{16} - a_{26})(\cos^2\phi - \sin^2\phi)\sin\phi\cos\phi$$

$$a'_{16} = [2a_{22}\sin^2\phi - 2a_{11}\cos^2\phi + (2a_{12} - a_{66})(\cos^2\phi - \sin^2\phi)]\sin\phi\cos\phi$$
$$+ a_{16}\cos^2\phi(\cos^2\phi - 3\sin^2\phi) + a_{26}\sin^2\phi(3\cos^2\phi - \sin^2\phi)$$

$$a'_{26} = [2a_{22}\cos^2\phi - 2a_{11}\sin^2\phi - (2a_{12}+a_{66})(\cos^2\phi - \sin^2\phi)]\sin\phi\cos\phi +$$
$$a_{16}\sin^2\phi(3\cos^2\phi - \sin^2\phi) + a_{26}\cos^2\phi(\cos^2\phi - 3\sin^2\phi)$$

$$a'_{45} = (a_{44} - a_{55})\sin\phi\cos\phi + a_{45}(\cos^2\phi - \sin^2\phi)$$

$$a'_{36} = 2(a_{23} - a_{13})\sin\phi\cos\phi + a_{36}(\cos^2\phi - \sin^2\phi)$$

$$a'_{14} = a_{14}\cos^3\phi + (a_{46} - a_{15})\sin\phi\cos^2 + (a_{24} - a_{56})\sin^2\phi\cos\phi - a_{25}\sin^3\phi$$

$$a'_{24} = a_{24}\cos^3\phi - (a_{46} + a_{25})\sin\phi\cos^2\phi + (a_{14} + a_{56})\sin^2\phi\cos\phi - a_{15}\sin^3\phi$$

$$a'_{25} = a_{25}\cos^3\phi + (a_{24} - a_{56})\sin\phi\cos^2\phi + (a_{15} - a_{46})\sin^2\phi\cos\phi + a_{14}\sin^3\phi$$

$$a'_{15} = a_{15}\cos^3\phi + (a_{14} + a_{56})\sin\phi\cos^2\phi + (a_{25} + a_{46})\sin^2\phi\cos\phi + a_{24}\sin^3\phi$$

$$a'_{46} = a_{46}\cos^3\phi + (-2a_{14} + 2a_{24} - a_{56})\sin\phi\cos^2\phi + (2a_{15} - 2a_{25} - a_{46})\sin^2\phi\cos\phi + a_{56}\sin^3\phi$$

$$a'_{56} = a_{56}\cos^3\phi + (-2a_{15} + 2a_{25} + a_{46})\sin\phi\cos^2\phi + (-2a_{14} + 2a_{24} - a_{56})\sin^2\phi\cos\phi - a_{46}\sin^3\phi$$

$$a'_{34} = a_{34}\cos\phi - a_{35}\sin\phi$$

$$a'_{35} = a_{35}\cos\phi + a_{34}\sin\phi$$

$$(4.7)$$

In the case of a hollow filament wound cylinder with winding angle ($\pm\,\alpha$), the winding angle is traditionally measured in the (θ-z) plane as a rotation about the radial direction (r). Angle (α) is measured in reference to the (z) axis. By contrast, in a laminated plate the in-plane fiber orientations are referenced to the (x)-axis and rotations occur about the (z)-axis. In effect we now require a change of coordinates to accommodate between the cylindrical system and the more familiar planar situation.

For a unidirectional lamina with the (x)-axis defining the fiber direction, the (x,y,z) rectilinear coordinates do not translate to (r,θ,z) but rather interchange to (z,θ,r) in the cylindrical system. Figure 4.1 illustrates.

148

Cylindrical system   Laminated Plate
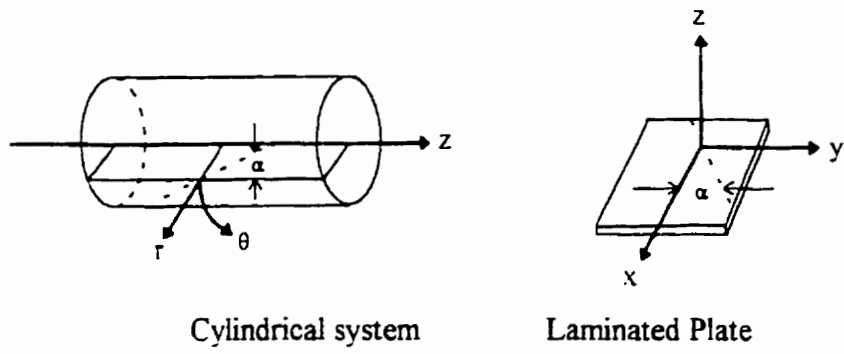
Figure 4.1 Angle measurements in different coordinate systems.

The on-axis orthotropic compliance terms originating from unidirectional (rectilinear) test data must be re-defined as in Table 4.2 and Figure (4.3) when referenced to the principal cylindrical coordinates.

Table 4.2 Axis definitions

Rectangular	1	2	3
	x	y	z
	↓	↓	↓
Cylindrical	z	θ	r
	3	2	1

Rectangular Coordinates   Cylindrical Coordinates

	σ_x	σ_y	σ_z	τ_{yz}	τ_{xz}	τ_{xy}
ε_x	a_{11}	a_{12}	a_{13}			a_{16}
ε_y	a_{21}	a_{22}	a_{23}			a_{26}
ε_z	a_{31}	a_{32}	a_{33}			a_{36}
γ_{yz}				a_{44}	a_{45}	
γ_{xz}				a_{54}	a_{55}	
γ_{xy}	a_{61}	a_{62}	a_{63}			a_{66}

$\Rightarrow$

	σ_r	σ_θ	σ_z	$\tau_{\theta z}$	τ_{rz}	$\tau_{r\theta}$
ε_r	a_{33}	a_{32}	a_{31}	a_{36}		
ε_θ	a_{23}	a_{22}	a_{21}	a_{26}		
ε_z	a_{13}	a_{12}	a_{11}	a_{16}		
$\gamma_{\theta z}$	a_{63}	a_{62}	a_{61}	a_{66}		
γ_{rz}					a_{55}	a_{54}
$\gamma_{r\theta}$					a_{45}	a_{44}

(a)   (b)

Figure 4.2 Compliance matrix conversions in switching from rectangular to cylindrical coordinates.

The fiber bands laid down in the filament winding process can be taken as as exhibiting a transversely isotropic character. In the very strictest sense the material being put down can be described as a coarse weave. the density of overlaps being related to the number of circuits per pattern chosen to achieve complete coverage. In practical terms this weave is so coarse that virtually all the areas exist in the form of "unidirectional" laminas, and the woven aspect can virtually be forgotten. (A look ahead to Figure 9.2 gives one an appreciation of the coarseness of this weave).

For the purpose of analysis, a total of 12 non-zero compliance terms, defined in material coordinate space as per equation (4.3), result in 20 terms subsequent to a rotation onto the principle axis as defined by equations (4.7). The components $a'_{14}, a'_{24}, a'_{46}, a'_{15}, a'_{25}, a'_{56}, a'_{34}, a'_{35}$ and their symmetric counterparts do not appear in Figure

150

4.2(a) since the a_{ij}'s defining these terms (equation 4.3) are zero on the RHS of equations (4.7).

The stress-strain relations in cylindrical coordinates can be written with indices (r,θ,z) replacing the cartesian descriptors (x,y,z), subject to the substitution scheme denoted in Table 4.2. Figure 4.2(b) indicates how the compliances referenced to the cylindrical coordinate system but originating from off-axis lamina properties need be replaced. This effectively eliminates the terms a_{16}, a_{26}, a_{36}, a_{45} for the transversely isotropic (filament wound) material defined in cylindrical coordinates. The resulting equations are constituted from 13 different a_{ij}'s for a total of 20 terms. In practice, the interwoven ($\pm\,\alpha$) plies laid down by the filament winding process effectively cancel the bulk or summed contribution of the terms multiplied by $\sin\phi\cos\phi$ (a_{16}, a_{26}, a_{36}, a_{45}) and their symmetric counterparts via continual sign changes in the term $\{\sin\phi\}$ for equations (4.7). Overall, with balanced angle ply windings, the combined $\pm$ layer pair properties are reduced to:

$$a_{11}' = a_{11}\cos^4\phi + a_{22}\sin^4\phi + (2a_{12} + a_{66})\sin^2\phi\cos^2\phi$$

$$a_{22}' = a_{11}\sin^4\phi + a_{22}\cos^2\phi + (2a_{12} + a_{66})\sin^2\phi\cos^2\phi$$

$$a_{33}' = a_{33}$$

$$a_{66}' = 4(a_{11} + a_{22} - 2a_{12} - a_{66})\sin^2\phi\cos^2\phi + a_{66}$$

$$a_{12}' = (a_{11} + a_{22} - 2a_{12} - a_{66})\sin^2\phi\cos^2\phi + a_{12}$$

$$a_{13}' = a_{13}\cos^2\phi + a_{23}\sin^2\phi$$

$$a_{23}' = a_{23}\cos^2\phi + a_{13}\sin^2\phi$$

$$a'_{44} = a_{44}\cos^2\phi + a_{55}\sin^2\phi$$

$$a'_{55} = a_{55}\cos^2\phi + a_{44}\sin^2\phi$$

<div align="right">(4.8)</div>

The above constitute a form identical to the orthotropic material case shown in (4.3). Equations (4.8) along with property determinations based on a micromechanics model described in Chapter 7 are used to calculate the 3-dimensional laminate compliances in the "Super Pressure - Vessel Designer" code.

4.2 Stress and Strain

Neglecting the transition regions near a cylindrical vessel's dome closures, the mid-section can be modeled as a finite number of orthotropic laminae. Strain and equilibrium equations for an element within such a lamina are well documented and presented below. (See for example Saada [161] chapters 4 and 6 on *Kinematics of Continuous Media.*)
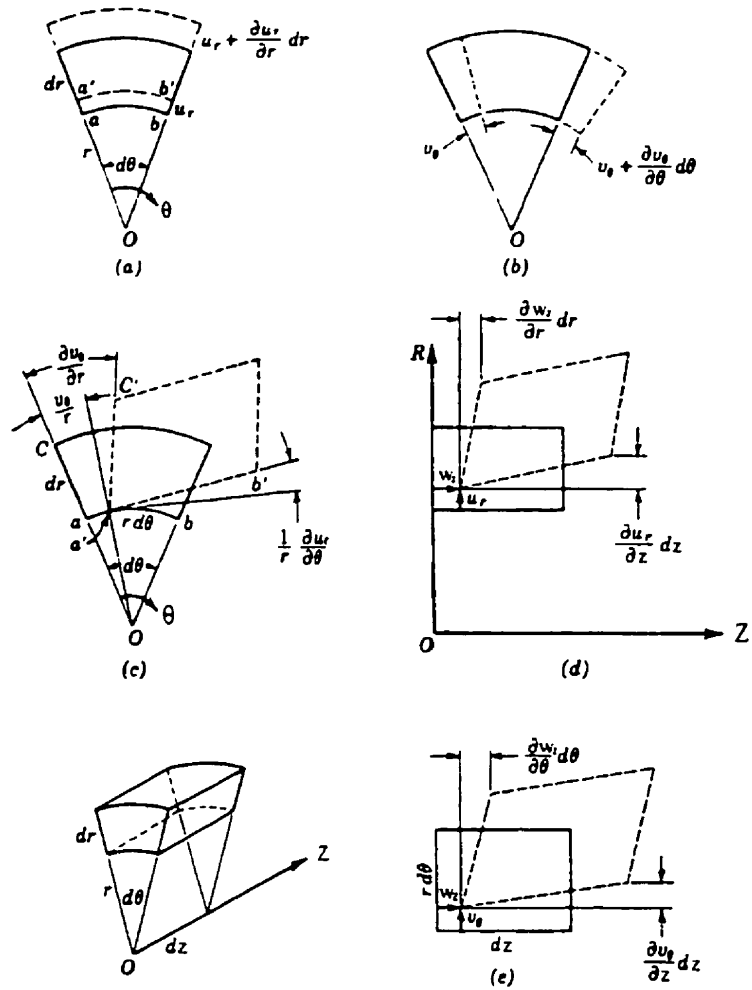
Figure 4.3 Components of strain in cylindrical coordinates [162].

Figure 4.3 shows an element subjected to displacements as indicated. Considering first the displacement u_r in the r direction, we see from Figure 4.3(a) that

$$\varepsilon_r = \frac{u_r + \left(\partial u_r / \partial r\right)\partial r - u_r}{\partial r} = \frac{\partial u_r}{\partial r}$$

From 4.3(a) we also see that pure radial displacement yields a strain in the θ direction, since the element has elongated in the θ direction. The length of the element

153

ab was originally $r\partial\theta$; but after the radial displacement u_r has taken place, this element has the position *a'b'* and the new length $(r + u_r)\partial\theta$. The tangential strain due to this displacement is therefore

$$\varepsilon_{\theta_1} = \frac{(r + u_r)\partial\theta - r\partial\theta}{r\partial\theta} = \frac{u_r}{r}$$

From Figure 4.3(b) the tangential displacement v_θ gives rise to a tangential strain equal to

$$\varepsilon_{\theta_2} = \frac{v_\theta + (\partial v_\theta / \partial\theta)\partial\theta - v_\theta}{r\partial\theta} = \frac{1}{r}\frac{\partial v_\theta}{\partial\theta}$$

and the total tangential strain ε_θ is equal to the sum of ε_{θ_1} and ε_{θ_2}, or

$$\varepsilon_\theta = \frac{u_r}{r} + \frac{1}{r}\frac{\partial v_\theta}{\partial\theta}$$

The normal strain in the axial or z direction is given by

$$\varepsilon_z = \frac{\partial w_z}{\partial z}$$

The shearing strain is given by the difference between the angle *cab* and *c'a'b'* in Figure 4.3(c).

$$\gamma_{r\theta} = \frac{1}{r}\frac{\partial u_r}{\partial\theta} + \frac{\partial v_\theta}{\partial r} - \frac{v_\theta}{r}$$

154

The first term comes from the change in radial displacement u_r in the tangential

direction; the second term comes from the change in the tangential displacement v_θ in

the radial direction; and the last term appears since part of the slope change of the line

$a'c'$ comes from the rotation of the element as a solid body about the axis O. From

Figures 4.3(d) and 4.3(e) the other two shearing strains $\gamma_{\theta z}$ and γ_{rz} may be obtained as

follows:

$$\gamma_{\theta z} = \frac{(\partial w_z / \partial \theta)\, d\theta}{r\, d\theta\, (1 + \partial v_\theta / \partial \theta)} + \frac{(\partial v_\theta / \partial z)\, dz}{dz\, (1 + \partial w_z / \partial z)}$$

$$\gamma_{\theta z} = \frac{1}{r}\frac{\partial w_z}{\partial \theta} + \frac{\partial v_\theta}{\partial z}$$

and

$$\gamma_{rz} = \frac{(\partial u_r / \partial z)\, dz}{dz\, (1 + \partial w_z / \partial z)} + \frac{(\partial w_z / \partial r)\, dr}{dr\, (1 + \partial u_r / \partial r)}$$

$$\gamma_{rz} = \frac{\partial u_r}{\partial z} + \frac{\partial w_z}{\partial r}$$

In the above we have assumed that the angles are equal to their tangents and that

the rate of change of displacement with respect to length is small compared to unity. It

must be stated that these equations are restricted to small displacements since they

comprise only the linear terms of the full set. Second order effects and small differences in

the definitions between tensorial and engineering strain bound the accuracy of all

155

equations developed forthcoming. These are standard "small displacement approximations". In summary for cylindrical coordinates, the strains are expressible as:

$$\varepsilon_r = \frac{\partial u}{\partial r}$$

$$\varepsilon_\theta = \frac{u}{r} + \frac{\partial v}{rd\theta}$$

$$\varepsilon_z = \frac{\partial w}{\partial z}$$

$$\gamma_{\theta z} = \frac{\partial w}{rd\theta} + \frac{\partial v}{dz}$$

$$\gamma_{rz} = \frac{\partial u}{\partial z} + \frac{\partial w}{dr}$$

$$\gamma_{rz} = \frac{\partial u}{\partial z} + \frac{\partial w}{dr}$$

$$\gamma_{r\theta} = \frac{\partial u}{rd\theta} + \frac{\partial v}{\partial r} - \frac{v}{r}$$

(4.9)

Figure 4.4 shows a cylindrical element. In the absence of body forces the equilibrium equations are derived by working out the balance of forces.

<u>Radial direction</u>

$$-\sigma_r(rd\theta)dz + (\sigma_r + \frac{\partial \sigma_r}{\partial r}dr)(r + dr)d\theta\, dz - \sigma_\theta dr \frac{d\theta}{2} dz$$

$$-(\sigma_\theta + \frac{\partial \sigma\theta}{\partial \theta}d\theta)dr \frac{d\theta}{2} dz - \tau_{r\theta}dr\, dz + (\tau_{r\theta} + \frac{\partial \tau_{r\theta}}{\partial \theta}d\theta)dr\, dz$$

$$-\tau_{rz}dr\, rd\theta + (\tau_{rz} + \frac{\partial \tau_{rz}}{\partial z}dz)dr\, rd\theta = 0$$

Expansion yields:
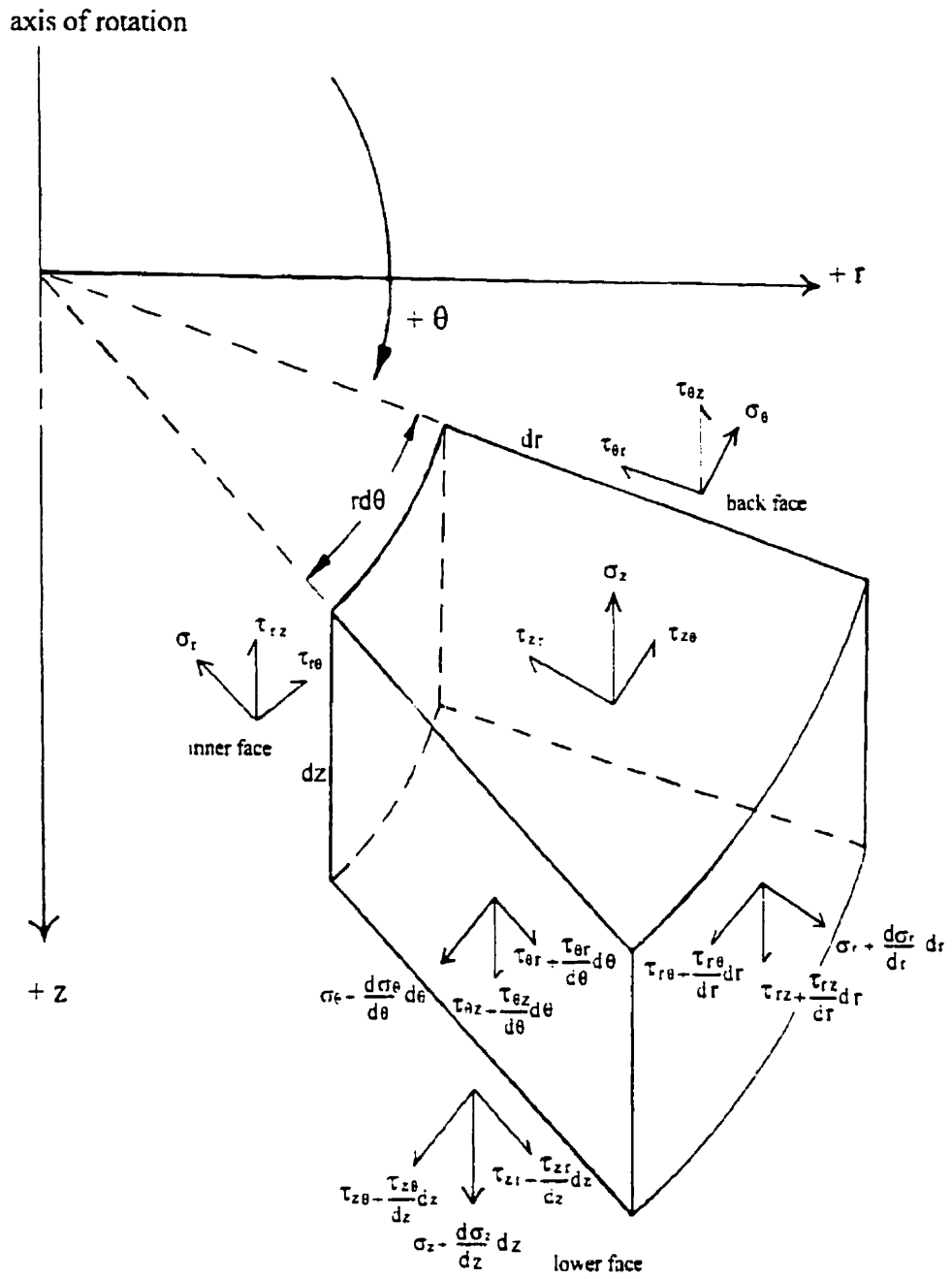
Figure 4.4 Cylindrical equilibrium element.

$$- \sigma_r r \, d\theta \, dz + \sigma_r r \, d\theta \, dz + r \frac{\partial \sigma_r}{\partial r} dr \, d\theta \, dz + \sigma_r \, dr \, d\theta \, dz +$$

$$\frac{\partial \sigma_r}{\partial r} dr \, dr \, d\theta \, dz - \sigma_\theta \, dr \frac{d\theta}{2} dz - \frac{\partial \sigma_\theta}{\partial \theta} d\theta \, dr \frac{d\theta}{2} dz - \sigma_\theta \, dr \frac{d\theta}{2} - \tau_{r\theta} \, dr \, dz +$$

$$\tau_{rz} \, dr \, dz + \frac{\partial \tau_{r\theta}}{\partial \theta r} dr \, d\theta \, dz - \tau_{rz} \, dr \, r d\theta + \tau_{rz} \, dr \, r d\theta + \frac{\partial \tau_{rz}}{\partial z} dz \, dr \, r d\theta = 0$$

Division by $(dr \, rd\theta \, dz)$ and neglecting 2nd order terms gives for the radial direction:

$$\frac{\partial \sigma_r}{\partial r} + \frac{\sigma_r - \sigma_\theta}{r} + \frac{\partial \tau_{rz}}{\partial z} + \frac{1}{r} \frac{\partial \tau_{r\theta}}{\partial \theta} = 0$$

Circumferential direction:

$$- \sigma_\theta \, dr \, dz + (\sigma_\theta + \frac{\partial \sigma_\theta}{\partial \theta} d\theta) \, dr \, dz - \tau_{r\theta} \, rd\theta \, dz +$$

$$(\tau_{r\theta} + \frac{\partial \tau_{r\theta}}{\partial r} dr)(r + dr) \, d\theta \, dz + \tau_{r\theta} \, dr \, dz \frac{d\theta}{2} +$$

$$(\tau_{r\theta} + \frac{\partial \tau_{r\theta}}{\partial \theta} d\theta) \, dr \, dz \frac{d\theta}{2} - \tau_{z\theta} \, rd\theta \, dr + (\tau_{z\theta} + \frac{\partial \tau_{z\theta}}{\partial z} dz) \, rd\theta \, dr = 0$$

Expansion yields:

$$- \sigma_\theta \, dr \, dz + \sigma_\theta \, dr \, dz + \frac{\partial \sigma_\theta}{\partial \theta} d\theta \, dr \, dz \quad \tau_{r\theta} \, rd\theta \, dz + \tau_{r\theta} \, rd\theta \, dz +$$

$$\tau_{r\theta} \, dr \, d\theta \, dz + \frac{\partial \tau_{r\theta}}{\partial r} dr \, r \, d\theta \, dz + \frac{\partial \tau_{r\theta}}{\partial r} dr \, dr \, d\theta \, dz + \tau_{r\theta} \, dr \, dz \frac{d\theta}{2} +$$

$$\tau_{r\theta} \, dr \, dz \frac{d\theta}{2} + \frac{\partial \tau_{r\theta}}{\partial \theta} d\theta \, dr \, dz \frac{d\theta}{2} - \tau_{z\theta} \, rd\theta \, dr + \tau_{z\theta} \, rd\theta \, dr + \frac{\partial \tau_{z\theta}}{\partial z} dz \, rd\theta \, dr = 0$$

Division by $(dr \, rd\theta \, dz)$ and neglecting 2nd order terms yields for the circumferential

direction:

$$\frac{1}{r} \frac{\partial \sigma_\theta}{\partial \theta} + \frac{2\tau_{r\theta}}{r} + \frac{\partial \tau_{r\theta}}{\partial r} + \frac{\partial \tau_{z\theta}}{\partial z} = 0$$

Axial direction:

158

$$- \sigma_z \, rd\theta \, dr + (\sigma_z + \frac{\partial \sigma_z}{\partial z} dz) \, rd\theta \, dr - \tau_{rz} \, rd\theta \, dz +$$

$$(\tau_{rz} + \frac{\partial \tau_{rz}}{\partial r} dr)(r + dr) \, d\theta \, dz - \tau_{\theta z} \, dr \, dz + (\tau_{\theta z} + \frac{\partial \tau_{\theta z}}{\partial \theta}) \, dr \, dz = 0$$

Expansion yields:

$$- \sigma_z + rd\theta \, dr + \sigma_z + rd\theta \, dr + \frac{\partial \sigma_z}{\partial z} dz \, rd\theta \, dr - \tau_{rz} \, rd\theta \, dz + \tau_{rz} \, rd\theta \, dz +$$

$$\frac{\partial \tau_{rz}}{\partial r} dr \, rd\theta \, dz + \tau_{rz} \, dr \, d\theta \, dz + \frac{\partial \tau_{rz}}{\partial r} dr \, dr \, d\theta \, dz - \tau_{\theta z} \, dr \, dz +$$

$$\tau_{\theta z} \, dr \, dz + \frac{\partial \tau_{\theta z}}{\partial \theta} d\theta \, dr \, dz = 0$$

Division by $(dr \, rd\theta \, dz)$ and neglecting 2nd order terms yields for the axial direction:

$$\frac{\partial \sigma_z}{\partial z} + \frac{\partial \tau_{rz}}{\partial r} + \frac{\tau_{rz}}{r} + \frac{1}{r} \frac{\partial \tau_{\theta z}}{\partial \theta} = 0$$

In many applied situations certain terms in the above equilibrium equations are from symmetry considerations and by Saint-Venant's principle taken to be invariant. This allows a degree of simplification. For example, barring unusual construction, in cylinders the elements attributing stress components due to variations along the axis can be set to zero.

The equilibrium equations in cylindrical coordinates are thus ordinarily expressed as:

$$\frac{\partial \sigma_r}{\partial r} + \frac{\partial \tau_{r\theta}}{rd\theta} + \frac{\sigma_r - \sigma_\theta}{r} = 0, \qquad \frac{\partial \tau_{r\theta}}{\partial r} + \frac{\partial \sigma_\theta}{rd\theta} + \frac{2\tau_{r\theta}}{r} = 0, \qquad \frac{\partial \tau_{rz}}{\partial r} + \frac{\partial \tau_{\theta z}}{rd\theta} + \frac{\tau_{rz}}{r} = 0$$

$$(4.10)$$

Equations (4.9) and (4.10) define the displacement and equilibrium equations respectively. Their combination into one or more unifying equation(s), called

159

compatibility relation(s), are a necessary step to arrive at equation(s) defining a physical problem amenable to a closed form solution. The *Method of Potentials* is one common technique among an assortment particularly suited to arrive at a solution for self-equilibrating stresses in plane strain / stress problems. The *Airy's stress function* belongs to this category and is resorted to subsequently.

4.3 Analysis

The orthotropic cylinder is of practical importance to analysis. For a typical filament wound construction adjacent, ($\pm \alpha$) angle wound layers are taken to behave as an orthotropic unit, given that the individual ply thickness is a small fraction of the whole lamina. Twisting, due to lack of exact symmetry in ply stacking, can be calculated on an individual layer basis using the methods presented by Sherrer [90] and as determined by Hoa [92] for specific constructions. Even under unrealistically extreme circumstances it was found that the resulting shear stresses remain about 4 orders of magnitude less than the principal stresses. The full implications of carrying forth without yielding to a ply-pair analysis can be appreciated by studying the equations brought forth in Chapter 5.

Local bending on the cylinder wall due to the end closures is neglected. This is acceptable for the mid-section of long cylinders where the end effects have died out. Generalized plane strain analysis can be invoked and in a first approximation it is assumed that the end sections are confined between fixed smooth rigid plates acted upon by a known force resulting from the endcaps. Hence the axial displacement is taken as a constant value at every cross-section (rather than zero). This can introduce small errors

because the restraint condition itself superposes its own stresses due to internal Possion action. Witherell [74] presents a 3 step axial strain equilibrating correction procedure for the plane-strain analysis method. First the conventional ($\varepsilon_z = 0$) plane-strain axial procedure is used to determine layer stresses due to the applied pressure. Then, in the correction, axial forces are applied to the individual layers such that each layer sees the same common axial strain initially assumed. In the third step, the gaps and overlaps resulting in the radial direction from the equilibrating layer stresses are used to compute additional inter-ply stresses which are finally added to the original pressure solution. In what follows the solution is obtained in a more direct manner.

Linear elasticity requires that the equations defining strains and displacements be simultaneously satisfied. It is necessary that in the process of deformation no voids or overlaps be created. This requires limitations upon the strains and mathematically such restrictions are defined as compatibility equations. (See for instance [161], pp. 89-91.) For the general case, six such restrictions exist, however when one condenses a problem to either plane stress or strain (variations in either strain or stress in the third direction are neglected) a single compatibility condition emerges. For generalized plane strain along the axis of a cylinder, the compatibility equation can be derived by taking appropriate partial derivatives of the stress - strain relations and making substitutions to eliminate displacements. A derivation of pertinent steps to this plane-strain elastic stress solution is detailed below.

For the condition of general anisotropy, in cylindrical coordinates, the system of equations to be solved can be organized in the following manner:

$$\varepsilon_r = a_{11}\,\sigma_r + a_{12}\,\sigma_\theta + a_{13}\,\sigma_z + a_{14}\,\tau_{\theta z} + a_{15}\,\tau_{rz} + a_{16}\,\tau_{r\theta}$$

$$\varepsilon_\theta = a_{21}\,\sigma_r + a_{22}\,\sigma_\theta + a_{23}\,\sigma_z + a_{24}\,\tau_{\theta z} + a_{25}\,\tau_{rz} + a_{26}\,\tau_{r\theta}$$

$$\varepsilon_z = a_{31}\,\sigma_r + a_{32}\,\sigma_\theta + a_{33}\,\sigma_z + a_{34}\,\tau_{\theta z} + a_{35}\,\tau_{rz} + a_{36}\,\tau_{r\theta}$$

$$\gamma_{\theta z} = a_{41}\,\sigma_r + a_{42}\,\sigma_\theta + a_{43}\,\sigma_z + a_{44}\,\tau_{\theta z} + a_{45}\,\tau_{rz} + a_{46}\,\tau_{r\theta}$$

$$\gamma_{rz} = a_{51}\,\sigma_r + a_{52}\,\sigma_\theta + a_{53}\,\sigma_z + a_{54}\,\tau_{\theta z} + a_{55}\,\tau_{rz} + a_{56}\,\tau_{r\theta}$$

$$\gamma_{r\theta} = a_{61}\,\sigma_r + a_{62}\,\sigma_\theta + a_{63}\,\sigma_z + a_{64}\,\tau_{\theta z} + a_{65}\,\tau_{rz} + a_{66}\,\tau_{r\theta}$$

(4.11)

By symmetry, strains must be the same at all cross-sections. It is sufficient to consider a slice between two sections a unit distance apart. Strains can be functions of r and θ, but not of axial distance z. In a generalized plane strain analysis ε_z is set equal to a constant rather than zero. Using this invariance of ε_z the equations can be further reduced by introducing C and the reduced coefficients β_{ij} in the following manner.

let:

$$\varepsilon_z = C = a_{13}\,\sigma_r + a_{23}\,\sigma_\theta + a_{33}\,\sigma_z + a_{34}\,\tau_{\theta z} + a_{35}\,\tau_{rz} + a_{36}\,\tau_{r\theta}$$

$$C - a_{33}\,\sigma_z = a_{13}\,\sigma_r + a_{23}\,\sigma_\theta + a_{34}\,\tau_{\theta z} + a_{35}\,\tau_{rz} + a_{36}\,\tau_{r\theta}$$

hence:

$$\sigma_z = \frac{C}{a_{33}} - \frac{1}{a_{33}}(a_{31}\,\sigma_r + a_{32}\,\sigma_\theta + a_{34}\,\tau_{\theta z} + a_{35}\,\tau_{rz} + a_{36}\,\tau_{r\theta})$$

(4.12)

Defining:

$$\beta_{ij} = a_{ij} - \frac{a_{i3}\,a_{j3}}{a_{33}} \qquad\qquad i,j = 1,2,4,5,6$$

(4.13)

Substitution of the definitions for σ_z and the β_{ij} coefficients into (4.11) allows regrouping of terms. Substitutions for ε_r are worked out below, the other 5 strains can be re-written identically.

$$\varepsilon_r = \frac{\partial u}{\partial r} = a_{11}\,\sigma_r + a_{12}\,\sigma_\theta + a_{14}\,\tau_{\theta z} + a_{15}\,\tau_{rz} + a_{16}\,\tau_{r\theta} +$$

$$a_{13}\left[\frac{C}{a_{33}} - \frac{1}{a_{33}}(a_{31}\,\sigma_r + a_{32}\,\sigma_\theta + a_{34}\,\tau_{\theta z} + a_{35}\,\tau_{rz} + a_{36}\,\tau_{r\theta})\right]$$

Collecting terms:

$$\varepsilon_r = \frac{a_{13}}{a_{33}}C + \sigma_r\left(a_{11} - \frac{a_{13}\,a_{31}}{a_{33}}\right) + \sigma_\theta\left(a_{12} - \frac{a_{13}\,a_{32}}{a_{33}}\right) + \tau_{\theta z}\left(a_{14} - \frac{a_{13}\,a_{34}}{a_{33}}\right) +$$

$$\tau_{rz}\left(a_{15} - \frac{a_{13}\,a_{35}}{a_{33}}\right) + \tau_{r\theta}\left(a_{16} - \frac{a_{13}\,a_{36}}{a_{33}}\right)$$

By the above, equations (4.11) can be given as:

$$\varepsilon_r = \frac{\partial u}{\partial r} = \beta_{11}\,\sigma_r + \beta_{12}\,\sigma_\theta + \beta_{14}\,\tau_{\theta z} + \beta_{15}\,\tau_{rz} + \beta_{16}\,\tau_{r\theta} + \frac{a_{13}}{a_{33}}C$$

$$\varepsilon_\theta = \frac{\partial v}{r\partial\theta} + \frac{u}{r} = \beta_{21}\,\sigma_r + \beta_{22}\,\sigma_\theta + \beta_{24}\,\tau_{\theta z} + \beta_{25}\,\tau_{rz} + \beta_{26}\,\tau_{r\theta} + \frac{a_{23}}{a_{33}}C$$

$$\varepsilon_z = \frac{\partial w}{\partial z} = C$$

$$\gamma_{\theta z} = \frac{\partial w}{r\partial\theta} + \frac{\partial v}{\partial z} = \beta_{41}\,\sigma_r + \beta_{42}\,\sigma_\theta + \beta_{44}\,\tau_{\theta z} + \beta_{45}\,\tau_{rz} + \beta_{46}\,\tau_{r\theta} + \frac{a_{43}}{a_{33}}C$$

$$\gamma_{rz} = \frac{\partial u}{\partial z} + \frac{\partial w}{\partial r} = \beta_{51}\,\sigma_r + \beta_{52}\,\sigma_\theta + \beta_{54}\,\tau_{\theta z} + \beta_{55}\,\tau_{rz} + \beta_{56}\,\tau_{r\theta} + \frac{a_{53}}{a_{33}}C$$

$$\gamma_{r\theta} = \frac{\partial u}{r\partial\theta} + \frac{\partial v}{\partial r} - \frac{v}{r} = \beta_{61}\,\sigma_r + \beta_{62}\,\sigma_\theta + \beta_{64}\,\tau_{\theta z} + \beta_{65}\,\tau_{rz} + \beta_{66}\,\tau_{r\theta} + \frac{a_{63}}{a_{33}}C$$

(4.14)

Methods of solution to the above problem are not obvious. One technique is via the method of potentials. This entails use of a stress function which satisfies the

163

equilibrium equations and also defines a relation between itself and body forces (if any). The quest is to find a solution to the compatibility equation, written out in terms of the stress function, that satisfies the boundary conditions. Stress functions for general cylindrical anisotropy are available. For instance Lekhnitskii [88] (section 23) or for isotropic cases Saada [161] (section 9.9) and Timoshenko [114] (chapter 12) with some specific cases being examined. Experience however determines which function applies itself well to particular boundary conditions.

Two stress functions, $F(r,\theta)$ for direct stresses and $\Psi(r,\theta)$ for shear, are introduced and define the stress components. These relations are applicable at the individual layer level but can also be used effectively to describe ply groups under specific circumstances.

Let:

$$\sigma_r = \frac{1}{r}\frac{\partial F}{\partial r} + \frac{1}{r^2}\frac{\partial^2 F}{\partial \theta^2} \quad , \quad \tau_{r\theta} = -\frac{\partial^2}{\partial r\,\partial\theta}\left(\frac{F}{r}\right)$$

$$\sigma_\theta = \frac{\partial^2 F}{\partial r^2}$$

$$\tau_{rz} = \frac{1}{r}\frac{\partial \Psi}{\partial \theta} \quad , \quad \tau_{\theta z} = -\frac{\partial \Psi}{\partial r}$$

By assuming homogeneous construction (within a group of ± angle windings) and realizing that angular symmetry in the (θ) direction implies stresses remain identical at all cross-sections, the problem can be simplified. The solution sought will be an equation in the form of functions of only one variable (r), without relation to angular position θ. Provided the cylinder is effectively built up from orthotropic ply groups (rather than considering each ply separately), and that there is no external axial torque applied,

coupling will not exist between normal and shear components, nor will there arise any

shear stresses to resisting an applied moment. The need for Ψ which relates specifically to

shear stress is eliminated. Under these conditions the stress components reduce to simply:

$$\sigma_r = \frac{1}{r}\frac{\partial F}{\partial r} \qquad \tau_{r\theta} = \tau_{\theta z} = \tau_{rz} = 0$$

$$\sigma_\theta = \frac{\partial^2 F}{\partial r^2} \qquad \sigma_z = \frac{C}{a_{33}} - \frac{1}{a_{33}}(a_{31}\sigma_r + a_{32}\sigma_\theta)$$

The governing equations of (4.14) can be simplified to:

$$\varepsilon_r = \frac{\partial u}{\partial r} = \beta_{11}\sigma_r + \beta_{12}\sigma_\theta + \frac{a_{13}}{a_{33}}C$$

$$\varepsilon_\theta = \frac{\partial v}{r\partial\theta} + \frac{u}{r} = \beta_{21}\sigma_r + \beta_{22}\sigma_\theta + \frac{a_{23}}{a_{33}}C$$

$$\varepsilon_z = \frac{\partial w}{\partial z} = C = \text{constant}$$

$$\gamma_{\theta z} = \gamma_{rz} = \gamma_{r\theta} = 0$$

(4.15)

A unifying relation can be derived by taking appropriate partial derivatives of $\gamma_{r\theta}$

as defined in (4.9) and making substitutions to eliminate the displacements in (4.15).

$$\gamma_{r\theta} = \frac{1}{r}\frac{\partial u}{\partial\theta} + \frac{\partial v}{\partial r} - \frac{v}{r}; \qquad r\gamma_{r\theta} = \frac{\partial u}{\partial\theta} + r\frac{\partial v}{\partial r} - v$$

$$\frac{\partial}{\partial r}(r\gamma_{r\theta}) = \frac{\partial^2 u}{\partial r\partial\theta} + \frac{\partial v}{\partial r} + r\frac{\partial^2 v}{\partial r^2} - \frac{\partial v}{\partial r}$$

$$\frac{\partial^2}{\partial r\partial\theta}(r\gamma_{r\theta}) = \frac{\partial^3 u}{\partial r\partial\theta^2} + r\frac{\partial^3 v}{\partial r^2\partial\theta}$$

(4.16)

A substitution for the first term in (4.16) is immediately obvious:

$$\frac{\partial}{\partial \theta}(\varepsilon_r) = \frac{\partial^2 u}{\partial r \partial \theta}$$

$$\frac{\partial^2}{\partial \theta^2}(\varepsilon_r) = \frac{\partial^3 u}{\partial r \partial \theta^2}$$

The second term can be generated equally. From (4.9)

$$r\varepsilon_\theta = \frac{\partial v}{\partial \theta} + u$$

$$\frac{\partial}{\partial r}(r\varepsilon_\theta) = \frac{\partial^2 v}{\partial r \partial \theta} + \frac{\partial u}{\partial r}$$

$$\frac{\partial}{\partial r^2}(r\varepsilon_\theta) = \frac{\partial^3 v}{\partial r^2 \partial \theta} + \frac{\partial^2 u}{\partial r^2}$$

thus: $\quad r\dfrac{\partial^3 v}{\partial r^2 \partial \theta} = r\left[\dfrac{\partial}{\partial r^2}(r\varepsilon_\theta) - \dfrac{\partial^2 u}{\partial r^2}\right]$

but: $\quad \dfrac{\partial}{\partial r}(\varepsilon_r) = \dfrac{\partial}{\partial r}\left(\dfrac{\partial u}{\partial r}\right) = \dfrac{\partial^2 u}{\partial r^2}$

The second term of (4.16) becomes:

$$r\left[\frac{\partial}{\partial r^2}(r\varepsilon_\theta) - \frac{\partial \varepsilon_r}{\partial r}\right]$$

Such that (4.16) can be expressed as:

$$\frac{\partial^2(r\gamma_{r\theta})}{\partial r \partial \theta} - \frac{\partial^2 \varepsilon_r}{\partial \theta^2} - r\frac{\partial}{\partial r^2}(r\varepsilon_\theta) + r\frac{\partial \varepsilon_r}{\partial r} = 0$$

$$(4.17)$$

The differential equation that must be satisfied is obtained by substituting the stress-strain relations (4.15) into relation (4.17) while expressing the stresses in terms of a stress function. Recalling that symmetry implies no variation with (θ) allows the reduction of (4.17) to:

$$\frac{\partial \varepsilon_r}{\partial r} - \frac{\partial}{\partial r^2}(r\varepsilon_\theta) = 0$$

<div align="right">(4.18)</div>

The second term of (4.18) is written as:

$$\frac{\partial}{\partial r^2}(r\varepsilon_\theta) = \frac{\partial}{\partial r^2}\left[\beta_{12}\left(\frac{\partial F}{\partial r}\right) + \beta_{22}\left(r\frac{\partial^2 F}{\partial r^2}\right) + r\frac{a_{23}}{a_{33}}C\right]$$

$$\frac{\partial}{\partial r^2}(r\varepsilon_\theta) = \frac{\partial}{\partial r}\left[\beta_{12}\left(\frac{\partial^2 F}{\partial r^2}\right) + \beta_{22}\left(\frac{\partial^2 F}{\partial r^2} + r\frac{\partial^3 F}{\partial r^3}\right) + \frac{a_{23}}{a_{33}}C\right]$$

$$\frac{\partial}{\partial r^2}(r\varepsilon_\theta) = \beta_{12}\left(\frac{\partial^3 F}{\partial r^3}\right) + \beta_{22}\left(\frac{\partial^3 F}{\partial r^3} + \frac{\partial^3 F}{\partial r^3} + r\frac{\partial^4 F}{\partial r^4}\right)$$

The first term of (4.18) is:

$$\frac{\partial(\varepsilon_r)}{\partial r} = \frac{\partial}{\partial r}\left[\beta_{11}\left(\frac{1}{r}\frac{\partial F}{\partial r}\right) + \beta_{12}\left(\frac{\partial^2 F}{\partial r^2}\right) + \frac{a_{13}}{a_{33}}C\right]$$

$$\frac{\partial(\varepsilon_r)}{\partial r} = \left[\beta_{11}\left(\frac{1}{r}\frac{\partial^2 F}{\partial r^2} - \frac{1}{r^2}\frac{\partial F}{\partial r}\right) + \beta_{12}\frac{\partial^3 F}{\partial r^3}\right]$$

Hence

$$\frac{\partial}{\partial r^2}(r\varepsilon_\theta) - \frac{\partial \varepsilon_r}{\partial r} = \beta_{22}\left(r\frac{\partial^4 F}{\partial r^4} + 2\frac{\partial^3 F}{\partial r^3}\right) - \beta_{11}\left(\frac{1}{r}\frac{\partial^2 F}{\partial r^2} - \frac{1}{r^2}\frac{\partial F}{\partial r}\right) = 0$$

The above reduces to the biharmonic equation:

$$\frac{\beta_{22}}{r}\frac{\partial^4 F}{\partial r^4} + 2\frac{\beta_{22}}{r}\frac{\partial^3 F}{\partial r^3} - \frac{\beta_{11}}{r^2}\frac{\partial^2 F}{\partial r^2} + \frac{\beta_{11}}{r^3}\frac{\partial F}{\partial r} = 0$$

<div align="right">(4.19)</div>

A solution to (4.19) requires that the boundary conditions of the problem be met.

Conditions on the cylindrical surface are:

When:
$$r = a ; \qquad \sigma_r = -P$$
$$r = b ; \qquad \sigma_r = -Q$$

where P and Q are internal and external pressures respectively. The substitutions outlined below permit solution via the biharmonic (Euler's) equation.

Let: $r = e^t$; $\quad t = \ln r$; $\quad \dfrac{dt}{dr} = \dfrac{1}{r}$; $\quad \dfrac{1}{r} = e^{-t}$

Then

$$F^I(r) = \frac{dF}{dr} = \frac{dF}{dt}\frac{dt}{dr} = \frac{dF}{dt}e^{-t} = \frac{1}{r}\frac{dF}{dt}$$

$$F^{II}(r) = \frac{d}{dr}[F^I(r)] = \frac{d}{dt}[F^I(r)]\frac{dt}{dr} = e^{-t}\frac{d}{dt}\left[e^{-t}\frac{dF}{dt}\right]$$

$$F^{II}(r) = e^{-t}\left(-e^{-t}\frac{dF}{dt} + e^{-t}\frac{d^2F}{dt^2}\right) = \frac{1}{r^2}\left(-\frac{dF}{dt} + \frac{d^2F}{dt^2}\right)$$

$$F^{III}(r) = \frac{d}{dr}[F^{II}(r)] = \frac{d}{dt}[F^{II}(r)]\frac{dt}{dr} = e^{-t}\frac{d}{dt}\left[e^{-2t}\frac{d^2F}{dt^2} - e^{-2t}\frac{dF}{dt}\right]$$

$$F^{III}(r) = e^{-t}\left[-2e^{-2t}\frac{d^2F}{dt^2} + e^{-2t}\frac{d^3F}{dt^3} + 2e^{-2t}\frac{dF}{dt} - e^{-2t}\frac{d^2F}{dt^2}\right]$$

$$F^{III}(r) = 2e^{-3t}\frac{dF}{dt} - 3e^{-3t}\frac{d^2F}{dt^2} + e^{-3t}\frac{d^3F}{dt^3} = \frac{2}{r^3}\frac{dF}{dt} - \frac{3}{r^3}\frac{d^2F}{dt^2} + \frac{1}{r^3}\frac{d^3F}{dt^3}$$

$$F^{IV}(r) = \frac{d}{dr}[F^{III}(r)] = \frac{d}{dt}[F^{III}(r)]\frac{dt}{dr} = e^{-t}\frac{d}{dt}\left[2e^{-3t}\frac{dF}{dt} - 3e^{-3t}\frac{d^2F}{dt^2} + e^{-3t}\frac{d^3F}{dt^3}\right]$$

$$F^{IV}(r) = e^{-t}\left[-6e^{-3t}\frac{dF}{dt} + 2e^{-3t}\frac{d^2F}{dt^2} + 9e^{-3t}\frac{d^2F}{dt^2} - 3e^{-3t}\frac{d^3F}{dt^3} - 3e^{-3t}\frac{d^3F}{dt^3} + e^{-3t}\frac{d^4F}{dt^4}\right]$$

$$F^{IV}(r) = \frac{-6}{r^4}\frac{dF}{dt} + \frac{11}{r^4}\frac{d^2F}{dt^2} - \frac{6}{r^4}\frac{d^3F}{dt^3} + \frac{1}{r^4}\frac{d^4F}{dt^4}$$

(4.20)

Substituting the first through the fourth derivatives of (4.20) into relation (4.19) yields:

$$\beta_{22}\left(\frac{1}{r^4}\frac{d^4F}{dt^4} - \frac{6}{r^4}\frac{d^3F}{dt^3} + \frac{11}{r^4}\frac{d^2F}{dt^2} - \frac{6}{r^4}\frac{dF}{dt}\right) + 2\frac{\beta_{22}}{r}\left(\frac{1}{r^3}\frac{d^3F}{dt^3} - \frac{3}{r^3}\frac{d^2F}{dt^2} + \frac{2}{r^3}\frac{dF}{dt}\right)$$

$$- \frac{\beta_{11}}{r^2}\left(\frac{1}{r^2}\frac{d^2F}{dt^2} - \frac{1}{r^2}\frac{dF}{dt}\right) + \frac{\beta_{11}}{r^3}\left(\frac{1}{r}\frac{dF}{dt}\right) = 0$$

Simplification yields:

168

$$\frac{1}{r^4}\left[\beta_{22}\frac{d^4F}{dt^4} - 4\beta_{22}\frac{d^3F}{dt^3} + (5\beta_{22} - \beta_{11})\frac{d^2F}{dt^2} + (-2\beta_{22} + 2\beta_{11})\frac{dF}{dt}\right] = 0$$

and division by β_{22} allows expression as:

$$\frac{1}{r^4}\left[\frac{d^4F}{dt^4} - 4\frac{d^3F}{dt^3} + \left(5 - \frac{\beta_{11}}{\beta_{22}}\right)\frac{d^2F}{dt^2} + 2\left(\frac{\beta_{11}}{\beta_{22}} - 1\right)\frac{dF}{dt}\right] = 0$$

(4.21)

The characteristic equation in terms of the roots is:

$$\lambda\left[\lambda^3 - 4\lambda^2 + \left(5 - \frac{\beta_{11}}{\beta_{22}}\right)\lambda + 2\left(\frac{\beta_{11}}{\beta_{22}} - 1\right)\right] = 0$$

The roots can be determined by long division. One method is to divide the above equation by a suspected root. $(\lambda - 2)$ as a divisor yields no remainder, hence it proves to be a root.

$$\lambda^2 - 2\lambda + 1 - \frac{\beta_{11}}{\beta_{22}}$$

$$(\lambda - 2)\sqrt{\lambda^3 - 4\lambda^2 + \left(5 - \frac{\beta_{11}}{\beta_{22}}\right)\lambda + 2\left(\frac{\beta_{11}}{\beta_{22}} - 1\right)}$$

$$\underline{\lambda^3 - 2\lambda^2}$$

$$-2\lambda^2 + \left(5 - \frac{\beta_{11}}{\beta_{22}}\right)\lambda$$

$$-2\lambda^2 - 4\lambda$$

$$\overline{\left(1 - \frac{\beta_{11}}{\beta_{22}}\right)\lambda}$$

$$\lambda - 2$$

$$\overline{-\frac{\beta_{11}}{\beta_{22}}\lambda + 2 + 2\left(\frac{\beta_{11}}{\beta_{22}} - 1\right)}$$

$$\underline{-\frac{\beta_{11}}{\beta_{22}}\lambda + 2\frac{\beta_{11}}{\beta_{22}}}$$

$$0$$

Two roots have already been extracted:

$$\lambda_1 = 0, \quad \lambda_2 = 2$$

The quadratic formula can be used to extract the remaining roots from the quotient above:

$$\lambda_3, \lambda_4 = \frac{2 \pm \sqrt{4 - 4(1 - \beta_{11}/\beta_{22})}}{2} = 1 \pm \sqrt{\beta_{11}/\beta_{22}}$$

Defining $\quad K = \sqrt{\beta_{11}/\beta_{22}}$

then $\quad \lambda_3 = (1 + K), \quad \lambda_4 = (1 - K)$

The solution of the differential equation takes the form:

$$F(t) = C_1 e^{\lambda_1 t} + C_2 e^{\lambda_2 t} + C_3 e^{\lambda_3 t} + C_4 e^{\lambda_4 t}$$

$$F(t) = C_1 e^{0t} + C_2 e^{2t} + C_3 e^{(1-k)t} + C_4 e^{(1-k)t}$$

Reverting to $F(r)$; where $r = e^t$

$$F(r) = C_1 + C_2 r^2 + C_3 r^{(1-K)} + C_4 r^{(1-K)}$$

$$(4.22)$$

One can check the validity of the solution found for the stress function:

From equation (4.22),

$$\frac{\partial F}{\partial r} = 2C_2 r + (1 + K)C_3 r^K + (1 - K)C_4 r^{-K}$$

$$\frac{\partial^2 F}{\partial r^2} = 2C_2 + K(1 + K)C_3 r^{K-1} - (1 - K)(K)C_4 r^{-1-K}$$

$$\frac{\partial^3 F}{\partial r^3} = K(1 + K)(K - 1)C_3 r^{K-2} + (1 - K)(K)(1 + K)C_4 r^{-2-K}$$

$$\frac{\partial^4 F}{\partial r^4} = K(1 + K)(K - 1)(K - 2)C_3 r^{K-3} - (1 - K)(K)(1 + K)(2 + K)C_4 r^{-3-K}$$

Substitution into (4.19) gives

170

$$0 = C_3 r^{K-3}(K)(1+K)(K-1)[(K-2)+2]\beta_{22} + C_4 r^{-K-3}(1-K)(K)(1+K)[(-2-K)+2]\beta_{22} +$$

$$C_3 r^{K-3}(1+K)(-K+1)\beta_{11} + C_4 r^{-K-3}(1-K)(K+1)\beta_{11} + \left(\frac{-2C_2}{r^2} + \frac{2C_2}{r^2}\right)\beta_{11}$$

$$0 = \beta_{22}(K^2)(1+K)(K-1)[C_3 r^{K-3} + C_4 r^{-K-3}] - \beta_{11}(1+K)(K-1)[C_3 r^{K-3} + C_4 r^{-K-3}]$$

$$0 = [C_3 r^{K-3} + C_4 r^{-K-3}](1+K)(K-1)[\beta_{22}(K^2) - \beta_{11}]$$

But $K^2 = \dfrac{\beta_{11}}{\beta_{22}}$, hence the equality holds

Appropriate boundary conditions, when applied to the stress function yield the stress distribution within the orthotropic cylinder.

$$\sigma_r = \frac{1}{r}\frac{\partial F}{\partial r} = \frac{1}{r}\left[2C_2 r + (1+K)C_3 r^K + (1-K)C_4 r^{-K}\right]$$

$$\sigma_r = 2C_2 + (1+K)C_3 r^{K-1} + (1-K)C_4 r^{-K-1}$$

$$\sigma_\theta = \frac{\partial^2 F}{\partial r^2} = 2C_2 + K(1+K)C_3 r^{K-1} + (1-K)(-K)C_4 r^{-K-1}$$

(4.23)

Looking back upon (4.22) and the partial derivatives that associate stresses with the stress function one can see that the choice for C_1 is not relevant to the stress distribution so it can be set to zero. However we are still left with 3 constants to solve for. There are two evident boundary conditions, namely the stresses at the inner and outer surfaces. We have at the boundary:

$$r = a, \quad \sigma_r = -P$$
$$r = b, \quad \sigma_r = -Q$$

where; P and Q are defined as internal and external pressures.

One must search for a third restraint upon the system, otherwise the third constant in the above equations cannot be determined. The system can also be solved if one arbitrarily assigns or finds justifiable reasons to assume that one of the remaining three constants must assume a value of zero. This is the approach taken in the work of many authors, including a publication on thick-wall pressure vessel analysis by A.K. Roy and S.W. Tsai [91]. Here C_2 is taken as zero. Unfortunately this approach is mathematically incorrect and it will be shown by Chapter 8 that such an assumption leads to a small error.

A third constraint condition can be developed in terms of displacements. From (4.15) and considering the absence of variation with respect to the θ direction we have:

$$\varepsilon_r = \frac{\partial u}{\partial r} = \beta_{11}\sigma_r + \beta_{12}\sigma_\theta + \frac{a_{13}}{a_{33}}C$$

$$\varepsilon_\theta = \frac{u}{r} = \beta_{21}\sigma_r + \beta_{22}\sigma_\theta + \frac{a_{23}}{a_{33}}C$$

but since $u = r\varepsilon_\theta$ and therefore $\dfrac{\partial u}{\partial r} = \dfrac{\partial}{\partial r}(r\varepsilon_\theta)$ we have

$$\frac{\partial}{\partial r}\left(\beta_{12}r\sigma_r + \beta_{22}r\sigma_\theta + \frac{a_{23}}{a_{33}}Cr\right) = \frac{\partial u}{\partial r}$$

so

$$\beta_{11}\sigma_r + \beta_{12}\sigma_\theta + \frac{a_{13}}{a_{33}}C - \frac{\partial}{\partial r}\left(\beta_{12}r\sigma_r + \beta_{22}r\sigma_\theta + \frac{a_{23}}{a_{33}}Cr\right) = 0$$

Substituting for the stresses from (4.23) yields

$$\beta_{11}\left[2C_2 + (1+K)C_3 r^{K-1} + (1-K)C_4 r^{-K-1}\right] +$$
$$\beta_{12}\left[2C_2 + K(1+K)C_3 r^{K-1} + (1-K)(-K)C_4 r^{-K-1}\right] + \frac{a_{13}}{a_{23}}C \longrightarrow$$

172

$$\beta_{12}\frac{\partial}{\partial r}\left[2C_2 r+(1+K)C_3 r^K+(1-K)C_4 r^{-K}\right]-$$

$$\beta_{22}\frac{\partial}{\partial r}\left[2C_2 r+K(1+K)C_3 r^K+(1-K)(-K)C_4 r^{-K}\right]-\frac{a_{23}}{a_{33}}C=0$$

which reduces to

$$2\beta_{11}C_2+\beta_{11}(1+K)C_3 r^{K-1}+(1-K)\beta_{11}C_4 r^{-K-1}+$$

$$2\beta_{12}C_2+K(1+K)\beta_{12}C_3 r^{K-1}+(1-K)(-K)\beta_{12}C_4 r^{-K-1}+\frac{a_{13}}{a_{33}}C-$$

$$2\beta_{12}C_2-\beta_{12}K(1+K)C_3 r^{K-1}-(-K)(1-K)\beta_{12}C_4 r^{-K-1}-$$

$$2\beta_{22}C_2-\beta_{22}K^2(1+K)C_3 r^{K-1}-\beta_{22}K^2(1-K)C_4 r^{-K-1}-\frac{a_{23}}{a_{33}}C=0$$

substituting $K^2=\dfrac{\beta_{11}}{\beta_{22}}$ we are left with

$$2C_2(\beta_{11}-\beta_{22})=\left(-\frac{a_{13}}{a_{33}}+\frac{a_{23}}{a_{33}}\right)C$$

hence the constraining relation becomes

$$2C_2=\left[\frac{a_{13}-a_{23}}{a_{33}(\beta_{22}-\beta_{11})}\right]C$$

defining

$$\chi=\frac{a_{13}-a_{23}}{(\beta_{22}-\beta_{11})a_{33}}$$

system (4.23) is restated as

$$\sigma_r=\chi C+(1+K)C_3 r^{K-1}+(1-K)C_4 r^{-K-1}$$

and

$$\sigma_\theta=\chi C+K(1+K)C_3 r^{K-1}-(1-K)K\,C_4 r^{-K-1}$$

173

Applying the stress boundary conditions at the inner and outer surfaces, the radial condition can be set as:

$$-\chi C - P = (1 + K)\, C_3 a^{K-1} + (1 - K)\, C_4 a^{-K-1}$$

$$-\chi C - Q = (1 + K)\, C_3 b^{K-1} + (1 - K)\, C_4 b^{-K-1}$$

$$(4.24)$$

Using matrix cofactors the constants C_3 and C_4 can be extracted.

$$C_3 = \frac{\begin{vmatrix} -P-\chi C & (1-K)a^{-K-1} \\ -Q-\chi C & (1-K)b^{-K-1} \end{vmatrix}}{\begin{vmatrix} (1+K)a^{K-1} & (1-K)a^{-K-1} \\ (1+K)b^{K-1} & (1-K)b^{-K-1} \end{vmatrix}} = \frac{(-\chi C - P)(1-K)b^{-1-K} + (Q+\chi C)(1-K)a^{-K-1}}{(1+K)(1-K)a^{K-1}\,b^{-1-K} - (1+K)b^{K-1}\,(1-K)a^{-K-1}}$$

$$C_4 = \frac{\begin{vmatrix} (1+K)a^{K-1} & -P-\chi C \\ (1+K)b^{K-1} & -Q-\chi C \end{vmatrix}}{\begin{vmatrix} (1+K)a^{K-1} & (1-K)a^{-K-1} \\ (1+K)b^{K-1} & (1-K)b^{-K-1} \end{vmatrix}} = \frac{(-\chi C - Q)(1+K)a^{K-1} + (P+\chi C)(1+K)b^{K-1}}{(1+K)(1-K)a^{K-1}\,b^{-1-K} - (1+K)b^{K-1}\,(1-K)a^{-K-1}}$$

Substitution back into equation (4.23) allows reduction to a more compact form. For σ_r:

$$\sigma_r = (1+K)r^{K-1}\left\{\frac{(-\chi C - P)(1-K)b^{-1-K} + (Q+\chi C)(1-K)a^{-K-1}}{(1+K)(1-K)a^{K-1}\,b^{-1-K} - (1+K)b^{K-1}\,(1-K)a^{-K-1}}\right\} +$$

$$(1-K)r^{-K-1}\left\{\frac{(-\chi C - Q)(1+K)a^{K-1} + (P+\chi C)(1+K)b^{K-1}}{(1+K)(1-K)a^{K-1}\,b^{-1-K} - (1+K)b^{K-1}\,(1-K)a^{-K-1}}\right\} + C\chi$$

$$\sigma_r = r^{K-1}\left\{\frac{-P(b)^{-1-K} + Q(a)^{-K-1}}{(a)^{K-1}(b)^{-1-K} - (b)^{K-1}(a)^{-K-1}}\right\} + r^{-K-1}\left\{\frac{-Q(a)^{K-1} + P(b)^{K-1}}{(a)^{K-1}(b)^{-1-K} - (b)^{K-1}(a)^{-1-K}}\right\}$$

$$+r^{K-1}\left\{\frac{-\chi C(b)^{-1-K} + \chi Ca^{-K-1}}{(a)^{K-1}(b)^{-1-K} - (b)^{K-1}(a)^{-K-1}}\right\} + r^{-K-1}\left\{\frac{-\chi C(a)^{K-1} + \chi C(b)^{K-1}}{(a)^{K-1}(b)^{-1-K} - (b)^{K-1}(a)^{-1-K}}\right\} + C\chi$$

174

factoring out b^{K-1} and b^{-K-1} from the denominator

$$\sigma_r = \left(\frac{r}{b}\right)^{K-1} \left\{\frac{-P(b)^{-1-K} + Q(a)^{-K-1}}{(a)^{K-1}(b)^{-2K} - (a)^{-K-1}}\right\} + \left(\frac{r}{b}\right)^{-K-1} \left\{\frac{-Q(a)^{K-1} + P(b)^{K-1}}{(a)^{K-1} - (b)^{2K}(a)^{-1-K}}\right\}$$

$$\left(\frac{r}{b}\right)^{K-1} \left\{\frac{-\chi C(b)^{-1-K} + \chi C(a)^{-K-1}}{(a)^{K-1}(b)^{-2K} - (a)^{-K-1}}\right\} + \left(\frac{r}{b}\right)^{-K-1} \left\{\frac{-\chi C(a)^{K-1} + \chi C(b)^{K-1}}{(a)^{K-1} - (b)^{2K}(a)^{-1-K}}\right\} + C\chi$$

Multiplying top and bottom terms by: $b^{-2K}a^{1-K}$

$$\sigma_r = \left(\frac{r}{b}\right)^{K-1} \left\{\frac{-P(b)^{-1-K}(a)^{K+1} + Q}{a^{2K}b^{-2K} - 1}\right\} + \left(\frac{r}{b}\right)^{-K-1} \left\{\frac{-Q(a)^{2K}(b)^{-2K} + P(b)^{-K-1}(a)^{1-K}}{(a)^{2K}(b)^{-2K} - 1}\right\} +$$

$$\left(\frac{r}{b}\right)^{K-1} \left\{\frac{-C\chi(b)^{-1-K}(a)^{K+1} + C\chi}{(a)^{2K}(b)^{-2K} - 1}\right\} + \left(\frac{r}{b}\right)^{-K-1} \left\{\frac{-C\chi(a)^{2K}(b)^{-2K} + C\chi(b)^{-K-1}(a)^{1-K}}{(a)^{2K}(b)^{-2K} - 1}\right\} + C\chi$$

$$\sigma_r = \left(\frac{r}{b}\right)^{K-1} \left\{\frac{-P(c)^{K-1} + Q}{(c)^{2K} - 1}\right\} + \left(\frac{r}{b}\right)^{-K-1} \left\{\frac{-Q(c)^{2K} + P(c)^{1-K}}{(c)^{2K} - 1}\right\} +$$

$$\left(\frac{r}{b}\right)^{K-1} \left\{\frac{-C\chi(c)^{K-1} + C\chi}{(c)^{2K} - 1}\right\} + \left(\frac{r}{b}\right)^{-K-1} \left\{\frac{-C\chi(c)^{2K} + C\chi(c)^{1+K}}{(c)^{2K} - 1}\right\} + C\chi$$

Defining:

$$W_1 = \left[1 - \left(\frac{r}{b}\right)^{K-1} \left\{\frac{1 - (c)^{K-1}}{1 - (c)^{2K}}\right\} - \left(\frac{r}{b}\right)^{-K-1} \left\{\frac{(1 - c^{K-1})(c)^{1-K}}{1 - (c)^{2K}}\right\}\right]$$

Then σ_r can be stated as:

$$\sigma_r = \left(\frac{r}{b}\right)^{K-1} \left\{\frac{-Pc^{K+1} + Q}{(c)^{2K} - 1}\right\} + \left(\frac{b}{r}\right)^{K-1} \left\{\frac{(-Qc^{K-1} + P)c^{K-1}}{(c)^{2K} - 1}\right\} + C\chi W_1$$

(4.25)

where; $c = (a/b)$

By similar method σ_θ is solved for.

175

$$\sigma_\theta = K(1+K)r^{K-1}\left\{\frac{(-\chi C-P)(1-K)b^{-1-K}+(Q+\chi C)(1-K)a^{-K-1}}{(1+K)(1-K)a^{K-1}b^{-1-K}-(1+K)b^{K-1}(1-K)a^{-K-1}}\right\}+$$

$$(-K)(1-K)r^{-K-1}\left\{\frac{(\chi C-Q)(1+K)a^{K-1}+(P+\chi C)(1+K)b^{K-1}}{(1+K)(1-K)a^{K-1}b^{-1-K}-(1+K)b^{K-1}(1-K)a^{-K-1}}\right\}$$

$$\sigma_\theta = (K)(r)^{K-1}\left\{\frac{-P(b)^{-1-K}+Q(a)^{-K-1}}{(a)^{K-1}(b)^{-1-K}-(b)^{K-1}(a)^{-K-1}}\right\}-(K)(r)^{-K-1}\left\{\frac{-Q(a)^{K-1}+P(b)^{K-1}}{(a)^{K-1}(b)^{-1-K}-(b)^{K-1}(a)^{-K-1}}\right\}+$$

$$(K)(r)^{K-1}\left\{\frac{-\chi C(b)^{-1-K}+\chi C(a)^{-K-1}}{(a)^{K-1}(b)^{-1-K}-(b)^{K-1}(a)^{-K-1}}\right\}-(K)(r)^{-K-1}\left\{\frac{-\chi C(a)^{K-1}+\chi C(b)^{K-1}}{(a)^{K-1}(b)^{-1-K}-(b)^{K-1}(a)^{-K-1}}\right\}+C\chi$$

factoring out b^{K-1} and b^{-K-1} from the denominator

$$\sigma_\theta = (K)\left(\frac{r}{b}\right)^{K-1}\left\{\frac{-P(b)^{-1-K}+Q(a)^{-K-1}}{(a)^{K-1}(b)^{-2K}-(a)^{-K-1}}\right\}-(K)\left(\frac{r}{b}\right)^{-K-1}\left\{\frac{-Q(a)^{K-1}+P(b)^{K-1}}{(a)^{K-1}-(b)^{2K}(a)^{-K-1}}\right\}+$$

$$(K)\left(\frac{r}{b}\right)^{K-1}\left\{\frac{-\chi C(b)^{-1-K}+\chi C(a)^{-K-1}}{(a)^{K-1}(b)^{-2K}-(a)^{-K-1}}\right\}-(K)\left(\frac{r}{b}\right)^{-K-1}\left\{\frac{-\chi C(a)^{K-1}+\chi C(b)^{K-1}}{(a)^{K-1}-(b)^{2K}(a)^{-K-1}}\right\}+C\chi$$

Multiplying top and bottom terms by: $b^{-2K}a^{1+K}$

$$\sigma_\theta = K\left(\frac{r}{b}\right)^{K-1}\left\{\frac{-P(b)^{-1-K}(a)^{K-1}+Q}{(a)^{2K}(b)^{-2K}-1}\right\}-(K)\left(\frac{r}{b}\right)^{-K-1}\left\{\frac{-Q(a)^{2K}(b)^{-2K}+P(b)^{-K-1}(a)^{1-K}}{(a)^{2K}(b)^{-2K}-1}\right\}+$$

$$K\left(\frac{r}{b}\right)^{K-1}\left\{\frac{-\chi C(b)^{-1-K}(a)^{K-1}+\chi C}{(a)^{2K}(b)^{-2K}-1}\right\}-(K)\left(\frac{r}{b}\right)^{-K-1}\left\{\frac{-\chi C(a)^{2K}(b)^{-2K}+\chi C(b)^{-K-1}(a)^{1-K}}{(a)^{2K}(b)^{-2K}-1}\right\}+C\chi$$

$$\sigma_\theta = K\left(\frac{r}{b}\right)^{K-1}\left\{\frac{-P(c)^{K-1}+Q}{(c)^{2K}-1}\right\}-(K)\left(\frac{r}{b}\right)^{-K-1}\left\{\frac{-Q(c)^{2K}+P(c)^{1-K}}{(c)^{2K}-1}\right\}+$$

$$K\left(\frac{r}{b}\right)^{K-1}\left\{\frac{-\chi C(c)^{K-1}+\chi C}{c^{2K}-1}\right\}-K\left(\frac{r}{b}\right)^{-K-1}\left\{\frac{-\chi C(c)^{2K}+\chi C(c)^{1+K}}{c^{2K}-1}\right\}+C\chi$$

Defining: $W_2 = \left[1 - K\left(\dfrac{r}{b}\right)^{K-1} \left\{ \dfrac{1-c^{K-1}}{1-c^{2K}} \right\} + K\left(\dfrac{r}{b}\right)^{-K-1} \left\{ \dfrac{\left(1-c^{K-1}\right)c^{K-1}}{1-c^{2K}} \right\} \right]$

Then σ_θ can be stated as:

$$\sigma_\theta = K\left(\dfrac{r}{b}\right)^{K-1} \left\{ \dfrac{-Pc^{K+1} + Q}{(c)^{2K} - 1} \right\} - (K)\left(\dfrac{b}{r}\right)^{K-1} \left\{ \dfrac{(-Qc^{K-1} + P)c^{1-K}}{(c)^{2K} - 1} \right\} + C\chi \; W_2$$

$$(4.26)$$

With knowledge of the stress distribution, the displacements of the cylinder are found. From equation (4.14), and knowing that F is a function of r only:

$$\varepsilon_\theta = \dfrac{u}{r}$$

$$u = \left(\beta_{21} \, \sigma_r + \beta_{22} \, \sigma_\theta + \dfrac{a_{23}}{a_{33}} \, C \right) r$$

$$(4.27)$$

From equation (4.9)

$$w = \int_0^l \varepsilon_z \, dz = \varepsilon_z l$$

$$(4.28)$$

where; (l) defines the length of the cylindrical section.

The radial displacement is found by expanding (4.27)

$$u = \dfrac{r}{\left(1-c^{2K}\right)} \left[\left(Pc^{K-1} - Q\right)\left(\beta_{21} + K\beta_{22}\right)\left(\dfrac{r}{b}\right)^{K-1} + c^{K-1}\left(P - Qc^{K-1}\right)\left(-\beta_{21} + K\beta_{22}\right)\left(\dfrac{b}{r}\right)^{K-1} \right] +$$

$$r\dfrac{a_{23}}{a_{33}} C + Cr\chi(\beta_{21} + \beta_{22}) + \dfrac{C\chi r}{\left(1-c^{2K}\right)}\left[(\beta_{21} + K\beta_{22})P^{K-1}\left(c^{K-1} - 1\right) + \left(-\beta_{21} + K\beta_{22}\right)P^{-K-1}\left(1-c^{K-1}\right)c^{K-1} \right]$$

$$(4.29)$$

Since the problem of interest is a laminated orthotropic cylinder constructed of many distinct layers, it is appropriate to introduce additional notation when carrying towards a general solution. With reference to Figure 4.5, the superscript and subscript (m)

denotes the successive layers (orthotropic units) from the inside to the outermost layer (n). Specific radii or surfaces upon which a pressure is acting are denoted by a and q with subscript (m). Because there exists one more definable surface than the actual number of layers (n), the innermost surface is defined at radius a_0 and consequently all successive surfaces are defined at the outer limit of each layer up to a_n, the vessel exterior.

$$(m) = 0,1,2,3,\dots n$$

$$c_m = \frac{a_{m-1}}{a_m} \quad ;$$

$a = a_0$; inside surface

$b = a_n$; outside surface

$$K_m = \left(\frac{\beta_{11}^{(m)}}{\beta_{22}^{(m)}} \right)^{1/2}$$

$a_m =$ outer surface of mth layer

The boundary conditions at the inside and outside of the cylinder are:

$$\sigma_r^{(o)} = -P$$
$$\sigma_r^{(n)} = -Q$$

Since adjacent layers are bonded, the following conditions must be fulfilled:

when; $r = a_{m-1}$; $\sigma_r^{(m-1)} = \sigma_r^{(m)}$

$$u^{(m-1)} = u^{(m)}$$

Furthermore, we define $q_{(m-1)}$ and $q_{(m)}$ as the normal forces acting on internal and external surfaces of the mth layer.

Cylindrical Wall

q_n

r

α

−α

z

F

F

q_o

End Closure

L

Configuration of the Pressure Vessel

b = a_n

θ

Layer (m+1) of ± α_{m+1}

Layer m of ± α

a_{m-1}

q_m

a_m

a_o

a_{m-1}

r

a_m

a_{m-1}

Enlarged View of the Cross Section
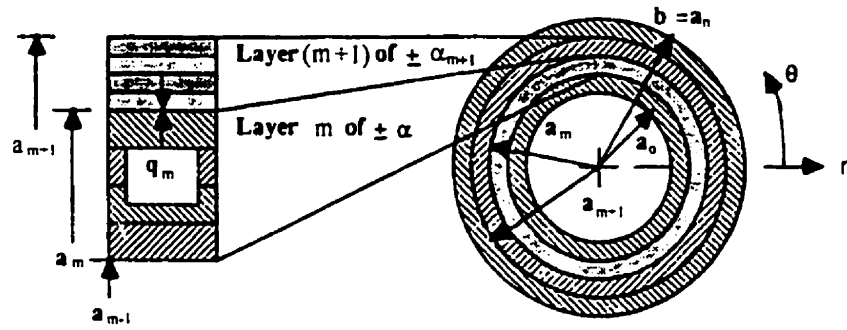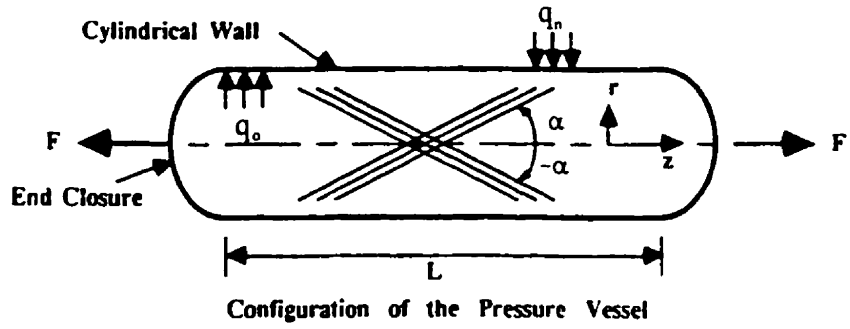
Figure 4.5 Cylindrical cross-section definitions. Adapted from [95].

The stresses and displacements for each layer can be expressed as:

$$\sigma_r^{(m)} = \frac{1}{1-c_m^{2K_m}}\left[\left(q_{m-1}\ c_m^{K_m-1} - q_m\right)\left(\frac{r}{a_m}\right)^{K_m-1} - \left(q_{m-1} - q_m\ c_m^{K_m-1}\right)\left(c_m^{K_m-1}\right)\left(\frac{a_m}{r}\right)^{K_m-1}\right] +$$

$$C\chi\left\{1-\left(\frac{r}{a_m}\right)^{K_m-1}\left(\frac{1-c^{K_m-1}}{1-c_m^{2K_m}}\right) - \left(\frac{r}{a_m}\right)^{-K_m-1}\left(\frac{1-c_m^{K_m-1}}{1-c_m^{2K_m}}\right)c_m^{K_m-1}\right\}$$

(4.30)

179

$$\sigma_\theta^{(m)} = \frac{K_m}{1-c_m^{2K_m}}\left[\left(q_{m-1}\,c_m^{\,K_m-1}-q_m\right)\left(\frac{r}{a_m}\right)^{K_m-1}+\left(q_{m-1}-q_m\,c_m^{\,K_m-1}\right)\left(c_m^{\,K_m-1}\right)\left(\frac{a_m}{r}\right)^{K_m-1}\right]+$$

$$C\chi\left\{1-K_m\left(\frac{r}{a_m}\right)^{K_m-1}\left(\frac{1-c_m^{\,K_m-1}}{1-c_m^{2K_m}}\right)+K_m\left(\frac{r}{a_m}\right)^{-K_m-1}\left(\frac{1-c_m^{\,K_m-1}}{1-c_m^{2K_m}}\right)c_m^{\,K_m-1}\right\}$$

$$\text{(4.31)}$$

From equation (4.12) the layer axial stress is:

$$\sigma_z^{(m)} = \left[\frac{C-a_{13}^{(m)}\sigma_r^{(m)}-a_{23}^{(m)}\sigma_\theta^{(m)}}{a_{33}^{(m)}}\right] = \left[\beta_{12}^{(m)}\sigma_r^{(m)}+\beta_{22}^{(m)}\sigma_\theta^{(m)}+\left(\frac{a_{23}}{a_{33}}\right)^{(m)}C\right]r$$

$$\text{(4.32)}$$

$$u^{(m)}=\varepsilon_\theta^{(m)}\,r=$$

$$u^{(m)}=\frac{a_m}{1-c_m^{2K_m}}\left[\left(q_{m-1}\,c_m^{\,K_m-1}-q_m\right)\left(\beta_{22}^{(m)}K^{(m)}+\beta_{12}^{(m)}\right)\left(\frac{r}{a_m}\right)^{K_m}+\right.$$

$$\left(q_{m-1}\,c_m^{\,K_m-1}-q_m\,c_m^{2K_m}\right)\left(\beta_{22}^{(m)}K^{(m)}-\beta_{12}^{(m)}\right)\left(\frac{a_m}{r}\right)^{K_m}\right]+\left(\frac{a_{23}}{a_{33}}\right)^{(m)}Cr+$$

$$Cr\chi^{(m)}\left(\beta_{21}^{(m)}+\beta_{22}^{(m)}\right)+\frac{C\chi^{(m)}a_m}{1-c_m^{2K_m}}\left[\left(\beta_{21}^{(m)}+K^{(m)}\beta_{22}^{(m)}\right)\left(\frac{r}{a_m}\right)^{K_m}\left(c_m^{\,K_m-1}-1\right)+\right.$$

$$\left.\left(-\beta_{21}^{(m)}+K^{(m)}\beta_{22}^{(m)}\right)\left(c_m^{\,K_m-1}-c_m^{2K_m}\right)\left(\frac{a_m}{r}\right)^{K_m}\right\}$$

$$\text{(4.33)}$$

The average axial traction on a closed cylinder is known by equilibrium. The integral of forces acting on the individual layers must sum up to this same quantity.

$$\sum_{m=1}^{n}2\pi\int_{a_{m-1}}^{a_m}\sigma_z\,rdr=\pi(q_o-q_n)a_o^2+F$$

$$\text{(4.34)}$$

On the right hand side of the equation is the force due to the endcap and F is an applied external force.

Equation (4.34) can be expanded by substituting from (4.32) and integrating appropriately. The result will be an expression for C as a function of the interface pressures "q_m". First substituting (4.30) and (4.31) into (4.32) expresses $\sigma_z^{(m)}$ as:

$$
\sigma_z^{(m)} = \frac{-q_{m-1}}{a_{33}^{(m)}(1-c_m^{2K_m})}\left[c_m^{K_m-1}\left(a_{13}^{(m)}+K_m a_{23}^{(m)}\right)\left(\frac{r}{a_m}\right)^{K_m-1} - \right.
$$

$$
\left.\left(c_m^{K_m-1}\right)\left(a_{13}^{(m)}-K_m a_{23}^{(m)}\right)\left(\frac{a_m}{r}\right)^{K_m-1}\right] - \frac{q_m}{a_{33}^{(m)}(1-c_m^{2K_m})}\left[-\left(a_{13}^{(m)}+K_m a_{23}^{(m)}\right)\left(\frac{r}{a_m}\right)^{K_m-1}+\right.
$$

$$
\left.\left(c_m^{2K_m}\right)\left(a_{13}^{(m)}-K_m a_{23}^{(m)}\right)\left(\frac{a_m}{r}\right)^{K_m-1}\right] + \frac{C}{a_{33}^{(m)}} - \frac{C\chi^{(m)}\left(a_{13}^{(m)}+a_{23}^{(m)}\right)}{\left(1-c_m^{2k_m}\right)a_{33}^{(m)}} -
$$

$$
\frac{C\chi^{(m)}\left(a_{13}^{(m)}+K_m a_{23}^{(m)}\right)}{a_{33}^{(m)}\left(1-c_m^{2K_m}\right)}\left[-\left(\frac{r}{a_m}\right)^{K_m-1}\left(1-c^{K_m-1}\right)\right] - \frac{C\chi^{(m)}\left(-a_{13}^{(m)}+K_m a_{23}^{(m)}\right)}{a_{33}^{(m)}\left(1-c_m^{2K_m}\right)}\left[\left(\frac{a_m}{r}\right)^{K_m-1}\left(1-c_m^{K_m-1}\right)c^{K_m-1}\right]
$$

(4.35)

Equation (4.34) can be restated as:

$$
\left(2\sum_{m=1}^{n}\int_{a_{m-1}}^{a_m} r\,\sigma_z\,dr\right) - \left((q_o-q_n)a_o^2+\frac{F}{\pi}\right) = 0
$$

Expansion of the summation term above, using $\sigma_z^{(m)}$ as expressed in (4.35), now yields:

$$
2\sum_{m=1}^{m}\left\{\frac{-q_{m-1}}{a_{33}^{(m)}(1-c_m^{2K_m})}\left[c_m^{K_m-1}\left(a_{13}^{(m)}+K_m a_{23}^{(m)}\right)\int_{a_{m-1}}^{a_m} r\left(\frac{r}{a_m}\right)^{K_m-1}dr - \right.\right.
$$

$$
\left.\left(c_m^{K_m-1}\right)\left(a_{13}^{(m)}-K_m a_{23}^{(m)}\right)\int_{a_{m-1}}^{a_m} r\left(\frac{a_m}{r}\right)^{K_m-1}dr\right] + \frac{-q_m}{a_{33}^{(m)}(1-c_m^{2K_m})}\left[-\left(a_{13}^{(m)}+K_m a_{23}^{(m)}\right)\cdot\right.
$$

$$
\left.\int_{a_{m-1}}^{a_m} r\left(\frac{r}{a_m}\right)^{K_m-1}dr + c_m^{2K_m}\left(a_{13}^{(m)}-K_m a_{23}^{(m)}\right)\int_{a_{m-1}}^{a_m} r\left(\frac{a_m}{r}\right)^{K_m-1}dr\right] + \frac{C}{a_{33}^{(m)}}\int_{a_{m-1}}^{a_m} rdr - \rightarrow
$$

$$\frac{C\chi^{(m)}\left(a_{13}^{(m)}+a_{23}^{(m)}\right)}{2a_{33}^{(m)}}\int_{a_{m-1}}^{a_m}r\,dr - \frac{C\chi^{(m)}\left(a_{13}^{(m)}+K_m a_{23}^{(m)}\right)}{\left(1-c_m^{2K_m}\right)}\left[\left(1-c^{K_m-1}\right)\int_{a_{m-1}}^{a_m}r\left(\frac{r}{a_m}\right)^{K_m-1}dr\right] -$$

$$\frac{C\chi^{(m)}\left(-a_{13}^{(m)}+K_m a_{23}^{(m)}\right)\left(1-c_m^{K_m-1}\right)c^{K_m-1}}{\left(1-c_m^{2K_m}\right)}\int_{a_{m-1}}^{a_m}r\left(\frac{a_m}{r}\right)^{K_m-1}dr\Bigg\}$$

<div align="right">(4.36)</div>

The integrals in (4.36) are developed. The first integral is:

$$\int_{a_{m-1}}^{a_m}r\left(\frac{r}{a_m}\right)^{K_m-1}dr = \left(\frac{1}{a_m}\right)^{K_m-1}\left(\frac{a_m^{K_m+1}-a_{m-1}^{K_m+1}}{K_m+1}\right) = \frac{a_m^2\left(1-\left(\frac{a_{m-1}}{a_m}\right)^{K_m-1}\right)}{K_m+1}$$

$$=\left(\frac{a_m^2\left(1-c_m^{K_m+1}\right)}{K_m+1}\right) = \frac{a_m^2\left(1-c_m^{K_m}\left(\frac{a_{m-1}}{a_m}\right)\right)}{K_m+1} = \frac{a_m\left(a_m-c_m^{K_m}a_{m-1}\right)}{K_m+1}$$

The second integral is:

$$\int_{a_{m-1}}^{a_m}r\left(\frac{a_m}{r}\right)^{K_m+1}dr = a_m^{K_m-1}\int_{a_{m-1}}^{a_m}r^{-K_m}dr = \frac{a_m^{K_m-1}(r)^{-K_m-1}}{-K_m+1}\bigg|_{a_{m-1}}^{a_m}$$

$$=\frac{a_m^2\left(\frac{a_m}{r}\right)^{K_m-1}}{1-K_m}\bigg|_{a_{m-1}}^{a_m} = \frac{a_m^2\left[\left(\frac{a_m}{a_m}\right)^{K_m-1}-\left(\frac{a_m}{a_{m-1}}\right)^{K_m-1}\right]}{1-K_m}$$

$$=\frac{a_m^2\left[1-\left(\frac{a_{m-1}}{a_m}\right)^{-K_m}\left(\frac{a_{m-1}}{a_m}\right)\right]}{1-K_m} = \frac{a_m^2\left[1-c_m^{-K_m}\left(\frac{a_{m-1}}{a_m}\right)\right]}{1-K_m} = \frac{a_m\left(a_m-c_m^{-K_m}a_{m-1}\right)}{1-K_m}$$

<div align="right">(4.37)</div>

The summation applied to (4.36) can now be written out. The first part expands to:

$$\frac{-q_{m-1}}{a_{33}^{(m)}\left(1-c_m^{2K_m}\right)}\left[c_m^{K_m+1}\left(a_{13}^{(m)}+K_m a_{23}^{(m)}\right)(a_m)\frac{\left(a_m-c_m^{K_m}a_{m-1}\right)}{K_m+1} - \right.$$

$$\left. \left(a_{13}^{(m)}-K_m a_{23}^{(m)}\right)\left(c_m^{K_m+1}\right)\frac{\left(a_m^2\left[1-c_m^{-K_m}\left(a_{m-1}/a_m\right)\right]\right)}{1-K_m}\right]$$

<div align="right">(4.38)</div>

<div align="center">182</div>

The tail end of the above equation can be simplified to:

$$\frac{c_m^{K_m-1}\left\{a_m^2\left[1-c_m^{-K_m}\left(\frac{a_{m-1}}{a_m}\right)\right]\right\}}{1-K_m} = \frac{\frac{a_{m-1}}{a_m}\left(a_m^2 c_m^{K_m} - \frac{a_{m-1} a_m^2}{a_m}\right)}{1-K_m} = \frac{a_{m-1}\left(a_m c_m^{K_m} - a_{m-1}\right)}{1-K_m}$$

The summation in (4.38) is revised to:

$$\frac{-q_{m-1}}{a_{33}^{(m)}\left(1-c_m^{2K_m}\right)}\left[c_m^{K_m-1}\left(a_{13}^{(m)} + K_m a_{23}^{(m)}\right)(a_m)\frac{\left(a_m - c_m^{K_m} a_{m-1}\right)}{K_m+1} - \left(a_{13}^{(m)} - K_m a_{23}^{(m)}\right)(a_{m-1})\frac{\left(a_m c_m^{K_m} - a_{m-1}\right)}{1-K_m}\right]$$

(4.39)

The second part of the summation term in (4.36) can be written as:

$$\frac{-q_m}{a_{33}^{(m)}\left(1-c_m^{2K_m}\right)}\left\{-\left(a_{13}^{(m)} + K_m a_{23}^{(m)}\right)(a_m)\frac{\left(a_m - c_m^{K_m} a_{m-1}\right)}{K_m+1} + \right.$$

$$\left. \left(a_{13}^{(m)} - K_m a_{23}^{(m)}\right)\left(c_m^{2K_m}\right)a_m^2\frac{\left[1-c_m^{-K_m}\left(a_{m-1}\,a_m\right)\right]}{1-K_m}\right\}$$

The last part of the above equation can be simplified to:

$$\frac{c_m^{2K_m}\left[a_m^2\left(1-c_m^{-K_m}\frac{a_{m-1}}{a_m}\right)\right]}{1-K_m} = \frac{c_m^{K_m}\left[a_m^2 c_m^{K_m} - a_m^2\left(\frac{a_{m-1}}{a_m}\right)\right]}{1-K_m} = \frac{c_m^{K_m} a_m\left(a_m c_m^{K_m} - a_{m-1}\right)}{1-K_m}$$

The second part of the summation in (4.36) can be revised to:

$$\frac{-q_m}{a_{33}^{(m)}\left(1-c_m^{2K_m}\right)}\left[-\left(a_{13}^{(m)} + K_m a_{23}^{(m)}\right)(a_m)\frac{\left(a_m - c_m^{K_m} a_{m-1}\right)}{K_m+1} + \right.$$

$$\left. \left(a_{13}^{(m)} - K_m a_{23}^{(m)}\right)\frac{\left(c_m^{K_m} a_m\right)\left(a_m c_m^{K_m} - a_{m-1}\right)}{1-K_m}\right]$$

(4.40)

And the last terms of (4.36) are:

$$\frac{C(a_m^2 - a_{m-1}^2)}{2a_{33}^{(m)}} - \frac{C\chi^{(m)}\left(a_{13}^{(m)} + a_{23}^{(m)}\right)\left(a_m^2 - a_{m-1}^2\right)}{2a_{33}^{(m)}\left(1 - c_m^{2K_m}\right)} + \frac{C\chi^{(m)}\left(a_{13}^{(m)} + K_m a_{23}^{(m)}\right)\left(1 - c_m^{K_m-1}\right)a_m\left(a_m - c_m^{K_m}a_{m-1}\right)}{a_{33}^{(m)}\left(1 - c_m^{2K_m}\right)(K_m + 1)} +$$

$$\frac{C\chi^{(m)}\left(a_{13}^{(m)} - K_m a_{23}^{(m)}\right)\left(1 - c_m^{K_m-1}\right)a_m\left(a_m - c_m^{-K_m}a_{m-1}\right)c_m^{K_m-1}}{a_{33}^{(m)}\left(1 - c_m^{2K_m}\right)(1 - K_m)}$$

defining:

$$W_1^{(m)} = \frac{\left(a_m^2 - a_{m-1}^2\right)}{2a_{33}^{(m)}}$$

$$W_2^{(m)} = \frac{\chi^{(m)}\left(a_{13}^{(m)} + a_{23}^{(m)}\right)\left(a_m^2 - a_{m-1}^2\right)}{2a_{33}^{(m)}\left(1 - c_m^{2K_m}\right)}$$

$$W_3^{(m)} = \frac{\chi^{(m)}\left(a_{13}^{(m)} + K_m a_{23}^{(m)}\right)\left(1 - c_m^{K_m-1}\right)a_m\left(a_m - c_m^{K_m}a_{m-1}\right)}{a_{33}^{(m)}\left(1 - c_m^{2K_m}\right)(K_m + 1)}$$

$$W_4^{(m)} = \frac{\chi^{(m)}\left(a_{13}^{(m)} - K_m a_{23}^{(m)}\right)\left(1 - c_m^{K_m-1}\right)a_m\left(a_m - c_m^{-K_m}a_{m-1}\right)c_m^{K_m-1}}{a_{33}^{(m)}\left(1 - c_m^{2K_m}\right)(1 - K_m)}$$

Defining δ_m as expresssion (4.39) with the multiplier $q_{(m-1)}$ removed and defining χ_m as expression (4.40) with the multiplier q_m removed, equation (4.34) can be recast:

$$2\sum_{m=1}^{n}\left[\delta_m q_{m-1} + \chi_m q_m + C\left[W_1^{(m)} - W_2^{(m)} + W_3^{(m)} + W_4^{(m)}\right]\right] - (q_o - q_n)a_o^2 - \frac{F}{\pi} = 0$$

(4.41)

Solving for C, we have:

$$C = \frac{(q_o - q_n)a_o^2 + \frac{F}{\pi} - 2\sum_{m=1}^{n}\left[\delta_m q_{m-1} + \chi_m q_m\right]}{2\sum_{m=1}^{n}\left[W_1^{(m)} - W_2^{(m)} + W_3^{(m)} + W_4^{(m)}\right]}$$

(4.42)

The constant axial strain C cannot be determined until the interface pressures q_m

are known. The condition of equal radial displacement u at the boundary between any two

adjacent layers permits additional equations allowing a determination of the interface

pressures.

$$u^{(m+1)} - u^{(m)} = 0$$

(4.43)

The boundary displacement, equation (4.43), can be expanded by substituting (4.33) and

putting $r = a_m$. This yields the following:

$$u^{(m+1)} - u^{(m)} = \frac{a_{m+1}}{1 - c_{m+1}^{2k_{m+1}}}\left[\left(q_m c_{m+1}^{K_{m+1}-1} - q_{m+1}\right)\left(\beta_{22}^{m+1}K^{m+1} + \beta_{12}^{m+1}\right)\left(\frac{a_m}{a_{m+1}}\right)^{K_{m+1}} + \right.$$

$$\left. \left(q_m c_{m+1}^{K_{m+1}-1} - q_{m+1}c_{m+1}^{2K_{m+1}}\right)\left(\beta_{22}^{m+1}K_{m+1} - \beta_{12}^{m+1}\right)\left(\frac{a_{m+1}}{a_m}\right)^{K_{m+1}}\right] -$$

$$\frac{a_m}{1 - c_m^{2k_m}}\left[\left(q_{m-1}c_m^{K_m+1} - q_m\right)\left(\beta_{22}^m K^m + \beta_{12}^m\right)\left(\frac{a_m}{a_m}\right)^{K_m} + \left(q_{m-1}c_m^{K_m-1} - q_m c_m^{2K_m}\right)\left(\beta_{22}^m K^m - \beta_{12}^m\right)\left(\frac{a_m}{a_m}\right)^{K_m}\right] +$$

$$+\left[\left(\frac{a_{23}}{a_{33}}\right)_{m+1} - \left(\frac{a_{23}}{a_{33}}\right)_m\right]a_m C + Ca_m\left[\chi^{m+1}\left(\beta_{21}^{m+1} + \beta_{22}^{m+1}\right) - \chi^m\left(\beta_{21}^m + \beta_{22}^m\right)\right]$$

The terms can be re-grouped:

$$\frac{C\chi^{m+1}a_{m+1}}{\left(1 - c_{m+1}^{2K_{m+1}}\right)}\left\{\left(\beta_{21}^{m+1} + K^{m+1}\beta_{22}^{m+1}\right)\left(\frac{a_m}{a_{m+1}}\right)^{K_{m+1}}\left(c_{m+1}^{K_{m+1}-1} - 1\right) + \left(-\beta_{21}^{m+1} + K^{m+1}\beta_{22}^{m+1}\right)\cdot\right.$$

$$\left. \left(c_{m+1}^{K_{m+1}-1} - c_{m+1}^{2K_{m+1}}\right)\left(\frac{a_{m+1}}{a_m}\right)^{K_{m+1}}\right\} -$$

$$\frac{C\chi^m a_m}{\left(1 - c_m^{2K_m}\right)}\left\{\left(\beta_{21}^m + K^m\beta_{22}^m\right)\left(\frac{a_m}{a_m}\right)^{K_m}\left(c_m^{K_m-1} - 1\right) + \left(-\beta_{21}^m + K^m\beta_{22}^m\right)\left(c_m^{K_m-1} - c_m^{2K_m}\right)\left(\frac{a_m}{a_m}\right)^{K_m}\right\}$$

Defining:

$$Y_1 = \left[\left(\frac{a_{23}}{a_{33}} \right)_{m-1} - \left(\frac{a_{23}}{a_{33}} \right)_m \right] a_m$$

$$Y_2 = a_m \left[\chi^{m-1} \left(\beta_{21}^{m+1} + \beta_{22}^{m+1} \right) - \chi^m \left(\beta_{21}^m + \beta_{22}^m \right) \right]$$

$$Y_3 = \frac{\chi^{m-1} a_{m+1}}{\left(1 - c_{m-1}^{2K_{m-1}} \right)} \left\{ \left(\beta_{21}^{m-1} + K^{m-1} \beta_{22}^{m-1} \right) \left(\frac{a_m}{a_{m+1}} \right)^{K_{m-1}} \left(c_{m-1}^{K_{m-1}-1} - 1 \right) + \left(-\beta_{21}^{m-1} + K^{m-1} \beta_{22}^{m+1} \right) \cdot \right.$$

$$\left. \left(c_{m-1}^{K_{m-1}-1} - c_{m-1}^{2K_{m-1}} \right) \left(\frac{a_{m+1}}{a_m} \right)^{K_{m-1}} \right\}$$

$$Y_4 = \frac{\chi^m a_m}{\left(1 - c_m^{2K_m} \right)} \left\{ \left(\beta_{21}^m + K^m \beta_{22}^m \right) \left(\frac{a_m}{a_m} \right)^{K_m} \left(c_m^{K_m-1} - 1 \right) + \left(-\beta_{21}^m + K^m \beta_{22}^m \right) \left(c_m^{K_m-1} - c_m^{2K_m} \right) \left(\frac{a_m}{a_m} \right)^{K_m} \right\}$$

$$u^{(m-1)} - u^{(m)} = \frac{q_m a_{m-1} c_{m-1}^{K_{m-1}-1}}{1 - c_{m-1}^{2K_{m-1}}} \left[(\beta_{22}^{(m+1)} K_{m-1} + \beta_{12}^{(m+1)}) \left(\frac{a_m}{a_{m+1}} \right)^{K_{m-1}} + \right.$$

$$\left. (-\beta_{12}^{(m-1)} + K_{m-1} \beta_{22}^{(m+1)}) \left(\frac{a_{m-1}}{a_m} \right)^{K_{m-1}} \right] - \frac{q_{m-1} a_{m+1}}{1 - c_{m+1}^{2K_{m-1}}} \left[(\beta_{22}^{(m+1)} K_{m-1} + \beta_{12}^{(m+1)}) \left(\frac{a_m}{a_{m+1}} \right)^{K_{m-1}} + \right.$$

$$\left. c_{m+1}^{2K_{m-1}} (-\beta_{12}^{(m-1)} + K_{m-1} \beta_{22}^{(m-1)}) \left(\frac{a_{m-1}}{a_m} \right)^{K_{m-1}} \right] - \frac{q_{m-1} a_m c_m^{K_m-1}}{1 - c_m^{2K_m}} \left[(\beta_{22}^{(m)} K_m + \beta_{12}^{(m)}) \left(\frac{a_m}{a_m} \right)^{K_m} + \right.$$

$$\left. (-\beta_{12}^{(m)} + K_m \beta_{22}^{(m)}) \left(\frac{a_m}{a_m} \right)^{K_m} \right] + \frac{q_m a_m}{1 - c_m^{2K_m}} \left[(\beta_{22}^{(m)} K_m + \beta_{12}^{(m)}) \left(\frac{a_m}{a_m} \right)^{K_m} + \right.$$

$$\left. c_m^{2K_m} (-\beta_{12}^{(m)} + K_m \beta_{22}^{(m)}) \left(\frac{a_m}{a_m} \right)^{K_m} \right] + C \left[Y_1^{(m)} + Y_2^{(m)} + Y_3^{(m)} + Y_4^{(m)} \right]$$

Redefining some of the coefficient terms is necessary. Using the substitutions

$a_{m-1} = c_{m-1}^{-1} a_m$ and $a_m = c_m^{-1} a_{m-1}$ the following form can be attained.

$$u^{(m+1)} - u^{(m)} = \frac{q_m\, a_m\, c_{m-1}^{K_{m-1}}}{1 - c_{m-1}^{2K_{m-1}}} \left[\left(\beta_{22}^{(m+1)} K_{m+1} + \beta_{12}^{(m+1)} \right) c_{m-1}^{K_{m-1}} + \right.$$

$$\left. \left(-\beta_{12}^{(m+1)} + K_{m+1}\, \beta_{22}^{(m-1)} \right) c_{m-1}^{-K_{m-1}} \right] - \frac{q_{m+1}\, a_{m+1}}{1 - c_{m+1}^{2K_{m+1}}} \left[\left(\beta_{22}^{(m+1)} K_{m+1} + \beta_{12}^{(m+1)} \right) c_{m+1}^{K_{m+1}} + \right.$$

$$\left. c_{m+1}^{2K_{m+1}} \left(-\beta_{12}^{(m+1)} + K_{m+1}\, \beta_{22}^{(m-1)} \right) c_{m+1}^{-K_{m+1}} \right] - \frac{q_{m-1}\, a_{m-1}\, c_m^{K_m}}{1 - c_m^{2K_m}} \left[\left(\beta_{22}^{(m)} K_m + \beta_{12}^{(m)} \right) + \right.$$

$$\left. \left(-\beta_{12}^{(m)} + K_m\, \beta_{22}^{(m)} \right) \right] + \frac{q_m\, a_m}{1 - c_m^{2K_m}} \left[\left(\beta_{22}^{(m)} K_m + \beta_{12}^{(m)} \right) + c^{2K_m} \left(-\beta_{12}^{(m)} + K_m\, \beta_{22}^{(m)} \right) \right] +$$

$$C \left[Y_1^{(m)} + Y_2^{(m)} + Y_3^{(m)} + Y_4^{(m)} \right]$$

where: C has been defined by (4.42).

Re-arranging and combining terms yields:

$$u^{(m+1)} - u^{(m)} = \frac{-q_{m-1}\, a_{m-1}\, c_m^{K_m}}{1 - c_m^{2K_m}} \left(2\beta_{22}^{(m)} K_m \right) - \frac{q_{m+1}\, a_{m+1}\, c_{m-1}^{K_{m-1}}}{1 - c_{m-1}^{2K_{m-1}}} \left(2\beta_{22}^{(m-1)} K_{m-1} \right) +$$

$$\frac{q_m\, a_m}{1 - c_m^{2K_m}} \left[\left(\beta_{22}^{(m)} K_m + \beta_{12}^{(m)} \right) + c_m^{2K_m} \left(-\beta_{12}^{(m)} + K_m\, \beta_{22}^{(m)} \right) \right] +$$

$$\frac{q_m\, a_m\, c_{m-1}^{K_{m-1}}}{1 - c_{m-1}^{2K_{m-1}}} \left[\left(\beta_{22}^{(m-1)} K_{m+1} + \beta_{12}^{(m-1)} \right) c_{m-1}^{K_{m-1}} + \left(-\beta_{12}^{(m+1)} + K_{m-1}\, \beta_{22}^{(m-1)} \right) c_{m-1}^{-K_{m-1}} \right] +$$

$$C \left[Y_1^{(m)} + Y_2^{(m)} + Y_3^{(m)} + Y_4^{(m)} \right]$$

$$(4.44)$$

The two terms with coefficients q_m in (4.44) can be rewritten as:

$$a_m\, q_m \left[\frac{1}{1 - c_m^{2K_m}} \left[\left(\beta_{22}^{(m)} K_m + \beta_{12}^{(m)} \right) + c^{2K_m} \left(-\beta_{12}^{(m)} + K_m\, \beta_{22}^{(m)} \right) \right] + \right.$$

$$\left. \frac{1}{1 - c_{m+1}^{2K_{m+1}}} \left[\left(\beta_{22}^{(m+1)} K_{m+1} + \beta_{12}^{(m+1)} \right) c_{m-1}^{2K_{m-1}} + \left(-\beta_{12}^{(m+1)} + K_{m-1}\, \beta_{22}^{(m-1)} \right) \right] \right]$$

rearrangement gives:

$$a_m\, q_m \left[\frac{1}{1 - c_m^{2K_m}} \left[(1 + c_m^{2K_m}) K_m\, \beta_{22}^{(m)} + (1 - c_m^{2K_m}) \beta_{12}^{(m)} \right] + \right.$$

$$\left. \frac{1}{1 - c_{m-1}^{2K_{m-1}}} \left[(1 + c_{m-1}^{2K_{m-1}}) K_{m+1}\, \beta_{22}^{(m-1)} + (c_{m+1}^{2K_{m-1}} - 1) \beta_{12}^{(m-1)} \right] \right]$$

187

After further simplification:

$$q_m a_m \left[\left[\left(\frac{(1+c_m^{2K_m})(K_m \beta_{22}^{(m)})}{1-c_m^{2K_m}} \right) + \beta_{12}^{(m)} \right] + \left[\left(\frac{(1+c_{m-1}^{2K_{m-1}})(K_{m-1}\beta_{22}^{(m-1)})}{1-c_{m-1}^{2K_{m-1}}} \right) - \beta_{12}^{(m-1)} \right] \right] $$

Defining the following two parameters:

$$\alpha_m = \frac{-c_m^{K_m}}{1-c_m^{2K_m}} \left(2\beta_{22}^{(m)} \right) K_m$$

$$\gamma_m = \left[\left[\left(\frac{(1+c_m^{2K_m})(K_m \beta_{22}^{(m)})}{1-c_m^{2K_m}} \right) + \beta_{12}^{(m)} \right] + \left[\left(\frac{(1+c_{m-1}^{2K_{m-1}})(K_{m-1}\beta_{22}^{(m-1)})}{1-c_{m-1}^{2K_{m-1}}} \right) - \beta_{12}^{(m-1)} \right] \right]$$

equation (4.44) can be reduced to:

$$0 = q_{m-1} a_{m-1} \alpha_m + q_m a_m \gamma_m + q_{m-1} a_{m+1} \alpha_{m-1} + C\left[Y_1^{(m)} + Y_2^{(m)} + Y_3^{(m)} + Y_4^{(m)} \right]$$

(4.45)

Making appropriate substitutions for C in (4.45) yields:

$$q_{m-1} a_{m-1} \alpha_m + q_m a_m \gamma_m + q_{m-1} a_{m-1} \alpha_{m-1} + \frac{\left[Y_1^{(m)} + Y_2^{(m)} + Y_3^{(m)} + Y_4^{(m)} \right]\left[(q_o - q_n)a_o^2 + \dfrac{F}{\pi} \right]}{2 \displaystyle\sum_{m=1}^{n} \left[W_1^{(m)} - W_2^{(m)} + W_3^{(m)} + W_4^{(m)} \right]} +$$

$$= \frac{2\left[Y_1^{(m)} + Y_2^{(m)} + Y_3^{(m)} + Y_4^{(m)} \right] \cdot \displaystyle\sum_{m=1}^{n} \left[\delta_m q_{m-1} + \chi_m q_m \right]}{2 \displaystyle\sum_{m=1}^{n} \left[W_1^{(m)} - W_2^{(m)} + W_3^{(m)} + W_4^{(m)} \right]}$$

(4.46)

where: $m = 1,2,3,\cdots (n\text{-}1)$

The preceding equation defines the interface pressure(s). However since in the general case many interfaces exist, a solution can only be obtained by writing out the

188

equality for all the interfaces and henceforth solving the equations simultaneously. Redefining some of the above quantities allows manipulation of the system into a matrix format. This provides a clearer view of the problem and renders solution via implementation of computer algorithms easier. The solution procedure used is outlined. Letting:

$$L = (q_o - q_n)a_o^2 + \frac{F}{\pi} \quad ; \quad \Delta = \sum_{m=1}^{n}\left[W_1^{(m)} - W_2^{(m)} + W_3^{(m)} + W_4^{(m)}\right]$$

Step 1:

L and Δ can be evaluated directly without knowledge of interface pressures, and thus become constants for any given problem.

Step 2:

With L and Δ known, two column matrices are defined:

$$[V] = \frac{2\left[Y_1^{(m)} + Y_2^{(m)} + Y_3^{(m)} + Y_4^{(m)}\right]}{\Delta}$$

$$m = 1,2,3,\ldots(n-1)$$

$$[F] = \frac{L\left[Y_1^{(m)} + Y_2^{(m)} + Y_3^{(m)} + Y_4^{(m)}\right]}{\Delta}$$

The above 2 column matrix values are defined for each interface, the number of interfaces being $(n-1)$ the number of layers (n).

Step 3:

The balance of equation (4.46) can also be broken into matrix format.

189

Defining: $[Q]$ a column matrix with $(n+1)$ terms

       $[D]$ a matrix of dimension $(n-1)$ $(n+1)$

       $[E]$ a matrix of dimension $(n-1)(n+1)$

The $[Q]$ matrix defines the pressures at each surface or interface.

$$[Q] = \begin{bmatrix} q_o \\ q_1 \\ q_2 \\ \Downarrow \\ q_n \end{bmatrix} \qquad \text{where: } q_m ; \quad m = 0,1,2,3...n$$

Each summation for $[\delta_i \ q_{i-1} + \chi_i \ q_i]$ represents a separate but

identical row in the $[D]$ matrix. The number of rows corresponds to the $(n-1)$ interfaces.

$$[D] = \begin{bmatrix} \delta_1, & (\chi_1 + \delta_2), & (\chi_2 + \delta_3), & (\chi_m + \delta_{m+1}), & \cdots & (\chi_{n-1} + \delta_n), & \chi_n \\ \delta_1, & (\chi_1 + \delta_2), & (\chi_2 + \delta_3), & (\chi_m + \delta_{m+1}), & \cdots & (\chi_{n-1} + \delta_n), & \chi_n \\ \Downarrow & \Downarrow & \Downarrow & \Downarrow & & \Downarrow & \Downarrow \end{bmatrix}$$

where for: $\delta_m . \chi_m ; \quad m = 1,2,3,...n \qquad ; \qquad n = $ number of layers

$$[E] = \begin{bmatrix} a_o \alpha_1 & a_1 \gamma_1 & a_2 \alpha_2 & 0 & 0 & 0 & 0 \\ 0 & a_1 \alpha_2 & a_2 \gamma_2 & a_3 \alpha_3 & 0 & 0 & 0 \\ 0 & 0 & a_{m-1} \alpha_m & a_m \gamma_m & a_{m+1} \alpha_{m+1} & 0 & 0 \\ 0 & 0 & 0 & \Downarrow & \Downarrow & \Downarrow & 0 \\ 0 & 0 & 0 & 0 & a_{n-1} \alpha_n & a_n \gamma_n & a_{n+1} \alpha_{n+1} \end{bmatrix}$$

where for: $a_m , \alpha_m , \gamma_m ; \quad m = 1,2,3,...n \qquad ; \qquad n = $ number of layers

The foregoing definitions permit writing equation (4.46) in a matrix form which

reduces as follows.

$$\{[V][D]\}[Q] - [E][Q] = [F]$$

$$[P][Q] = [F]$$

$$[P^*][Q^*] = [F^*]$$

$[E][Q]$ and $\{[V][D]\}[Q]$ each produce $(n\text{-}1)$ equations with $(n\div 1)$ terms. Thus the left hand side (*LHS*) can be combined and represented by the matrix $[P]$. In $[Q]$, q_o and q_n are known (internal and external pressure) hence when $[P][Q]$ is multiplied out the first and last columns of the *LHS* result in knowns that can be subtracted from the matrix $[F]$ (consisting entirely of knowns). The matrices resulting from this subtraction are represented by $[P^*],[Q^*]$ and $[F^*]$. Since $[P^*]$ is square (dimension $(n\text{-}1)(n\text{-}1)$) and each of column matrices $[Q^*]$ and $[F^*]$ is size $(n\text{-}1)$, the system becomes amenable to solution.

The "Super Pressure Vessel Designer" program uses LU decomposition with partial pivoting (ref. [164]) to solve for the interface pressures represented by $[Q^*]$. The program then employs equation (4.42) to compute the constant axial displacement C and thereafter calculates the individual layer stresses via equations (4.30), (4.31), (4.32) for σ_r σ_θ, and σ_z respectively.

Chapter 5

Generalized Plane Strain and Closed-Form Variable Property Solutions

5.0 Generalized Plane Strain Cylindrical Relations

This chapter explores the cylindrical elasticity relations with the aim of bringing some clarity to origins of the equations, implicit assumptions and details not found in any of the texts or papers cited in the references. To this aim the results are constructed from basics. It is felt that many researchers have neglected such a tedious task and thereby also fallen victim to either typographic errors as present in Lekhnitskii's work *Anisotropic Bodies* [88] or misapplied / misinterpreted the equations, especially as concerns the undetermined constants of integration. In virtually all cases, because of the simplifying assumptions made (though perhaps not necessarily understood) the outcome is unaffected. As we will see, a true layer by layer solution is far more complex as it involves shear stresses and twisting effects that must be solved simultaneous with axial contractions. This is a daunting endeavor for a multilayered vessel. Here the equations are presented in full for only one such layer.

Elasticity relations in cylindrical coordinates are usually stated without considering fully the possibility of deformations in the axial coordinate direction z. A definition of the generalized plane strain condition is that it entails lateral forces to act in planes normal to the axis (generators) and not to vary along the length of the assumed infinite body. A

192

primary consequence is that stresses and strains (but not necessarily displacements) must show no variation in z. This eliminates $\partial/\partial z$ from the equilibrium equation (4.10).

If there are planes of elastic symmetry normal to the generators, the cross-sections remain plane under loading, the case of pure plane strain. If however there are planes of elastic symmetry but none of them lie parallel to the r-θ plane, and particularly in the case of anisotropy, the deformation is no longer plane strain. In this case it is not possible to satisfy all equations and conditions of the theory of elasticity with the assumption that axial displacement $w = 0$; the cross-sections will warp and / or twist but all identically. This kind of deformation is described as *generalized plane strain*, in distinction with pure plane strain. In generalized plane strain the restriction $w = 0$ is loosened to $\varepsilon_z = \partial w/\partial z =$ *constant*. This implies that $w = Dz + W_1(r,\theta)$. Axial displacement is thus permitted as a function of z and as a more general function of r and θ. For a body of finite length, the deformation is not strictly generalized plane strain since the displacements will depend on z unless the forces acting over the ends are distributed in a manner identical to the internal stresses $\tau_{rz}, \tau_{\theta z}, \sigma_z$ present within a cross-section of the infinite body.

Figure 5.1 depicts resultant stresses, forces and moments acting over the ends of a long cylinder. However on the basis of Saint-Venant's principle, it is known that the exact stress distribution over the ends present in a finite body will assume those of an infinite body at some characteristic distance from a local abnormality. In composites this distance is much greater because stresses are channeled along the fibers, nevertheless it exists, and for a typical graphite-epoxy such as T300/5208 it is approximately 4 times greater than the characteristic thickness dimension that would normally associated with an isotropic case of

the same geometry [104]. If the ends of a finite body are free from forces and are not

fixed, the following exact conditions must be met at the ends: $\tau_{rz} = \tau_{\theta z} = \tau_{r\theta} = 0$.

Alternately these conditions may be replaced by appropriate ones requiring that the

resultant force vector and resultant moment of the forces at the ends equal zero. If there

exist resulting moments or forces acting over the ends of a finite body, then solutions for

the infinite case can be utilized (excluding local end regions) by equating the external

resultants with the undetermined constants of integration entering the solution for

displacements to be presented subsequently.
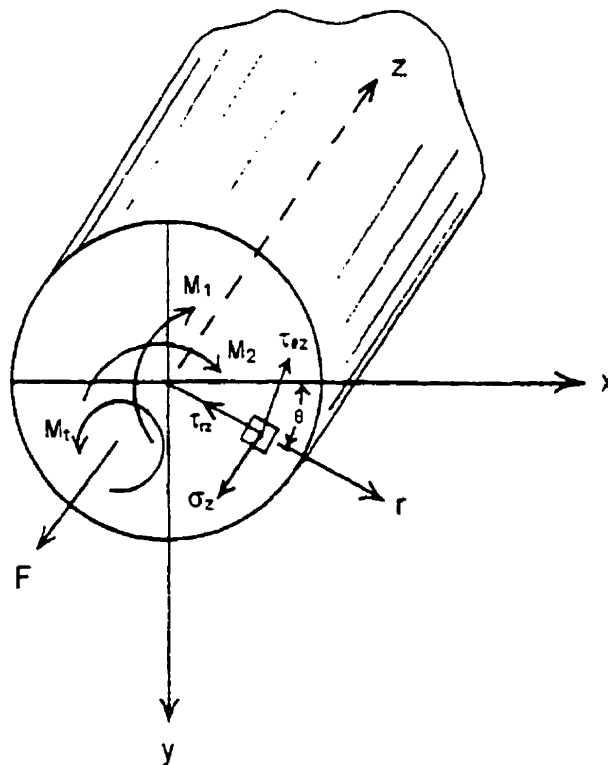
Figure 5.1 End conditions for cylindrical body

Equations (4.9) and (4.11) combine to give:

$$\varepsilon_r = \frac{\partial u}{\partial r} = a_{11}\sigma_r + a_{12}\sigma_\theta + a_{13}\sigma_z + \ldots + a_{16}\tau_{r\theta}$$

$$\varepsilon_\theta = \frac{1}{r}\frac{\partial v}{\partial \theta} + \frac{u}{r} = a_{21}\sigma_r + a_{22}\sigma_\theta + a_{23}\sigma_z + \ldots + a_{26}\tau_{r\theta}$$

$$\varepsilon_z = \frac{\partial w}{\partial z} = a_{31}\sigma_r + a_{32}\sigma_\theta + a_{33}\sigma_z + a_{34}\tau_{\theta z} + a_{35}\tau_{rz} + a_{36}\tau_{r\theta} = D$$

$$\gamma_{\theta z} = \frac{1}{r}\frac{\partial w}{\partial \theta} + \frac{\partial v}{\partial z} = a_{41}\sigma_r + a_{42}\sigma_\theta + \ldots + a_{46}\tau_{r\theta}$$

$$\gamma_{rz} = \frac{\partial w}{\partial r} + \frac{\partial u}{\partial z} = a_{51}\sigma_r + a_{52}\sigma_\theta + \ldots + a_{56}\tau_{r\theta}$$

$$\gamma_{r\theta} = \frac{1}{r}\frac{\partial u}{\partial \theta} + \frac{\partial v}{\partial r} - \frac{v}{r} = a_{61}\sigma_r + a_{62}\sigma_\theta + \ldots + a_{66}\tau_{r\theta}$$

(5.1)

as such, σ_z can be expressed separately:

$$\sigma_z = \frac{D}{a_{33}} - \frac{1}{a_{33}}\left(a_{31}\sigma_r + a_{32}\sigma_\theta + a_{34}\tau_{\theta z} + a_{35}\tau_{rz} + a_{36}\tau_{r\theta}\right)$$

(5.2)

Thus

$$\varepsilon_r = a_{11}\sigma_r + a_{12}\sigma_\theta + a_{13}\left(\frac{D}{a_{33}} - \frac{1}{a_{33}}\left(a_{31}\sigma_r + a_{32}\sigma_\theta + a_{34}\tau_{\theta z} + a_{35}\tau_{rz} + a_{36}\tau_{r\theta}\right)\right) + a_{14}\tau_{\theta z} + a_{15}\tau_{rz} + a_{16}\tau_{r\theta}$$

$$\varepsilon_r = \left(a_{11} - \frac{a_{13}a_{31}}{a_{33}}\right)\sigma_r + \left(a_{12} - \frac{a_{13}a_{32}}{a_{33}}\right)\sigma_\theta + \left(a_{14} - \frac{a_{13}a_{34}}{a_{33}}\right)\tau_{\theta z} + \left(a_{15} - \frac{a_{13}a_{35}}{a_{33}}\right)\tau_{rz} +$$

$$\left(a_{16} - \frac{a_{13}a_{36}}{a_{33}}\right)\tau_{r\theta} + \frac{a_{13}}{a_{33}}D$$

Defining the reduced coefficient β_{ij},

where: $\beta_{ij} = a_{ij} - \dfrac{a_{i3}a_{3j}}{a_{33}} = \beta_{ji}$

195

$$\varepsilon_r = \beta_{11}\sigma_r + \beta_{12}\sigma_\theta + \beta_{14}\tau_{\theta z} + \beta_{15}\tau_{rz} + \beta_{16}\tau_{r\theta} + \frac{a_{13}}{a_{33}}D$$

Similarly, the same substitutions can be applied to the entire system and (5.1) is transformed to:

$$\frac{\partial u}{\partial r} = \beta_{11}\sigma_r + \beta_{12}\sigma_\theta + \beta_{14} + \ldots + \beta_{16}\tau_{r\theta} + \frac{a_{13}}{a_{33}}D$$

$$\frac{1}{r}\frac{\partial v}{\partial \theta} + \frac{u}{r} = \beta_{21}\sigma_r + \beta_{22}\sigma_\theta + \ldots + \beta_{26}\tau_{r\theta} + \frac{a_{23}}{a_{33}}D$$

$$\frac{\partial w}{\partial z} = D$$

$$\frac{1}{r}\frac{\partial w}{\partial \theta} + \frac{\partial v}{\partial z} = \beta_{41}\sigma_r + \beta_{42}\sigma_\theta + \ldots + \beta_{46}\tau_{r\theta} + \frac{a_{34}}{a_{33}}D$$

$$\frac{\partial u}{\partial z} + \frac{\partial w}{\partial r} = \beta_{51}\sigma_r + \beta_{52}\sigma_\theta + \ldots + \beta_{56}\tau_{r\theta} + \frac{a_{35}}{a_{33}}D$$

$$\frac{1}{r}\frac{\partial u}{\partial \theta} + \frac{\partial v}{\partial r} - \frac{v}{r} = \beta_{61}\sigma_r + \beta_{62}\sigma_\theta + \ldots + \beta_{66}\tau_{r\theta} + \frac{a_{36}}{a_{33}}D$$

(5.3)

5.1 Rigid Body Rotations

Before proceeding we must consider rigid body displacements and rotations. With reference to Figure 5.2 ; $\omega_1, \omega_2, \omega_3$ represent *small* rotations of the body (in radians) about directions r, θ, z respectively. Let u_0, v_0, w_0 be translations. The following relations can be written for point O representing an arbitrary location on the cylinder. The components of motion resolved to u', v', w' can be stated as:
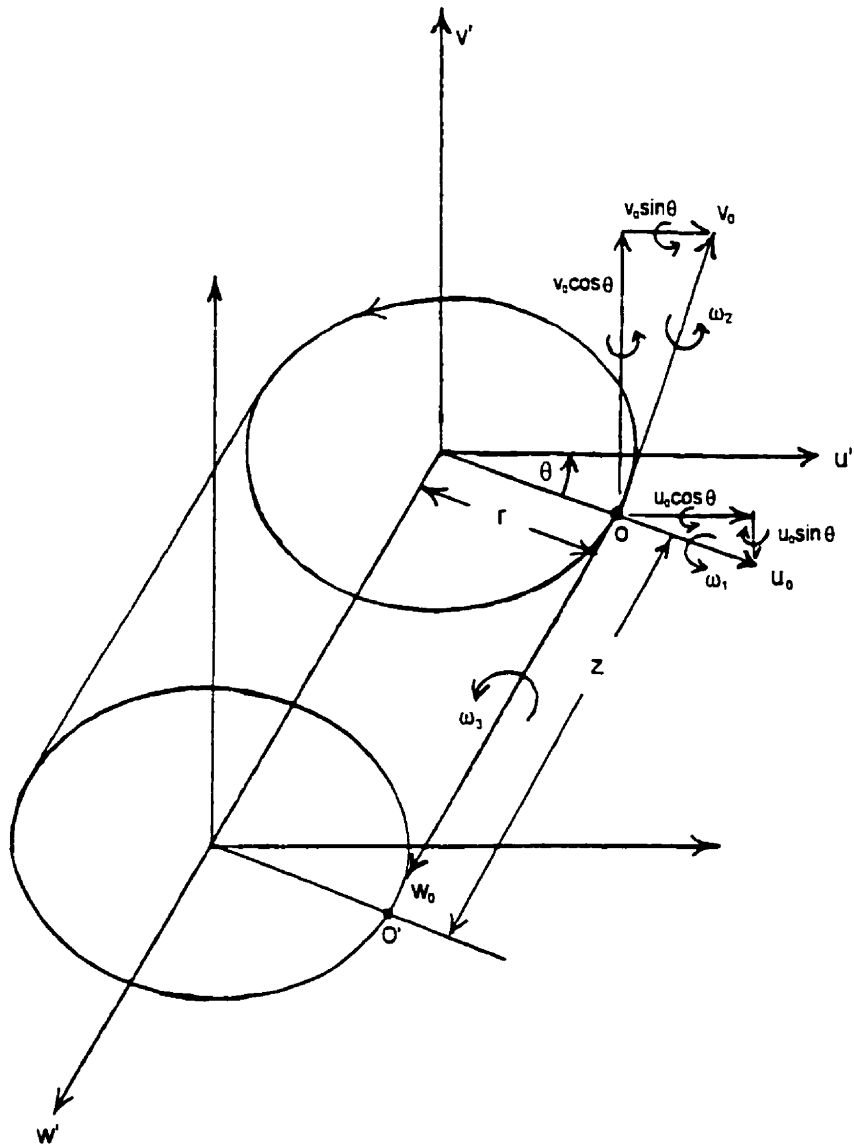
Figure 5.2 Rigid body motion nomenclature

$$u' = \omega_2 \, z \cos\theta - \omega_1 \, z \sin\theta + u_0 \cos\theta + v_0 \sin\theta$$

$$v' = \omega_3 \, r - \omega_1 \, z \cos\theta - \omega_2 \, z \sin\theta + v_0 \cos\theta - u_0 \sin\theta$$

$$w' = \omega_1 \, r \sin\theta - \omega_2 \, r \cos\theta + w_0$$

$$(5.4)$$

With reference to Figure 5.2, rigid body motion in equation (5.4) for direction u' has both

translation and rotation components. The translation components for point O constitute

the horizontal components from normal displacement vectors v_0 and u_0

($u_0 \cos\theta$ and $v_0 \sin\theta$ respectively). The body can also be rotating, and this rotation is

described by components $\omega_1, \omega_2, \omega_3$. These too can be resolved into their trigonometric

components along the u_0 and v_0 directions as indicated by the circular arrows on the

diagram. Taking the body's center of rotation at arbitrary point O and imagining a point

displaced from this location by a distance z at location O', the rotation components about

the v' axis would constitute of two parts: $\{\omega_2 \cos\theta$ and $-\omega_1 \sin\theta\}$. Since the rotations

and displacements are restricted to being small quantities in this analysis, the

corresponding movement in the u' direction is simply the arm z multiplied by the net

rotation $\{\omega_2 \cos\theta - \omega_1 \sin\theta\}$. The other terms for v' and w' are constituted similarly, with

the addition that a point can also be imagined as being displaced from location O by a

distance along the r direction to O'.

We can now define more general functions for displacements $\{U_1, V_1, W_1\}$ allowing

both strains and rigid body rotation / translation. With the concept of generalized plane

strain introduced earlier, position along the z direction is not a factor and we can exclude

from (5.4) the terms involving z. Adding to these yet undetermined general functions of

displacement we attain the form

$$U_1(r,\theta) = U(r,\theta) + u_0 \cos\theta + v_0 \sin\theta$$

$$V_1(r,\theta) = V(r,\theta) + \omega_3 r + v_0 \cos\theta - u_0 \sin\theta$$

$$W_1(r,\theta) = W(r,\theta) - r(\omega_2 \cos\theta - \omega_1 \sin\theta) + w_0$$

<div align="right">(5.5)</div>

Here $U(r,\theta)$, $V(r,\theta)$, $W(r,\theta)$ indicate displacements other than those introduced due to rigid body movements and these do not involve z. It will later become evident they arise from internal strains. The objective is to extract an encompassing form for D and further to arrive at equations describing in a general sense the displacements of a cylindrical body.

From (5.1), $\dfrac{\partial w}{\partial z} = D$, so we integrate

$$w = Dz + W_1(r,\theta) \qquad \text{where:} \quad W_1(r,\theta) \text{ takes its form from (5.5).}$$

The fourth of (5.3) can be stated as:

$$\frac{\partial v}{\partial z} = \beta_{41}\sigma_r + \beta_{42}\sigma_\theta + \beta_{44}\tau_{\theta z} + \beta_{45}\tau_{rz} + \beta_{46}\tau_{r\theta} + \frac{a_{34}}{a_{33}}D - \frac{1}{r}\frac{\partial w}{\partial \theta}$$

$$v = \int\left(\beta_{41}\sigma_r + \beta_{42}\sigma_\theta + \beta_{44}\tau_{\theta z} + \beta_{45}\tau_{rz} + \beta_{46}\tau_{r\theta} - \frac{a_{34}}{a_{33}}D - \frac{1}{r}\frac{\partial w}{\partial \theta}\right)dz$$

$$v = \left[\beta_{41}\sigma_r + \beta_{42}\sigma_\theta + \beta_{44}\tau_{\theta z} + \beta_{45}\tau_{rz} + \beta_{46}\tau_{r\theta} - \frac{a_{34}}{a_{33}}D\right]z - \int \frac{1}{r}\frac{\partial}{\partial \theta}(Dz + W_1(r,\theta))dz$$

$$v = z\left[\beta_{41}\sigma_r + \beta_{42}\sigma_\theta + \beta_{44}\tau_{\theta z} + \beta_{45}\tau_{rz} + \beta_{46}\tau_{r\theta} + \frac{a_{34}}{a_{33}}D - \frac{1}{r}\frac{\partial W_1(r,\theta)}{\partial \theta}\right] + V_1(r,\theta) - \frac{1}{r}\frac{z^2}{2}\frac{\partial D}{\partial \theta}$$

<div align="right">Where: V_1 is the integration constant.   (5.6)</div>

The fifth of (5.3) can be stated as:

$$\frac{\partial u}{\partial z} = \beta_{51}\sigma_r + \beta_{52}\sigma_\theta + \beta_{54}\tau_{\theta z} + \beta_{55}\tau_{rz} + \beta_{56}\tau_{r\theta} + \frac{a_{35}}{a_{33}}D - \frac{\partial w}{\partial r}$$

$$u = \int\left[\beta_{51}\sigma_r + \beta_{52}\sigma_\theta + \beta_{54}\tau_{\theta z} + \beta_{55}\tau_{rz} + \beta_{56}\tau_{r\theta} + \frac{a_{35}}{a_{33}}D - \frac{\partial}{\partial r}(Dz + W_1(r,\theta))\right]dz$$

$$u = z\left[\beta_{51}\sigma_r + \beta_{52}\sigma_\theta + \beta_{54}\tau_{\theta z} + \beta_{55}\tau_{rz} + \beta_{56}\tau_{r\theta} + \frac{a_{35}}{a_{33}}D - \frac{\partial W_1(r,\theta)}{\partial r}\right] - \frac{z^2}{2}\frac{\partial D}{\partial r} + U_1(r,\theta)$$

<div align="right">Where: U_1 is the integration constant.   (5.7)</div>

Substituting the above expression into the first of (5.3) and equating terms:

$$\varepsilon_r = \frac{\partial u}{\partial r} = z \frac{\partial}{\partial r}\left[\beta_{51}\sigma_r + \beta_{52}\sigma_\theta + \beta_{54}\tau_{\theta z} + \beta_{55}\tau_{rz} + \beta_{56}\tau_{r\theta} + \frac{a_{35}}{a_{33}}D - \frac{\partial W_1(r,\theta)}{\partial r}\right] -$$

$$\frac{z^2}{2}\frac{\partial^2 D}{\partial r^2} + \frac{\partial U_1(r,\theta)}{\partial r} = \beta_{11}\sigma_r + \beta_{12}\sigma_\theta + \beta_{14}\tau_{\theta z} + \beta_{15}\tau_{rz} + \beta_{16}\tau_{r\theta} + \frac{a_{13}}{a_{33}}D$$

Since $z \neq 0$, the terms multiplied by z and z^2 must themselves $= 0$.

hence:

$$\frac{\partial^2 D}{\partial r^2} = 0$$

and

$$\frac{\partial}{\partial r}\left[\beta_{51}\sigma_r + \beta_{52}\sigma_\theta + \beta_{54}\tau_{\theta z} + \beta_{55}\tau_{rz} + \beta_{56}\tau_{r\theta} + \frac{a_{35}}{a_{33}}D - \frac{\partial W_1(r,\theta)}{\partial r}\right] = 0$$

(5.8)

so:

$$\frac{\partial U_1(r,\theta)}{\partial r} = \beta_{11}\sigma_r + \beta_{12}\sigma_\theta + \dots + \beta_{16}\tau_{r\theta} + \frac{a_{13}}{a_{33}}D$$

(5.9)

Similarly for the second of (5.3)

$$\varepsilon_\theta = \frac{1}{r}\frac{\partial v}{\partial \theta} + \frac{u}{r} = \frac{1}{r}\frac{\partial}{\partial \theta}\left[z\left(\beta_{41}\sigma_r + \beta_{42}\sigma_\theta + \dots + \frac{a_{34}}{a_{33}}D - \frac{1}{r}\frac{\partial W_1(r,\theta)}{\partial \theta}\right)\right] + \frac{1}{r}\frac{\partial V_1(r,\theta)}{\partial \theta} -$$

$$\frac{1}{r}\frac{z^2}{2}\frac{\partial^2 D}{r\partial\theta\partial r} + \frac{U_1(r,\theta)}{r} = \beta_{21}\sigma_r + \beta_{22}\sigma_\theta + \dots + \beta_{26}\tau_{r\theta} + \frac{a_{23}}{a_{33}}D$$

Equating z and z^2 coefficients we learn that

$$\frac{1}{r}\frac{\partial}{\partial \theta}\left[\frac{\partial D}{\partial r}\right] = 0 \qquad \text{and} \qquad \frac{1}{r}\frac{\partial}{\partial \theta}\left(\beta_{41}\sigma_r + \beta_{42}\sigma_\theta + \dots \frac{a_{34}}{a_{33}}D - \frac{1}{r}\frac{\partial W_1(r,\theta)}{\partial \theta}\right) = 0$$

(5.10)

200

thus

$$\frac{\partial V_1(r,\theta)}{r\partial\theta} + \frac{U_1(r,\theta)}{r} = \beta_{21}\sigma_r + \beta_{22}\sigma_\theta + \ldots \beta_{26}\tau_{r\theta} + \frac{a_{23}}{a_{33}}D$$

(5.11)

From the 6th of (5.3) we have

$$\frac{1}{r}\frac{\partial u}{\partial\theta} + \frac{\partial v}{\partial r} - \frac{v}{r} = \frac{1}{r}\frac{\partial}{\partial\theta}\left[z\left(\beta_{51}\sigma_r + \beta_{52}\sigma_\theta + \ldots + \frac{a_{35}}{a_{33}}D - \frac{\partial W_1(r,\theta)}{\partial r}\right)\right] - \frac{z^2}{2}\frac{\partial}{r\partial\theta}\left(\frac{\partial D}{\partial r}\right) + \frac{\partial U_1(r,\theta)}{r\partial\theta} +$$

$$\frac{\partial}{\partial r}\left[z\left(\beta_{41}\sigma_r + \beta_{42}\sigma_\theta + \ldots + \frac{a_{34}}{a_{33}}D - \frac{1}{r}\frac{\partial W_1(r,\theta)}{\partial\theta}\right)\right] - \frac{z^2}{2}\frac{\partial}{\partial r}\left[\frac{\partial D}{r\partial\theta}\right] + \frac{\partial}{\partial r}V_1(r,\theta) -$$

$$\frac{1}{r}\left[z\left(\beta_{41}\sigma_r + \beta_{42}\sigma_\theta + \ldots + \frac{a_{34}}{a_{33}}D - \frac{1}{r}\frac{\partial W_1(r,\theta)}{\partial\theta}\right) + V_1(r,\theta) - \frac{z^2}{2}\frac{\partial D}{r\partial\theta}\right] = \beta_{61}\sigma_r + \beta_{62}\sigma_\theta + \ldots + \beta_{66}\tau_{r\theta} + \frac{a_{36}}{a_{33}}D$$

equating coefficients z^2 we see that

$$\left[\frac{\partial}{r\partial\theta}\left(\frac{\partial D}{\partial r}\right) + \frac{\partial}{\partial r}\left(\frac{\partial D}{r\partial\theta}\right) - \frac{1}{r^2}\frac{\partial D}{\partial\theta}\right] = 0$$

(5.12)

equating coefficients with z we have

$$\left[\frac{\partial}{r\partial\theta}\left(\beta_{51}\sigma_r + \beta_{52}\sigma_\theta + \ldots + \frac{a_{35}}{a_{33}}D - \frac{\partial W_1(r,\theta)}{\partial r}\right) + \left(\frac{\partial}{\partial r} - \frac{1}{r}\right)\left(\beta_{41}\sigma_r + \beta_{42}\sigma_\theta + \ldots + \frac{a_{34}}{a_{33}}D - \frac{1}{r}\frac{\partial W_1(r,\theta)}{\partial\theta}\right)\right] = 0$$

(5.13)

The remaining terms are:

$$\frac{\partial}{r\partial\theta}[U_1(r,\theta)] + \left(\frac{\partial}{\partial r} - \frac{1}{r}\right)[V_1(r,\theta)] = \beta_{61}\sigma_r + \beta_{62}\sigma_\theta + \ldots + \beta_{66}\tau_{r\theta} + \frac{a_{36}}{a_{33}}D$$

(5.14)

One must solve for all possible forms of D. From the expressions in (5.8), (5.10) and

(5.12), the following 3 conditions must be satisfied:

201

1) $\dfrac{\partial^2 D}{\partial r^2} = 0$

2) $\dfrac{1}{r}\dfrac{\partial}{\partial \theta}\left[\dfrac{\partial D}{\partial r}\right] = 0$

3) $\dfrac{\partial}{r\partial \theta}\left[\dfrac{\partial D}{\partial r}\right] + \left[\dfrac{\partial}{\partial r} - \dfrac{1}{r}\right]\dfrac{\partial D}{r\partial \theta} = 0$

(5.15)

Beginning with the 3rd condition, it can be cast as:

$$\dfrac{1}{r}\dfrac{\partial}{\partial \theta}\left(\dfrac{\partial D}{\partial r}\right) - \dfrac{1}{r^2}\dfrac{\partial D}{\partial \theta} + \dfrac{1}{r}\dfrac{\partial}{\partial \theta}\left(\dfrac{\partial D}{\partial r}\right) - \dfrac{1}{r^2}\dfrac{\partial D}{\partial \theta} = 0$$

or

$$\dfrac{2}{r}\dfrac{\partial}{\partial \theta}\left(\dfrac{\partial D}{\partial r}\right) - \dfrac{2}{r^2}\dfrac{\partial D}{\partial \theta} = 0$$

or

$$\dfrac{1}{r}\dfrac{\partial}{\partial \theta}\left(\dfrac{\partial D}{\partial r}\right) = \dfrac{1}{r^2}\dfrac{\partial D}{\partial \theta}$$

(5.18)
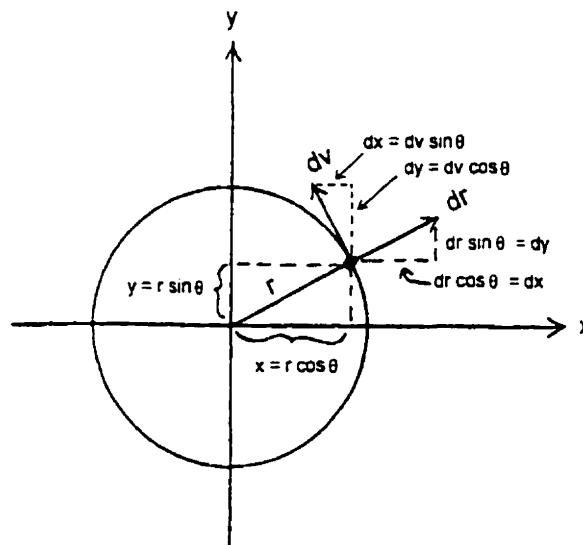
Figure 5.3 Polar to rectangular conversions

With the help of Figure 5.3 we recognize that $rd\theta = dv$ and the second condition of (5.15) is cast in rectangular as:

$$\frac{\partial}{\partial v}\left[\frac{\partial D}{\partial r}\right] = 0$$

$$\frac{\partial}{\partial y}\frac{\partial y}{\partial v}\left[\frac{\partial D}{\partial x}\frac{\partial x}{\partial r}\right] = 0$$

$$\frac{\partial}{\partial y}\cos\theta\left[\frac{\partial D}{\partial x}\cos\theta\right] = 0$$

$$\cos^2\theta\frac{\partial}{\partial y}\left[\frac{\partial D}{\partial x}\right] = 0$$

since: $\quad \cos^2\theta \neq 0, \qquad \frac{\partial}{\partial y}\left[\frac{\partial D}{\partial x}\right] = 0$

Integrating with respect to (y) gives:

$$\frac{\partial D}{\partial x} = C_1 + C_2\, f_1(x)$$

Integrating wrt (x) gives:

$$D = C_1 x + \int C_2 f_1(x)\,dx + C_3 f_2(y) + C_4 \tag{5.16}$$

Since the order of differentiation must be immaterial, we can state that:

$$\frac{\partial}{\partial x}\left[\frac{\partial D}{\partial y}\right] = 0$$

Integrating wrt. (x) gives:

$$\frac{\partial D}{\partial y} = C_1^* + C_2^* f_2(y)$$

Integrating wrt. (y) gives:

$$D = C_1^* y + \int C_2^* f_2^*(y) \, dy + C_3^* f_3^*(x) + C_4^*$$

(5.17)

The first condition of (5.15) is examined and cast into rectangular coordinates.

$$\frac{\partial}{\partial r}\left[\frac{\partial D}{\partial r}\right] = 0$$

$$\frac{\partial}{\partial x}\frac{\partial x}{\partial r}\left[\frac{\partial D}{\partial x}\frac{\partial x}{\partial r}\right] = 0$$

$$\cos^2\theta \frac{\partial}{\partial x}\left[\frac{\partial D}{\partial x}\right] = 0$$

since:

$$\cos^2\theta \neq 0 \quad , \quad \frac{\partial}{\partial x}\left[\frac{\partial D}{\partial x}\right] = 0$$

integrating wrt.(x) gives:

$$\frac{\partial D}{\partial x} = C_5 + C_6 \, f(y)$$

integrating again wrt.(x) gives:

$$D = C_5 x + x C_6 \, f(y) + C_7 \, f^*(y) + C_8$$

(5.18)

Comparing equations (5.16), (5.17) and (5.18), each expressing possible solutions for D,

we note that the coefficients C_2, C_2^* and C_6 must equal zero since they are unique and

have no counterpart amongst the various expressions.

Further, similarity requires that $C_4 = C_4^* = C_8 = C$.

$$C_1 x = C_3 \, f(x) = C_5 x \qquad \text{only if} \qquad f(x) = x \qquad \text{and} \qquad C_1 = C_3 = C_5 = A$$

also

204

$$C_3 \, f(y) = C_1^* \, y = C_7 \, f^*(y) \qquad \text{only if} \qquad f(y) = f^*(y) = y \quad \text{and} \quad C_1^* = C_3 = C_7 = B$$

If one does not impose the conditions above for both the unspecified functions of (x), (y) and the coefficients, only a trivial solution results.

We conclude that the only possible form is:

$$D = Ax + By + C$$

reverting back to polar:

$$D = Ar \cos\theta + Br \sin\theta + C$$

$$\tag{5.19}$$

Finally the 3rd condition of (5.15) can be used to check the solution above for possibly being restrictive.

$$\frac{\partial}{r\partial\theta}\left[\frac{\partial D}{\partial r}\right] = \frac{1}{r^2}\frac{\partial D}{\partial \theta}$$

$$\frac{\partial}{r\partial\theta}\left[\frac{\partial}{\partial r}(Ar \cos\theta + Br \sin\theta + C)\right] = \frac{1}{r^2}\frac{\partial}{\partial\theta}(Ar \cos\theta + Br \sin\theta + C)$$

$$\frac{\partial}{r\partial\theta}(A\cos\theta + B\sin\theta) = \frac{1}{r^2}(-Ar\sin\theta + Br\cos\theta)$$

$$\frac{1}{r}(-A\sin\theta + B\cos\theta) = \frac{1}{r}(-A\sin\theta + B\cos\theta)$$

One must conclude that the solution found for D is not restrictive.

(5.8) can be stated as:

$$\frac{\partial}{\partial r}\left(\beta_{s1}\sigma_r + \beta_{s2}\sigma_\theta + \ldots + \frac{a_{35}}{a_{33}}D\right) = \frac{\partial^2 W_1}{\partial r^2}$$

The above can be expressed as

$$\frac{\partial}{\partial r}\left(\beta_{51}\sigma_r + \beta_{52}\sigma_\theta + \ldots + \frac{a_{35}}{a_{33}}D\right) = \frac{\partial}{\partial r}\left(\frac{\partial}{\partial r}\left[W - r(\omega_2 \cos\theta - \omega_1 \sin\theta) + w_0\right]\right)$$

$$(5.20) .$$

giving

$$\frac{\partial}{\partial r}\left(\beta_{51}\sigma_r + \beta_{52}\sigma_\theta + \ldots + \frac{a_{35}}{a_{33}}D\right) = \frac{\partial}{\partial r}\left(\frac{\partial W}{\partial r}\right)$$

integration then yields

$$\left(\beta_{51}\sigma_r + \beta_{52}\sigma_\theta + \ldots + \frac{a_{35}}{a_{33}}D\right) + f(\theta) + C^* = \frac{\partial W}{\partial r}$$

Where C^* is an integration constant.

$$(5.21)$$

(5.10) can be expressed as

$$\frac{\partial}{r\partial\theta}\left(\beta_{41}\sigma_r + \beta_{42}\sigma_\theta + \ldots + \frac{a_{34}}{a_{33}}D\right) = \frac{\partial}{r\partial\theta}\left(\frac{\partial}{r\partial\theta}\left[W - r(\omega_2 \cos\theta - \omega_1 \sin\theta) + w_0\right]\right)$$

$$(5.22)$$

From Figure 5.3 one can use the substitutions

$$\frac{\partial}{r\partial\theta} = \frac{\partial}{\partial v} = \frac{\partial}{\partial y}\frac{\partial y}{\partial v} = \frac{\partial}{\partial y}\cos\theta , \qquad x = r\cos\theta , \qquad y = r\sin\theta$$

and the second part of the *RHS* can be transformed to

$$\cos^2\theta\frac{\partial^2}{\partial y^2}\left[-\omega_2 x + \omega_1 y\right]$$

since this derivative evaluates to zero we have

$$\frac{\partial}{r\partial\theta}\left(\beta_{41}\sigma_r + \beta_{42}\sigma_\theta + \ldots + \frac{a_{34}}{a_{33}}D\right) = \frac{\partial}{r\partial\theta}\left(\frac{\partial W}{r\partial\theta}\right)$$

and by integration

$$\left(\beta_{41}\sigma_r + \beta_{42}\sigma_\theta + \ldots + \frac{a_{34}}{a_{33}}D\right) + f(r) + C^{**} = \frac{1}{r}\frac{\partial W}{\partial\theta}$$

Where: C^{**} is an integration constant. (5.23)

Substituting (5.20) and (5.22) into (5.13)

$$\frac{\partial}{r\partial\theta}\left[\beta_{51}\sigma_r+\beta_{52}\sigma_\theta+....+\frac{a_{35}}{a_{33}}D-\left(\beta_{51}\sigma_r+\beta_{52}\sigma_\theta+....+\frac{a_{35}}{a_{33}}D\right)-f(\theta)-C^*\right]+$$

$$\left(\frac{\partial}{\partial r}-\frac{1}{r}\right)\left[\beta_{41}\sigma_r+\beta_{42}\sigma_\theta+....+\frac{a_{34}}{a_{33}}D-\left(\beta_{41}\sigma_r+\beta_{42}\sigma_\theta+....+\frac{a_{34}}{a_{33}}D\right)-f(r)-C^{**}\right]=0$$

reduced to:

$$\frac{\partial}{r\partial\theta}\left[f(\theta)+C^*\right]+\left(\frac{\partial}{\partial r}-\frac{1}{r}\right)\left[f(r)+C^{**}\right]=0$$

(5.24)

$$\frac{\partial}{r\partial\theta}\left[f(\theta)\right]+\underset{\downarrow}{\frac{\partial C^*}{r\partial r}}+\frac{\partial}{\partial r}f(r)-\frac{f(r)}{r}+\underset{\downarrow}{\frac{\partial C^{**}}{\partial r}}-\frac{C^{**}}{r}=0$$

$$\quad\quad\quad 0\quad\quad\quad\quad\quad\quad\quad\quad 0$$

$$\frac{1}{r}\left[\frac{\partial}{\partial\theta}f(\theta)-C^{**}\right]+\left[\frac{\partial f(r)}{\partial r}+\frac{f(r)}{r}\right]=0$$

and we know that $f(\theta)$ must be a periodic function otherwise we would have multi-valued displacements. Differentiation will not make it disappear thus the only possible solution becomes

$$C^{**}=0\quad,\quad f(\theta)=0\quad\quad\text{and}\quad\quad f(r)=\pm 9r$$

Since C^* is immaterial to the outcome, we set it equal zero. From (5.21)

$$\frac{\partial W}{\partial r}=\left(\beta_{51}\sigma_r+\beta_{52}\sigma_\theta+....+\frac{a_{35}}{a_{33}}D\right)$$

(5.25)

and

207

$$\frac{1}{r}\frac{\partial W}{\partial \theta} = \left(\beta_{41}\sigma_r + \beta_{42}\sigma_\theta + \ldots + \frac{a_{34}}{a_{33}}D\right) - \vartheta r$$

$$(5.26)$$

Two equivalent forms of $\dfrac{1}{r}\dfrac{\partial^2 W}{\partial \theta \partial r}$ can be written. From (5.25)

$$\frac{\partial}{r\partial \theta}\left(\frac{\partial W}{\partial r}\right) = \frac{\partial^2 W}{r\partial \theta \partial r} = \frac{\partial}{r\partial \theta}\left(\beta_{51}\sigma_r + \beta_{52}\sigma_\theta + \ldots + \beta_{62}\tau_{r\theta}\right) + \frac{a_{35}}{a_{33}}\frac{\partial}{r\partial \theta}\left(Ar\cos\theta + Br\sin\theta + C\right)$$

$$\frac{1}{r}\frac{\partial^2 W}{\partial \theta \partial r} = \frac{\partial}{r\partial \theta}\left(\beta_{51}\sigma_r + \beta_{52}\sigma_\theta + \ldots + \beta_{62}\tau_{r\theta}\right) + \frac{1}{r}\frac{a_{35}}{a_{33}}\left(B\cos\theta - A\sin\theta\right)$$

$$(5.27)$$

however

$$\frac{\partial}{\partial r}\left(\frac{1}{r}\frac{\partial W}{\partial \theta}\right) = \frac{1}{r}\frac{\partial^2 W}{\partial \theta \partial r} - \frac{1}{r^2}\frac{\partial W}{\partial \theta}$$

so

$$\frac{1}{r}\frac{\partial^2 W}{\partial \theta \partial r} = \frac{\partial}{\partial r}\left(\frac{1}{r}\frac{\partial W}{\partial \theta}\right) + \frac{1}{r^2}\frac{\partial W}{\partial \theta}$$

$$(5.28)$$

using (5.26)

$$\frac{\partial}{\partial r}\left(\frac{1}{r}\frac{\partial W}{\partial \theta}\right) = \frac{\partial}{\partial r}\left(\beta_{41}\sigma_r + \beta_{42}\sigma_\theta + \ldots + \beta_{46}\tau_{r\theta}\right) + \frac{\partial}{\partial r}\left[\frac{a_{34}}{a_{33}}\left(Ar\cos\theta + Br\sin\theta + C\right)\right] +$$

$$\frac{\partial}{\partial r}\left(\frac{1}{r}\frac{\partial W}{\partial \theta}\right) = \frac{\partial}{\partial r}\left(\beta_{41}\sigma_r + \beta_{42}\sigma_\theta + \ldots + \beta_{46}\tau_{r\theta}\right) + \frac{a_{34}}{a_{33}}\left(A\cos\theta + B\sin\theta\right) - \vartheta$$

$$(5.29)$$

substituting (5.26) and (5.29) into (5.28)

$$\frac{1}{r}\frac{\partial^2 W}{\partial \theta \partial r} = \frac{\partial}{\partial r}\left(\beta_{41}\sigma_r + \beta_{42}\sigma_\theta + \ldots + \beta_{46}\tau_{r\theta}\right) + \frac{a_{34}}{a_{33}}\left(A\cos\theta + B\sin\theta\right) - \vartheta +$$

208

$$\frac{1}{r}\left(\beta_{41}\sigma_r + \beta_{42}\sigma_\theta + \ldots + \beta_{46}\tau_{r\theta}\right) + \frac{1}{r}\frac{a_{34}}{a_{33}}\left(Ar\cos\theta + Br\sin\theta + C\right) + \frac{1}{r}(-\vartheta r)$$

<div align="right">(5.30)</div>

equating (5.27) and (5.30), separating differential terms to one side

$$\frac{\partial}{r\partial\theta}\left(\beta_{51}\sigma_r + \beta_{52}\sigma_\theta + \ldots + \beta_{56}\tau_{r\theta}\right) - \left(\frac{\partial}{\partial r} + \frac{1}{r}\right)\left(\beta_{41}\sigma_r + \beta_{42}\sigma_\theta + \ldots + \beta_{46}\tau_{r\theta}\right) = \frac{C}{r}\frac{a_{34}}{a_{33}} -$$

$$2\vartheta + \frac{\left(2a_{34}A - a_{35}B\right)}{a_{33}}\cos\theta + \frac{\left(2a_{34}B + a_{35}A\right)}{a_{33}}\sin\theta$$

<div align="right">(5.31)</div>

A relation to combine u and v is sought. The first, second and sixth relations in (4.9) are restated below.

$$\varepsilon_r = \frac{\partial u}{\partial r}$$

$$\varepsilon_\theta = \frac{1}{r}\frac{\partial v}{\partial\theta} + \frac{u}{r}$$

$$\gamma_{r\theta} = \frac{1}{r}\frac{\partial u}{\partial\theta} + \frac{\partial v}{\partial r} - \frac{v}{r}$$

The approach taken is to solve for $\gamma_{r\theta}$ as a combination of ε_θ and ε_r. We take a derivative $\partial^2/\partial r\partial\theta$ upon $\gamma_{r\theta}$ and attempt to substitute derivatives of ε_r and ε_θ to establish an equality.

$$r\varepsilon_\theta = \frac{\partial v}{\partial\theta} + u$$

$$r\gamma_{r\theta} = \frac{\partial u}{\partial\theta} + \frac{r\partial v}{\partial r} - v$$

$$\frac{\partial^2}{\partial r\partial\theta}\left(r\gamma_{r\theta}\right) = \frac{\partial}{\partial r}\left[\frac{\partial^2 u}{\partial\theta^2} + \frac{r\partial^2 v}{\partial r\partial\theta} - \frac{\partial v}{\partial\theta}\right] = \frac{\partial^3 u}{\partial r\partial\theta^2} + \frac{\partial^2 v}{\partial r\partial\theta} + r\frac{\partial^3 v}{\partial r^2\partial\theta} - \frac{\partial^2 v}{\partial r\partial\theta}$$

<div align="center">209</div>

$$\frac{\partial^2}{\partial r \partial \theta}\left(r\gamma_{r\theta}\right) = \frac{\partial^3 u}{\partial r \partial \theta^2} + r\frac{\partial^3 v}{\partial r^2 \partial \theta}$$

(5.32)

The first term above is simply

$$\frac{\partial^2}{\partial \theta^2}\left(\varepsilon_r\right) = \frac{\partial^3 u}{\partial r \partial \theta^2}$$

(5.33)

for the second term of (5.32)

$$\frac{\partial^2}{\partial r^2}\left(r\varepsilon_\theta\right) = \frac{\partial^2}{\partial r^2}\left[\frac{\partial v}{\partial \theta} + u\right] = \frac{\partial^3 v}{\partial r^2 \partial \theta} + \frac{\partial^2 u}{\partial r^2}$$

multiply by r

$$r\frac{\partial^2}{\partial r^2}\left(r\varepsilon_\theta\right) = r\frac{\partial^3 v}{\partial r^2 \partial \theta} + r\frac{\partial^2 u}{\partial r^2}$$

(5.34)

but

$$r\frac{\partial}{\partial r}\left(\varepsilon_r\right) = r\frac{\partial^2 u}{\partial r^2}$$

hence

$$r\frac{\partial^2}{\partial r^2}\left(r\varepsilon_\theta\right) - r\frac{\partial}{\partial r}\left(\varepsilon_r\right) = r\frac{\partial^3 v}{\partial r^2 \partial \theta}$$

(5.35)

Substituting (5.33) and (5.35) into (5.32) yields:

$$\frac{\partial^2}{\partial \theta^2}\left(\varepsilon_r\right) + \frac{r\partial^2}{\partial r^2}\left(r\varepsilon_\theta\right) - r\frac{\partial}{\partial r}\left(\varepsilon_r\right) = \frac{\partial^2}{\partial r \partial \theta}\left(r\gamma_{r\theta}\right)$$

which is recast as:

$$\left(\frac{\partial^2}{\partial \theta^2} - r\frac{\partial}{\partial r}\right)\varepsilon_r + r\frac{\partial^2}{\partial r^2}\left(r\varepsilon_\theta\right) - \frac{\partial^2}{\partial r \partial \theta}\left(r\gamma_{r\theta}\right) = 0$$

(5.36)

210

from (5.1) relations for $\varepsilon_r, \varepsilon_\theta, \gamma_{r\theta}$ are put into (5.36).

$$\left(\frac{\partial^2}{\partial\theta^2} - r\frac{\partial}{\partial r}\right)\left(\beta_{11}\sigma_r + \beta_{12}\sigma_\theta + \ldots + \beta_{16}\tau_{r\theta} + \frac{a_{13}}{a_{33}}D\right) + r\frac{\partial^2}{\partial r^2}\left[r\left(\beta_{21}\sigma_r + \beta_{22}\sigma_\theta + \ldots + \beta_{26}\tau_{r\theta} + \frac{a_{23}}{a_{33}}D\right)\right] -$$

$$\frac{\partial}{\partial r\partial\theta}\left[r\left(\beta_{61}\sigma_r + \beta_{62}\sigma_\theta + \ldots + \beta_{66}\tau_{r\theta} + \frac{a_{36}}{a_{33}}D\right)\right] = 0$$

(5.37)

Expansion and separation of differential terms to one side gives:

$$\left(\frac{\partial^2}{\partial\theta^2} - r\frac{\partial}{\partial r}\right)\left(\beta_{11}\sigma_r + \beta_{12}\sigma_\theta + \ldots + \beta_{16}\tau_{r\theta}\right) + r\frac{\partial^2}{\partial r^2}\left[r\left(\beta_{21}\sigma_r + \beta_{22}\sigma_\theta + \ldots + \beta_{26}\tau_{r\theta}\right)\right] -$$

$$\frac{\partial^2}{\partial r\partial\theta}\left[r\left(\beta_{61}\sigma_r + \beta_{62}\sigma_\theta + \ldots + \beta_{66}\tau_{r\theta}\right)\right] = -\left(\frac{\partial^2}{\partial\theta^2} - r\frac{\partial}{\partial r}\right)\frac{a_{13}}{a_{33}}[Ar\cos\theta + Br\sin\theta + C] -$$

$$r\frac{\partial^2}{\partial r^2}\left[r\frac{a_{23}}{a_{33}}[Ar\cos\theta + Br\sin\theta + C]\right] + \frac{\partial^2}{\partial r\partial\theta}\left[r\frac{a_{36}}{a_{33}}[Ar\cos\theta + Br\sin\theta + C]\right]$$

(5.38)

For displacements using (5.5) we have:

$$w = Dz + W_1 = z(Ar\cos\theta + Br\sin\theta + C) + W(r,\theta) - r(\omega_2\cos\theta - \omega_1\sin\theta) + w_0$$

$$w = z(Ar\cos\theta + Br\sin\theta + C) + W(r,\theta) + w'$$

(5.39)

where; w' = rigid body motion akin to (5.4)

From (5.7) using (5.20) and (5.5)

$$u = \frac{-z^2}{2}\frac{\partial}{\partial r}(Ar\cos\theta + Br\sin\theta + C) + U(r,\theta) + u_0\cos\theta + v_0\sin\theta +$$

$$z\left(\beta_{51}\sigma_r + \beta_{52}\sigma_\theta + \ldots + \frac{a_{35}}{a_{33}}D - \frac{\partial}{\partial r}(W - r(\omega_2\cos\theta - \omega_1\sin\theta) + w_0)\right)$$

$$u = \frac{-z^2}{2}\frac{\partial}{\partial r}\left(Ar\cos\theta + Br\sin\theta + C\right) + U(r,\theta) + u_0\cos\theta + v_0\sin\theta +$$

$$z\left(\beta_{51}\sigma_r + \beta_{52}\sigma_\theta + \dots + \frac{a_{35}}{a_{33}}D - \left(\beta_{51}\sigma_r + \beta_{52}\sigma_\theta + \dots + \frac{a_{35}}{a_{33}}D\right) + \left(\omega_2\cos\theta - \omega_1\sin\theta\right)\right)$$

$$u = \frac{-z^2}{2}\left(A\cos\theta + B\sin\theta\right) + U(r,\theta) + z\left(\omega_2\cos\theta - \omega_1\sin\theta\right) + u_0\cos\theta + v_0\sin\theta$$

$$u = \frac{-z^2}{2}\left(A\cos\theta + B\sin\theta\right) + U(r,\theta) + u'$$

(5.40)

<div align="center">where; u' = rigid body motion akin to (5.4)</div>

From (5.6) using (5.22) and (5.5)

$$v = \frac{-z^2}{2}\frac{\partial}{r\partial\theta}\left(Ar\cos\theta + Br\sin\theta + C\right) + V(r,\theta) + \omega_3 r + v_0\cos\theta - u_0\sin\theta +$$

$$z\left(\beta_{41}\sigma_r + \beta_{42}\sigma_\theta + \dots + \frac{a_{34}}{a_{33}}D - \frac{\partial}{r\partial\theta}\left(W - r(\omega_2\cos\theta - \omega_1\sin\theta) + w_0\right)\right)$$

$$v = \frac{-z^2}{2}\frac{\partial}{r\partial\theta}\left(Ar\cos\theta + Br\sin\theta + C\right) + V(r,\theta) + \omega_3 r + v_0\cos\theta - u_0\sin\theta +$$

$$z\left(\beta_{41}\sigma_r + \beta_{42}\sigma_\theta + \dots + \frac{a_{34}}{a_{33}}D - \left(\beta_{41}\sigma_r + \beta_{42}\sigma_\theta + \dots + \frac{a_{34}}{a_{33}}D - \vartheta r\right) + \left(\omega_2\sin\theta + \omega_1\cos\theta\right)\right)$$

$$v = \frac{-z^2}{2}\left(B\cos\theta - A\sin\theta\right) + \vartheta rz + V(r,\theta) - z\left(\omega_1\cos\theta + \omega_2\sin\theta\right) + v_0\cos\theta - u_0\sin\theta$$

$$v = \frac{-z^2}{2}\left(B\cos\theta - A\sin\theta\right) + \vartheta rz + V(r,\theta) + v'$$

(5.41)

<div align="center">where; v' = rigid body motion akin to (5.4)</div>

5.1.1 Examination of Constants

Apart from rigid body translations and rotations, the cylinder's internal displacements (deformations) are described via u, v and w. The four constants A, B, C, ϑ describe global deformations arising from the internal strains. By inspection it is evident that ϑ represents twist, A and B bending deformations in mutually perpendicular directions and C represents axial displacement. Additionally one can see that for a finite length cylinder under bending, the coordinate $z = 0$ is to be taken at the middle of its length for the displacement equations to apply correctly.

If we assume from symmetry considerations that there is no variation in displacement wrt. θ, then the angular variation of circumferential distortion $\left(\frac{\partial v}{\partial \theta}\right)$, warpage characteristic of bending $\left(\frac{\partial w}{\partial \theta}\right)$ and radial distortion characteristic of squashing $\left(\frac{\partial u}{\partial \theta}\right)$ disappear. From equation (5.40) we note that lengthwise taper $\left(\frac{\partial u}{\partial z}\right)$ does not exist since all derivatives on the *RHS* equate to zero except for deformations resulting from constants A and B dependent on angle θ which simply reflect gross bending. The direct radial deformation characteristic of pressure $\left(\frac{\partial u}{\partial r}\right)$ and axial deformation characteristic of end loading $\left(\frac{\partial w}{\partial z}\right)$ exists. Also warpage characteristic of axial shear $\left(\frac{\partial w}{\partial r}\right)$, distortion of the radii characteristic of twisting $\left(\frac{\partial v}{\partial r}\right)$, and lengthwise twist $\left(\frac{\partial v}{\partial z}\right)$ remain.

Examining a single filament wound layer, and using Figure (4.2b) along with the stress function introduced for (4.15), we note that only remaining shear stress is $\tau_{\theta z}$.

However $a_{15}....a_{45}$ and $a_{16}....a_{46} = 0$, thus $\gamma_{rz} = \gamma_{r\theta} = 0$. This leads to the conclusion that

213

$\partial w/\partial r = 0$ and $\left(\partial v/\partial r - v/r\right) = 0$. Therefore $\partial v/\partial r \neq 0$ and distortion of the radii characteristic of twisting takes place. Lengthwise twist is present, a direct result of $\partial v/\partial z \neq 0$.

A more practical view takes into consideration that filament wound layers do not generally exist in isolation but as interwoven $\pm$ angle pairs. In effect the lay-up is symmetrical both about the midplane and wrt. the generators. This eliminates $a_{14} \ldots a_{34}$ and lengthwise twisting $\left(\partial v/\partial z\right)$ effectively ceases. It is with this assumption that the methods of Chapter 4 are quite justifiable, however a complete understanding does require a look at the general case.

5.2 Extraction of "L" Terms

The differential equations (5.31) and (5.38) can be solved using the stress functions presented in Chapter 4. For clarity they are repeated below.

$$\sigma_r = \frac{1}{r}\frac{\partial F}{\partial r} + \frac{1}{r^2}\frac{\partial^2 F}{\partial \theta^2}$$

$$\sigma_\theta = \frac{\partial^2 F}{\partial r^2}$$

$$\tau_{r\theta} = \frac{-\partial^2}{\partial r \partial \theta}\left(\frac{F}{r}\right)$$

$$\tau_{rz} = \frac{1}{r}\frac{\partial \Psi}{\partial \theta}$$

$$\tau_{\theta z} = -\frac{\partial \Psi}{\partial r}$$

The *LHS* of (5.38) can be expressed in terms of the stress function.

$$\left(\frac{\partial^2}{\partial \theta^2} - r\frac{\partial}{\partial r}\right)\left[\beta_{11}\left(\frac{1}{r}\frac{\partial F}{\partial r} + \frac{1}{r^2}\frac{\partial^2 F}{\partial \theta^2}\right) + \beta_{12}\left(\frac{\partial^2 F}{\partial r^2}\right) + \beta_{14}\left(\frac{-\partial \Psi}{\partial r}\right) + \beta_{15}\left(\frac{1}{r}\frac{\partial \Psi}{\partial \theta}\right) + \right.$$

$$\beta_{16}\left(\frac{-\partial^2}{\partial r\partial\theta}\left(\frac{F}{r}\right)\right)\Bigg] + r\frac{\partial^2}{\partial r^2}\left[r\beta_{21}\left(\frac{1}{r}\frac{\partial F}{\partial r} + \frac{1}{r^2}\frac{\partial^2 F}{\partial\theta^2}\right) + \right.$$

$$\left. r\beta_{22}\left(\frac{\partial^2 F}{\partial r^2}\right) + r\beta_{24}\left(\frac{-\partial\Psi}{\partial r}\right) + r\beta_{25}\left(\frac{1}{r}\frac{\partial\Psi}{\partial\theta}\right) + r\beta_{26}\left(\frac{-\partial^2}{\partial r\partial\theta}\left(\frac{F}{r}\right)\right)\right] -$$

$$\frac{\partial^2}{\partial r\partial\theta}\left[r\beta_{61}\left(\frac{1}{r}\frac{\partial F}{\partial r} + \frac{1}{r^2}\frac{\partial^2 F}{\partial\theta^2}\right) + r\beta_{62}\left(\frac{\partial^2 F}{\partial r^2}\right) + r\beta_{64}\left(\frac{-\partial\Psi}{\partial r}\right) + r\beta_{65}\left(\frac{1}{r}\frac{\partial\Psi}{\partial\theta}\right) + r\beta_{66}\left(\frac{-\partial}{\partial r\partial\theta}\left(\frac{F}{r}\right)\right)\right]$$

$$(5.42)$$

The 1$^{\text{st}}$ term in (5.42) expands to:

$$\beta_{11}\frac{1}{r}\frac{\partial^3 F}{\partial\theta^2\partial r} + \beta_{11}\frac{1}{r^2}\frac{\partial^4 F}{\partial\theta^4} + \beta_{12}\frac{\partial^4 F}{\partial\theta^2\partial r^2} - \beta_{14}\frac{\partial^3\Psi}{\partial\theta^2\partial r} + \beta_{15}\frac{1}{r}\frac{\partial^3\Psi}{\partial\theta^3} + \beta_{16}\frac{1}{r^2}\frac{\partial^3 F}{\partial\theta^3} - \beta_{16}\frac{1}{r}\frac{\partial^4 F}{\partial r\partial\theta^3}$$

The 2$^{\text{nd}}$ term in (5.42) expands to:

$$-r\left[-\beta_{11}\frac{1}{r^2}\frac{\partial F}{\partial r} + \beta_{11}\frac{1}{r}\frac{\partial^2 F}{\partial r^2} + \beta_{11}\frac{-2}{r^3}\frac{\partial^2 F}{\partial\theta^2} + \beta_{11}\frac{1}{r^2}\frac{\partial^3 F}{\partial r\partial\theta^2} + \beta_{12}\frac{\partial^3 F}{\partial r^3} - \right.$$

$$\left. \beta_{14}\frac{\partial^2\Psi}{\partial r^2} - \beta_{15}\frac{1}{r^2}\frac{\partial\Psi}{\partial\theta} + \beta_{15}\frac{1}{r}\frac{\partial^2\Psi}{\partial r\partial\theta} - \beta_{16}\frac{2}{r^3}\frac{\partial F}{\partial\theta} + \beta_{16}\frac{1}{r^2}\frac{\partial^2 F}{\partial r\partial\theta} + \beta_{16}\frac{1}{r^2}\frac{\partial^2 F}{\partial r\partial\theta} - \beta_{16}\frac{1}{r}\frac{\partial^3 F}{\partial r^2\partial\theta}\right]$$

The 3$^{\text{rd}}$ term of (5.42) expands to:

$$r\left[\beta_{21}\frac{\partial^3 F}{\partial r^3} + \beta_{21}\frac{\partial}{\partial r}\left(\frac{-1}{r^2}\frac{\partial^2 F}{\partial\theta^2} + \frac{1}{r}\frac{\partial^3 F}{\partial\theta^2\partial r}\right) + \beta_{22}\frac{\partial}{\partial r}\left(\frac{\partial^2 F}{\partial r^2} + r\frac{\partial^3 F}{\partial r^3}\right) + \right.$$

$$\left. \beta_{24}\frac{\partial}{\partial r}\left(-\frac{\partial\Psi}{\partial r} - r\frac{\partial^2\Psi}{\partial r^2}\right) + \beta_{25}\frac{\partial^3\Psi}{\partial r^2\partial\theta} + \frac{\partial}{\partial r}\left(-\beta_{26}\frac{1}{r^2}\frac{\partial F}{\partial\theta} + \beta_{26}\frac{1}{r}\frac{\partial^2 F}{\partial r\partial\theta} - \beta_{26}\frac{\partial^3 F}{\partial r^2\partial\theta}\right)\right]$$

rewritten as

$$r\left[\beta_{21}\frac{\partial^3 F}{\partial r^3} + \beta_{21}\frac{2}{r^3}\frac{\partial^2 F}{\partial\theta^2} - \beta_{21}\frac{1}{r^2}\frac{\partial^3 F}{\partial r\partial\theta^2} - \beta_{21}\frac{1}{r^2}\frac{\partial^3 F}{\partial\theta^2\partial r} + \beta_{21}\frac{1}{r}\frac{\partial^4 F}{\partial\theta^2\partial r^2} + \right.$$

$$\beta_{22}\frac{\partial^3 F}{\partial r^3} + \beta_{22}\frac{\partial^3 F}{\partial r^3} + \beta_{22}r\frac{\partial^4 F}{\partial r^4} - \beta_{24}\frac{\partial^2\Psi}{\partial r^2} - \beta_{24}\frac{\partial^2\Psi}{\partial r^2} - \beta_{24}r\frac{\partial^3\Psi}{\partial r^3} +$$

$$\left. \beta_{25}\frac{\partial^3\Psi}{\partial r^2\partial\theta} + \beta_{26}\frac{2}{r^3}\frac{\partial F}{\partial\theta} - \beta_{26}\frac{1}{r^2}\frac{\partial^2 F}{\partial r\partial\theta} - \beta_{26}\frac{1}{r^2}\frac{\partial^2 F}{\partial r\partial\theta} + \beta_{26}\frac{1}{r}\frac{\partial^3 F}{\partial r^2\partial\theta} - \beta_{26}\frac{\partial^4 F}{\partial r^3\partial\theta}\right]$$

215

The 4ᵗʰ term of (5.42) expands to:

$$-\left[\frac{\partial}{\partial r}\left(\beta_{61}\frac{\partial^2 F}{\partial r\partial\theta}+\beta_{61}\frac{1}{r}\frac{\partial^3 F}{\partial\theta^3}\right)+\frac{\partial}{\partial r}\left(\beta_{62}r\frac{\partial^3 F}{\partial\theta\partial r^2}\right)+\frac{\partial}{\partial r}\left(-\beta_{64}r\frac{\partial^2\Psi}{\partial r\partial\theta}\right)+\beta_{65}\frac{\partial^3\Psi}{\partial r\partial\theta^2}+\right.$$

$$\left.\frac{\partial}{\partial\theta}\left(-\beta_{66}\frac{1}{r^2}\frac{\partial F}{\partial\theta}+\beta_{66}\frac{1}{r}\frac{\partial^2 F}{\partial r\partial\theta}-\beta_{66}\frac{\partial^3 F}{\partial r^2\partial\theta}\right)\right]$$

rewritten as

$$-\left[\beta_{61}\frac{\partial^3 F}{\partial r^2\partial\theta}-\beta_{61}\frac{1}{r^2}\frac{\partial^3 F}{\partial\theta^3}+\beta_{61}\frac{1}{r}\frac{\partial^4 F}{\partial\theta^3\partial r}+\beta_{62}\frac{\partial^3 F}{\partial\theta\partial r^2}+\beta_{62}r\frac{\partial^4 F}{\partial\theta\partial r^3}-\beta_{64}\frac{\partial^2\Psi}{\partial r\partial\theta}-\right.$$

$$\left.r\beta_{64}\frac{\partial^3\Psi}{\partial r^2\partial\theta}+\beta_{65}\frac{\partial^3\Psi}{\partial r\partial\theta^2}-\beta_{66}\frac{1}{r^2}\frac{\partial^2 F}{\partial\theta^2}+\beta_{66}\frac{1}{r}\frac{\partial^3 F}{\partial r\partial\theta^2}-\beta_{66}\frac{\partial^4 F}{\partial r^2\partial\theta^2}\right]$$

Grouping terms for F & Ψ :

$$r^2\beta_{22}\frac{\partial^4 F}{\partial r^4}-2r\beta_{26}\frac{\partial^4 F}{\partial r^3\partial\theta}+\left(2\beta_{12}+\beta_{66}\right)\frac{\partial^4 F}{\partial r^2\partial\theta^2}-\frac{2}{r}\beta_{16}\frac{\partial^4 F}{\partial r\partial\theta^3}+\frac{1}{r^2}\beta_{11}\frac{\partial^4 F}{\partial\theta^4}+2r\beta_{22}\frac{\partial^3 F}{\partial r^3}$$

$$-\frac{1}{r}\left(2\beta_{12}+\beta_{66}\right)\frac{\partial^3 F}{\partial r\partial\theta^2}+\frac{2}{r^2}\beta_{16}\frac{\partial^3 F}{\partial\theta^3}-\beta_{11}\frac{\partial^2 F}{\partial r}-\frac{2}{r}\left(\beta_{16}+\beta_{26}\right)\frac{\partial^2 F}{\partial r\partial\theta}+\frac{1}{r^2}\left(2\beta_{11}+2\beta_{12}-\beta_{66}\right)\frac{\partial^2 F}{\partial\theta^2}+$$

$$\frac{1}{r}\beta_{11}\frac{\partial F}{\partial r}+\frac{2}{r^2}\left(\beta_{16}+\beta_{26}\right)\frac{\partial F}{\partial\theta}+r^2\left(\beta_{24}\right)\frac{\partial^3\Psi}{\partial r^3}+r\left(\beta_{25}+\beta_{64}\right)\frac{\partial^3\Psi}{\partial r^2\partial\theta}-\left(\beta_{14}+\beta_{65}\right)\frac{\partial^3\Psi}{\partial r\partial\theta^2}+$$

$$\beta_{15}\frac{1}{r}\frac{\partial^3\Psi}{\partial\theta^3}+r\left(\beta_{14}-2\beta_{24}\right)\frac{\partial^2\Psi}{\partial r^2}+\left(\beta_{64}-\beta_{15}\right)\frac{\partial^2\Psi}{\partial r\partial\theta}+\beta_{15}\frac{1}{r}\frac{\partial\Psi}{\partial\theta}=RHS$$

(5.43)

Dividing the whole expression by r^2 we can express it as $L_4'F+L_3'\Psi=RHS$.

where: L_4' Represents all differentials wrt. F

L_3' Represents all differentials wrt. Ψ

Equation (5.31) can be treated equally. Expansion gives:

$$\frac{1}{r}\frac{\partial}{\partial\theta}\left[\beta_{51}\left(\frac{1}{r}\frac{\partial F}{\partial r}+\frac{1}{r^2}\frac{\partial^2 F}{\partial\theta^2}\right)+\beta_{52}\left(\frac{\partial^2 F}{\partial r^2}\right)+\beta_{54}\left(\frac{-\partial\Psi}{\partial r}\right)+\beta_{55}\left(\frac{1}{r}\frac{\partial\Psi}{\partial\theta}\right)+\beta_{56}\left(\frac{-\partial^2}{\partial r\partial\theta}\left(\frac{F}{r}\right)\right)\right]-$$

$$\left(\frac{\partial}{\partial r}+\frac{1}{r}\right)\left[\beta_{41}\left(\frac{1}{r}\frac{\partial F}{\partial r}+\frac{1}{r^2}\frac{\partial^2 F}{\partial\theta^2}\right)+\beta_{42}\left(\frac{\partial^2 F}{\partial r^2}\right)+\beta_{44}\left(\frac{-\partial\Psi}{\partial r}\right)+\beta_{45}\left(\frac{1}{r}\frac{\partial\Psi}{\partial\theta}\right)+\beta_{46}\left(\frac{-\partial^2}{\partial r\partial\theta}\left(\frac{F}{r}\right)\right)\right]=RHS$$

(5.44)

Further expansion yields:

$$\left[\beta_{51}\left(\frac{1}{r^2}\frac{\partial^2 F}{\partial r\partial\theta}+\frac{1}{r^3}\frac{\partial^3 F}{\partial\theta^3}\right)+\beta_{52}\left(\frac{1}{r}\frac{\partial^3 F}{\partial\theta\partial r^2}\right)-\beta_{45}\left(\frac{1}{r}\frac{\partial^2\Psi}{\partial r\partial\theta}\right)+\right.$$

$$\left.\beta_{55}\frac{1}{r^2}\frac{\partial^2\Psi}{\partial\theta^2}+\beta_{56}\left(\frac{1}{r^3}\frac{\partial^2 F}{\partial\theta^2}-\frac{1}{r^2}\frac{\partial^3 F}{\partial r\partial\theta^2}\right)\right]-$$

$$\left[\beta_{41}\left(-\frac{1}{r^2}\frac{\partial F}{\partial r}+\frac{1}{r}\frac{\partial^2 F}{\partial r^2}-\frac{2}{r^3}\frac{\partial^2 F}{\partial\theta^2}+\frac{1}{r^2}\frac{\partial^3 F}{\partial r\partial\theta^2}\right)+\beta_{42}\left(\frac{\partial^3 F}{\partial r^3}\right)-\beta_{44}\left(\frac{\partial^2\Psi}{\partial r^2}\right)+\right.$$

$$\left.\beta_{45}\left(\frac{-1}{r^2}\frac{\partial\Psi}{\partial\theta}+\frac{1}{r}\frac{\partial^2\Psi}{\partial r\partial\theta}\right)+\beta_{46}\left(\frac{-2}{r^3}\frac{\partial F}{\partial\theta}+\frac{1}{r^2}\frac{\partial^2 F}{\partial r\partial\theta}+\frac{1}{r^2}\frac{\partial^2 F}{\partial r\partial\theta}-\frac{1}{r}\frac{\partial^3 F}{\partial r^2\partial\theta}\right)\right]-$$

$$\frac{1}{r}\left[\beta_{41}\left(\frac{1}{r}\frac{\partial F}{\partial r}+\frac{1}{r^2}\frac{\partial^2 F}{\partial\theta^2}\right)+\beta_{42}\left(\frac{\partial^2 F}{\partial r^2}\right)+\beta_{44}\left(-\frac{\partial\Psi}{\partial r}\right)+\beta_{45}\left(\frac{1}{r}\frac{\partial\Psi}{\partial\theta}\right)+\beta_{46}\left(\frac{1}{r^2}\frac{\partial F}{\partial\theta}-\frac{1}{r}\frac{\partial^2 F}{\partial r\partial\theta}\right)\right]=RHS$$

Grouping terms:

$$-\beta_{42}\frac{\partial^3 F}{\partial r^3}+\frac{1}{r}\left(\beta_{52}+\beta_{46}\right)\frac{\partial^3 F}{\partial r^2\partial\theta}-\frac{1}{r^2}\left(\beta_{56}+\beta_{41}\right)\frac{\partial^3 F}{\partial r\partial\theta^2}+\frac{1}{r^3}\beta_{51}\frac{\partial^3 F}{\partial\theta^3}-\frac{1}{r}\left(\beta_{41}+\beta_{42}\right)\frac{\partial^2 F}{\partial r^2}+$$

$$\frac{1}{r^2}\left(\beta_{51}-\beta_{46}\right)\frac{\partial^2 F}{\partial r\partial\theta}+\frac{1}{r^3}\left(\beta_{56}+\beta_{41}\right)\frac{\partial^2 F}{\partial\theta^2}+\beta_{46}\frac{1}{r^3}\frac{\partial F}{\partial\theta}+$$

$$\beta_{44}\frac{\partial^2\Psi}{\partial r^2}-2\beta_{45}\frac{1}{r}\frac{\partial^2\Psi}{\partial r\partial\theta}+\beta_{55}\frac{1}{r^2}\frac{\partial^2\Psi}{\partial\theta^2}+\frac{1}{r}\beta_{44}\frac{\partial\Psi}{\partial r}=RHS$$

(5.45)

The equation can be expressed as:

$$L_3^{''}F+L_2^{'}\Psi=RHS$$

where: $L_3^{''}$ represents all the differentials with respect to F

$L_2^{'}$ represents all the differentials with respect to Ψ

217

In summary, the system of differential equations to be solved is:

$$L_4'F + L_3'\Psi = \frac{2}{a_{33}}\left[A(a_{13} - a_{23}) + Ba_{36}\right]\frac{\cos\theta}{r} + \frac{2}{a_{33}}\left[B(a_{13} - a_{23}) + Aa_{36}\right]\frac{\sin\theta}{r}$$

$$L_3''F + L_2'\Psi = \frac{1}{a_{33}}(2a_{34}A - a_{35}B)\cos\theta + \frac{1}{a_{33}}(2a_{34}B + a_{35}A)\sin\theta + \frac{a_{34}C}{a_{33}r} - 2\vartheta$$

$$(5.46)$$

5.3 Variable Material Coefficients

We examine next the case for variable material coefficients in a pressure vessel constructed of a set of off-axis orthotropic layers. Recalling previous discussion concerning the possibility of bending deformations, and since in this case there are no externally applied bending moments to react, we note that the arbitrary constants of integration A & $B = 0$.

For this case (5.31) and (5.38) immediately simplify to:

$$\frac{1}{r}\frac{\partial}{\partial\theta}\left[\beta_{51}\sigma_r + \beta_{52}\sigma_\theta + \beta_{54}\tau_{\theta z} + \beta_{55}\tau_{rz} + \beta_{56}\tau_{r\theta}\right] - \left(\frac{\partial}{\partial r} + \frac{1}{r}\right)\left[\beta_{41}\sigma_r + \beta_{42}\sigma_\theta + \beta_{44}\tau_{\theta z} + \beta_{45}\tau_{rz} + \beta_{46}\tau_{r\theta}\right] =$$

$$\frac{a_{34}C}{a_{33}r} - 2\vartheta$$

and

$$\left(\frac{\partial^2}{\partial\theta^2} - r\frac{\partial}{\partial r}\right)\left[\beta_{11}\sigma_r + \beta_{12}\sigma_\theta + \beta_{14}\tau_{\theta z} + \beta_{15}\tau_{rz} + \beta_{16}\tau_{r\theta}\right] +$$

$$r\frac{\partial^2}{\partial r^2}\left[r(\beta_{21}\sigma_r + \beta_{22}\sigma_\theta + \beta_{24}\tau_{\theta z} + \beta_{25}\tau_{rz} + \beta_{26}\tau_{r\theta})\right] -$$

$$\frac{\partial^2}{\partial r\partial\theta}\left[r(\beta_{61}\sigma_r + \beta_{62}\sigma_\theta + \beta_{64}\tau_{\theta z} + \beta_{65}\tau_{rz} + \beta_{66}\tau_{r\theta})\right] = RHS = 0$$

218

Seeing that filament wound construction also entails rotational symmetry, we can set

$$\frac{\partial}{\partial \theta} = 0$$

We are left with:
$$\sigma_r = \frac{1}{r}\frac{\partial F}{\partial r} \qquad \tau_{r\theta} = \tau_{rz} = 0$$

$$\sigma_\theta = \frac{\partial^2 F}{\partial r^2}$$

$$\tau_{\theta z} = -\frac{\partial \Psi}{\partial r}$$

Also for the rotated off-axis lamina the coefficients $\beta_{15}, \beta_{25}, \beta_{45}, \beta_{16}, \beta_{26}, \beta_{36}$ and their

symmetric counterparts equal zero.

The system (5.46) is now:

$$-\left(\frac{\partial}{\partial r} + \frac{1}{r}\right)\left[\beta_{14}\frac{1}{r}\frac{\partial F}{\partial r} + \beta_{24}\frac{\partial^2 F}{\partial r^2} + \beta_{44}\frac{-\partial \Psi}{\partial r}\right] = \frac{C}{r}\frac{a_{34}}{a_{33}} - 2\vartheta$$

and

$$\left(-r\frac{\partial}{\partial r}\right)\left[\beta_{11}\frac{1}{r}\frac{\partial F}{\partial r} + \beta_{12}\frac{\partial^2 F}{\partial r^2} + \beta_{14}\frac{-\partial \Psi}{\partial r}\right] + r\frac{\partial^2}{\partial r^2}\left[r\left(\beta_{12}\frac{1}{r}\frac{\partial F}{\partial r} + \beta_{22}\frac{\partial^2 F}{\partial r^2} + \beta_{24}\frac{-\partial \Psi}{\partial r}\right)\right] =$$

$$r\frac{\partial}{\partial r}\left(\frac{a_{13}}{a_{33}}C\right) - r\frac{\partial^2}{\partial r^2}\left[r\frac{a_{23}}{a_{33}}C\right]$$

$$(5.47)$$

If the material coefficients are *fixed* the first part is:

$$-\left(\beta_{14}\frac{-1}{r^2}\frac{\partial F}{\partial r} + \beta_{14}\frac{1}{r}\frac{\partial^2 F}{\partial r^2} + \beta_{14}\frac{1}{r^2}\frac{\partial F}{\partial r}\right) - \beta_{24}\left(\frac{\partial^3 F}{\partial r^3} + \frac{1}{r}\frac{\partial^2 F}{\partial r^2}\right) + \beta_{44}\left(\frac{\partial^2 \Psi}{\partial r^2} + \frac{1}{r}\frac{\partial \Psi}{\partial r}\right) = \frac{C}{r}\frac{a_{34}}{a_{33}} - 2\vartheta$$

which simplifies to

$$-\beta_{24}\frac{\partial^3 F}{\partial r^3} - \frac{1}{r}(\beta_{14} + \beta_{24})\frac{\partial^2 F}{\partial r^2} + \beta_{44}\left(\frac{\partial^2 \Psi}{\partial r^2} + \frac{1}{r}\frac{\partial \Psi}{\partial r}\right) = \frac{C}{r}\frac{a_{34}}{a_{33}} - 2\vartheta$$

$$(5.48)$$

and the second part is:

219

$$-r\left[\beta_{11}\left(\frac{-1}{r^2}\frac{\partial F}{\partial r}+\frac{1}{r}\frac{\partial^2 F}{\partial r^2}\right)+\beta_{12}\frac{\partial^3 F}{\partial r^3}-\beta_{14}\frac{\partial^2 \Psi}{\partial r^2}\right]+r\frac{\partial}{\partial r}\left[\beta_{12}\frac{\partial^2 F}{\partial r^2}+\beta_{22}\frac{\partial^2 F}{\partial r^2}+r\beta_{22}\frac{\partial^3 F}{\partial r^3}-\right.$$

$$\left.\beta_{24}\left(\frac{\partial\Psi}{\partial r}+r\frac{\partial^2\Psi}{\partial r^2}\right)\right]=RHS$$

rewriting,

$$\beta_{11}\frac{1}{r}\frac{\partial F}{\partial r}-\beta_{11}\frac{\partial^2 F}{\partial r^2}-r\beta_{12}\frac{\partial^3 F}{\partial r^3}+r\beta_{14}\frac{\partial^2\Psi}{\partial r^2}+r\beta_{12}\frac{\partial^3 F}{\partial r^3}+r\beta_{22}\frac{\partial^3 F}{\partial r^3}+r\beta_{22}\frac{\partial^3 F}{\partial r^3}+$$

$$r^2\beta_{22}\frac{\partial^4 F}{\partial r^4}-r\beta_{24}\frac{\partial^2\Psi}{\partial r^2}-r\beta_{24}\frac{\partial^2\Psi}{\partial r^2}-r^2\beta_{24}\frac{\partial^3\Psi}{\partial r^3}=RHS$$

or

$$\beta_{22}\left(r^2\frac{\partial^4 F}{\partial r^4}+2r\frac{\partial^3 F}{\partial r^3}\right)+\beta_{11}\left(\frac{-\partial^2 F}{\partial r^2}+\frac{1}{r}\frac{\partial F}{\partial r}\right)-r^2\beta_{24}\frac{\partial^3\Psi}{\partial r^3}+r(\beta_{14}-2\beta_{24})\frac{\partial^2\Psi}{\partial r^2}=RHS$$

$$(5.49)$$

If the material coefficients are *variable* and expressible as a function of (r) they are then subject to differentiation. A simple yet powerful variation can be set using power functions (though any other suitable functions could be utilized for this purpose). Applying the power function form to the general case:

$$a_{ij}=\alpha_{ij}r^{-n}$$
$$\beta_{ij}=\gamma_{ij}r^{-n}$$

Then (5.47) can be stated as:

$$-\gamma_{24}r^{-n}\frac{\partial^3 F}{\partial r^3}-[\gamma_{14}+\gamma_{24}(1-n)]r^{-n-1}\frac{\partial^2 F}{\partial r^2}+\gamma_{14}nr^{-n-2}\frac{\partial F}{\partial r}+\gamma_{44}r^{-n}\frac{\partial^2\Psi}{\partial r^2}+\gamma_{44}(1-n)r^{-n-1}\frac{\partial\Psi}{\partial r}=\frac{C\alpha_{34}}{r\alpha_{33}}-2\vartheta$$

$$(5.50)$$

Dividing both sides by r^{-n} we can write

$$-\gamma_{24}\frac{\partial^3 F}{\partial r^3}-\frac{(\gamma_{14}+\gamma_{24}(1-n))}{r}\frac{\partial^2 F}{\partial r^2}+\frac{n\gamma_{14}}{r^2}\frac{\partial F}{\partial r}+\gamma_{44}\left(\frac{\partial^2\Psi}{\partial r^2}+\frac{(1-n)}{r}\frac{\partial\Psi}{\partial r}\right)=C\frac{\alpha_{34}}{\alpha_{33}}r^{n-1}-2\vartheta r^n$$

$$(5.50a)$$

similarly (5.38) becomes

$$-r\frac{\partial}{\partial r}\left[\gamma_{11}r^{-n-1}\frac{\partial F}{\partial r}+\gamma_{12}r^{-n}\frac{\partial^2 F}{\partial r^2}-\gamma_{14}r^{-n}\frac{\partial \Psi}{\partial r}\right]+r\frac{\partial^2}{\partial r^2}\left[r\left(\gamma_{21}r^{-n-1}\frac{\partial F}{\partial r}+\gamma_{22}r^{-n}\frac{\partial^2 F}{\partial r^2}-\gamma_{24}r^{-n}\frac{\partial \Psi}{\partial r}\right)\right]$$

$$=r\frac{\partial}{\partial r}\left(\frac{\alpha_{13}}{\alpha_{33}}C\right)-r\frac{\partial^2}{\partial r^2}\left[r\frac{\alpha_{23}}{\alpha_{33}}C\right]$$

(5.51)

Divide both sides of (5.51) by $r\dfrac{\partial}{\partial r}$ and we have

$$-\left[\gamma_{11}r^{-n-1}\frac{\partial F}{\partial r}+\gamma_{12}r^{-n}\frac{\partial^2 F}{\partial r^2}-\gamma_{14}r^{-n}\frac{\partial \Psi}{\partial r}\right]+\frac{\partial}{\partial r}\left[r\left(\gamma_{21}r^{-n-1}\frac{\partial F}{\partial r}+\gamma_{22}r^{-n}\frac{\partial^2 F}{\partial r^2}-\gamma_{24}r^{-n}\frac{\partial \Psi}{\partial r}\right)\right]$$

$$=\frac{\alpha_{13}}{\alpha_{33}}C-\frac{\partial}{\partial r}\left[r\frac{\alpha_{23}}{\alpha_{33}}C\right]$$

or

$$-\gamma_{11}r^{-n-1}\frac{\partial F}{\partial r}-\gamma_{12}r^{-n}\frac{\partial^2 F}{\partial r^2}+\gamma_{14}r^{-n}\frac{\partial \Psi}{\partial r}-\gamma_{21}nr^{-n-1}\frac{\partial F}{\partial r}+\gamma_{22}(-n+1)r^{-n}\frac{\partial^2 F}{\partial r^2}-$$

$$\gamma_{24}(-n+1)r^{-n}\frac{\partial \Psi}{\partial r}+\gamma_{12}r^{-n}\frac{\partial^2 F}{\partial r^2}+\gamma_{22}r^{-n-1}\frac{\partial^3 F}{\partial r^3}-\gamma_{24}r^{-n-1}\frac{\partial^2 \Psi}{\partial r^2}=\left(\frac{\alpha_{13}-\alpha_{23}}{\alpha_{33}}\right)C$$

Collecting terms:

$$\gamma_{22}r^{-n-1}\frac{\partial^3 F}{\partial r^3}+\gamma_{22}(-n+1)r^{-n}\frac{\partial^2 F}{\partial r^2}-(\gamma_{11}+n\gamma_{21})r^{-n-1}\frac{\partial F}{\partial r}-\gamma_{24}r^{-n-1}\frac{\partial^2 \Psi}{\partial r^2}+$$

$$\left[\gamma_{14}-\gamma_{24}(-n+1)\right]r^{-n}\frac{\partial \Psi}{\partial r}=\left(\frac{\alpha_{13}-\alpha_{23}}{\alpha_{33}}\right)C$$

(5.52)

Multiplying both sides by $\dfrac{r^{n-1}}{\gamma_{22}}$

$$\frac{\partial^3 F}{\partial r^3}+\frac{(-n+1)}{r}\frac{\partial^2 F}{\partial r^2}-\frac{(\gamma_{11}+n\gamma_{21})}{r^2\gamma_{22}}\frac{\partial F}{\partial r}-\frac{\gamma_{24}}{\gamma_{22}}\frac{\partial^2 \Psi}{\partial r^2}+\frac{\left[\gamma_{14}-\gamma_{24}(-n+1)\right]}{\gamma_{22}}\frac{1}{r}\frac{\partial \Psi}{\partial r}=\left(\frac{\alpha_{13}-\alpha_{23}}{\gamma_{22}\alpha_{23}}\right)Cr^{n-1}$$

(5.52a)

221

Making the substitution: $\qquad \dfrac{\partial F}{\partial r} = \phi, \qquad \dfrac{\partial \Psi}{\partial r} = \varphi$

The equations (5.50a) and (5.52a) can be reduced by 1 order of magnitude:

$$-\gamma_{24}\frac{\partial^2\phi}{\partial r^2} - \frac{1}{r}\left(\gamma_{14} + \gamma_{24}(1-n)\right)\frac{\partial\phi}{\partial r} + \frac{n}{r^2}\gamma_{14}\,\phi + \gamma_{44}\left(\frac{\partial\varphi}{\partial r} + \frac{1-n}{r}\varphi\right) = C\frac{\alpha_{34}}{\alpha_{33}}r^{n-1} - 2\vartheta r^n$$

$$\frac{\partial^2\phi}{\partial r^2} + \left(\frac{-n+1}{r}\right)\frac{\partial\phi}{\partial r} - \frac{(\gamma_{11} + n\gamma_{12})}{r^2\gamma_{22}}\phi - \frac{\gamma_{24}}{\gamma_{22}}\frac{\partial\varphi}{\partial r} + \left[\frac{\gamma_{14} + \gamma_{24}(n-1)}{\gamma_{22}}\right]\frac{1}{r}\varphi = \left[\frac{\alpha_{13} - \alpha_{23}}{\gamma_{22}\alpha_{33}}\right]Cr^{n-1}$$

$$\text{(5.53)}$$

Recognize that:

$$\frac{\partial\varphi}{\partial r} + \frac{1-n}{r}\varphi = \frac{1}{r^{1-n}}\frac{\partial}{\partial r}\left(r^{1-n}\varphi\right) = \frac{1}{r^{1-n}}\left(r^{1-n}\frac{\partial\varphi}{\partial r} + (1-n)r^{-n}\varphi\right)$$

Therefore:

$$\gamma_{44}\frac{1}{r^{1-n}}\frac{\partial}{\partial r}\left(r^{1-n}\varphi\right) = C\frac{\alpha_{34}}{\alpha_{33}}r^{n-1} - 2\vartheta r^n + \gamma_{24}\frac{\partial^2\phi}{\partial r^2} + \frac{1}{r}\left(\gamma_{14} + (1-n)\gamma_{24}\right)\frac{\partial\phi}{\partial r} - \frac{n\gamma_{14}}{r^2}\phi$$

multiplying by $\left(\dfrac{r^{1-n}}{\gamma_{44}}\right)$

$$\frac{\partial}{\partial r}\left(r^{1-n}\varphi\right) = \frac{C\alpha_{34}}{\gamma_{44}\alpha_{33}} - \frac{2\vartheta r}{\gamma_{44}} + r^{1-n}\frac{\gamma_{24}}{\gamma_{44}}\frac{\partial^2\phi}{\partial r^2} + r^{-n}\frac{\left(\gamma_{14} + (1-n)\gamma_{24}\right)}{\gamma_{44}}\frac{\partial\phi}{\partial r} - \frac{n\gamma_{14}}{\gamma_{44}}r^{-n-1}\phi$$

$$r^{1-n}\varphi = \int\left(C\frac{\alpha_{34}}{\gamma_{44}\alpha_{33}} - \frac{2\vartheta r}{\gamma_{44}} + r^{1-n}\frac{\gamma_{24}}{\gamma_{44}}\frac{\partial^2\phi}{\partial r^2} + r^{-n}\frac{\left(\gamma_{14} + (1-n)\gamma_{24}\right)}{\gamma_{44}}\frac{\partial\phi}{\partial r} - \frac{n\gamma_{14}}{\gamma_{44}}r^{-n-1}\phi\right)dr$$

$$r^{1-n}\varphi = C\frac{\alpha_{34}r}{\gamma_{44}\alpha_{33}} - \frac{2\vartheta r^2}{2\gamma_{44}} + \frac{\gamma_{24}}{\gamma_{44}}\int\left(r^{1-n}\frac{\partial^2\phi}{\partial r^2} + (1-n)r^{-n}\frac{\partial\phi}{\partial r}\right)dr + \frac{\gamma_{14}}{\gamma_{44}}\int\left(r^{-n}\frac{\partial\phi}{\partial r} - nr^{-n-1}\phi\right)dr$$

$$r^{1-n}\varphi = \frac{Cr}{\gamma_{44}}\frac{\alpha_{34}}{\alpha_{33}} - \frac{\vartheta r^2}{\gamma_{44}} + \frac{\gamma_{24}}{\gamma_{44}}r^{1-n}\frac{\partial\phi}{\partial r} + \frac{\gamma_{14}}{\gamma_{44}}r^{-n}\phi$$

multiplying by r^{n-1}

222

$$\varphi = \frac{Cr^n}{\gamma_{44}}\frac{\alpha_{34}}{\alpha_{33}} - \frac{9r^{n-1}}{\gamma_{44}} + \frac{\gamma_{24}}{\gamma_{44}}\frac{\partial\phi}{\partial r} + \frac{1}{r}\frac{\gamma_{14}}{\gamma_{44}}\phi$$

Substituting the expression for φ back into (5.53)

$$\frac{\partial^2\phi}{\partial r^2} + \left(\frac{-n+1}{r}\right)\frac{\partial\phi}{\partial r} - \frac{(\gamma_{11}+n\gamma_{12})}{\gamma_{22}}\frac{1}{r^2}\phi - \frac{\gamma_{24}}{\gamma_{22}}\left[\frac{C\alpha_{34}nr^{n-1}}{\gamma_{44}\alpha_{33}} - \frac{(n+1)9r^n}{\gamma_{44}} + \frac{\gamma_{24}}{\gamma_{44}}\frac{\partial^2\phi}{\partial r^2} - \right.$$
$$\left.\frac{\gamma_{14}}{\gamma_{44}}\frac{1}{r^2}\phi + \frac{\gamma_{14}}{\gamma_{44}}\frac{1}{r}\frac{\partial\phi}{\partial r}\right] + \left[\frac{\gamma_{14}+\gamma_{24}(n-1)}{\gamma_{22}}\right]\left[\frac{C\alpha_{34}r^{n-1}}{\gamma_{44}\alpha_{33}} - \frac{9r^n}{\gamma_{44}} + \frac{1}{r}\frac{\gamma_{24}}{\gamma_{44}}\frac{\partial\phi}{\partial r} + \frac{1}{r^2}\frac{\gamma_{14}}{\gamma_{44}}\phi\right] =$$
$$\left[\frac{\alpha_{13}-\alpha_{23}}{\gamma_{22}\alpha_{33}}\right]Cr^{n-1}$$

Collecting terms:

$$\frac{\partial^2\phi}{\partial r^2}\left[1 - \frac{\gamma_{24}^2}{\gamma_{22}\gamma_{44}}\right] + \frac{1}{r}\frac{\partial\phi}{\partial r}\left[(-n+1) - \frac{\gamma_{24}}{\gamma_{22}}\frac{\gamma_{14}}{\gamma_{44}} + \frac{\gamma_{14}\gamma_{24}}{\gamma_{44}\gamma_{22}} + \frac{\gamma_{24}^2}{\gamma_{22}\gamma_{44}}(n-1)\right] - $$
$$\frac{\phi}{r^2}\left[\frac{(\gamma_{11}+n\gamma_{12})}{\gamma_{22}} - \frac{\gamma_{24}\gamma_{14}}{\gamma_{22}\gamma_{44}} - \frac{\gamma_{14}^2}{\gamma_{22}\gamma_{44}} - \frac{\gamma_{14}\gamma_{24}(n-1)}{\gamma_{22}\gamma_{44}}\right] = $$
$$-\left[\frac{-n\gamma_{24}}{\gamma_{22}}\left(\frac{C\alpha_{34}r^{n-1}}{\gamma_{44}\alpha_{33}}\right) + \left(\frac{\gamma_{14}}{\gamma_{22}} + (n-1)\frac{\gamma_{24}}{\gamma_{22}}\right)\left(\frac{C\alpha_{34}r^{n-1}}{\gamma_{44}\alpha_{33}}\right)\right] + \frac{Cr^{n-1}}{\alpha_{33}}\left[\frac{\alpha_{13}-\alpha_{23}}{\gamma_{22}}\right] + $$
$$9r^n\left[\frac{-\gamma_{24}(n+1)}{\gamma_{22}\gamma_{44}} + \frac{\gamma_{14}}{\gamma_{22}\gamma_{44}} + \frac{\gamma_{24}(n-1)}{\gamma_{22}\gamma_{44}}\right]$$

rearranging

$$\frac{\partial^2\phi}{\partial r^2}\left[\frac{\gamma_{24}\gamma_{44}-\gamma_{24}^2}{\gamma_{22}\gamma_{44}}\right] + \frac{1}{r}\frac{\partial\phi}{\partial r}\left[\frac{(-n+1)\gamma_{22}\gamma_{44}-\gamma_{24}^2(-n+1)}{\gamma_{22}\gamma_{44}}\right] - $$
$$\frac{\phi}{r^2}\left[\frac{\gamma_{11}\gamma_{44}+n\gamma_{12}\gamma_{44}-\gamma_{24}\gamma_{14}-\gamma_{14}^2+\gamma_{14}\gamma_{24}-n\gamma_{14}\gamma_{24}}{\gamma_{22}\gamma_{44}}\right] = $$
$$\frac{-Cr^{n-1}}{\alpha_{33}}\left[\frac{\gamma_{14}\alpha_{34}}{\gamma_{22}\gamma_{44}} - \frac{\gamma_{24}\alpha_{34}}{\gamma_{22}\gamma_{44}}\right] + \frac{Cr^{n-1}}{\alpha_{33}}\left[\frac{\alpha_{13}-\alpha_{23}}{\gamma_{22}}\right] + 9r^n\left[\frac{\gamma_{14}-2\gamma_{24}}{\gamma_{22}\gamma_{44}}\right]$$

or

223

$$\frac{\partial^2 \phi}{\partial r^2}\left[\frac{\gamma_{24}\gamma_{44}-\gamma_{24}^2}{\gamma_{22}\gamma_{44}}\right] + \frac{(-n+1)}{r}\frac{\partial \phi}{\partial r}\left[\frac{\gamma_{22}\gamma_{44}-\gamma_{24}^2}{\gamma_{22}\gamma_{44}}\right] - \frac{\phi}{r^2}\left[\frac{\gamma_{11}\gamma_{44}-\gamma_{14}^2-rr_{14}\gamma_{24}+rr_{12}\gamma_{44}}{\gamma_{22}\gamma_{44}}\right] =$$

$$\frac{Cr^{n-1}}{\alpha_{33}}\left[\frac{(\alpha_{13}-\alpha_{23})\gamma_{44}+\alpha_{34}(\gamma_{24}-\gamma_{14})}{\gamma_{22}\gamma_{44}}\right] + 9r^n\left[\frac{\gamma_{14}-2\gamma_{24}}{\gamma_{22}\gamma_{44}}\right]$$

Dividing by $\dfrac{\gamma_{24}\gamma_{44}-\gamma_{24}^2}{\gamma_{24}\gamma_{44}}$

$$\frac{\partial^2 \phi}{\partial r^2} + \left(\frac{-n+1}{r}\right)\frac{\partial \phi}{\partial r} - \frac{\phi}{r^2}\left[\frac{\gamma_{11}\gamma_{44}-\gamma_{14}^2-rr_{14}\gamma_{24}+rr_{12}\gamma_{44}}{\gamma_{22}\gamma_{44}-\gamma_{24}^2}\right] =$$

$$\frac{Cr^{n-1}}{\alpha_{33}}\left[\frac{(\alpha_{13}-\alpha_{23})\gamma_{44}+\alpha_{34}(\gamma_{24}-\gamma_{14})}{\gamma_{22}\gamma_{44}-\gamma_{24}^2}\right] + 9r^n\left[\frac{\gamma_{14}-2\gamma_{24}}{\gamma_{22}\gamma_{44}-\gamma_{24}^2}\right]$$

$$(5.54)$$

The system (5.46) has now been collapsed into the single Euler equation above. Next we must find solution to the homogeneous part in (5.54).

let:
$$\phi = r^\lambda$$
$$\phi' = \lambda r^{\lambda-1}$$
$$\phi'' = \lambda(\lambda-1)r^{\lambda-2}$$

The *LHS* of (5.54) becomes

$$\lambda(\lambda-1)r^{\lambda-2} + \left(\frac{1-n}{r}\right)\lambda r^{\lambda-1} - \frac{r^\lambda}{r^2}\left[\frac{\gamma_{11}\gamma_{44}-\gamma_{14}^2-rr_{14}\gamma_{24}+rr_{12}\gamma_{44}}{\gamma_{22}\gamma_{44}-\gamma_{24}^2}\right] = 0$$

or

$$r^{\lambda-2}\left[\lambda^2-\lambda+\lambda-n\lambda-\left(\frac{\gamma_{11}\gamma_{44}-\gamma_{14}^2-rr_{14}\gamma_{24}+rr_{12}\gamma_{44}}{\gamma_{22}\gamma_{44}-\gamma_{24}^2}\right)\right] = 0$$

Since $r^{\lambda-2} \neq 0$

$$\lambda^2-n\lambda-\left(\frac{\gamma_{11}\gamma_{44}-\gamma_{14}^2-rr_{14}\gamma_{24}+rr_{12}\gamma_{44}}{\gamma_{22}\gamma_{44}-\gamma_{24}^2}\right) = 0$$

$$\lambda = \frac{n \pm \sqrt{n^2 + \dfrac{4\left(\gamma_{11}\gamma_{44} - \gamma_{14}^2 - n\gamma_{14}\gamma_{24} + n\gamma_{12}\gamma_{44}\right)}{\gamma_{22}\gamma_{44} - \gamma_{24}^2}}}{2}$$

$$\lambda_{1,2} = \frac{n \pm \sqrt{n^2 + 4\gamma_n}}{2} \qquad \text{where;} \qquad \gamma_n = \frac{\gamma_{11}\gamma_{44} - \gamma_{14}^2 - n\left(\gamma_{14}\gamma_{24} - \gamma_{12}\gamma_{44}\right)}{\gamma_{22}\gamma_{44} - \gamma_{24}^2}$$

The solution is: $\phi = C_1 r^{\lambda_1} + C_2 r^{\lambda_2}$

alternately if $\lambda_1 = s$, $\quad \lambda_2 = t$

then

$$\phi = C_1 r^s + C_2 r^t$$

The *RHS* terms of (5.54) dictate the particular solution:

let: $\qquad g_n = \left[\dfrac{\left(\alpha_{13} - \alpha_{23}\right)\gamma_{44} + \alpha_{34}\left(\gamma_{24} - \gamma_{14}\right)}{\gamma_{22}\gamma_{44} - \gamma_{24}^2}\right]$, $\quad f_n = \left[\dfrac{\gamma_{14} - 2\gamma_{24}}{\gamma_{22}\gamma_{44} - \gamma_{24}^2}\right]$

then: $\qquad RHS = \dfrac{g_n C r^{n-1}}{\alpha_{33}} + \vartheta r^n f_n$

the Wronskian: $\varpi = y_1 y_2^1 - y_1^1 y_2$

$$\varpi = tr^s r^{t-1} - sr^{s-1} r^t \qquad\qquad \text{where:} \quad y_1 = r^s \quad , \quad y_2 = r^t$$

$$\varpi = r^{s+t-1}\left(t - s\right)$$

$$y_P = -y_1 \int \frac{y_2}{\varpi}\left(\frac{Cg_n r^{n-1}}{\alpha_{33}}\right) dr + y_2 \int \frac{y_1}{\varpi}\left(\frac{Cg_n r^{n-1}}{\alpha_{33}}\right) dr$$

$$y_P = -r^s \int \frac{r^t\left(Cg_n r^{n-1}\right)}{r^{s+t-1}\left(t - s\right)\alpha_{33}} dr + r^t \int \frac{r^s\left(Cg_n r^{n-1}\right)}{r^{s+t-1}\left(t - s\right)\alpha_{33}} dr$$

$$y_P = \frac{Cg_n}{\left(t - s\right)\alpha_{33}}\left[-r^s \int r^{n-s} dr + r^t \int r^{n-t} dr\right]$$

$$y_A = \frac{Cg_n}{(t-s)\alpha_{33}} \left[\frac{-r^s(r^{n-s-1})}{(n-s+1)} + \frac{r^t(r^{n-t-1})}{n-t+1} \right]$$

$$y_A = \frac{Cg_n}{(t-s)\alpha_{33}} \left[\frac{-r^{n-1}}{n-s+1} + \frac{r^{n-1}}{n-t+1} \right] = \frac{Cg_n r^{n-1}}{(t-s)\alpha_{33}} \left[\frac{-1}{n-s+1} + \frac{1}{n-t+1} \right]$$

$$y_A = \frac{Cg_n r^{n-1}}{(t-s)\alpha_{33}} \left[\frac{-n+t-1+n-s+1}{(n-s+1)(n-t+1)} \right] = \frac{Cg_n r^{n-1}}{(t-s)\alpha_{33}} \left[\frac{(t-s)}{(n-s+1)(n-t+1)} \right]$$

$$y_A = \frac{Cg_n r^{n-1}}{\alpha_{33}(n-s+1)(n-t+1)}$$

but: $\quad s = 5n + 5\sqrt{n^2 + 4\gamma_n}$

$\quad\quad\quad t = 5n - 5\sqrt{n^2 + 4\gamma_n}$

so

$$(n-s+1)(n-t+1) = \left(n - 5n - 5\sqrt{n^2 + 4\gamma_n} + 1 \right)\left(n - 5n + 5\sqrt{n^2 + 4\gamma_n} + 1 \right)$$

$$(n-s+1)(n-t+1) = \left(5n - 5\sqrt{n^2 + 4\gamma_n} + 1 \right)\left(5n + 5\sqrt{n^2 + 4\gamma_n} + 1 \right)$$

$$(n-s+1)(n-t+1) = .25n^2 + 25n\sqrt{n^2 + 4\gamma_n} + 5n - 25n\sqrt{n^2 + 4\gamma_n} - 25(n^2 + 4\gamma_n) - $$

$$5\sqrt{n^2 + 4\gamma_n} + 5n + 5\sqrt{n^2 + 4\gamma_n} + 1$$

$$(n-s+1)(n-t+1) = 1 + n - \gamma_n$$

therefore

$$y_A = \frac{Cg_n r^{n-1}}{\alpha_{33}(1 + n - \gamma_n)}$$

A similar treatment for the second paricular solution gives

$$y_{P_2} = \frac{f_n \vartheta}{(t-s)} \left[-r^s \int_{r^{s-t-1}}^{} \frac{r^t r^n}{r^{s-t-1}} \, dr + r^t \int_{r^{s-t-1}}^{} \frac{r^s r^n}{r^{s-t-1}} \, dr \right]$$

$$y_{P_2} = \frac{f_n \vartheta}{(t-s)} \left[\frac{-r^s\left(r^{n-s-2}\right)}{n-s+2} + \frac{r^t\left(r^{n-t-2}\right)}{n-t+2} \right] + C_3$$

$$y_{P_2} = \frac{f_n \vartheta}{(t-s)} \left[\frac{-r^{n+2}}{n-s+2} + \frac{r^{n+2}}{n-t+2} \right] + C_3$$

$$y_{P_2} = \frac{f_n \vartheta r^{n-2}}{(t-s)} \left[\frac{-n+t-2+n-s+2}{(n-s+2)(n-t+2)} \right] + C_3 = \frac{2f_n \vartheta r^{n-2}}{(t-s)} \left[\frac{(t-s)}{(n-s+2)(n-t+2)} \right] + C_3$$

$$y_{P_2} = \frac{f_n \vartheta r^{n-2}}{(n-s+2)(n-t+2)} + C_3$$

Re-examining y_{P_1}:

$$y_{P_1} = \frac{Cr^{n-1}}{\alpha_{33}} \cdot \frac{g_n}{1+n-\gamma_n} = \frac{Cr^{n-1}}{\alpha_{33}} \cdot \frac{\dfrac{(\alpha_{13}-\alpha_{23})\gamma_{44} + \alpha_{34}(\gamma_{24}-\gamma_{14})}{\gamma_{22}\gamma_{44} - \gamma_{24}^2}}{1+n - \left(\dfrac{\gamma_{11}\gamma_{44} - \gamma_{14}^2 - n(\gamma_{14}\gamma_{24} + \gamma_{12}\gamma_{44})}{\gamma_{22}\gamma_{44} - \gamma_{24}^2} \right)}$$

$$y_{P_1} = \frac{Cr^{n-1}}{\alpha_{33}} \cdot \frac{\dfrac{(\alpha_{13}-\alpha_{23})\gamma_{44} + \alpha_{34}(\gamma_{24}-\gamma_{14})}{\gamma_{22}\gamma_{44} - \gamma_{24}^2}}{\dfrac{\gamma_{22}\gamma_{44} - \gamma_{24}^2 + n\gamma_{22}\gamma_{44} - n\gamma_{24}^2 - \gamma_{11}\gamma_{44} + \gamma_{14}^2 + n\gamma_{14}\gamma_{24} + n\gamma_{12}\gamma_{44}}{\gamma_{22}\gamma_{44} - \gamma_{24}^2}}$$

Defining

$$\chi_{1_n} = \frac{(\alpha_{13}-\alpha_{23})\gamma_{44} + \alpha_{34}(\gamma_{24}-\gamma_{14})}{\left(\gamma_{22}\gamma_{44} - \gamma_{24}^2\right) - \left(\gamma_{11}\gamma_{44} - \gamma_{14}^2\right) + n\left[\gamma_{22}\gamma_{44} - \gamma_{24}^2 + \gamma_{14}\gamma_{24} + \gamma_{12}\gamma_{44}\right]}$$

$$\chi_{1_n} = \frac{(\alpha_{13}-\alpha_{23})\gamma_{44} + \alpha_{34}(\gamma_{24}-\gamma_{14})}{(n+1)\left(\gamma_{22}\gamma_{44} - \gamma_{24}^2\right) + n\left(\gamma_{14}\gamma_{24} + \gamma_{12}\gamma_{44}\right) - \left(\gamma_{11}\gamma_{44} - \gamma_{24}^2\right)}$$

then

$$y_{P_1} = \frac{Cr^{n-1}\chi_{1_n}}{\alpha_{33}}$$

Re-examining y_{p_2}:

$$y_{p_2} = \frac{f_n\, 9 r^{n+2}}{(n-s+2)(n-t+2)} + C_3$$

using

$$s = .5n + .5\sqrt{n^2 + 4\gamma_n}$$

$$t = .5n - .5\sqrt{n^2 + 4\gamma_n}$$

we note that

$$(n-s+2)(n-t+2) = \left(n - .5n - .5\sqrt{n^2+4\gamma_n} + 2\right)\left(n - .5n + .5\sqrt{n^2+4\gamma_n} + 2\right)$$

$$(n-s+2)(n-t+2) = \left(.5n - .5\sqrt{n^2+4\gamma_n} + 2\right)\left(.5n + .5\sqrt{n^2+4\gamma_n} + 2\right)$$

$$(n-s+2)(n-t+2) = .25n^2 + .25n\sqrt{n^2+4\gamma_n} + n - .25n\sqrt{n^2+4\gamma_n} - .25(n^2+4\gamma_n) - 1\sqrt{n^2+4\gamma_n} +$$
$$n + 1\sqrt{n^2+4\gamma_n} + 4$$

$$(n-s+2)(n-t+2) = 2n - \gamma_n + 4$$

$$(n-s+2)(n-t+2) = 2(n+2) - \gamma_n$$

therefore

$$y_{p_2} = \left(9 r^{n+2}\right)\frac{\dfrac{\gamma_{14} - 2\gamma_{24}}{\gamma_{22}\gamma_{44} - \gamma_{24}^2}}{2n + 4 - \left(\dfrac{\gamma_{11}\gamma_{44} - \gamma_{14}^2 - n(\gamma_{14}\gamma_{24} - \gamma_{12}\gamma_{44})}{\gamma_{22}\gamma_{44} - \gamma_{24}^2}\right)} + C_3$$

$$y_{p_2} = \left(9 r^{n+2}\right)\frac{\gamma_{14} - 2\gamma_{24}}{2n(\gamma_{22}\gamma_{44} - \gamma_{24}^2) + 4(\gamma_{22}\gamma_{44} - \gamma_{24}^2) - (\gamma_{11}\gamma_{44} - \gamma_{14}^2) + n(\gamma_{14}\gamma_{24} - \gamma_{12}\gamma_{44})}$$

$$y_{p_2} = \left(9 r^{n-2}\right)\frac{\gamma_{14} - 2\gamma_{24}}{4(\gamma_{22}\gamma_{44} - \gamma_{24}^2) - (\gamma_{11}\gamma_{44} - \gamma_{14}^2) + n\left[2(\gamma_{22}\gamma_{44} - \gamma_{24}^2) + \gamma_{14}\gamma_{24} - \gamma_{12}\gamma_{44}\right]}$$

228

$$y_{P_2} = \left(\vartheta r^{n+2}\right)\frac{\gamma_{14} - 2\gamma_{24}}{2(n+2)\left(\gamma_{22}\gamma_{44} - \gamma_{24}^2\right) + n\left(\gamma_{14}\gamma_{24} - \gamma_{12}\gamma_{44}\right) - \left(\gamma_{11}\gamma_{44} - \gamma_{14}^2\right)}$$

Defining:

$$\mu_{1_n} = \frac{\left(\gamma_{14} - 2\gamma_{24}\right)}{2(n+2)\left(\gamma_{22}\gamma_{44} - \gamma_{24}^2\right) + n\left(\gamma_{14}\gamma_{24} - \gamma_{12}\gamma_{44}\right) - \left(\gamma_{11}\gamma_{44} - \gamma_{14}^2\right)}$$

then

$$y_{P_2} = \vartheta\mu_{1_n} r^{n+2} + C_3$$

The complete solution is:

$$\phi = C_1 r^s + C_2 r^t + \frac{Cr^{n+1}}{\alpha_{33}}\chi_{1_n} + \vartheta\mu_{1_n} r^{n+2} + C_3$$

Thus

$$\varphi = \frac{C\alpha_{34} r^n}{\alpha_{33}\gamma_{44}} - \frac{\vartheta r^{n-1}}{\gamma_{44}} + \frac{\gamma_{24}}{\gamma_{44}}\left[sC_1 r^{s-1} + tC_2 r^{t-1} + (n+1)\frac{Cr^n\chi_{1_n}}{\alpha_{33}} + (n+2)\vartheta\mu_{1_n} r^{n-1}\right] +$$

$$\frac{\gamma_{14}}{\gamma_{44}}\left[C_1 r^{s-1} + C_2 r^{t-1} + \frac{Cr^n\chi_{1_n}}{\alpha_{33}} + \vartheta\mu_{1_n} r^{n+1} + \frac{C_3}{r}\right]$$

another form is

$$\varphi = \frac{\gamma_{14}}{\gamma_{44}}\frac{C_3}{r} + \frac{Cr^n}{\alpha_{33}}\left[\frac{\alpha_{34}}{\gamma_{44}} + \frac{\left((n+1)\gamma_{24} + \gamma_{14}\right)}{\gamma_{44}}\chi_{1_n}\right] +$$

$$\vartheta r^{n-1}\left[\frac{-1}{\gamma_{44}} + \frac{\left((n+2)\gamma_{24} + \gamma_{14}\right)}{\gamma_{44}}\mu_{1_n}\right] + C_1 r^{s-1}\left[\frac{s\gamma_{24} + \gamma_{14}}{\gamma_{44}}\right] + C_2 r^{t-1}\left[\frac{t\gamma_{24} + \gamma_{14}}{\gamma_{44}}\right]$$

let: $g_s = \left(\frac{\gamma_{14} + s\gamma_{24}}{\gamma_{44}}\right)$, $g_t = \left[\frac{\gamma_{14} + t\gamma_{24}}{\gamma_{44}}\right]$

let: $\chi_{2_n} = \left[\dfrac{\alpha_{34}}{\gamma_{44}} + \dfrac{((n+1)\gamma_{24}+\gamma_{14})\chi_{1_n}}{\gamma_{44}} \right]$

let: $\mu_{2_n} = \left[\dfrac{-1}{\gamma_{44}} + \dfrac{((n+2)\gamma_{24}+\gamma_{14})\mu_{1_n}}{\gamma_{44}} \right]$

$$\chi_{2_n} = \frac{\alpha_{34}}{\gamma_{44}} + \frac{((n+1)\gamma_{24}+\gamma_{14})}{\gamma_{44}} \left[\frac{(\alpha_{13}-\alpha_{23})\gamma_{44}+\alpha_{34}(\gamma_{24}-\gamma_{14})}{(n+1)(\gamma_{22}\gamma_{44}-\gamma_{24}^2)+n(\gamma_{14}\gamma_{24}-\gamma_{12}\gamma_{44})-(\gamma_{11}\gamma_{44}-\gamma_{14}^2)} \right]$$

(5.55)

The numerator above can be expanded:

$(n+1)\alpha_{34}(\gamma_{22}\gamma_{44}-\gamma_{24}^2)+n\alpha_{34}(\gamma_{14}\gamma_{24}-\gamma_{12}\gamma_{44})-\alpha_{34}(\gamma_{11}\gamma_{44}-\gamma_{14}^2)+$

$(n+1)\gamma_{24}\gamma_{44}(\alpha_{13}-\alpha_{23})+\gamma_{14}\gamma_{44}(\alpha_{13}-\alpha_{23})+(n+1)\alpha_{34}\gamma_{24}^2-$

$(n+1)\alpha_{34}\gamma_{24}\gamma_{14}-\alpha_{34}\gamma_{14}^2+\alpha_{34}\gamma_{14}\gamma_{24}$

further expansion gives

$n\alpha_{34}\gamma_{22}\gamma_{44}-n\alpha_{34}\gamma_{24}^2+\alpha_{34}\gamma_{22}\gamma_{44}-\alpha_{34}\gamma_{24}^2+n\alpha_{34}\gamma_{14}\gamma_{24}-n\alpha_{34}\gamma_{12}\gamma_{44}-$

$\alpha_{34}\gamma_{11}\gamma_{44}+\alpha_{34}\gamma_{14}^2+(n+1)(\gamma_{24}\gamma_{44})(\alpha_{13}-\alpha_{23})+$

$\gamma_{14}\gamma_{44}\alpha_{13}-\gamma_{14}\gamma_{44}\alpha_{23}+n\alpha_{34}\gamma_{24}^2+\alpha_{34}\gamma_{24}^2-n\alpha_{34}\gamma_{24}\gamma_{14}-\alpha_{34}\gamma_{24}\gamma_{14}-\alpha_{34}\gamma_{14}^2+\alpha_{34}\gamma_{14}\gamma_{24}$

canceling terms and grouping

$$\chi_{2_n} = \frac{\gamma_{44}\left[\alpha_{34}(\gamma_{22}-\gamma_{11})+n\alpha_{34}(\gamma_{22}-\gamma_{12})+\gamma_{14}(\alpha_{13}-\alpha_{23})+(n+1)\gamma_{24}(\alpha_{13}-\alpha_{23})\right]}{\gamma_{44}\left[(n+1)(\gamma_{22}\gamma_{44}-\gamma_{24}^2)+n(\gamma_{14}\gamma_{24}-\gamma_{12}\gamma_{44})-(\gamma_{11}\gamma_{44}-\gamma_{14}^2)\right]}$$

with simplification

$$\chi_{2_n} = \frac{\left[\gamma_{14}+(n+1)\gamma_{24}\right](\alpha_{13}-\alpha_{23})+n\alpha_{34}(\gamma_{22}-\gamma_{12})+\alpha_{34}(\gamma_{22}-\gamma_{11})}{\left[(n+1)(\gamma_{22}\gamma_{44}-\gamma_{24}^2)+n(\gamma_{14}\gamma_{24}-\gamma_{12}\gamma_{44})-(\gamma_{11}\gamma_{44}-\gamma_{14}^2)\right]}$$

For the term μ_{2_n}

230

$$\mu_{2_n} = \frac{-1}{\gamma_{44}} + \frac{\left((n+2)\gamma_{24} + \gamma_{14}\right)\left(\gamma_{14} - 2\gamma_{24}\right)}{\left[2(n+2)\left(\gamma_{22}\gamma_{44} - \gamma_{24}^2\right) + n\left(\gamma_{14}\gamma_{24} - \gamma_{12}\gamma_{44}\right) - \left(\gamma_{11}\gamma_{44} - \gamma_{14}^2\right)\right]\gamma_{44}}$$

with expansion

$$\mu_{2_n} = \frac{-2(n+2)\left(\gamma_{22}\gamma_{44} - \gamma_{24}^2\right) + \left((n+2)\gamma_{24} + \gamma_{14}\right)\left(\gamma_{14} - 2\gamma_{24}\right) - n\left(\gamma_{14}\gamma_{24} - \gamma_{12}\gamma_{44}\right) + \left(\gamma_{11}\gamma_{44} - \gamma_{14}^2\right)}{\gamma_{44}\left(2(n+2)\left(\gamma_{22}\gamma_{44} - \gamma_{24}^2\right) + n\left(\gamma_{14}\gamma_{24} - \gamma_{12}\gamma_{44}\right) - \left(\gamma_{11}\gamma_{44} - \gamma_{14}^2\right)\right)}$$

further expansion

$$\mu_{2_n} = \frac{\begin{array}{c} -2n\gamma_{22}\gamma_{44} - 4\gamma_{22}\gamma_{44} + 2n\gamma_{24}^2 + 4\gamma_{24}^2 + n\gamma_{24}\gamma_{14} - 2n\gamma_{24}^2 + 2\gamma_{24}\gamma_{14} - 4\gamma_{24}^2 + \rightarrow \\ \rightarrow \gamma_{14}^2 - 2\gamma_{14}\gamma_{24} - n\gamma_{14}\gamma_{24} + n\gamma_{12}\gamma_{44} + \gamma_{11}\gamma_{44} - \gamma_{14}^2 \end{array}}{\gamma_{44}\left(2(n+2)\left(\gamma_{22}\gamma_{44} - \gamma_{24}^2\right) + n\left(\gamma_{14}\gamma_{24} - \gamma_{12}\gamma_{44}\right) - \left(\gamma_{11}\gamma_{44} - \gamma_{24}^2\right)\right)}$$

canceling terms

$$\mu_{2_n} = \frac{\gamma_{44}\left(-2n\gamma_{22} - 4\gamma_{22} + n\gamma_{12} + \gamma_{11}\right)}{\gamma_{44}\left(2(n+2)\left(\gamma_{22}\gamma_{44} - \gamma_{24}^2\right) + n\left(\gamma_{14}\gamma_{24} - \gamma_{12}\gamma_{44}\right) - \left(\gamma_{11}\gamma_{44} - \gamma_{24}^2\right)\right)}$$

rearrangement

$$\mu_{2_n} = \frac{\left[\gamma_{11} - 4\gamma_{22} - n\left(2\gamma_{22} - \gamma_{12}\right)\right]}{2(n+2)\left(\gamma_{22}\gamma_{44} - \gamma_{24}^2\right) + n\left(\gamma_{14}\gamma_{24} - \gamma_{12}\gamma_{44}\right) - \left(\gamma_{11}\gamma_{44} - \gamma_{24}^2\right)}$$

The solution for φ is:

$$\varphi = \frac{\gamma_{14}}{\gamma_{44}}\frac{C_3}{r} + \frac{Cr^n}{\alpha_{33}}\chi_{2_n} + C_1 g_s r^{s-1} + C_2 g_t r^{t-1} + 9\mu_{2_n} r^{n-1}$$

(5.56)

The stresses are:

231

$$\sigma_r = \frac{1}{r}\phi = C_1 r^{s-1} + C_2 r^{t-1} + \frac{Cr^n}{\alpha_{33}}\chi_{1_n} + \vartheta\,\mu_{1_n} r^{n+1} + \frac{C_3}{r}$$

$$\sigma_\theta = \frac{\partial\phi}{\partial r} = C_1 sr^{s-1} + C_2 tr^{t-1} + (n+1)\frac{Cr^n}{\alpha_{33}}\chi_{1_n} + (n+2)\vartheta\,\mu_{1_n} r^{n+1}$$

$$\tau_{\theta z} = -\phi = \frac{-\gamma_{14}}{\gamma_{44}}\frac{C_3}{r} - \frac{Cr^n}{\alpha_{33}}\chi_{2_n} - C_1 g_s r^{s-1} - C_2 g_t r^{t-1} - \vartheta\,\mu_{2_n} r^{n+1}$$

(5.57)

From previous discussion, we know that in the absence of externally applied bending

moments, the coefficients A & $B = 0$. Essentially this implies no variation with θ. Of the

original 4, two unknown integration constants (C and ϑ) remain to be determined. From

(5.1) and (5.19)

$$\varepsilon_z = a_{31}\sigma_r + a_{32}\sigma_\theta + a_{33}\sigma_z + a_{34}\tau_{\theta z} = Ar\cos\theta + Br\sin\theta + C$$

$$\downarrow \qquad\qquad \downarrow$$
$$0 \qquad\qquad 0$$

If material coefficients can be defined by a single function of (r), we have:

$$r^{-n}(\alpha_{31}\sigma_r + \alpha_{32}\sigma_\theta + \alpha_{33}\sigma_z + \alpha_{34}\tau_{\theta z}) = C$$

$$C - \sigma_z\alpha_{33}r^{-n} = (\alpha_{31}\sigma_r + \alpha_{32}\sigma_\theta + \alpha_{34}\tau_{\theta z})r^{-n}$$

$$\sigma_z = \frac{C - r^{-n}(\alpha_{31}\sigma_r + \alpha_{32}\sigma_\theta + \alpha_{34}\tau_{\theta z})}{\alpha_{33}r^{-n}}$$

$$\sigma_z = \frac{Cr^n}{\alpha_{33}} - \frac{1}{\alpha_{33}}(\alpha_{31}\sigma_r + \alpha_{32}\sigma_\theta + \alpha_{34}\tau_{\theta z})$$

(5.58)

Displacements simplify to:

$$\varepsilon_r = \frac{\partial u}{\partial r} = r^{-n}(\gamma_{11}\sigma_r + \gamma_{12}\sigma_\theta + \gamma_{14}\tau_{\theta z}) + \frac{\alpha_{13}}{\alpha_{33}}C$$

$$\varepsilon_\theta = \frac{u}{r} = r^{-n}(\gamma_{21}\sigma_r + \gamma_{22}\sigma_\theta + \gamma_{24}\tau_{\theta z}) + \frac{\alpha_{23}}{\alpha_{33}}C$$

232

so

$$u = r^{-n-1}\left(\gamma_{21}\sigma_r + \gamma_{22}\sigma_\theta + \gamma_{24}\tau_{\theta z}\right) + \frac{\alpha_{23}}{\alpha_{33}}C$$

Equating the above expressions for displacement (u):

$$r^{-n}\left(\gamma_{11}\sigma_r + \gamma_{12}\sigma_\theta + \gamma_{14}\tau_{\theta z}\right) + \frac{\alpha_{13}}{\alpha_{33}}C - \frac{\partial}{\partial r}\left(r^{-n-1}\left(\gamma_{21}\sigma_r + \gamma_{22}\sigma_\theta + \gamma_{24}\tau_{\theta z}\right) + r\frac{\alpha_{23}}{\alpha_{33}}C\right) = 0$$

$$r^{-n}\left(\gamma_{11}\sigma_r + \gamma_{12}\sigma_\theta + \gamma_{14}\tau_{\theta z}\right) - \frac{\partial}{\partial r}\left(r^{-n-1}\left(\gamma_{21}\sigma_r + \gamma_{22}\sigma_\theta + \gamma_{24}\tau_{\theta z}\right)\right) = \left(\frac{\alpha_{23}-\alpha_{13}}{\alpha_{33}}\right)C$$

substituting for the stresses

$$C_1\, r^{s-n-1}\left[\gamma_{11} + s\gamma_{12} - g_s\gamma_{14} - (s-n)\left(\gamma_{12} + s\gamma_{22} - g_s\gamma_{24}\right)\right] +$$
$$C_2\, r^{t-n-1}\left[\gamma_{11} + t\gamma_{12} - g_t\gamma_{14} - (t-n)\left(\gamma_{12} + t\gamma_{22} - g_t\gamma_{24}\right)\right] +$$
$$\frac{C}{\alpha_{33}}\left[\gamma_{11}\chi_{1_n} + \gamma_{12}(n+1)\chi_{1_n} - \gamma_{14}\chi_{2_n} - \left(\gamma_{12}\chi_{1_n} + \gamma_{22}(n+1)\chi_{1_n} - \gamma_{24}\chi_{2_n}\right)\right] +$$
$$9r\left[\gamma_{11}\mu_{1_n} + (n+2)\mu_{1_n}\gamma_{12} - \gamma_{14}\mu_{2_n} - 2\left(\gamma_{12}\mu_{1_n} + (n+2)\mu_{1_n}\gamma_{22} - \gamma_{24}\mu_{2_n}\right)\right] +$$
$$C_3 r^{-n-1}\left[\gamma_{11} - \frac{\gamma_{14}^2}{\gamma_{44}} - (-n)\left(\gamma_{12} - \frac{\gamma_{14}\gamma_{24}}{\gamma_{44}}\right)\right] = \left(\frac{\alpha_{23}-\alpha_{13}}{\alpha_{33}}\right)C$$

$$(5.59)$$

Substituting for each term of (5.59) in brackets, we have: (1st term)

$$\gamma_{11} + s\gamma_{12} - \left(\frac{\gamma_{14} + s\gamma_{24}}{\gamma_{44}}\right)\gamma_{14} + (n-s)\left(\gamma_{12} + s\gamma_{22} - \frac{(\gamma_{14} + s\gamma_{24})}{\gamma_{44}}\gamma_{24}\right)$$

which expands to

$$\frac{\gamma_{11}\gamma_{44} + s\gamma_{12}\gamma_{44} - \gamma_{14}^2 - s\gamma_{24}\gamma_{14} + n\gamma_{12}\gamma_{44} + ns\gamma_{22}\gamma_{44} - n\gamma_{14}\gamma_{24} - ns\gamma_{24}^2 - s\gamma_{12}\gamma_{44} - s^2\gamma_{22}\gamma_{44} + s\gamma_{14}\gamma_{24} + s^2\gamma_{24}^2}{\gamma_{44}}$$

The numerator above is

$$\gamma_{11}\gamma_{44} - \gamma_{14}^2 + s^2\left(\gamma_{24}^2 - \gamma_{22}\gamma_{44}\right) - ns\left(\gamma_{24}^2 - \gamma_{22}\gamma_{44}\right) + n\left(\gamma_{12}\gamma_{44} - \gamma_{14}\gamma_{24}\right)$$

233

and can be expressed as

$$\gamma_{11}\gamma_{44} - \gamma_{14}^2 + \left(s^2 - ns\right)\left(\gamma_{24}^2 - \gamma_{22}\gamma_{44}\right) + n\left(\gamma_{12}\gamma_{44} - \gamma_{14}\gamma_{24}\right)$$

but: $s = .5n + .5\sqrt{n^2 + 4\gamma_n}$

so

$$s^2 - ns = \left(.5n + .5\sqrt{n^2 + 4\gamma_n}\right)\left(.5n + .5\sqrt{n^2 + 4\gamma_n}\right) - .5n^2 - .5n\sqrt{n^2 + 4\gamma_n}$$

$$s^2 - ns = .25n^2 + .5n\sqrt{n^2 + 4\gamma_n} + .25\left(n^2 + 4\gamma_n\right) - .5n^2 - .5n\sqrt{n^2 + 4\gamma_n}$$

$$s^2 - ns = \gamma_n$$

recall: $\gamma_n = \dfrac{\gamma_{11}\gamma_{44} - \gamma_{14}^2 - n\left(\gamma_{14}\gamma_{24} - \gamma_{12}\gamma_{44}\right)}{\gamma_{22}\gamma_{44} - \gamma_{24}^2}$

the numerator of the first term in equation (5.59) becomes

$$\left(\gamma_{11}\gamma_{44} - \gamma_{14}^2\right) + \dfrac{\left(\gamma_{11}\gamma_{44} - \gamma_{14}^2 - n\left(\gamma_{14}\gamma_{24} - \gamma_{12}\gamma_{44}\right)\right)\left(\gamma_{24}^2 - \gamma_{22}\gamma_{44}\right)}{\left(\gamma_{22}\gamma_{44} - \gamma_{24}^2\right)} + n\left(\gamma_{12}\gamma_{44} - \gamma_{14}\gamma_{24}\right)$$

Hence all terms cancel and the numerator = 0. No constraints arise.

For the second term in equation (5.59), replacing s by t in the above equation:

$$t = .5n - .5\sqrt{n^2 + 4\gamma_n}$$

$$t^2 - nt = \left(.5n - .5\sqrt{n^2 + 4\gamma_n}\right)\left(.5n - .5\sqrt{n^2 + 4\gamma_n}\right) - .5n^2 + .5n\sqrt{n^2 + 4\gamma_n}$$

$$t^2 - nt = .25n^2 - .5n\sqrt{n^2 + 4\gamma_n} + .25\left(n^2 + 4\gamma_n\right) - .5n^2 + .5n\sqrt{n^2 + 4\gamma_n}$$

$$t^2 - nt = \gamma_n$$

similarly we conclude that the numerator = 0; no constraints arise.

For the 3rd term of (5.59), with rearrangement

$$\left(\gamma_{11} + n\gamma_{12} - \gamma_{22}(n+1)\right)\chi_{1_n} + \left(\gamma_{24} - \gamma_{14}\right)\chi_{2_n}$$

substitution for stresses yields

$$\frac{\left[\left(\gamma_{11} - \gamma_{22}\right) + n\left(\gamma_{12} - \gamma_{22}\right)\right]\left[\left(\alpha_{13} - \alpha_{23}\right)\gamma_{44} + \alpha_{34}\left(\gamma_{24} - \gamma_{14}\right)\right] + \rightarrow}{\rightarrow \left(\gamma_{24} - \gamma_{14}\right)\left[\left((n+1)\gamma_{24} + \gamma_{14}\right)\left(\alpha_{13} - \alpha_{23}\right) + n\alpha_{34}\left(\gamma_{22} - \gamma_{12}\right) + \alpha_{34}\left(\gamma_{22} - \gamma_{11}\right)\right]}{(n+1)\left(\gamma_{22}\gamma_{44} - \gamma_{24}^2\right) + n\left(\gamma_{14}\gamma_{24} - \gamma_{12}\gamma_{44}\right) - \left(\gamma_{11}\gamma_{44} - \gamma_{14}^2\right)}$$

Expansion of the numerator yields:

$$\left(\gamma_{11}\gamma_{44} - \gamma_{22}\gamma_{44}\right)\left(\alpha_{13} - \alpha_{23}\right) + \alpha_{34}\left(\gamma_{24} - \gamma_{14}\right)\left(\gamma_{11} - \gamma_{22}\right) + n\left(\gamma_{12}\gamma_{44} - \gamma_{22}\gamma_{44}\right)\left(\alpha_{13} - \alpha_{23}\right) +$$
$$n\left(\gamma_{12} - \gamma_{22}\right)\left(\gamma_{24} - \gamma_{14}\right)\alpha_{34} + (n+1)\left(\gamma_{24}^2 - \gamma_{14}\gamma_{24}\right)\left(\alpha_{13} - \alpha_{23}\right) + \left(\gamma_{24}\gamma_{14} - \gamma_{14}^2\right)\left(\alpha_{13} - \alpha_{23}\right) +$$
$$n\alpha_{34}\left(\gamma_{24} - \gamma_{14}\right)\left(\gamma_{22} - \gamma_{12}\right) + \alpha_{34}\left(\gamma_{24} - \gamma_{14}\right)\left(\gamma_{22} - \gamma_{11}\right)$$

canceling and regrouping terms

$$\left[(n+1)\gamma_{24}^2 + (n+1)\left(-\gamma_{22}\gamma_{44}\right) + n\gamma_{12}\gamma_{44} - n\gamma_{14}\gamma_{24} + \gamma_{11}\gamma_{44} - \gamma_{14}^2\right]\left(\alpha_{13} - \alpha_{23}\right)$$

with further rearrangement and grouping, the 3rd term can be set to

$$\frac{-\left(\alpha_{13} - \alpha_{23}\right)\left[(n+1)\left(\gamma_{22}\gamma_{44} - \gamma_{24}^2\right) + n\left(\gamma_{14}\gamma_{24} - \gamma_{12}\gamma_{44}\right) - \left(\gamma_{11}\gamma_{44} - \gamma_{14}^2\right)\right]}{(n+1)\left(\gamma_{22}\gamma_{44} - \gamma_{24}^2\right) + n\left(\gamma_{14}\gamma_{24} - \gamma_{12}\gamma_{44}\right) - \left(\gamma_{11}\gamma_{44} - \gamma_{14}^2\right)}$$

which reduces to

$$= -\left(\alpha_{13} - \alpha_{23}\right)$$

Thus the 3rd term satisfies the *RHS* of (5.59).

For the 4th term of (5.59), the numerator is:

$$\left[\left(\gamma_{11} + n\gamma_{12} - 2(n+2)\gamma_{22}\right)\mu_{1_n} + \left(2\gamma_{24} - \gamma_{14}\right)\mu_{2_n}\right]$$

restated as

$$\left[\left(\gamma_{11} - 4\gamma_{22}\right) + n\left(\gamma_{12} - 2\gamma_{22}\right)\right]\mu_{1_n} + \left(2\gamma_{24} - \gamma_{14}\right)\mu_{2_n}\right]$$

expanding, the entire term can be written as

$$\frac{\left[(\gamma_{11}-4\gamma_{22})+n(\gamma_{12}-2\gamma_{22})\right](\gamma_{14}-2\gamma_{24})+(2\gamma_{24}-\gamma_{14})\left[\gamma_{11}-4\gamma_{22}-n(2\gamma_{22}-\gamma_{12})\right]}{2(n+2)(\gamma_{22}\gamma_{44}-\gamma_{24}^2)+n(\gamma_{14}\gamma_{24}-\gamma_{12}\gamma_{44})-(\gamma_{14}\gamma_{44}-\gamma_{24}^2)}$$

The numerator however works out as

$$\gamma_{11}\gamma_{14}-2\gamma_{11}\gamma_{24}-4\gamma_{22}\gamma_{14}+8\gamma_{22}\gamma_{24}+n\gamma_{12}\gamma_{14}-2n\gamma_{12}\gamma_{24}-2n\gamma_{22}\gamma_{14}+4n\gamma_{22}\gamma_{24}+$$
$$2\gamma_{11}\gamma_{24}-8\gamma_{22}\gamma_{24}-\gamma_{14}\gamma_{11}+4\gamma_{14}\gamma_{22}-4n\gamma_{22}\gamma_{24}+n\gamma_{24}\gamma_{12}+2n\gamma_{14}\gamma_{22}-n\gamma_{14}\gamma_{12}=0$$

No constraints are imposed due to this term.

The 5th term of (5.59) would then require the condition

$$C_3 r^{-n-1}\left[\frac{\gamma_{11}\gamma_{44}-\gamma_{14}^2+n(\gamma_{12}\gamma_{44}-\gamma_{14}\gamma_{24})}{\gamma_{44}}\right]=0$$

Since the γ's are not zero, we must set the integration constant $C_3=0$

The final solution can be summarized as:

$$\sigma_r=\frac{C}{\alpha_{33}}r^n\chi_{1_n}+C_1 r^{s-1}+C_2 r^{t-1}+\vartheta\,\mu_{1_n}r^{n-1}$$

$$\sigma_\theta=(n+1)\frac{C}{\alpha_{33}}r^n\chi_{1_n}+C_1 sr^{s-1}+C_2 tr^{t-1}+(n+2)\vartheta\,\mu_{1_n}r^{n-1}$$

$$\tau_{\theta z}=\frac{-C}{\alpha_{33}}r^n\chi_{2_n}-C_1 g_s r^{s-1}-C_2 g_t r^{t-1}-\vartheta\,\mu_{2_n}r^{n-1}$$

$$\sigma_z=\frac{C}{\alpha_{33}}r^n-\frac{1}{\alpha_{33}}(\alpha_{31}\sigma_r+\alpha_{32}\sigma_\theta+\alpha_{34}\tau_{\theta z})$$

(5.60)

Making additional simplifications

let:　　$(n+1)\chi_{1_n}=\chi_{3_n}$　　,　　and　　$\frac{C}{\alpha_{33}}=C_0$　,　　and　　$(n+2)\mu_{1_n}=\mu_{3_n}$

Thus:

$$\sigma_r=C_0 r^n\chi_{1_n}+C_1 r^{s-1}+C_2 r^{t-1}+\vartheta\,\mu_1 r^{n-1}$$
$$\sigma_\theta=C_0 r^n\chi_{3_n}+C_1 sr^{s-1}+C_2 tr^{t-1}+\vartheta\,\mu_{3_n}r^{n-1}$$
$$\tau_{\theta z}=-C_0 r^n\chi_{2_n}-C_1 g_s r^{s-1}-C_2 g_t r^{t-1}-\vartheta\,\mu_{2_n}r^{n-1}$$

$$\sigma_z = C_0 r^{-n} - \frac{1}{\alpha_{33}}(\alpha_{13}\sigma_r + \alpha_{23}\sigma_\theta + \alpha_{34}\tau_{\theta z})$$

(5.61)

5.4 Solving for the Constants C_0 and ϑ

With functionally dependent material properties in a rotated orthotropic lamina

two equations for two unknowns C and ϑ must be solved. First however C_1 and C_2 can

be solved in terms of the known stresses:

Applying boundary conditions for internal and external surface

@ $\left.\begin{array}{ll} r = a, & \sigma_r = -P \\ r = b, & \sigma_r = -Q \end{array}\right\}$ in opposition to external pressure which is defined as (+)

where: P = internal pressure

Q = external pressure

$$-C_0\chi_{1_n}a^n - \vartheta\,\mu_1 a^{n-1} - P = C_1 a^{s-1} + C_2 a^{t-1}$$

$$-C_0\chi_{n1}b^n - \vartheta\,\mu_1 b^{n-1} - Q = C_1 b^{s-1} + C_2 b^{t-1}$$

$$C_1 = \frac{\begin{vmatrix} \left(C_0\chi_{1_n}a^n - \vartheta\,\mu_1 a^{n-1} - P\right) & a^{t-1} \\ \left(-C_0\chi_{1_n}b^n - \vartheta\,\mu_1 b^{n-1} - Q\right) & b^{t-1} \\ a^{s-1} & a^{t-1} \\ b^{s-1} & b^{t-1} \end{vmatrix}}{\begin{vmatrix} a^{s-1} & a^{t-1} \\ b^{s-1} & b^{t-1} \end{vmatrix}} = \frac{\begin{array}{l} -C_0\chi_{1_n}a^n b^{t-1} - \vartheta\,\mu_1 a^{n-1}b^{t-1} - P\,b^{t-1} + \to \\ \to C_0\chi_{1_n}b^n a^{t-1} + \vartheta\,\mu_1 b^{n-1}a^{t-1} + Q a^{t-1} \end{array}}{a^{s-1}\,b^{t-1} - b^{s-1}\,a^{t-1}}$$

$$C_2 = \frac{\begin{vmatrix} a^{s-1} & \left(-C_0\chi_{n1}a^n - \vartheta\,\mu_1 a^{n-1} - P\right) \\ b^{s-1} & \left(-C_0\chi_{1_n}b^n - \vartheta\,\mu_1 b^{n-1} - Q\right) \\ a^{s-1} & a^{t-1} \\ b^{s-1} & b^{t-1} \end{vmatrix}}{\begin{vmatrix} a^{s-1} & a^{t-1} \\ b^{s-1} & b^{t-1} \end{vmatrix}} = \frac{\begin{array}{l} -C_0\chi_{1_n}b^n a^{s-1} - \vartheta\,\mu_1 b^{n-1}a^{s-1} - Q a^{s-1} + \to \\ \to C_0\chi_{1_n}a^n b^{s-1} + \vartheta\,\mu_1 a^{n-1}b^{s-1} + P\,b^{s-1} \end{array}}{a^{s-1}\,b^{t-1} - b^{s-1}\,a^{t-1}}$$

The above constants C_1, C_2 can each be expressed as a sum of 3 constituents denoted by subscripts such that:

$$C_1 = C_{1_{pq}} + C_{1\chi} + C_{1\vartheta}$$

$$C_2 = C_{2_{pq}} + C_{2\chi} + C_{2\vartheta}$$

These terms above can be expressed as:

$$C_{1_{pq}} = \frac{-P b^{t-1} + Q a^{t-1}}{a^{s-1} b^{t-1} - b^{s-1} a^{t-1}} \qquad C_{2_{pq}} = \frac{-Q a^{s-1} + P b^{s-1}}{a^{s-1} b^{t-1} - b^{s-1} a^{t-1}}$$

$$C_{1\chi} = \frac{-C_0 \chi_{1_n} a^n b^{t-1} + C_0 \chi_{1_n} b^n a^{t-1}}{a^{s-1} b^{t-1} - b^{s-1} a^{t-1}} \qquad C_{2\chi} = \frac{-a^{s-1} C_0 \chi_{1_n} b^n + b^{s-1} C_0 \chi_{1_n} a^n}{a^{s-1} b^{t-1} - b^{s-1} a^{t-1}}$$

$$C_{1\vartheta} = \frac{-\vartheta \mu_1 a^{n+1} b^{t-1} + \vartheta \mu_1 b^{n+1} a^{t-1}}{a^{s-1} b^{t-1} - b^{s-1} a^{t-1}} \qquad C_{2\vartheta} = \frac{-\vartheta \mu_1 b^{n+1} a^{s-1} + \vartheta \mu_1 a^{n+1} b^{s-1}}{a^{s-1} b^{t-1} - b^{s-1} a^{t-1}}$$

by factoring out b^{s-1}, b^{t-1}

$$C_{1\chi} = \frac{C_0 \chi_{1_n}}{b^{s-1} b^{t-1}} \left(\frac{-a^n b^{t-1} + b^n a^{t-1}}{\dfrac{a^{s-1}}{b^{s-1}} - \dfrac{a^{t-1}}{b^{t-1}}} \right) \qquad C_{2\chi} = \frac{C_0 \chi_{1_n}}{b^{s-1} b^{t-1}} \left(\frac{-a^{s-1} b^n + b^{s-1} a^n}{\dfrac{a^{s-1}}{b^{s-1}} - \dfrac{a^{t-1}}{b^{t-1}}} \right)$$

$$C_{1\chi} = \frac{C_0 \chi_{1_n}}{b^{s-1}} \left(\frac{-a^n + b^n c^{t-1}}{c^{s-1} - c^{t-1}} \right) \qquad C_{2\chi} = \frac{C_0 \chi_{1_n}}{b^{t-1}} \left(\frac{-c^{s-1} b^n + a^n}{c^{s-1} - c^{t-1}} \right)$$

$$C_{1\chi} = \frac{C_0 \chi_{1_n}}{b^{s-1}} \left(\frac{-ca^n + c^t b^n}{c^s - c^t} \right) \qquad C_{2\chi} = \frac{C_0 \chi_{1_n}}{b^{t-1}} \left(\frac{-b^n c^{s-1} + a^n}{c^{s-1} - c^{t-1}} \right)$$

$$C_{1\chi} = \frac{C_0 \chi_{1_n}}{b^{s-1}} \left(\frac{c^t b^n - ca^n}{c^s - c^t} \right) \qquad C_{2\chi} = \frac{C_0 \chi_{1_n}}{b^{t-1}} \left(\frac{ca^n - b^n c^s}{c^s - c^t} \right)$$

Similarly for the other terms

$$C_{1_{pq}} = \frac{1}{b^{s-1}b^{t-1}} \left(\frac{-P b^{t-1} + \underline{Q} a^{t-1}}{\dfrac{a^{s-1}}{b^{s-1}} - \dfrac{a^{t-1}}{b^{t-1}}} \right) \qquad C_{2_{pq}} = \frac{1}{b^{s-1}b^{t-1}} \left(\frac{-\underline{Q} a^{s-1} + P b^{s-1}}{\dfrac{a^{s-1}}{b^{s-1}} - \dfrac{a^{t-1}}{b^{t-1}}} \right)$$

$$C_{1_{pq}} = \frac{1}{b^{s-1}} \left(\frac{-P + \underline{Q} c^{t-1}}{c^{s-1} - c^{t-1}} \right) \qquad C_{2_{pq}} = \frac{1}{b^{t-1}} \left(\frac{-\underline{Q} c^{s-1} + P}{c^{s-1} - c^{t-1}} \right)$$

$$C_{1_{pq}} = \frac{1}{b^{s-1}} \left(\frac{-P c + \underline{Q} c^{t}}{c^{s} - c^{t}} \right) \qquad C_{2_{pq}} = \frac{1}{b^{t-1}} \left(\frac{-\underline{Q} c^{s} + P c}{c^{s} - c^{t}} \right)$$

and

$$C_{19} = \frac{9\mu_{1}}{b^{s-1}b^{t-1}} \left(\frac{-a^{n-1}b^{t-1} + b^{n-1}a^{t-1}}{\dfrac{a^{s-1}}{b^{s-1}} - \dfrac{a^{t-1}}{b^{t-1}}} \right) \qquad C_{29} = \frac{9\mu_{1}}{b^{s-1}b^{t-1}} \left(\frac{-b^{n-1}a^{s-1} + a^{n-1}b^{s-1}}{\dfrac{a^{s-1}}{b^{s-1}} - \dfrac{a^{t-1}}{b^{t-1}}} \right)$$

$$C_{19} = \frac{9\mu_{1}}{b^{s-1}} \left(\frac{-a^{n-1} + b^{n-1}c^{t-1}}{c^{s-1} - c^{t-1}} \right) \qquad C_{29} = \frac{9\mu_{1}}{b^{t-1}} \left(\frac{-b^{n-1}c^{s-1} + a^{n-1}}{c^{s-1} - c^{t-1}} \right)$$

$$C_{19} = \frac{9\mu_{1}}{b^{s-1}} \left(\frac{-a^{n-1}c + b^{n-1}c^{t}}{c^{s} - c^{t}} \right) \qquad C_{29} = \frac{9\mu_{1}}{b^{t-1}} \left(\frac{-b^{n-1}c^{s} + a^{n-1} + c}{c^{s} - c^{t}} \right)$$

Solving for stresses

$$\sigma_{r} = C_{0}\chi_{1_{n}} r^{n} + \left(\frac{r}{b}\right)^{s-1} \left(\frac{c^{t}\underline{Q} - c P}{c^{s} - c^{t}}\right) + \left(\frac{r}{b}\right)^{t-1} \left(\frac{c P - c^{s}\underline{Q}}{c^{s} - c^{t}}\right) +$$

$$C_{0}\chi_{1_{n}} \left(\frac{r}{b}\right)^{s-1} \left(\frac{c^{t}b^{n} - c a^{n}}{c^{s} - c^{t}}\right) + C_{0}\chi_{1_{n}} \left(\frac{r}{b}\right)^{t-1} \left(\frac{c a^{n} - c^{s}b^{n}}{c^{s} - c^{t}}\right) +$$

$$9\mu_{1_{n}} \left(\frac{r}{b}\right)^{s-1} \left(\frac{c^{t}b^{n-1} - c a^{n-1}}{c^{s} - c^{t}}\right) + 9\mu_{1_{n}} \left(\frac{r}{b}\right)^{t-1} \left(\frac{c a^{n-1} - c^{s}b^{n-1}}{c^{s} - c^{t}}\right) + 9\mu_{1} r^{n-1}$$

expressed better as

$$\sigma_{r} = \rho^{s-1} \left(\frac{c^{t}\underline{Q} - c P}{c^{s} - c^{t}}\right) + \rho^{t-1} \left(\frac{c P - c^{s}\underline{Q}}{c^{s} - c^{t}}\right) +$$

239

$$C_0 \chi_{1_n} \left[r^n + \rho^{s-1}\left(\frac{c^t b^n - c a^n}{c^s - c^t}\right) + \rho^{t-1}\left(\frac{c a^n - c^s b^n}{c^s - c^t}\right) \right] +$$

$$\vartheta \mu_{1_n} \left[r^{n+1} + \rho^{s-1}\left(\frac{c^t b^{n+1} - c a^{n+1}}{c^s - c^t}\right) + \rho^{t-1}\left(\frac{c a^{n+1} - c^s b^{n+1}}{c^s - c^t}\right) \right]$$

(5.62)

where: $\left(\dfrac{r}{b}\right) = \rho$

Similarly for σ_θ:

$$\sigma_\theta = s\rho^{s-1}\left(\frac{c^t \underline{Q} - c P}{c^s - c^t}\right) + t\rho^{t-1}\left(\frac{c P - c^s \underline{Q}}{c^s - c^t}\right) +$$

$$C_0 \left[\chi_{3_n} r^n + \chi_{1_n}\left[s\rho^{s-1}\left(\frac{c^t b^n - c a^n}{c^s - c^t}\right) + t\rho^{t-1}\left(\frac{c a^n - c^s b^n}{c^s - c^t}\right) \right] \right] +$$

$$\vartheta \left[\mu_{3_n} r^{n+1} + \mu_{1_n}\left[s\rho^{s-1}\left(\frac{c^t b^{n+1} - c a^{n+1}}{c^s - c^t}\right) + t\rho^{t-1}\left(\frac{c a^{n+1} - c^s b^{n+1}}{c^s - c^t}\right) \right] \right]$$

(5.63)

also

$$\tau_{\theta z} = -g_s\rho^{s-1}\left(\frac{c^t \underline{Q} - c P}{c^s - c^t}\right) - g_t\rho^{t-1}\left(\frac{c P - c^s \underline{Q}}{c^s - c^t}\right) -$$

$$C_0 \left[\chi_{2_n} r^n + \chi_{1_n}\left[g_s\rho^{s-1}\left(\frac{c^t b^n - c a^n}{c^s - c^t}\right) + g_t\rho^{t-1}\left(\frac{c a^n - c^s b^n}{c^s - c^t}\right) \right] \right] -$$

$$\vartheta \left[\mu_{2_n} r^{n+1} + \mu_{1_n}\left[g_s\rho^{s-1}\left(\frac{c^t b^{n+1} - c a^{n+1}}{c^s - c^t}\right) + g_t\rho^{t-1}\left(\frac{c a^{n+1} - c^s b^{n+1}}{c^s - c^t}\right) \right] \right]$$

(5.64)

Solving for the constants C_0 and ϑ

First boundary condition (net axial pressure load):

$$P(b^2 - a^2)\pi = \int_a^b \sigma_z \, 2\pi r \, dr$$

(5.65)

$$\frac{P}{2}(b^2 - a^2) = \int_a^b \sigma_z r \, dr$$

Second boundary condition (lack of external twisting moment):

$$M = \int_a^b (\tau_{\theta z} r) 2\pi r \, dr = 0$$

$$M = 2\pi \int_a^b \tau_{\theta z} r^2 dr = 0$$

For the first integral:

$$\frac{P}{2}(b^2 - a^2) = \int_a^b r \left(C_0 - \frac{1}{\alpha_{33}} (\alpha_{31}\sigma_r + \alpha_{32}\sigma_\theta + \alpha_{34}\tau_{\theta z}) \right) dr$$

$$\frac{P}{2}(b^2 - a^2) = C_0 \frac{(b^2 - a^2)}{2} - \frac{1}{\alpha_{33}} \int_a^b r(\alpha_{31}\sigma_r + \alpha_{32}\sigma_\theta + \alpha_{34}\tau_{\theta z}) dr$$

Essentially there are only 4 integrals to evaluate, since they repeat throughout the

equations for $\sigma_r, \sigma_\theta, \tau_{\theta z}$.

$$\int_a^b \rho^{s-1} r \, dr \quad , \qquad \int_a^b \rho^{t-1} r \, dr \quad , \qquad \int_a^b r r^n \, dr \quad , \qquad \int_a^b r r^{n-1}$$

$$\Downarrow \qquad\qquad \Downarrow \qquad\qquad \Downarrow \qquad\qquad \Downarrow$$

$$\frac{1}{b^{s-1}} \int_a^b r^s \, dr \quad , \qquad \frac{1}{b^{t-1}} \int_a^b r^t \, dr \quad , \qquad \frac{b^{n+2} - a^{n+2}}{n+2} \quad , \qquad \frac{b^{n-3} - a^{n-3}}{n+3}$$

$$\Downarrow \qquad\qquad \Downarrow \qquad\qquad \Downarrow \qquad\qquad \Downarrow$$

$$\frac{1}{b^{s-1}} \left.\frac{r^{s-1}}{s+1}\right|_a^b \quad , \qquad \frac{1}{b^{t-1}} \left.\frac{r^{t-1}}{t+1}\right|_a^b \quad , \qquad \frac{b^{n-2}(1 - c^{n-2})}{n+2} \quad , \qquad \frac{b^{n-3}(1 - c^{n-3})}{n+3}$$

$$\Downarrow \qquad\qquad\qquad \Downarrow$$

$$\frac{b^{-s-1}(b^{s-1} - a^{s-1})}{s+1} , \qquad \frac{b^{-t-1}(b^{t-1} - a^{t-1})}{t+1}$$

$$\Downarrow \qquad\qquad\qquad \Downarrow$$

$$\frac{b^2(1 - a^{s-1} b^{-s-1})}{s+1} , \qquad \frac{b^2(1 - a^{t-1} b^{-t-1})}{t+1} \qquad \text{where: } c = \frac{a}{b}$$

$$\Downarrow \qquad\qquad\qquad\qquad \Downarrow$$

$$\frac{b^2\left(1-c^{s+1}\right)}{s+1} \quad , \qquad\qquad \frac{b^2\left(1-c^{t+1}\right)}{t+1}$$

The above equation is written out as:

$$\frac{P}{2}\left(b^2-a^2\right)=C_0\,\frac{\left(b^2-a^2\right)}{2}-C_0\,b^{n+2}\,\frac{\left(1-c^{n+2}\right)}{(n+2)}\left[\frac{\alpha_{13}}{\alpha_{33}}\chi_{1_n}+\frac{\alpha_{23}}{\alpha_{33}}\chi_{3_n}-\frac{\alpha_{34}}{\alpha_{33}}\chi_{2_n}\right]-$$

$$\vartheta\,\frac{b^{n+3}\left(1-c^{n+3}\right)}{(n+3)}\left[\frac{\alpha_{13}}{\alpha_{33}}\mu_{1_n}+\frac{\alpha_{23}}{\alpha_{33}}\mu_{3_n}-\frac{\alpha_{34}}{\alpha_{33}}\mu_{2_n}\right]-$$

$$\frac{b^2\left(1-c^{s+1}\right)}{s+1}\left[\frac{\alpha_{13}}{\alpha_{33}}+s\frac{\alpha_{23}}{\alpha_{33}}-g_s\frac{\alpha_{34}}{\alpha_{33}}\right]\left(\frac{c^t Q-cP}{c^s-c^t}\right)-\frac{b^2\left(1-c^{t+1}\right)}{t+1}\left[\frac{\alpha_{13}}{\alpha_{33}}+t\frac{\alpha_{23}}{\alpha_{33}}-g_t\frac{\alpha_{34}}{\alpha_{33}}\right]\left(\frac{cP-c^s Q}{c^s-c^t}\right)-$$

$$C_0\,\frac{b^2\left(1-c^{s+1}\right)}{s+1}\left[\frac{\alpha_{13}}{\alpha_{33}}\chi_{1_n}+s\frac{\alpha_{23}}{\alpha_{33}}\chi_{1_n}-g_s\frac{\alpha_{34}}{\alpha_{33}}\chi_{1_n}\right]\left(\frac{c^t b^n-ca^n}{c^s-c^t}\right)-$$

$$C_0\,\frac{b^2\left(1-c^{t+1}\right)}{t+1}\left[\frac{\alpha_{13}}{\alpha_{33}}\chi_{1_n}+t\frac{\alpha_{23}}{\alpha_{33}}\chi_{1_n}-g_t\frac{\alpha_{34}}{\alpha_{33}}\chi_{1_n}\right]\left(\frac{ca^n-c^s b^n}{c^s-c^t}\right)-$$

$$\vartheta\,\frac{b^2\left(1-c^{s+1}\right)}{s+1}\left[\frac{\alpha_{13}}{\alpha_{33}}\mu_{1_n}+s\frac{\alpha_{23}}{\alpha_{33}}\mu_{1_n}-g_s\frac{\alpha_{34}}{\alpha_{33}}\mu_{1_n}\right]\left(\frac{c^t b^{n+1}-ca^{n+1}}{c^s-c^t}\right)-$$

$$\vartheta\,\frac{b^2\left(1-c^{t+1}\right)}{t+1}\left[\frac{\alpha_{13}}{\alpha_{33}}\mu_{1_n}+t\frac{\alpha_{23}}{\alpha_{33}}\mu_{1_n}-g_t\frac{\alpha_{34}}{\alpha_{33}}\mu_{1_n}\right]\left(\frac{ca^{n+1}-c^s b^{n+1}}{c^s-c^t}\right)$$

Separating out C_0 and ϑ, the above is recast.

$$\frac{P}{2}\left(b^2-a^2\right)+\frac{b^2\left(1-c^{s+1}\right)}{s+1}\left[\frac{\alpha_{13}}{\alpha_{33}}+s\frac{\alpha_{23}}{\alpha_{33}}-g_s\frac{\alpha_{34}}{\alpha_{33}}\right]\left(\frac{c^t Q-cP}{c^s-c^t}\right)+$$

$$\frac{b^2\left(1-c^{t+1}\right)}{t+1}\left[\frac{\alpha_{13}}{\alpha_{33}}+t\frac{\alpha_{23}}{\alpha_{33}}-g_t\frac{\alpha_{34}}{\alpha_{33}}\right]\left(\frac{cP-c^s Q}{c^s-c^t}\right)=$$

$$C_0\left\{\frac{b^2-a^2}{2}+\frac{b^{n+2}}{n+2}\left(1-c^{n+2}\right)\left[\frac{\alpha_{13}}{\alpha_{33}}\chi_{1_n}+\frac{\alpha_{23}}{\alpha_{33}}\chi_{3_n}-\frac{\alpha_{34}}{\alpha_{33}}\chi_{2_n}\right]-\right.$$

$$\frac{b^2\left(1-c^{s+1}\right)}{s+1}\left[\frac{\alpha_{13}}{\alpha_{33}}\chi_{1_n}+s\frac{\alpha_{23}}{\alpha_{33}}\chi_{1_n}-g_s\frac{\alpha_{34}}{\alpha_{33}}\chi_{1_n}\right]\left(\frac{c^t b^n-ca^n}{c^s-c^t}\right)--\rightarrow$$

$$\frac{b^2\left(1-c^{t+1}\right)}{t+1}\left[\frac{\alpha_{13}}{\alpha_{33}}\chi_{1_n}+t\frac{\alpha_{23}}{\alpha_{33}}\chi_{1_n}-g_t\frac{\alpha_{34}}{\alpha_{33}}\chi_{1_n}\right]\left(\frac{c\,a^n-c^s b^n}{c^s-c^t}\right)\Biggr\}-$$

$$\vartheta\Biggl\{\frac{b^{n+3}\left(1-c^{n-3}\right)}{n+3}\left[\frac{\alpha_{13}}{\alpha_{33}}\mu_{1_n}+\frac{\alpha_{23}}{\alpha_{33}}\mu_{3_n}-\frac{\alpha_{34}}{\alpha_{33}}\mu_{2_n}\right]+$$

$$\frac{b^2\left(1-c^{s+1}\right)}{s+1}\left[\frac{\alpha_{13}}{\alpha_{33}}\mu_{1_n}+s\frac{\alpha_{23}}{\alpha_{33}}\mu_{1_n}-g_s\frac{\alpha_{34}}{\alpha_{33}}\mu_{1_n}\right]\left(\frac{c^t b^{n-1}-c\,a^{n-1}}{c^s-c^t}\right)+$$

$$\frac{b^2\left(1-c^{t+1}\right)}{t+1}\left[\frac{\alpha_{13}}{\alpha_{33}}\mu_{1_n}+t\frac{\alpha_{23}}{\alpha_{33}}\mu_{1_n}-g_t\frac{\alpha_{34}}{\alpha_{33}}\mu_{1_n}\right]\left(\frac{c\,a^{n-1}-c^s b^{n+1}}{c^s-c^t}\right)\Biggr\}$$

This last form can be expressed as:

$$\wedge_1=C_0\wedge_2+\vartheta\wedge_3\qquad\text{where:}\qquad\begin{array}{l}\wedge_1\text{ represents the }LHS,\\[4pt]\wedge_2\text{ bracket terms multiplying }C_0,\\[4pt]\wedge_3\text{ bracket terms multiplying }\vartheta\,.\end{array}$$

$$(5.66)$$

For the second boundary condition

$$\frac{M}{2\pi}=0=\int_a^b\tau_{\theta z}r^2\,dr$$

The integrals to solve are:

$$\frac{1}{b^{s-1}}\int_a^b r^2 r^{s-1}\,dr\qquad\frac{1}{b^{t-1}}\int_a^b r^2 r^{t-1}\,dr\qquad\int_a^b r^2 r^n\,dr\qquad\int_a^b r^2 r^{n-1}\,dr$$

$$\Downarrow\qquad\qquad\qquad\Downarrow\qquad\qquad\qquad\Downarrow\qquad\qquad\qquad\Downarrow$$

$$\frac{1}{b^{s-1}}\int_a^b r^{s-1}\,dr\qquad\frac{b^3\left(1-c^{t-2}\right)}{t+2}\qquad\int_a^b r^{n-2}\,dr\qquad\int_a^b r^{n-3}\,dr$$

$$\Downarrow\qquad\qquad\qquad\qquad\qquad\qquad\qquad\Downarrow\qquad\qquad\qquad\Downarrow$$

$$\frac{1}{b^{s-1}}\cdot\frac{r^{s-2}}{s+2}\Bigg|_a^b\qquad\qquad\qquad\qquad\frac{b^{n+3}-a^{n+3}}{n+3}\qquad\frac{b^{n+4}-a^{n+4}}{n+4}$$

$$\Downarrow\qquad\qquad\qquad\qquad\qquad\qquad\qquad\Downarrow\qquad\qquad\qquad\Downarrow$$

$$\frac{1}{b^{s-1}}\cdot\frac{b^{s-2}-a^{s-2}}{(s+2)}\qquad\qquad\qquad\frac{b^{n-3}\left(1-c^{n-3}\right)}{n+3}\qquad\frac{b^{n-4}\left(1-c^{n-4}\right)}{n+4}$$

$$\Downarrow$$

$$\frac{b^3\left(b^{s-2}-a^{s-2}\right)}{b^3\;b^{s-1}(s+2)}$$

$$\Downarrow$$

$$\frac{b^3\left(b^{s-2}-a^{s-2}\right)}{b^{s-2}(s+2)}$$

$$\Downarrow$$

$$\frac{b^3\left(1-c^{s-2}\right)}{(s+2)}$$

using these integrals we can write

$$0=\left[-g_s\frac{b^3\left(1-c^{s-2}\right)}{s+2}\left(\frac{c^t\underline{Q}-cP}{c^s-c^t}\right)-g_t\frac{b^3\left(1-c^{t-2}\right)}{t+2}\left(\frac{cP-c^s\underline{Q}}{c^s-c^t}\right)\right]-$$

$$C_0\left[\chi_{2_n}b^{n-3}\frac{\left(1-c^{n-3}\right)}{n+3}+\chi_{1_n}\left[g_s\frac{b^3\left(1-c^{s-2}\right)}{s+2}\left(\frac{c^tb^n-ca^n}{c^s-c^t}\right)+g_t\,b^3\left(\frac{1-c^{t-2}}{c^s-c^t}\right)\left(\frac{ca^n-c^sb^n}{c^s-c^t}\right)\right]\right]-$$

$$\vartheta\left[\mu_{2_n}b^{n-4}\frac{\left(1-c^{n-4}\right)}{n+4}+\mu_{1_n}\left[g_s\frac{b^3\left(1-c^{s-2}\right)}{s+2}\left(\frac{c^tb^{n-1}-ca^{n-1}}{c^s-c^t}\right)+g_t\frac{b^3\left(1-c^{t-2}\right)}{t+2}\left(\frac{ca^{n-1}-cb^{n-1}}{c^s-c^t}\right)\right]\right]$$

The above can be expressed as:

$$\Gamma_1=C_0\,\Gamma_2+\vartheta\,\Gamma_3 \qquad \text{where:} \quad \Gamma_1 \text{ represents the } LHS, \text{ (first term above with } P \text{ and } Q\text{)}$$

$$\Gamma_2 \text{ bracket terms multiplying } C_0,$$

$$\Gamma_3 \text{ bracket terms multiplying } \vartheta.$$

(5.67)

The solution to the constants C_0 and ϑ is found by Cramer's rule applied to the system (5.66) & (5.67).

244

$$\Gamma_1 = C_0 \Gamma_2 + \vartheta \Gamma_3$$
$$\wedge_1 = C_0 \wedge_2 + \vartheta \wedge_3$$

(5.68)

$$C_0 = \frac{\Gamma_1 \wedge_3 - \wedge_1 \Gamma_3}{\Gamma_2 \wedge_3 - \wedge_2 \Gamma_3} \quad , \quad \vartheta = \frac{\Gamma_2 \wedge_1 - \wedge_2 \Gamma_1}{\Gamma_2 \wedge_3 - \wedge_2 \Gamma_3}$$

5.4.1 Subset of Variable Property Solution Using n = 0

It is useful also to compare this equation set with the work presented by

Lekhnitskii [88], the later which is plagued by a few typographic errors. The simplest case,

that of an off-axis orthotropic layer, is solved for fixed material coefficients.

Equation (5.47) is restated for clarity.

$$-r\frac{\partial}{\partial r}\left[\beta_{11}\frac{1}{r}\frac{\partial F}{\partial r} + \beta_{12}\frac{\partial^2 F}{\partial r^2} - \beta_{14}\frac{\partial \Psi}{\partial r}\right] + r\frac{\partial^2}{\partial r^2}\left[r\left(\beta_{12}\frac{1}{r}\frac{\partial F}{\partial r} + \beta_{22}\frac{\partial^2 F}{\partial r^2} - \beta_{24}\frac{\partial \Psi}{\partial r}\right)\right] =$$
$$\frac{r\partial}{\partial r}\left(\frac{a_{13}}{a_{33}}C\right) - r\frac{\partial^2}{\partial r^2}\left[r\frac{a_{23}}{a_{33}}C\right]$$

Dividing by $r\dfrac{\partial}{\partial r}$

$$-\beta_{11}\frac{1}{r}\frac{\partial F}{\partial r} - \beta_{12}\frac{\partial^2 F}{\partial r^2} + \beta_{14}\frac{\partial \Psi}{\partial r} + \frac{\partial}{\partial r}\left[r\left(\beta_{12}\frac{1}{r}\frac{\partial F}{\partial r} + \beta_{22}\frac{\partial^2 F}{\partial r^2} - \beta_{24}\frac{\partial \Psi}{\partial r}\right)\right] = \frac{a_{13}C}{a_{33}} - \frac{\partial}{\partial r}\left[r\frac{a_{23}}{a_{33}}C\right]$$

which works out as

$$-\beta_{11}\frac{1}{r}\frac{\partial F}{\partial r} - \beta_{12}\frac{\partial^2 F}{\partial r^2} + \beta_{14}\frac{\partial \Psi}{\partial r} + \beta_{12}\frac{\partial^2 F}{\partial r^2} + \beta_{22}\frac{\partial^2 F}{\partial r^2} + \beta_{22}r\frac{\partial^3 F}{\partial r^3} - \beta_{24}\frac{\partial \Psi}{\partial r} - \beta_{24}r\frac{\partial^2 \Psi}{\partial r^2} = \left(\frac{a_{13} - a_{23}}{a_{33}}\right)C$$

Gathering terms

245

$$r\beta_{22}\frac{\partial^3 F}{\partial r^3}+\left(\beta_{22}-\beta_{12}+\beta_{12}\right)\frac{\partial^2 F}{\partial r^2}-\frac{\beta_{11}}{r}\frac{\partial F}{\partial r}+\left(\beta_{14}-\beta_{24}\right)\frac{\partial \Psi}{\partial r}-\beta_{24}r\frac{\partial^2 \Psi}{\partial r^2}=\left(\frac{a_{13}-a_{23}}{a_{33}}\right)C$$

simplifying

$$\frac{\partial^3 F}{\partial r^3}+\frac{1}{r}\frac{\partial^2 F}{\partial r^2}-\frac{\beta_{11}}{\beta_{22}}\frac{1}{r^2}\frac{\partial F}{\partial r}-\frac{\beta_{24}}{\beta_{22}}\frac{\partial^2 \Psi}{\partial r^2}+\frac{\left(\beta_{14}-\beta_{24}\right)}{\beta_{22}}\frac{1}{r}\frac{\partial \Psi}{\partial r}=\frac{C}{r}\left(\frac{a_{13}-a_{23}}{a_{33}\beta_{22}}\right)$$

Using the substitutions:

$$\frac{\partial F}{\partial r}=\phi$$

$$\frac{\partial \Psi}{\partial r}=\varphi$$

yields

$$\frac{\partial^2 \phi}{\partial r^2}+\frac{1}{r}\frac{\partial \phi}{\partial r}-\frac{\beta_{11}}{\beta_{22}}\frac{1}{r^2}\phi-\frac{\beta_{24}}{\beta_{22}}\frac{\partial \varphi}{\partial r}+\left(\frac{\beta_{14}-\beta_{24}}{\beta_{22}}\right)\frac{1}{r}\varphi=\frac{C}{r}\left(\frac{a_{13}-a_{23}}{\beta_{22}a_{33}}\right)$$

(5.69)

also, restating (5.48) for clarity

$$-\beta_{24}\frac{\partial^3 F}{\partial r^3}-\frac{1}{r}\left(\beta_{14}+\beta_{24}\right)\frac{\partial^2 F}{\partial r^2}+\beta_{44}\left(\frac{\partial^2 \Psi}{\partial r^2}+\frac{1}{r}\frac{\partial \Psi}{\partial r}\right)=\frac{C}{r}\frac{a_{34}}{a_{33}}-2\vartheta$$

reducing the differentials an order of magnitude by substitution

$$-\beta_{24}\frac{\partial^2 \phi}{\partial r^2}-\frac{1}{r}\left(\beta_{14}+\beta_{24}\right)\frac{\partial \phi}{\partial r}+\beta_{44}\left(\frac{\partial \varphi}{\partial r}+\frac{1}{r}\varphi\right)=\frac{C}{r}\frac{a_{34}}{a_{33}}-2\vartheta$$

Another form is

$$\beta_{44}\frac{1}{r}\frac{\partial}{\partial r}\left(r\varphi\right)=\frac{C}{r}\frac{a_{34}}{a_{33}}-2\vartheta+\beta_{24}\frac{\partial^2 \phi}{\partial r^2}+\frac{1}{r}\left(\beta_{14}+\beta_{24}\right)\frac{\partial \phi}{\partial r}$$

simplifying

$$\frac{\partial}{\partial r}\left(r\varphi\right)=\frac{Ca_{34}}{\beta_{44}a_{33}}-\frac{2\vartheta r}{\beta_{44}}+\frac{\beta_{24}}{\beta_{44}}r\frac{\partial^2 \phi}{\partial r^2}+\left(\frac{\beta_{14}+\beta_{24}}{\beta_{44}}\right)\frac{\partial \phi}{\partial r}$$

Integrating

$$r\varphi = \int\left(\frac{Ca_{34}}{\beta_{44}a_{33}} - \frac{2\vartheta r}{\beta_{44}} + \frac{\beta_{24}}{\beta_{44}}r\frac{\partial^2\phi}{\partial r^2} + \frac{\beta_{14}}{\beta_{44}}\frac{\partial\phi}{\partial r} + \frac{\beta_{24}}{\beta_{44}}\frac{\partial\phi}{\partial r}\right)dr$$

$$r\varphi = \frac{Ca_{34}}{\beta_{44}a_{33}}r - \frac{2\vartheta r^2}{2\beta_{44}} + \frac{\beta_{24}}{\beta_{44}}r\frac{\partial\phi}{\partial r} + \frac{\beta_{14}}{\beta_{44}}\phi$$

$$\varphi = \frac{Ca_{34}}{\beta_{44}a_{33}} - \frac{\vartheta r}{\beta_{44}} + \frac{\beta_{24}}{\beta_{44}}\frac{\partial\phi}{\partial r} + \frac{1}{r}\frac{\beta_{14}}{\beta_{44}}\phi$$

$$(5.70)$$

Substituting (5.70) back into (5.69) results in a single equation:

$$\frac{\partial^2\phi}{\partial r^2} + \frac{1}{r}\frac{\partial\phi}{\partial r} - \frac{\beta_{11}}{\beta_{22}}\frac{1}{r^2}\phi - \frac{\beta_{24}}{\beta_{22}}\frac{\partial}{\partial r}\left[\frac{Ca_{34}}{\beta_{44}a_{33}} - \frac{\vartheta r}{\beta_{44}} + \frac{\beta_{24}}{\beta_{44}}\frac{\partial\phi}{\partial r} + \frac{1}{r}\frac{\beta_{14}}{\beta_{44}}\phi\right] +$$

$$\left(\frac{\beta_{14}-\beta_{24}}{\beta_{22}}\right)\frac{1}{r}\left[\frac{Ca_{34}}{\beta_{44}a_{33}} - \frac{\vartheta r}{\beta_{44}} + \frac{\beta_{24}}{\beta_{44}}\frac{\partial\phi}{\partial r} + \frac{1}{r}\frac{\beta_{14}}{\beta_{44}}\phi\right] = \frac{C}{r}\left(\frac{a_{13}-a_{23}}{\beta_{22}a_{33}}\right)$$

Expanding:

$$\frac{\partial^2\phi}{\partial r^2} + \frac{1}{r}\frac{\partial\phi}{\partial r} - \frac{\beta_{11}}{\beta_{22}}\frac{1}{r^2}\phi - \frac{\beta_{24}}{\beta_{22}}\left[0 - \frac{\vartheta}{\beta_{44}} + \frac{\beta_{24}}{\beta_{44}}\frac{\partial^2\phi}{\partial r^2} - \frac{\beta_{14}}{\beta_{44}}\frac{1}{r^2}\phi + \frac{\beta_{14}}{\beta_{44}}\frac{1}{r}\frac{\partial\phi}{\partial r}\right] +$$

$$\left(\frac{\beta_{14}-\beta_{24}}{\beta_{22}}\right)\left[\frac{Ca_{34}}{r\beta_{44}a_{33}} - \frac{\vartheta}{\beta_{44}} + \frac{\beta_{24}}{\beta_{44}}\frac{1}{r}\frac{\partial\phi}{\partial r} + \frac{\beta_{14}}{\beta_{44}}\frac{1}{r^2}\phi\right] = \frac{C}{r}\frac{(a_{13}-a_{23})}{\beta_{22}a_{33}}$$

grouping terms

$$\frac{\partial^2\phi}{\partial r^2}\left[1 - \frac{\beta_{24}^2}{\beta_{22}\beta_{44}}\right] + \frac{1}{r}\frac{\partial\phi}{\partial r}\left[1 - \frac{\beta_{14}\beta_{24}}{\beta_{22}\beta_{44}} + \frac{(\beta_{14}-\beta_{24})}{\beta_{22}}\frac{\beta_{24}}{\beta_{44}}\right] -$$

$$\frac{1}{r^2}\phi\left[\frac{\beta_{11}}{\beta_{22}} - \frac{\beta_{14}\beta_{24}}{\beta_{22}\beta_{44}} - \frac{(\beta_{14}-\beta_{24})}{\beta_{22}}\frac{\beta_{14}}{\beta_{44}}\right] = \frac{C}{r}\left[\frac{(a_{13}-a_{23})}{\beta_{22}a_{33}} - \frac{(\beta_{14}-\beta_{24})}{\beta_{22}}\frac{a_{34}}{\beta_{44}a_{33}}\right] + \vartheta\left[\frac{-\beta_{24}}{\beta_{22}\beta_{44}} + \frac{(\beta_{14}-\beta_{24})}{\beta_{22}\beta_{44}}\right]$$

Re-writing:

$$\left[\frac{\beta_{22}\beta_{44}-\beta_{24}^2}{\beta_{22}\beta_{44}}\right]\frac{\partial^2\phi}{\partial r^2} + \frac{1}{r}\frac{\partial\phi}{\partial r}\left[\frac{\beta_{22}\beta_{44}-\beta_{14}\beta_{24}+\beta_{14}\beta_{24}-\beta_{24}^2}{\beta_{22}\beta_{44}}\right] -$$

247

$$\frac{1}{r^2}\phi\left[\frac{\beta_{11}\beta_{44}-\beta_{14}\beta_{24}-\beta_{14}^2+\beta_{14}\beta_{24}}{\beta_{22}\beta_{44}}\right]=\frac{C}{a_{33}r}\left[\frac{(a_{13}-a_{23})\beta_{44}-a_{34}(\beta_{14}-\beta_{24})}{\beta_{22}\beta_{44}}\right]-\vartheta\left[\frac{2\beta_{24}-\beta_{14}}{\beta_{22}\beta_{44}}\right]$$

Dividing both sides by $\dfrac{\beta_{22}\beta_{44}-\beta_{24}^2}{\beta_{22}\beta_{44}}$

$$\frac{\partial^2\phi}{\partial r^2}+\frac{1}{r}\frac{\partial\phi}{\partial r}-\frac{1}{r^2}\phi\left[\frac{(\beta_{11}\beta_{44}-\beta_{14}^2)}{(\beta_{22}\beta_{44}-\beta_{24}^2)}\right]=\frac{C}{a_{33}\,r}\left[\frac{(a_{13}-a_{23})\beta_{22}-a_{34}(\beta_{14}-\beta_{24})}{\beta_{22}\beta_{44}-\beta_{24}^2}\right]-\vartheta\left[\frac{(2\beta_{24}-\beta_{14})}{\beta_{22}\beta_{44}-\beta_{24}^2}\right]$$

$$(5.71)$$

For purposes of clarity, we define the bracketed terms above as:

$$d_1=\left[\frac{(a_{13}-a_{23})\beta_{44}-a_{34}(\beta_{14}-\beta_{24})}{\beta_{22}\beta_{44}-\beta_{24}^2}\right],\qquad d_2=\left[\frac{(2\beta_{24}-\beta_{14})}{\beta_{22}\beta_{44}-\beta_{24}^2}\right]$$

Solving the homogeneous part of this Euler equation

let: $\phi=r^\lambda$

$$\phi'=\lambda r^{\lambda-1}$$

$$\phi''=\lambda(\lambda-1)r^{\lambda-2}$$

then the *LHS* of (5.71) becomes

$$\lambda(\lambda-1)r^{\lambda-2}+\frac{1}{r}\lambda r^{\lambda-1}-\frac{1}{r^2}r^\lambda\left[\frac{\beta_{11}\beta_{44}-\beta_{14}^2}{\beta_{22}\beta_{44}-\beta_{24}^2}\right]=0$$

$$r^{\lambda-2}\left[\lambda^2-\lambda+\lambda-\frac{\beta_{11}\beta_{44}-\beta_{14}^2}{\beta_{22}\beta_{44}-\beta_{24}^2}\right]=0$$

$$r^{\lambda-2}\left[\lambda^2-\frac{\beta_{11}\beta_{44}-\beta_{14}^2}{\beta_{22}\beta_{44}-\beta_{24}^2}\right]=0$$

$$\lambda^2=\frac{\beta_{11}\beta_{44}-\beta_{14}^2}{\beta_{22}\beta_{44}-\beta_{24}^2}$$

$$\lambda_{1,2} \pm \sqrt{\frac{\beta_{11}\beta_{44} - \beta_{14}^2}{\beta_{22}\beta_{44} - \beta_{24}^2}} \quad \text{or} \quad \lambda_{1,2} = \pm K \quad \text{where:} \quad K = \sqrt{\frac{\beta_{11}\beta_{44} - \beta_{24}^2}{\beta_{22}\beta_{44} - \beta_{24}^2}}$$

The final form is

$$\phi = C_1 r^{\lambda_1} + C_2 r^{\lambda_2} = C_1 r^K + C_2 r^{-K}$$

$$(5.72)$$

In solving for the particular solution, we note that the homogeneous part takes the form:

$$y_h = C_1 y_1(r) + C_2 y_2(r)$$

The particular solution can thus be determined as:

where:

$$y_p = -y_1 \int \frac{y_2(RHS)}{\varpi} dr + y_2 \int \frac{y_1(RHS)}{\varpi} dr$$

$$y_1 = r^K, \quad y_2 = r^{-K}$$

$$y_p = -r^K \int \frac{r^{-K}(RHS)}{-2Kr^{-1}} dr + r^{-K} \int \frac{r^K(RHS)}{-2Kr^{-1}} dr$$

$$\varpi = y_1 y_2' - y_1' y_2 \quad \text{(Wronskian)}$$

$$\varpi = r^K(-K)r^{-K-1} - Kr^{K-1}r^{-K}$$

$$y_p = \frac{r^K}{2K} \int r^{1-K}(RHS) dr - \frac{r^{-K}}{2K} \int r^{1-K}(RHS) dr$$

$$(RHS) = RHS \text{ of eqn. } (5.71)$$

Substituting first the d_1 term

$$y_A = \frac{r^K}{2K} \int r^{1-K}\left(\frac{C}{a_{33}r} d_1\right) dr - \frac{r^{-K}}{2K} \int r^{1-K}\left(\frac{C}{a_{33}r} d_1\right) dr$$

$$y_A = \frac{r^K}{2K} \frac{Cd_1}{a_{33}} \int r^{-K} dr - \frac{r^{-K}}{2K} \frac{Cd_1}{a_{33}} \int r^K dr$$

$$y_A = \frac{r^K}{2K} \frac{r^{-K-1}}{(-K+1)} \frac{Cd_1}{a_{33}} - \frac{r^{-K}}{2K} \frac{r^{K-1}}{(K+1)} \frac{Cd_1}{a_{33}}$$

$$y_A = \frac{Cd_1}{a_{33}} \frac{r}{2K}\left(\frac{1}{-K+1} - \frac{1}{K+1}\right)$$

$$y_A = \frac{Cd_1}{a_{33}} \frac{r}{2K} \frac{(K+1)-(-K+1)}{(K+1)(-K+1)}$$

$$y_{P_1} = \frac{Cd_1}{a_{33}} \frac{r}{2K} \left(\frac{2K+1-1}{(K+1)(-K+1)} \right)$$

$$y_{P_1} = \frac{Cd_1 r}{a_{33}\left(-K^2 - K + K + 1\right)}$$

$$y_{P_1} = \frac{Cd_1 r}{a_{33}\left(1 - K^2\right)}$$

but:

$$1 - K^2 = 1 - \frac{\beta_{11}\beta_{44} - \beta_{14}^2}{\beta_{22}\beta_{44} - \beta_{24}^2} = \frac{\left(\beta_{22}\beta_{44} - \beta_{24}^2\right) - \left(\beta_{11}\beta_{44} - \beta_{14}^2\right)}{\beta_{22}\beta_{44} - \beta_{24}^2}$$

$$y_{P_1} = \frac{Cr}{a_{33}} \left[\frac{(a_{13} - a_{23})\beta_{44} - a_{34}(\beta_{14} - \beta_{24})}{\left(\beta_{22}\beta_{44} - \beta_{24}^2\right) - \left(\beta_{11}\beta_{44} - \beta_{14}^2\right)} \right]$$

$$y_{P_1} = \frac{C\chi_1 r}{a_{33}}$$

where: $$\chi_1 = \left[\frac{(a_{13} - a_{23})\beta_{44} - a_{34}(\beta_{14} - \beta_{24})}{\left(\beta_{22}\beta_{44} - \beta_{24}^2\right) - \left(\beta_{11}\beta_{44} - \beta_{14}^2\right)} \right]$$

The second portion of the *RHS* is solved in the same manner.

$$y_{P_2} = \frac{r^K}{2K} \int \left(r^{1-K} d_2\right) dr - \frac{r^{-K}}{2K} \int \left(r^{1-K} d_2\right) dr$$

$$y_{P_2} = \frac{r^K}{2K} \left(\frac{r^{2-K}}{2-K} \right) d_2 - \frac{r^{-K}}{2K} \left(\frac{r^{2+K}}{2+K} \right) d_2 + C_3$$

$$y_{P_2} = \frac{d_2}{2K} \left(\frac{r^2}{2-K} - \frac{r^2}{2+K} \right) + C_3$$

$$y_{P_2} = \frac{d_2}{2K} \frac{r^2(2+K) - r^2(2-K)}{(2-K)(2+K)} + C_3$$

$$y_{P_2} = \frac{d_2 r^2}{2K} \frac{(2-2+K+K)}{4-2K+2K-K^2} + C_3$$

$$y_{P_2} = \frac{r^2 (2K) d_2}{(2K)(4-K^2)} + C_3$$

but:

$$4-K^2 = 4 - \frac{\beta_{11}\beta_{44} - \beta_{14}^2}{\beta_{22}\beta_{44} - \beta_{24}^2} = \frac{4(\beta_{22}\beta_{44} - \beta_{24}^2) - (\beta_{11}\beta_{44} - \beta_{14}^2)}{\beta_{22}\beta_{44} - \beta_{24}^2}$$

substituting for d_2

$$y_{P_2} = \frac{r^2 \vartheta (-2\beta_{24} + \beta_{14})}{(4-K^2)(\beta_{22}\beta_{44} - \beta_{24}^2)} + C_3$$

substituting for $(4-K^2)$

$$y_{P_2} = \frac{r^2 \vartheta (-2\beta_{24} + \beta_{14})}{4(\beta_{22}\beta_{44} - \beta_{24}^2) - (\beta_{11}\beta_{44} - \beta_{14}^2)} + C_3$$

$$y_{P_2} = r^2 \vartheta \mu_1 + C_3$$

where:
$$\mu_1 = \frac{(-2\beta_{24} + \beta_{14})}{4(\beta_{22}\beta_{44} - \beta_{24}^2) - (\beta_{11}\beta_{44} - \beta_{14}^2)}$$

- -

The complete solution for ϕ is:

$$\phi = C_1 r^K + C_2 r^{-K} + \frac{C\chi_1 r}{a_{33}} + \mu_1 r^2 \vartheta + C_3$$

(5.73)

Solving for φ, from (5.70)

$$\varphi = \frac{Ca_{34}}{\beta_{44}a_{33}} - \frac{\vartheta r}{\beta_{44}} + \frac{\beta_{24}}{\beta_{44}} \frac{\partial}{\partial r}\left[C_1 r^K + C_2 r^{-K} + \frac{C\chi_1 r}{a_{33}} + \mu_1 r^2 \vartheta + C_3 \right] +$$

$$\frac{1}{r} \frac{\beta_{14}}{\beta_{44}}\left[C_1 r^K + C_2 r^{-K} + \frac{C\chi_1 r}{a_{33}} + \mu_1 r^2 \vartheta + C_3 \right]$$

251

expansion

$$\varphi = \frac{C}{a_{33}} \frac{a_{34}}{\beta_{44}} - \frac{\vartheta r}{\beta_{44}} + \frac{\beta_{24}}{\beta_{44}} KC_1 r^{K-1} + C_2 \frac{\beta_{24}}{\beta_{44}} (-K) r^{-K-1} + \frac{\beta_{24}}{\beta_{44}} \frac{C\chi_1}{a_{33}} + \frac{\beta_{24}}{\beta_{44}} 2\mu_1 r \vartheta +$$
$$\frac{\beta_{14}}{\beta_{44}} C_1 r^{K-1} + \frac{\beta_{14}}{\beta_{44}} C_2 r^{-K-1} + \frac{\beta_{14}}{\beta_{44}} \frac{C\chi_1}{a_{33}} + \frac{\beta_{14}}{\beta_{44}} \mu_1 r \vartheta + \frac{1}{r} \frac{\beta_{14}}{\beta_{44}} C_3$$

$$(5.74)$$

collecting terms:

$$\varphi = \frac{1}{r} \frac{\beta_{14}}{\beta_{44}} C_3 + \frac{C}{a_{33}} \left(\frac{a_{34}}{\beta_{44}} + \frac{\beta_{24}}{\beta_{44}} \chi_1 + \frac{\beta_{14}}{\beta_{44}} \chi_1 \right) + \vartheta r \left(\frac{-1}{\beta_{44}} + \frac{2\beta_{24}}{\beta_{44}} \mu_1 + \frac{\beta_{14}}{\beta_{44}} \mu_1 \right) +$$
$$C_1 r^{K-1} \left(\frac{\beta_{24} K}{\beta_{44}} + \frac{\beta_{14}}{\beta_{44}} \right) + C_2 r^{-K-1} \left(\frac{-K\beta_{24}}{\beta_{44}} + \frac{\beta_{14}}{\beta_{44}} \right)$$

Defining: $\quad g_K = \dfrac{\beta_{14} + K\beta_{24}}{\beta_{44}} \quad , \quad g_{-K} = \dfrac{\beta_{14} - K\beta_{24}}{\beta_{44}}$

$$(5.75)$$

also

$$\chi_2 = \frac{a_{34} + \chi_1(\beta_{14} + \beta_{24})}{\beta_{44}} \quad = \quad \frac{a_{34}}{\beta_{44}} + \left[\frac{(a_{13} - a_{23})\beta_{44} - a_{34}(\beta_{14} - \beta_{24})}{(\beta_{22}\beta_{44} - \beta_{24}^2) - (\beta_{11}\beta_{44} - \beta_{14}^2)} \right] \frac{(\beta_{14} + \beta_{24})}{\beta_{44}}$$

$$\chi_2 = \frac{a_{34}(\beta_{22}\beta_{44} - \beta_{24}^2) - a_{34}(\beta_{11}\beta_{44} - \beta_{14}^2) + (a_{13} - a_{23})\beta_{44}(\beta_{14} + \beta_{24}) - a_{34}(\beta_{14} - \beta_{24})(\beta_{14} + \beta_{24})}{\beta_{44}\left[(\beta_{22}\beta_{44} - \beta_{24}^2) - (\beta_{11}\beta_{44} - \beta_{14}^2) \right]}$$

$$\chi_2 = \frac{\begin{array}{l} a_{34}\beta_{22}\beta_{44} - a_{34}\beta_{24}^2 - a_{34}\beta_{11}\beta_{44} + a_{34}\beta_{14}^2 + a_{13}\beta_{14}\beta_{44} + a_{13}\beta_{24}\beta_{44} - \rightarrow \\ \rightarrow a_{23}\beta_{14}\beta_{44} - a_{23}\beta_{24}\beta_{44} - a_{34}\beta_{14}^2 - a_{34}\beta_{14}\beta_{24} + a_{34}\beta_{24}^2 + a_{34}\beta_{24}\beta_{14} \end{array}}{\beta_{44}\left[(\beta_{22}\beta_{44} - \beta_{24}^2) - (\beta_{11}\beta_{44} - \beta_{14}^2) \right]}$$

$$\chi_2 = \frac{(a_{13} - a_{23})(\beta_{14}\beta_{44} + \beta_{24}\beta_{44}) + a_{34}(\beta_{22}\beta_{44} - \beta_{11}\beta_{44})}{\beta_{44}\left[(\beta_{22}\beta_{44} - \beta_{24}^2) - (\beta_{11}\beta_{44} - \beta_{14}^2) \right]}$$

$$\chi_2 = \frac{(a_{13} - a_{23})(\beta_{14} + \beta_{24}) + a_{34}(\beta_{22} - \beta_{11})}{(\beta_{22}\beta_{44} - \beta_{24}^2) - (\beta_{11}\beta_{44} - \beta_{14}^2)}$$

$$(5.77)$$

252

lastly, defining

$$\mu_2 = \left[\frac{-1}{\beta_{44}} + \frac{(2\beta_{24} + \beta_{14})\mu_1}{\beta_{44}} \right]$$

$$\mu_2 = \frac{1}{\beta_{44}} \left[-1 + (2\beta_{24} + \beta_{14})\mu_1 \right]$$

$$\mu_2 = \frac{1}{\beta_{44}} \left[\frac{-4(\beta_{22}\beta_{44} - \beta_{24}^2) + (\beta_{11}\beta_{44} - \beta_{14}^2) + (2\beta_{24} + \beta_{14})(-2\beta_{24} + \beta_{14})}{4(\beta_{22}\beta_{44} - \beta_{24}^2) - (\beta_{11}\beta_{44} - \beta_{14}^2)} \right]$$

$$\mu_2 = \frac{1}{\beta_{44}} \left[\frac{-4\beta_{22}\beta_{44} + 4\beta_{24}^2 + \beta_{11}\beta_{44} - \beta_{14}^2 - 4\beta_{24}^2 - 2\beta_{14}\beta_{24} + 2\beta_{14}\beta_{24} + \beta_{14}^2}{4(\beta_{22}\beta_{44} - \beta_{24}^2) - (\beta_{11}\beta_{44} - \beta_{14}^2)} \right]$$

$$\mu_2 = \left[\frac{\beta_{11} - 4\beta_{22}}{4(\beta_{22}\beta_{44} - \beta_{24}^2) - (\beta_{11}\beta_{44} - \beta_{14}^2)} \right]$$

(5.78)

Applying the definitions derived for coefficient quantities, (5.74) becomes

$$\omega = \frac{1}{r} \frac{\beta_{14}}{\beta_{44}} C_3 + \frac{C}{a_{33}} \chi_2 + \mu_2 \vartheta\, r + C_1 g_K r^{K-1} + C_2 g_{-K} r^{-K-1}$$

(5.79)

To find expressions for the stresses, the stress functions are applied. Recall

$$\frac{\partial F}{\partial r} = \phi \qquad \text{also} \qquad \frac{1}{r} \frac{\partial F}{\partial r} = \sigma_r$$

$$\frac{\partial \Psi}{\partial r} = \varphi \qquad\qquad \frac{\partial^2 F}{\partial r^2} = \sigma_\theta$$

$$\frac{-\partial \Psi}{\partial r} = \tau_{\theta z}$$

hence $\quad \sigma_r = \frac{1}{r}\phi$

$$\sigma_\theta = \frac{\partial \phi}{\partial r}$$

$$\tau_{\theta z} = -\varphi$$

Substitution of (5.73) and (5.79) into the above expressions yields:

$$\sigma_r = \frac{C\chi_1}{a_{33}} + C_1 r^{K-1} + C_2 r^{-K-1} + \mu_1 r\vartheta + \frac{C_3}{r}$$

$$\sigma_\theta = \frac{C\chi_1}{a_{33}} + KC_1 r^{K-1} - C_2 K r^{-K-1} + 2\mu_1 r\vartheta$$

$$\tau_{\theta z} = \frac{-1}{r}\frac{\beta_{14}}{\beta_{44}}C_3 - \frac{C}{a_{33}}\chi_2 - C_1 g_K r^{K-1} - C_2 g_{-K} r^{-K-1} - \mu_2 r\vartheta$$

$$\sigma_z = \frac{C}{a_{33}} - \frac{1}{a_{33}}\left(a_{13}\sigma_r + a_{23}\sigma_\theta + a_{34}\tau_{\theta z}\right)$$

(5.79)

The above is a simple case ($n = 0$) of the more general solution derived previously. It should be evident that application of the expressions for displacements , as was done in the procedure leading from equations (5.58) to (5.60) will also result with $C_3 = 0$.

5.4.2 Evaluating the Constants for the Case of $n = 0$

The general solution for an off-axis orthotropic layer, present within a cylinder, requires the evaluation of two constants C and ϑ. The seemingly complete solutions presented in advanced works by most authors (for example: Adali,Verijenko et al. [165]) are correct only for the situation where a layer of the cylinder or vessel is *prevented* from twisting (yet not restrained axially). Generally only the constant C is solved for without regard to ϑ. Setting $\vartheta = 0$ means that no twist is present, however this condition is a constraint (similar to fixed ends so as to allow no axial displacement) which is not natural to a single layer. The condition $\vartheta = 0$ is *approximately* held true with the condition that adjacent layers are oriented opposite and cancel out net twist. This is never exactly true

since the individual oppositely oriented plies have their mean at slightly different radial locations. For a filament wound construction with multiple circuits per path the lay-up is interwoven so on a whole the twist is more likely to cancel completely, however on a local basis (between sections where fibers cross-over) the twist and additional stress it causes remain. The condition of $\vartheta = 0$ would also be applicable to a case with entirely fixed ends. In the strictest sense, evaluation of these constants requires simultaneous application of two boundary conditions and solving a system with two unknowns.

If setting $\vartheta = 0$ (by whatever justification) only the more familiar axial boundary condition is required.

$$\frac{L}{2\pi} = \int_a^b \sigma_z r\, dr = \int_a^b r \left[\frac{C}{a_{33}} - \frac{1}{a_{33}} \left(a_{13}\sigma_r + a_{23}\sigma_\theta + a_{34}\tau_{\theta z} \right) \right] dr$$

where: L = axial load

(5.80)

Substituting the relations for stresses:

$$\frac{L}{2\pi} = \int_a^b \left(\frac{C}{a_{33}} r \right) dr - \int_a^b \left(\frac{a_{13}}{a_{33}} r \sigma_r + \frac{a_{23}}{a_{33}} r \sigma_\theta + \frac{a_{34}}{a_{33}} r \tau_{\theta z} \right) dr$$

$$\frac{L}{2\pi} = \frac{C}{a_{33}} \frac{\left(b^2 - a^2 \right)}{2} - \int_a^b \left(\frac{a_{13}}{a_{33}} r \sigma_r + \frac{a_{23}}{a_{33}} r \sigma_\theta + \frac{a_{34}}{a_{33}} r \tau_{\theta z} \right) dr$$

$$\frac{L}{2\pi} = \frac{C b^2}{a_{33}} \frac{\left(1 - c^2 \right)}{2} - \int_a^b \left(\frac{a_{13}}{a_{33}} r \sigma_r + \frac{a_{23}}{a_{33}} r \sigma_\theta + \frac{a_{34}}{a_{33}} r \tau_{\theta z} \right) dr$$

(5.81)

Evaluating terms of the integration, one must first substitute the stresses. Expressions for the stresses are obtained by a procedure analogous to the steps followed in arriving at equations (5.62), (5.63) and (5.64), the result being:

$$\sigma_r = C_0 \chi_1 \left[1 - \rho^{K-1} \left(\frac{1-c^{K+1}}{1-c^{2K}} \right) - \rho^{-K-1} \left(\frac{1-c^{K-1}}{1-c^{2K}} \right) c^{K-1} \right] \div$$

$$\left[\rho^{K-1} \left(\frac{Pc^{K-1}-Q}{1-c^{2K}} \right) + \rho^{-K-1} \left(\frac{Qc^{K-1}-P}{1-c^{2K}} \right) c^{K-1} \right]$$

(5.82)

$$\sigma_\theta = C_0 \chi_1 \left[1 - K\rho^{K-1} \left(\frac{1-c^{K+1}}{1-c^{2K}} \right) + K\rho^{-K-1} \left(\frac{1-c^{K-1}}{1-c^{2K}} \right) c^{K-1} \right] +$$

$$\left[K\rho^{K-1} \left(\frac{Pc^{K-1}-Q}{1-c^{2K}} \right) - K\rho^{-K-1} \left(\frac{Qc^{K-1}-P}{1-c^{2K}} \right) c^{K-1} \right]$$

(5.83)

$$\tau_{\theta z} = -g_K \rho^{K-1} \left(\frac{Pc^{K+1}-Q}{1-c^{2K}} \right) - g_{-K} \rho^{-K-1} \left(\frac{Qc^{K-1}-P}{1-c^{2K}} \right) c^{K+1} +$$

$$+ C_0 \left[-\chi_2 + \chi_1 \left[\rho^{K-1} g_K \left(\frac{1-c^{K-1}}{1-c^{2K}} \right) + \rho^{-K-1} g_{-K} \left(\frac{1-c^{K-1}}{1-c^{2K}} \right) c^{K-1} \right] \right]$$

(5.84)

Essentially there are only 2 integrals to evaluate:

$$\int_a^b \rho^{K-1} r \, dr \qquad \text{and} \qquad \int_a^b \rho^{-K-1} r \, dr$$

$$\Downarrow \qquad\qquad\qquad\qquad\qquad \Downarrow$$

$$b^{-K-1} \int_a^b r^{K-1} \cdot r \, dr \qquad\qquad b^{K-1} \int_a^b r^{-K-1} r \, dr$$

$$\Downarrow \qquad\qquad\qquad\qquad\qquad \Downarrow$$

$$b^{-K-1} \int r^K \, dr \qquad\qquad b^{K-1} \int_a^b r^{-K} \, dr$$

$$\Downarrow \qquad\qquad\qquad\qquad\qquad \Downarrow$$

$$b^{-K-1} \left. \frac{r^{K-1}}{K+1} \right|_a^b \qquad\qquad b^{K-1} \left. \frac{r^{-K-1}}{(-K+1)} \right|_a^b$$

$$\Downarrow \qquad\qquad\qquad\qquad\qquad \Downarrow$$

$$b^{-K-1} \frac{\left(b^{K-1} - a^{K-1} \right)}{(K+1)} \qquad\qquad b^{K-1} \frac{b^{-K-1} - a^{-K-1}}{(-K+1)}$$

256

$$\Downarrow$$

$$\frac{b^2 - a^{K-1}b^{-K-1}}{K+1}$$

$$\Downarrow$$

$$\frac{b^2\left(1 - a^{K+1}b^{-K-1}\right)}{K+1}$$

$$\Downarrow$$

$$\frac{b^2\left(1 - c^{K-1}\right)}{K+1}$$

$$\Downarrow$$

$$\frac{b^2 - b^{K-1}a^{-K-1}}{-K+1}$$

$$\Downarrow$$

$$\frac{b^2\left(1 - b^{K-1}a^{-K-1}\right)}{-K+1}$$

$$\Downarrow$$

$$\frac{b^2\left(1 - c^{-K-1}\right)}{-K+1}$$

Substitution of these integrals into (5.81) gives

$$\frac{L}{2\pi} = C_0 b^2 \frac{\left(1-c^2\right)}{2} - C_0\left[\frac{a_{13}}{a_{33}}\chi_1 + \frac{a_{23}}{a_{33}}\chi_1 - \frac{a_{34}}{a_{33}}\chi_2\right]\int_a^b r\, dr -$$

$$\left\{\frac{C_0\chi_1}{a_{33}}\left[-a_{13} - Ka_{23} + a_{34}g_K\right]\left(\frac{1-c^{K-1}}{1-c^{2K}}\right)\frac{b^2\left(1-c^{K-1}\right)}{K+1} + \frac{C_0\chi_1}{a_{33}}\left[-a_{13} + Ka_{23} + g_{-K}a_{34}\right]\cdot\right.$$

$$\frac{b^2\left(1-c^{-K-1}\right)}{-K+1}\left(\frac{1-c^{K-1}}{1-c^{2K}}\right)c^{K-1} + \frac{1}{a_{33}}\left[\frac{b^2\left(1-c^{K-1}\right)}{K+1}\frac{\left(Pc^{K-1}-Q\right)}{\left(1-c^{2K}\right)}\right]\left(a_{13} + Ka_{23} - a_{34}g_K\right) +$$

$$\left.\frac{1}{a_{33}}\left[\frac{b^2\left(1-c^{-K-1}\right)}{-K+1}\frac{\left(Qc^{K-1}-P\right)}{\left(1-c^{2K}\right)}c^{K-1}\right]\left(a_{13} - Ka_{23} - a_{34}g_{-K}\right)\right\}$$

rearranged as

$$\frac{L}{2\pi} = \frac{C_0 b^2\left(1-c^2\right)}{2} - \frac{b^2\left(1-c^2\right)}{2}\frac{C_0}{a_{33}}\left(a_{13}\chi_1 + a_{23}\chi_1 - a_{34}\chi_2\right) -$$

$$\frac{C_0\chi_1 b^2}{a_{33}}\left(-a_{13} - Ka_{23} + a_{34}g_K\right)\left(\frac{1-c^{K+1}}{1-c^{2K}}\right)\frac{\left(1-c^{K-1}\right)}{K+1} - \frac{C_0\chi_1 b^2}{a_{33}}\left(-a_{13} + Ka_{23} + g_{-K}a_{34}\right)\cdot$$

$$\left(\frac{1-c^{K-1}}{1-c^{2K}}\right)\frac{\left(1-c^{-K-1}\right)}{-K+1} - \frac{b^2\left(1-c^{K-1}\right)}{a_{33}(K+1)}\frac{\left(Pc^{K-1}-Q\right)}{\left(1-c^{2K}\right)}\left(a_{13} + Ka_{23} - a_{34}g_K\right) -$$

$$\frac{b^2\left(1-c^{-K-1}\right)}{a_{33}(-K+1)}\frac{\left(Qc^{K-1}-P\right)}{\left(1-c^{2K}\right)}c^{K-1}\left(a_{13} - Ka_{23} - a_{34}g_{-K}\right)$$

$$(5.85)$$

257

The axial extension constant is:

$$C_0 = \frac{\dfrac{L}{2\pi} + \dfrac{b^2(1-c^{K-1})}{a_{33}(K+1)}\dfrac{(Pc^{K-1}-Q)}{(1-c^{2K})}(a_{13}+Ka_{23}-a_{34}g_K)+ \rightarrow}{\dfrac{b^2(1-c^2)}{2}-\dfrac{b^2(1-c^2)}{2a_{33}}(a_{13}\chi_1+a_{23}\chi_1-a_{34}\chi_2)-\dfrac{b^2\chi_1}{a_{33}}(-a_{13}-Ka_{23}+a_{34}g_K)\cdot \rightarrow}$$

$$\rightarrow \dfrac{b^2(1-c^{-K-1})}{a_{33}(-K+1)}\dfrac{(Qc^{K-1}-P)}{(1-c^{2K})}c^{K-1}(a_{13}-Ka_{23}-a_{34}g_{-K})$$

$$\rightarrow \dfrac{(1-c^{K-1})}{(1-c^{2K})}\dfrac{(1-c^{K-1})}{(K+1)}-\dfrac{b^2\chi_1}{a_{33}}(-a_{13}+Ka_{23}+a_{34}g_{-K})\dfrac{(1-c^{K-1})}{(1-c^{2K})}\dfrac{(1-c^{-K-1})c^{K-1}}{(-K+1)}$$

(5.86)

Thus from (5.57)

$$\sigma_z = C_0 - \frac{C_0}{a_{33}}\left[\chi_1(a_{13}+a_{23})-\chi_2 a_{34}\right]-\frac{C_0\chi_1}{a_{33}}\left[-a_{13}-Ka_{23}+a_{34}g_K\right]\frac{(1-c^{K-1})}{(1-c^{2K})}\rho^{K-1}-$$

$$\frac{C_0\chi_1}{a_{33}}\left[-a_{13}+Ka_{23}+g_{-K}a_{34}\right]\frac{(1-c^{K-1})}{(1-c^{2K})}c^{K-1}\rho^{-K-1}-\frac{1}{a_{33}}\frac{(Pc^{K-1}-Q)}{(1-c^{2K})}\left[a_{13}+Ka_{23}-a_{34}g_K\right]\rho^{K-1}-$$

$$\frac{1}{a_{33}}\frac{(Qc^{K-1}-P)}{(1-c^{2K})}c^{K-1}(a_{13}-Ka_{23}-a_{34}g_{-K})\rho^{-K-1}$$

(5.87)

Solution for $\sigma_r, \sigma_\theta, \tau_{\theta z}$ follow simply by substituting the expression for C_0 in (5.86) into (5.81) through (5.83).

The more general case with fixed material coefficients puts no restriction on twisting so the constant 9 is determined with the help of the additional boundary condition set below.

$$\frac{M}{2\pi} = 0 = \int_a^b \tau_{\theta z} r^2 dr$$

Drawing from (5.84) and (5.64) the shear is:

$$\tau_{\theta z} = -\frac{Pc^{K+1}-Q}{1-c^{2K}}g_K\,\rho^{K-1} - \frac{Qc^{K-1}-P}{1-c^{2K}}g_{-K}\,c^{K+1}\rho^{-K-1} +$$

$$C_0\left[-\chi_2 + \chi_1\left(\frac{1-c^{K+1}}{1-c^{2K}}g_K\,\rho^{K-1} + \frac{1-c^{K-1}}{1-c^{2K}}g_{-K}\,c^{K-1}\rho^{-K-1}\right)\right] +$$

$$\vartheta b\left[\mu_2\rho + \mu_1\left(\frac{1-c^{K-2}}{1-c^{2K}}g_K\,\rho^{K-1} + \frac{1-c^{K-2}}{1-c^{2K}}g_{-K}\,c^{K-2}\rho^{-K-1}\right)\right]$$

$$(5.88)$$

Solving for the integrals:

$$\frac{1}{b^{K-1}}\int_a^b r^{K-1}r^2\,dr \qquad\qquad \frac{1}{b^{-K-1}}\int_a^b r^{-K-1}r^2\,dr \qquad\qquad \frac{1}{b}\int_a^b r\cdot r^2\,dr$$

$$\Downarrow \qquad\qquad\qquad\qquad \Downarrow \qquad\qquad\qquad\qquad \Downarrow$$

$$\frac{1}{b^{K-1}}\int_a^b r^{K+1}\,dr \qquad\qquad \frac{1}{b^{-K-1}}\int r^{-K-1}\,dr \qquad\qquad \frac{1}{b}\cdot\frac{r^4}{4}\Big|_a^b$$

$$\Downarrow \qquad\qquad\qquad\qquad \Downarrow \qquad\qquad\qquad\qquad \Downarrow$$

$$\left(\frac{1}{b^{K-1}}\right)\frac{r^{K+2}}{K+2}\Big|_a^b \qquad\qquad \left(\frac{1}{b^{-K-1}}\right)\frac{r^{K-2}}{(-K+2)}\Big|_a^b \qquad\qquad \frac{1}{b}\cdot\frac{b^4-a^4}{4}$$

$$\Downarrow \qquad\qquad\qquad\qquad \Downarrow \qquad\qquad\qquad\qquad \Downarrow$$

$$\frac{b^{K+2}-a^{K+2}}{b^{K-1}(K+2)} \qquad\qquad \left(\frac{1}{b^{-K-1}}\right)\frac{\left(b^{-K-2}-a^{-K-2}\right)}{(-K+2)} \qquad\qquad \frac{1}{b}\cdot\frac{b^4\left(1-c^4\right)}{4}$$

$$\Downarrow \qquad\qquad\qquad\qquad \Downarrow$$

$$\frac{b^3\left(b^{K-2}-a^{K-2}\right)}{b^3\left(b^{K-1}\right)(K+2)} \qquad\qquad \frac{b^3\left(b^{-K-2}-a^{-K-2}\right)}{b^{-K-2}(-K+2)}$$

$$\Downarrow \qquad\qquad\qquad\qquad \Downarrow$$

$$\frac{b^3\left(b^{K-2}-a^{K-2}\right)}{b^{K-2}(K+2)} \qquad\qquad \frac{b^3\left(b^{-K-2}-a^{-K-2}\right)}{b^3 b^{-K-1}(-K+2)}$$

$$\Downarrow \qquad\qquad\qquad\qquad \Downarrow$$

$$\frac{b^3\left(1-c^{K-2}\right)}{K+2} \qquad\qquad \frac{b^3 b^{-K-2}\left(1-c^{-K-2}\right)}{b^{-K-2}(-K+2)}$$

$$\Downarrow$$

259

$$\frac{b^3\left(1-c^{-K+2}\right)}{(-K+2)}$$

Using the integrals we write: (1st of system)

$$0 = \frac{-\left(Pc^{K+1}-Q\right)}{1-c^{2K}}g_K\frac{b^3\left(1-c^{K+2}\right)}{K+2}-\frac{\left(Qc^{K-1}-P\right)}{1-c^{2K}}g_{-K}\,c^{K+1}\frac{b^3\left(1-c^{-K+2}\right)}{-K+2}+$$

$$C_0\left[-\chi_2+\chi_1\left(\frac{1-c^{K+1}}{1-c^{2K}}g_K\frac{b^3\left(1-c^{K+2}\right)}{K+2}\right)+\frac{1-c^{K-1}}{1-c^{2K}}g_{-K}\,c^{K-1}\frac{b^3\left(1-c^{-K+2}\right)}{-K+2}\right]+$$

$$\vartheta\left[\mu_2\frac{b^4\left(1-c^4\right)}{4}+\mu_1\left(\frac{1-c^{K+2}}{1-c^{2K}}g_K\frac{b^4\left(1-c^{K+2}\right)}{K+2}+\frac{1-c^{K-2}}{1-c^{2K}}g_{-K}\,c^{K-2}\frac{b^4\left(1-c^{-K+2}\right)}{-K+2}\right)\right]$$

$$(5.89)$$

For the condition of axial force:

$$\text{axial load } = \int_a^b\sigma_z\cdot2\pi r\,dr$$

$$\pi(P-Q)a^2 = 2\pi\int_a^b\sigma_z r\,dr$$

$$(P-Q)\frac{a^2}{2} = \int_a^b\sigma_z r\,dr$$

$$\sigma_z = \frac{C}{a_{33}}-\frac{1}{a_{33}}\left(a_{13}\sigma_r+a_{23}\sigma_\theta+a_{34}\tau_{\theta z}\right)$$

$$(P-Q)\frac{a^2}{2} = \int_a^b\left[C_0 r-\frac{r}{a_{33}}\left(a_{13}\sigma_r+a_{23}\sigma_\theta+a_{34}\tau_{\theta z}\right)\right]dr \qquad (5.90)$$

The individual terms derived from (5.82), (5.83), (5.84) and (5.62), (5.63), (5.64) are as follow:

$$\sigma_r = \frac{\left(Pc^{K-1} - Q\right)}{1 - c^{2K}}\rho^{K-1} + \frac{\left(Qc^{K-1} - P\right)}{1 - c^{2K}}c^{K+1}\rho^{-K-1} +$$

$$C_0\left[\chi_1 - \chi_1\frac{\left(1 - c^{K-1}\right)}{1 - c^{2K}}\rho^{K-1} - \chi_1\frac{\left(1 - c^{K-1}\right)}{1 - c^{2K}}c^{K+1}\rho^{-K-1}\right] +$$

$$\vartheta\left[\mu_1\rho b - \mu_1 b\frac{\left(1 - c^{K-2}\right)}{1 - c^{2K}}\rho^{K-1} - \mu_1 b\frac{\left(1 - c^{K-2}\right)}{1 - c^{2K}}c^{K+2}\rho^{-K-1}\right]$$

(5.91)

$$\sigma_\theta = \frac{\left(Pc^{K-1} - Q\right)}{1 - c^{2K}}K\rho^{K-1} - \frac{\left(Qc^{K-1} - P\right)}{1 - c^{2K}}Kc^{K+1}\rho^{-K-1} +$$

$$C_0\left[\chi_1 - \chi_1\frac{\left(1 - c^{K-1}\right)}{1 - c^{2K}}K\rho^{K-1} + \chi_1\frac{\left(1 - c^{K-1}\right)}{1 - c^{2K}}Kc^{K+1}\rho^{-K-1}\right] +$$

$$\vartheta\left[2\mu_1 b\rho - \mu_1 b\frac{\left(1 - c^{K-2}\right)}{1 - c^{2K}}K\rho^{K-1} + \mu_1 b\frac{\left(1 - c^{K-2}\right)}{1 - c^{2K}}Kc^{K+2}\rho^{-K-1}\right]$$

(5.92)

$$\tau_{\theta z} = \frac{-\left(Pc^{K+1} - Q\right)}{1 - c^{2K}}g_K\,\rho^{K-1} - \frac{\left(Qc^{K-1} - P\right)}{1 - c^{2K}}g_{-K}\,c^{K+1}\rho^{-K-1} +$$

$$C_0\left[-\chi_2 + \chi_1\frac{\left(1 - c^{K-1}\right)}{1 - c^{2K}}g_K\,\rho^{K-1} + \chi_1\frac{\left(1 - c^{K-1}\right)}{1 - c^{2K}}g_{-K}\,c^{K-1}\rho^{-K-1}\right] +$$

$$\vartheta\left[\mu_2 b\rho + \mu_1 b\frac{\left(1 - c^{K+2}\right)}{1 - c^{2K}}g_K\,\rho^{K-1} + \mu_1 b\frac{\left(1 - c^{K-2}\right)}{1 - c^{2K}}g_{-K}\,c^{K-2}\rho^{-K-1}\right]$$

(5.93)

The integrals required in (5.90), solved previously, are restated for clarity

$$\frac{1}{b^{K-1}}\int_a^b r\cdot r^{K-1}dr \qquad\qquad \int_a^b r\,dr \qquad\qquad \frac{1}{b^{K-1}}\int_a^b r\cdot r^{-K-1}dr$$

$$\Downarrow \qquad\qquad\qquad\qquad \Downarrow \qquad\qquad\qquad\qquad \Downarrow$$

$$\frac{b^2\left(1 - c^{K-1}\right)}{K+1} \qquad\qquad \frac{b^2\left(1 - c^2\right)}{2} \qquad\qquad \frac{b^2\left(1 - c^{-K-1}\right)}{-K+1}$$

Substituting back gives:

261

$$(P-Q)\frac{a^2}{2} = C_0 \frac{b^2\left(1-c^2\right)}{2} - C_0 \frac{b^2\left(1-c^2\right)}{2}\left[\frac{a_{13}}{a_{33}}\chi_1 + \frac{a_{23}}{a_{33}}\chi_1 - \frac{a_{34}}{a_{33}}\chi_2\right] -$$

$$\vartheta\left[\frac{a_{13}}{a_{33}}\mu_1 + \frac{a_{23}}{a_{33}}2\mu_1 + \frac{a_{34}}{a_{33}}\mu_2\right]\frac{b^3\left(1-c^3\right)}{3} -$$

$$C_0\left[-\frac{a_{13}}{a_{33}}\chi_1 - \frac{a_{23}}{a_{33}}\chi_1 K + \frac{a_{34}}{a_{33}}\chi_1 g_K\right]\frac{(1-c^{K-1})}{(1-c^{2K})}\frac{b^2\left(1-c^{K-1}\right)}{K+1} -$$

$$\vartheta\left[-\frac{a_{13}}{a_{33}}\mu_1 b - \frac{a_{23}}{a_{33}}K\mu_1 b + \frac{a_{34}}{a_{33}}g_K\mu_1 b\right]\frac{(1-c^{K-2})}{(1-c^{2K})}\frac{b^2\left(1-c^{K-1}\right)}{K+1} -$$

$$C_0\left[-\frac{a_{13}}{a_{33}}\chi_1 + \frac{a_{23}}{a_{33}}\chi_1 K + \frac{a_{34}}{a_{33}}\chi_1 g_{-K}\right]\frac{(1-c^{K-1})}{(1-c^{2K})}\frac{c^{K-1}b^2\left(1-c^{-K-1}\right)}{-K+1} -$$

$$\vartheta\left[-\frac{a_{13}}{a_{33}}\mu_1 b + \frac{a_{23}}{a_{33}}K\mu_1 b + \frac{a_{34}}{a_{33}}g_{-K}\mu_1 b\right]\frac{(1-c^{K-2})}{(1-c^{2K})}\frac{c^{K+2}b^2\left(1-c^{-K-1}\right)}{-K+1} -$$

$$\left[\frac{a_{13}}{a_{33}} + K\frac{a_{23}}{a_{33}} - g_K\frac{a_{34}}{a_{33}}\right]\frac{(Pc^{K-1}-Q)}{(1-c^{2K})}\frac{b^2\left(1-c^{K-1}\right)}{K+1} -$$

$$\left[\frac{a_{13}}{a_{33}} - K\frac{a_{23}}{a_{33}} - g_{-K}\frac{a_{34}}{a_{33}}\right]\frac{(Qc^{K-1}-P)}{(1-c^{2K})}\frac{c^{K-1}b^2\left(1-c^{-K-1}\right)}{-K+1}$$

Separating C_0 and ϑ from the above expression

$$(P-Q)\frac{a^2}{2} + \left[\frac{a_{13}}{a_{33}} + K\frac{a_{23}}{a_{33}} - g_K\frac{a_{34}}{a_{33}}\right]\frac{(Pc^{K-1}-Q)}{(1-c^{2K})}\frac{b^2\left(1-c^{K-1}\right)}{K+1} +$$

$$\left[\frac{a_{13}}{a_{33}} - K\frac{a_{23}}{a_{33}} - g_K\frac{a_{34}}{a_{33}}\right]\frac{(Qc^{K-1}-P)}{(1-c^{2K})}\frac{c^{K-1}b^2\left(1-c^{-K-1}\right)}{-K+1} =$$

$$C_0\left[\frac{b^2\left(1-c^2\right)}{2} - \frac{b^2\left(1-c^2\right)}{2}\left[\frac{a_{13}}{a_{33}}\chi_1 + \frac{a_{23}}{a_{33}}\chi_1 \frac{a_{34}}{a_{33}}\chi_2\right] + \left[\frac{a_{13}}{a_{33}}\chi_1 + \frac{a_{23}}{a_{33}}K\chi_1 - \frac{a_{34}}{a_{33}}g_K\chi_1\right] \cdot\right.$$

$$\left.\frac{(1-c^{K-1})}{(1-c^{2K})}\frac{b^2\left(1-c^{K-1}\right)}{K+1} + \left[\frac{a_{13}}{a_{33}}\chi_1 - \frac{a_{23}}{a_{33}}K\chi_1 - \frac{a_{34}}{a_{33}}g_{-K}\chi_1\right]\frac{(1-c^{K-1})}{(1-c^{2K})}\frac{c^{K-1}b^2\left(1-c^{-K-1}\right)}{-K+1}\right] +$$

$$\vartheta\left[-\left[\frac{a_{13}}{a_{33}}\mu_1 + 2\frac{a_{23}}{a_{33}}\mu_1 + \frac{a_{34}}{a_{33}}\mu_2\right]\frac{b^3\left(1-c^3\right)}{3} + \left[\frac{a_{13}}{a_{33}}\mu_1 b + \frac{a_{23}}{a_{33}}K\mu_1 b - \frac{a_{34}}{a_{33}}g_K\mu_1 b\right] \cdot\right.$$

$$\left.\frac{(1-c^{K-2})}{(1-c^{2K})}\frac{b^2\left(1-c^{K-1}\right)}{K+1} + \left[\frac{a_{13}}{a_{33}}\mu_1 b - \frac{a_{23}}{a_{33}}K\mu_1 b - \frac{a_{34}}{a_{33}}g_{-K}\mu_1 b\right]\frac{(1-c^{K-2})}{(1-c^{2K})}\frac{c^{K-2}b^2\left(1-c^{-K-1}\right)}{-K+1}\right]$$

$$(5.94)$$

Solution methodology is easier when terms are grouped. For equation (5.94)

Letting: $\wedge_1' = LHS$ of (5.94) containing the terms P and Q.

$\wedge_2' =$ term multiplying C_0

$\wedge_3' =$ term multiplying ϑ

A compact form of (5.94) is

$$\wedge_1' = C_0 \wedge_2' + \vartheta \wedge_3'$$

(5.95)

For equation (5.89):

Letting: $\Gamma_1' =$ LHS of equation (5.89) containing the terms P and Q.

$\Gamma_2' =$ term multiplying C_0

$\Gamma_3' =$ term multiplying ϑ

A compact form of (5.89) is

$$\Gamma_1' = C_0 \Gamma_2' + \vartheta \Gamma_3'$$

(5.96)

Solution of the system (5.95) & (5.96) by determinants yields:

$$C_0 = \frac{\wedge_1' \Gamma_3' - \Gamma_1' \wedge_3'}{\wedge_2' \Gamma_3' - \Gamma_2' \wedge_3'} \quad , \quad \vartheta = \frac{\wedge_2' \Gamma_1' - \Gamma_2' \wedge_1'}{\wedge_2' \Gamma_3' - \Gamma_2' \wedge_3'}$$

(5.97)

Back-substitution into the equations for the stresses completes the solution.

The main cases involving a single layer have been solved in the preceding derivations. In summary the general case is described by equation (5.67) for radially variable material properties. Given fixed material properties, the case with unrestrained twisting and axial extension is (5.97) while the simpler case devoid of twist has solutions presented in (5.81), (5.82), (5.83), (5.84) & (5.87).

263

Obviously if the materials are on-axis orthotropic or presumed to behave as such macroscopically due to a balanced pair ± lay-up, the terms a_{14}, a_{24}, a_{34} drop out. As a consequence the system of differential equations in (5.67) becomes uncoupled. An enormous collapse of complexity results, eliminating the terms $g_K, g_{-K}, \mu_{1_n}, \mu_{2_n}$ and greatly simplifying $\chi_{1_n}, \chi_{2_n}, \lambda_{1,2}$. This case has already been analyzed in Chapter 4.

A further case, more complex, can be built as an extension upon the general solution derived in (5.67) for radially variable properties. This is the topic of the next chapter.

Chapter 6

Numerical Solution Method for Variable Properties

6.0 Introduction

Building on the Chapter 5 derivations, which are founded on first principles and presented the problem in its simplest variable property form, this section deals with the topic at a practical level required for design.

Chapter 5 presented solutions for discrete layer analysis where off-axis orthotropic layer behavior was analyzed. For this case the twisting term in concert with the axial displacement term was calculated without neglecting either the contribution to the overall stress state or the interdependence among these terms. Some omissions, as with supposed complete analysis published earlier [166][74][165], violate the mathematical foundations in subtle ways. They do not address the twisting phenomena and employ simplifying assumptions without exposing which effects are being neglected or why there might be justification for doing so.

6.1 Identifying the Constraints

Though challenging in the mathematical sense and useful for analyzing flawed designs or otherwise special purpose constructions, unbalanced anisotropic constituents are not mainstream building blocks in vessel design. The problem of designing for optimal stress distributions in conventional balanced lay-ups was not looked at from a practical

perspective in the last chapter. The elegant closed form solution for radial property variations has a fundamental flaw. No materials known have properties that can follow these variation rates for each of the independent elastic "constants" that describe behavior. In fact the micromechanics models used to interpolate properties for fiber composites actually disallow this condition simply by the form of the equations themselves.

To look at matters logically, one can perform a simple thought experiment: The near perfect carbon / graphite fiber can be viewed as constituted from many sheets of graphite, each highly wrinkled and then the assembly rolled up into a scroll. For more crystalline sheets axial alignment is improved, there are effectively fewer "bonds" across the basal planes of adjacent sheets hence fiber transverse modulus falls to a minimum as axial modulus approaches the theoretical maximum of 1060 GPa. Clearly the transverse and shear moduli behave in opposition to the axial modulus. A matrix will dampen the effect but cannot make it go away. A single equal and monotonic variation rate for all moduli cannot account for nor model this behavior.

The above "experiment" limits itself to current technology working with fiber composites of one base constituent. Future engineering might allow one to build custom materials atom by atom, mixing different constituents in a fashion that permits tailoring to virtually any mathematical prescribed variation and limited only by atomic bonding rules.

6.2 Examination of Real Materials

For the present, being restricted to properties exhibited by common materials of construction, it is necessary to adapt mathematically the solutions for stress distribution so as to mimic property variations achievable. This complicates the math and dilutes the clarity of the effects originating from an individual property on the overall. Most important however is identifying the major player(s) so as to proceed in establishing criteria for them to assert greater control over the final stress distribution. Contributions to the stress pattern resulting from less influential material properties would then be of diminished consequence. Another method of extracting some information on this topic is to simplify the boundary conditions from those of a pressure vessel to that of a pipe. This eliminates one physical dimension in the mathematical sense and reduces the problem from 6 to 3 rates of property variation.

In the mathematics that follow, various situations are considered and a finite difference numerical technique is used to solve the general case.

6.2.1 Modeling the Material

One of the complications discovered during the programming of these methods has little to do with resolving the differential equations but is perhaps just as challenging. This hidden riddle is that of modeling a multi-layer vessel as a continuum. After a multi-dimensional minimization algorithm [164] (Procedure Ameoba in unit Compmath.pas) was

implemented to best-fit discrete ply properties to individual power functions, smoothness of fit became exceedingly elusive. For any continuum method to reflect what can be achieved in physical construction with today's technology of discrete layer construction, the mathematical fit of the parameters one might assume to be governing has to be reasonably good.

As an engineer, it is customary to work with the concept of material stiffnesses and after many years of practicing the art one can get a rather good feel for such quantities. Composites are quite complex and contain many mutually influencing stiffness quantities, some of which are rather difficult to visualize and attach physical significance to. The mathematics used require translating these quantities to compliances 'a_{ij}' and mathematical groupings of compliances 'β_{ij}'. Such terms share less physical feel for their magnitudes. Further, because fiber composites are mainly used in off-axis orientations, fourth order tensor transformations are needed to describe their characteristics under these circumstances. Such transforms are near impossible for the mind to follow.

Imagine one starting out on a design, the objective being to vary smoothly a specific quantity that one can attach some physical significance to (say A_{22}). A particular radial variation rate is thought to be beneficial. Drawing from experience the engineer can synthesize a collection of layers constituting different materials, winding angles, fiber concentrations and thicknesses. The choices are not random but directed by some knowledge of the governing parameters that control circumferential stiffness A_{22}. Inverting the quantities to establish a_{22} it is quickly found that the smooth variation so carefully designed has deteriorated enormously. Further when the equivalent cylindrical compliance

variation β_{22} is computed not only is the smooth variation gone, but also the rate of change sought might have become contrary to the sense actually desired. To come up with a design that follows a prescribed mathematical variation for the β_{22} quantity has now become exceedingly difficult because it is impossible to foresee the mathematical interactions from start to finish. The dilemma is that no mathematical technique is known to work the problem backwards. The situation is compounded by the fact that one might be required to fit as many as 6 properties simultaneously.

6.2.2 Program Features

How then can such a problem be tackled? The key to the enigma is to give the designer a tool to assess instantly if an alteration made will help or hinder his objective. For this purpose the "Super Pressure - Vessel Designer" program is equipped with an interactive graphic design screen that allows perturbations in constituent properties of the building layers. These are driven by the arrow keys where one can switch material, fiber angles, volume fraction and layer thicknesses and see the outcome in real time, saving results if desired. Smooth fits can be achieved in a matter of minutes. Fitting multiple properties simultaneously is also possible but requires compromising between the goodness of fit among many possibilities. Obviously this can take longer. Examples are forthcoming in Chapter 8.

6.3 Closed Form Solutions

Another aspect to consider in practical design is along the line of identifying which properties are influential, which are controllable, and flagging the ones that do not matter. Unfortunately the closed form mathematical solutions existent for differential equations of the Cauchy-Euler type or its close relatives are quite limited. Of the nearly 5000 closed solutions catalogued in a landmark work by Polyanim & Zatsev [167] only a handful are similar to the Cauchy-Euler form. In $\left\{ x^2 y'' + f(x)y'x + g(x)y = r(x) \right\}$ some have simple polynomials for $f(x)$ and $g(x)$, others constitute Bessel or modified Bessel forms and yield to series solutions. For most polynomial variants, the terms in $f(x)$ and $g(x)$ are forcibly related, unless the terms are exceedingly simple. Finding an encompassing closed form that models that which is possible to achieve, at least approximately, with discrete layering is difficult and perhaps not quite attainable.

6.4 Micromechanics Issues

An item inferred in previous sections but not addressed directly is how one can effectively manipulate material properties of the constituents. The literature holds an assortment of basic data on planar constituent ply properties but few studies give complete characterizations for 3-dimensional material constants. In fact such measurements are quite complex and usually rely on a combination of mechanical and ultrasonic tests. Typically some of the more difficult to measure properties are inferred by back-calculating

270

terms. The calculations often originate from different types of tests in an effort to bracket the terms more closely. This is done because individual test methods are not precise enough to bound the values closely. Because of the complexity involved in getting a full and accurate set of data for any one material, the designer cannot hope to come up with the property data required in designing a vessel simply by looking into a handbook. One way to overcome this impasse is to synthesize the properties using accurate micromechanical models. These same models can also be used to dissect the more commonly available unidirectional ply data and quantify the intrinsically difficult to measure 3-D fiber properties. The vessel design program implements a model put forward by Hashin [168], Christensen [169] and others known as the Composite Cylinders Model (CCM). Here unidirectional ply data from 3-D tests are input along with neat matrix properties. The program extracts the fiber properties and saves them for later use in a synthesis operation where new elastic constants for composites composed of different fiber/matrix fractions and type are computed. These computations are implemented automatically and transparently as one directs the synthesis through the interactive interface of the vessel design program described in the previous section. More on the development of this technique is presented in Chapter 7.

6.5 Individually Variable Properties - Off-axis Orthotropic Case

Radial variations in each constituent material property can be described by power functions as follows:

271

Let:

$$\beta_{11} = \gamma_{11} r^{-l}$$

$$\beta_{12} = \gamma_{12} r^{-m}$$

$$\beta_{22} = \gamma_{22} r^{-d}$$

$$\beta_{14} = \gamma_{14} r^{-s}$$

$$\beta_{24} = \gamma_{24} r^{-p}$$

$$\beta_{44} = \gamma_{44} r^{-q}$$

Let:

$$\alpha_{34} = a_{34} r^{-h}$$

$$\alpha_{33} = a_{33} r^{-k}$$

$$\alpha_{13} = a_{13} r^{-i}$$

$$\alpha_{23} = a_{23} r^{-j}$$

Let:

$$\frac{\alpha_{34}}{\alpha_{33}} r^{-h+k} = \frac{\alpha_{34}}{\alpha_{33}} r^{-e}$$

$$\frac{\alpha_{13}}{\alpha_{33}} r^{-i-k} = \frac{\alpha_{13}}{\alpha_{33}} r^{-u}$$

$$\frac{\alpha_{23}}{\alpha_{33}} r^{-j-k} = \frac{\alpha_{23}}{\alpha_{33}} r^{-v}$$

The first of (5.47) becomes:

$$-\left(\frac{\partial}{\partial r} + \frac{1}{r}\right)\left[\gamma_{14} r^{-s-1} \frac{\partial F}{\partial r} + \gamma_{24} r^{-p} \frac{\partial^2 F}{\partial r^2} - \gamma_{44} r^{-q} \frac{\partial \Psi}{\partial r}\right] = \frac{C\alpha_{34} r^{-e-1}}{\alpha_{33}} - 2\vartheta$$

which expands to

$$(-s-1)\gamma_{14} r^{-s-2} \frac{\partial F}{\partial r} + \gamma_{14} r^{-s-1} \frac{\partial^2 F}{\partial r^2} - p\gamma_{24} r^{-p-1} \frac{\partial^2 F}{\partial r^2} + \gamma_{24} r^{-p} \frac{\partial^3 F}{\partial r^3} + q\gamma_{44} r^{-q-1} \frac{\partial \Psi}{\partial r} -$$

$$\gamma_{44} r^{-q} \frac{\partial^2 \Psi}{\partial r^2} + \gamma_{14} r^{-s-2} \frac{\partial F}{\partial r} + \gamma_{24} r^{-p-1} \frac{\partial^2 F}{\partial r^2} - \gamma_{44} r^{-q-1} \frac{\partial \Psi}{\partial r} = \frac{C\alpha_{34} r^{-e-1}}{\alpha_{33}} - 2\vartheta$$

and rearranges to

$$-\left[\gamma_{24} r^{-p} \frac{\partial^3 F}{\partial r^3} + \frac{\gamma_{14} r^{-s} + (1-p)\gamma_{24} r^{-p}}{r} \frac{\partial^2 F}{\partial r^2} + \frac{\gamma_{14}(1+(-s-1))}{r^2} \frac{\partial F}{\partial r} - \gamma_{44} r^{-q} \frac{\partial^2 \Psi}{\partial r^2} +\right.$$

$$\left. \frac{\gamma_{44}(q-1) r^{-q}}{r} \frac{\partial \Psi}{\partial r}\right] = \frac{C\alpha_{34} r^{-e-1}}{\alpha_{33}} - 2\vartheta$$

Dividing by r^{-p}

$$-\gamma_{24} \frac{\partial^3 F}{\partial r^3} - \frac{\gamma_{14} r^{-s+p} + \gamma_{24}(1-p)}{r} \frac{\partial^2 F}{\partial r^2} + \frac{s\gamma_{14} r^{-s-p}}{r^2} \frac{\partial F}{\partial r} +$$

$$\gamma_{44}\left(r^{-q-p} \frac{\partial^2 \Psi}{\partial r^2} - \frac{(1-q)}{r} r^{-q-p} \frac{\partial \Psi}{\partial r}\right) = \frac{C\alpha_{34} r^{p-e-1}}{\alpha_{33}} - 2\vartheta r^p$$

reducing 1 order of magnitude by substitutions

272

$$\frac{\partial F}{\partial r} = \phi \qquad \text{and} \qquad \frac{\partial \Psi}{\partial r} = \phi$$

$$-\gamma_{24}\frac{\partial^2 \phi}{\partial r^2} - \frac{\gamma_{14}r^{-s-p}+\gamma_{24}(1-p)}{r}\frac{\partial \phi}{\partial r} + \frac{s\gamma_{14}r^{-s-p}}{r^2}\phi + \gamma_{44}r^{-q-p}\left[\frac{\partial \phi}{\partial r} - \frac{(1-q)}{r}\phi\right] = \frac{C\alpha_{34}r^{p-e-1}}{\alpha_{33}} - 2\vartheta r^{p}$$

$$(6.1)$$

The second of (5.47) translates to:

$$r\gamma_{22}r^{-d}\frac{\partial^3 F}{\partial r^2} + \gamma_{22}r^{-d}(-d+1)\frac{\partial^2 F}{\partial r^2} - \frac{1}{r}\frac{\partial F}{\partial r}\left(\gamma_{11}r^{-1} + m\gamma_{12}r^{-m}\right) - r\gamma_{24}r^{-p}\frac{\partial^2 \Psi}{\partial r^2} +$$

$$\frac{\partial \Psi}{\partial r}\left[\gamma_{14}r^{-s} - \gamma_{24}r^{-p}(-p+1)\right] = C\left[\frac{\alpha_{13}}{\alpha_{33}}r^{-u} - (1-v)\frac{\alpha_{23}}{\alpha_{33}}r^{-v}\right]$$

$$(6.2)$$

Equation (6.2) can equally be reduced one order of magnitude and by multiplying both

sides by $\dfrac{r^{d-1}}{\gamma_{22}}$ we get

$$\frac{\partial^2 \phi}{\partial r^2} + \left(\frac{-d+1}{r}\right)\frac{\partial \phi}{\partial r} - \frac{1}{r^2}\left(\frac{\gamma_{11}r^{d-1} + m\gamma_{12}r^{d-m}}{\gamma_{22}}\right)\phi - \left(\frac{\gamma_{24}}{\gamma_{22}}r^{d-p}\right)\frac{\partial \phi}{\partial r} + \left[\frac{\gamma_{14}r^{d-s} - \gamma_{24}r^{d-p}(-p+1)}{\gamma_{22}}\right]\frac{\phi}{r} =$$

$$C\left[\frac{\alpha_{13}}{\alpha_{33}\gamma_{22}}r^{d-u-1} - (1-v)\frac{\alpha_{23}}{\alpha_{33}\gamma_{22}}r^{d-v-1}\right]$$

$$(6.3)$$

Recognizing that the last term on the *LHS* of equation (6.1) can be expressed as:

$$\gamma_{44}\frac{r^{-q+p}}{r^{1-q}}\frac{\partial}{\partial r}\left(r^{1-q}\phi\right) = \gamma_{44}\frac{r^{-q+p}}{r^{1-q}}\left[(1-q)r^{-q}\phi + r^{1-q}\frac{\partial \phi}{\partial r}\right] = \gamma_{44}r^{-q+p}\left[\frac{(1-q)}{r}\phi + \frac{\partial \phi}{\partial r}\right]$$

so (6.1) can be cast as

$$\gamma_{44}r^{p-1}\frac{\partial}{\partial r}\left(r^{1-q}\phi\right) = C\frac{\alpha_{34}}{\alpha_{33}}r^{-e-p-1} - 2\vartheta r^{p} + \gamma_{24}\frac{\partial^2 \phi}{\partial r^2} + \frac{\gamma_{14}r^{-s-p}+\gamma_{24}(1-p)}{r}\frac{\partial \phi}{\partial r} - \frac{s\gamma_{14}r^{-s-p}}{r^2}\phi$$

multiplying by $\dfrac{r^{-p+1}}{\gamma_{44}}$

273

$$\frac{\partial}{\partial r}\left(r^{1-q}\varphi\right) = C\frac{\alpha_{34}}{\gamma_{44}\alpha_{33}}r^{-e} - \frac{2\vartheta r}{\gamma_{44}} + \frac{\gamma_{24}}{\gamma_{44}}r^{-p+1}\frac{\partial^2\phi}{\partial r^2} + \frac{\gamma_{14}r^{-s}+\gamma_{24}(1-p)r^{-p}}{\gamma_{44}}\frac{\partial\phi}{\partial r} - \frac{s\gamma_{14}r^{-s-1}}{\gamma_{44}}\phi$$

integrating

$$r^{1-q}\varphi = \frac{C\alpha_{34}}{\gamma_{44}\alpha_{33}}\frac{r^{-e+1}}{(1-e)} - \frac{2\vartheta r^2}{2\gamma_{44}} + \frac{\gamma_{24}}{\gamma_{44}}\int\left(r^{-p+1}\frac{\partial^2\phi}{\partial r^2}+(1-p)r^{-p}\frac{\partial\phi}{\partial r}\right)dr + \frac{\gamma_{14}}{\gamma_{24}}\int\left(r^{-s}\frac{\partial\phi}{\partial r}-sr^{-s-1}\phi\right)dr$$

which evaluates to

$$r^{1-q}\varphi = \frac{C\alpha_{34}}{\gamma_{44}\alpha_{33}}\frac{r^{-e+1}}{(1-e)} - \frac{\vartheta r^2}{\gamma_{44}} + \frac{\gamma_{24}}{\gamma_{44}}r^{1-p}\frac{\partial\phi}{\partial r} + \frac{\gamma_{14}}{\gamma_{44}}r^{-s}\phi$$

or

$$\varphi = \frac{C\alpha_{34}}{\gamma_{44}\alpha_{33}}\frac{r^{-e+q}}{(1-e)} - \frac{\vartheta r^{q-1}}{\gamma_{44}} + \frac{\gamma_{24}}{\gamma_{44}}r^{q-p}\frac{\partial\phi}{\partial r} + \frac{\gamma_{14}}{\gamma_{44}}r^{q-s-1}\phi$$

$$(6.4)$$

Substituting (6.4) into (6.3) yields a single differential equation for the system.

$$\frac{\partial^2\phi}{\partial r^2} + \left(\frac{-d+1}{r}\right)\frac{\partial\phi}{\partial r} - \frac{1}{r^2}\left(\frac{\gamma_{11}r^{d-l}+m\gamma_{12}r^{d-m}}{\gamma_{22}}\right)\phi -$$

$$\frac{\gamma_{24}}{\gamma_{22}}r^{d-p}\left[\frac{C\alpha_{34}(-e+q)r^{-e+q-1}}{\gamma_{44}\alpha_{33}(1-e)} - \frac{(q+1)\vartheta r^q}{\gamma_{44}} + \frac{(q-p)\gamma_{24}r^{q-p-1}}{\gamma_{44}}\frac{\partial\phi}{\partial r} + \frac{\gamma_{24}r^{q-p}}{\gamma_{44}}\frac{\partial^2\phi}{\partial r^2} + \right.$$

$$\left. \frac{(q-s-1)\gamma_{14}r^{q-s-2}}{\gamma_{44}}\phi + \frac{\gamma_{14}r^{q-s-1}}{\gamma_{44}}\frac{\partial\phi}{\partial r}\right] +$$

$$\frac{\gamma_{14}r^{d-s}+(1-p)\gamma_{24}r^{d-p}}{r\gamma_{22}}\left[\frac{C\alpha_{34}r^{-e+q}}{\gamma_{44}\alpha_{33}(1-e)} - \frac{\vartheta r^{q+1}}{\gamma_{44}} + \frac{\gamma_{24}}{\gamma_{44}}r^{q-p}\frac{\partial\phi}{\partial r} + \frac{\gamma_{14}}{\gamma_{44}}r^{q-s-1}\phi\right] =$$

$$C\left[\frac{\alpha_{13}}{\alpha_{33}\gamma_{22}}r^{d-u-1} - (1-v)\frac{\alpha_{23}}{\alpha_{33}\gamma_{22}}r^{d-v-1}\right]$$

collecting terms

274

$$\frac{\partial^2 \phi}{\partial r^2}\left[1 + \frac{\gamma_{24}^2 r^{d-q-2p}}{\gamma_{44}\gamma_{22}}\right] +$$

$$\frac{\partial \phi}{\partial r}\left[\frac{1-d}{r} - \frac{\gamma_{24}^2(q-p)r^{q-2p-d-1}}{\gamma_{22}\gamma_{44}} - \frac{\gamma_{14}\gamma_{24}r^{d-p+q-s-1}}{\gamma_{22}\gamma_{44}} + \frac{\gamma_{14}\gamma_{24}r^{d-s+q-p-1}}{\gamma_{22}\gamma_{44}} + \frac{\gamma_{24}^2(1-p)r^{d-2p+q-1}}{\gamma_{22}\gamma_{44}}\right] -$$

$$\phi\left[\frac{\gamma_{11}r^{d-l-2} + m\gamma_{12}r^{d-m-2}}{\gamma_{22}} + \frac{(q-s-1)\gamma_{14}\gamma_{24}r^{d-p+q-s-2}}{\gamma_{22}\gamma_{44}} - \frac{\gamma_{14}^2 r^{d-2s-q-2}}{\gamma_{22}\gamma_{44}} - \frac{\gamma_{24}\gamma_{14}(1-p)r^{d-p+q-s-2}}{\gamma_{22}\gamma_{44}}\right] =$$

$$C\left[\frac{\alpha_{13}r^{d-u-1}}{\alpha_{33}\gamma_{22}} - \frac{\alpha_{23}(1-v)r^{d-v-1}}{\alpha_{33}\gamma_{22}} + \frac{\alpha_{34}\gamma_{24}(-e+q)r^{d-p+e+q-1}}{\gamma_{22}\gamma_{44}\alpha_{33}(1-e)} - \frac{\alpha_{34}\gamma_{14}r^{d-s-e+q-1}}{\gamma_{22}\gamma_{44}\alpha_{33}(1-e)} - \frac{\alpha_{34}\gamma_{24}(1-p)r^{d-p+e+q-1}}{\gamma_{22}\gamma_{44}\alpha_{33}(1-e)}\right] +$$

$$\vartheta\left[\frac{-\gamma_{24}(q+1)r^{q+d-p}}{\gamma_{22}\gamma_{44}} + \frac{\gamma_{14}r^{d-s-q}}{\gamma_{22}\gamma_{44}} + \frac{\gamma_{24}(1-p)r^{d-p-q}}{\gamma_{22}\gamma_{44}}\right]$$

rearranging

$$\frac{\partial^2 \phi}{\partial r^2}\left[\gamma_{44}\gamma_{22} + \gamma_{24}^2 r^{d+q-2p}\right] +$$

$$\frac{1}{r}\frac{\partial \phi}{\partial r}\left[(1-d)\gamma_{22}\gamma_{44} + \gamma_{14}\gamma_{24}\left(r^{d-s-q-p} - r^{q-s-d-p}\right) + \gamma_{24}^2(1-p)r^{d-p+q-p}(q-p)r^{q-2p-d}\right] -$$

$$\frac{\phi}{r^2}\left[\gamma_{11}\gamma_{44}r^{d-l} + m\gamma_{12}\gamma_{44}r^{d-m} + \gamma_{14}\gamma_{24}\left((q-s-1)r^{d-p+q-s} - (1-p)r^{d-p+q-s}\right) - \gamma_{14}^2 r^{d-2s-q}\right] =$$

$$\frac{C}{r\alpha_{33}}\left[\alpha_{13}\gamma_{44}r^{d-u} - \alpha_{23}\gamma_{44}(1-v)r^{d-v} + \alpha_{34}\gamma_{24}\left(\frac{(q-e)r^{d-p-e+q}}{1-e} - \frac{(1-p)r^{d-p-e+q}}{1-e}\right) + \frac{\alpha_{34}\gamma_{14}r^{d-s-e+q}}{1-e}\right] +$$

$$\vartheta\left[\gamma_{24}\left((1-p)r^{d-p-q} - (q+1)r^{q+d-p}\right) + \gamma_{14}r^{d-s-q}\right]$$

(6.5)

Considering the case of a filament wound composite pressure vessel, the terms β_{14}, β_{24} are effectively zero since the layers consist of plies with a balanced number of (+) and (−) direction lamina. It is thus more practical to consider first solving such a case where β_{14} and β_{24} do not play a role. Namely for any layer build-up with a large number of intermingled and balanced set of plies.

This restriction simplifies the differential equation to:

275

$$\frac{\partial^2 \phi}{\partial r^2} + \left(\frac{-d+1}{r}\right)\frac{\partial \phi}{\partial r} - \left(\frac{\gamma_{11}r^{d-l} + m\gamma_{12}r^{d-m}}{\gamma_{22}}\right)\frac{\phi}{r^2} = \frac{C}{\alpha_{33}\gamma_{22}r}\left[\alpha_{13}r^{d-u} - (1-v)\alpha_{23}r^{d-v}\right]$$

(6.6)

Resolving the above is not straight-forward for two reasons.

1) The powers of r are not whole, rather real numbers.

2) A particular solution is required because of the boundary condition that defines C.

From previous solutions we know that the *RHS* arises from the axial boundary condition when movement in this direction is free. For the case of fixed axial boundaries the *LHS* equates to zero and we have the thick pipe problem (pure plane strain). This simpler case is tackled first.

Before proceedings it is important to examine the exponents of the power functions. For the case when all radial variations occur at the same rate "n" the expression of the β_{ij} ' s in terms of their γ_{ij} r^{-n} equivalents is straight forward. However when individual rate variations are assigned to each a_{ij}, replacement of reduced compliance β_{ij} ' s by single power function equivalents based on the α_{ij} ' s powers is not possible. This is illustrated below.

Case of all properties varying equally: general case:

$$a_{ij} = \alpha_{ij}r^{-n}$$

$$\beta_{ij} = \left(\alpha_{ij}r^{-n} - \frac{\alpha_{i3}r^{-n}\alpha_{j3}r^{-n}}{\alpha_{33}r^{-n}}\right)$$

$$\beta_{ij} = \left(\alpha_{ij} - \frac{\alpha_{i3}\alpha_{j3}}{\alpha_{33}}\right)r^{-n} = \gamma_{ij}r^{-n}$$

example: $\beta_{11} = \gamma_{11}r^{-n}$

Case of each property varying separately: (shown for γ_{11}, other cases similar)

$$a_{11} = \alpha_{11}r^{-w}$$

$$a_{13} = \alpha_{13}r^{-i}$$

$$a_{33} = \alpha_{33}r^{-k}$$

$$\beta_{11} = \left(\alpha_{11}r^{-w} - \frac{\alpha_{13}r^{-i}\alpha_{13}r^{-i}}{\alpha_{33}r^{-k}}\right)$$

$$\beta_{11} = \alpha_{11}r^{-w} - \frac{\alpha_{13}^2}{\alpha_{33}}r^{k-2i} = \gamma_{11}r^{-l}$$

276

Such complications can be addressed in two ways. Either reformulate the differential equation in terms of the α_{ij} ' s, which complicates the symbolic mathematics, or compute a new γ_{ij} r^{-n} type representations for each β_{ij}. The later method can be carried out using the individual ply data, computing a similar least squares approximation to the power function as was done with $a_{ij} = \alpha_{ij} r^{-n}$. This is the method followed in the subsequent derivations. For either approach it must be remembered that the power function representation of the material properties serve only an approximation to real constructions (which are discreetly layered). The mathematical purpose of the power representation is to affect the character of the stress function ϕ. This is in turn descriptive of the stress distributions developed in the pressurized thick cylinder. To restate, the design objective is to bracket the principal power function(s) influencing the stress function ϕ and allow the minor variables to fall as they will. A real vessel, no matter how precisely constructed, can only ever approach the situation as modeled. However one will attain a clearer objective of what is desirable.

The fundamental flaw of design techniques previous to this analysis has been the lack of a modeling equation that bridges from individual layer stresses to the whole. However now there is an emerging mathematical objective, namely massaging the stress function into a shape that distributes the circumferential stress more uniformly. Control parameters are the rate functions linked to the material properties. The distribution of stresses required is also dependent on the material's strength. Because strength depends on state of stress, changes in the stress function ϕ will have a secondary influence on the

277

strength itself. Iteration will always be required because there are no direct rules linking

strength to stiffness as one progresses from one material to the next. A treatment for

laminate stiffnesses and strengths, taken from a micromechanical prediction to a laminate

within the vessel, is a subject deferred to Chapter 7.

Also it must be noted that the differential equation for the stress function ϕ in

equation (6.6) has no known closed form solution. Numerical methods can be used to find

a solution for ϕ. The complete differential equation (6.6) can be classified as a two point

boundary value problem with an additional integral boundary constraint.

6.6 Numerical Methods Solution

An approach to the solution of equation (6.6) is to employ numerical techniques.

For boundary value problems various (almost standard) algorithms exist. These methods

can in a broad sense be classified as "shooting" or "relaxation" [164]. For equations where

the objective is to minimize a specific variational property, Rayleigh-Ritz algorithms are

useful. No single technique is universal for all problems and sometimes custom adaptations

are necessary. Further classification of algorithms distinguishes between linear and

nonlinear forms of the differential equation to be solved [160]. The shooting methods

require breaking down higher order differential equations to a system of coupled first

order equations but generally show an advantage in speed of convergence and inherent

small error provided they converge. Relaxation techniques are simple in concept. These

replace the differentials by finite difference formulations and set up a mesh of points over

the interval of interest. The objective is to adjust the values on the mesh via iteration

(called relaxation) bringing the values into successively closer agreement with the finite difference equations and simultaneously with the boundary conditions. Convergence is relatively slow but stable. Relaxation works better than shooting when the boundary conditions are especially delicate or subtle, or where they involve complicated algebraic relations that cannot easily be solved in closed form.

For the problem at hand a finite difference approach was chosen. Because the boundary conditions also involve an integral relation for σ_z when the *RHS* of the equation is considered, the technique lends itself well. An outline of the algorithm used, some customizations and details for iteration on the σ_z boundary condition are presented below.

6.7 Finite Difference Algorithm

A linear finite difference technique was employed, outlined in a text by Burden, Faires and Reynolds [160]. The core of the method utilizes center difference formulas derived from 3rd degree Taylor polynomial expansions to replace the derivatives. Truncation error for these estimates is a small fraction of the step size squared, considered adequate for the purpose. Equation (6.6) can be written (with two of its boundary conditions) in the form

$$y'' = p(x)y' + q(x)y + r(x), \qquad a \le x \le b, \qquad y(a) = \alpha, \qquad y(b) = \beta$$

(6.7)

where:

$$q(x) = \left(\frac{\gamma_{11} r^{d-l} + m\gamma_{12} r^{d-m}}{r^2 \gamma_{22}} \right) \qquad , \qquad p(x) = \left(\frac{d-1}{r} \right)$$

279

$$r(x) = \frac{C}{\alpha_{33}\gamma_{22}r} \left[\alpha_{13} r^{d-u} - (1-v)\alpha_{23} r^{d-v} \right] \quad , \quad y = \phi = \frac{\sigma_r}{r}$$

The interval of interest can be divided up into sufficiently small parts by picking an integer N which represents the number of interior meshpoints. The surface boundary conditions represent 2 additional points. With this scheme N+1 subintervals result, whose endpoints are the known boundary meshpoints.

$$x_i = a + ih, \quad \text{for} \quad i = 0,1,2,3,...N+1, \quad \text{where} \quad h = \frac{(b-a)}{N+1}$$

for the interior meshpoints $x_i = 1,2,3...N$ the differential equation to be approximated is

$$y''(x_i) = p(x_i)y'(x_i) + q(x_i)y(x_i) + r(x_i)$$

The Taylor expansion gives estimates for the derivatives as

$$y'(x_i) = \frac{1}{2h}\left[y(x_{i-1}) - y(x_{i-1}) \right]$$

(6.8)

$$y''(x_i) = \frac{1}{h^2}\left[y(x_{i-1}) - 2y(x_i) + y(x_{i-1}) \right]$$

(6.9)

Equation (6.7) can be rewritten as

$$\frac{\left[y(x_{i-1}) - 2y(x_i) + y(x_{i-1}) \right]}{h^2} = p(x_i)\left[\frac{y(x_{i-1}) - y(x_{i-1})}{2h} \right] + q(x_i)y(x_i) + r(x_i)$$

(6.10)

letting w_i represent the solution points, the endpoint conditions can be represented by

$$w_0 = \alpha, \quad w_{N+1} = \beta,$$

and for each interior meshpoint one can write

280

$$\left(\frac{2w_i - w_{i+1} - w_{i-1}}{h^2}\right) + p(x_i)\left(\frac{w_{i+1} - w_{i-1}}{2h}\right) + q(x_i)w_i = -r(x_i)$$

For solution a re-arranged form is needed

$$-\left(1 + \frac{h}{2}p(x_i)\right)w_{i-1} + \left(2 + h^2q(x_i)\right)w_i - \left(1 - \frac{h}{2}p(x_i)\right)w_{i+1} = -h^2r(x_i)$$

$$(6.11)$$

Written out for each interior meshpoint, (6.11) takes the form of an $N \times N$ tridiagonal matrix.

$$\begin{bmatrix} 2 + h^2q(x_1) & -1 + \frac{h}{2}p(x_1) & 0 & 0 & 0 \\ -1 - \frac{h}{2}p(x_2) & 2 + h^2q(x_2) & -1 + \frac{h}{2}p(x_2) & \vdots & 0 \\ \vdots & \vdots & \vdots & \vdots & \vdots \\ 0 & \vdots & \vdots & \vdots & -1 + \frac{h}{2}p(x_{N-1}) \\ 0 & \vdots & \vdots & -1 - \frac{h}{2}p(x_N) & 2 + h^2q(x_N) \end{bmatrix}$$

$$\times \begin{bmatrix} w_1 \\ w_2 \\ \vdots \\ w_{N-1} \\ w_N \end{bmatrix} = \begin{bmatrix} -h^2r(x_1) + \left(1 + \frac{h}{2}p(x_1)\right)w_0 \\ -h^2r(x_2) \\ \vdots \\ -h^2r(x_{N-1}) \\ -h^2r(x_N) + \left(1 + \frac{h}{2}p(x_N)\right)w_{N+1} \end{bmatrix}$$

$$(6.12)$$

Given that p,q,r are continuous on the interval and $q(x) \geq 0$ on $[a, b]$, then the tridiagonal linear system (6.12) has a unique solution provided $h < 2/L$ where

$$L = \max_{a \leq x \leq b}|p(x)| \quad [160].$$

The "Super Pressure - Vessel Designer" program implements a solution to the above set of equations using Crout's reduction method [160] which is specifically efficient for tridiagonal linear systems. Even with $N = 100$, execution times on an $i80486$ based machine take under 1 second. Typically 10-20 subintervals provide more than enough accuracy. Procedure FiniteD under unit compmath.pas contains the code.

Solution however consists not simply of solving the above matrix, but also of fitting the 3rd boundary condition. This is achieved by first setting the constant C in (6.6) to zero (i.e.: $r(x) = 0$) and solving the system. Next the σ_z stress is calculated via numerical integration over the entire interval.

$$\text{axial force} = \int_a^b \sigma_z 2\pi r dr = (P - Q)\pi a^2$$

From equation (5.58) and the definitions for variable properties found in Section 6.5

$$\sigma_z = \frac{C}{\alpha_{33}}r^k - \frac{\alpha_{13}}{\alpha_{33}}r^{-u}\sigma_r - \frac{\alpha_{23}}{\alpha_{33}}r^{-v}\sigma_\theta$$

(6.13)

Since the stress function ϕ contains the stresses via

$$\frac{\phi}{r} = \sigma_r \qquad \text{and} \qquad \frac{\partial \phi}{\partial r} = \sigma_\theta$$

Using these expressions with (6.13) and the axial constraint above, we have

$$(P - Q)\pi a^2 = \int_a^b \left[\frac{Cr^k}{\alpha_{33}} - \frac{\alpha_{13}r^{-u}(\phi)}{\alpha_{33}} - \frac{\alpha_{23}r^{-v}\left(\frac{\partial \phi}{\partial r}\right)}{\alpha_{33}} \right] 2\pi r \, dr$$

simplifying

$$(P - Q)\frac{a^2}{2} = \int_a^b \left[\frac{Cr^{k-1}}{\alpha_{33}} - \frac{\alpha_{13}r^{-u-1}(\phi)}{\alpha_{33}} - \frac{\alpha_{23}r^{-v-1}\left(\frac{\partial \phi}{\partial r}\right)}{\alpha_{33}} \right] dr$$

integrating partially

$$(P-Q)\frac{a^2}{2} = C\left[\frac{b^{k+2}-a^{k+2}}{\alpha_{33}(k+2)}\right] - \int_a^b\left[\frac{\alpha_{13}r^{-u-1}(\phi)}{\alpha_{33}} + \frac{\alpha_{23}r^{-v-1}\left(\partial\phi/\partial r\right)}{\alpha_{33}}\right]dr$$

solving for C

$$C = \frac{\alpha_{33}(k+2)}{b^{k+2}-a^{k+2}}\left[(P-Q)\frac{a^2}{2} + \int_a^b\left[\frac{\alpha_{13}r^{-u-1}(\phi)}{\alpha_{33}} + \frac{\alpha_{23}r^{-v-1}\left(\partial\phi/\partial r\right)}{\alpha_{33}}\right]dr\right]$$

(6.14)

The remaining integral in equation (6.14) can be evaluated numerically using results from

the solution to the matrix system (6.12). At the interior mesh points $\phi = w_i$ and derivatives

can be evaluated for the term $\left(\partial\phi/\partial r\right)$ utilizing equation (6.8). However at the exterior

meshpoints one-sided difference formulas are required. For the inner and outer surfaces

respectively the following expressions were used.

$$w_0' = \frac{1}{2h}\left[-3w_0 + 4(w_0+h) - (w_0+2h)\right] \qquad \text{(inside)}$$

and

$$w_0' = \frac{1}{2h}\left[(w_0-2h) - 4(w_0-h) + 3w_0\right] \qquad \text{(outside)}$$

The integration is then carried forth using the trapezoidal rule

$$\int_a^b f(r)dr \cong \sum_{n=a}^{b-h}\frac{h}{2}\left[f(r_n) + f(r_{n-h})\right]$$

Having done this allows estimation of the constant C according to (6.14) and establishes a

non-zero value for $r(x)$. This estimate of C, (rather than zero) is subsequently used within

system (6.12) and the finite difference equations are re-computed. This form of fixed point

283

iteration continues until a tolerance for successive evaluations of C is met. Practice shows that setting the tolerance to 10^{-6} (1 microstrain) achieves convergence in about 2 or 3 iterations.

The vessels design program implements the above calculations transparently via a graphical user interface. Pressing the arrow keys allows alterations to any of 12 parameters (two to describe each of the 6 variable material power functions) and computes the 3 principle stresses. These are updated and displayed instantly. Examples are forthcoming in Chapter 8.

Chapter 7

Micromechanics, Damage and Post FPF Design

7.0 Micromechanics

The concept of using micromechanical based predictions to estimate composite lamina characteristics has been established for many years. Rarely however is it used for design purposes, rather engineers still rely on test data, especially in applications where certification to a standard or acceptance by a governing body is requisite. Much of this stems from a limited ability to predict strengths via micromechanics, and thereby also failure. But inadequate strength predictions alone should not discount the utility of micromechanics, rather be seen as an area where a much deeper understanding remains to be gained. A second point, expanded upon in a subsequent section, is that the polynomial failure theory(s) in broadest use (i.e.: Tsai-Wu) appear to be based on a fundamental mis-interpretation of Hill's work [170][259]. Although controversial, to say the least, forward thinking authors have brought out failure criteria more in line with physical reality [112] [114][117]. The combination of weak strength predictions coupled to inadequate failure theories have contributed to a maligning of micromechanics in the eyes of engineers and designers. Also, the variety of micromechanics taught in many texts [171][172][173] [174][175][176] is empirical in nature, contributing an appearance that it lacks good theoretical foundation.

Practical application of micromechanics is made in this work, not so much for strength but rather for the close estimation of elastic properties it allows. Reference [171]

gives a short history of efforts up to about 1968 which lead to the now renowned Halpin-Tsai relations. For completeness, and also for contrast with more current methods this still popular form is presented briefly below. Essentially Halpin and Tsai showed that a good approximation of the many models presented to that date could be reduced to an approximate empirical relation for design.

$$E_1 \cong E_f \upsilon_f + E_m \upsilon_m \quad \text{(rule of mixtures)}$$

where: subscripts f = fiber

$$\nu_{12} = \nu_f \upsilon_f + \nu_m \upsilon_m$$

m = matrix

and

$$\frac{M}{M_m} = \frac{1 + \xi \eta \upsilon_f}{1 - \eta \upsilon_f}$$

(7.1)

where:

$$\eta = \frac{\left(\dfrac{M_f}{M_m}\right) - 1}{\left(\dfrac{M_f}{M_m}\right) + \xi} \quad \text{in which:}$$

M = composite modulus E_2, G_{12}, ν_{23}

M_f = corresponding fiber modulus E_f, G_f, ν_f

M_m = corresponding matrix modulus E_m, G_m, ν_m

(7.2)

and ξ is a measure of fiber reinforcement of the composite that depends on the fiber geometry, packing geometry, and loading conditions. The values of ξ are obtained by comparing equations (7.1) and (7.2) with exact elasticity solutions and assigning a value of, or function for, ξ by curve fitting.

The difficulty in using these equations is determination of a suitable factor for ξ. Experience has shown that $\xi = 2$ gives reasonable predictions of transverse moduli E_2,

286

and $\xi = 1$ for the calculation of shear modulus G_{12}. The accuracy of the predictions vary

mildly within a reasonable range of the fiber volume fractions and the fiber packing array

assumed. More difficulty is encountered with shear modulus predictions and the

approximation $\xi = 1 + 40\upsilon_f^{10}$ can be used with some success.

Some physical insight into the Halpin-Tsai equations can be gained by examining

their behavior for a range of values of ξ and η. When $\xi = 0$,

$$\frac{1}{M} = \frac{\upsilon_f}{M_f} + \frac{\upsilon_m}{M_m}$$

which is the series connected model generally associated with the lower bound of a

composite modulus. When $\xi = \infty$,

$$M = \upsilon_f M_f + \upsilon_m M_m$$

which is the parallel-connected model, known as the rule of mixtures, generally associated

with the upper bound of a composite modulus. Thus ξ is a measure of the reinforcement

of the composite by the fiber. For small values of ξ, the fibers are not very effective,

whereas for large values of ξ, the fibers are extremely effective in increasing the

composite stiffness above the matrix stiffness. The limiting values for η can be shown to

be $\eta = 1$ for rigid inclusions, $\eta = 0$ for homogeneous material, and for voids, $\eta = -1/\xi$.

The term $\eta\upsilon_f$ in equation (7.1) can be interpreted as a "reduced fiber volume fraction",

since $\eta \leq 1$. Practical values of $\eta\upsilon_f$ are less than 0.6, and curves for various

combinations of "reduced fiber volume fraction" $\eta\upsilon_f$ versus relative "fiber to matrix

stiffness ratios" M/M_m are plotted for a range of ξ in Figure 7.1 below [173].
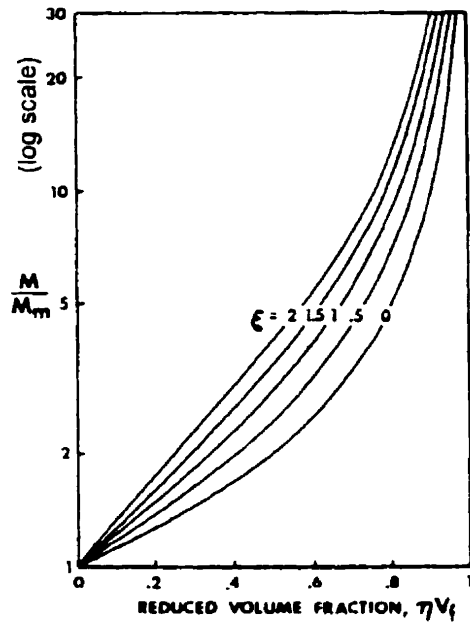
Figure 7.1 Influence of matrix stiffness upon transverse properties [173].

Alternative semi-analytical predictions were furthered somewhat more recently by

Tsai [174][175][176] and others. The essentials are still based on back-calculating "stress

partitioning parameters" η_s, η_y, η_k, η_G for in plane shear, in plane transverse, transverse

bulk, and transverse shear moduli, respectively. The results appear to give fair estimates.

Advantages of these formulations being mainly their relative ease of use. However,

considering the proliferation of desktop computational power, fewer constraints now exist

towards employing results of deeply analytical solutions.

The method of choice for the present endeavor is based on formulations published

by Z. Hashin [168]. Expressions for bounds on the 5 effective (transversely isotropic)

elastic moduli of a unidirectional fiber composite, consisting of transversely isotropic

288

fibers and matrix can be derived. A review on the topic, published by R.M. Christensen is

followed, and further details can be sought elsewhere [169]. The composite cylinders

geometric model initially introduced by Hashin and Rosen consists of *isotropic* fibers

represented by infinitely long circular cylinders embedded in a continuous matrix phase.

With each individual fiber of radius "a" there is associated an annulus of matrix material

of radius "b". Each individual cylinder combination of this type is referred to as a

composite cylinder, and the absolute values of radii "a" and "b" vary with each composite

cylinder such that a volume filling combination is obtained. The ratio of a/b is however

required to be constant for all composite cylinders. Naturally the absolute size of

individual cylinders must vary down to infinitesimal. A displacement type problem can be

posed to determine the upper bound and a stress type problem to establish the lower

bound of each of the moduli. The utility of this model results from the fact that analysis of

an individual cylinder suffices to determine exactly 4 of the 5 effective transversely

isotropic elastic moduli for the representative volume element. A solution is exact when

the upper and lower bounds coincide. The most difficult property to determine is G_{23} and

it is found that except for very small or very large fiber volume fractions the bounds do

not coincide. No concise solution for G_{23} has yet been found for the Composite Cylinders

Assemblage (CCA) , also referred to as the Composite Cylinders Model. A way around

this problem has been to solve a closely related model, the 3 phase cylinder model, known

also as the Generalized Self Consistent Scheme (GSCS). Here all but a single composite

cylinder is replaced by an equivalent homogeneous media. This allows a concise, though

complex, determination for G_{23}. It is not known whether G_{23} so determined is or is not

the solution for the CCA, but it is an exact result for G_{23} of the 3 phase model. For practical purposes one can take the 4 exact solutions for the CCA ($E_{11}, v_{12}, G_{12}, K_{23}$) along with the 3 phase model result for G_{23}. Evaluations of possible alternative forms for G_{23} using the Generalized Self-Consistent Scheme point to the conclusion that results from the above methods yield physically possible results at the extremums whilst other competitive methods break down [116]. The body of work by Hashin, Christensen and others also evaluates the practical application of results to single size fiber composites, with comparisons to numerical solutions of hexagonal arrays and also indicating which bound of the CCA is most appropriate under specific circumstances should one choose to avoid the complex equations comprising the closed form solutions to G_{23} from the 3 phase model.

Without digressing further, to synthesize the 3-dimensional material properties requisite for analysis in a thick-walled vessel, the formulations that follow were coded into the "Super Pressure - Vessel Designer" program. This particular equation set (the work of Z. Hashin [168]) was chosen because it appears to be one of the most advanced models at present and extends the standard CCA model using a replacement scheme under plane strain conditions for bulk modulus k and shear modulus G, modifying the equations to allow for the fact that the phase constituents are often *transversely isotropic* themselves. Here, because of the assumption of transverse isotropy for the constituents all directional properties can be described in terms of two directions, axial *(A)* and transverse *(T)*.

In keeping with the notation in use by the aforementioned authors, the stress-strain relations of a transversely isotropic *lamina* akin to the system in (4.1) can be presented in the following form [168]:

$$\sigma_{11} = n\varepsilon_{11} + l(\varepsilon_{22} + \varepsilon_{33})$$
$$\sigma_{22} = l\varepsilon_{11} + (k_T + G_T)\varepsilon_{22} + (k_T - G_T)\varepsilon_{33}$$
$$\sigma_{33} = l\varepsilon_{11} + (k_T - G_T)\varepsilon_{22} + (k_T + G_T)\varepsilon_{33}$$
$$\tau_{44} = 2G_T\gamma_{44}$$
$$\tau_{55} = 2G_A\gamma_{55}$$
$$\tau_{66} = 2G_A\gamma_{66}$$

Note: Tensorial shear strain is being used in this section.

where: k_T = transverse bulk modulus (K_{23})

G_T = transverse shear modulus (G_{23})

G_A = axial shear modulus (G_{12})

n = axial modulus (A_{11})

l = Poisson moduli (A_{12}, A_{13})

(7.3)

Other important elastic moduli are:

E_A = axial Young' modulus (E_{11})

v_A = axial Poisson's ratio (v_{12})

E_T = transverse Young's modulus (E_{22})

v_T = transverse Poisson's ratio (v_{23})

These are related to the moduli in (7.3) by relations:

$$E_A = n - 4k_T v_A^2$$

(7.4)

$$v_A = l/2k_T$$

(7.5)

$$E_T = \frac{4k_T G_T}{k_T + mG_T} = 2(1 + \nu_T)G_T = \frac{4}{\dfrac{1}{G_T} + \dfrac{1}{k_T} + \dfrac{4\nu_A^2}{E_A}}$$

(7.6)

$$\nu_T = \frac{k_T - mG_T}{k_T + mG_T}$$

(7.7)

where: $m = 1 + \dfrac{4k_T \nu_A^2}{E_A}$

Using additional subscripts (f) & (m) to denote respectively fiber and matrix properties,

υ to denote volume fraction, solution of the Composite Cylinders Assembly gives [168]

$$k_T = \frac{k_{Tm}(k_{Tf} + G_{Tm})\upsilon_m + k_{Tf}(k_{Tm} + G_{Tm})\upsilon_f}{(k_{Tf} + G_{Tm})\upsilon_m + (k_{Tm} + G_{Tm})\upsilon_f} = k_{Tm} + \frac{\upsilon_f}{\dfrac{1}{k_{Tf} - k_{Tm}} + \dfrac{\upsilon_m}{k_{Tm} + G_{Tm}}}$$

(7.7)

$$E_A = E_{Am}\upsilon_m + E_{Af}\upsilon_f + \frac{4(\nu_{Af} - \nu_{Am})^2 \upsilon_m \upsilon_f}{\upsilon_m / k_{Tf} + \upsilon_{Tf} / k_m + 1/G_{Tm}}$$

(7.8)

$$\nu_A = \nu_{Am}\upsilon_m + \nu_{Af}\upsilon_f + \frac{(1/k_{Tm} - 1/k_{Tf})(\nu_{Af} - \nu_{Am})\upsilon_m \upsilon_f}{\upsilon_m / k_{Tf} + \upsilon_f / k_{Tm} + 1/G_{Tm}}$$

(7.9)

$$G_A = G_{Am}\frac{G_{Am}\upsilon_m + G_{Af}(1 + \upsilon_f)}{G_{Am}(1 + \upsilon_f) + G_{Af}\upsilon_m} = G_{Am} + \frac{\upsilon_f}{\dfrac{1}{G_{Af} - G_{Am}} + \dfrac{\upsilon_m}{2G_{Am}}}$$

(7.10)

$$G_T^{(-)} = G_{Tm} + \frac{\upsilon_f}{\dfrac{1}{G_{Tf} - G_{Tm}} + \dfrac{k_{Tm} + 2G_{Tm}}{2G_{Tm}(k_{Tm} + G_{Tm})}\upsilon_m}$$

(7.11)

$$G_T^{(+)} = G_{Tm}\left[1 + \frac{\left(1+\beta_m\right)\upsilon_f}{\rho - \upsilon_f\left(1 + \frac{3\beta_m^2\upsilon_m^2}{\alpha\upsilon_f^3 + 1}\right)}\right]$$

<div align="right">(7.12)</div>

where:

$$\alpha = \frac{\beta_m - \gamma\beta_f}{1 + \gamma\beta_f}, \qquad \rho = \frac{\gamma + \beta_m}{\gamma - 1}, \qquad \beta_m = \frac{k_{Tm}}{k_{Tm} + 2G_{Tm}}, \qquad \beta_f = \frac{k_{Tf}}{k_{Tf} + 2G_{Tf}}, \qquad \gamma = \frac{G_{Tf}}{G_{Tm}}$$

Equations (7.11) and (7.12) represent the lower and upper bounds of the transverse shear modulus. The 3 phase model discussed earlier provides a solution for G_T slightly closer to the lower bound and can be found in references [169][116]. The careful reader will note that the formulation above differ slightly from their isotropic counterparts found in the above references, due to the replacement scheme used by Hashin whereby:

$$k_{Tf} \Rightarrow k_f = \lambda^* + G_f = \frac{3k_f - 2G_f}{3} + G_f = k_f + \frac{G_f}{3} = \frac{G_f}{1 - 2v_f} = \frac{G_f^2}{3G_f - E_f}$$

$G_{Tf} \Rightarrow G_f$, therefore: $\qquad k_{Tm} = \frac{3k_m - 2G_m}{3} + G_m = k_m + \frac{G_m}{3}$

<div align="right">(7.13)</div>

Where: $\qquad k_{Tf}$ = plane strain bulk modulus of fiber

k_{Tm} = plane strain bulk modulus of matrix

k_f, k_m = conventional bulk modulus, fiber or matrix

G_{Tf} = transverse shear modulus

G_f = isotropic shear modulus

λ^* = Lamé's constant

Using values representative of a graphite epoxy composite, the upper and lower bounds for the transverse shear modulus turn out to be very close to one another ($\approx$ 5%). Analysis by the aforementioned authors has shown that when the fibers are stiffer than the matrix ($k_f > k_m$ and $G_f > G_m$) the bounds are as given, however it should be noted that signs on the bounds are reversed in the case where the matrix stiffness exceeds the transverse stiffness of the fibers. This can be the case for some organic fibers, for example Spectra® 900.

For practical applications, the formulations as presented above are of no direct value since most of the quantities required are immeasurable, especially as concerns the fiber properties. But without accurate 3-D composite properties input, the pressure vessel elasticity equations derived in previous chapters would hardly be worth the exercise. To synthesize a design requires a firm handle on all elastic properties of constituent layers, not just approximations or values randomly extracted from diverse studies which are unlikely to meet the property relations underlying the transverse isotropy implicit to laminates used in calculating the vessel stresses.

What is really required amounts to a database of *fiber* properties. Reverse micromechanics was the method used to achieve the result in the present work. Equations (7.7)-(7.12) can be reformulated to extract fiber properties from uniaxial composite test data. In this way many diverse test results available in the literature can be examined, constituted of different matrix, fiber volume fractions and preparation methods. Provided the matrix properties are known or can be closely estimated and the test methods employed extract accurate data for lamina characteristics, fiber properties can be derived

from a broad basis. In theory, the back-calculated fiber properties should converge to specific values for each type, class or grade of fiber. The reverse formulations are derived:

From (7.7)

$$k_T = \frac{k_{Tm}k_{Tf}\upsilon_m + k_{Tm}G_{Tm}\upsilon_m + k_{Tf}\upsilon_f\left(G_{Tm} + k_{Tm}\right)}{k_{Tf}\upsilon_m + G_{Tm}\upsilon_m + \left(k_{Tm} + G_{Tm}\right)\upsilon_f}$$

$$k_T\left(k_{Tf}\upsilon_m\right) + k_T\left[G_{Tm}\upsilon_m + \left(k_{Tm} + G_{Tm}\right)\upsilon_f\right] = k_{Tf}\left(k_{Tm}\upsilon_m + G_{Tm}\upsilon_m + k_{Tm}\upsilon_f\right) + k_{Tm}G_{Tm}\upsilon_m$$

$$k_{Tf}\left[k_T\upsilon_m - \left(k_{Tm}\upsilon_m + G_{Tm}\upsilon_m + k_{Tm}\upsilon_f\right)\right] = k_{Tm}G_{Tm}\upsilon_m - k_T\left[G_{Tm}\upsilon_m + \left(k_{Tm} + G_{Tm}\right)\upsilon_f\right]$$

The transverse plane strain bulk modulus of the fiber is

$$k_{Tf} = \frac{k_{Tm}G_{Tm}\upsilon_m - k_T\left[G_{Tm}\upsilon_m + \left(k_{Tm} + G_{Tm}\right)\upsilon_f\right]}{\left[k_T\upsilon_m - \left(k_{Tm}\upsilon_m + G_{Tm}\upsilon_m + k_{Tm}\upsilon_f\right)\right]}$$

(7.14)

From (7.8)

$$E_{Af} = \frac{E_{Am} - E_m\upsilon_m - \left[\dfrac{4\left(v_{Af} - v_{Am}\right)^2 \upsilon_m\upsilon_f}{\upsilon_m/k_{Tf} + \upsilon_{Tf}/k_{Tm} + 1/G_{Tm}}\right]}{\upsilon_f}$$

Directly from (7.9)

let:
$$R = \left[\frac{\left(1/k_{Tm} - 1/k_{Tf}\right)\upsilon_m\upsilon_f}{\upsilon_m/k_{Tf} + \upsilon_f/k_{Tm} + 1/G_{Tm}}\right]$$

$$v_A - v_{Am}\upsilon_m = v_{Af}\left(\upsilon_f + R\right) - \upsilon_m R$$

Axial Poisson ratio of the fiber is

$$v_{Af} = \frac{v_A + v_{Am}\left(R - \upsilon_m\right)}{\upsilon_f + R}$$

(7.15)

From (7.10)

$$G_A G_{Am}(1 + \upsilon_f) + G_{Af} G_A \upsilon_m = G_{Am}^2 \upsilon_m + G_{Af} G_{Am} + G_{Af} G_{Am} \upsilon_f$$

$$G_A G_{Am}(1 + \upsilon_f) - G_{Am}^2 \upsilon_m = G_{Af}(G_{Am} + \upsilon_f G_{Am} - G_A \upsilon_m)$$

Axial shear modulus of the fiber is

$$G_{Af} = \frac{G_A G_{Am}(1 + \upsilon_f) - G_{Am}^2 \upsilon_m}{(G_{Am} + \upsilon_f G_{Am} - G_A \upsilon_m)}$$

(7.16)

From the lower bound (7.11)

let: $$Q = \frac{k_m + 2G_{Tm}}{2G_{Tm}(k_m + G_{Tm})} \upsilon_m$$

then

$$\frac{G_T - G_{Tm}}{\upsilon_f} = \frac{1}{\dfrac{1}{G_{Tf} - G_{Tm}} \div Q}$$

$$\frac{1}{G_{Tf} - G_{Tm}} = \frac{\upsilon_f}{G_T - G_{Tm}} - Q$$

The transverse shear modulus of the fiber (lower bound) is

$$G_{TF}^{(-)} = G_{Tm} + \frac{1}{\left(\dfrac{\upsilon_f}{G_T - G_{Tm}} - Q \right)}$$

(7.17)

The upper bound of the transverse shear modulus is rather complicated and involves

solution to a quadratic form. Equation (7.12) is formulated as

296

$$\frac{G_T^{(-)}}{G_{Tm}} - 1 = \frac{(1+\beta_m)\upsilon_f}{\rho - \upsilon_f\left(1 + \frac{3\beta_m^2\upsilon_m^2}{\alpha\upsilon_f^3 + 1}\right)}$$

rearranging

$$\rho - \upsilon_f\left(1 + \frac{3\beta_m^2\upsilon_m^2}{\alpha\upsilon_f^3 + 1}\right) = \frac{(1+\beta_m)\upsilon_f}{\dfrac{G_T^{(-)}}{G_{Tm}} - 1}$$

let: $\quad X = \dfrac{(1+\beta_m)\upsilon_f}{\dfrac{G_T^{(-)}}{G_{Tm}} - 1}$ $\qquad , \qquad Y = 3\beta_m^2\upsilon_m^2$

then

$$\rho - \upsilon_f\left(1 + \frac{Y}{\alpha\upsilon_f^3 + 1}\right) = X$$

substitute for ρ and expanding terms

$$\frac{\gamma + \beta_m}{\gamma - 1} - \upsilon_f\left(1 + \frac{Y}{\left(\dfrac{\beta_m - \gamma\beta_f}{1 + \gamma\beta_f}\right)\upsilon_f^3 + 1}\right) = X$$

$$\frac{\gamma + \beta_m}{\gamma - 1} - \upsilon_f\left(1 + \frac{Y}{\left(\dfrac{\beta_m\upsilon_f^3 - \gamma\beta_f\upsilon_f^3 + 1 + \gamma\beta_f}{1 + \gamma\beta_f}\right)}\right) = X$$

$$\frac{\gamma + \beta_m}{\gamma - 1} - \upsilon_f\left(1 + \frac{Y + Y\gamma\beta_f}{(\beta_m\upsilon_f^3 + 1) + \gamma(-\beta_f\upsilon_f^3 + \beta_f)}\right) = X$$

$$\frac{\gamma + \beta_m}{\gamma - 1} - \upsilon_f\left(\frac{(\beta_m\upsilon_f^3 + 1) + \gamma(-\beta_f\upsilon_f^3 + \gamma\beta_f) + Y + Y\gamma\beta_f}{(\beta_m\upsilon_f^3 + 1) + \gamma(-\beta_f\upsilon_f^3 + \beta_f)}\right) = X$$

$$\frac{\gamma + \beta_m}{\gamma - 1} - \left(\frac{(\beta_m \upsilon_f^4 + \upsilon_f + Y\upsilon_f) + \gamma(-\beta_f \upsilon_f^4 + \beta_f \upsilon_f + Y\beta_f \upsilon_f)}{(\beta_m \upsilon_f^3 + 1) + \gamma(-\beta_f \upsilon_f^3 + \beta_f)} \right) = X$$

$$\frac{\gamma + \beta_m}{\gamma - 1} = \left(\frac{(\beta_m \upsilon_f^4 + \upsilon_f + Y\upsilon_f) + \gamma(-\beta_f \upsilon_f^4 + \beta_f \upsilon_f + Y\beta_f \upsilon_f)}{(\beta_m \upsilon_f^3 + 1) + \gamma(-\beta_f \upsilon_f^3 + \beta_f)} \right) + X$$

$$\frac{\gamma + \beta_m}{\gamma - 1} = \left(\frac{(\beta_m \upsilon_f^4 + \upsilon_f + Y\upsilon_f) + \gamma(-\beta_f \upsilon_f^4 + \beta_f \upsilon_f + Y\beta_f \upsilon_f) + (\beta_m \upsilon_f^3 X + X) + \gamma(-\beta_f \upsilon_f^3 X + \beta_f X)}{(\beta_m \upsilon_f^3 + 1) + \gamma(-\beta_f \upsilon_f^3 + \beta_f)} \right)$$

$$\frac{\gamma + \beta_m}{\gamma - 1} = \left(\frac{(\beta_m \upsilon_f^4 + \upsilon_f + Y\upsilon_f + \beta_m \upsilon_f^3 X + X) + \gamma(-\beta_f \upsilon_f^4 + \beta_f \upsilon_f + Y\beta_f \upsilon_f - \beta_f \upsilon_f^3 X + \beta_f X)}{(\beta_m \upsilon_f^3 + 1) + \gamma(-\beta_f \upsilon_f^3 + \beta_f)} \right)$$

let:
$$A = (-\beta_f \upsilon_f^4 + \beta_f \upsilon_f + Y\beta_f \upsilon_f - \beta_f \upsilon_f^3 X + \beta_f X)$$
$$B = (\beta_m \upsilon_f^4 + \upsilon_f + Y\upsilon_f + \beta_m \upsilon_f^3 X + X)$$
$$C = (-\beta_f \upsilon_f^3 + \beta_f)$$
$$D = (\beta_f \upsilon_f^3 + 1)$$

then

$$\frac{\gamma + \beta_m}{\gamma - 1} = \frac{\gamma(A) + B}{\gamma(C) + D}$$

Solving for γ

$$\gamma^2 C + \beta_m \gamma C + \gamma D + \beta_m D = \gamma^2 A - \gamma A + \gamma B - B$$

$$\gamma^2(C - A) + \gamma(\beta_m C + D + A - B) + \beta_m D + B = 0$$

$$\gamma^2 + \gamma \left(\frac{\beta_m C + D + A - B}{(C - A)} \right) + \frac{\beta_m D + B}{(C - A)} = 0$$

let:
$$b = \frac{\beta_m C + D + A - B}{(C - A)} \qquad , \qquad c = \frac{\beta_m D + B}{(C - A)}$$

the solution for γ is

$$\gamma = \frac{-b \pm \sqrt{b^2 - 4c}}{2} \qquad \text{(use positive value)}$$

and hence the transverse fiber modulus is

$$G_{Tf}^{(-)} = \gamma G_{Tm}$$

(7.18)

The "Super Pressure - Vessel Designer" program makes use of the foregoing

micromechanics equation sets to build a database of constituent materials. The software

runs in either direction at a keystroke, enabling the user both to break down mechanical

test data, extracting fiber properties, and rebuilding laminate values from the

aforementioned extracted properties. Much of the code that handles these tasks can be

found in unit compmath.pas, procedure GenerateMatProp and in unit failure.pas,

procedure Calculate_Prop. The utility comes about from the fact that diverse test results

from samples using the same fiber type can be compared. Additionally, if matrix properties

are underestimated, during decomposition certain transverse moduli will come out

negative. This is also true when improper (theoretically impossible) combinations of

moduli are input for decomposition. It is not obvious, but rather experience in working

with this segment of code has shown that a very considerable proportion of 3-D material

property combinations found in the literature does *not* degenerate properly, resulting in

some negative transverse moduli. Usually the problem is related to a slight over estimation

of in plane transverse tensile moduli or a mismatched transverse shear moduli. The most

notorious aspect however is that most data sets available for a particular material are

incomplete. Either they lack the basic strength data (axial tensile & compressive,

299

transverse tensile & compressive, in plane shear) or are missing at least one of the 5

fundamental independent properties. Additionally it must be noted that values of bulk

modulus k_T are not habitually published, v_T is also rarely measured. Nevertheless

techniques have been developed to skirt these difficulties. Firstly relations (7.4)-(7.7) are

made use of to handle input of material property combinations different from the ones

$(k_T, v_T, E_A, G_T, G_A)$ required by the micromechanics formulas. Namely the program

accepts the first 5 non-blank entries out of a possible 7 $(E_{11}, v_{12}, G_{12}, E_{22}, v_{23}, G_{23}, K_{23})$

laminate measurements, and automatically converts to the required quantities internally. A

choice can be made between the case of isotropic or transversely isotropic fiber properties

and the transverse bound will automatically be chosen according to relative stiffness of

matrix as compared to fiber. Another feature is that for cases where the input data is over-

determined, in that values specified for E_{22} and G_{23} cannot both be reconstituted from

fiber-matrix properties, an iterative procedure can be invoked that will select k_T to

minimize the relative error between the computed E_{22}, G_{23} respective to the values

specified initially. The decomposition / reconstitution procedure can be invoked as often

as desired and the values obtained edited at either the laminate or decomposed state. A

very short example outlining the basics is presented in Chapter 8. Naturally, fiber volume

fraction and matrix properties can be altered and their effects determined. Laminate tensile

strengths X are handled by a rule of mixtures approach, while a slightly modified formula,

taken from Tsai [174], is used for compressive strength X'. The form for this is

$$\frac{X'}{X'^0} = \left[\frac{G_{12}}{G_{12}^0}\right]^{0.2}\left(\frac{v_f}{v_f^0}\right)$$

Where: Superscript (^{0}) describes the initial.

(7.19)

300

Transverse and shear strength are assumed to rely solely on the matrix and remain independent of fiber volume fraction.

Use of the Composites Cylinders Assembly as a representative volume element for unidirectional fiber composites, even when the interface is rather imperfect, has been studied by G.P. Tandon [177]. It was concluded that volume fractions as high as 80% can be modeled and so long as the fibers are not in contact, the actual location of the fibers has little significant effect on the moduli.

With a little practice, 3-D laminate data can usually be decomposed and reconstituted within 4-6 attempts, yielding both theoretically acceptable fiber properties and reconstituted results very close to the test data inputs. It should be noted that the formulas for decomposition are *very sensitive* to the inputs whereas in working the micromechanics equations in the forward direction the opposite is true. Such a characteristic makes it easy to predict material elastic characteristics from constituents, but not vice-versa. M. Battley [178] has published some discussion of the back-calculation method using various models and correctly concluded that this is a difficult task.

Table 7.1 is a summary of results for 18 different materials analyzed in this study, the results of which are available to other components of the "Super Pressure - Vessel Designer" program. The data presented in the figure represents a compilation of test results gathered from a wide range of sources. Result for any single material represented cannot be attributed exclusively to the findings in any particular paper, book or technical data sheet, but rather were chosen to represent the median of values being used in the literature. For some popular materials the results are compiled from 5-6 different

publications, for others there was barely enough information available to make up one data set. References [37][45][55][65][74][94][108][124][184][191][215][[234-244] along with manufacturers data sheets comprise the majority of this data. It must at the same time be noted that in many instances laminate values have seen some alterations because the quoted literature values gave impossible decomposition results. This does not necessarily indicate that the experimentally measured results are entirely inaccurate, rather test methods may be biasing the data, or the presence of voids, fiber waviness, inhomogeneities and other factors unaccounted in the CGA model are responsible. Rifts between the ideal mathematically determined transversely isotropic character and reality are ever present. There is subjectivity involved in forward / back calculation of the micromechanics equations since the user has to judge what balance of properties at the fiber level are reasonable whenever the input combination chosen shows that negative moduli would be required to achieve the result. Obviously to do this well requires a large and precise lot of input data. Diversity in test methods, from ultrasound and mechanical coupon tests to single fiber studies, are beneficial because each has their bias and the differing points of view can serve as a reality cross-check. The micromechanics formulations however provide a point of reference at a very basic level. Table 7.1 is unique in the sense that the values tabulated conform to the assumptions inherent in transverse isotropy at both fiber and laminate level, something not likely to be found elsewhere, especially when adopting values either randomly from the literature or taking mechanical test results at face value.

Table 7.1 Micromechanics database

Material	E_glass	S-glass	KEV_49	Spec_900	KEV_149	T300_34C	AS_3501	T300_5208	G_30
E11 (GPa)	45	55	87.1	40	107	124	138.6	140.9	127.9
V12 (GPa)	0.265	0.28	0.341	0.32	0.34	0.31	0.313	0.325	0.331
G12 (GPa)	4.61	6.26	2.14	1.1	2.2	4.8	6.05	4.85	3.94
E22 (GPa)	13.94	18.81	5.72	2.7	6.2	9.4	11.1	9.17	7.95
V23 (ratio)	0.335	0.337	0.529	0.42	0.558	0.55	0.543	0.48	0.487
G23 (GPa)	5.22	7.04	1.87	0.95	1.99	3.03	3.6	3.1	2.67
K23 (GPa)	11.22	15.42	6.27	2.38	7.23	10.79	12.58	9.06	7.96
Em (GPa)	3.64	5.05	3.75	3.4	3.4	3.6	4.4	3.8	4
Vm (ratio)	0.35	0.35	0.35	0.35	0.35	0.35	0.35	0.35	0.35
XT (MPa)	1020	1620	1540	1070	1450	1234	1587	1347	1590
XC (MPa)	620	960	234	91	260	1234	1447	1181	1284
YT (MPa)	40	60	27	8	27	72.9	51.7	47.6	45
YC (MPa)	140	140	93	44	110	258	206	199.3	200
SS (MPa)	60	60	47	17	57	71.4	93	94.5	106
ff (%)	60	60	66	50	60	67.2	66	62	55
Fiber									
EI (Gpa)	72.5	88.3	130	76.59	176.1	182.8	207.7	224.9	229.3
VI (ratio)	0.22	0.243	0.336	0.28	0.334	0.294	0.298	0.312	0.319
GI (GPa)	29.73	35.5	2.71	0.96	3.35	15.45	23.86	23.58	15.4
Et (GPa)	72.55	88.27	6.73	1.90	8.85	15.93	18.79	16.26	13.48
Vt (ratio)	0.22	0.243	0.542	0.35	0.627	0.664	0.649	0.514	0.502
Gt (GPa)	29.73	35.5	2.18	0.70	2.72	4.79	5.7	5.37	4.49
Kt (GPa)	53.09	69.11	7.53	1.48	12.24	24.83	28.04	17.24	13.88

Material	AS4_3502	T300_TSAI	IM6_SCI	T1000	IM7_9772	G_50	Boron	P75S	P100S
E11 (GPa)	144.8	180	182.2	189.4	173	193	204	274	497
V12 (GPa)	0.31	0.28	0.25	0.25	0.29	0.27	0.271	0.27	0.31
G12 (GPa)	4.8	7.17	4.48	4.48	5.52	4.13	5.75	3.58	5.6
E22 (GPa)	9.6	10.3	8.96	8.96	7.58	6.96	17.96	6.21	5.3
V23 (ratio)	0.461	0.451	0.378	0.38	0.426	0.4	0.375	0.416	0.458
G23 (GPa)	3.29	3.55	3.25	3.22	2.66	2.48	6.53	2.19	1.82
K23 (GPa)	9.12	9.54	7.28	7.25	6.69	5.86	14.67	5.34	4.91
Em (GPa)	4.2	3.8	3.4	3.8	4.5	3.8	5.34	3.2	3.8
Vm (ratio)	0.35	0.35	0.35	0.35	0.35	0.35	0.35	0.35	0.35
XT (MPa)	1932	1500	2875	3614	2820	1240	1260	966	1242
XC (MPa)	1656	1500	1896	2379	1613	937	2500	150	290
YT (MPa)	60	40	37.9	74	75	37.9	61	33	18
YC (MPa)	200	246	138	128	200	200	202	150	150
SS (MPa)	100	68	102	102	109	90.3	67	55	34.5
ff (%)	62	70	66	66	58	62	50	52	62
Fiber									
EI (Gpa)	231	255.5	274.3	285	295	308.9	402.6	523.9	799.3
VI (ratio)	0.289	0.255	0.206	0.205	0.249	0.225	0.21	0.203	0.286
GI (GPa)	16.06	68.55	15.56	12.04	42.45	12.19	166.36	69.51	79.05
Et (GPa)	15.99	16.47	15.2	13.77	10.12	9.39	402.6	10.6	5.98
Vt (ratio)	0.458	0.449	0.291	0.29	0.344	0.308	0.21	0.294	0.406
Gt (GPa)	5.49	5.68	5.89	5.34	3.76	3.59	166.36	4.1	2.13
Kt (GPa)	15.07	15.18	10.79	9.75	7.76	6.82	286.84	7.52	5.05

7.1 Structural Properties of Fibers

The structural properties of reinforcing fibers present a large subject matter. Since the carbon / graphite variety is of exceeding importance a very brief discussion follows. Diamond is isotropic with a modulus of 1200 GPa and represents the tightest packed form of carbon and the hardest material known. Unfortunately it is metastable and converts to graphite when heated to about $1500°$ C in a vacuum. In the process it decreases in density from 3.300 g/cm^3 to 2.265 g/cm^3 and if the resulting graphite has no preferred orientation the Young's modulus drops to only 7 GPa. However if there is a preferred orientation imparted, a value near the modulus of diamond can be recovered along the basal plane. Figure 7.2 shows the unit cell of a graphite crystal and Figure 7.3 attaches numerical values to the elastic constants associated with such a crystalline structure.
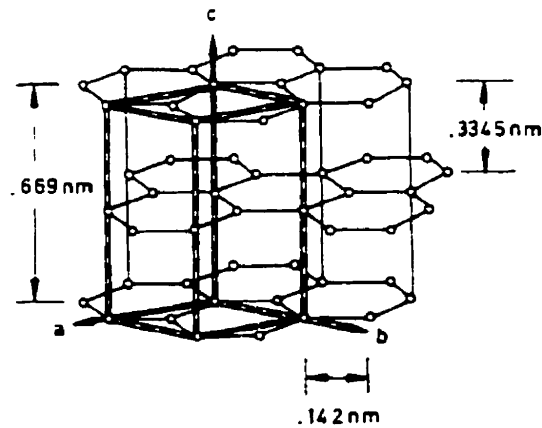
Figure 7.2 The structure of graphite and its unit cell [179].

There are essentially 2 possible stacking sequences, the form illustrated in Figure 7.2 where successive basal planes shift ± one bond length resulting in *ababab* stacking and another form whereby basal planes always shift + one bond length giving *abcabc* stacking. There is also another less ordered form known as turbostractic carbon whereby the graphite layer planes may be rotated individually around the *c* axis to form a "crystal" in which the layer planes, while still parallel, are not ordered with respect to each other. In commercial fiber production the precursors are Polyacrylonitrile fibers (PAN) and mesophase pitch (MP). In both cases the processing usually involves hot stretching and heat treatment techniques to improve the orientation and internal structure of the product. Studies have shown a great possible variety in the internal structures, however the common goal is always improved orientation of the crystallites and decreasing crystallite imperfections, especially on the fiber surface. No property improvement over amorphous graphite is seen unless layer orientation is less than 20° away from the tensile axis. A very good product will show alignment on the order of 5° mis-orientation. Most of this ordering takes place on the surface of the fiber, the interior being less so.
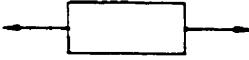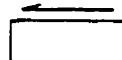
Elastic compliance (GPa^{-1})		Crystal directions	Elastic constant (GPa)	
s_{11}	0.00098	Pure tension parallel to the basal planes	c_{11}	1060
s_{33}	0.0275	Pure tension across the basal planes	c_{33}	36.5
s_{44}	0.25	Shear between basal planes	c_{44}	4
s_{12}	−0.00016	Shear within a basal plane	c_{12}	180
s_{13}	−0.00033	Shear through basal planes	c_{13}	15

Figure 7.3 Graphite single crystal elastic constants [179].

Typically such a structure, as shown in Figure 7.4, constitutes many highly curved

interlocking sheets of layer planes and in the case of very high processing temperatures

may be sheathed by a circumferentially oriented jacket of larger and more highly oriented

crystallites. The crystallites are mainly turbostractic. The interior folded layer orientation

can be considered either random or perhaps somewhat radial in nature for certain cases. It is this structure obviously that controls both the transverse and axial elastic properties.
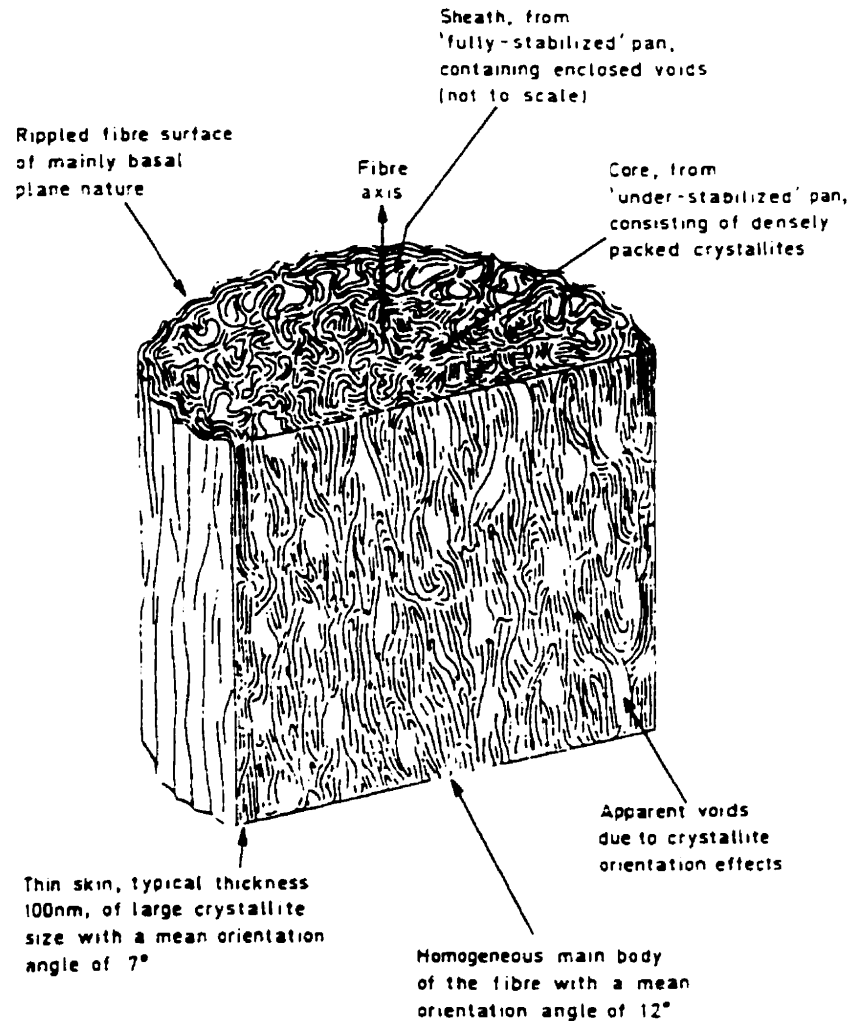
Figure 7.4 Graphite fiber internal structure [179].

Other transversely isotropic materials, some polymer based like aramid fibers (Kevlar®) and crystalline polyethylene (Spectra®), have their own particular internal structures that likewise determine their elastic moduli. As with carbon fibers many variants

exist and similarly trade-offs between axial and transverse elastic moduli (and strengths) need to be considered.

The reference book *Strong Fibers* [179] presents data from many researchers, dealing mainly with the crystallographic structures responsible for elastic moduli and strengths of advanced fibers. Figure 7.2, 7.3, 7.4 and Table 7.2 are drawn from this text.

Table 7.2 Calculated and observed preferred orientation parameters for carbon fibers [179].

Nominal heat treatment temperature ^{0}C	Fiber type	Young's modulus (GPa)	Torsional modulus (GPa)	Calculated S_{44} (GPa)$^{-1}$	Calculated mean angle ϕ^o	Observed angles 1	2	3
2500	1	428	14	0.143	7	8	8	5
1500	2	245	24	0.083	15	17	12	
1000	3	197	26	0.077	18	19	14	

It is interesting to compare briefly Table 7.1 computations with some values on fiber moduli obtained by independent sources. What should become evident is that the micromechanical predictions are of the right order. Tests have shown that when PAN fibers are carbonized and heat treated the torsional modulus increases sharply from 1.5 GPa to 18 GPa after heating to 1000°C. Heating the fibers between 1000°C - 2500°C, corresponding to temperatures at which Type 3, Type 2 and Type 1 carbon/graphite are produced, the torsional modulus remained almost constant. Subsequent heating to 2800°C makes it fall to 15 GPa. Other researchers approaching the problem differently appear to be coming up with similar results, for example Tsai's [174] predictions for the transverse

modulus of T-300 fiber which are based on a semi-analytic variant of the Halpin-Tsai

formulations, back-calculate a value of 18.7 GPa for this material.

Another set of published values can be found in *Carbon Fibers* [180]. Some of this

data is recompiled in Table 7.3 below. The test methods are varied.

Table 7.3 Properties of polyacrylonitrile and mesophase
pitch based carbon fibers [180].

Manufacturer	Fiber Designation	Tensile Modulus (GPa)	Shear Modulus (GPa)	Transverse Modulus (GPa)
PAN Fibers				
Hercules	AS4	221	17	
Toray	T-40	290	17.5	4.0
Toray	T-50	390	14-15	
Toray	T-300	231	15	3.21
MP Fibers				
Amoco	P-55S	380	6.6-7.0	
Amoco	P-75	520	8.0-9.0	
Amoco	P-100	758	4.7-5.0	
DuPont	E-35	262	8.0-8.5	
DuPont	E-75	524	5.7-6.0	
DuPont	E-105	717	5.0-5.5	

The Poisson's ratio of three different high strength carbon fibers has also been

measured with a laser diffraction technique [180]. The average values are in the range of

0.26 - 0.28 with a claimed accuracy of 5.7%. For dog-bone shaped fiber cross-sections the

Poisson's ratio is anisotropic around the fiber perimeter. The Poisson's ratio for Toray

T-300 and Amoco P-55 were found to be 0.22 and 0.10 respectively as measured by

photographic techniques. Table 7.4, also drawn from reference [180] was computed from

dynamic mechanical measurements on laminates. Despite the great difficulties in attaining

Table 7.4 Computed properties of some Amoco carbon fibers [180].

Fiber	E_a [GPa]	G_a [GPa]	v_a	E_t [GPa]	G_t [GPa]	α_a [ppm]	α_t [ppm]
P-55-H	305	15.6	0.32	10.8	3.0	−1.37	12.1
P-55-L	300	12.9	0.29	10.7	3.2	−1.37	11.6
P-75-H	450	13.3	0.24	8.8	2.5	−1.49	12.2
P-75-L	449	12.7	0.23	8.8	2.5	−1.44	12.7
P-100-H	770	23.6	0.30	7.1	2.1	−1.48	9.4
P-100-L	775	20.6	0.22	6.8	2.0	−1.47	9.5
T-50-H	358	18.1	0.13	10.3	3.3	−1.28	6.6
T-50-L	354	16.4	0.15	10.2	3.3	−1.17	6.8
T-300X	341	19.0	0.13	10.3	3.5	−1.20	7.0
T-300	204	22.2	0.26	14.7	5.0	−0.67	8.9
T-300	205	23.4	0.27	14.4	4.9	−0.67	8.8
T-650	243	23.1	0.29	13.8	5.0	−0.84	7.8

Notes: H = high resin volume fraction; L = low resin volume fraction; T-300X = heat treated T-300; two samples of T-300; the higher modulus PAN-type fibers heat treated at a higher temperature relative to the lower modulus PAN-type fibers. E_a, E_t, Young's modulus in the axial and transverse direction; G, shear modulus; n, Poisson's ratio; a, coefficient of thermal expansion.

any sort of accuracy in such measurements, the similarity with previous results should be noted. To date the only properties directly measurable by mechanical means are single fiber axial tensile modulus E_{Af}, and axial shear modulus G_{Af} by torsion pendulum.

Diametrical compression tests can also be done to measure transverse response. Such mechanical tests, as done by Kawabata [181], among others appear to give lower moduli than results computed on the basis of ultrasonic techniques (combined with analytic models) as with the work of Smith [182], Dean and Turner [183], or Vong and Verchery [184].

It cannot be stated with any certainty that the values in Table 7.1 derived on the basis of reverse micromechanics are correct, however we can be reasonably certain that they are representative on the overall. The key point to comprehend is that although transverse fiber properties can change greatly, the continuous phase (transversely) is the

matrix and it exerts the strongest influence overall on shear and through thickness response. In terms of pressure vessel design one important point is that a high fiber volume fraction and a stiff matrix are crucial factors towards the goal of attaining a higher through-thickness stiffness, necessary for efficient load transmission towards the outer layers. This yields strong influence over the factor K (chapter 4). When this is not attainable, then an increasing rate of change in the circumferential stiffness is required to enforce a more level stress distribution. Of course no material is infinitely stiff hence the *thickness limit* to a prescribed optimal stress distribution is reached sooner for transversely compliant material. It should also be noted from the above figures and tables that axial fiber stiffness generally varies inversely with transverse fiber stiffness within a given material when various internal structures are possible.

The employment of micromechanics for the program "Super Pressure - Vessel Designer" has the greater goal of encompassing the "what if" questions arising when in search of new, better, hypothetical materials, or comparisons with or possible modifications of parameters associated with existent materials. With the goal of achieving a smooth variation in properties demanded by the continuum theory, the micromechanics module is in place to facilitate that effort.

A discussion of micromechanics inevitably raises the question of strengths. Being there are as of yet few practical means of going from fiber morphology to single fiber strengths to lamina characteristics, it is better to resort to standard uniaxial lamina tests and thereon devise failure criteria for a laminate. This leads to the subject of the next section.

7.2 Failure Theories

Application of proper failure theories to composite structures is a subject of endless debate. Critical reviews are widespread and the reader is encouraged to seek out publications by Hart-Smith [170][185][186][187] as an eye-opener to the many shortfalls presented by the classic quadratic interaction form, which is widely taught in texts and repeatedly examined in experimental studies. The later are slated to extract the all elusive interaction parameters. A review of classic theories and their experimental correlation is covered by R.E. Rowlands within a book chapter [188]. Moreover numerous studies and theories have been forwarded over the years, only a few of which can be mentioned in this space.

An important concept in composites is that failure cannot be defined as only one thing, rather it is a sequence of events and modes. Some of these are progressive sub-critical failures like matrix microcracking, in contrast with gross delamination at interfaces which must be recognized as an independent mode. These facts are plainly stated in an early publication by Tsai and Hahn [189] so it appears somewhat far reaching to see their quadratic interaction criterion now being extended well past the first ply failure predictions it was originally intended for by applying alterations to interaction terms and assigning matrix degradation's without evaluating how these changes affect the 3-dimensional character of a laminate's behavior. Although the concept appears warranted in principle, the details and underlying assumptions need to be examined and understood if extensions and refinement of the basic method are to proceed.

Quoted from reference [189]: "More work is needed in the effects of the first ply failure on the subsequent structural behavior under various loading and environmental conditions". ... "Delamination, which is unique to composite laminates should be recognized as an independent failure mode and treated accordingly".

"On the whole, more effort should be directed toward the investigation of formation and propagation of sub-critical failures in composite laminates. Much study remains to be done for effects of these sub-critical failures on the overall structural performance. This understanding is essential to a full utilization of composites because composite usage will be limited mostly by the matrix and / or interface failures rather than by fiber failure".

Without doubt, the quadratic interaction theorem, like any other failure theory is an exercise in curve fitting to experimental data. The anchor points to one such plot are deduced from uniaxial, shear and biaxial tests. Typically these involve the quantities (X,X',Y,Y',S,F_{12}). Because the tensor form is truncated to second order terms, the resulting curve in 2 dimensional space is an ellipse shifted from the origin. The terms above represent strengths obtained from, axial tensile, axial compressive, transverse tensile, transverse compressive, in plane shear and an interaction parameter evaluated from a biaxial test, respectively.

Obviously with more anchor points and inclusion of higher order terms a mathematical curve can always be made to fit the data a lot better. This essentially is the case for the cubic tensor polynomial form as presented by R.C. Tennyson et. al. [120]. Naturally, attaining closure for the failure envelope becomes a complex process and the

evaluation requires, in addition to the anchor points mentioned above, 2 more biaxial load tests. Alternatively closure conditions can be invoked to reduce the number of biaxial load tests however this only serves to bracket the interaction terms between limits [121].

With due regard for the efforts placed in trying to describe laminate failure by a single equation with interactions between the various possible modes, one must still consider the probing question posed by Hart-Smith, "Should Fiberous Composite Failure Modes be Interacted or Superimposed?" [170]. A key to the applicability of any mathematical model is that it reflects accurately underlying physical phenomenon. One must then ask oneself where does the tensor polynomial form come from, why was it selected? Hill's classical work on the plasticity of slightly orthotropic metals is at the root [259]. Hill was able to use smooth continuous envelopes only because he was dealing with *homogeneous* material for which the mechanism of yield was the *same* regardless of the state of combined stresses. Fiber composites, on the other hand, are *heterogeneous* and the mode of failure *varies* greatly with the nature of the applied stresses. Composite materials may legitimately be homogenized into an equivalent substance for the purpose of calculating the elastic constants (because these are seen macroscopically), but this represents a physically unrealistic oversimplification in regard to predicting strength (a microscopic phenomena). The application of Hill's theory to a heterogeneous material should have required separate failure envelopes for every possible mode of failure for each of the constituents. These envelopes should then have been superimposed with the governing failure envelope defined by the minimum common area. If we are to follow Hill's inspiration, one can separate the failures into two subgroups, one for each

mechanism at work (fibers = brittle fracture; matrix = ductile yielding) and draw a tensor polynomial based curve through the different measured strengths yet still considering each of the constituents separately.

The above should not be seen as a very radical departure from past practices, but as a more precisely directed approach aimed at modeling the mechanisms underlying, rather than forcefully curve fitting with an ever greater number of parameters.

Only recently have serious attempts been made along this line of thought. Firstly it must be realized that the maximum stress and maximum strain criteria are an elementary form of "non-interactive" criteria. Hart-Smith has extended these forms to arrive at truncated envelopes that encompass shear and biaxial loading. These envelopes do not use a polynomial form, but rely on the superposition of many separate failure modes. The underlying assumption however is strongly based on the discussion of Hill's work above.

A higher level of analysis has been carried out by W.W. Feng [117][119] and R.M. Christensen [112][113]114][169][190]. These authors, among others like T.R. Guess [124], S.R. Swanson and A.P. Christoforou [191], have recognized the need to separate failure along lines marked by matrix and fiber effects. Each has devised means to separate out the contribution of matrix and fibers with regard to the failure of a single unidirectional lamina. Common to Feng's and Christensen's formulations is use of two quadratic envelopes, one each for fiber and matrix. Feng's approach is strain based, while Christensen's most recent is stress based. A brief summary of each is presented below.

Feng's failure criterion [117] is based upon the strain invariants of finite elasticity, i.e. small strains. The criterion assumes that the material is transversely isotropic and that

315

failure occurs when the strain energy density reaches its maximum value. The fiber and matrix failure modes can be decoupled provided one assumes that the single interaction term A_{15} present in the failure surface is negligible. The form for the failure surface based on the 5 invariants is:

$$A_1(I_1-3)+A_{11}(I_1-3)^2+A_2(I_2-3)+A_4(I_4-1)+A_5(I_5-1)+A_{55}(I_5-1)^2+A_{15}(I_1-3)(I_5-1)-1=0$$

Where: I_j = Cauchy strain invariants (defined in Feng's paper [117])

A_{ij} = Unknown strength (quantities to be determined)

Decoupling is then possible since the invariants I_1, I_2, I_3 are not functions of fiber orientations while I_4, I_5 are functions of fiber orientation.

Therefore for the matrix mode the criterion is

$$A_1(I_1-3)+A_{11}(I_1-3)^2+A_2(I_2-3)-1=0$$

(7.20)

and the fiber criterion is

$$A_5(I_5-1)+A_{55}(I_5-1)^2+A_4(I_4-1)-1=0$$

(7.21)

Using infinitesimal strains to approximate the Cauchy strains, the equivalent invariants are

$$J_1 = \varepsilon_{11}+\varepsilon_{22}+\varepsilon_{33}$$

$$J_2 = \frac{1}{6}\left[(\varepsilon_{11}-\varepsilon_{22})^2+(\varepsilon_{22}-\varepsilon_{33})^2+(\varepsilon_{33}-\varepsilon_{11})^2+\varepsilon_{12}^2+\varepsilon_{23}^2+\varepsilon_{13}^2\right]$$

$$J_4 = \varepsilon_{12}^2+\varepsilon_{13}^2$$

$$J_5 = \varepsilon_{11}$$

The strain invariants I are related to J by

$$J_1 = \frac{1}{2}(I_1 - 3)$$

$$J_2 = \frac{1}{12}(I_1^2 - 3I_2)$$

$$J_4 = \frac{1}{4}(I_4 - I_3^2)$$

$$J_5 = \frac{1}{2}(I_5 - 1)$$

Substituting these, the failure criterion for infinitesimal strains can be written as

$$A_1 J_1 + A_{11} J_1^2 + A_2 J_2 + A_4 J_4 + A_5 J_5 + A_{55} J_{55}^2 + A_{15} J_1 J_5 = 1$$

(7.21)

Again, neglecting interaction, matrix dominated failure for infinitesimal strains is

$$A_1 J_1 + A_{11} J_1^2 + A_2 J_2 - 1 = 0$$

(7.22)

and fiber dominated failure is

$$A_4 J_4 + A_{55} J_{55}^2 + A_5 J_5 - 1 = 0$$

(7.23)

To evaluate the A terms for a unidirectional composite six quantities, the axial tensile and compressive failure strains $X_\varepsilon, X_\varepsilon'$, the transverse tensile and compressive failure strains $Y_\varepsilon, Y_\varepsilon'$, and the axial and transverse shear failure strains $S_\varepsilon, S_\varepsilon'$ are required. Substituting these strains one at a time into the failure criterion yields 6 equations.

For   Equation
⇓   ⇓

$$\varepsilon_{23} = S_\varepsilon', \quad A_2 S_\varepsilon'^2 - 1 = 0$$

(7.24)

$$\varepsilon_{22} = Y_\varepsilon, \quad A_1(1 - v_{21} - v_{23})Y_\varepsilon + A_{11}(1 - v_{21} - v_{23})^2 Y_\varepsilon^2 + \frac{A_2}{6}\left[(1 + v_{12})^2 + (v_{21} - v_{23})^2 + (1 + v_{23})^2\right]Y_\varepsilon^2 - 1 = 0$$

(7.25)

$$\varepsilon_{22} = Y_\varepsilon', \quad A_1(1 - v_{21} - v_{23})Y_\varepsilon' + A_{11}(1 - v_{21} - v_{23})^2 Y_\varepsilon'^2 + \frac{A_2}{6}\left[(1 + v_{12})^2 + (v_{21} - v_{23})^2 + (1 + v_{23})^2\right]Y_\varepsilon'^2 - 1 = 0$$

317

$$\varepsilon_{12} = S_\varepsilon \quad , \quad A_4 S_\varepsilon^2 - 1 = 0 \tag{7.26}$$

$$\varepsilon_{11} = X_\varepsilon \; , \quad A_5 X_\varepsilon + A_{55} X_\varepsilon^2 - 1 = 0 \tag{7.27}$$

$$\varepsilon_{11} = X_\varepsilon' \; , \quad A_5 X_\varepsilon' + A_{55} X_\varepsilon'^2 - 1 = 0 \tag{7.28}$$

$$\tag{7.29}$$

The first 3 equations above are associated with the matrix failure mode, the second 3 equations relate to the fiber failure mode. For infinitesimal strains $S_\varepsilon' = S_\varepsilon$ so that $A_2 = A_4$, and the unknowns reduce to 5. The equations above can be solved in sets of two (7.25 & 7.26), (7.28 & 7.29) to yield all the unknown coefficients explicitly.

There is physical meaning attached to each term. The A_2, A_4 terms represent energy terms that govern the distortional failure criterion. The A_{11}, A_{55} terms are the energy terms that govern the dilational failure criterion. The A_1, A_5 terms consider the difference between the tensile and compressive strengths of the material. These are zero when tensile and compressive failure strains are equal.

The two resulting ellipses for failure are superposed, with the overlapping region describing the intact condition whilst a damaged but yet not completely failed lamina might exist within a laminate for the intermediate region between the matrix failure and the fiber fracture envelope.

Christensen's work is motivated from different reasoning but leads to a remarkably similar form. He addresses the issues in two ways. One approach is somewhat similar in principle to Hart-Smith's premise in where it is argued that the number of (strength) parameters necessary to describe failure is related to the number of independent material

properties necessary to fully describe the elastic properties of the system [113]. More specifically, the five elastic properties of idealized transverse isotropy are actually an approximation to the nine properties form for orthotropy. These average macro-properties are in turn an approximation to the micro-scale properties which control behavior. The idealization of transverse isotropy can be taken one step further by reducing the 5 elastic constants to 4, for a sub-class of transverse isotropy still applicable to typical polymeric composite fiber / matrix composites. There exist six distinct sub-classes of transverse isotropy which can occur on the possible path to isotropy (described by 2 independent constants). A reduction to isotropy requires:

$$a_{11} = a_{22}$$
$$a_{12} = a_{23}$$
$$a_{66} = \frac{a_{22} - a_{23}}{2}$$

(7.30)

These can be subdivided into:

(i) Isotropy of extensional effects

(ii) Isotropy of Poisson's ratio effects

(iii) Isotropy of shear effects

(iv) Combinations of the above

Total isotropy is confirmed when the first 3 conditions of (7.30) are met. The case of importance for typical fiber composites is the isotropy of Poisson's ratios effects.

In practical terms, the outcome of Christensen's analysis provides the following expressions which are extremely helpful in estimating out of plane properties for cases where no further data is available.

319

$$v_{23} = v_{12}\left(\dfrac{1 - v_{12}\dfrac{E_{22}}{E_{11}}}{1 - v_{12}}\right) = v_{12}\left(\dfrac{1 - v_{21}}{1 - v_{12}}\right)$$

(7.23)

Other forms of the same relation are obtained by employing the identities between

properties for general transverse isotropy (7.4)-(7.7). Such alternate forms are given by

$$G_{23} = (1 - 2v_{12})k_{23} = \dfrac{(1 - v_{12})E_{22}}{2\left(1 - v_{12}^2 \dfrac{E_{22}}{E_{11}}\right)}$$

or

$$\dfrac{2v_{12}k_{23}}{k_{23} - G_{23}} = v_{12} + \dfrac{1 - v_{12}^2 \dfrac{E_{22}}{E_{11}}}{1 + v_{12}} = 1$$

(7.24)

Christensen is by no means alone in postulating that for most practical cases 4

independent properties suffice. T.P. Philippidis and P.S. Theocaris [239] examined a novel

thermal method for extracting v_{23} and compared Christensen's formulation to their own

earlier results based on spectral decomposition of the compliance tensor, along with the

new thermal method they developed. Each of these 3 approaches yielded similar results.

Interestingly, this phenomena is not restricted to composites. Lekhnitskii [88] reporting on

the work of Russian researchers S.A. Batugin and R.K. Nirenburg (circa 1972) who

examined anisotropic rocks, presented a similar type of relation with 4 independent

constants that applied itself rather accurately in 45 out of the 47 cases examined.

Parallels can be drawn between the failure characterization of isotropic materials and transversely isotropic ones. Taking for the isotropic material a polynomial expansion of second degree on the stress tensor gives the possible failure form as

$$\alpha_1 \sigma_{kk} + \alpha_2 \sigma_{kk}^2 + \alpha_3 \sigma_{ij} \sigma_{ij} = 1$$

where σ_{ij} is the stress tensor and the α's are the failure parameters. Eliminating the possibility of failure by hydrostatic compression, this can be reduced to

$$\alpha \sigma_{kk} + \beta s_{ij} s_{ij} = 1$$

where $\alpha \geq 0, \beta \geq 0$ and s_{ij} is the deviatoric stress tensor. Thus failure can be described by 2 parameters; this associates and coordinates with the 2 elastic properties form of isotropic materials. (i.e.: For each distinct elastic property there is an associated strength.) Similarly in the case of transverse isotropy, the expansion into a polynomial form of second degree is composed of the following 7 terms.

$$\sigma_{11}, \sigma_{ii}, \sigma_{11}^2, \sigma_{ii}^2, \sigma_{11}\sigma_{ii}, \sigma_{1i}\sigma_{1i}, \sigma_{ij}\sigma_{ij} \qquad i, j = 2,3$$

This is the well known form of the Tsai-Wu criterion. With arguments taken from the second viewpoint described below, the 7 parameters form can be divided into two modes of failure under conditions of strong anisotropy. These are matrix dominated (Mode I) and fiber dominated (Mode II). Grouping the terms we have 4 containing the index (1), and 3 containing the index (i,j). The associate parameter count, totaling 7 is:

Mode I : 4 parameters

Mode II: 3 parameters

Taking an imposing physical condition of allowing failure under states of hydrostatic tension, but disallowing failure under states of hydrostatic compression reduces the parameter count for each mode by 1, leaving:

Mode I : 3 parameters

Mode II: 2 parameters

Thus there are 5 failure parameters, the same as the number of elastic properties, analogous to the case of isotropy. With reference to the approximations presented for a 4 independent constants description of the material where we have isotropy of Poisson's ratio effects, an analogous simplification to the failure criteria should be possible whereby:

Mode I : 2 parameters

Mode II: 2 parameters

A second viewpoint takes a micromechanical approach to discriminate between stresses that are, and those that are not interactive with σ_{11} on a micro-scale. Here it is pointed out with the help of the Generalized Self-Consistent Scheme that there is a very large stress concentration effect (30-40 times) in the matrix phase for the longitudinal and transverse shear cases, not present in longitudinal extension or contraction. In a relative sense there is a very energetic and non-uniform state in the matrix phase in axial or transverse shear (or transverse extension or contraction) whereas in the case of uni-axial stress in the fiber direction, there is a low energy state in the matrix. Consequently it is appropriate to adopt the hypothesis that the state in the matrix due to macro-stress σ_{11} is of insufficient magnitude to interact with the state in the matrix due to the other components of the macro-stress, even though the macro-stress σ_{11} is very large due to the

322

fiber contribution. Christensen takes this to motivate the broader point of view which distinguishes the modes of yield that involve stress component σ_{11} with other modes of yield involving the other components of stress which themselves are not interactive with σ_{11} on the micro-scale. Without digressing into derivations that are presented elsewhere [113][114] the applicable formulas are: Matrix dominated criterion, Mode I (2 parameters):

$$\alpha_1 k_1 (\sigma_{22} + \sigma_{33}) + (1 + 2\alpha_1) \left[\tfrac{1}{4} (\sigma_{22} - \sigma_{33})^2 + \sigma_{23}^2 \right] + (\sigma_{12}^2 - \sigma_{31}^2) = k_1^2$$

(7.25)

where:

$$k_1 = \sigma_{12}^r = \frac{|\sigma_{22}^C|}{2}$$

(7.26)

and

$$\alpha_1 = \frac{1}{2} \left(\frac{|\sigma_{22}^C|}{\sigma_{22}^r} - 1 \right)$$

(7.28)

The fiber dominated criterion, Mode II (2 parameters) is:

$$-\alpha_2 k_2 \sigma_{11} + \tfrac{1}{4}(1 + 2\alpha_2)\sigma_{11}^2 - \frac{(1 - \alpha_2)^2}{2} \left(\frac{\sigma_{22} + \sigma_{33}}{2} \right) \sigma_{11} = k_2^2$$

(7.29)

where:

$$k_2 = \sigma_{12}^r = \frac{\sigma_{11}^r}{2}$$

(7.30)

and

$$\alpha_2 = \frac{1}{2} \left(\frac{\sigma_{11}^r}{|\sigma_{11}^C|} - 1 \right)$$

(7.31)

The 4 parameter failure form given above contains the restriction in (7.26) that

$$|\sigma_{22}^C| = 2\sigma_{12}^r$$

323

This restriction relating axial shear stress at failure to transverse normal stress in compressive failure can be relaxed by including another parameter in the matrix dominated form giving

$$\alpha_1 k_1 (\sigma_{22} + \sigma_{33}) + (1 + 2\alpha_1)\left[\tfrac{1}{4}(\sigma_{22} - \sigma_{33})^2 + \sigma_{23}^2\right] + \beta_1(\sigma_{12}^2 + \sigma_{31}^2) = k_1^2$$

(7.32)

where:

$$k_1 = \frac{|\sigma_{22}^C|}{2} \quad , \quad \beta_1 = \left(\frac{\sigma_{22}^C}{2\sigma_{12}^r}\right)^2 \quad , \quad \alpha_1 = \frac{1}{2}\left(\frac{|\sigma_{22}^C|}{\sigma_{22}^T} - 1\right)$$

(7.33)

Both Feng's (7.22 & 7.23) and Christensen's (7.29 & 7.32) criteria were coded into "Super Pressure - Vessel Designer" (along with Tsai-Wu) for comparative purposes.

To make practical use of the formulas seen above, the classic safety factor concept was applied to each equation set prior to translating into code. This permits the program to display failure in graphical form as a relative quantity. The screen shows miniature "thermometers" that climb up and eventually change shade as they surpass first ply failure. Chapter 8 is complete with some examples.

To illustrate the safety factor concept, Mode I failure in Christensen's theory is given, Feng's equations were treated in an identical manner. Let: R = Safety factor by which applied loading can be multiplied before causing failure.

Assuming a linear response:

$\sigma_{22} = R\sigma_{22}^*$
$\sigma_{33} = R\sigma_{33}^*$
$\sigma_{31} = R\sigma_{31}^*$ where: σ^* represents an actual stress within the lamina
$\sigma_{23} = R\sigma_{23}^*$
$\sigma_{12} = R\sigma_{12}^*$

Equation (7.32) can be expressed as

$$\alpha_1 k_1 \left(\sigma_{22}^* + \sigma_{33}^* \right) + \left(1 + 2\alpha_1 \right) \left[\tfrac{1}{4} R^2 \left(\sigma_{22}^* - \sigma_{33}^* \right)^2 + R^2 \sigma_{23}^{*2} \right] + R^2 \beta_1 \left(\sigma_{12}^{*2} + \sigma_{31}^{*2} \right) = k_1^2$$

recast as

$$R^2 \left[\beta_1 \left(\sigma_{12}^{*2} + \sigma_{31}^{*2} \right) + \left(1 + 2\alpha_1 \right) \left(\tfrac{1}{4} \left(\sigma_{22}^* - \sigma_{33}^* \right)^2 + \sigma_{23}^{*2} \right) \right] + R \left[\alpha_1 k_1 \left(\sigma_{22}^* - \sigma_{33}^* \right) \right] - k_1^2 = 0$$

$$R = \frac{-B \pm \sqrt{B^2 - 4AC}}{2A}$$

(7.34)

where:

$$A = \beta_1 \left(\sigma_{12}^{*2} + \sigma_{31}^{*2} \right) + \left(1 + 2\alpha_1 \right) \left(\tfrac{1}{4} \left(\sigma_{22}^* - \sigma_{33}^* \right)^2 + \sigma_{23}^{*2} \right)$$

$$B = \alpha_1 k_1 \left(\sigma_{22}^* - \sigma_{33}^* \right)$$

$$C = k_1^2$$

After some examination of computed results and further review of the literature, a subjective evaluation was made. Computed laminate safety factors from a pressure vessel design (drawn from the example case *gtank1.ves* presented in Chapter 8) are given in Table 7.5 and Table 7.6. The internal pressure applied is 60 MPa. Predictions from the two foregoing theories are compared with other popular criteria.

Table 7.5 Comparison of safety factor predictions from different failure criteria.

Layer No.	Material file	Angle ±	Christensen Fiber	Christensen Matrix	Feng Fiber	Feng Matrix	Tsai-Wu FPF	Tsai Matrix
1	T_1000	50	8.13	2.35	5.30	2.45	1.93	5.60
2	Kev_49	71	3.72	5.23	4.91	1.82	1.92	3.48
3	T300_520	57	4.05	5.36	3.03	9.33	2.89	5.89
4	AS4_3502	59	5.87	5.94	4.47	11.61	3.68	6.48
5	IM6_SCI	57	7.80	5.10	6.37	10.76	3.87	6.86
6	IM7_9772	56	8.74	5.66	5.95	55.30	4.60	5.38
7	P75S	49	2.47	3.76	2.40	171.31	2.32	3.27
8	P100S	42	2.71	1.38	1.52	6.89	1.93	1.38

Table 7.6 Safety factors based on maximum strain and maximum stress.

Layer No.	Material file	Angle ±°	M. Strain ε_x	M. Strain ε_y	M. Strain ε_s	M. Stress σ_x	M. Stress σ_y	M. Stress σ_s
1	T_1000	50	8.58	5.98	5.41	8.96	-14.51	5.41
2	Kev_49	71	5.12	-429.80	7.98	5.59	-1.45	7.98
3	T300_520	57	4.19	6.71	4.79	4.40	-14.63	4.79
4	AS4_3502	59	6.01	11.77	6.05	6.21	-154.05	6.05
5	IM6_SCI	57	8.00	7.64	7.59	8.14	-493.77	7.58
6	IM7_9772	56	8.94	16.3	5.61	9.06	26.87	5.61
7	P75S	49	2.57	5.51	4.35	2.59	6.13	4.35
8	P100S	42	2.71	2.73	2.02	2.71	2.33	2.02

Clearly for this loading case Feng's theory appears less capable of anticipating matrix failure. A part of this is due to the fact that the formulation is essentially 2-dimensional. In computation, layer strains are determined from layer stresses. These strains are then resolved into local material coordinates from which lamina stresses are computed via the material stiffness matrix. Compressive radial strain (out of plane) can yield a dominating influence over transverse in plane strain in the material coordinates (acting through the stiffness matrix) causing a reversal in sign of the in plane stress transverse to the fiber axis. This is evidenced in the foregoing table with the difference in sign seen on some of the safety factors as measured via maximum stress as opposed to the maximum strain criteria. V.K. Choo and D. Hull [193] have found that this compressive stress influence can delay the onset of matrix "plastic" deformation.

Feng's theory neglects out of plane strain entirely whereas the stress based theories account for it partially since the stiffness matrix used to determine the stress mixes in a contribution from the out of plane component. Feng's criteria also give some rather low

fiber failure predictions relative to the maximum strain theory. Experimental work with regard to using either Feng's envelope, Tsai-Wu, Tsai-Hill, maximum stress or maximum strain under 3-dimensional loading using pressurized tubes under combinations of axial load and torsion have been carried out by M.A. Zocher et al. [119]. In this study, ultimate failure predictions of all theories (with the exception of maximum fiber strain theory upon ignoring failures in non-critical directions) is notoriously bad. The wide discrepancies found between experiment and the mathematical envelopes are quite noteworthy and should be a sobering reminder to all who put excessive faith into the numbers being generated.

Christensen's equations for fiber failure gives results close to the maximum fiber strain ε_x, or maximum fiber stress σ_x, a good indicator. Experimental studies on pressure vessels have long shown this to be approximately the case [194][174][124]. Matrix failure predictions with Christensen's criteria are generally less conservative than the Tsai-Wu envelope but do not stray unduly far from either maximum shear strain or maximum transverse strain predictions. S.R. Swanson and A.P. Christoforou [194][191] have experimented with biaxial testing using tubular specimens and lay-ups typical of filament wound pressure vessels. Their results are in part reproduced in Figure 7.5 showing last ply failure (LPF) as predicted by Tsai-Wu, a maximum fiber strain envelope, and a maximum fiber strain envelope incorporating a non-linear shear estimate analogous to equation (7.88), section 7.5. Figure 7.6 presents Swanson's replot of data complied by T.R. Guess [124] showing the approximate correlation with maximum fiber strain theory [191], and Figure 7.7 shows the apparent insensitivity of the biaxial stress ratio upon fiber failure.
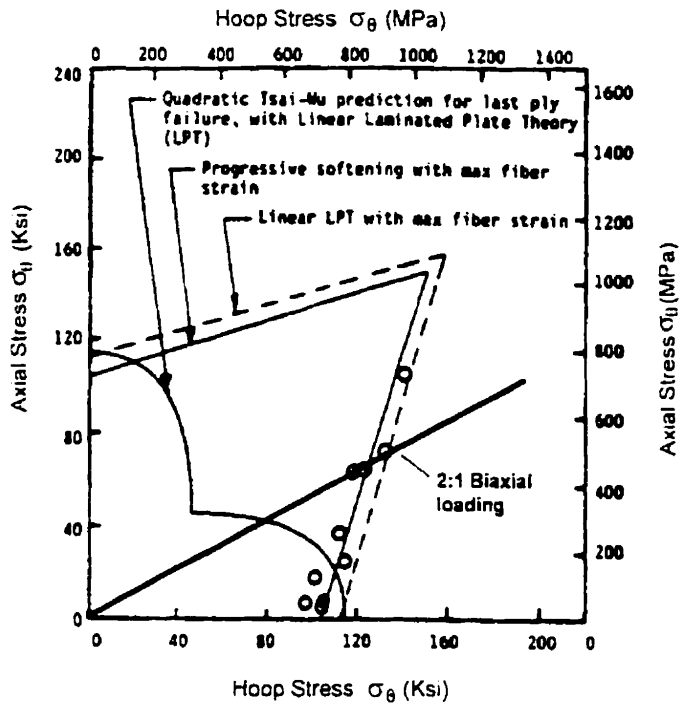
Figure 7.5 Comparison of measured biaxial failure stresses with
failure theories for [90/±45/0]ₛ AS4/3501-6. [194]
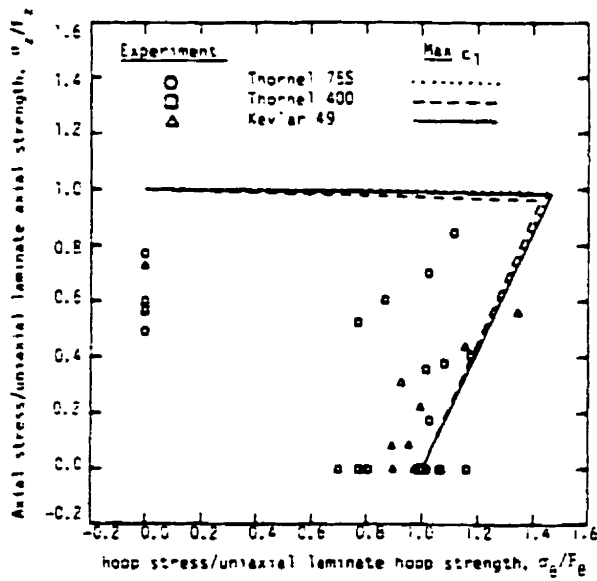
Figure 7.6 Experimental strength data for [±30/90]ₛ laminates [191].
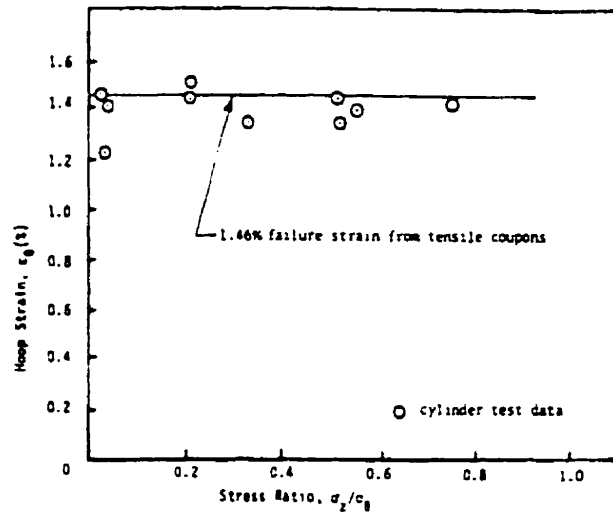
Figure 7.7 Measured failure strain of [90/±45/0]$_s$
AS4/3501-6 under biaxial loading [194].

Judging by the above figures, quadratic interaction fails to capture the essence. It is

perhaps a good predictor of initial failures but even this is unclear since it has also been

suggested by none other than HT. Hahn, J.B. Erikson and S.W. Tsai [195] that a better

predictor of matrix failure is

$$F_2\sigma_2 + F_{22}\sigma_2^2 + F_{66}\tau_{12}^2 = 1$$

Where: F_{ij} are the standard Tsai-Wu theory strength parameters.

This equation is the basis for the right-most column in Table 7.5. The results appear not

too dissimilar from Christensen's matrix failure predictions in many cases.

Swanson and co-authors have gained a clearer understanding and sum their

experience: "On the whole one must differentiate between laminates and test conditions

where matrix failure coincides or leads to ultimate laminate failure, and those conditions

where matrix failure merely tends to redistribute the stresses within the plies. The latter

329

case is often referred to as fiber dominated. In general, tests in which matrix failure coincides with ultimate failure appear to be reasonably well modeled by the Tsai-Wu polynomial or perhaps modifications suggested to it by Hahn, Erikson and Tsai." .... "On the other hand previous results also seem to suggest that laminate failure due to fiber failure is not well modeled by the Tsai-Wu quadratic formula." They give many examples from studies other than their own to support these conclusions.

In this author's opinion the method put forth by Christensen may be a better predictor both for the onset of matrix cracking and fiber fracture. It should also be pointed out that the "Super Pressure - Vessel Designer" source code contains the Tsai-Wu failure envelope equations, as well as Feng's and Christensen's. Results from all three can and have been used to evaluate failures but Christensen's may well be the most representative. Such a determination remains a subject for experimental studies of the future. As a measure of simplicity, the analysis in Chapter 8 is based on the Christensen criteria, but a change in compiler directives can invoke Feng's or Tsai-Wu since the procedures remain present in the code.

To recap the forgoing discussions, it should be made clear that this design program makes an attempt to go beyond a linear analysis into the murky region of gradual matrix failure. For high pressure vessel designs, proof testing takes place, often far past the realm of first ply failure. To this end the matrix failure criteria mark the beginning of a highly nonlinear process that persists with further pressurization until a Mode II failure (fiber fracture) occurs. Although dependent on vessel wall construction, the event of matrix damage is unlikely to precipitate catastrophic failure, but it will certainly lead to a

substantial change in the internal stress distribution of the wall layers, something one cannot anticipate from linear elastic design. Upon unloading the damage remains and the elastic response in subsequent loading cycles is affected. It would be desirable to have trustworthy and proven failure criteria, especially equations derived from a full 3-dimensional perspective. Unfortunately the art is not well enough advanced presently to encompass these wishes so one can at best proceed on the basis of the most recent findings.

The next section describes in further detail the experimental / theoretical background and equations used to assess laminate damage level as a function of loading past initial failure.

7.3 Damage Modeling

The quest to ascertain what is happening inside a "failed" lamina and how it affects the continued existence or catastrophic destruction of the whole laminate is a continuing one. Few subjects are as confusing and complex. The search for answers has lead to voluminous publications, few if any definitive methods useful to the designer exist as of yet.

Exploitation of laminates past the onset of matrix failure can be quite rewarding. Typically as little as one-third the strain potential is being used for the case of designs based on first ply failure theory. Early on it was recognized that the reduction in stiffness of laminated composites containing failed layers was a *gradual* process. Failure however is a subjective term. While matrix cracking may be an important event in the structural

integrity of the laminate, it is still quite different than fiber failure. It is ultimately for the designer to decide what level of failure can be tolerated. Researchers H.T. Hahn and S.W. Tsai [196], studying the behavior of laminates after initial failure, proposed a simple bilinear theory whereby stiffness reductions were modeled on the basis of a rule of mixtures approach to failed and yet un-failed portions of the lamina. Efforts in the field have since seen a multiplicity of approaches from fracture mechanics studies to intensive computer methods including simulation of crack initiation and growth in laminates with specified layups. Nonetheless it must be remembered that much modeling is based on linear assumptions, although the post damage behavior of the constituent materials is often highly non-linear.

A particular case in point, and a fact often questioned by the uninitiated, is that at first glance containment of pressures exceeding the uniaxial transverse compressive failure stress of a lamina appears patently impossible. Obviously this is erroneous, for in reviewing the development work presented in Chapter 2 there have been many well documented cases of ultra-high pressure composite vessels far exceeding this imagined limit. The stress-strain behavior of angle ply Kevlar$^{\circledR}$ laminates in compression along the thickness direction, documented by A.A. Fahmy [197], reveals how this is possible. For his study 1000 ply thick ($5'' - 5\frac{1}{2}''$ or 250 -275 mm) $\pm$ angle laminates were constructed, cut into rectangular specimens and subjected to compressive tests. One such result is shown in Figure 7.8. Although uniaxial compression tests produced a matrix dominated shear failure in expectation with uniaxial lamina strength predictions, a highly non-linear
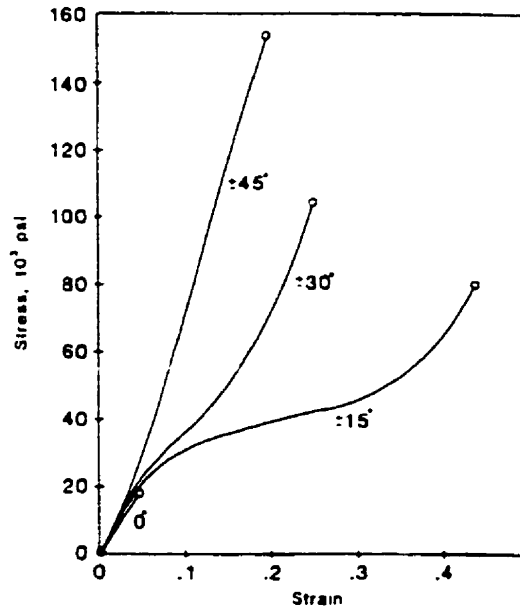
Figure 7.8 Through-thickness compressive properties
of angle ply Kevlar® lay-ups [197].

behavior emerges whereby the mode of failure shifts from matrix to fiber dominated as the

lamination angle progresses from unidirectional to cross-ply.

In fact, for the cross-ply failing at an incredible 154,000 psi (1062 MPa),

destruction was explosive with sideways ejection of plies. Undoubtedly had the test

specimen taken the form of a cylinder, higher pressures still would have been achieved.

The micrographic evidence showed a transverse collapse of the fibers into a ribbon like

state, with modulus loss and ultimately a gain in transverse stiffness highly dependent on

the laminate's orientation angle. From Figure 7.8 and the experiences related in building

50,000 psi containment vessels found in reference [45], it is evident that in exercising

construction techniques aimed at limiting fiber rotations which instigate the drastic loss of

through-thickness moduli, stable "radial compaction" can place in the 20,000 to 35,000

333

psi (138-241 MPa) range. Clearly such behavior is important and adds yet more confusion to the picture emerging for damage occurring as result of simple in-plane loading.

Present three dimensional constitutive theories are based on linear elasticity [190] and hence have no ability to model effects such as the one described above. The best one can hope to achieve at this point is to draw as much knowledge as possible from (tensile) in-plane damage theories and apply it. To this end it is pertinent to review briefly some of the studies that have been considered while broaching the subject of modeling damage. Discussion of particular model details is beyond the scope of the present treatise however a qualitative feel for the ground that has been covered is deemed important in light of the post first ply failure analysis presented subsequently.

The major damage that develops in laminates under static or cyclic loading is in the form of interlaminar and intralaminar cracks. The former develop in between plies mainly during the final destruction phase of the laminate. The latter appear earlier on and quite suddenly, in large numbers within plies where the stresses have reached a critical value, defined perhaps by the first ply failure criteria of the ply. These are families of cracks in the fiber direction (but usually transverse or inclined to the principal load direction) and their macroscopic effect is a reduction of the in-plane stiffness of the laminate. The analysis of stiffness reduction has seen repeated attention, but the complexity of the matter has in large part limited the analytical treatments to cross-ply laminates of the $[0_m/90_n]_s$ configuration in which only the 90 degree plies are cracked. The main methods of analysis employ some variant of shear lag theory (1-2-3 dimensional), self-consistent approximation schemes to assess ply stiffness reductions in conjunction with classical

334

laminate analysis, or variational (energy) methods. Other approaches are classic fracture

mechanics, non-linear viscoelastic analysis, internal state variables (thermodynamic basis),

or general boundary value problem solutions for special crack geometries (both analytical

and via finite elements). The methods used overlap but each have be shown to coincide at

some level with experimental data.

Z. Hashin [198] used a variational approach to show how transverse laminate

stiffness and Poisson's ratio varies with increasing crack density for combinations of

transverse and longitudinal cracks in two different cross-ply layups for glass and graphite

epoxies. The solutions are lower bound. His derivations also provide numerical estimates

on the magnitudes and distribution of out of plane and interlaminar shear stresses

$\left(\sigma_z, \tau_{xz}, \tau_{yz}\right)$ which is unique to this method. Unfortunately, as with many techniques,

crack density is a requisite input parameter and the solution derived is limited to the [0/90]

layups examined.

G. Devorak and N. Laws [199] favor a fracture mechanics approach. Their studies

brought forth that the mechanism of cracking between thin and thick plies is different.

Thin plies tend to propagate transverse cracks which are parallel to the fiber axis and grow

through the thickness (T) direction of the lamina, whereas thick plies also show crack

growth on planes that are perpendicular to the midplane of the ply and can be described as

running longitudinal (L) slit type cracks following the fiber axis. Clearly a crack can extend

either in the (T) or (L) direction or simultaneously in both. The corresponding energy

release rate or alternately toughness can be expressed as $G_c(T)$, and $G_c(L)$ with critical

crack widths $\delta_c(T), \delta_c(L)$, etc. It is estimated that the Mode *II (longitudinal shear)* to

Mode I *(transverse tensile)* fracture toughness ratio is $^{K_{IIc}}/_{K_{IC}} \cong 5$ in typical laminates. For

mixed mode fracture, as takes place within a lamina, the difference in toughness values for

both (L) and (T) type cracks is not as severe between each mode, and it is estimated that

$\delta_{IC}(T) < \delta_{IC}(L)$ by about a factor of two. Therefore, because it is energetically favorable,

first ply failure in thick plies occurs as a result of type (T) cracking followed by type (L)

cracking. In thin plies the through thickness dimension falls below the critical value and

hence the strength becomes related only to the onset of unstable type (L) cracking, much

as the strength of a thick ply was related to type (T) cracking. The transition was found to

occur at 0.5 mm ply thickness for an E-glass/epoxy material with $G_{IC}(L) = 250 \, J/M^2$.

Additionally it was found that the angle of lay-ups constraining the 90° plies did not have

any great influence on the transition of strengths between thin and thick plies. Figure 7.9,

reproduced from reference [199], illustrates the limiting lower strength as ply thickness

increases. A consequent conclusion was that initial surface flaws present either due to

machining, impact or internal flaws as a by-product of manufacturing can provide seed

points for type (T) cracks and substantially lower or altogether eliminate any advantages

that thin ply construction may have in raising the initial matrix failure stress. Unfortunately

neither the absolute or even relative quantities of the fracture toughness parameters are

documented well enough to make any real design oriented use of such approaches. These

studies however do lead to an understanding of why a transition occurs between the

apparent strength of finely dispersed plies as opposed to thicker lamina lay-ups.

An earlier study by D. Flaggs and M. Kural [209] found a weak relation between

the orientation angle of the ± constraining layers and the strength enhancement effect

these layers lent to the transverse plies. The [0/90] type layups showed the greatest

enhancement effect while [±30/90] and [±60/90] constructions had somewhat milder

enhancement effects respectively for any given transverse ply thickness. However as

expected, with transverse ply thicknesses progressing from one to 8 layers (1 mm), the in

situ strengths dropped by approximately a factor of two, and for the eight layer case were

only 13% higher than for a unidirectional sample.
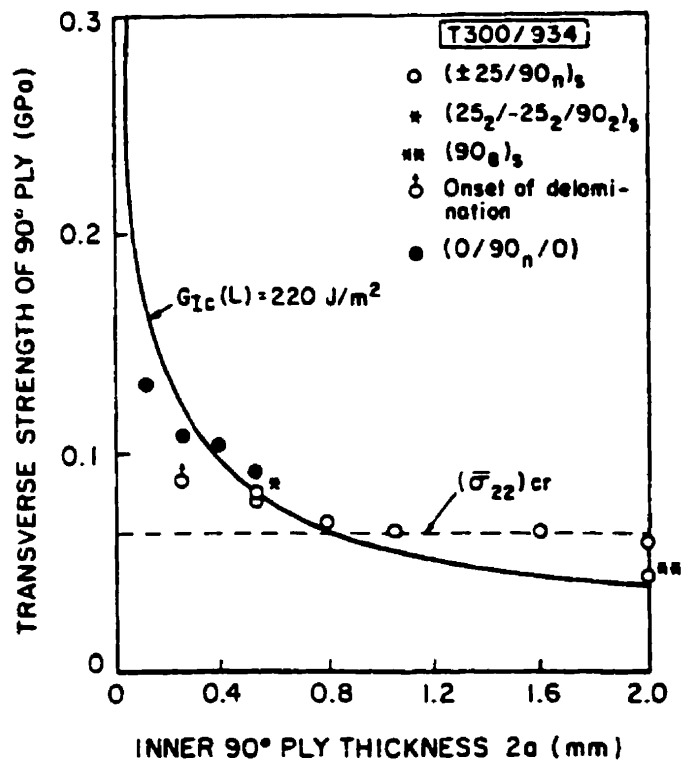
Figure 7.9 Strength vs. ply thickness [199].

Further analysis and testing by Flaggs [192] looked at mixed mode fractures in

laminates of the $[0_2/\pm\theta]_s$ variety where lamination angle θ took values of 70, 80 and 90

degrees. It was pointed out that one-point stress failure theory such as the Tsai-Wu

337

criterion and others were underestimating and entirely inadequate in modeling the failure process responsible for tensile matrix failure, especially in the finely interspersed lay-ups examined.

Quite early on investigators had realized that crack spacing tended to be quite uniform but also strongly dependent on the thickness of the transverse layers undergoing this damage [201]. For instance in glass laminates (which are easier to study because of their transparency) crack initiation occurs at about 0.4% strain, whilst at 0.8% strain it was found that the crack patterns stabilized to a remarkable uniformity, and also that initiation sites concentrated where fibers were nearly or actually in contact or in areas fraught with voids. These same investigations correlated the onset of acoustic emissions with transverse microcracking and also showed that just prior to delamination and complete failure, the transverse cracks were beginning to penetrate the adjacent plies and starting to branch out at ±45° from ply interfaces, following the fiber directions in adjacent plies. It was also determined that the crack spacing approaches an apparent lower limit commensurate with the thickness of the constrained ply. The crack spacing saturates as the interfacial shear strength across the layers is broached which leads to extensive delamination and hence an altogether new mode of failure, generally catastrophic.

Concerning acoustic emissions, it should be emphasized that there does not yet appear to be any great success in differentiating between intralaminar and interlamina cracking with acoustic techniques, however recent studies have shown it is capable of assessing quite conclusively whether prior impact damage exists within pressure vessels (using a proof test depressurization cycle) and specific test guidelines have been published.

Low frequency "friction" waveform signatures have been identified that can be correlated to the presence of impact damage in such tests [202][203].

The concept of a Characteristic Damage State (*CDS*) was introduced by K.L. Reifsnider and co-authors. This effect is now recognized widely and researchers have accepted that damaged laminates will always tend towards a lower bound of the transverse crack spacing, characteristic of the material and lay-up.

Over the years many closed form solutions to the crack spacing in terms of applied load and lamina properties have been derived. This in turn allows the prediction of reductions in transverse stiffness. Many of the models are based in one form or another on shear-lag theory with additional parameters like probability density functions for strength or assumed stress distributions between adjacent cracks determining the onset of subsequent cracks. Simpler solutions employ only specimen geometry and shear moduli rather than a full fracture mechanics approach to the "first ply failure stress" so they do not depend on evaluations of the energy release rate of the lamina [204]. Although such approaches are helpful, the analysis tend to be geometry specific and the procedures requires an integration for every load increment. A useful feature of at least one such simplified method, presented in reference [204], is that it could lend itself to modeling fatigue damage accumulation given *S-N* curves for the constituent plies as input.

A concept analogous with classical fracture mechanics is the use of a resistance curve (*R*-curve) where the curve represents the composite's resistance to transverse crack initiation, multiplication and growth [205][206]. It was found that such curves are basically independent of the stiffness of the constraining layers, especially if the thickness

ratio of the 90° layers to the constraining layers remains constant. Such approaches have been applied to predict crack growth and stiffness reductions [206].

One advantage of fracture mechanics based models is that the matrix toughness effects can be seen reflected upon predictions of the stress levels necessary to cause changes in transverse properties such as Poisson's ratio for damaged laminates, and that this limit is far higher for the toughened matrix material [208].

Some model refinements that have proven useful to the shear-lag type analysis are inclusion of a separate interlaminar shear layer (resin rich area) [209] and accounting for the effects of built in thermo-elastic stresses resulting from the cure process, especially as concerns graphite-epoxy laminates. Useful test methods for estimating thermal stresses experimentally are via antisymmetric lamina curvature changes during cooling and such measurements can be used in conjunction with these models. Details describing one technique are available in reference [209]. N. Takeda and S. Ogihara [210] have employed a novel method to test for residual thermal curing strains in laminates without resorting to special layups. They call the technique the "ply separation method". A sample cut from the symmetric laminate is ground on one face to remove a layer and the resulting curvature is measured in order to back-calculate the residual strains. With either method it turns out that the strain values are only about one half those predicted using published thermal expansion coefficients and curing temperatures. This is expected since the resin gelation point is a key factor determining the zero stress temperature, however in practice difficult to determine other than by actual testing.

P. Gudmunson and S. Ostlund [211] have shown results pertaining to both thin and thick laminates under a *dilute* crack density assumption (crack stress fields do not interact with another). Their calculations, derived on the basis of elasticity theory, are formulated using the change in elastic energy of a laminate with the appearance of a crack to arrive at a stiffnesses reduction matrix described by a dimensionless crack density η_k. The resulting stiffness reduction matrix constituted of α_{ij}'s is solved for. Solutions to the cracked geometry stiffness have also been obtained by finite element modeling of laminates with layups $\left[(\theta, -\theta)_n \right]$ typical of filament winding. One of the most interesting revelations being that for both the glass/epoxy and AS4/3502 graphite materials studied, the $\pm$ lay-up angle played little role in the relative stiffness change due to cracking when normalized against a cross-ply arrangement undergoing the same cracking. Figure 7.10 is reproduced from reference [211] to illustrate this finding.
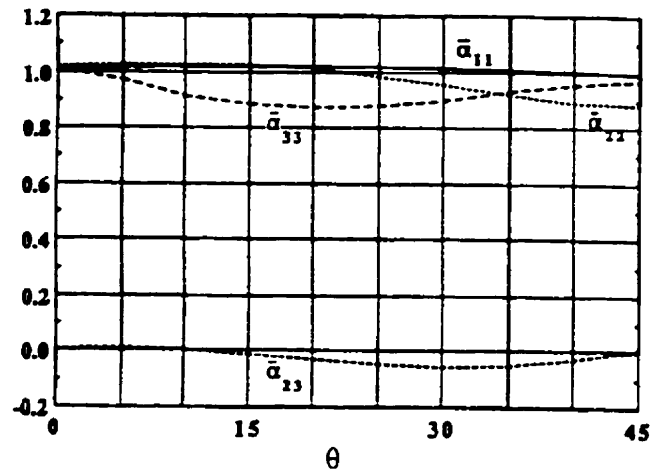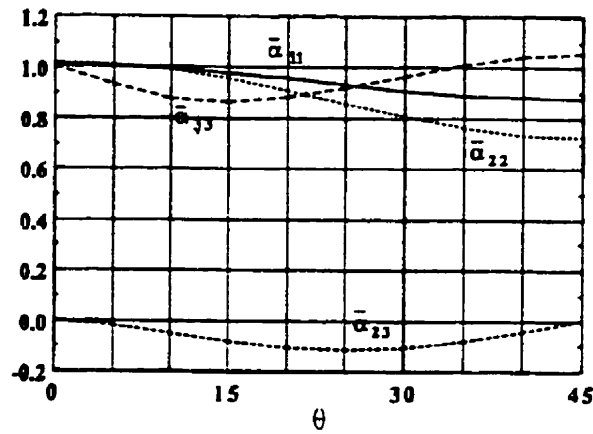
Figure 7.10 Normalized coefficients $\bar{\alpha}_{ij}$ as functions of the ply angle θ for an internal matrix crack in a GFRP (a) and CFRP (b) $\left[(\theta,-\theta)_n\right]$ laminate [211].

The relatively small variations in $\bar{\alpha}_{ij}$ lead to the conclusion that if an average value is chosen, the maximum error in stiffness reduction predictions is on the order of 15% for any angle. This certainly simplifies predictions where high accuracy is not needed. Even though a dilute approximation was made, applying up to about $\frac{1}{2}\eta_k$ (half the saturation

crack density), a non-dilute analysis using a finite element calculation for each individual crack was also performed and showed similar results.

S.R. Swanson and B.C. Trask [212] carried out experiments on quasi-isotropic tubular specimens in measuring and modeling the development of matrix cracks in the absence of the free edge effect. They also noted that in their tubular laminates, delivered fiber strains at failure were very close to fiber strains at failure in unidirectional coupon tests where no transverse matrix cracks existed.

R.J. Numiser and S.C. Tan [213] developed a model for a cracked composite lamina subjected to general in plane loading (as opposed to uniaxial loading) and their elasticity formulations showed that the cracked lamina compliances were dependent on the laminate within which the damaged ply is contained. The effects were more noticeable for shear moduli when compared to a self-consistent (laminate independent) model. This partly contradicts other researchers who claim the dependence on the constraining layers is weak.

Many matrix cracking models are based on some type of shear-lag theory. Unfortunately one must then assume an adjustable shear-lag parameter. Laws and Devorak [214] proposed a method for extracting this parameter given the fracture toughness G_c, first ply failure stress, thermal curing stress, elastic moduli and some geometric parameters defining the layup.

An Internal State Variable (ISV) approach is described by J.W. Lee and co-authors [215] to arrive at a damaged stiffness matrix for cross-ply layups. Essentially the (ISV) is a quantity which represents the contribution of the crack opening displacement to the

343

observable strain which can be measured from a specimen with matrix cracks under uniaxial tensile loading. The equations however need crack spacing as an input parameter, a quantity not readily available from a design point of view.

From an experimental perspective, J.W. Hoover et al. [216] performed a remarkably detailed study of crack development under slow loading for glass fiber composites of varied lay-ups. They identified 3 distinct stages of stiffness reduction. The first stage occurred *before* any transverse cracks appeared and was unexpected because stiffness degradation was thought to result from transverse cracks. The effects were attributed to presence of residual strains which may relax and subcritical damage that occurs at around 0.2% to 0.3% strain. The subcritical damage was postulated to occur in two forms: Microcracking and microdebonding. Microcracks are small cracks in the matrix that consolidate at higher strains to produce transverse cracks, microdebonding is the separation of the fibers and matrix. The first observable damage occurred in stage 2 where there was a region of linear stiffness reduction that continued until the crack density reached values of 0.5 cracks mm^{-1}. This feature of the stiffness reduction curve occurred over the greatest range of crack densities and continued up until reaching the Characteristic Damage State (*CDS*) providing such a state was attained. For some laminates this was not fully achieved. The stage 3 reduction is identified by a large decrease in stiffness at a high crack density. The effect is evident with laminates having ±25° and ±45° constraining layers where for very small changes in crack density there occurs a tremendous stiffness reduction. Consequently there develops constraining ply cracking, delamination and fiber failure. In this region transverse cracking is not the only

damage mode and the transverse crack density does not represent the amount of accumulated damage therefore should not be used to model a stiffness reduction. It can be labeled the final (catastrophic) failure region.

A recent experimental study on crack growth in *quasi-isotropic* laminates by J. Tong et al. [217] followed crack development in *all* the plies. It was noted in this study that with ply thicknesses greater than 0.5 mm the transverse ply failure strain appears to be approximately constant for laminates of different lay-ups and similar to the transverse failure strain of a unidirectional lay-up, after the thermal curing strains had been taken into account. Although the exact initiation point for transverse cracking was slightly different between cross-ply and quasi-isotropic lay-ups, the form of the curves plotting crack density with strain show remarkably similar character. This important concept will be revisited later. Figures 7.11 and 7.12, reproduced from [217] illustrate some detail.
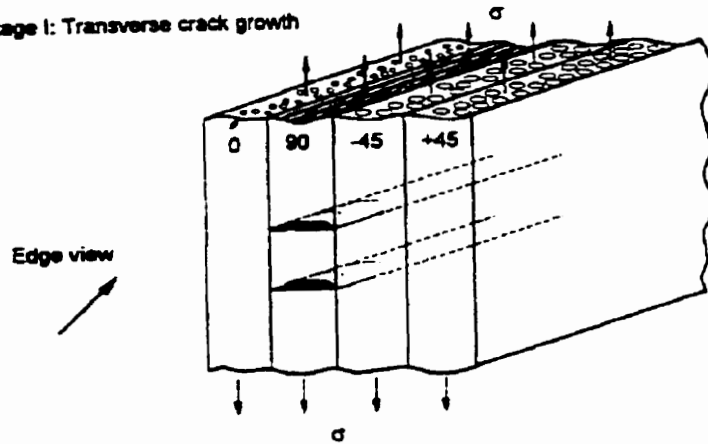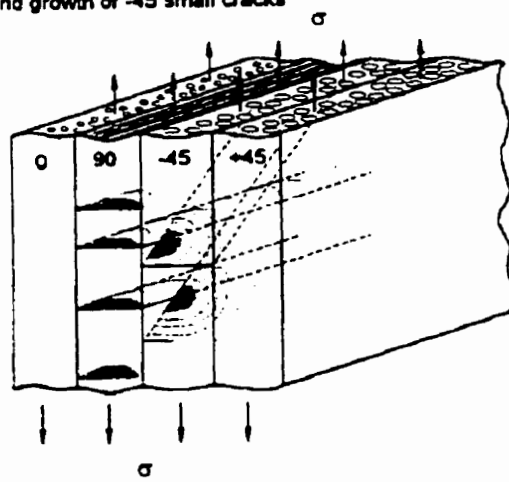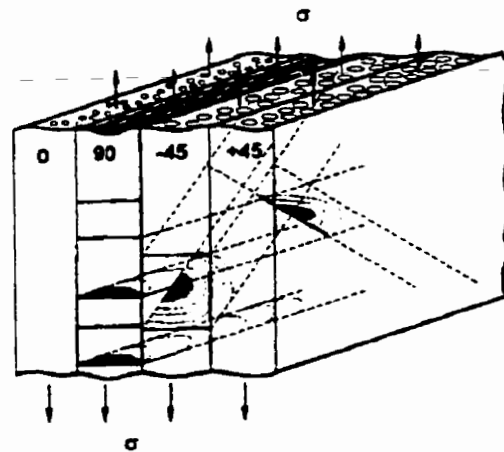
Figure 7.11 Crack growth process from transverse to off-axis plies [217].
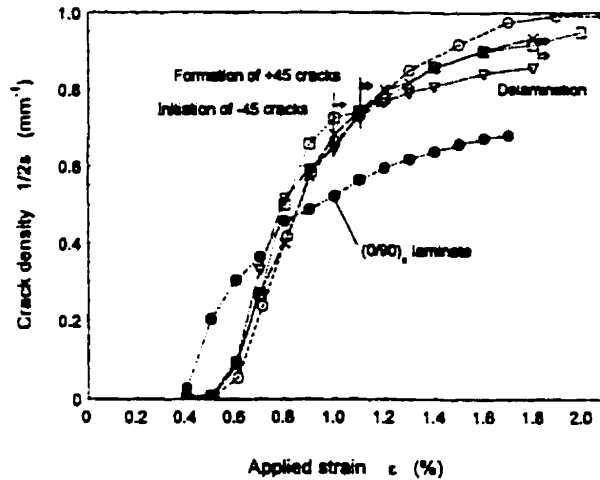
Figure 7.12 Crack density vs. applied strain for cross-ply & quasi-isotropic lay-ups [217].

The existence of a crack saturation effect or Characteristic Damage State (CDS) has long been seen to exist, however it is not always fully developed before the laminate destructs due to fiber breakage or massive delamination. The precise mechanism underlying its development has been the subject of debate. One explanation, put forward by J.F. Caron and A. Ehrlacher [218] is that small delaminations begin to appear at the tips of cracks between the plies at high stress levels. This stops all new load transfer by slow interface destruction and hence brings about a damage saturation phenomena. They have photographed evidence that leads to such a conclusion.

S.E. Groves et al. [219] recorded two different types of transverse matrix cracks. These are straight cracks and curved cracks including partial angled cracks. It was determined that these appeared in a particular order (straight first) and subsequently the straight cracks were flanked by the curved variety. The straight cracks appeared suddenly (brittle type fracture) while the angled cracks came about later and were always located

347

nearby. A curved crack is a matrix crack that initially forms as a partial angled crack and grows towards the straight crack, often joining up at the middle with another to form a curved crack. Because the growth rate of these partial angled cracks is much slower than that of the straight crack, a ductile fracture mode is suggested. The authors explained the process from the point of view of local stress distibutions in the vicinity of the straight cracks and used finite elements to verify. However the saturation effect may also be related to a phenomena whereby the fracture mode appears to be slowly changing to one with a slightly more ductile character as the strain level increases. The appearance of curved cracks was very pronounced for thick transverse plies yet practically non-existent for finely laminated lay-ups. Figure 7.13 illustrates schematically.

Schematic of the matrix crack pattern in a
[0/90₂]ₛ laminate
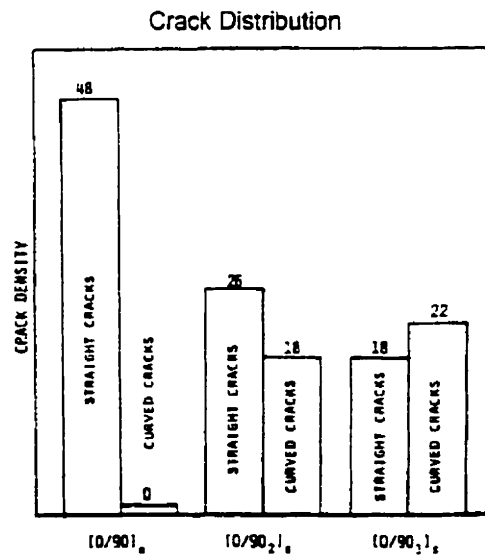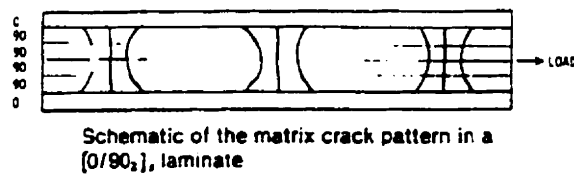
Figure 7.13 Crack patterns and distribution with increasing ply thickness [219].

348

V. Kominar and H.D. Wagner [220] studied the effects of using flexibilized resins to elevate the strain levels seen at first cracking. An interesting fact reported is that changing the resin flexibility from 2% to 70% (35X) results in an increase of first damage strain from .2% to 1% (5X) for a unidirectional glass laminate. However for a complex lay-up the translation into improved laminate strains is far greater than what would be expected on the basis of uniaxial tests. Conversely the interfacial bond strength suffers greatly with flexibilized resins and results in an earlier appearance of non-linearity in the stress-strain curve along with stress-whitening. This lowers the transverse stress at which debonding begins and there is also more debonding prior to cracking and failing. Naturally such resins are also limited to a lower service temperature.

Most of the modeling to date has concentrated on transverse stiffness predictions, and some authors have noted that few if any reliable experimental data appears available to test predictions for shear modulus reductions due to transverse ply cracking [200].

The most primitive of modeling techniques for laminates having experienced first ply failures is the "ply discount method". Obviously, and with reference to the studies mentioned above, this approach is very conservative, and can at best predict the sequence of *first ply* failures in the laminate, however is near useless to estimate *ultimate* properties. S.W. Tsai in his composite design series texts [174][176] advanced the notion of using a matrix and fiber degradation factor along with a modified form of the quadratic interaction criterion to enable an estimation of the sequence of events leading to failure and also the final failure load. The concept of the matrix degradation factor is based on the *CDS* described earlier and can be taken as meaning that macroscopically approximately 15% of

349

the matrix moduli is retained in the damaged state. With fiber breakage in a layer, only 1% of fiber stiffness is retained. These matrix and fiber factors are then entered into semi-empirical micromechanics equations to result with transverse stiffness predictions for composite moduli E_{22}, G_{12}, in plane Poisson's ratio v_{12} and so forth. Axial compressive strength is also modified on the basis that the fiber looses support from the surrounding matrix and this is termed "loss of the foundation shear modulus". The best fitting matrix degradation factors vary with the lay-up and materials of construction and optimal values range from 0.02 to 0.30. Table 7.7, a summary of matrix degradation values taken from S.W. Tsai's design text [176], shows that these empirical factors encompass a wide range.

Table 7.7 Matrix degradation factors [176].

Material	Lay-up	Permissible Range	Recomended Degradation Factor
T-300/5208	[0/90]	0.0 - 0.40	⇓
T-300/5208	[0/90$_2$]	0.0 - 0.40	avg: 0.20
T-300/5208	[π/4]	0.07 - 0.34	
T-300/5208	[0$_2$/±45]	0.16 - 0.47	⇑
AS/3501	[0/90]	0.0 - 0.40	0.20
IM6/epoxy	[0/90]	0.0 - 0.20	0.10
Boron/5505	[0/90]	0.0 - 0.60	0.30
AS/Peek	[0/90]	0.0 - 0.20	0.10
E-glass/epoxy	[0/90]	0.0 - 0.14	0.065
Kevlar/epoxy	[0/90]	0.0 - 0.04	0.020

The post first ply failure evaluations can take place in an iterative loop or directly in a single step provided one is willing to forego some detail on the sequence of events leading to rupture. The concept is simple enough to use but also suffers in many regards, not least of which is the failure criterion. Hart-Smith [185] was very critical, but rightly noted that the interaction criterion being used for this progressive failure analysis

350

effectively eliminates the interaction term F_{12} once the matrix "degrades". Also failure plot

anchor points are affected by this process. To paraphrase his concerns: Effectively the

criteria becomes non-interactive and the contribution of matrix dominated terms is

suppressed in order to accentuate the fiber contribution. The technique is a subtle path

towards applying separate failure envelopes, one matrix dominated, the other fiber

dominated and in the limit this approaches maximum stress / maximum strain theory.

Nonetheless the present author believes that the overall degradation modeling

advanced by S.W. Tsai et al. is well enough founded to warrant building a second

generation approach for 3 reasons: Firstly, separate failure envelope theories already exist

hence there is no need to employ something that needs heavy modification in the face of

matrix damage. Secondly, Tsai's design approach to assigning a matrix degradation factor

was drawn in part from early (1980) fatigue tests conducted by A.L. Highsmith and K.L.

Reifsnider [221]. Later it was updated by work drawn from his (1992) Ph.D. student who

was modeling the damage process and Characteristic Damage State limit properties. It is

documented that crack patterns resulting from fatigue damage show a different character

than those obtained under monotonic tensile loading [217]. More recent models have been

proposed which quantify the expected state of damage developed at any point during the

damage process without knowledge of the crack spacing apriori, so there is a stong

incentive to move past earlier techniques. Thirdly, fully analytical micromechanics models

are well developed and have been shown to give accurate predictions of 3-dimensional

properties. There is little need to go through an intermediate step of assigning a "degraded

matrix property" whilst the damage models are predicting some of the laminate stiffness reductions directly.

From this rationale a revised post first ply failure computation was developed for predicting the laminate response and the results incorporated into the code of "Super Pressure - Vessel Designer". Details are presented in the following section.

7.4 Post First Ply Failure

Much of the information that has been gained in the area of damage modeling remains disconnected. Few models exist that predict crack density from loading and thereby estimate the damaged moduli, rather most techniques rely on an input of crack density to establish the damaged moduli. Full 3-dimensional damaged property characteristics are even harder to ascertain. One facet the research has brought forth is that within a class of lay-ups and material the development of transverse cracks and the commensurate softening of certain moduli follows a defined pattern which is not sensitive to details in construction. The postulated Characteristic Damage State (*CDS*) is in part evidence of such a trait. One particular researcher who has tried to draw together certain aspects, in a manner of normalizing such data, is Luo-Yu Xu. In a series of papers [222][223][224][225][226][227] presented over the past few years an attempt has been made at compressing his own data and that of other researchers into an "equivalence" form such that a wide range of tests from disparate sources can be treated. This author calls the normalized resultant quantity an "equivalent residual lamina stiffness", which is in

turn based on the concept of "equivalent crack density" and "equivalent applied loading".

Amongst all the models and techniques reviewed, the above method with some

adaptations was chosen for implementation. Key reasons for this choice are:

1) The concept is general and does not rely entirely on specific lamina lay-ups or

materials although it can be refined by including crack growth data from particular

laminates and may also use fracture toughness results to improve accuracy.

2) Crack spacing needs not be known apriori, since their formation can be

estimated directly from the loading.

3) The equivalence concept allows use of data from many published sources.

4) A small database of test results using various materials and laminate

constructions has already been analyzed and compressed into useable form.

5) Application is through a one-step process, requiring no stepwise integration to

sum on a crack by crack basis, so computational time becomes insignificant.

The concept is developed briefly below.

It is assumed that the growth of transverse matrix cracks is related not only to the

cracking stress state but rather governed by distributive initial defects. Therefore strictly

analytical models are insufficient and probabilistic methods are employed instead. For

simplicity we assume that in a brittle matrix the initiation of transverse cracks can be

simulated by some distribution of effective flaws. The size or length of these effective

flaws is of an unknown distribution and their maximum and minimum value are a_{max} and

a_{min}. A non-dimensional variable, the *"equivalent crack length"* a_{eq} is defined to describe the range of possible values.

$$a_{eq} = \frac{a - a_{min}}{a_{max} - a}$$

$$(7.35)$$

From linear elastic fracture mechanics we have an equation of the form

$$G_{IC}^{MC} = \zeta \sigma^2 \pi a$$

$$(7.36)$$

where G_{IC}^{MC} represents the intralaminar fracture toughness (transverse matrix cracking), ζ is a geometry parameter and σ the applied stress. The equation can be cast in terms of applied strain ε rather than stress, whereby the critical flaw length a is expressed in the form.

$$a = \frac{\zeta_M \zeta_S}{\varepsilon^2}$$

$$(7.37)$$

Here ζ_M represents a material parameter, ζ_S is a structural parameter. The material parameter stays constant for different laminates constructed of the same material under the same cure process, and can be considered a property just as Young's modulus, etc. The structural parameter can vary from one cracking state to another in the same laminate. Substituting the form (7.37) into equation (7.35) yields

$$a_{eq} = \frac{\dfrac{\zeta_M \zeta_S}{\varepsilon^2} - \dfrac{\zeta_M \zeta_S^{CS}}{\varepsilon_{CS}^2}}{\dfrac{\zeta_M \zeta_S^{Cl}}{\varepsilon_{Cl}^2} - \dfrac{\zeta_M \zeta_S}{\varepsilon^2}}$$

$$(7.38)$$

354

As the loading is increased a small population of large pre-existent flaws form the first cracks. As these initiation sites are consumed smaller remaining flaws subsequently become the origin of further matrix cracks, commensurate with increasing load.

The $_{CI}$ and $_{CS}$ notation stands for crack initiation and crack saturation respectively. Therefore a_{min} represents attainment of the saturated crack state and a_{max} is related to pre-existent defect density at crack initiation. A rearrangement and canceling of terms reduces the above to

$$a_{eq} = \frac{\varepsilon_{CI}^2 \left(\varepsilon_{CS}^2 - K_{CSS}\varepsilon^2\right)}{\varepsilon_{CS}^2\left(K_{CIS}\varepsilon^2 - \varepsilon_{CI}^2\right)} = \varepsilon_{eq}^2$$

(7.39)

where:

$$K_{CSS} = \frac{\zeta_{zs}^{CS}}{\zeta_{s}}, \qquad \text{and} \qquad K_{CIS} = \frac{\zeta_{zs}^{CI}}{\zeta_{s}}$$

Here ε_{eq} is defined as "equivalent applied loading". Another form is

$$\varepsilon_{eq} = \frac{\varepsilon_{CI}}{\varepsilon_{CS}} \sqrt{\frac{\varepsilon_{CS}^2 - K_{CSS}\varepsilon^2}{K_{CIS}\varepsilon^2 - \varepsilon_{CI}^2}}$$

(7.40)

In view of the fact that many studies have shown the structural effects to be secondary (insensitivity to constraining layer arrangement and exact location of transverse plies within laminate) one can also extend this interpretation as meaning that the variation in the structural parameter is small from initiation to saturation states. Hence $K_{CSS} \cong K_{CIS} \cong 1$. Equation (7.40) simplifies to

$$\varepsilon_{eq} = \frac{\varepsilon_{CI}}{\varepsilon_{CS}} \sqrt{\frac{\varepsilon_{CS}^2 - \varepsilon^2}{\varepsilon^2 - \varepsilon_{CI}^2}}$$

$$(7.41)$$

Considering a length of lamina L in which matrix cracks will appear, containing a total of

N_T effective flaws. At an applied loading level ε_{eq}, the number of effective flaws that will

have formed into matrix cracks is:

$$N = N_T \int_{a_{eq}}^{\infty} f(a_{eq}) da_{eq}$$

$$(7.42)$$

where $f(a_{eq})$ is the *probability density function* describing the equivalent crack length.

Normalizing (7.42) with respect to lamina length L defines the matrix crack density and

the *saturation crack density* as $D = N/L$, $D_{CS} = N_T/L$ and the equation may be restated

as

$$D = D_{CS} \int_{a_{eq}}^{\infty} f(a_{eq}) da_{eq}$$

Introducing a non-dimensional parameter, the *equivalent crack density* $D_{eq} = D/D_{CS}$

$$D_{eq} = \int_{a_{eq}}^{\infty} f(a_{eq}) da_{eq} = F(\infty) - F(a_{eq}) = 1 - F_{\varepsilon}(\varepsilon_{eq})$$

$$(7.43)$$

where $F_{\varepsilon}(\varepsilon_{eq})$ represents the *distribution function* expressed in terms of the equivalent

applied loading (instead of equivalent crack length) which can be extracted by curve-fitting

to experimental data. For example: Figure 7.14 shows a plot of equivalent loading ε_{eq}^2

against the equivalent crack density D_{eq}.

356
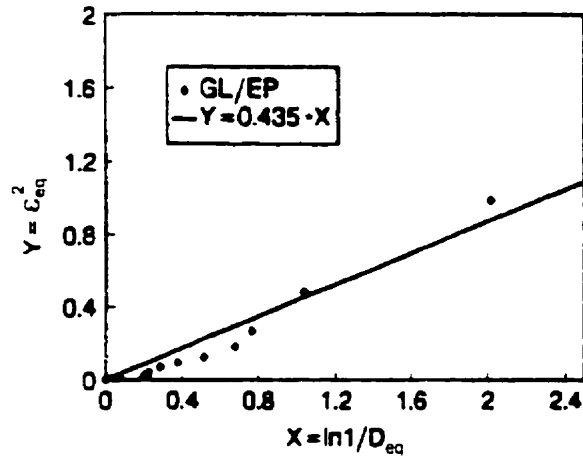
Figure 7.14 Parameter transformation relationship between the equivalent loading and equivalent crack density. Values are for a $[90_3/0]_s$ glass/epoxy laminate [222].

The data plots out well using a semi-log scale, and directly from the figure we get

$$\varepsilon_{eq}^2 = 0.425 \ln\left(\frac{1}{D_{eq}}\right)$$

therefore the equivalent crack density is

$$D_{eq} = e^{-\left(\frac{\varepsilon_{eq}^2}{0.435}\right)} = e^{-\left(\frac{\varepsilon_{eq}}{0.659}\right)^2}$$

(7.44)

Labeling the proportionality constant 0.659 as a (material cracking) parameter ε_{eq}^c and

applying this quantity to (7.43) the distribution function is determined

$$F_c(\varepsilon_{eq}) = 1 - e^{-\left(\frac{\varepsilon_{eq}}{\varepsilon_{eq}^c}\right)^2}$$

(7.45)

357

This is essentially a Rayleigh cumulative distribution function [261], a single operative variable case of the more encompassing 2 parameter Weibull distribution. Equation (7.44) can be cast into the more general two parameter form

$$D_{eq} = e^{-\left(\frac{\epsilon_{eq}}{\epsilon_{eq}^{CW}}\right)^{CK}}$$

(7.46)

where the two Weibull curve fitting parameters ϵ_{eq}^{CW} and CK are extracted from experimental data in a fashion similar to that presented in Figure 7.14.

Reviewing some data taken from reference [222], Figure 7.15(a) compares "*characteristic curves*" generated using crack densities gathered from both cross-ply and quasi-isotropic AS4 graphite fiber based laminates. It is evident that there is a slightly different response between these two classes of lay-ups however they both follow the basic trend rather closely. Figures 7.15(b) -7.15(d) are for cross-ply lay-ups, each with a different matrix. The curve fits appear reasonably good and experience has shown that it remains so provided one does not stray too far in the type of fiber and lay-up. Some data for glass epoxies is plotted in Figure 7.16. Compiling the test results of many researchers, Luo-Yu Xu has put into evidence that although the saturation crack density in different laminates might vary widely, and that the matrix crack growth processes can be quite different as a result of loading history (fatigue vs. static) and / or the lay-up sequence, the final residual laminate stiffnesses seem insensitive to such differences. Generally the thin 90° layer laminates had the high initiation loading and matrix crack growth rate and the big final saturation crack density. However the final stiffness reductions were about equal

regardless if there were several separate thin layers or only a unitary one. Once the loading

and crack density parameters are normalized and transformed into non-dimensional

quantities, the plots appear as a family of curves. The fitting parameters or "characteristic

parameters" will provide an accurate prediction for the same material / under the same

cure process, allowing some estimation for similar materials and lay-ups under similar

processing.
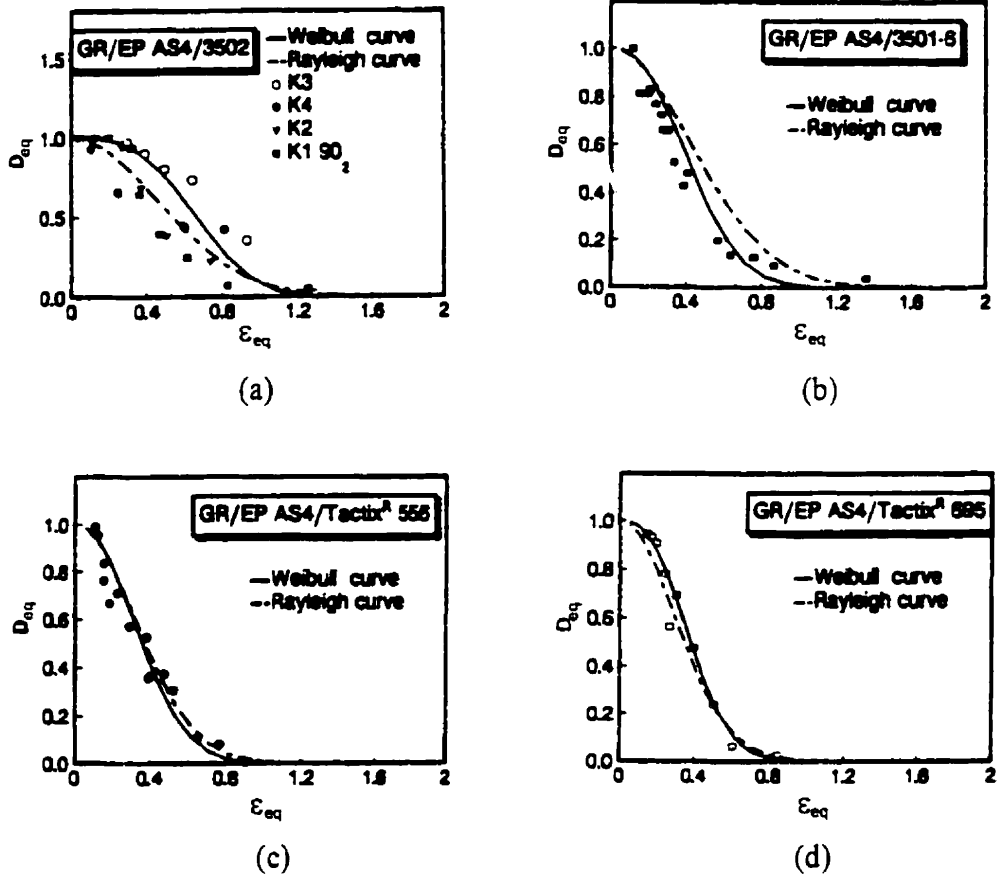
Figure 7.15 Characteristic curves for graphite epoxy with different resin systems [222].
For Figure (a) Laminates: K1 = [0/90]₄ₛ ; K2 = [0₄/90₄]ₛ
K3 = [45/90/-45/90/45/90/-45/90]ₛ ; K4 = [60/90/-60/90/60/90/-60/90]ₛ
For Figures (b) through (d) laminates are all [0₂/90₂]ₛ

A secondary feature in evidence from the above figures is the fact that the curve resulting

from a highly rubberized matrix Tactix 695 with $G_{IC} = 1250\,J/m^2$ shows less difference

than one might expect in comparison to a conventional resin 3501-6 with

$G_{IC} = 220\,J/m^2$ [208]. The G_{IC} value is $343\,J/m^2$ for the Tactix 556 system.

(a)   (b)
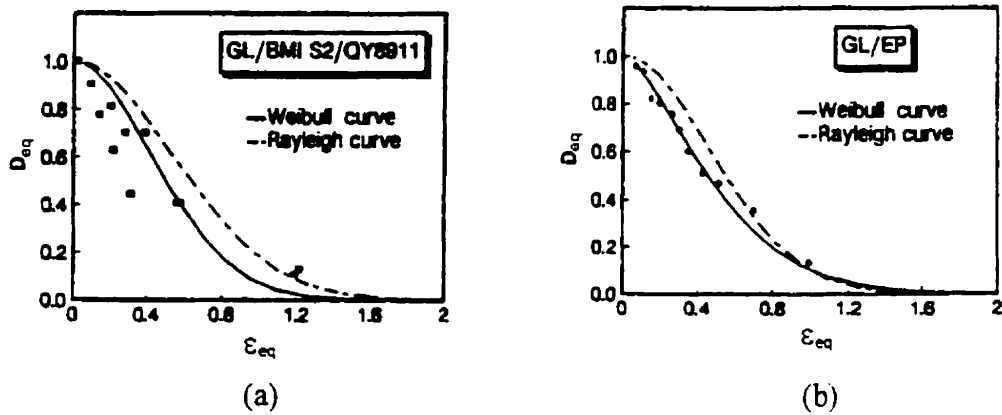
Figure 7.16 Characteristic curves for (a): [0/90₂/0₂/90]ₛ and (b): [0₃/90]ₛ glass-epoxy
laminates [222].

Fitting parameters for different materials evaluated in reference [222] are presented in

Table 7.8. For Rayleigh curves the "*characteristic equivalent loading*" ε_{eq}^c varies from

0.4 - 0.8 for different materials. The correlation between this parameter and other material

constants such as the transverse tensile strength or fracture toughness is not yet clear.

Table 7.8 Fitting parameters for characteristic curves [222].

Material	Lay-up	$CK = \beta$	ε_{eq}^{CW}	ε_{eq}^{C}	α_R	α_W
AS4/3502	[0₄/90₄]s etc.	3.09	0.744	0.643	2.42	2.49
AS4/3501-6	[0₂/90₂]s	2.39	0.500	0.600	2.78	5.24
AS4/TA556	[0₂/90₂]s	2.17	0.427	0.452	4.89	6.33
AS4/TA696	[0₂/90₂]s	2.53	0.441	0.417	5.75	7.43
T300/QY8911	[0₂/F/90₄]s etc.*	1.17	0.952	0.787	1.61	1.06
S2/QY8911	[0₂/90₂/0₂/90]s	1.96	0.606	0.763	1.72	2.67
GL/EP	[0₃/90]s	1.51	0.579	0.659	2.30	2.28
SiC/CAS	[0₁₂]s	2.60	0.450	0.460	4.73	7.97

* 'F' indicates film adhesive layer

In an effort to expand somewhat on the meaning Luo-Yu Xu's parameters consider the shape of Weibull curves and the equation of this density function presented in the Figure 7.17 below.
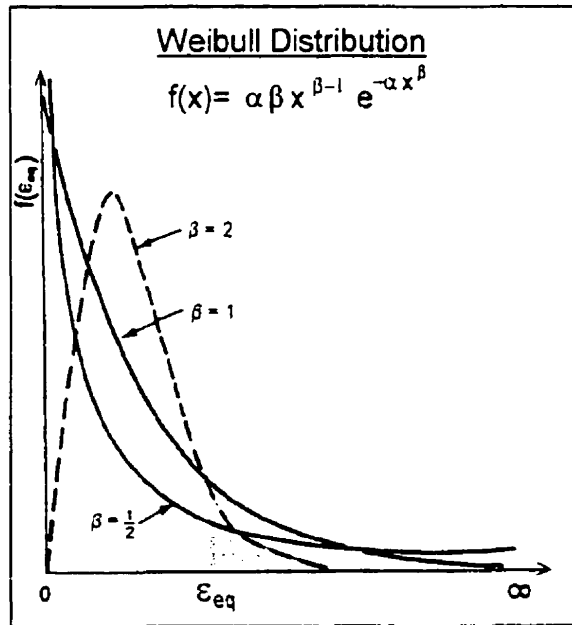
Figure 7.17 Probability distribution functions for a random variable [229].
Rayleigh distribution when $\beta = 2$,
Exponential distribution for $\beta = 1$,
Weibull distribution when α and β are free parameters.

Probability of failure (occurrence of damage) can be computed as follows. The definition of a Weibull density distribution, with ε_{eq} as the functional parameter, is:

$$f(\varepsilon_{eq}) = \alpha\beta\varepsilon_{eq}^{\beta-1}e^{-\alpha\varepsilon_{eq}^\beta}$$

$$(7.47)$$

The probability of a crack forming depends on the integral of this function over the load range in question. For a relatively small load, assuming $\beta = 2$, $\alpha = 1$, this integral would represent the shaded area in Figure 7.17. Here it must be remembered that large values of ε_{eq} represent small loads, similar to large values of a_{eq} representing the small loads necessary to propagate cracks from large initial flaws. The probability for failure or damage occurring is thus represented by the integral

$$D_{eq} = \int_{\varepsilon_{eq}}^{\infty} f(\varepsilon_{eq})d\varepsilon_{eq}$$

$$(7.48)$$

We note that any probability function integrated over the entire range ($0 \rightarrow \infty$) yields unity. Thus if we plot D_{eq} as a function of the lower limit of integration ε_{eq} one can expect to get a reverse "S" shaped curve with $D_{eq} = 1$ as the load increases to the breaking point $\left(\varepsilon_{eq} \rightarrow 0\right)$.

A variation of parameters can be used to simplify the integral,

let: $\quad y = \varepsilon_{eq}^\beta \qquad\qquad$ then $\qquad dy = \beta\varepsilon_{eq}^{\beta-1}d\varepsilon_{eq}$

$$D_{eq} = \int\limits_{\varepsilon_{eq}^0}^{\infty} \alpha e^{-\alpha y} dy = -e^{-\alpha y}\Big|_{\varepsilon_{eq}}^{\infty} = 0 - \left(-e^{-\alpha \varepsilon_{eq}^{\beta}}\right) = e^{-\alpha \varepsilon_{eq}^{\beta}}$$

(7.49)

Further, to examine the implication of parameters α and β one must start with the definition of a probability density function.

$$f(\varepsilon_{eq}) = Z(\varepsilon_{eq}) \cdot R(\varepsilon_{eq})$$ where: Z is a rate function

R is a reliability function

(7.50)

The reliability function is defined as

$$R(\varepsilon_{eq}) = e^{-\int\limits_0^{\varepsilon_{eq}} Z(y)dy}$$

(7.51)

where the integration limits reflect the reliability side rather than the failure side of the curve.

For a Weibull probability density function the *rate* function Z is defined as

$$Z(\varepsilon_{eq}) = \alpha\beta\varepsilon_{eq}^{\beta-1}$$

(7.52)

Essentially this is a smoothly increasing / decreasing type of power function with β as the major shape controlling parameter while α acts as a scaling parameter. Figure 7.18 plots the rate function for various values of β with $\alpha = 1$, (B and a in the Figure 7.18) .

CRACK RATE CURVES
a = 1
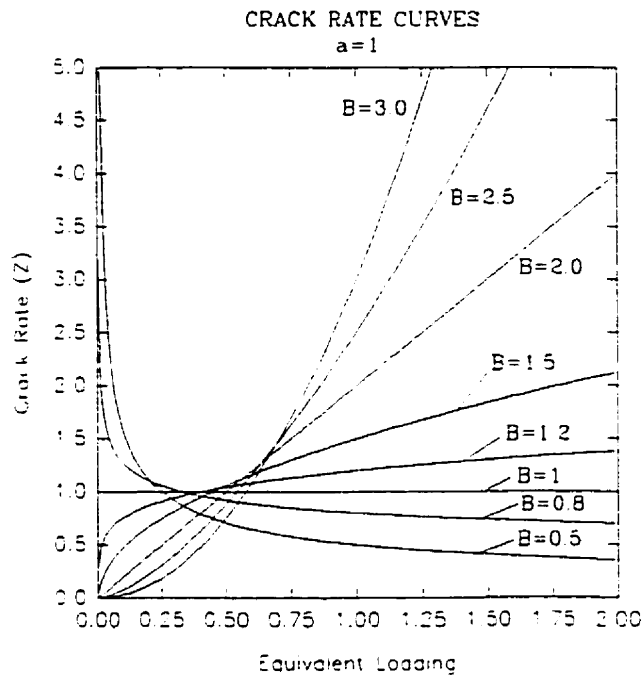
Figure 7.18 Crack rate curves for fitting parameter β (B in figure) when α = 1 .

Comparing equation (7.46) with (7.49) it is obvious that $\beta = CK$ and looking back to

Table 7.8 we note that $CK > 1$, so one can state outright that the rate of crack generation

tends to zero as the equivalent loading increases to the breaking point ($\varepsilon_{eq} \to 0$). A high

value of β implies that an increased amount of cracking takes place at lower loads while a

lower value indicates the crack generation rate is slow early on, reaching saturation at a

pace that begins dropping to zero only at a load close to rupture, and then very quickly.

Scaling parameter α serves to rotate these curves CCW with increasing values. We note

also that putting $\beta = 2$ sets a linear decrease to the crack generation rate and we recover

the Rayleigh form, equation (7.44). In terms of the probability density shown in Figure

7.17, increasing β skews the curves to the right, meaning more crack generation at relatively low strains above *FPF* with respect to the ultimate strain capability of the laminate.

Luo-Yu Xu's parameters ε_{eq}^{CW} and ε_{eq}^{C} are actually $\alpha^{-\frac{1}{\beta}}$ and $\alpha^{-\frac{1}{2}}$ respectively. Table 7.8 also gives α_W and α_R which are values of α back-calculated from Luo-Yu's fitting parameters above for the Weibull and Rayleigh curves. The Rayleigh curve implies a linear decrease in the crack generation rate so the α fitting parameter is the best fit approximation to this slope. A higher value meaning that the rate decreases faster per unit loading. This rate is also approximately inversely proportional to Luo-Yu Xu's ε_{eq}^{CW} and ε_{eq}^{C} terms, so a low value of Luo-Yu Xu's parameters means that the overall steepness of the characteristic curve is more pronounced.

The characteristic curves should be read from right to left. The presence of a high ε_{eq} value indicates cracks are being initiated at a relatively low load. Using a toughened matrix suppresses the onset of cracking and ε_{eq} is thereby smaller when cracking does commence. In turn the crack development phase is then quite abrupt making the D_{eq} vs. ε_{eq} curve rather steep. This results in commensurably lower values for ε_{eq}^{C} or ε_{eq}^{CW} since this constant is related to the inverse of the slope. It appears that materials and lay-ups which show a great strain range over which damage can occur before final fracture such as glass-epoxies (because the strain limit for glass is high) or multidirectional lay-ups which degrade rather gradually and commence cracking early on will tend towards a high

value of ε_{eq}^C. High strength type graphite epoxies appear to occupy the middle to high

range values indicating that as they fail the damage develops gradually. For the Weibull

fitting parameters the effect of ε_{eq}^{CW} is analogous to ε_{eq}^C as it describes the overall

steepness of the center portion of the curve, and the parameter CK modifies the curl of

these reverse "S" curves near the extremities, with higher values causing greater

roundness. Thus the combination of a high CK value coupled with low ε_{eq}^{CW} would

indicate a situation where crack growth rate is extremely high at some intermediate value

of equivalent load, for example the Tactix 696 system.

Certainly more work needs to be done in this area to quantify which fitting

parameters are most appropriate and relate best to the types of laminates under study. The

"Super Pressure - Vessel Designer" code uses one set of Weibull curve fitting parameters

throughout. The ones chosen were those obtained for quasi-isotropic AS4/3502 lay-ups.

The material behavior is shown in Figure 7.15(a) and listed under the first row of Table

7.8. Ideally if more extensive data were available, fitting parameters for damage

development could be included as part of the database and applied individually to each

material. Numerical methods for extracting Weibull parameters are available in reference

[229].

There are however still two other factors that need to be determined, namely crack

initiation and saturation strains, before the method discussed above can be applied. Crack

initiation strains are optimally determined from a fracture mechanics approach. From linear

elastic fracture mechanics the critical strain energy release rate is equal to the intralaminar

fracture toughness at crack initiation.

$$U = \frac{1}{2}\int_V \sigma_i \varepsilon_i dV \qquad\qquad G_{IC}^{MC} = \frac{dU}{t\,da}\bigg|_{a\to a_c}$$

(7.53)

Where U is the strain energy for the laminate with the matrix crack, often expressed as a

function of the matrix crack density or the flaw length. The maximum strength approach

assumes that the stress of the off-axis lamina attains its critical strength value when the

matrix crack initiates. However due to the in situ strength effect in a laminate, this critical

strength of the lamina is *not* a material constant. Another view considers strength as a

probabilistic phenomena. These theories are available in the literature [230][231].

However from a simpler standpoint the matrix crack initiation can still be predicted well

enough by analytical models. Shear-lag approaches are followed by many analysts,

including the work of N. Laws and G. Dvorak [214], J.W. Lee and I.M. Daniel [204],

and Luo-Yu Xu [223]. Ultimately they come up with an equation describing the relation

between the matrix crack initiation strain and the shear-lag parameter K_t (along with

material constants and geometry). For cross-ply laminates the form used by Luo-Yu Xu

[222], adapted from [214] can be expressed as

$$\varepsilon_{cr} = \sqrt{\frac{K_t t_0 E_{11} G_{IC}^{MC}}{(E_{11}t_0 + E_{22}t_{90})E_{22}}} - \varepsilon_{90}^R$$

(7.54)

where ε_{90}^R is the residual strain of the 90° plies in the applied load direction, t defines

lamina thicknesses and K_t is given by

$$K_t = \sqrt{\frac{(\alpha +1)G_{23}(E_{11}t_0 + E_{22}t_{90})}{E_{11}E_{22}t_0 t_{90}^2}}$$

(7.55)

367

Here G_{23}, E_{11}, E_{22} are elastic moduli and α is the assumed shape index of the crack

opening displacement, which varies among models due to different assumptions for

longitudinal displacements [223]. P.A. Smith and J.R. Wood [232] concur, indicating that

for a parabolic distribution $\alpha = 3$, for a linear variation of displacement $\alpha = 1$. In the case

of in plane shear loading the shear-lag parameter takes a similar form

$$K_s = \sqrt{\frac{(\alpha + 1)\left(G_{12}^0 t_0 + G_{12}^{90} t_{90}\right)}{G_{12}^0 t_0 t_{90}^2}}$$

(7.56)

where G_{12}^0 and G_{12}^{90} are in plane shear moduli of the $0°$ and $90°$ layers respectively. For

$[0_n/90_m]_s$ laminates the value of α may range from 0.5 to 2.5 but most often takes on a

value of 0.9-1.1 [214]. Such equations are useable provided intralaminar fracture

toughness data is available. However for designers this is often not the case. Moreover

how to treat lay-ups with arbitrary orientations remains unanswered.

Y.M. Han, H.T. Hahn and R.B. Croman [205] note that such fracture based *FPF*

predictions tend to deviate from experimental results as the ply thickness increases. This

observation indicates that the mode of transverse ply cracking is therefore also changing.

When the $90°$ ply is thin, the assumption of the inherent flaw being a through-thickness

type is reasonable. However as the $90°$ ply becomes thicker, the same assumption is not

likely to hold true. Since the analytical models are based on the presence of a through-the-

thickness flaw, their predictions are expected to become worse as the $90°$ ply thickness

increases. For typical prepreg thicknesses the transition starts to occur when the number

of plies n is about 3. For thick plies, one may use an inherent flaw that is neither through-the-thickness nor through-the-width.

Considering that for pressure vessels of thick wall construction it would be highly unusual from a manufacturing standpoint to employ a very thin ply layering sequence which would require the calculation of in situ strength magnification effects, we are then back to strength based failure criterion's to define FPF. The "Super Pressure - Vessel Designer" software uses only standard uniaxial strength values, rather than requiring ply fracture toughness input. At worst this makes the FPF predictions slightly conservative in relation to fracture mechanics predictions, not necessarily a bad thing from a design or safety perspective.

The last undetermined factor concerns evaluating the crack saturation strain. When the first transverse matrix crack appears in the 90° (or other off-axis) layer, given the coordinate origin is located at the first matrix crack, the total normal or in-plane shear stress of the 90° layer can be obtained by analytical models. Generally it can be written in a form

$$\overline{\sigma}_{90} = \overline{\sigma}_{90}^{o}\left(1 - \sigma_{(x)}\right) \qquad \text{where for:} \quad x = 0, \quad \sigma_{(x)} = 1; \quad x \to \infty, \quad \sigma_{(x)} \to 0 \tag{7.57}$$

Here $\overline{\sigma}_{90}^{o}$ is the far-field stress of the 90° layer and $\sigma_{(x)}$ represents an undetermined stress function over distance (x) with the behavioral characteristics given above. Although there are numerous approaches to solving the problem, by far the most common is based on shear-lag theory. With this approach the solution takes the form

$$\overline{\sigma}_{90} = \overline{\sigma}_{90}^{o}\left(1 - e^{-K_r x}\right) \tag{7.58}$$

where K_r is the so-called shear-lag parameter (also known as ξ in some literature) of the laminate. Determination of such has been given earlier in equations (7.54 & 7.55). Physically the parameter K_r represents the recovery "rate" of the stress near a crack. See Figure 7.19. Some researchers such as K.L. Reifsnider imply that the "saturation crack spacing" is the shortest distance from the original crack to the position at which the stress reaches its original undisturbed level. A refined view of this concept must extend to include the flaw distribution within the cracking lamina. When cracking first occurs, the most severe initial flaws will control the process, but since these large flaws represent only a very small proportion ($\cong 1\%$) of the total they are quickly consumed. The load needs to be steadily higher to propagate the ever more numerous smaller flaws into cracks and the cracking rate is heightened because the density of these small flaws is much greater. At some point the influence of the shear lag zone becomes the rate controlling parameter.
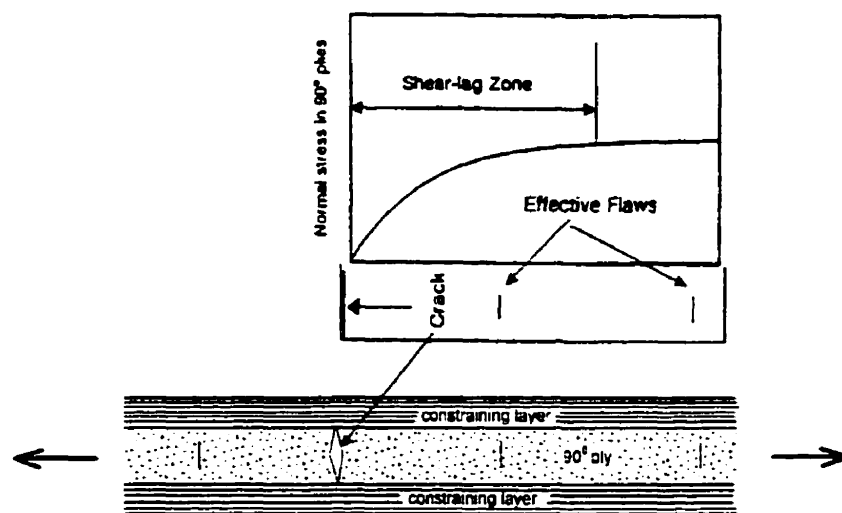
Figure 7.19 Characteristic damage state development.
Adapted in part from [223].

Consider two flaws as depicted in Figure 7.19, their lengths are considered to be approximately the same, one exists inside the shear lag zone, the other outside. For a given applied stress the flaw outside is likely to propagate a crack whilst the flaw inside is effectively shielded due to the lower stress in that region. Eventually as flaws of a given size are consumed there is leveling-off effect with load because further crack propagation requires reaching deeper and deeper inside the shear lag zone. The characteristic spacing establishes itself when a disproportionately high load increase is requisite to project sufficient stress within the shear-lag zone to reach the ever smaller remaining flaws.

Based on equation (7.58) the final saturation spacing of matrix cracks L_{cs} can be determined by (crack density $D_{cs} = 1/L_{cs}$)

$$1 - e^{-K_f L_{cs}} = 1 - D_c \qquad \text{where: } D_c \leq 0.15 \qquad \text{(from experiments)}$$

(7.59)

D_c is a material constant with probabilistic meaning, which represents the total effect of distributive defects which are able to form matrix cracks. It should be a constant for laminates of the same material undergoing the same cure process. Because D_c is taken as a constant, the effective longitudinal modulus of each cracked 90° layer will reach the same value. This value is dependent on the material property but independent of the laminate lay-up, especially the constraining effect of the adjacent plies. Furthermore, the effective longitudinal modulus of each cracked 90° ply will have a lower boundary value. This lower boundary seems to be independent of the material property and it has been

verified by many experimental results, moreover this concept extends to the effective

Poisson's ratio and shear modulus.

Therefore in the limit as the saturation crack density is approached

$$D_{CS} = -K_t/\ln D_\epsilon$$

(7.60)

For a cross-ply laminate with matrix cracks within the 90° layer, the ratio of the

longitudinal moduli of the laminates with and without matrix cracks can be given by a

shear-lag analysis, or similarly by other techniques [206][214][204][223][232]. With

derivation details deferred to reference [223][225][226] an approximate solution to the

problem can be expressed as

$$E_{22}(D) = E_{22}\left(1 - \frac{2D}{K_t}\tanh\left(\frac{K_t}{2D}\right)\right)$$

(7.61)

where $E_{22}(D)$ represents the damaged transverse modulus. Two non-dimensional

parameters, the "equivalent crack density" $D_{eq} = D/D_{CS}$ and the equivalent residual

lamina stiffness $RS_{eq} = E_{22}(D)/E_{22}$ can be introduced.

$$RS_{eq} = 1 - \frac{2D_{eq}}{\ln D_\epsilon}\tanh\left(\frac{\ln D_\epsilon}{2D_{eq}}\right)$$

(7.62)

When the matrix crack density attains the saturation value D_{CDS}, then $D_{eq} = 1$ and we

have

$$RS_{eq} = 1 - \frac{2}{\ln D_\epsilon}\tanh\left(\frac{\ln D_\epsilon}{2}\right) \geq 0.2 \quad \text{for} \quad D_\epsilon \leq 0.15$$

(7.63)

372

Figure 7.20 plots the generic shape of these residual stiffness curves with differing values

of material constant D_ε. It can be seen that in the limit, residual stiffness ranges from about

20% - 40% the initial values depending on the choice of D_ε.
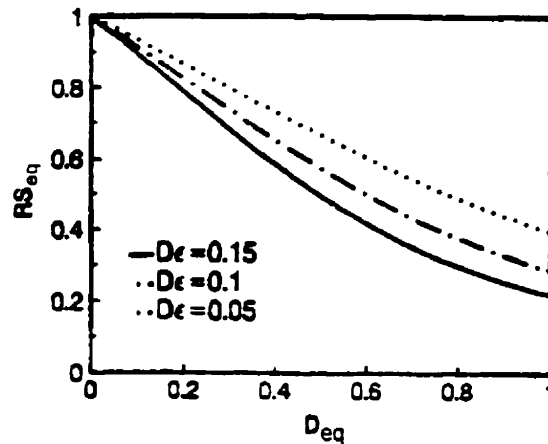
Figure 7.20 Characteristic curves for stiffness degradation
expressed by the equivalent residual stiffness
and the equivalent crack density for a range of D_{eq} [224].

Similarly shear moduli reductions follow an identical form except that K_s would

be used in the equations. Figure 7.21 presents results from a few sources in the literature,

re-plotted using the residual stiffness concept. Considering the diversity of the data, these

plots reinforce the predictive power of the method. Table 7.9 gives a summary of

predicted lower bound (superscript LB) values for a selection of cross-ply laminates at

their characteristic damage state. The agreement with measured final (superscrift F)

longitudinal Young's modulus values is excellent [224]. The "Super Pressure - Vessel

Designer" code uses equation (7.62) to estimate residual stiffness beyond first ply failure

and sets D_c at 0.15 to be conservative.
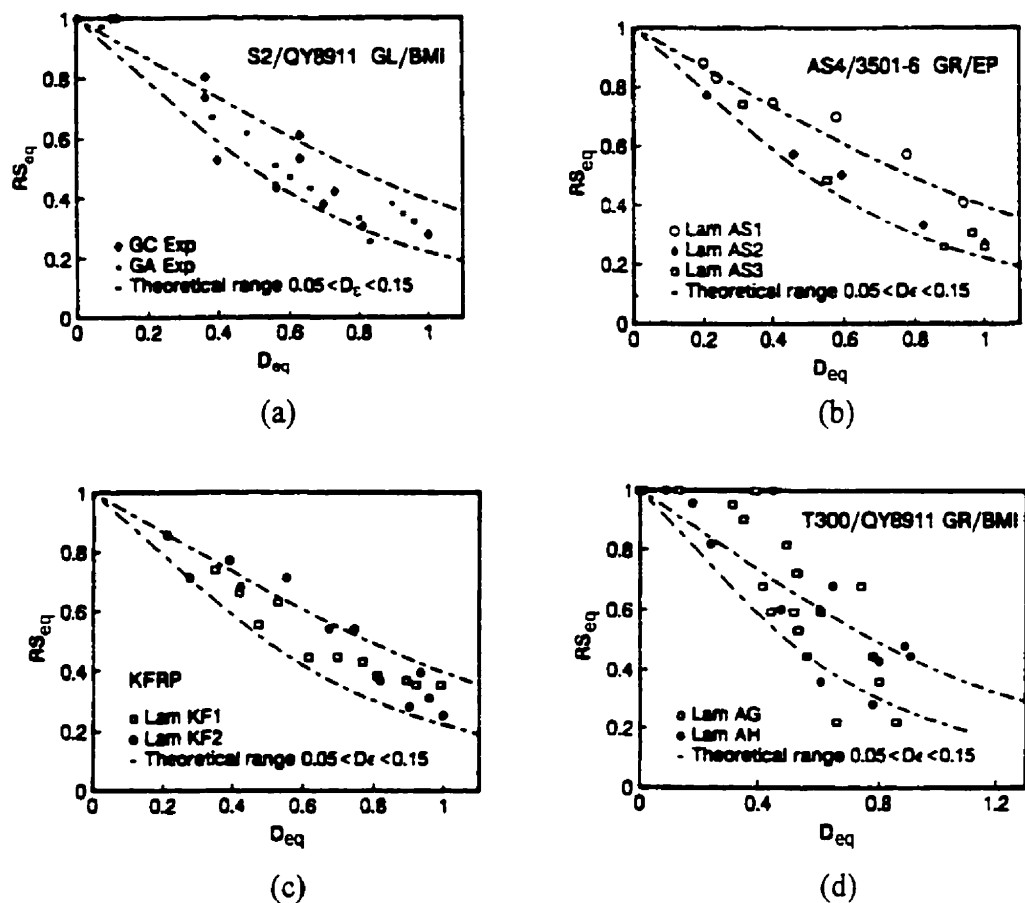
Figure 7.21 The characteristic curves of stiffness degradation for various laminates [224].

    (a)   GA: $[0_3/90_3]_s$, GC: $[0/90_2/0_2/90]_s$

    (b)   AS1: $[0/90_3]_s$, AS2: $[0/90_2]_s$, AS3: $[0_2/90_2]_s$

    (c)   KF1: $[0/90_2]_s$, KF2: $[0/90]_s$

    (d)   AG: $[0/F/90_4]_s$, AH: $[0/F/90_4/F/0]_s$ where: F = film adhesive layer

Table 7.9 Predicted failure (F) and measured lower boundary (LB)
values of the longitudinal Young's modulus ratio [224].

Material	Lay-Up	E_x^F/E_x^0	E_x^{LB}/E_x^0
S2/QY8911	$[0_3/90_3]_s$	0.789	0.782
S2/QY8911	$[0_3/90_2/0]_s$	0.772	0.782
S2/QY8911	$[0_2/90_3/0_2/90]_s$	0.790	0.782
T300/QY8911	$[0_2/90_4]_s$	0.918	0.908
T300/QY8911	$[0/90_4/0]_s$	0.924	0.908
T300/QY8911	$[0_2/F/90_4]_s$	0.916	0.908
T300/QY8911	$[0/F/90_4/F/0]_s$	0.926	0.908
KFRP	$[0/90_2]_3$	0.916	0.896
KFRP	$[0/90]_s$	0.948	0.944
AS4/3502	$[0/90_3]_s$	0.902	0.867
AS4/3502	$[0/90_2]_s$	0.915	0.907
AS4/3502	$[0_2/90_2]_s$	0.954	0.950
AS4/3502	$[0/90]_s$	0.969	0.950
GL/EP	$[0/90_3]_s$	0.580	0.613
GL/EP	$[0/90]_s$	0.829	0.800
GL/EP	$[90_3/0]_s$	0.612	0.613
GL/EP	$[0/90]_s$	0.870	0.840

Although we have a good idea of what the limit state represents in terms of

property retention, the crack saturation strain has not yet been quantified. To this end one

must look at experimental data and use some intuitive knowledge. Luo-Yu Xu notes that

for most glass fiber and graphite fiber based composites the saturation strain value is in

excess of 1.4%. In fact to measure the saturation strain in graphite epoxies it is suggested

that the 90° lamina be constrained in a hybrid composite for the test since this value is

generally bigger than the ultimate strain of the 0° graphite fibers that control the final

fracture. In practice the saturation crack spacing in glass based laminates can be achieved

and one need not look far, for example A.L. Highsmith and K.L. Reifsneider [221] or the

collection of literature results compiled by Luo-Yu Xu [223]. Saturation is attained

because the ultimate fiber failure strain is high relative to the (constrained) strain capability

of the resin systems employed. Graphite epoxy composites, constituted from the same

resin systems as their glass counterparts usually suffer "premature" failure prior to

developing a fully saturated crack state, perhaps with exception of expensive high strength

fibers as Torayca T1000. The crack saturation strains seem to have a high correlation with

the matrix toughness. For example, comparing with a quite different system, crack

saturation of a ceramic matrix composite SiC/CAS is easily attained at only about 0.5%

strain. One must be mindful that the saturation strain represents more of a property related

to the matrix / fiber combination than any influence attributable to lay-up. Figures 7.22 -

7.25, drawn from the literature, each show curves exhibiting the strain levels necessary to

attain a saturated damage state. Often the limit state is not fully attained but visually

projecting the plots enables some estimation. Clearly the response is a strong function of

the matrix / fiber combination. For the purpose of comparative design evaluations the

"Super Pressure - Vessel Designer" code presently fixes the saturation strain at 3 times the

initiation strain. The main reason for this approximation is that it appears approximately

correct for intermediate strength graphite fibers (AS4, T300, etc.) which constitute main

building blocks for commercial high performance pressure vessels. An assumption of 5X

or 7X *FPF* strain might be deemed more applicable to glass and Kevlar[®] based laminates

respectively, however it must be stated that an absolute value of strain, rather than one

linked to the failure initiation point might be just as good. Too little is known at this point.

Obviously since this quantity is a material parameter, it would best be read into the

program as part of the material file (along with the "characteristic curve" fitting parameters). Clearly such hard data is still lacking and better correlation's with the matrix fracture toughness and bond strength would be very desirable. Only test data from more material samples can refine the predictions any further.
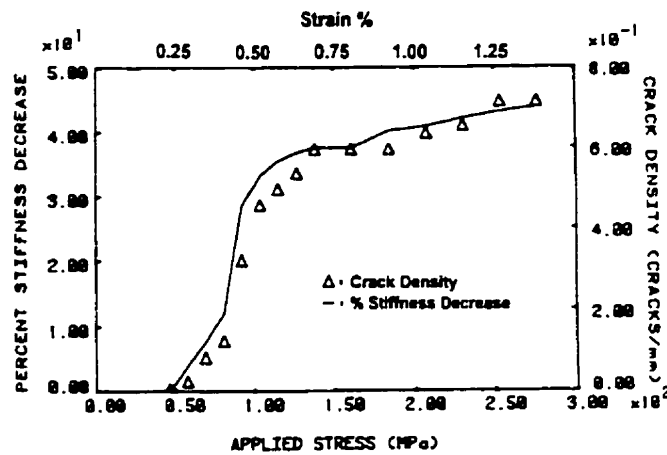
Figure 7.22 Stiffness decrease and crack density vs. stress or strain level for a [0/90₃]ₛ laminate. Adapted from Highsmith and Reifsnider [221].
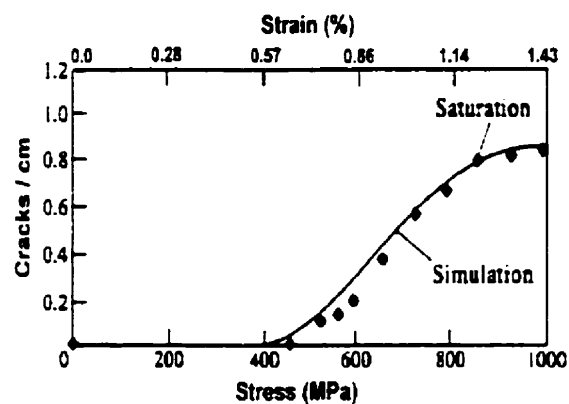
Figure 7.23 Transverse cracking for a T300/N174 graphite epoxy [0₂/90₂] laminate. Adapted from Caron and Ehrlacher [218].
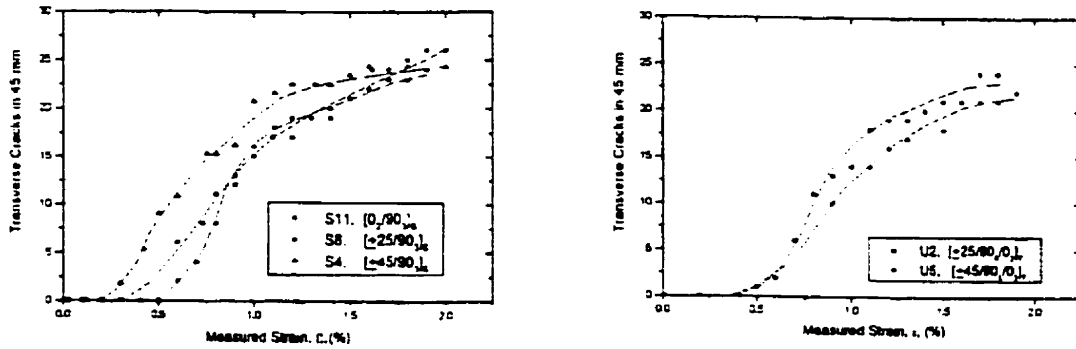
Figure 7.24 Transverse cracks attaining a saturation level in Scotchply
1003 (glass-epoxy) laminates. Adapted from J.W. Hoover et al. [216].
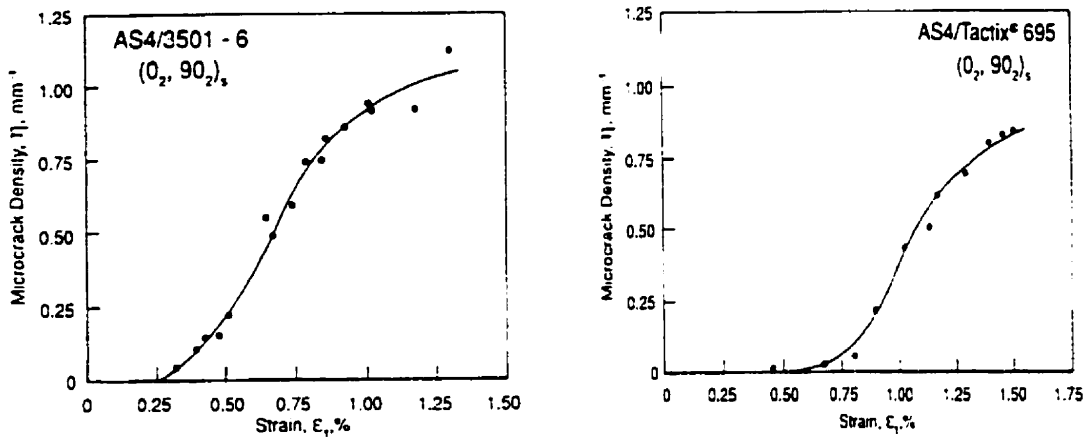
Figure 7.25 Density of the transverse microcracks in the 90° layer plotted against axial
strain. Saturated state is approached but never develops fully before the 0°
fibers attain their strain limit. A more brittle matrix would be expected to
exhibit the saturated state more clearly prior to laminate destruction. Source
R. Talreja et al. [208].

378

7.5 Elastic Moduli Reductions

The final topic concerns extension of the laminate transverse moduli degradation determined in the previous section for application in a more general sense to the 3-dimensional elasticity theory upon which the composite pressure vessel analysis is based. This is by no means an easy task. It essentially involves bridging from an empirical formulation to a strictly mathematical form. However there exists a body of research that can guide in this regard. Namely, effects on axial moduli, shear moduli and in-plane Poisson's ratio due to transverse matrix cracking have been studied in conjunction with the transverse stiffness reductions discussed earlier. P.A. Smith and J.R. Wood for instance suggested using changes in Poisson's ratio to quantify the stiffness reductions in cross-ply laminates since it can be measured by a strain gage rather than requiring means of measuring crack densities [232]. It is known or at least strongly suspected that shear moduli and Poisson's ratio reductions are commensurate with transverse moduli reductions. In fact the equations developed often take the same form [206][224] and differ mainly by a constant such as the shear-lag parameter (K_s or K_t) to reflect upon the loading condition imposed. Y.M. Han and H.T. Hahn [206] note that very few models exist to predict crack initiation under shear or general in plane loading. Data to substantiate theory is even more scarce. Figure 7.26 and Figure 7.27, borrowed from Han and Hahn [206], depict Poisson ratio and shear moduli reductions derived from a shear-lag model applicable to generalized in-plane loading. The equations used are essentially identical to Luo-Yu Xu's.
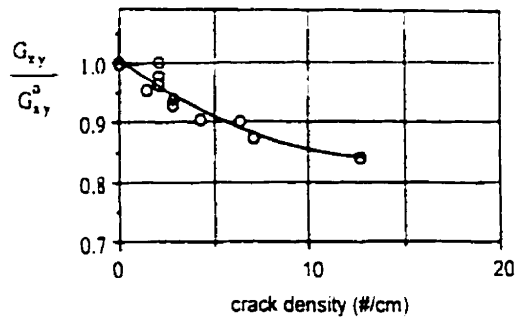
Figure 7.26 Poisson's ratio reduction in AS4/3501-6 $[0/90]_s$
with transverse cracking [206].
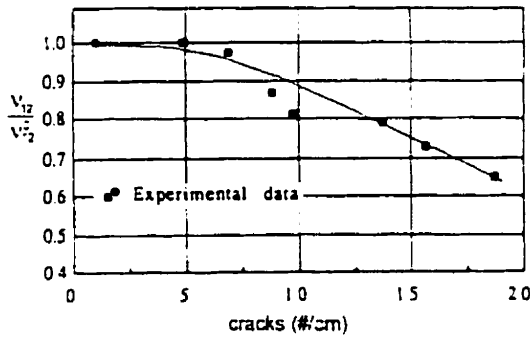
Figure 7.27 Shear moduli reduction vs. crack density.
Laminate: AS4-3502 $[0_2/90_2]_s$
Adapted from Han & Hahn [206].

Many other authors have shown similar trends. Accepting for the moment that the

expected shear modulus and Poisson's ratio reductions resulting from matrix cracking are

of the same order as the transverse moduli, we now look at through thickness properties.

Obviously for the case of a pressure vessel the through-thickness stresses are

compressive and any flaws present would close up rather than grow. Intuition tells us that the elastic response in this direction should be virtually independent of the transverse crack density. Figure 7.28 makes this more clear. As far as the out-of plane stress is concerned, there is no discontinuity and the cracks only serve to channel yet do not cause any effective decrease in area nor force a detour path into another layer as happens with the transverse stress.
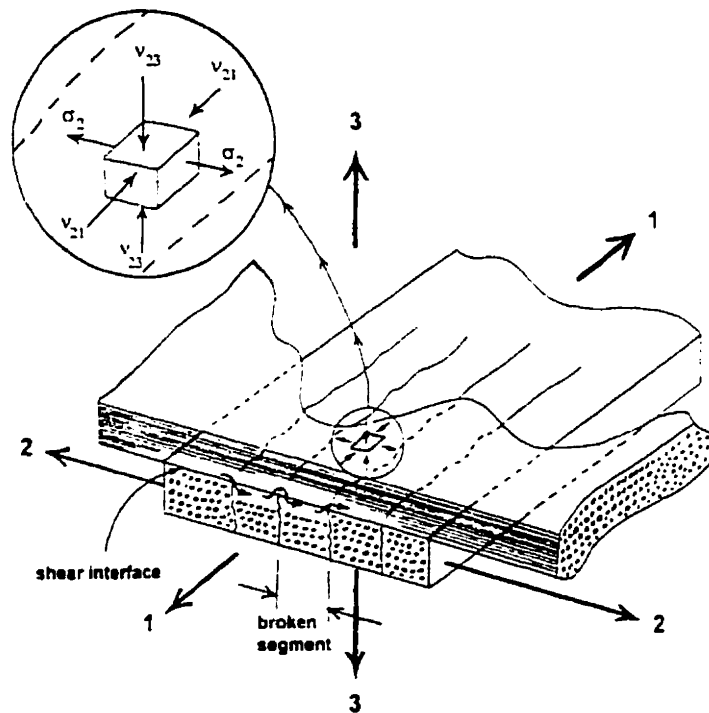
Figure 7.28   Cracked laminate schematic for lamina stiffness degradation scheme.
Effect of stress σ_2 is magnified.

One big problem with mechanical experiments on composites is that they indicate *engineering stiffness* properties. These are *not* the components of stiffness requisite in elasticity formulations. Furthermore there are two other factors. The idealization of

transverse isotropy must be entirely eradicated under cases of matrix cracking and because the effects of crack opening are felt only for tensile loads the stiffness constants lose independence from the sign on stress (bilinear behavior). Thus the starting point for stiffness equations must be the orthotropic equation set (4.3) and that which is derived below is applicable foremost (but not exclusively) to tensile in plane and compressive out of plane loading.

For an undamaged transversely isotropic medium the generalized Hooke's law reduces to 5 *elastic moduli* (A_{11}, A_{12}, A_{22}, A_{23}, A_{66}) which designate the 5 independent effective properties of the media [88]. In the case of a non-homogeneous body these coefficients are functions of position and can be named *elastic characteristics*. Specifically these relations, using the tensorial shear strain convention of Section 7.1 are expressed in a lamina reference frame as

$$
\begin{aligned}
\sigma_{11} &= A_{11}\varepsilon_{11} + A_{12}\varepsilon_{22} + A_{12}\varepsilon_{33} \\
\sigma_{22} &= A_{12}\varepsilon_{11} + A_{22}\varepsilon_{22} + A_{23}\varepsilon_{33} \\
\sigma_{33} &= A_{12}\varepsilon_{11} + A_{23}\varepsilon_{22} + A_{22}\varepsilon_{33} \\
\sigma_{31} &= 2A_{66}\varepsilon_{31} \\
\sigma_{23} &= \left(A_{22} - A_{23}\right)\varepsilon_{23} \\
\sigma_{12} &= 2A_{66}\varepsilon_{12}
\end{aligned}
\qquad \text{where:} \qquad
\begin{aligned}
A_{12} &= A_{13} \\
A_{22} &= A_{33}
\end{aligned}
$$

$$(7.64)$$

A matrix inversion of this equation set yields relations between the stiffness moduli A_{ij} and the compliance components a_{ij} used in equation (4.4) and more generally throughout the derivations in Chapters 4-6.

Consider a uniaxial state of stress specified by $\sigma_{11} \neq 0$ and

$\sigma_{22} = \sigma_{33} = \tau_{12} = \tau_{23} = \tau_{31} = 0$ typical of a mechanical tensile test. Using these

conditions imposed on (7.64) it is readily found that

$$\sigma_{11} = E_{11}\varepsilon_{11}$$

where: $E_{11} = A_{11} - \dfrac{2A_{12}^2}{A_{22} + A_{23}}$

$$(7.65)$$

Modulus E_{11} is called the *uniaxial modulus*, and it is this quantity that is directly

measurable by the mechanical test. The lateral contraction that accompanies the state of

uniaxial stress is used to define Poisson's ratio through

$$v_{12} = \frac{-\varepsilon_{22}}{\varepsilon_{11}} \qquad \text{and} \qquad v_{13} = \frac{-\varepsilon_{33}}{\varepsilon_{11}}$$

$$(7.66)$$

where in the convention v_{ij}, the first index i refers to the coordinate of the *imposed*

stress or strain and the second index j refers to the *response* direction. Solution to the

system (7.64) also yields

$$v_{12} = v_{13} = \frac{A_{12}}{A_{22} + A_{23}}$$

$$(7.67)$$

Next consider the state specified by

$\varepsilon_{11} = 0$ and $\varepsilon_{22} = \varepsilon_{33} = \varepsilon$

Let

$\sigma_{22} = \sigma_{33} = \sigma$

Under these conditions (7.64) yields

$$\sigma = 2K_{23}\varepsilon$$

where

$$K_{23} = \tfrac{1}{2}\left(A_{22} + A_{23}\right)$$

(7.68)

Modulus K_{23} is designated the *plane strain bulk modulus*. The directly measurable shear

moduli are defined as

$$G_{12} = G_{31} = A_{66} \qquad \text{and} \qquad G_{23} = \tfrac{1}{2}\left(A_{22} - A_{23}\right)$$

(7.69)

Relation (7.65) - (7.69) can be inverted to give

$$A_{11} = E_{11} + 4v_{12}^2 K_{23}$$
$$A_{12} = 2K_{23}v_{12}$$
$$A_{22} = G_{23} + K_{23} \qquad\qquad K_{23} = k_T = \text{transverse bulk modulus}$$
$$A_{23} = -G_{23} + K_{23}$$
$$A_{66} = G_{12}$$

(7.70)

These relations are identical to the definitions presented in (7.3)-(7.5).

By no means are the properties defined above the only measurable ones. For

example in a transverse tensile test the condition imposed is

$$\sigma_{22} \neq 0, \quad \sigma_{11} = \sigma_{33} = \sigma_{12} = \sigma_{23} = \sigma_{31} = 0.$$ From (7.64) it is found that

$$\sigma_{22} = E_{22}\varepsilon_{22}$$

where:

$$E_{22} = A_{22} + \frac{A_{12}^2\left(A_{23} - A_{22}\right) + A_{23}\left(A_{12}^2 - A_{11}A_{23}\right)}{A_{11}A_{22} - A_{12}^2}$$

(7.71)

Defining Poisson's ratios

$$v_{21} = \frac{-\varepsilon_{11}}{\varepsilon_{22}} \qquad \text{and} \qquad v_{23} = \frac{-\varepsilon_{33}}{\varepsilon_{22}}$$

(7.72)

system (7.64) yields

$$v_{21} = \frac{A_{12}(A_{22} - A_{23})}{A_{11}A_{22} - A_{23}^2} \qquad \text{and} \qquad v_{23} = \frac{A_{11}A_{23} - A_{12}^2}{A_{11}A_{22} - A_{12}^2}$$

(7.73)

From transverse isotropy (2 and 3 directional properties are equal) it follows that

$$v_{31} = v_{21} \qquad \text{and} \qquad v_{32} = v_{23}$$

(7.74)

However $v_{12} \neq v_{21}$ but the relation

$$\frac{v_{12}}{E_{11}} = \frac{v_{21}}{E_{22}}$$

(7.75)

can be verified by substitution.

Turning to the orthotropic equivalent of (7.4) and most specifically examining the case of a uniformly transversely cracked lamina confined between plies which are able to transmit tensile stress across the shear interface between these lamine, a procedure outlining an equivalence between engineering property changes and elastic moduli reductions will be followed. The lessons are interesting.

For the orthotropic material the elasticity equation set is as per Table 7.10.

Table 7.10 Orthotropic stiffness components

	ε_{11}	ε_{22}	ε_{33}	ε_{23}	ε_{31}	ε_{12}
σ_{11}	A_{11}	A_{12}	A_{13}			
σ_{22}	A_{21}	A_{22}	A_{23}			
σ_{33}	A_{31}	A_{32}	A_{33}			
σ_{23}				A_{44}		
σ_{31}					A_{55}	
σ_{12}						A_{66}

Referring back to Figure 7.28, and remembering the intrinsic meaning attached to the index of each stiffness component (more accurately named *influence coefficient* by the Russian terminology [88]), one must envision the following. A uniformly distributed stress applied in the (1) fiber direction or through thickness direction (3) should see no significant impediment since the cracks only channel these stresses along their original path. The only way the transversely cracked layer can resist a stress in the (2) direction is by channeling and then bridging this stress across the shear interface into the constraining layer and back again as indicated by the arrows on the diagram. Consequently one can take stiffness A_{22} to reflect the degradation directly whilst A_{11} and A_{33} should reflect their original value. Now with regard to stiffnesses of mixed index, careful reasoning is requisite. Take A_{12} for example. By definition it is the stiffness in the (2) direction, or the *response* direction, due to an applied stress in the (1) or *imposed* direction. Looking at Figure 7.28 one can envision that each broken segment receives its portion of the uniformly distributed stress directly and that the response in the (2) direction, due to the internal Poisson action within that segment, must be transmitted outward across the shear interface for its actions to be felt globally. A_{21} represents a mirror action, it is a stiffness contribution arising from a stress imposed in the (2) direction. However to get this stress to exist within a segment of broken lamina it must first be diverted across the shear interface from the constraining layer before acting via a Poisson effect which causes an action in the response direction (1). This action is shown magnified in Figure 7.28. Clearly stiffness A_{21} is degraded. Similarly A_{23} indicates the through-thickness response resulting from a stress imposed in the (2) direction. The same torturous path for the

stress input to the broken segment must be followed before the Poisson effect can result an out-of-plane response. This is also true of A_{32} since the uniformly distributed stress in the (3) direction feeds each broken lamina segment directly and the (2) response occurs but can only be felt globally if its action is transmitted across the shear interface to the undamaged constraining layer. (If the Poisson response remained in plane then its action would be lost to altering the crack opening displacement). In sum the lesson is that only stiffness components with an *imposed* or *response* index of (2) should be affected by the presence of these transverse matrix cracks. Logically, stiffnesses involving combinations of direction index (1) and (3) would be immune to the effect of cracks since neither their imposed or response paths are altered.

Consider next the action of direct stress in direction (2). First, for a broken element to see such stress it must be transmitted via shear from the adjacent constraining layer into the element. Secondly the element's resistance to dimensional change must be reflected back across the same boundary for its effect to be felt globally. This path differs from the Poisson effects described earlier where the shear boundary is used *once* to create the tensile stress in the broken element but *not* relied on to make its contribution to the Poisson effect felt, or conversely, where the stress might be applied directly and the resultant Poisson action of the broken element then transmitted *once* across the shear interface. The difference being that when both imposed and response direction are (2), the shear interface is exploited to perform two actions simultaneously rather than one. It would therefore be logical to expect a stronger degradation of the tensile influence coefficient in comparison with Poisson coefficients.

Lastly, looking at shear, one can visualize the broken segments with the cracked surfaces sliding past another when the imposed stresses are either σ_{12} or σ_{23}. This does not happen for stress σ_{13} since the angular deformation on each cracked face should be equal and in the same sense provided that the shear applied to each segment is identical (which it should be since the loads are assumed to be uniformly distributed). In another way of looking, shear σ_{13} can be resolved into a combination of imposed stresses constituted from σ_{11} and σ_{33}. There is no involvement of stress from the (2) direction, unlike what occurs when shears σ_{12} and σ_{23} are synthesized from tensile stresses. It follows that A_{44} and A_{66} should be degraded but not A_{55}.

In testing the above reasoning, values computed for the engineering constants of damaged laminates (physically measurable quantities) should agree with expected behavior. For instance the changes in the various Poisson's ratios should follow what is known from experiment, and obvious results like virtual independence of axial modulus E_{11} and E_{33} from matrix cracking must never be violated. Also the engineering moduli cannot be seen to be increasing with the onset of damage.

With a little thought, the conclusions reached above can be extended to the case of subsequent fiber breakage where a shear transfer to adjacent layers becomes requisite to bridge the point of fracture. In this case the direct stiffness component with an imposed and response stress index of (1) can be set to a low value, typically the reduction ought to be at a level commensurate with the stiffness of the surrounding damaged matrix. In addition, with fiber breakage, the Poisson related stiffnesses containing the (1) direction would also need to resort to a shear transfer to the constraining material and

consequently their contribution to the laminate would be expected to drop by approximately the same factor as for the case when either the imposed or response direction is (2).

The effect of assigning stiffness reductions to the matrix terms in Table 7.10 as postulated can easily be examined by assigning actual values for a damaged laminate and then comparing the resulting engineering constants to those of an undamaged laminate. Also trends with Poisson's ratios can be considered in view with available experimental evidence. If the results meet with physical expectations the method can be deemed successful, otherwise it must be rejected.

For the purpose of example, engineering material values for unidirectional T300_5208 at 60% volume fraction were taken from the material database of Table 7.1. The "Super Pressure - Vessel Designer" program's facility for calling up the stiffness and compliance matrix at any orientation angle was used to generate the virgin stiffness values. These are presented in Table 7.11 below. The engineering properties associated with this unidirectional lamina are given in Table 7.12.

Table 7.11 Virgin stiffness matrix T300_5208 (GPa)

	ε_{11}	ε_{22}	ε_{33}	ε_{23}	ε_{31}	ε_{12}
σ_{11}	140.22	5.75	5.75			
σ_{22}	5.75	11.84	5.80			
σ_{33}	5.75	5.80	11.84			
σ_{23}				6.04		
σ_{31}					9.22	
σ_{12}						9.22

389

Table 7.12 Engineering properties T300_5208 (GPa)

Property	Composite	Matrix
E_{11}	136.47	3.80
E_{22}	8.933	
ν_{12}	.325	.35
ν_{23}	.479	
G_{12}	4.612	
G_{23}	3.018	
K_{23}	8.82	

The engineering properties for the composite are generated by applying the terms in Table 7.11 to equations (7.65)-(7.73). Similarly for the damaged lamina the effective engineering constants can be determined, however the equations carry extra terms since there are now more than 5 independent constants. For illustration purposes let us assume 2 distinct, sequential stages of damage. The first is a condition at or near the saturation crack density, and from Figure 7.20 let us assign an engineering stiffness degradation amounting to a 25% retention of the original value. A second and more severe subsequent damage condition to model is that when fiber breakage occurs after the matrix stiffness degradation phase. The moduli reductions to choose for this event is not well researched but one does know it must be very severe and reduction of the principal moduli to the effective level of the surrounding damaged matrix seems reasonable.

The relations between the engineering properties and the elastic moduli for the orthotropic form (7.76) can be determined. For an imposed uniaxial state of stress

specified by $\sigma_{11} \neq 0$ and $\sigma_{22} = \sigma_{33} = \tau_{12} = \tau_{23} = \tau_{31} = 0$ the pertinent elasticity

equations are:

$$\sigma_{11} = A_{11}\varepsilon_{11} + A_{12}\varepsilon_{22} + A_{13}\varepsilon_{33}$$
$$0 = A_{21}\varepsilon_{11} + A_{22}\varepsilon_{22} + A_{23}\varepsilon_{33}$$
$$0 = A_{31}\varepsilon_{11} + A_{32}\varepsilon_{22} + A_{33}\varepsilon_{33}$$

$$(7.76)$$

the second and third equations of (7.76) reduce to

$$\varepsilon_{22} = -\left(\frac{A_{21}\varepsilon_{11} + A_{23}\varepsilon_{33}}{A_{22}}\right) \quad \text{and} \quad \varepsilon_{33} = -\left(\frac{A_{31}\varepsilon_{11} + A_{32}\varepsilon_{22}}{A_{33}}\right)$$

solving for ε_{22} and ε_{33} gives

$$\varepsilon_{22} = -\frac{A_{21}\varepsilon_{11}}{A_{22}} - \frac{A_{23}}{A_{22}}\left(\frac{-A_{31}\varepsilon_{11}}{A_{33}} - \frac{A_{32}\varepsilon_{22}}{A_{33}}\right)$$

$$\varepsilon_{22}\left(1 - \frac{A_{23}A_{32}}{A_{22}A_{33}}\right) = \varepsilon_{11}\left(\frac{-A_{21}}{A_{22}} + \frac{A_{23}A_{31}}{A_{22}A_{33}}\right)$$

$$\varepsilon_{22} = \frac{\varepsilon_{11}\left(\dfrac{A_{23}A_{31}}{A_{22}A_{33}} - \dfrac{A_{21}}{A_{22}}\right)}{\left(1 - \dfrac{A_{23}A_{32}}{A_{22}A_{33}}\right)}$$

$$\varepsilon_{22} = \varepsilon_{11}\frac{A_{23}A_{31} - A_{21}A_{33}}{A_{22}A_{33} - A_{23}A_{32}}$$

$$(7.77)$$

and

$$\varepsilon_{33} = -\frac{A_{31}\varepsilon_{11}}{A_{33}} - \frac{A_{32}}{A_{33}}\left(\frac{-A_{21}\varepsilon_{11}}{A_{22}} - \frac{A_{23}\varepsilon_{33}}{A_{22}}\right)$$

$$\varepsilon_{33}\left(1 - \frac{A_{32}A_{23}}{A_{33}A_{22}}\right) = \varepsilon_{11}\left(\frac{A_{32}A_{21}}{A_{33}A_{22}} - \frac{A_{31}}{A_{33}}\right)$$

$$\varepsilon_{33} = \frac{\varepsilon_{11}\left(\dfrac{A_{32}A_{21}}{A_{33}A_{22}} - \dfrac{A_{31}}{A_{33}}\right)}{\left(1 - \dfrac{A_{32}A_{23}}{A_{33}A_{22}}\right)}$$

$$\varepsilon_{33} = \varepsilon_{11}\frac{A_{32}A_{21} - A_{31}A_{22}}{A_{33}A_{22} - A_{32}A_{23}}$$

(7.78)

substituting into the first of (7.78)

$$\sigma_{11} = \varepsilon_{11}\left[A_{11} + \frac{A_{12}\left(A_{23}A_{31} - A_{21}A_{33}\right) + A_{13}\left(A_{32}A_{21} - A_{31}A_{22}\right)}{\left(A_{22}A_{33} - A_{23}A_{32}\right)}\right]$$

so $\sigma_{11} = \varepsilon_{11}E_{11}$ where:

$$E_{11} = A_{11} + \frac{A_{12}\left(A_{23}A_{31} - A_{21}A_{33}\right) + A_{13}\left(A_{32}A_{21} - A_{31}A_{22}\right)}{\left(A_{22}A_{33} - A_{23}A_{32}\right)}$$

(7.79)

from the definition of Poisson's ratio we rearrange (7.78) and (7.79) to get

$$v_{12} = \frac{-\varepsilon_{22}}{\varepsilon_{11}} = \frac{A_{33}A_{21} - A_{23}A_{31}}{A_{33}A_{22} - A_{32}A_{23}}$$

(7.80)

$$v_{13} = \frac{-\varepsilon_{33}}{\varepsilon_{11}} = \frac{A_{31}A_{22} - A_{32}A_{21}}{A_{33}A_{22} - A_{32}A_{23}}$$

(7.81)

Using the imposed stress state $\sigma_{22} \neq 0$, $\sigma_{11} = \sigma_{33} = \sigma_{23} = \sigma_{31} = \sigma_{12} = 0$, by identical

technique to the above we find

$$E_{22} = A_{22} + \frac{A_{21}\left(A_{13}A_{32} - A_{12}A_{33}\right) + A_{23}\left(A_{13}A_{31} - A_{32}A_{11}\right)}{A_{33}A_{11} - A_{31}A_{13}}$$

$$v_{21} = \frac{-\varepsilon_{11}}{\varepsilon_{22}} = \frac{A_{12}A_{33} - A_{13}A_{32}}{A_{11}A_{33} - A_{13}A_{31}}$$

$$(7.83)$$

$$v_{23} = \frac{-\varepsilon_{33}}{\varepsilon_{22}} = \frac{A_{32}A_{11} - A_{13}A_{31}}{A_{33}A_{11} - A_{31}A_{13}}$$

$$(7.84)$$

Finally using imposed stress state $\sigma_{33} \neq 0$, $\sigma_{11} = \sigma_{22} = \sigma_{23} = \sigma_{31} = \sigma_{12} = 0$, the engineering constants compute as

$$E_{33} = A_{33} + \frac{A_{31}(A_{12}A_{23} - A_{13}A_{22}) + A_{32}(A_{21}A_{13} - A_{23}A_{11})}{A_{11}A_{22} - A_{12}A_{21}}$$

$$(7.85)$$

$$v_{31} = \frac{-\varepsilon_{11}}{\varepsilon_{33}} = \frac{A_{23}A_{11} - A_{21}A_{13}}{A_{22}A_{11} - A_{21}A_{12}}$$

$$(7.86)$$

$$v_{32} = \frac{-\varepsilon_{22}}{\varepsilon_{33}} = \frac{A_{23}A_{11} - A_{21}A_{13}}{A_{22}A_{11} - A_{21}A_{12}}$$

$$(7.87)$$

The engineering constants, equations (7.79)-(7.87) can be solved in our example case with various moduli reduction schemes imposed upon the A_{ij} terms. To this end a considerable amount of time was spent trying to find proportionate values one could use to alter the respective moduli and not violate the basic premises discussed earlier. This turns out to be a lot more difficult than one would assume. After many unsatisfactory trials by manual means, two routines were coded, one to generate the engineering constants from the stiffnesses via equations (7.79)-(7.87) and an inverse procedure to generate the stiffnesses from engineering constants (adapted from R.M. Jones [173]).

These short routines are called procedure stiffness and stiffinv, and can be found in unit failure.pas. The code was run repeatedly using a range of inputs deemed reasonable. The quest to attain a valid stiffness reduction scheme would be trivial provided one knew the simultaneous behavior of all engineering constants under transverse cracking, but such data was not found in any of the literature reviewed. After examining the parameters at play the following guidelines were set forth:

1) Engineering moduli in undamaged directions must not change.

2) Principle stiffness moduli in undamaged directions must not change.

3) Poisson's ratios not involving damaged directions must remain constant.

4) Poisson related stiffness moduli can only decrease but must remain positive.

5) Individual lamina Poisson's ratios cannot become negative.

6) The stiffness matrix remains symmetric (Forces are conservative, path independent).

7) Affected Poisson's moduli should be decreased, preferably by a common factor.

In practice these criteria are easily violated, especially the first three. Initially all reduction schemes tested failed because principle moduli E_{33} and / or E_{11} always ended up increasing, something deemed impossible. These early schemes were based on using the same reduction factor for both principle moduli E_{22} and the associated Poisson related moduli. There were many other short comings such as reversals in the trends on the resulting Poisson's ratios depending on the level of stiffness reduction being modeled in the transverse direction. Also it was impossible to keep Poisson ratios v_{13} and v_{31} constant (condition 3) and simultaneously not violating other factors. With

some clues provided by the inverse code that generated stiffness matrix values from assumed degraded engineering properties, a reduction scheme emerged that managed to meet conditions (1-7). The reduction factors and corresponding moduli for various levels of damage are presented in Table 7.13 for the T300_5208 material.

Table 7.13 Proposed moduli reductions for progressive matrix failure, T300_5208.

$ij = 22$ factor	$ij = 12,23$ factor	E_{11}	E_{22}	E_{33}	v_{12}	v_{21}	v_{13}	v_{31}	v_{23}	v_{32}
1.00	1.00	136.47	8.93	8.933	0.325	0.0213	0.325	0.0213	0.479	0.479
0.85	0.92	136.48	7.61	8.948	0.352	0.0196	0.327	0.0214	0.440	0.519
0.75	0.87	136.46	6.70	8.911	0.379	0.0186	0.324	0.0211	0.414	0.556
0.60	0.77	136.49	5.40	8.968	0.417	0.0164	0.328	0.0216	0.365	0.615
0.50	0.71	136.46	4.48	8.914	0.464	0.0152	0.324	0.0211	0.334	0.681
0.35	0.59	136.48	3.16	8.951	0.548	0.0126	0.327	0.0215	0.275	0.808
0.25	0.50	136.47	2.26	8.936	0.652	0.0107	0.326	0.0213	0.230	0.959

The reduction factors utilized above were only set to the second decimal place, however virtually perfect matches to the criteria can be achieved by further refinement. Shown in Table 7.14 for contrast is an example of a failed moduli reduction scheme whereby all conditions are identical to those in Table 7.13 except that the factor 0.25 was used throughout. In this case moduli E_{11} and E_{33} have exceeded the undamaged values, and the various Poisson's ratios are all changing quite unpredictably.

Table 7.14 Failed moduli reduction scheme for matrix damage, T300_5208.

$ij = 22$ factor	$ij = 12,23$ factor	E_{11}	E_{22}	E_{33}	v_{12}	v_{21}	v_{13}	v_{31}	v_{23}	v_{32}
0.25	0.25	137.23	2.80	10.94	0.263	0.0053	0.453	0.036	0.105	0.472

The bigger test involves selecting randomly different materials, applying this same scheme and seeing whether it was specific only to the T300_5208 data set or if it can be applied rather universally. Table 7.15 applies the same moduli reduction scheme to IM7_9772, Kev_49 and E_glass. Base material properties for these are available in Table 7.1. Obviously the conditions (1-7) are entirely fulfilled, and we must conclude that the scheme shows merit. It stands to reason that other moduli reduction combinations may work equally or better however it is likely that experiments will be needed to confirm behavior to a level more precise than currently postulated. At minimum, one can have confidence that the with the present simple prediction scheme, violations from actual behavior should not be too severe.

Table 7.15 Effect of proposed stiffness reduction scheme on various materials.

Material: IM7_9772 @ 58% fiber volume									
$ij=22$ factor	$ij=12,23$ factor	E_{11}	E_{22}	E_{33}	v_{12}	v_{21}	v_{13}	v_{31}	v_{23}	v_{32}
1.00	1.00	173.00	7.585	7.585	0.290	0.0127	0.290	0.0127	0.426	0.426
0.75	0.87	172.99	5.681	7.569	0.337	0.0111	0.289	0.0126	0.369	0.494
0.50	0.71	172.99	3.793	7.571	0.413	0.0090	0.289	0.0126	0.300	0.605
0.25	0.50	173.00	1.905	7.585	0.580	0.0063	0.290	0.0127	0.208	0.851
Material: Kev_49 @ 66% fiber volume									
$ij=22$ factor	$ij=12,23$ factor	E_{11}	E_{22}	E_{33}	v_{12}	v_{21}	v_{13}	v_{31}	v_{23}	v_{32}
1.00	1.00	87.10	5.718	5.718	0.340	0.0223	0.340	0.0223	0.529	0.529
0.75	0.87	87.09	4.284	5.679	0.396	0.0194	0.338	0.0221	0.457	0.614
0.50	0.71	87.09	2.872	5.699	0.485	0.0159	0.338	0.0221	0.368	0.751
0.25	0.50	87.10	1.457	5.718	0.681	0.0111	0.340	0.0225	0.252	1.058
Material: E_Glass @ 60% fiber volume									
$ij=22$ factor	$ij=12,23$ factor	E_{11}	E_{22}	E_{33}	v_{12}	v_{21}	v_{13}	v_{31}	v_{23}	v_{32}
1.00	1.00	45.00	13.94	13.94	0.265	0.082	0.265	0.082	0.335	0.335
0.75	0.87	44.99	10.47	13.92	0.307	0.071	0.264	0.082	0.286	0.389
0.50	0.71	45.00	7.02	13.93	0.376	0.058	0.264	0.082	0.225	0.476
0.25	0.50	45.00	3.56	13.94	0.529	0.041	0.265	0.082	0.144	0.671

Some experimental data exists to compare changes in a laminate's Poisson ratio

as a function of damage accumulation. Figures 7.26 and 7.27 indicate that a significant

reduction is expected, along with the shear modulus. It can be seen that since v_{21} is

steadily decreasing with damage its effect will be transferred to the laminate as a whole.

For example: Using properties from T300_5208 for a [0/90]$_s$ laminate and adding up the

stiffness matrices of two layers, one virgin and the other at saturation damage, one gets

the laminate response. By inverting this stiffness matrix it can be verified that the overall

v_{12} value of the laminate will decrease from 0.040 to 0.030 (for crack saturation).
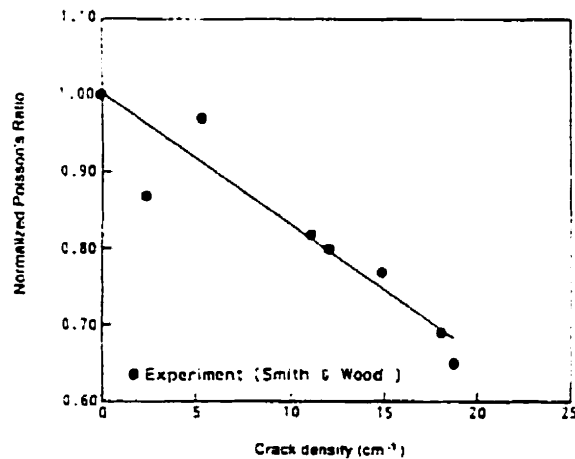
Figure 7.29 Poisson's ratio reduction as a function of crack density.
Adapted from Jhang, Fan & Soutis [200], data from Smith & Wood [232].

This 25% reduction compares favorably with similar materials experimented upon

by others as evidenced in Figures 7.26 and 7.29. Also from these same figures one would

expect shear moduli reductions on the order of the Poisson related stiffness moduli and hence such a factor was assigned to shear stiffness terms A_{44} and A_{66}.

Luo-Yu Xu [224], Smith and Wood [232], Han and Hahn [206] and others indicate that v_{21} is dependent on matrix cracking in a manner similar to the transverse stiffness reduction and G_{12} is expected to behave identically with the exception of using a different shear-lag parameter. The majority of experiments however find Poisson moduli reductions to exceed theoretical predictions. In fact Smith and Wood [232] discovered cases where the reductions exceeded 50%, the maximum reduction possible according to ply-discount. They noted significant damage parallel to the longitudinal plies in the form of slits and splits. This type of damage can account for the remaining 50% reduction possible until the splitting develops uniformly and Poisson's ratio drops to zero. The values for v_{13} and v_{31} would *not* be expected to change with transverse cracking since they involve stresses that act in a direct line on each broken element and thereby circumvent a shear transfer mechanism altogether.

A further refinement to the scheme was necessary to establish the effective properties of a laminate after fiber fracture. It turns out that assigning a stiffness reduction factor on the remaining Poisson terms containing the (1) direction along with reducing the principle moduli A_{11} to a value near that of the surrounding damaged matrix achieves a steady E_{33} value. Experience has shown that reducing A_{11} to exactly the stiffness of the surrounding matrix may cause various negative Poisson's ratios and significant deviations in E_{33}. Multiplier values on the degraded matrix modulus ranging between 1.0 −1.3 give an effective principle stiffness A_{11} that results in a through-

thickness engineering modulus E_{33} that remains virtually unchanged. The higher the

multiplier, the greater the residual value of E_{22} and E_{11}, and also the difference between

them. Table 7.16 presents the computed engineering constants for 4 different materials at

maximum matrix degradation coupled with fiber failure. The additional degradation's

assigned to moduli associated with the (1) direction are indicated and were chosen for

good fit.

Table 7.16 Moduli degradation factors for fully damaged matrix + broken fiber.

Material	$ij = 22$ factor	$ij = 12,23$ factor	$ij = 13$ factor	$A_{11} = f \cdot A_{22}$ $f = factor$	E_{11}	E_{22}	E_{33}	ν_{12}	ν_{21}	ν_{13}	ν_{31}	ν_{23}	ν_{32}
T300_5208	0.25	0.50	0.50	1.10	0.463	0.407	8.99	0.965	0.849	0.006	0.126	0.039	0.857
IM7_9772	0.25	0.50	0.50	1.10	0.952	0.835	7.54	0.800	0.702	0.035	0.278	0.070	0.631
Kevlar_49	0.25	0.50	0.55	1.30	0.404	0.385	5.74	1.034	0.766	0.014	0.205	0.006	0.866
E_Glass	0.25	0.50	0.50	1.10	2.33	2.08	13.97	0.681	0.609	0.056	0.338	0.072	0.485

Methods presented above to estimate the 3-D property variations that arise from

transverse cracking phenomena were coded into "Super Pressure - Vessel Designer". The

program calculates the degraded properties within an iterative loop that computes the

stresses acting on the entire vessel. As a laminate begins to fail, the current overload

factor (defined as $\frac{1}{R}$ in equation (7.34)) is compared to the load of first ply failure ($R = $

1) according to the failure criterion. The difference between this quantity and the crack

saturation limit sets the "equivalent loading" for equation (7.41) which in combination

with the fitting parameters of Table 7.8 and equation (7.46) enables determination of the

"equivalent residual stiffness" as defined by (7.63). Effectively equation (7.41) is

transformed to:

$$\varepsilon_{eq} = \frac{1}{3}\sqrt{\frac{3^2 - \left(\frac{1}{R}\right)^2}{\left(\frac{1}{R}\right)^2 - 1}} \qquad \text{Where: } \varepsilon_{cs} = 3\left(\varepsilon_{ci}\right) \quad \text{and} \quad \varepsilon_{ci} = R = 1$$

(7.88)

Knowing this reduction factor allows implementation of the stiffness reduction scheme

described above and subsequently a re-evaluation of the 3-D material properties for each

constituent layer experiencing some level of damage. The vessel stresses are then re-

computed and the new "overload" in each layer is compared to that of the previous

iteration. If the difference in the overload factor compared with the previous computation

meets a relative tolerance (0.1%) the solution is considered converged for that layer,

otherwise a midpoint strain between the newly computed and previous iteration is used in

subsequent re-calculations for damaged material parameters. This midpoint approach to

estimating the degradation for subsequent iterations provides added stability and has

eliminated oscillation about 2 solution points. If the failure criterion indicates that fiber

breakage occurs, then the appropriate stiffness reductions (indicated in Table 7.16 and

Figure 7.30) are incorporated. Evaluation continues until all layers have met the relative

tolerance. Screen graphics showing the stresses and relative safety factors throughout the

vessel wall are updated and displayed with each iteration. Examples are given in Chapter

8.

Practice has shown the algorithm operates in stable fashion and usually requires 5-

7 iterations before converging on a solution for cases where there is severe matrix

damage and / or layers containing broken fibers. More normal situations are usually

resolved in 1-3 iterations, on the whole a matter of a few seconds for modest desktop

computers such as those based on an *i486 - series* processor.
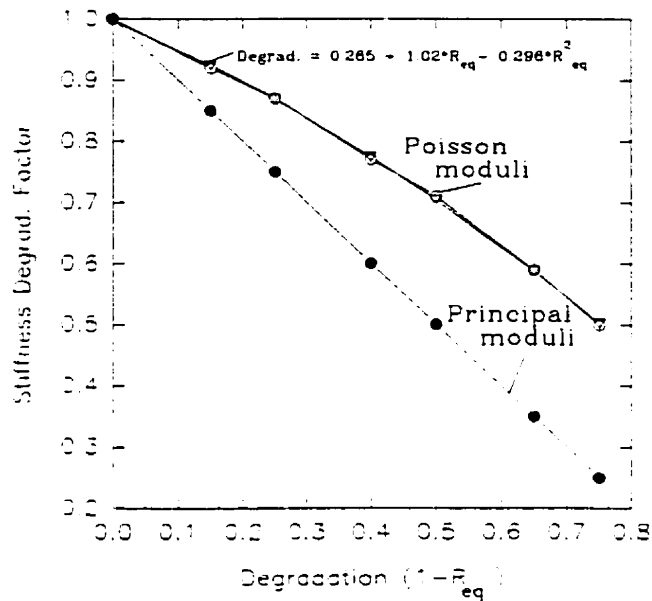
Figure 7.30 Moduli reduction scheme for matrix damage.
Program uses the curve-fit equation given in the diagram to
adjust Poisson related moduli along with the condition
$A_{11} = 1.1\left(A_{22}^{damaged}\right)$ after fiber breakage.

As a final item, it is well known that unidirectional composite laminates under test

essentially exhibit a non-linear shear behavior. (Note: The effect is *not* related to

transverse cracking in any regard). This topic was investigated by S.R. Swanson and co-

authors [233][194], both for devising a test to quantify the effect and in relation to

modeling the response of laminates under biaxial stress. Different empirical relations were

presented, one of which was adapted to the current work. These researchers found that such approximations improved the correlation with failure theories in biaxially loaded tubes and that the analytical relations were indeed able to mimic the actual stress-strain curves quite closely. In lieu of such evidence the formulation

$$G_{12}^N = \frac{\tau}{\gamma} = \frac{G_{12}^0}{\left[1 + \left(\frac{G_{12}^0 \gamma}{\tau_b}\right)\right]^{\frac{1}{2}}}$$

where: G_{12}^N = actual non-linear shear modulus

G_{12}^0 = initial shear modulus

τ_b = ultimate shear strength

γ = actual shear strain

(7.89)

was used as a correction factor to the initial shear modulus. A more complete form of this equation utilizing the actual strain at failure is also available [233]. This correction presents itself in the same loop described earlier for re-calculating moduli on the basis of damage due to transverse crack formation. The correction is invoked only prior to a ply's matrix failure initiation point, thereafter moduli reductions are governed by the damage parameter. For this reason at least one iteration occurs in all stress computations using a non-linear shear approximation regardless of whether damage due to cracking has begun at any point. This effect can play a noticeable role in raising the load required for the onset of matrix cracking, ($\cong 10\%$) but has no action upon the computed burst pressure. The software allows evaluations with or without inclusion of this correction factor so one can see the difference it causes.

To summarize, each topic presented throughout this work has been incorporated into the design software. Computation of stress distributions as per Chapters 4 - 6, or the winding parameters as per Chapter 3, are by themselves insufficient in providing guidance through to building a performant pressure vessel. To close the circle one needs to look at strength. But strength is a dependent phenomenon, related to loading history and damage accumulation. This damage affects the elastic characteristics which in turn alters the stress distributions. By combining the different elements of Chapter 7 one can estimate the level to which elastic properties are affected. In turn, the elasticity solutions described in the earlier chapters can be re-invoked to assess these new and altered stress distributions and also used to predict remaining strength. The design software written executes these computations automatically every time the load is incremented. Its capabilities are presented next.

Chapter 8

Description of Software with Examples

8.0 Super Pressure - Vessel Designer

In this section we devote our attention to the pressure vessel design process insofar as describing how the various segments of software operate and interconnect as a system to implement the various topics discussed in the foregoing chapters. A hypothetical vessel design is used as an example and followed through to demonstrate features of the program.

The software to assist in pressure vessel design has been developed over a number of years and has evolved and existed in many incarnations. Each new version was labeled sequentially, *ves_1*, *ves_2*, ... eventually there were so many generations of code that *ves_9.exe* (the present filename) was fixed and the name "Super Pressure-Vessel Designer" was coined. The source code (Appendix B) continues to be updated, seeing improvement and changes on a regular basis. The code in Appendix B was created with Borland's Turbo Pascal® 5.5 and constitutes a compilation of approximately 11 thousand lines of executable code. Considerably more was written for the project. Not every element coded is active for the compiled version in the included diskette. Elements seeing continued development or used for code verification and auxiliary routines related to different failure envelopes and degradation schemes have been commented out making these portions invisible to the compiler. The version on diskette is a functional package which can be run directly from the MS DOS® prompt or an MS DOS® window under the

404

MS Windows® environment. Because of memory requirements and organizational concerns the code is subdivided into different "overlays", each containing multiple "units", with each of these in turn holding an assortment of procedures (subroutines) and / or function calls. Generally the procedures are grouped into categories with the name of the unit somewhat indicative of the procedures contained within. The main program loads the overlay manager first (which initiates EMS memory if present) and subsequently loads the interface section of each unit. The code required for execution is then transparently made available whilst not wasting memory by loading unnecessary portions. The source code has limited commentary within, sufficient to jog the programmer's memory, but not meant for the casual reader who is trying to follow execution without the code tracing ability of the integrated debugger environment (IDE) used during development.

The program is designed to handle 15 distinct ± angle pair layers (referred to simply as layers henceforth), a practical number considering that construction techniques essentially limit high quality lay-ups to an outer/inner diameter ratio of around 1.25. This translates to on average 1.67% of the vessel's inner radii per layer, about 0.067″ (1.7 mm) for an 8″ (200 mm) inside diameter unit. Practically speaking, on a typical small filament winder using a 0.5″(13 mm) bandwidth with about 5-10 fiber tows such dimensions are on the order of two layer pairs. This is a reasonable value. Another point to consider is that the diameter to wall thickness ratio (d/t) of such a layer is $\cong$ 120:1 and well into the range where thin wall approximations (constant stress through the layer) are the accepted norm. But in no place are we using thin-wall approximations, only the full solution. Finding the optimal number of layers is esentially a question related to how one subdivides

the natural stress gradient into a sufficient number of layers to limit the maximums at the inner face of each. Because these gradients are steepest at the inner surface of any vessel, one would simply assign thinner dimensions to the innermost layer(s) in an attempt to lessen the difference between the stresses at the radial extremities of each of these. The requirement for a large number of layers is not actual from a stress analysis point of view but rather the benefit could come about via considerations of stable radial compaction and limitations arising from the manufacturing techniques where one must cope with winding around the dome enclosures.

The magnitude of the stress gradients can be evaluated by examining some of the forthcoming figures and taking note for instance of the difference between the maximum and minimum hoop stress. To illustrate we can momentarily flip forward to an example case presented subsequently. We have in Figure 8.20 an 8 layer vessel loaded to near failure at 150 MPa internal pressure. The layer stresses for this loading are given in Table 8.4. The data shows the hoop stress (sigma θ) variation to be about 2.6% of the average stress in one lamina. The overall stress reduction achievable through flattening this variation by subdividing any one layer into sub-layers and optimizing for example the winding angles could only reduce the inner surface stress by at most half this amount (1.3%). This is not very consequential. The through-thickness stress gradients of σ_θ, although significant on the large scale because they are continuous (30-50% reductions through the wall), are not very contributory individually once they are subdivided into smaller elements and staggered appropriately. So the need for a vast number of layers to more evenly distribute the load through the wall is thus essentially a fallacy.

The mathematical portion of the code is not restricted to 15 layer designs. The maximum number of layers is defined by a global constant in the code. Fifteen layer pairs is an artificial constraint based on the 640 x 480 pixel resolution of one graphics screen and its ability to clearly display the results while providing space for interactive editing. Scrolling and zooming graphics or a Windows® implementation could be employed to overcome this limitation and may be addressed in the future.

Program operation is quite simple and it can be run from nearly any personal computer with an Intel® 8086 based processor or better (80386, 80486, Pentium ...). 640 KB memory is sufficient and no math coprocessor is required on the very early generation PC's because the software is set to emulate its presence. Numeric data types are 6 bit real with 11-12 significant digits, covering the range $2.9E^{-39}$ to $1.7E^{38}$. Extended memory is a benefit but not required. From the DOS prompt calling the batch file "SPVD" starts the program, which flashes an opening screen and then defaults to the main menu. The available selections are at screen bottom, invoked by highlighted <ALT-letter> combinations. Other active keys used to navigate through the program are highlighted with a red background at the top of the screen whenever these keys are active. A chart showing branches of the menu tree can be studied in Figure 8.1. From this chart the sequence of operations necessary for program operation is not yet imediately evident however before getting deeper into the details of the program an overview of the structure and description of the main functions are in order. More concise instructions for operation follows afterwards.

The code is subdivided into different modules, each to handle or enable study of

different aspects related the pressure vessel design. The various elements communicate

with one another by creating and modifying text files which are written to disk and
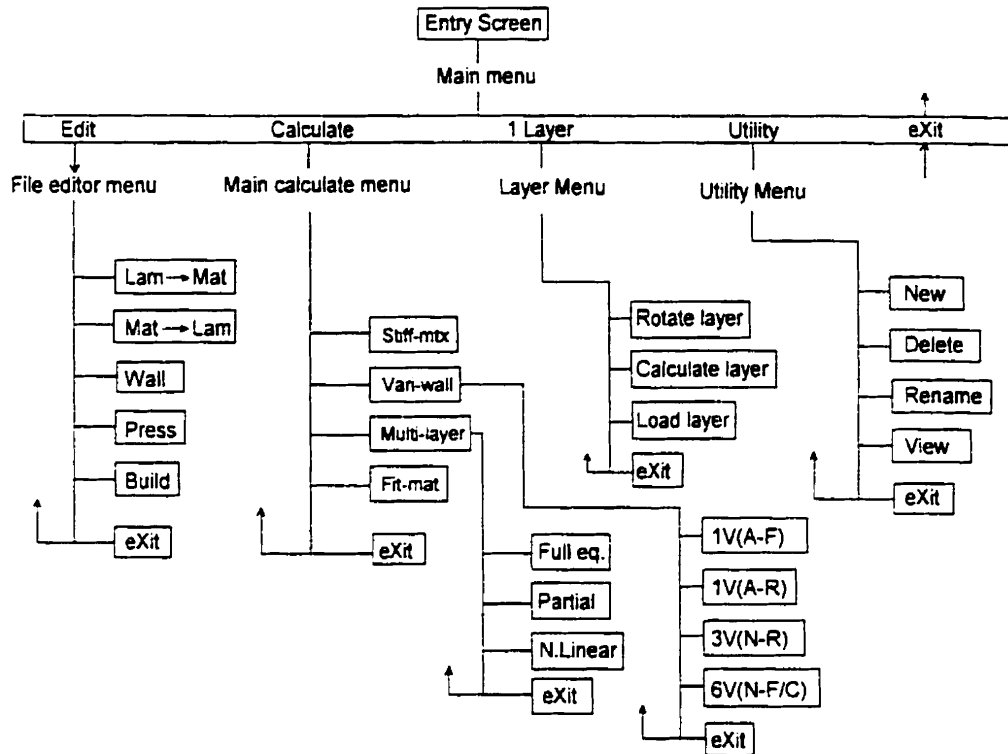
Figure 8.1 Menu chart for "Super Pressure -Vessel Designer"

subsequently read by other segments of the program. The basic idea is to first create all

the necessary building blocks, in this case the support files, needed to analyse cases. For

example: Material property files {.mat}, vessel wall lay-up files {.wal}, dimensions and

loading files {.prs}. Once this has been done the case to be analysed is synthesized by

combining a wall lay-up, within which material files are embedded, and the loading /

dimensions into a master file that contains all the information necessary to define the

construction {.*ves*}. From this point 3 different modules are available, each of which has the capability both to analyse and also to modify the material and construction parameters of the case under examination. The 3 modules are (Vari-wall), (Fit-mat) and (Multi-layer).

8.1 Description of Program Modules

Different approaches to vessel design are possible. One possibility is the desire to achieve a particular stress distribution through a wall. (Vari-wall) has 4 different mathematical solutions that define a wall as a continuum (rather than individual layers). Here stress distributions are depicted for such hypothetical variable material property walls. The power functions describing these hypothetical material parameters can be varied (via cursor keys) and the resulting stress distributions are given (graphically). Having from the above gained an idea of the property variation rates necessary to achieve a particular stress distribution, another module (Fit-mat) is used to bridge between the hypothetical contiuum and the discrete material lay-ups constituting real vessels.

In (Fit-mat) mathematical curve-fits are generated showing how well the elastic properties of discrete materials in the chosen lay-up conform to the ideal variation rates responsible for desirable stress distributions determined earlier. Here the wall construction file can be edited incrementally (via the cursor keys) to approach the elastic parameter variations required. Once a satisfactory combination is found, the 3rd module (Multi-layer) can be invoked to check how closely the stresses in a real vessel would follow the theoretical distribution initially sought.

Within the (Multi-layer) module there also exists an extensive editing facility for the materials / lay-up and a depiction of the relative failure load of the matrix and fiber within each layer. Here again the design can be altered to adjust the stresses in individual layers or through sucessive perturbations one can arrive at other situations. These would encompass simultaneous fiber fracture in all layers, minimization of matrix damage or fail-safe design whereby pressure overloads would result in highly visible fractured exterior surface whilst maintaining enough structural integrity to avert rupture. The (Multi-layer) module can also simulate loading increments / decrements and can mimic proof tests, maintaining degraded material properties in memory to compute changes in stress distributions comensurate with the occurance of damage.

Now, to look at the individual program elements more closely, it is best to have the program running alongside the forthcomeing descriptions and follow along while running through the individual segments.

The (Edit) menu selection branches to a variety of file management tasks, including setting up the input files, a prerequisite to running the calculations under the (Calculate) menu. All input and output files are text format, therefore contents within can be viewed using any text editor or the file viewer available under the (Utility) menu.

The less significant menu items will be discussed first and some are remnant from earlier work and are useful as tools to analyze specific aspects of laminate behavior in test cases. Briefly, under the main menu, the (1 Layer) option is meant to give a feel for how materials behave in isolation. The option permits input of a ± lay-up angle for a set of plies thereby allowing a view of the *effective* stiffness and compliance matrices of the angle-ply

pair. Figure 8.2 illustrates the above being used to study a ± 59° lamination angle on

IM7_9772 graphite epoxy. To do this, select the 1 layer menu by typing <ALT-L> (hold

down Alt key and then press L). A new menu appears from which one selects <ALT-C>

to calculate the properties of a layer. This same screen will then automatically show a list

of all available files that one can choose from. Using <PgUp> <PgDn> allows scrolling

through all the available files. The file under consideration is highlighted and pressing

<INS> copies this file to the entry location. Once satisfied with the selection, hitting

<Enter> prompts the program to come up with a screen similar to Figure 8.2. This screen

gives the stiffness and compliance matrices for a unidirectional ply of the material selected.

Further, the matrices can be computed for any ± θ lamination angle as would be typical of

a filament wound layer pair. For this select <ALT-R> (Rotate layer) to enter the rotation

angle and hit <Enter> when done. A new set of stiffness matrices will appear

representing the ± θ sub-laminate. Lastly, supposing one were to design a filament wound

vessel using only this one particular ± θ lay-up angle then the resulting stresses and

displacements of such a vessel can be computed by further selecting < ALT-L> (Load

layer) and entering dimensions and pressure loads to define such a vessel. Figure 8.3

shows the result after the 4 input parameters (Outside diameter, inside diameter, internal

pressure, external pressure) have been typed in and <Enter> has been hit to invoke the

calculations. The example shown in Figure 8.3. is for a ± 59° lamination angle on

IM7_9772 material. The equations being solved by the computer are contained within

(4.30) - (4.42) and the radial displacement is made available via (4.29).

"Avoidance" (bottom of screen) is a name which has been coined to describe the

parameter K (used throughout Chapters 4 & 5). Defined in terms of the global stiffness coordinates of the layer pair, we have:

$$K = \sqrt{\frac{\beta_{11}}{\beta_{22}}} = \sqrt{\frac{(1 - v_{rz}v_{zr})E_\theta}{(1 - v_{\theta z}v_{z\theta})E_r}}$$

Substituting engineering quantities into the definition, it becomes clear that this parameter is effectively related to the circumferential to radial stiffness ratio. It can be viewed as a measure of the effectiveness of any laminate in suppressing transfer of stress onto the outer layers. Thus it defines the ability of any sub-laminate or even the whole laminate to avoid the through-thickness transmission of in-plane loads resulting from pressure upon laminations beneath or above. A high value of K indicates that the layer is relatively compressible radially. The innermost fibers of such a layer will be absorbing a high proportion of the load (since they lack support from behind) and thus the stress gradient within such a layer will be steep. The laminations providing support from behind will be effectively isolated from load leading to inefficiency in wall construction. The value of K depends on the winding angle and it increases from unity up to a maximum for the material as the winding angles progresses from $0°$ (polar) to $90°$ (hoop). This points to the theory that for an efficient single material vessel one must arrange the winding angles in a fashion so as not to cause a discontinuity in the rate at which the radial load is being absorbed through the wall. Otherwise the layer(s) behind can never be fully stressed. This facet will be examined further via an example at the end of the chapter.

For different materials the maximum value of K ranges widely. Table 8.1 presents examples at various $\pm \alpha$ lamination angles.

Table 8.1 Value of '*K*' in various materials as a function of lamination angle

Material	0°	30°	45°	55°	70°	90°
S-glass	1.00	1.02	1.11	1.19	1.32	1.40
Kev_49	1.00	1.28	1.88	2.35	2.97	3.32
AS4_3502*	1.00	1.33	1.96	2.45	3.09	3.45
IM6_SCI	1.00	1.45	2.28	2.92	3.73	4.18
T1000	1.00	1.46	2.32	2.97	3.80	4.26
P100S	1.00	2.45	4.46	5.87	7.63	8.61

*also T300_5208

Looking back upon Chapters 4-5 one can see that K is the primary variable governing the rate at which stresses diminishes with radial distance through a single layer. Isotropic material have $K = 1$, obviously the planar dominated stiffness of composites, graphite epoxy in particular, will exhibit much greater decay rates since E_r is comparatively small.
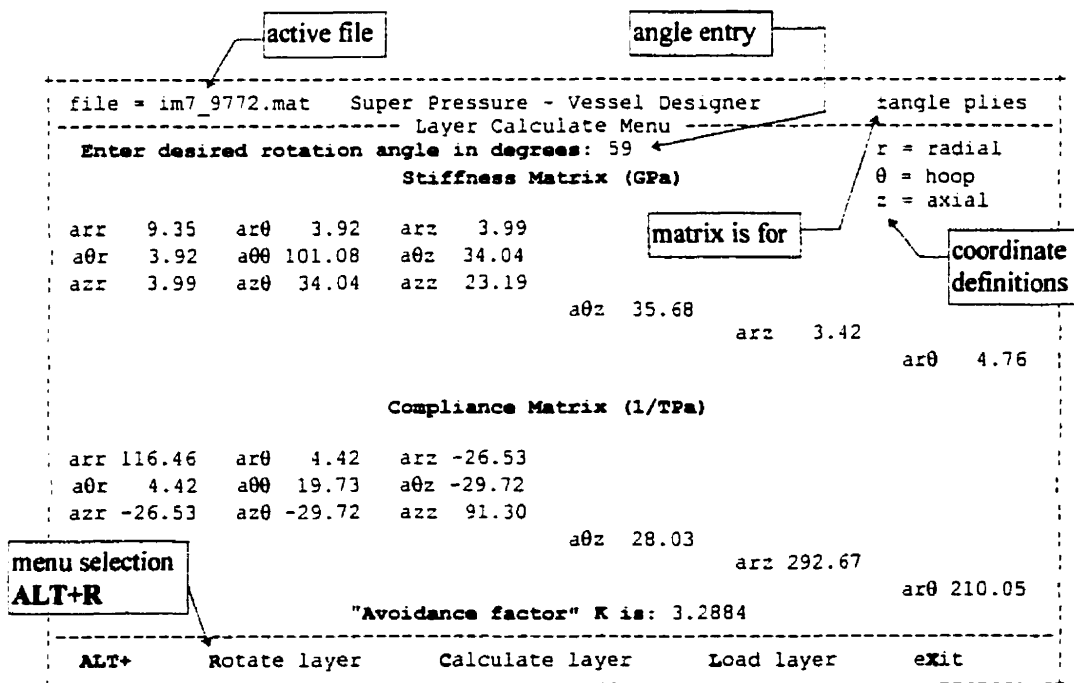
Figure 8.2 Rotated matrix stiffness and compliance values for ± angle ply pair.

413

```
+-----------------------------------------------------------------------------
: file = im7_9772.mat   Super Pressure - Vessel Designer                      :
:------------------------------- Layer Calculate Menu ------------------------:
:   Outside diameter (mm):300   ▲    +--------+                               :
:                                 /----|entries |                             :
:   Inside diameter (mm):150    /      +--------+                             :
:                               /      "Avoidance factor" K: 3.28837          :
:   Internal pressure (MPa):100 |                          ▼                  :
:                                                           \     +--------+  :
:   External pressure (MPa):10  ▼                            \----|β₁₁/β₂₂ |  :
:                                                                 +--------+  :
:   Parameter                   Inside        Middle        Outside           :
:                                                                             :
:   Sigma (θ) MPa:              320.636       48.8915       1.48300           :
:                                                                             :
:   Sigma (r)  MPa:             -100.00       -20.138       -10.000           :
:                                                                             :
:   Sigma (z)  MPa:             91.3885       26.1347       13.6483           :
:                                                                             :
:   Radial Disp. (mm):          0.23765       0.01114       -0.0630           :
:                                                                             :
:   Hoop strain (%):            0.3169        0.0099        -0.0421           :
:------------------------------------------------------------------------------
:   ALT+      Rotate layer    Calculate layer    Load layer      eXit         :
+-----------------------------------------------------------------------------
```

Figure 8.3 Stress distribution in single layer vessel upon loading

Under the (Edit) menu are contained operations for setting up the files requisite for

the design of a pressure vessel. A key aspect involves establishing a materials database,

which presently contains about 20 laminate varieties. (Edit) contains two program

elements that perform exactly each other's inverse fuction. These are (Lam→Mat) and

(Mat→Lam). The idea here is to extract and accumulate data on 3-dimensional fiber

properties by decomposing via micromechanical formulations the properties of a

unidirectional lamina. (Lam→Mat) performs such a task. Once this objective is achieved

new materials can be synthesized, either with different resin properties, volume fractions

or even imagined fiber properties not currently available. The program element

(Mat→Lam) carries out this reconstitution. For some more popular fibers, for instance T-

300, different data sets are available and as such each can be used to estimate the fiber

properties via the micromechanical back-calculation and conversely also investigate the

sensitivity of fiber engineering moduli towards the lamina characteristics . These will in

turn influence the stress distributions in the vessel.

```
+-----------------------------------------------------------------------+
: Ins & Enter          Super Pressure - Vessel Designer    PgUp:PgDn:Home:End :
:--------------------------- File Editor Menu ----------------------------:
: Enter filename or select:
:                                      [hot keys]
: AS4_3502.LAM    T300_34C.LAM
: AS3501_5.LAM    T300_520.LAM
, KEV_149.LAM     A_6061T6.LAM
: AS_3501.LAM     BR_S2_GL.LAM
: BORON_TS.LAM    BR_KV_49.LAM
: T300_TSA.LAM    SAN_KEV.LAM
: G_50.LAM        KEV_SCI.LAM
: E_GLASS.LAM     S2_SCI.LAM    <-----------[filenames in database]
: IM6_SCI.LAM                               [are listed automatically]
: IM7_9772.LAM
: G_30.LAM
: P100S.LAM
: KEV_49.LAM
: P75S.LAM
: SPEC900.LAM
: S_GLASS.LAM
: T1000.LAM
:------------------------------------------------------------------------:
: ALT+    Lam->Mat    Mat->Lam    Wall    Press    Build    eXit
+-----------------------------------------------------------------------+
```

Figure 8.4 File editor menu. Laminate name is entered to open file.

```
                              [hot keys & navigation]
+-----------------------------------------------------------------------+
: AS3501_5.LAM         Super Pressure - Vessel Designer    ↑:↓:Tab:Shift-Tab :
:--------------------------- File Editor Menu ----------------------------:
:       [laminate file]      Lamina Properties
:
: Modulus E11       (GPa)  142.00   L. Tens. Strength  (MPa)   1545.0
:
: Poisson V12       (ratio) 0.300   L. Comp. Strength  (MPa)   1565.0
:
: Modulus G12       (ratio) 4.480   T. Tens. Strength  (MPa)   52.00
:
: * Modulus E22 *   (GPa)   9.850 <-  T. Comp. Strength  (MPa)   118.00
:
: * Poisson V23 *   (ratio) 0.461   L. Shear Strength  (MPa)   72.00
:
: * Modulus G23 *   (GPa)   3.369   Fiber Vol. Fraction  (%)   70.50
:
: * Modulus K23 *   (GPa)   9.361 <-  Fiber Model <T-iso><iso>    T-iso
:
: Matrix Modulus E  (GPa)   3.726   Fit E12 & G12   <Yes><No>  [defaults to "No"]
:                                                            <-
: Matrix Poisson V  (ratio) 0.350   Metal ?         <Yes><No>
:------------------------------------------------------------------------:
: ALT+    Lam->Mat    Mat->Lam    Wall    Press    Build    eXit
+-----------------------------------------------------------------------+
```

Figure 8.5 Entry of unidirectional lamina data. For parameters denoted by * the
first two non-zero entries out of four will be utilized. Reverse
micromechanics is instigated by choosing the Lam→Mat option.

415

```
                        ┌──────────────────────┐
                        │ constituent material file │
        ┌──────────────┤                      ├────────────────────────────┐
        │ AS3501_5.MAT    Super Pressure - Vessel Designer    ↑:↓:Tab:Shift-Tab  │
        │------------------------- File Editor Menu -----------------------│
        │                   Fiber & Matrix Properties      ┌──────────┐    │
        │                                                  │navigation│    │
        │ Fib. Modulus El    (GPa)   199.85    L. Tens. Strength  (MPa) 1545.0 │
        │                                                                 │
        │ Fib. Poisson Vl    (ratio)  0.282    L. Comp. Strength  (MPa) 1565.0 │
        │                                                                 │
        │ Fib. Shear   Gl    (GPa)   9.676     T. Tens. Strength  (MPa) 52.000 │
        │                                                                 │
        │ * F. Modulus Et *  (GPa)   15.304    T. Comp. Strength  (MPa) 118.00 │
        │                                                                 │
        │ * F. Poisson Vt *  (ratio)  0.468    Shear Strength     (MPa) 72.000 │
        │                                                                 │
        │ * F. Shear   Gt *  (GPa)   5.211     Fiber Volume Fraction (%) 70.500 │
        │                                                                 │
        │ * F. Modulus Kt *  (GPa)   14.728    Fiber Model  <T-iso><iso>  T-iso │
        │                                                                 │
        │ Matrix Modulus Em  (GPa)   3.726     Fit E12 & G12    <Yes><No> │
        │                                                                 │
        │ Matrix Poisson Vm  (ratio)  0.350    Metal ?          <Yes><No> │
        │-----------------------------------------------------------------│
        │ ALT+    Lam→Mat    Mat→Lam    Wall    Press    Build    eXit    │
        └─────────────────────────────────────────────────────────────────┘
```

Figure 8.6 Material file generated with the command <ALT-L>. Values
here can be adjusted if so desired and then changes to laminate
properties may be reexamined by invoking the (Mat→Lam) option.

If one wishes to create an entirely new material entry, the first step is to also create

a new filename. For this one must switch to the (Utility) menu <ALT-U> and then select

(New) <ALT-N>. Existing filenames, sorted by file extension are listed automatically.

This helps avoid overwriting old files. When the list of existing files is longer than the

space on the screen the keys <PgDn> <PgUp> will scroll through the entries. For

example one could combine data for AS/3501-5 from Masters and Reifsnider [245],

Highsmith and Reifsnider [246] and adapt strengths from Tsai [174], to create a file

named AS3501_5.lam. One must type in the filename with its appropriate extension, in

this case (.lam) since it is unidirectional laminate data that will be entered. Hitting

<Enter> registers the filename. Next one must navigate back to the (Edit) menu via

416

<ALT-X> and then <ALT-E>. To view or edit a laminate, selecting (Lam→Mat) <ALT-L> will bring forth an entry screen as appears in Figure 8.4. The filename just created (AS3501-5.lam) can now be selected from the list that appears automatically on the bottom of the screen. Filename selection is via <PgUp> <PgDn>. Using the <INS> key copies the highlighted selection to the curser location, <Enter> then invokes action. A new screen will apear as per Figure 8.5.

After keying in or modifying the data (using keys <←↑↓→> and <Tab / Shift-Tab> to navigate) and entering "T-iso" for fiber type, selecting (Lam→Mat) for a second time invokes computation of the extracted fiber properties via the micromechanics equations of Section 7.2 (equations 7.14 - 7.17). Hitting <Enter> or any of the <Alt> + letter combinations will automatically save the entries, while <Esc> aborts and <Alt-X> returns a higher level menu. Figures 8.6 illustrates the screen one would see going from the laminate test data just entered (or modified) to the fiber properties that have been back-calculated. The fiber data, or matrix values can then also be edited if desired. Subsequently selecting the inverse operation (Mat→Lam) reconstitutes laminate properties from the fiber/matrix data and returns one back to the entry screen for laminate quantities.

Once satisfied with the contents of the material database, the next step consists of designing a prototype vessel (Wall) lay-up by selecting this menu item. All layers constitute (± angle) pairs with 0° indicating axial alignment and 90° indicating hoop windings. Existing wall construction filenames are shown immediately. If a new wall is being developed it must first be created using (New) under the (Utility) menu and typing

in a filename using a .wal extension. Existing files are best selected by navigating through available files using the active keys (indicated in red background on the top screen corners). As noted before, the list of available files can be scrolled with <**Home**> and <**End**> should they exceed the display capacity of the screen. <**PgUp**> and <**PgDn**> moves the selection curser and hitting <**Ins**> copies the selected file to the entry location. Subsequently hitting <**Enter**> invokes action. Alternately a desired filename can always be typed in. This is a common file entry feature used throughout the program.

Under the (**Wall**) option the materials available for construction are listed on the bottom of the screen once a valid .wal filename has been entered. Figure 8.7 is typical of such an entry screen. Navigation between fields within this screen is identical to that of other edit screens (<**Tab** / **Shift-Tab**> and <←↑↓→> keys). Again, action keys are indicated in red background at the top of the screen. Filenames for the available materials can be selected and pasted to the entry location without typing them. A prototype vessel wall can thus easily be designed with a minimum of keystrokes. The design parameters chosen need not be too exact but some general guidelines would be to select a sufficient number of layers, putting the lower stiffness / high strength materials on the inside (layer #1) and attempting to graduate subsequent layers stiffnesses with the aim of putting the highest stiffness (usually lowest strength) material as the last (outer) layer. Thicknesses can be entered at will and are not interpreted literally but scaled relative to one another in order to conform to a desired overall wall thickness (defined later). Winding angles are always taken as refering to a layer pair. When unsure of where to start, 55° is a good reference point, more interspersed winding angles will likely be necessary due to

```
                        ┌─────────────────────┐
              ____──────│navigation & hot keys│──────_____
             /          └─────────────────────┘          \
+-----------/------------------------------------------------\----------+
| Tab:S-Tab:Ins:Enter    Super Pressure - Vessel Designer    PgUp:PgDn:Home:End |
|------------------------------ Wall Construction-----------------------------|
|    Layer            Material        Angle       Thickness    Fiber Volume    |
|     (#)            (filename)       (+/-)°        (mm)        (percent)      |
|      1              T300_34C          55            2             67          |
|      2              AS_3501           53            3             60          |
|      3              t300_520          70            2             63          |
|      4              G_50              40            1             55          |
|      5              im7_9772          50            2             64          |
|      ▲        ▲                                                              |
|      │         \         ┌─────────┐                                        |
|      │          \────────│paste to │──────────                             |
|      │                   │location │          │                           |
|      │    ┌──────────────────┐      └─────────┘                           |
|      │────│up to 15 layers    │                                           |
|      │    └──────────────────┘   ┌────────────┐                           |
|      │                 ┌─────────│materials in │──┘                       |
|      │                /          │database     │                          |
|      ▼       ▲        /           └────────────┘                          |
|                                                                            |
|   T300_34C.MAT   AS3501_5.MAT   G_50.MAT     P75S.MAT     T300_520.MAT     |
|   T1000.MAT      S_GLASS.MAT    SPEC900.MAT  A_6061T6.MAT P100S.MAT        |
|--------------------------------------------------------------------------- |
| ALT+      Lam→Mat      Mat→Lam      Wall      Press     Build      eXit     |
+----------------------------------------------------------------------------+
```

Figure 8.7 Format of a *.wal file. The available materials in the database
can be viewed and selected from the lower half of the screen and
pasted to the curser location with <Ins>.

manufacturing considerations or the stable radial compaction phenomena described in

Section 7.3. Fiber volume fractions must also be specified. Since all these parameters

including the insertion or deletion of layers are adjustable later on, any reasonable guess

will suffice at this point. Hitting <Enter> completes the procedure.

Under the (Edit) menu, the (Press) <ALT-P> menu item edits a .prs file which

stores the pressure loading and vessel dimensions. Again, if a file does not yet exist it must

first be created using (New) or (Rename) or can be purged with (Del) if so desired under

the (Utility) menu. Units used throughout the program are metric and indicated where

applicable. A pressure loading of 10 MPa ($\approx$1,450 psi) or some fraction or multiple

thereof is often a good starting point. External pressure can be applied if applicable, and

the thickness entered here will govern calculations, over-riding individual layer thicknesses

```
+-----------------------------------------------------------------------+
: file = TEST1.LDS      Super Pressure - Vessel Designer   Arrow Keys:Enter :
:----------------------------Pressures & Dimensions------------------/-------:
:                                                          +----------+ /    :
:                                                          | hot keys |-/     :
: Inside diameter   (mm) 80     +------------+                                :
: Wall thickness    (mm) 20  <--|loading &   |----+                          :
: Internal press. (MPa) 30     |dimensions  |     :                          :
: External press. (MPa) 0      +------------+     :                          :
:                                                 :                          :
-                                                 :                         -
:                                                 :                          :
:                                                 :                          :
:-------------------------------------------------+-------------------------- :
: ALT+    Lam->Mat     Mat->Lam     Wall     Press     Build      eXit       :
+-----------------------------------------------------------------------+
```
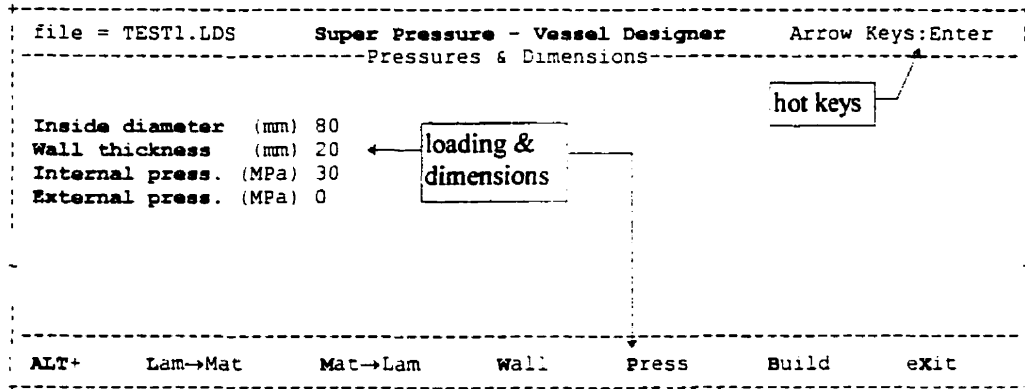
Figure 8.8 Loading file under creation.

entered in the .wall file by scaling them to the value specified in the .prs file. Figure 8.8

depicts the entry screen for such a loading file.

Finally, selecting (Build) creates a vessel loading case which becomes the basis for

subsequent analysis. The user is prompted to enter a combination of .wall and .prs files to

be assigned a new name with extension .ves. Once these preliminary file management tasks

are complete the vessel wall design features mentioned earlier can be utilized. These are

described in Section 8.2, forthcomming.

Finally, a small additional feature, from the main menu selection of the (Calculate)

option brings up the screen shown in Figure 8.9.

```
+-----------------------------------------------------------------------+
: file = Unknown        Super Pressure - Vessel Designer                    :
:-------------------------- Main Calculate Menu --------------------------- :
:             +----------+             +--------------+                     :
:            -|laminate  |         +---|design options|----+               :
-            / |analysis  |        /   +--------------+    :               -
:           /  +----------+       /                        :               :
:          /                     /                         :               :
:         /                     /                          :               :
:--------+---------------------+---------------------------+--------------- :
: ALT+   Stiff-Mtx    Vari-wall    Multi-layer    Fit-mat    eXit          :
+-----------------------------------------------------------------------+
```
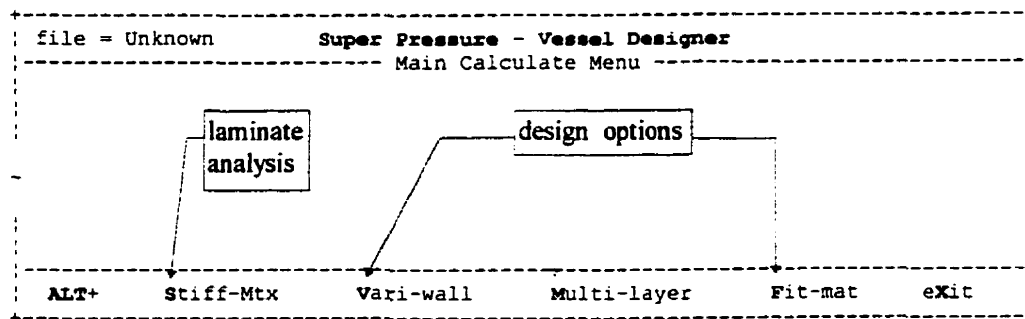
Figure 8.9 Options under the (Calculate) menu.

Selection of (Stiff-Mtx) <Alt-S> brings forth a list of available (.ves) files. Upon

entering the desired file name the global stiffness (combined stiffness matrix) and

compliance of an entire vessel laminate can be viewed. The computation is performed on

the basis of laminated plate theory. Results are presented in a cylindrical reference frame.

Its purpose is mainly to get a feel for the numbers involved in describing the laminate as a

whole in comparison with the stiffness maticies of individual layer pairs. Figure 8.10

shows the stiffness and compliance matrix of the 5 layer vessel design given in Figure 8.7.

```
+-------------------------------------------------------------------------+
: file = NEW1.VES      Super Pressure - Vessel Designer     Laminate Matrix :
:--------------------------- Main Calculate Menu -------------+-------------:
:                                                            / r = radial   :
:                            Stiffness Matrix (GPa)         / θ = hoop      :
:                                                          /  z = axial     :
: Arr  12.36   ArӨ   5.97   Arz   6.12      |denotes which| /                :
: AӨr   5.97   AӨӨ  74.82   AӨz  32.95      |matrix        |                 :
: Azr   6.12   AzӨ  32.95   Azz  33.30                                       :
:                                      AӨz  32.34                            :
:                                             Arz   3.77                     :
:                                                    ArӨ    4.43             :
:                                                                           :
:                            Compliance Matrix (1/TPa)                      :
:                                                                           :
: arr  88.99   arθ   0.20   arz -16.56                                       :
: aθr   0.20   aθθ  23.69   aθz -23.48                                       :
: azr -16.56   azθ -23.48   azz  56.32                                       :
:                                      aθz  30.92                            :
:                                             arz 265.45                     :
:                                                    arθ 225.75             :
:                                                                           :
:-------------------------------------------------------------------------: :
: ALT+     stiff-Mtx     Vari-wall     Multi-layer     Fit-mat     eXit    :
+-------------------------------------------------------------------------+
```

Figure 8.10 Global stiffness and compliance matrices for newl.ves file of Figure 8.7.

8.2 Variable Property Design

The core feature of the vessel design program revolves around the 3 selections named (Var_wall), (Fit-mat) and (Multi-layer). Each choice demands input of a vessel filename (.ves), available selections appearing at the bottom of the screen. A graphics mode screen appears and interactive editing of variables is made available via <←↑↓→ >, <PgUp>, <PgDn>, <Ins>, <Del>, <Tab>, <Esc> and other hot keys, most of which are listed at the screen bottom.

The selection (Fit-mat) <Alt-F> plots out a series of curves which are generated by a multi-parameter curve-fitting algorithm {amoeba.pas}, each being a best fit approximation to the ideal of smoothly varying material properties based on the individual layer values. Such a plot can be viewed by looking at Figure 8.11. Each stiffness or compliance property is represented by a different color, listed in the legend at bottom left. The thickness dimension through the vessel wall is represented by the graph abscissa, the ordinate plots moduli, compliance or reduced compliance. The top of the graph has tick marks indicating the boundary of individual layers which are listed numerically on the right hand side of the screen. The first layer (left-most on the graph) is defined as the inner-most (# 1). Parameters such as material type, winding angle, thickness and fiber volume fraction (cyan colored) can be edited for each layer. A light-blue cursor moves with the arrow keys and values can be incremented / decremented via.<Up-arrow / Dn-arrow>. When the desired changes have been made hitting <Ins> will update the calculations and refresh the screen. The numerically determined fitting parameters for any one graph are
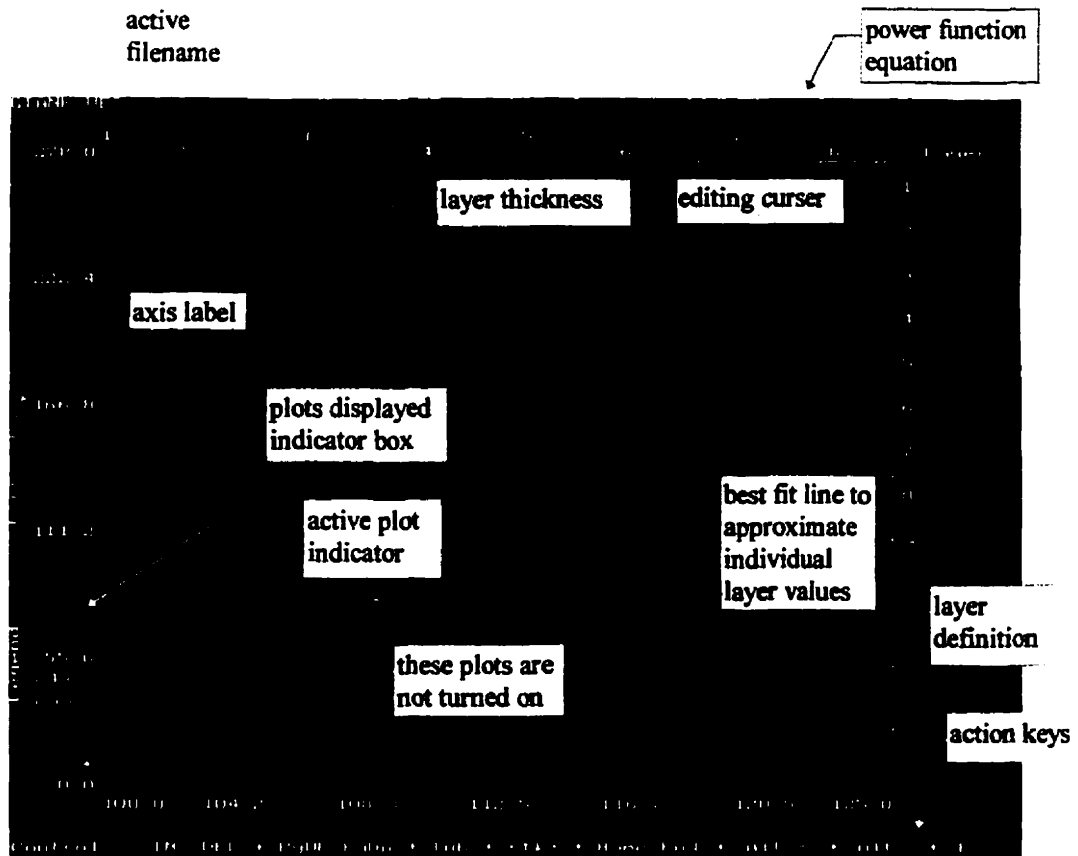
Figure 8.11 Preliminary property variations plot.

shown at top right. The initial screen defaults to the best fit for A_{11} and a box surrounds

this value in the legend. A small white cursor next to this box is controlled by <PgUp /

PgDn>, and moving it serves to indicate which plot one wishes to see. Pressing <Ins>

selects the plot <Del> de-selects the plot. All selected plots are surrounded by a colored

box.

The fitting parameters shown are always those for the "boxed" parameter next to

the white cursor. Multiple plots can be selected, and the ordinate will automatically scale

itself to the highest value amongst these. The <Tab> key cycles the graphs through stiffness $\left(A_{ij}\right)$, compliance $\left(a_{ij}\right)$ and reduced compliance $\left(\beta_{ij}\right)$ values.

With this tool the designer can check to see how well the wall construction conforms to an idealized variable property form. Naturally it is difficult to come up with a "perfect" wall, especially from the outset, however this not a problem. It is only necessary to remember that good fitting is requisite for a controlling parameter (like β_{22}) and that the less influential or uncontrollable ones can be left to fall as they will. For example $\left(A_{11}\right)$, the radial stiffness, is invariant with winding angle and depends mostly on the transverse moduli of fiber, resin selection and volume fraction. One could choose to optimize this quantity but it would lead to selecting composite laminas with nicely progressive through-thickness moduli, likely incompatible with a desired circumferential stiffness variation rate that may be exhibiting the opposite tendency.

8.2.1 General Examples

In the remaining set of figures example cases are put forth and sucessively modified. To start, a preliminary vessel wall can be proposed. For illustration the wall construction file *strong.wal* will be used in what follows. A corresponding loading case (*big.lds*) describing a 200 mm diameter by 25 mm thick wall with 60 MPa internal pressure was joined to it using the (Build) menu option as shown in Figure 8.12 to define a new vessel file (*gtank.ves*). Figure 8.13 indicates the initial choices for this wall construction. This is the lay-up upon which the curve-fitting seen in Figure 8.11 was

performed. Ordinarily it would be unusual to proceed with so many different materials, thicknesses and fiber volume fractions, however this is an illustratory case so there is no harm.

```
+----------------------------------------------------------------------+
: Arrow keys:Ins:Enter  Super Pressure - Vessel Designer    PgUp:PgDn:Home:End :
:------------------------------ File Editor Menu --------------------------:
:                                                                          :
:  Load    (.LDS)  input file:  BIG.LDS          ┌─entry location ─┐       :
:  Wall    (.WAL)  input file:  STRONG.WAL  ◄     └──────────────────┘      :
:  Vessel  (.VES)  output file:  gtank.ves                                 :
:                                                                          :
:  TEST1.LDS       SCI_GR.WAL       NEW1.VES      ┌─list of existing files─┐ :
:  BIG.LDS         TEST.WAL         GTANK.VES     └────────────────────────┘ :
:  VERIFY1.LDS     BEST.WAL         BEST1.VES  ◄                            :
:  EXP2.LDS        SN006.WAL        SAN_50K.VES                             :
:  TEST2.LDS       SN009.WAL        SAN_55K.VES                             :
:  B35_55.LDS      SN008.WAL        SN006.VES                              :
:  B40_76.LDS      SN011.WAL        SN008.VES                              :
:  B40_61.LDS      SAN_50K.WAL      SN009.VES                              :
:  B40_94.LDS      SAN_55K.WAL      SN011.VES              ┌──────────────┐ :
:  SANDIA50.LDS    SCI.WAL          SCI_GR2.VES     ──────│menu bar item │ :
:  SANDIA55.LDS    DD.WAL           SCI_GR.VES             └──────────────┘ :
:  EXP1.LDS        TTEST.VES        SCI.VES                                 :
:  STRONG.WAL      GTANK2.VES       GTANK1.VES                             :
:  NEW.WAL         GTANK3.VES                                              :
:------------------------------------------------------------------------:
: ALT+     Lam→Mat      Mat→Lam      Wall     Press     Build     eXit    :
+----------------------------------------------------------------------+
```

Figure 8.12 Entry screen under (Build) option to combine appropriate files.

```
                           ┌──action keys──┐
                      ┌────┤               ├────┐
                     /     └───────────────┘     \
+------------------/------------------------------\-----------+
: Tab:S-Tab:Ins:Enter   Super Pressure - Vessel Designer   PgUp:PgDn:Home:End :
:------------------------------ Wall Construction-------------------------:
:   Layer         Material      Angle      Thickness     Fiber Volume     :
:    (#)         (filename)     (+/-)°       (mm)         (percent)       :
:     1            T1000          53          1              69           :
:     2            kev_49         54          2              67           :
:     3            T300_520       55          3              66           :
:     4            as4_3502       56          2              65           :
:     5            im6_sci        57          2              64           :
:     6            IM7_9772       58          2              63           :
:     7            p75s           59          2.5            62           :
:     8            p100s          60          1.5            60           :
:                                                                        :
:                  ┌─material files─┐                                    :
:             /────│available       │                                    :
:            /     └────────────────┘                                    :
:           ◄                                                            :
:  T300_34C.MAT   AS3501_5.MAT   G_50.MAT      P75S.MAT      T300_520.MAT :
:  T1000.MAT      S_GLASS.MAT    SPEC900.MAT   A_6061T6.MAT  P100S.MAT    :
:----------------------------------------------------------------------:
: ALT+     Lam→Mat      Mat→Lam      Wall     Press     Build     eXit    :
+----------------------------------------------------------------------+
```

Figure 8.13 Initial choice of lay-up for wall construction. File: *strong.wal.*

425

From Figure 8.11 one can see that some of the desired effect of having a smoothly

varying circumferential stiffness is being achieved but obviously the fit to the curve is far

from as good as it could be. That however can easily be fixed by adjusting the layer

parameters on the right of the screen. The easiest way to progress is by starting with the

layer deviating most from the curve and making a small perturbation in winding angle or

volume fraction and then hitting <Ins> to inspect the result. Within a few minutes the

modifications shown in Figure 8.14 can be obtained. Here, for illustration, the principal

reduced compliance β_{22} has been plotted rather than the stiffnesses (use <Tab> key to
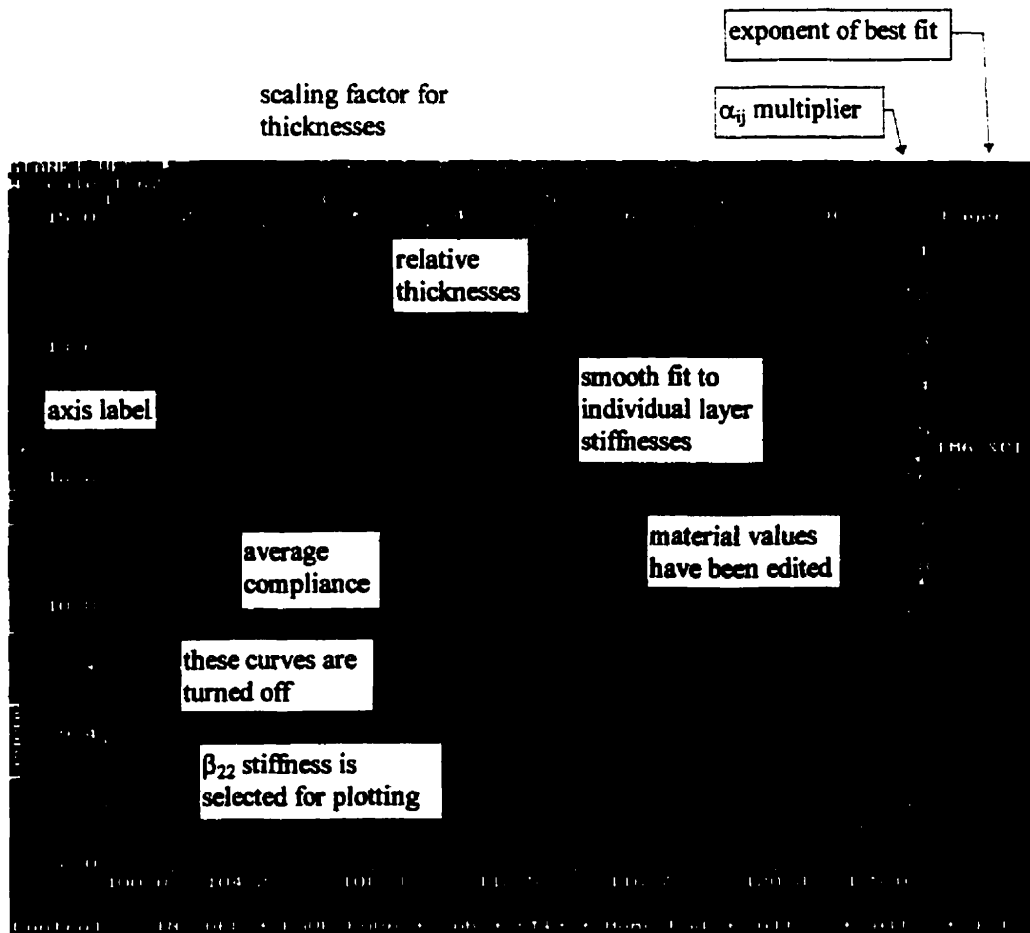
Figure 8.14 Goodness of fit for reduced circumferential stiffness β_{22} after some
manipulation of the material parameters.

page screens and <PgUp / PgDn> & <Del> key to turn off the plots not required). The average compliance value for every curve plotted is marked on the left inside of the graph, and the wall scaling factor (over the relative thicknesses input) is shown at the top left corner.

Once satisfied with the results, a file can be saved under a new name. In this case the name *gtankl.ves* was created by pressing <Alt-S> which prompts for a filename. This file will form the basis of our example case.

Till now we have implicitly assumed that the curve to fit is the one shown on the screen. This is not the case, the curve being plotted is merely the one calculated as a best fit to the individual layer quantities entered (via the layer parameters). In other words, the curve follows the layer data, it does not lead it. The actual rate being sought will be discussed later under the (Var-wall) option. The exponent describing this variation rate is shown in the top right corner of the figure above. At any time the 2 fitting parameters describing the curve being considered (marked by the white cursor and boxed in the legend) are displayed at the top right of the screen. The exponent determines the slope of the curve, while the α_y multiplier is simply the stiffness or compliance value at the outside of the vessel where the relative radius $\rho = 1$. The specific variation rate sought must be guided by these values. The most effective method for significantly altering these fitting parameters is by making changes first to the inner and outer layers to direct the slope of the curve. (Use arrow keys to select and increment or decrement parameters of the highlighted value). Subsequently the intermediate layer parameters can be adjusted to better the fit. The user will quickly note the *high sensitivity* to winding angle variations

and to a lesser extent that of fiber volume fraction. The individual layer thicknesses or material selection can be altered by moving the light-blue background cursor under these parameters also. The user can then scroll (arrow keys) through all the available materials in the database and select a new one. Such further options are not explored here but their actions should be obvious.

Up to this point no mention has been made as how to determine what a potentially desirable elastic property variation rate might actually be. For this one must turn to the (Var-wall) menu option, discussed next.

8.2.2 Solutions Types

The (Var-wal) option <Alt-V> presents a submenu as per Figure 8.15 allowing a choice of variable properties type solutions.
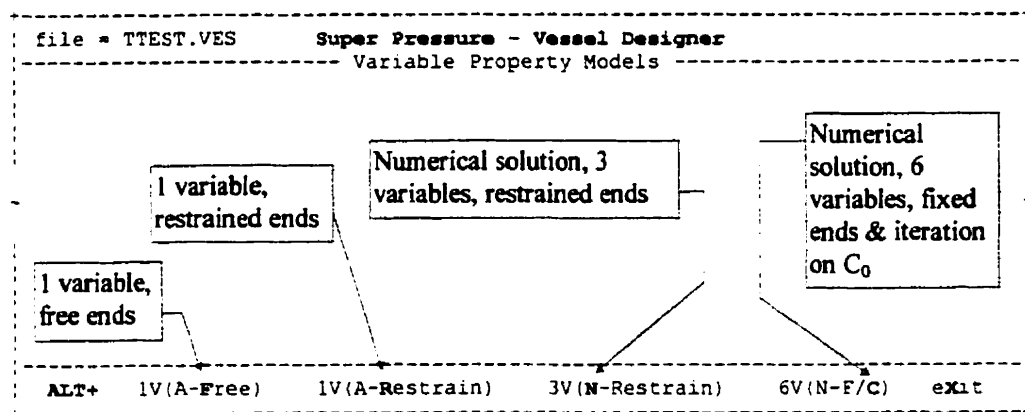
Figure 8.15 Four solutions available under (Var-Mat) option.

428

In all cases solved below $\vartheta = 0$ as twist is not a factor for $\pm$ angle ply-pairs. The choices are: {1} Closed form solution with all properties varying at rate "n" as presented in Chapter 5 equations (5.61) with $C_0 = 0$, (restrained boundary). {2} Solution via equations (5.61) with C_0 computed from the axial force boundary condition (5.65) applied to σ_z. {3} Finite difference approach using 3 individually variable elasticities (power functions) with fixed end condition $C = 0$. The solution is obtained by solving the system (6.23). {4} Finite difference method with 6 variable material properties coupled to an iterative solution for the free ends with the addition of equations (6.24)-(6.26).

Each solution is based on a different set of assumptions hence one should not expect to see the same outcome. The methods are all based on modeling the cylinder wall as a continuously variable elastic material. Realistically, only the finite difference methods permit modeling property variation rates that can be achieved in actual constructions, nevertheless it is interesting to see how these solutions differ from those of previous researchers and we can note the limitations of these earlier efforts.

The most coarse assumption is being able to vary all properties at the same rate "n". This case can be examined with the menu selection <ALT-R> or <ALT-F>, the difference being whether the cylinder ends are (Restrained) or (Free) to move. Turning back to our example case *gtankl.ves*, the stress distribution expected within a vessel constructed of such hypothetical material would be as shown in Figures 8.16 and 8.17 respectively.
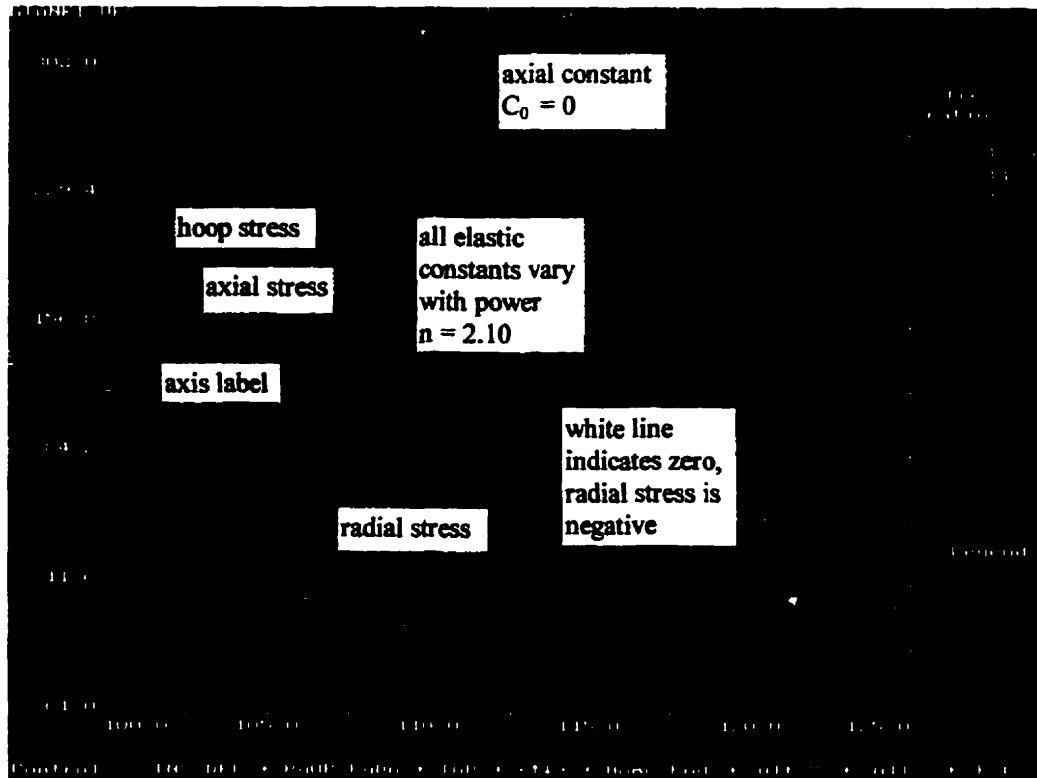
Figure 8.16 Expected stress distribution with all elastic constants varying
at the same rate n. The end conditions are as per a pipe
constrained between rigid walls.

By contrast, Figure 8.18 shows the plot of a thick vessel constructed from a single

material, in this case T300_5208, with constant properties ($n = 0$) through the thickness.

Obviously the stress distribution and even the governing stress between the first

two cases is vastly different due to the end constraint. The global variation rate "n" plotted

for each analysis is by default taken to be that of the curve fitted to the reduced

compliance β_{22} under the <Plot> option. Using the <arrow keys> , <PgUp / PgDn> the

exponent of this power function can be altered and hitting <Ins> will recompute the stress

distribution. With a few trials one can easily arrive at an elastic property variation rate that

provides a virtually constant circumferential stress through the thickness.
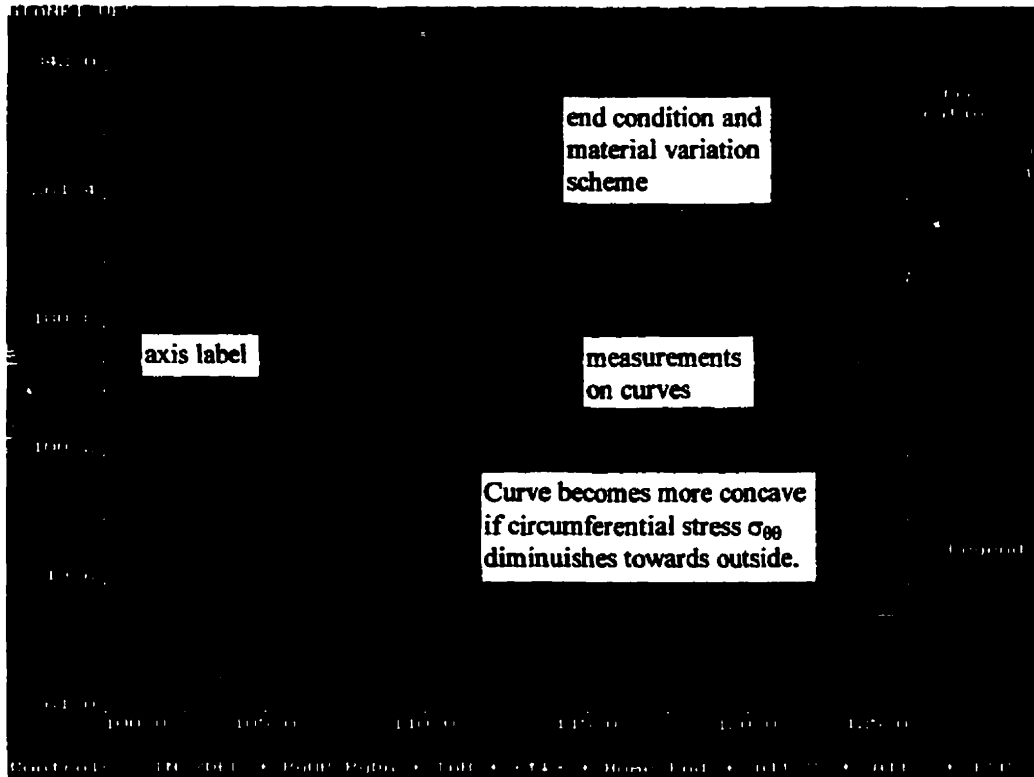
Figure 8.17 Stress distribution for example case using "free ends".
Axial constraint is removed allowing movement as in a
pressure vessel. Stress distributions change remarkably.

This may not be anywhere near optimal for a final design but might provide some idea of a

starting point. The numerical parameters shown as "Stress ratio" are a relative measure for

gaging the difference between the minimum and maximum stress with respect to the

average stress at the endpoints for σ_z and σ_θ. For σ_r the percentage shown is a measure

of deviation from linearity of the centerpoint, with negative values indicating concavity of

the curve, whilst positive values result when the σ_r curve is convex and the wall retains

its greatest stress away from the inside surface.
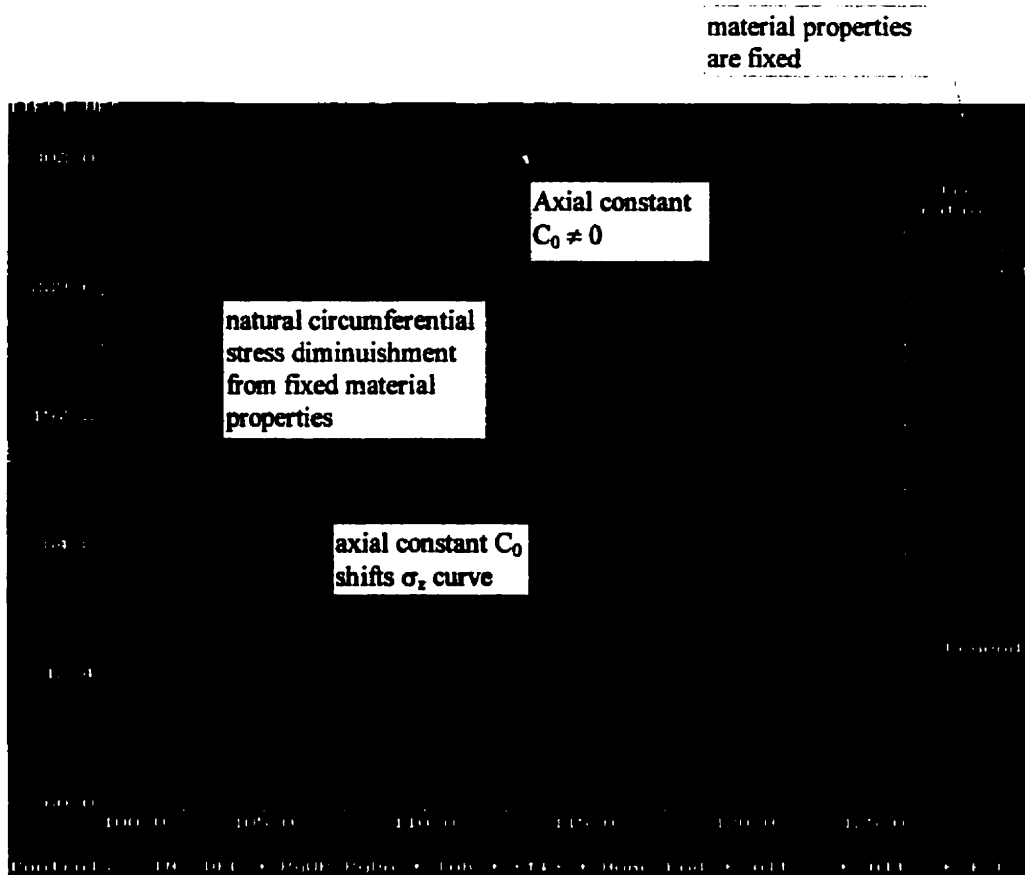
Figure 8.18 Stress distribution in a single material vessel built from ± 60° T300_5208 with fixed properties. The end conditions affect mainly σ_{zz} but not the distribution of $\sigma_{\theta\theta}$. Axial stress is about 1/3 lower given restrained ends.

In Figure 8.18 the T300_5208 material shown is one with a relatively low "avoidance" factor K for a given lamination angle and hence is nominally considered to be superior at carrying stress to the outer portions of the wall. Clearly, from the figure the ability even of a "good" composite is quite poor as approximately 1/3 of the hoop stress is lost through a 1" (25 mm) thick wall. The real aim in designing a multi-layer vessel is to ward off a composite's natural "avoidance" in transmitting stress in the through-thickness

direction. From these coarse first approximations it should now be more apparent that careful consideration is requisite in the design of any multi-layer / multi-material vessel.

8.2.3 Individually Variable Property Solutions

To exemplify and expand on the above, stress distributions have been found to be rather sensitive to some of the elastic constants and the individual variation rates assigned to them. This fact becomes evident when we examine the results of a numerical solution. Figure 8.19 presents a 3 variable properties numerical solution to our example case. The graph shown in Figure 8.19 can be invoked by selecting <Alt-N > under the (Calculate) sub-menu. The results are so different from Figures 8.16 and 8.17 that one first hardly recognizes it to be a solution to the same problem (*gtank1.ves*).

In fact the validity of the numerical solutions was in question and to resolve this dilemma test cases were run to parallel the method with the closed form solution for common variation rate "*n*" to ensure identical results. These test case value alterations are still in the numerical methods code but commented out. In turn, the code for the common variation rate "*n*" was tested against code for constant material properties "*K*" written specifically for one layer (as seen in Figure 8.3) and also compared to the results of the code for multilayer solutions (Full eqns & Partial eqns, discussed in the next section) when reduced to solving for the single layer case. In all, 7 independent segments of code using both "free-ends" and "fixed ends" boundaries were run to cross-check results. The numerical solution was accurate to the 2rd decimal place or better for the stresses

433

objective is to get σ_r
stress distribution even,
preferably with a flat σ_z
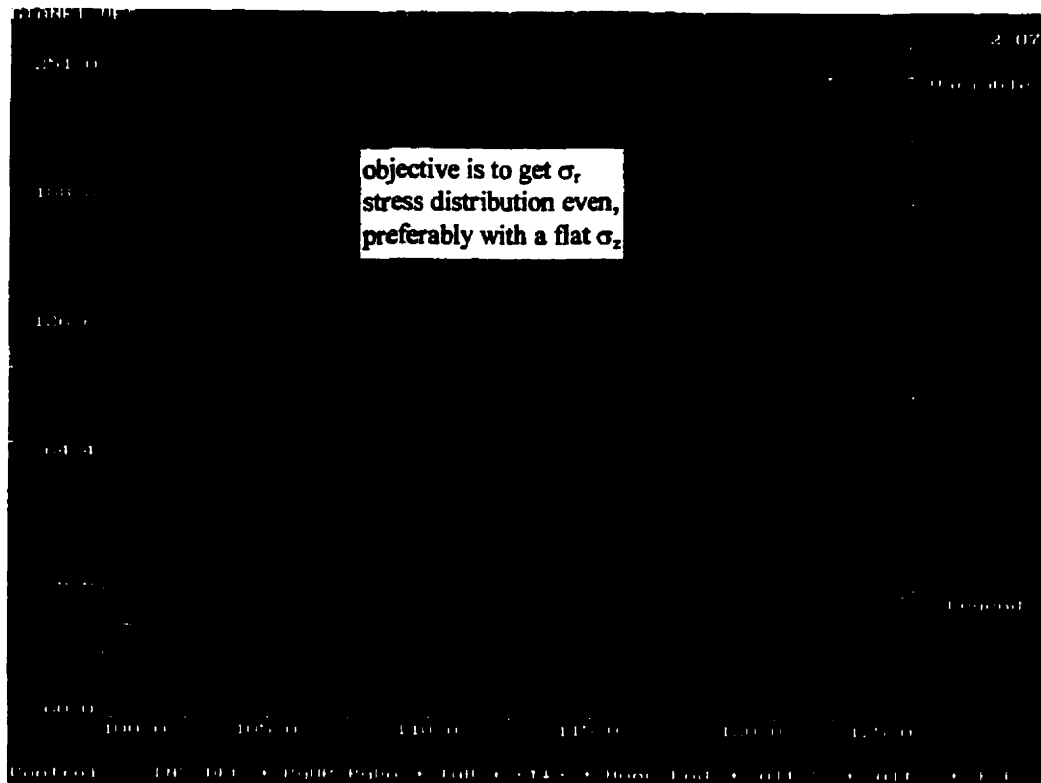
Figure 8.19 Numerical solution to gtankl.ves using fixed boundary conditions.
Restrained ends are not of drastic consequence, serving mostly to
affect an increase in the circumferential stress near the outside surface.

(measured in MPa) when compared to the closed form equations. Further the multi-layer

solution was laboriously hand checked for 1, 2 and 3 layer cases in parallel with the source

code debugger through every step of execution.

Considering the above results, one will note that the numerical solution with 3

individual property variation rates, namely those on the LHS of differential equation (6.6)

(Figure 8.19), falls somewhere within the extremes of when the problem was solved with

all properties obeying the same variation rate "n" both with (Figure 8.16) and without

(Figure 8.17) an end constraint. The 3 variable properties solution above should also be

contrasted to the well known constant material properties case (Figure 8.18). Comparing

434

amongst these figures one may note that σ_z sees the most drastic change in magnitude

and tendency. This ought be expected since σ_z is controlled mainly by the end constraint

and Poisson related stiffnesses which are in turn dependent on winding angle and other

factors unrelated to the specific circumferential moduli variation rates sought earlier. By

contrast the numerical solution approximating all 6 material constants in variable property

form (Figure 8.20), including those on the *RHS* of equation (6.6) differs little from the

simpler "3 variable" homogeneous solution given in (8.19). The influence of the free

boundary is present but now only moderately so.
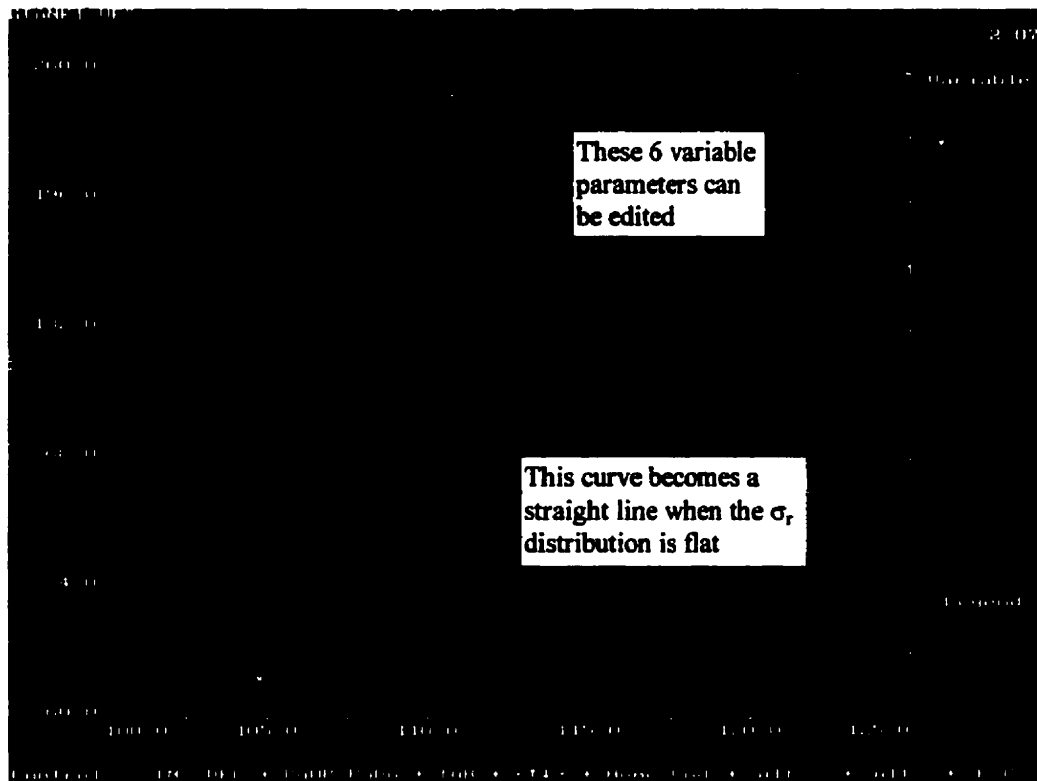
Figure 8.20 Numerical variable properties solution to *gtankl.ves* with free end conditions.

In each of the foregoing variable properties solutions the power functions

describing the material can be edited via the cursor keys $<\leftarrow\uparrow\downarrow\rightarrow>$ to select either the

exponent or mantissa and increment / decrement the values, and then pressing <Ins> to

recompute the distribution. <Home> and <End> serve respectively to reset either all

parameters or the currently edited one to its original value. In this way one can quickly

search out the parameters which carry the most influence upon the design of a desirable

stress distribution and aim to modify these to conform when designing a lay-up under the

(Plot) option.

An explanation of the most prominent effects resulting from perturbations upon

each parameter is listed in Table 8.2. It helpful to remember that the form of the property

variation given in the graphs is $\beta_{ij} = \gamma_{ij}\rho^{xx}$. Since the value of ρ (normalized radius)

ranges from $c = a/b \rightarrow 1$, negative values of the exponent xx serve to increase the

property at the inside of the cylinder wall relative to the outside. The reverse is true for

positive exponents. Because we are effectively looking at compliances, large negative

exponents imply less stiffness on the inside relative to the outside. The mantissa $\left(\gamma_{ij}\right)$ for

each reduced stiffness term $\left(\beta_{ij}\right)$ has a sign (either positive or negative) and essentially

this sign will not change with alterations to the winding angle, material, etc., only the

magnitude of the term is affected. For the compliance term (α_{13}) the sign is dependent on

winding angle so one must be careful when making interpretations.

The form of the differential equation for the stress function ϕ is quite similar given

the case of all properties expressed as individually variable quantities and for the situation

where they are all taken to vary at the same radial rate. The main difference is that an

analytical solution exists for the later but only a numerical one for the more general case.

Table 8.2 Effect of compliance variation on stress distribution for "free ends".

Parameter	Sign	Mantissa (γ_{ij})	Exponent (xx)
β_{11}	+	Lowest possible value best. Low values help stress transmit outward and minimize curvature in σ_θ plot. Low values here also demand a less negative exponent for β_{22} to result in a flat σ_θ plot.	Effect is very weak. For high value of the mantissa large exponents raise hoop stress marginally on outside surface.
β_{12}	−	Affects curvature in σ_θ plot. High negative values lower inner hoop stress. Practically this value is always a small negative quantity and not really a major player.	Effect is weak. Large negative exponents can lower inside surface hoop stress.
β_{22}	+	Moderate influence upon circumferential stress distribution. Lower values can promote increased curvature in the center of the σ_θ plot and promote a lowering of the stress in that location.	Main controlling influence upon σ_θ plot. Large negative values shift hoop stress outward. Values in the range -1.6 to -2.0 give a nearly level stress distribution for common lay-ups.
α_{11}	±	Strong influence on σ_z plot. Large negative values near inside surface lower stress there at expense of increased axial stress on outer surface (common case). For most material, winding angles in the range of 14° - 42° result in a positive mantissa	Large exponents of either sign may result due to curve fitting since winding angle determines sign of mantissa in each layer. Low winding angles can contribute to unusually large σ_z due to this fact.
α_{22}	−	Very strong influence on σ_θ plot. Large negative values decrease σ_z on outside surface and influence σ_θ in a similar though lesser fashion. Winding angles can extort radical influence.	Large positive exponents magnify axial stress on outside surface
α_{33}	+	Some effect on overall axial stress level (shifts σ_z plot vertically). Large influence on shape of σ_z curve. Big values usually tend to lower both hoop and axial stress on outside surface.	Exponent values near zero flatten out curvature in all plots. Large negative values promote a high σ_z stress on the outside surface.

Since all stress computations stem from the stress function it is well to understand

how the variation rates affect its shape. Looking back to equations (5.54) and (6.6) and

eliminating the terms containing the index 4 and the twist coefficient 9 in the former we

can simplify and place the two equations side by side.

$$\frac{\partial^2 \phi}{\partial r^2} + \left(\frac{-n+1}{r}\right)\frac{\partial \phi}{\partial r} - \left[\frac{\gamma_{11} + m\gamma_{12}}{\gamma_{22}}\right]\frac{\phi}{r^2} = \frac{Cr^{n-1}}{\alpha_{33}\gamma_{22}}\left[(\alpha_{13} - \alpha_{23})\right]$$

(8.1)

$$\frac{\partial^2 \phi}{\partial r^2} + \left(\frac{-d+1}{r}\right)\frac{\partial \phi}{\partial r} + \left(\frac{\gamma_{11}r^{d-1} + m\gamma_{12}r^{d-m}}{\gamma_{22}}\right)\frac{\phi}{r^2} = \frac{Cr^{d-1}}{\alpha_{33}\gamma_{22}}\left[\alpha_{13}r^{-u} - (1-v)\alpha_{23}r^{-v}\right]$$

(8.2)

Solution for ϕ in the first takes the form

$$\phi = C_1 r^s + C_2 r^t + \frac{Cr^{n+1}}{\alpha_{33}}\chi_{1.}$$

For the second equation the solution is unknown however the shape of ϕ should show

similarity given the equations are so close.

Also remembering that

$$\sigma_r = \frac{\phi}{r} \quad , \qquad \sigma_\theta = \frac{\partial \phi}{\partial r} \quad , \qquad \sigma_z = \frac{C}{\alpha_{33}}r^k - \frac{\alpha_{13}}{\alpha_{33}}r^{-u}\sigma_r - \frac{\alpha_{23}}{\alpha_{33}}r^{-v}\sigma_\theta$$

it is easier to comprehend the influence derived from each term. Basically if we desire a

constant hoop stress, integration of ϕ leads to the form $\sigma_r = A + B/r$. This indicates that

the corresponding σ_r must plot as a hyperbola and that the rate at which radial pressure is

absorbed will vary inversely with the radial position. If we desire uniform absorbtion of the

radial pressure across the thickness (σ_r plots as a straight line) then it works out that σ_θ

must have a positive slope of twice the magnitude by which radial pressure is being

absorbed per unit thickness. (ie: σ_θ is higher on the outside of the cylinder). The group of

terms $\alpha_{13}, \alpha_{23}, \alpha_{33}$ affect mainly σ_z because they reside on the *RHS* of the differential

equation and dictate the particular solution. The *d* exponent and γ_{22} term have direct

438

influence on the first derivative (σ_θ) and a secondary effect on all the other terms where they mix with other factors. The term γ_{11} raised to its exponent l multiplies ϕ so a heavy influence upon the radial stress should be expected. γ_{12} tends to be of small magnitude, its effects are subtle but act mainly on σ_r. If the hoop stress is constant, then the second derivative will be zero. For the free boundary situation, as in any vessel, interactions always occur due to the fact that the particular solution (*RHS*) must be satisfied. Compliance α_{33} plays a significant roll because the numerator constituting terms α_{13}, α_{23} are of different magnitudes and these quantities do not cancel except under rare circumstance. The *RHS* then extends some influence over σ_θ since the second derivative must play a role in satisfying these terms and it will only manifest itself when curvature exists in the σ_θ plot. This is why altering the *RHS* terms causes a secondary change in the σ_θ curvature.

Even without this mathematical insight making alterations to the stress distribution is not a difficult matter, rather a little bit of experimentation goes a long way towards attaining a feel for what is possible.

8.3 Discrete Multi-layer Design

The final and most revealing function of "Super Pressure - Vessel Designer" is found under the (Multi-layer) sub-menu selection. The idea behind this program segment is not only to solve for the resultant static stress distribution at a given pressure but also to render an idea of how a pressure vessel's stress distribution will change under the

influence of damage resulting from an accumulation of matrix micro-cracking which becomes incipient at some level of loading. Naturally the accuracy of such predictions are dependent wholly on the underlying failure criterions, damage and stiffness reduction models. None of these are well proven, yet they are among the better ones currently available. Taken together they are expected to provide more insight than anything short of lengthy incremental finite element approaches incorporating fracture mechanics (CODSTRAN) as with some of the impact damage assessment studies, typical of those carried out by Minnetyan and Chamis [260] on behalf of NASA for thin walled vessels.

A choice of three solution methods is available, each of which solves the layer by layer problem. The first two choices labeled (Full eqns) and (Partial eqns) differentiate as to the completeness of the elasticity equations used to render a solution. (Partial) refers to the approximate method presented by Roy and Tsai [56] where the constant $2C_2$ in (4.23) was assigned a value of zero, rather than assuming the correct value of χC as with the (Full) implementation. All three options carry forth via solution to the matrix system (4.46) and implement Christensen's separate failure criteria for matrix and fibers upon
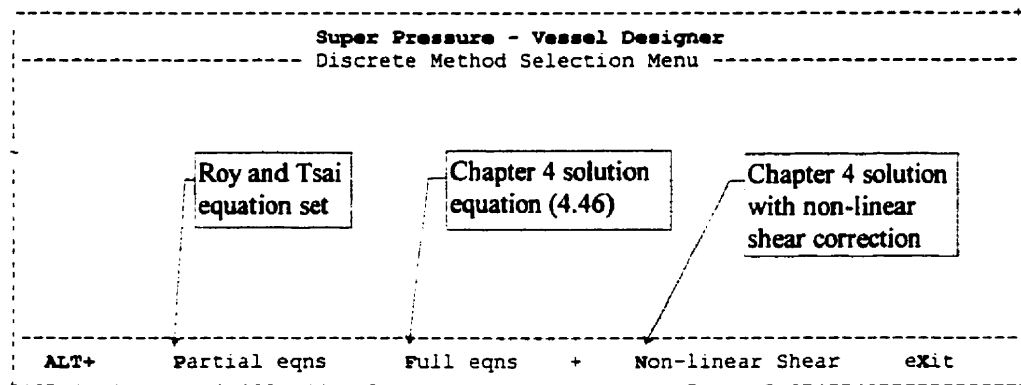
Figure 8.21 Menu selections under the multi-layer solution option.

each layer as described in (7.34). Thereupon Luo-Yu Xu's damage modeling is invoked as presented in Section 7.4 and elastic moduli reductions are computed via Tables 7.13 and Figure 7.30. The third option (Non-linear shear) carries forward with the addition of equation (7.88) and is coupled with the (Full) analytical method. Because the damage effects are highly non-linear the elasticity solution has to be solved in an iterative loop. With each iteration and for every layer the error between the matrix safety factor R (matrix overload indicator) after matrix failure initiation is compared to the overload factor from the previous cycle. A new matrix safety factor is estimated and the damage level and consequent stress distribution is re-computed until the relative error between successive iterations in the computed over-load factor matches to within 0.1% for all layers. Both the intermediate and final solutions are output in graphical format during this process.

For (Non-linear shear) the shear corrections are invoked in each layer up until matrix failure is reached, thereon this correction stays constant and further reductions depend on the residual equivalent stiffness coupled with the moduli reduction scheme. Figure 8.22 illustrates the graphical output format. The screen plots the three principal stresses, differentiated by color, for each layer. An observant reader should note the similarity in trend between this plot and those of Figures 8.19 and 8.20. The vertical dotted lines mark the individual layers and each layer is flanked by a set of small "thermometers" color coded for matrix and fiber, as per the legend. The height of these "thermometers" at the middle and layer extremities represent the inverse of the safety factor R determined via equation (7.34). The lower horizontal yellow dotted line across

441
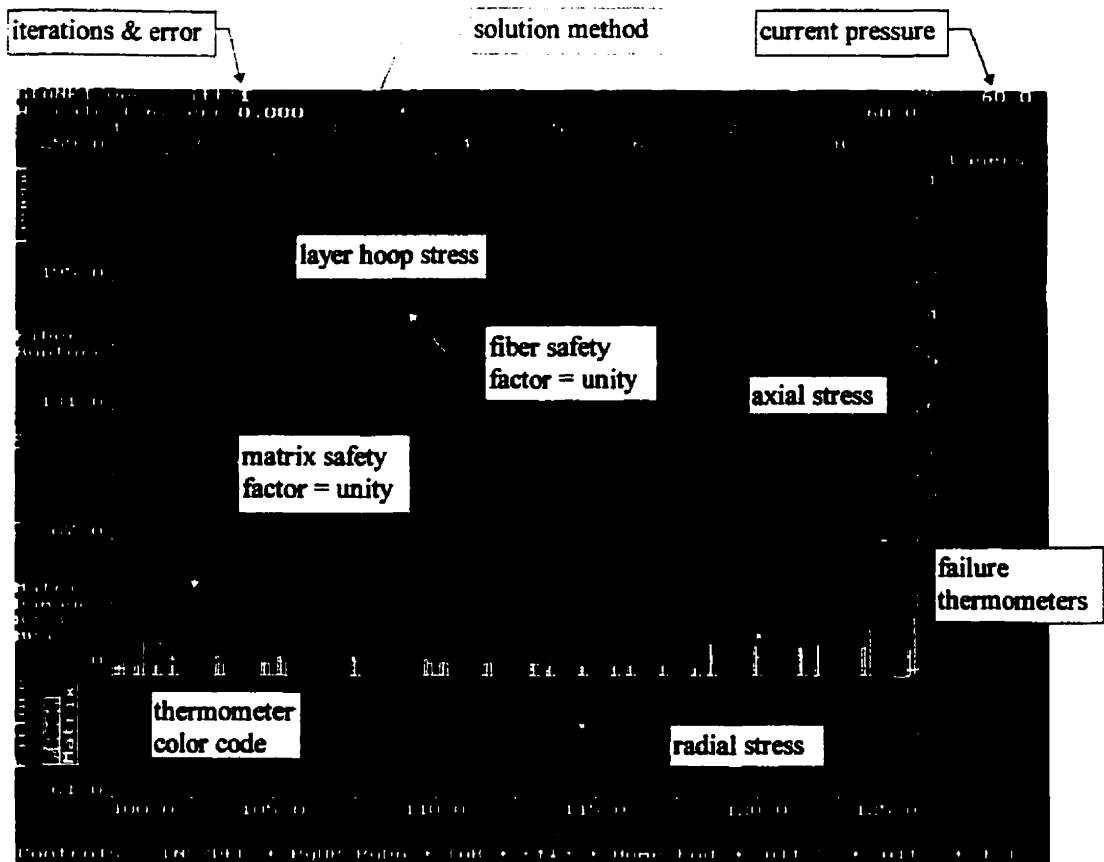
Figure 8.22 Plot of the discrete layer stress distribution using the (Partial eqns) option.

the plot marks a safety factor of unity. Imposed pressure is at the top right corner and can

be incremented / decremented (±0.1 MPa) via <PgUp>/<PgDn> or (±1.0 MPa) via

<Home /End>. The plot is regenerated upon pressing <Enter>.

Parameters describing the wall construction can be edited just as under the (Plot)

option described earlier. In addition layers can be inserted or deleted using <Alt-I> (to

inset below cursor) or <Ins> (to insert above cursor) and <Del> to delete at the cursor

location. Proof pressure at the top of the screen records the highest pressure attained, as

the damaged conditions within each layer are retained when one unloads the vessel. The

442

number of iterations and error between successive estimates (red background) can be followed during execution at the top of the screen. The error pertaining to the non-linear shear correction, denoted by **ers** operates only when the option <**Alt-N**> is selected. Wall thicknesses are always scaled from values given in the *.wal* file to the overall thickness defined in the *.lds* file from which the *.ves* file stems. This is to ensure that when editing individual wall thicknesses that one will not waste time adding and subtracting from different layers to maintain constant net thickness. It is important in order to ensure one is comparing designs with the same relative thickness ratio "*c*". The applicable scaling factor is at top left on the screen.

An estimate of first matrix damage appears in yellow next to the $R = 1$ line. As the load is increased via the <**PgUp / Home**> keys, the thermometers rise and the vertical axis is re-scaled every time one hits <**Enter**> to re-compute. Should either matrix failure or fiber fracture occur, the height of the thermometer(s) will extend beyond the $R = 1$ line and light up to a higher intensity, remaining lit even if the pressure is later lowered in order to remind one of the damage state present. The height of each matrix thermometer once it reaches beyond the matrix damage initiation line represents the inverse of the damage parameter as measured by the residual equivalent stiffness RS_{eq} defined in equation (7.61). The upper dotted yellow line marks the attainment of the characteristic damage state. This level may or may not be reached by the matrix indicator since it requires that the fiber itself remains intact. If the failure criterion predicts fiber fracture at any point then both damage indicators (matrix and fiber) are simultaneously assigned to this level. Since damage is permanent and assumed to be equal throughout the layer, the thermometer

indicators will all assume the same height at damage onset, which is different from the safety factor display (un-lit) where elasticity equations assign differing safety factors according to the radial position within the layer. Once damage has begun the program will iterate and flash intermediate "solutions" on screen until it settles.

The progress to convergence can be monitored by watching **itt, err** and **ers.** The number of iterations depends on many factors, typically taking longer with large pressure increments and walls with many damaged layers. Rarely does it run more than 10 and the program will automatically halt at 30 iterations and display. If the initial pressure denoted in the *.lds* file is high enough to cause damage immediately, then the first damage estimate will display "999.0" to warn that no valid computation is possible, since this estimate requires a linear elasticity approach. This situation is easily rectified by lowering the pressure via <PgDn / End> and then saving under the same or a new filename via <Alt-S>. an action that would also be called upon to save any other desirable changes made after editing the construction parameters. Should it be desired to restart the analysis at any loading point, pressing <Tab> will reset the material properties to their original undamaged values and revert to the last conditions saved to file, or simply the original file. This feature is convenient if some failure event was "missed" by having incremented the load too quickly.

For this particular example the solution option of (Full eqns) via <Alt-F> gives virtually the same results, only that first damage occurs at approximately 0.5 MPa higher than with the (Partial eqns) option. This brings into evidence that in practical terms the simplified solution put forward by Roy and Tsai [91] appears sufficient.

The example case presented in Figure 8.22 is the same lay-up studied previously.

This was designed purely on the merits of what was *assumed* to perhaps approximate a

desirable variation rate based on the (Plot) curve-fitting module. More interesting

however is the fact that although the stresses were relatively well balanced to begin with,

the distribution begins to suffer greatly once the loading is sufficient to cause damage.

This progressive distortion of the distribution and eventual unloading of some layers as

they break can be studied via Figure 8.23.
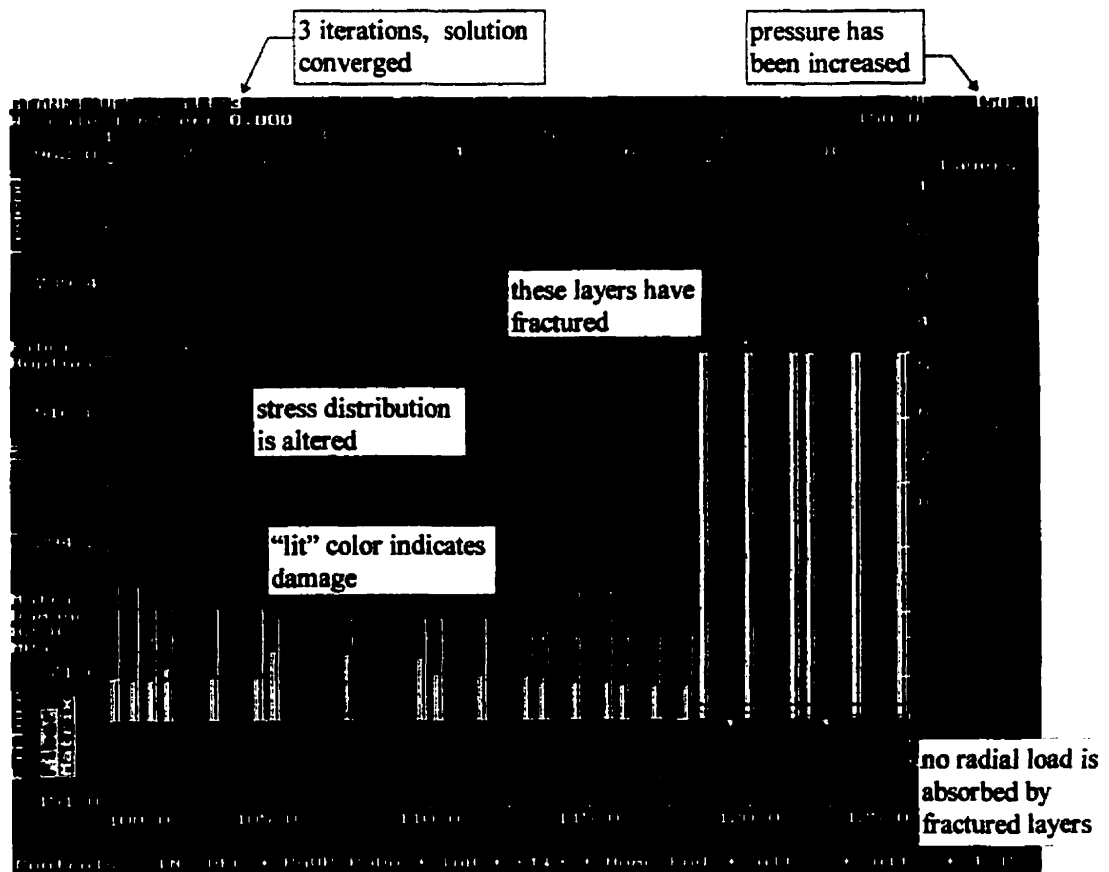
Figure 8.23 Example case loaded to the point where the two outer layers have broken. Matrix failure is evident everywhere and appears to be causing a disproportionate unloading of the Kevlar® layer hoop stresses.

445

Obviously in this case the two outer materials were badly chosen from the fiber

strength point of view. Although the matrix had begun to fail in both the inner and

outermost layer, the P75S material fractured first at 149 MPa, propagating to the adjacent

P100S ply, but the damage was computed to be non-fatal and halted by itself. As a

consequence of this upset the inner layer has become the most heavily loaded, whilst

matrix damage has relieved the Kevlar® layer from much of its load as well. Continuing

with the loading one can predict that the T300 layer will fracture next since already the

fibers are much nearer failure than the matrix, something almost expected for a layer

wound near the "netting" 54.7°. Figure 8.24 below predicts the next stage.
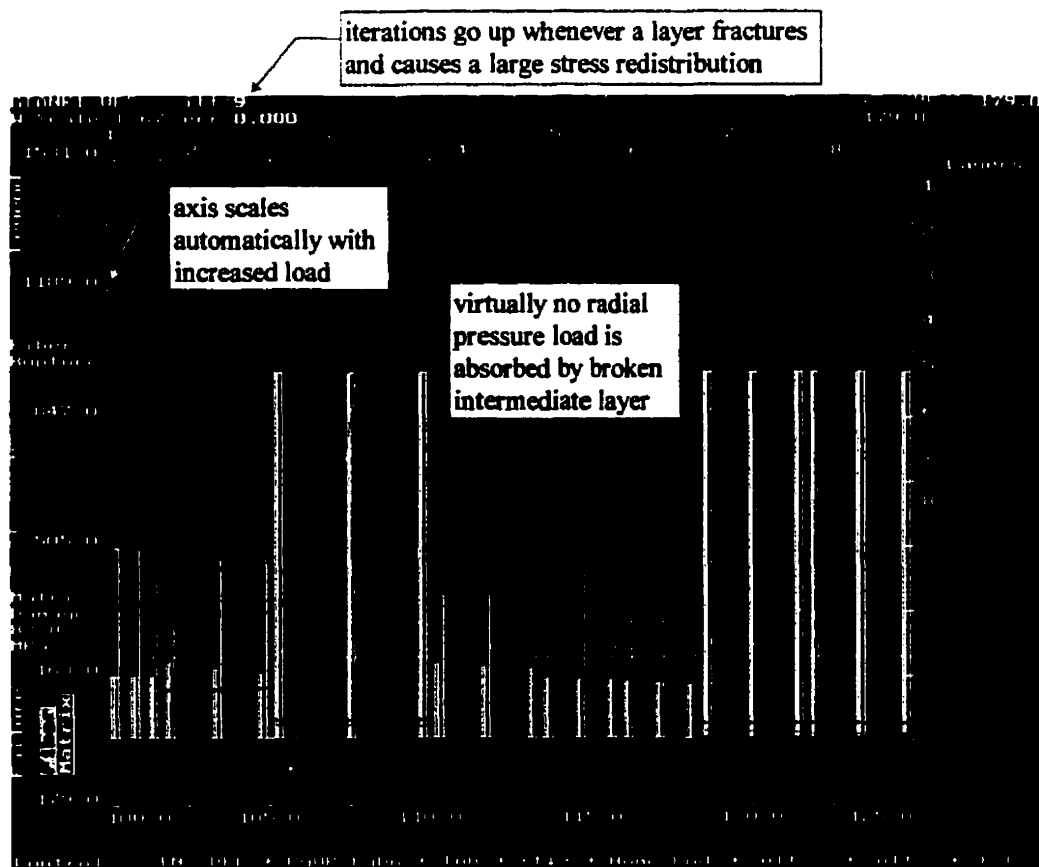
Figure 8.24 Vessel with a third layer fractured. Breakage occurred at 179 MPa.

446

Surprisingly even with the third layer fractured the failure is not yet catastrophic, but one can see clearly by the slope of the radial stress curve that the fraction of pressure being absorbed by the first two layers is quite extreme. With just an increment in loading the Kevlar® and AS4 layers approach fiber fracture almost simultaneously, and in turn precipitate catastrophic failure throughout. The thermometers then all show maximum degradation which corresponds to the upper yellow dotted line. At this point the program halts as it has detected fiber failure in all layers and displays an estimated failure load, bracketing the last known pressure it survived and the last increment which it did not. The end result is given in Figure 8.25, with the burst estimate shown at the top. The stress distribution depicted at this point is meaningless since the program has aborted .
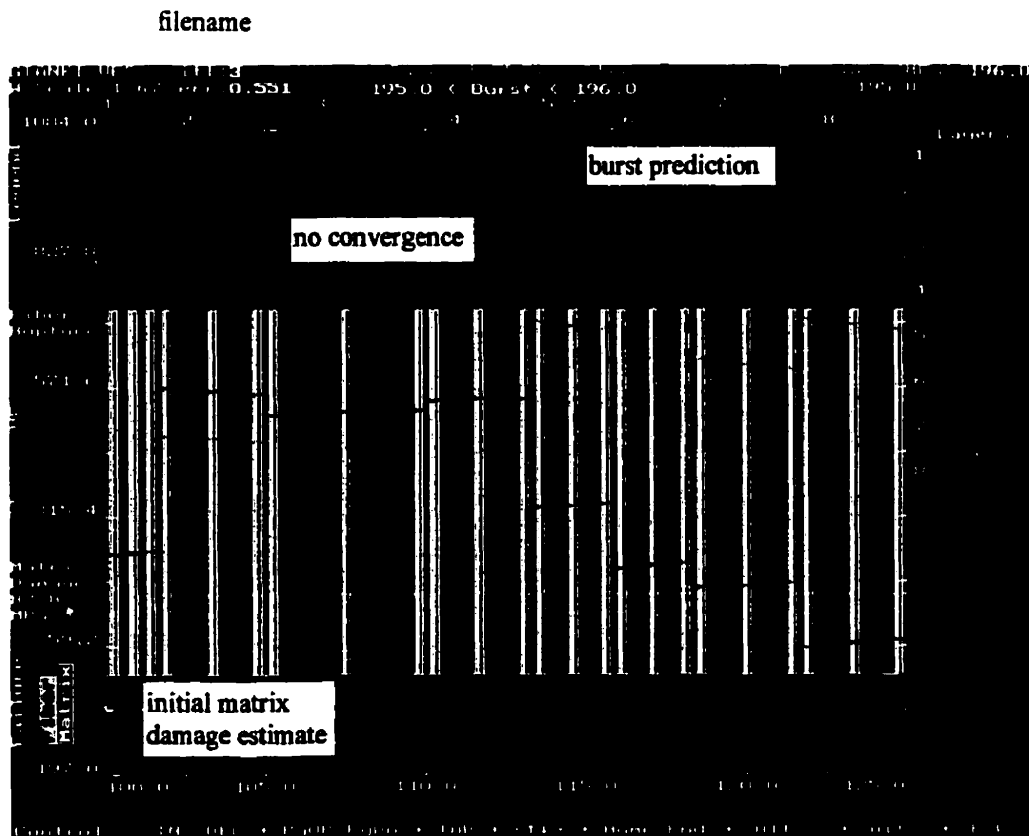
Figure 8.25 Poorly designed vessel of example case; burst at 195 MPa (28,300 psi).

447

Naturally the exact sequence and pressure level at which events occur depends on the accuracy of both the damage model parameters and the constants entered into the materials database. To further exemplify such sensitivity one need only consider what happens when we use the third option <Alt-N> which invokes the non-linear shear approximation. Here the interesting part is that the estimates for first damage keep moving to progressively higher levels (for the example case being studied) as one drives the program to calculate according to the initial estimate. Eventually damage does result but the level at which it occurs can be significantly higher than first anticipated. For this particular case we end up seeing a first damage estimate of 93.6 MPa an increase of 13% over the linear estimate (82.8 MPa). To attain this estimate one must not exceed the damage load predicted on the previous iteration. Single iterations can also be forced at constant load by hitting <Enter> without incrementing the applied pressure. A final damage prediction is recorded upon detection of matrix failure in any one layer. This is the value then displayed in yellow on the leftmost portion of the screen.

In using the non-linear shear computations the effect on the overall failure (burst) of the vessel is virtually nil since the shear correction is invoked only in the elastic response regime. From the standpoint of designing a good stress distribution near but not beyond the first damage point, the non-linear calculations can help one optimize a design. For instance by comparing Figure 8.26 with Figure 8.22 it can be seen that the outermost layer (P100S) in the case being studied has suffered a little unloading due to non-linear shear. This could be rectified by altering material parameters slightly to compensate.

It is as easy to adjust the wall lay-up in this screen as under the (Plot) menu and in
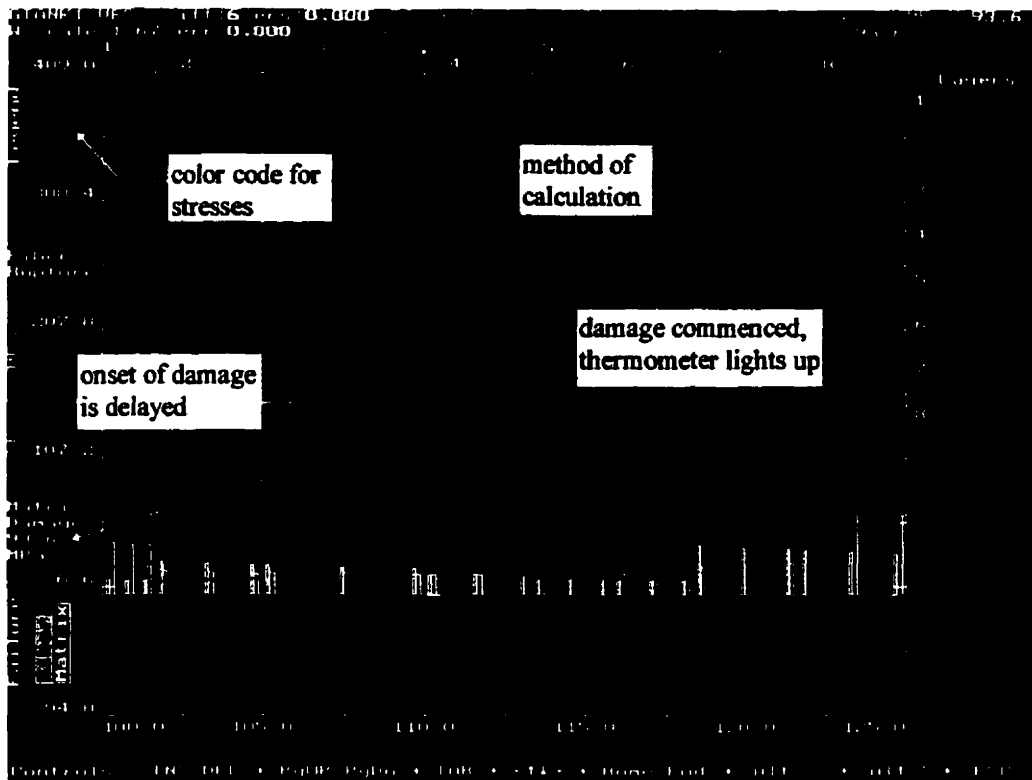
Figure 8.26 Initiation of matrix damage being suppressed due to modeling the non-linear shear response. Fracture sequence for the layers and final rupture is similar to the case modeled using linear response.

fact a design problem can be worked both ways in an effort to extract the property

variation rates conducive to an optimal stress distribution. Additionally, at any stage of

loading the numbers underlying the graphics can be saved to file or output directly to a

printer with the keystroke <Alt-F> and <Alt-P> respectively. The data filenames

generated for later inspection are numbered sequentially with the extension .d##. These

flash up momentarily when such an action is invoked. For example with the source file

gtankl.ves, recalling the 3rd saved-to-file loading state one would search for the filename

gtankl.d3 and open it with any standard text editor, or select the file viewing option

(View) under the (Utility) menu. The content of one such file, commensurate with the

449

loading shown in Figure 8.23 (except that non-linear analysis was used) is presented in

Tables 8.3 - 8.7 below.

Table 8.3 Vessel construction, loading and degradation

```
                    Super Pressure - Vessel Designer
                    Vessel Filename: gtankl.ves
                    Calculation Method: NL Shear / Full equations
                    Current Pressure (MPa): 150.0
                    Proof Pressure (MPa): 150.0
                    First Damage (MPa): 93.6
                    Rupture: FALSE
                    Wall Thickness (mm): 25.0
                    Inside Diameter (mm): 200.0
                    Wall Scaling Factor: 1.667
```

Lay No.	Material Name	Thick (mm)	Angle (-/-)	Fiber Percent	Matrix Safety	Fiber Safety	Matrix Degrad.	Fiber Degrad.	Shear Red.
1	t1000	1	50	63	0.715	2.012	0.595	1.000	0.917
2	kev_49	2	71	69	0.789	1.605	0.704	1.000	0.837
3	t300_520	3	57	66	0.834	1.199	0.776	1.000	0.666
4	as4_3502	2	59	65	0.838	1.812	0.784	1.000	0.714
5	im6_sci	1.5	57	64	0.740	2.227	0.630	1.000	0.830
6	im7_9772	1.5	56	63	0.952	2.401	0.974	1.000	0.703
7	p75s	2	49	56	0.221	0.221	0.221	0.221	0.998
8	p100s	2	42	62	0.221	0.221	0.221	0.221	0.825

Table 8.4 Stresses and strains along vessel primary axis

Layer no.	Sigma (r) inside	mid.	outer	Sigma (θ) inside	mid.	outer	Sigma (z) inside	mid.	outer
1	-150.0	-140.8	-131.9	966.5	953.3	940.8	687.7	680.2	673.1
2	-131.9	-119.4	-107.7	661.9	629.6	600.1	73.0	73.6	74.3
3	-107.7	-85.8	-65.5	851.7	820.1	793.0	391.0	383.8	378.1
4	-65.5	-52.3	-39.7	828.7	811.2	795.6	347.9	345.3	343.2
5	-39.7	-29.6	-19.9	889.5	878.5	868.7	413.3	410.7	408.5
6	-19.9	-10.0	-0.4	910.9	901.9	892.9	472.7	471.0	469.8
7	-0.4	-0.3	-0.2	9.0	8.7	8.4	24.5	24.6	24.6
8	-0.2	-0.1	0.0	7.0	6.6	6.3	24.2	24.3	24.4

Layer no.	Epsilon (r) % inside	mid.	outer	Epsilon (θ) % inside	mid.	outer	Epsilon (z) % inside	mid.	outer
1	-2.067	-1.970	-1.875	0.907	0.883	0.860	0.942	0.942	0.942
2	-2.474	-2.295	-2.130	0.860	0.808	0.760	0.942	0.942	0.942
3	-1.616	-1.420	-1.241	0.760	0.707	0.660	0.942	0.942	0.942
4	-1.203	-1.088	-0.979	0.660	0.633	0.609	0.942	0.942	0.942
5	-0.892	-0.789	-0.689	0.609	0.593	0.579	0.942	0.942	0.942
6	-0.831	-0.722	-0.616	0.579	0.564	0.551	0.942	0.942	0.942
7	-0.185	-0.183	-0.180	0.551	0.541	0.531	0.942	0.942	0.942
8	-0.197	-0.194	-0.191	0.531	0.521	0.512	0.942	0.942	0.942

Table 8.5 Stresses in material coordinates

Layer no.	Sigma (1) inside	mid.	outer	Sigma (2) inside	mid.	outer
1	1635.5	1612.8	1591.3	18.7	20.7	22.7
2	741.7	705.3	672.1	-6.8	-2.2	2.2
3	1199.4	1153.5	1113.8	43.2	50.5	57.3
4	1115.5	1091.1	1069.1	61.1	65.5	69.7
5	1256.0	1239.8	1225.2	46.8	49.4	52.0
6	1312.9	1298.1	1285.1	70.7	74.2	77.6
7	13.1	13.0	12.9	20.4	20.3	20.2
8	12.4	12.3	12.3	18.7	18.6	18.5

Layer no.	Sigma (3) inside	mid.	outer	Sigma (6) inside	mid.	outer
1	-150.0	-140.8	-131.9	-1.0	-1.7	-2.4
2	-131.9	-119.4	-107.7	-0.8	-1.3	-1.7
3	-107.7	-85.8	-65.5	-5.3	-6.8	-8.1
4	-65.5	-52.3	-39.7	-8.1	-8.8	-9.5
5	-39.7	-29.6	-19.9	-8.5	-8.9	-9.3
6	-19.9	-10.0	-0.4	-14.6	-15.2	-15.8
7	-0.4	-0.3	-0.2	-7.3	-7.5	-7.7
8	-0.2	-0.1	0.0	-9.0	-9.2	-9.4

Table 8.6 Strains in material coordinates

Layer no.	Epsilon (1) % inside	mid.	outer	Epsilon (2) % inside	mid.	outer
1	0.922	0.907	0.894	0.928	0.918	0.908
2	0.869	0.822	0.779	0.933	0.928	0.923
3	0.814	0.777	0.744	0.888	0.872	0.859
4	0.735	0.715	0.697	0.867	0.860	0.854
5	0.708	0.697	0.687	0.843	0.839	0.834
6	0.692	0.682	0.673	0.828	0.824	0.820
7	0.719	0.714	0.708	0.774	0.769	0.765
8	0.758	0.754	0.749	0.715	0.710	0.704

Layer no.	Epsilon (3) % inside	mid.	outer	Epsilon (6) % inside	mid.	outer
1	-2.067	-1.970	-1.875	-0.034	-0.058	-0.081
2	-2.474	-2.295	-2.130	-0.051	-0.083	-0.112
3	-1.616	-1.420	-1.241	-0.167	-0.215	-0.257
4	-1.203	-1.088	-0.979	-0.249	-0.272	-0.294
5	-0.892	-0.789	-0.689	-0.304	-0.319	-0.332
6	-0.831	-0.722	-0.616	-0.337	-0.350	-0.362
7	-0.185	-0.183	-0.180	-0.387	-0.397	-0.407
8	-0.197	-0.194	-0.191	-0.409	-0.418	-0.428

Table 8.7 Stiffness matrices

```
Local Stiffness Matrix [Cij] (MPa), Layer: 1

        182.81    2.78    3.62
          2.78    6.11    3.08
          3.62    3.08   10.25
                                3.03
                                       4.20
                                              2.96


Local Stiffness Matrix [Cij] (MPa), Layer: 2

         93.84    3.63    4.33
          3.63    5.82    3.75
          4.33    3.75    8.27
                                2.08
                                       2.18
                                              1.53


Local Stiffness Matrix [Cij] (MPa), Layer: 3

        153.75    5.44    6.19
          5.44    9.96    5.54
          6.19    5.54   12.83
                                4.42
                                       5.39
                                              3.16


Local Stiffness Matrix [Cij] (MPa), Layer: 4

        155.19    5.14    5.81
          5.14   10.07    5.32
          5.81    5.32   12.84
                                4.75
                                       5.14
                                              3.24


Local Stiffness Matrix [Cij] (MPa), Layer: 5

        178.61    2.85    3.61
          2.85    6.48    3.15
          3.61    3.15   10.29
                                3.34
                                       4.27
                                              2.80


Local Stiffness Matrix [Cij] (MPa), Layer: 6

        189.74    3.80    3.88
          3.80    9.32    3.95
          3.88    3.95    9.57
                                5.37
                                       6.32
                                              4.35


Local Stiffness Matrix [Cij] (MPa), Layer: 7

          0.42    1.38    0.32
          1.38    1.72    1.51
          0.32    1.51    7.78
                                0.21
                                       3.98
                                              1.89


Local Stiffness Matrix [Cij] (MPa), Layer: 8

          0.36    1.45    0.34
          1.45    1.48    1.47
          0.34    1.47    6.72
                                0.01
                                       5.60
                                              2.20
```

452

As mentioned at the beginning of this chapter, the concept of equal stress design is not necessarily the ideal in most practical situations since in going from one material to the next strengths change, often dramatically. There is no rule connecting material strengths to their elastic properties. In such cases it is better to design in a manner of equalizing failure initiation rather than strength. How to define the failure is a matter of interpretation based on the design objective. Generally two situations arise, and a balance must be struck between them. The first issue is that one may want to minimize the amount of matrix damage in the interest of good fatigue life characteristics, volumetric expansion concerns or simply out of prudence. The second objective, more obvious, is to maximize the burst pressure. The means to achieve either are not via unique solutions, rather it has been found that a good visual tool allowing for the effect of perturbations on basic designs is fast and effective in extracting the necessary design parameters. Below, simple cases of achieving either of these objectives (maximize matrix damage initiation pressure / maximize burst pressure) are presented based on the lay-up of the example case followed throughout the chapter.

For the purpose of showing what can be achieved with a slightly more optimized design in terms of burst pressure, we can eliminate the 3 materials that have low strength and fracture prematurely, then re-adjust the lay-up slightly to compensate the resultant stresses for differences in strength between layers, aiming for near simultaneous layer fracture rather than uniform stress. Such a vessel using the same relative thickness as before is shown in Figure 8.27 just prior to burst.

matrix damage is pronounced and
commences at a relatively low load
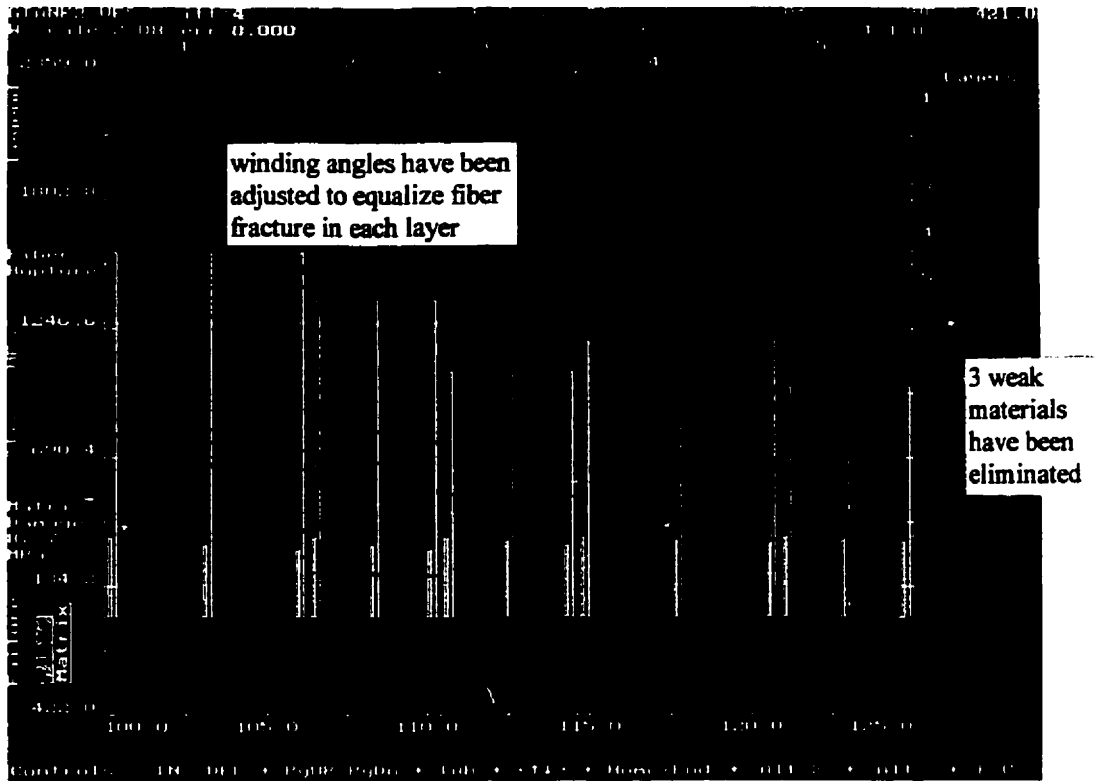
Figure 8.27 Five layer vessel based on materials used in example case designed for
higher burst pressure. Burst is predicted at 422 MPa (63,240 psi) but
damage begins at relatively low load.

Similarly vessels can as easily be designed to achieve a high pressure for the onset

of first ply failure (at the expense of lowered burst pressures) by shifting stresses in a

fashion to minimize matrix loading. There are no set rules for achieving this, it essentially

becomes a matter of trial and error, however the instant visual interpretation of any

perturbations quickly directs one to achieving a situation whereby the matrix loading in

each layer is lowered to the greatest extent possible. An example, using the same materials

and layer thicknesses as in the above case, with this criteria in mind is shown in Figure

8.28 below. The trials to achieve this took less than 10 minutes.
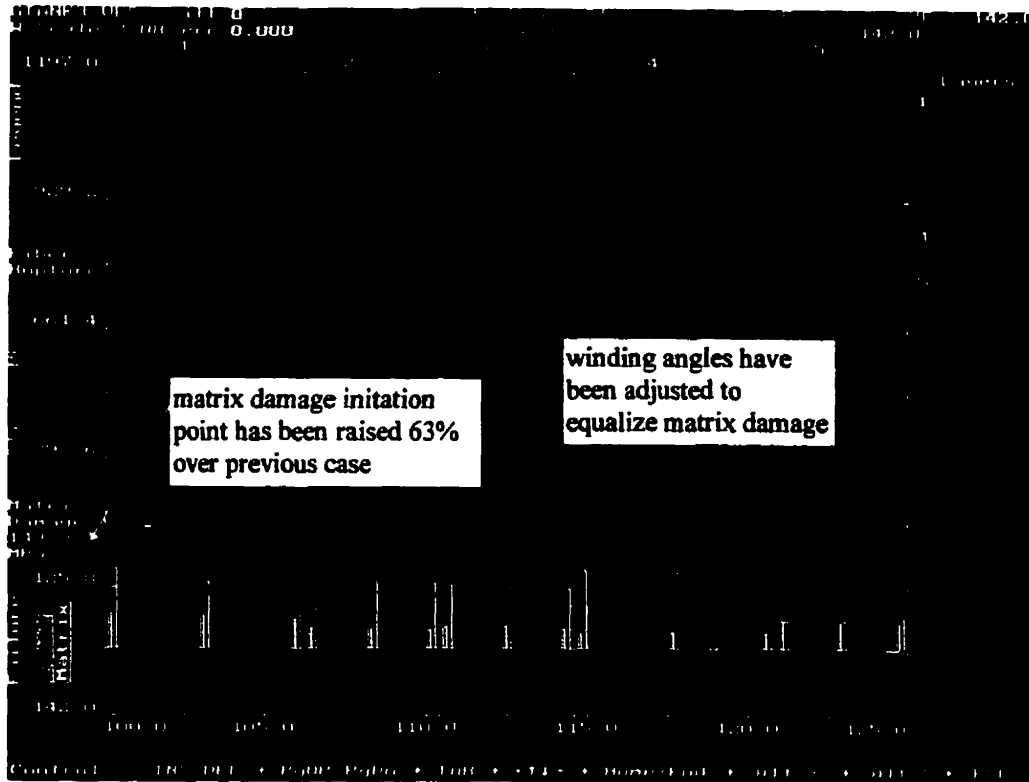
Figure 8.28 Five layer vessel designed with objective of raising the *FPF* pressure.
Damage starts at 143 MPa (20,780 psi) and burst is predicted
at 310 MPa, (42,840 psi).

8.4 Practical Design Examples

Let us consider the relatively simple problem of designing a pressure vessel for

which we limit ourselves to a single material. We can set the radius to thickness ratio at a

practical limit for construction using $b/a = 1.25$, as in the previous examples. A very

standard material of relatively low cost can be selected, in this case AS4_3502. The design

problem posed is to select a lay-up that will maximize the burst pressure. We shall

commence in the usual fashion by entering the construction parameters for a .wal file and combining it with a loading case (.lds) to create a .ves file. These steps, nor the keystrokes for what follows will be detailed as it is assumed that the basics of program operation are understood. To begin with, an 8 layer design following a conventional winding pattern that alternates hoop windings with helical layers is examined. At this point, to help evaluate the results. a few additional features within the program have been turned on. The top right of the screen (Figure 8.29) presents two additional numbers. One denotes the predicted burst pressure based on the most highly loaded fiber layer (B:), the other is a factor named "fiber strength usage efficiency". It estimates how close the material throughout the entire wall is to rupture. This factor (labeled E:) is effectively computed as:

$$\left[\frac{\text{min. fiber safety factor}}{\sum_{1}^{n} (\text{fiber safety factors}) / n} * 100 \right]$$ and expressed as a percentage. If the fibers at every

point were equally close to failure then the E factor would be 100%. Additionally the layer within which the fibers are most highly stressed "lights up" to a higher intensity in order to emphasize its location. Obviously, to attain the design goal, the strength usage efficiency should be as high as possible. This reflects upon the ultimate pressure capability of the vessel but the two quantities are not linked directly. For some non-optimal designs there may exist marginally higher burst pressures at the expense of lower strength usage efficiency however this is an exception and generally the two factors vary in tandem.

The design shown in Figure 8.29 has seen many iterations in an effort to balance the layer loadings. As a result of experimenting with the program, a few important
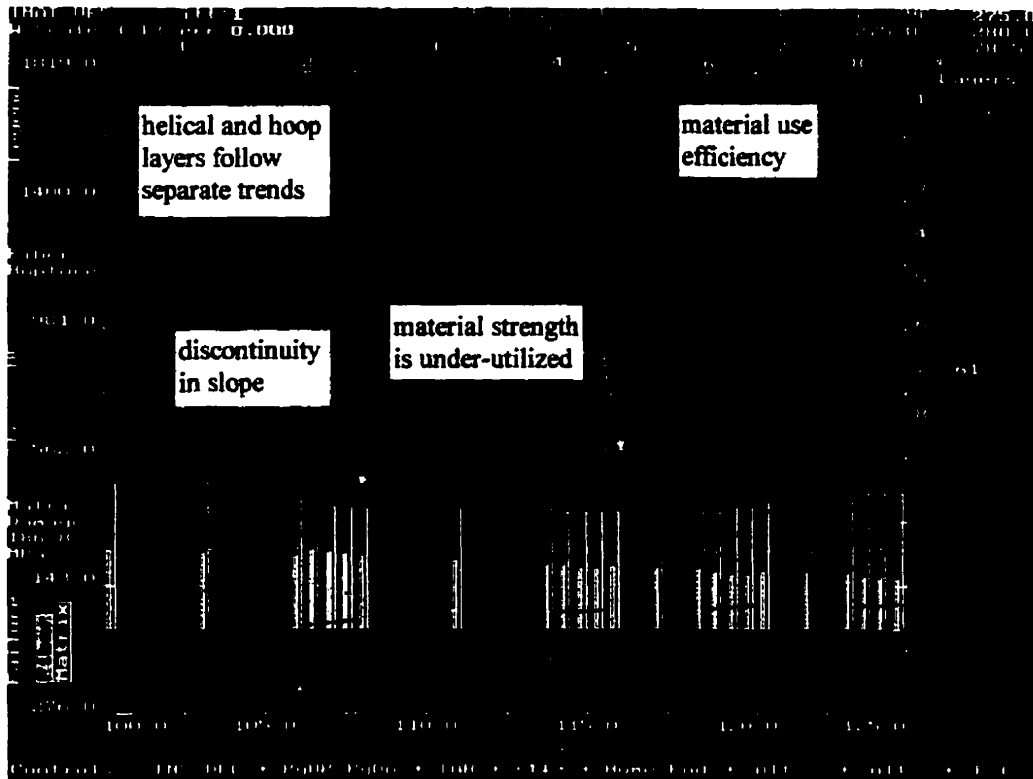
Figure 8.29 Single material vessel using interspersed hoop and helical
windings optimized for maximum burst pressure.

observations have been made. It is always possible to balance the loadings in the two

innermost layers (by altering the winding angles) but the problem thereafter is that the

remaining layers may be shielded from sufficient strain to maximize their usage efficiency.

No amount of re-arrangement of the outer winding angles can then raise the usage

efficiency or ultimate pressure capability further. Different configurations can be attempted

with interspersed hoop and helical windings. Another variation is shown in Figure 8.30.

The situation described, visible both in Figures 8.29 and 8.30 appears to be a fundamental

limitation or at least a major impediment when using alternating helical and hoop layers.

This may be overcome by switching to stiffer materials in the outer layers. However we

notice that in the foregoing two quasi-optimized designs, the stresses σ_r and σ_z

nevertheless follow a smooth trend when one considers the hoop and helical portions of

the winding separately. This trend was not designed purposely but evolved through the

iteration process which was aimed at maximizing burst pressure.
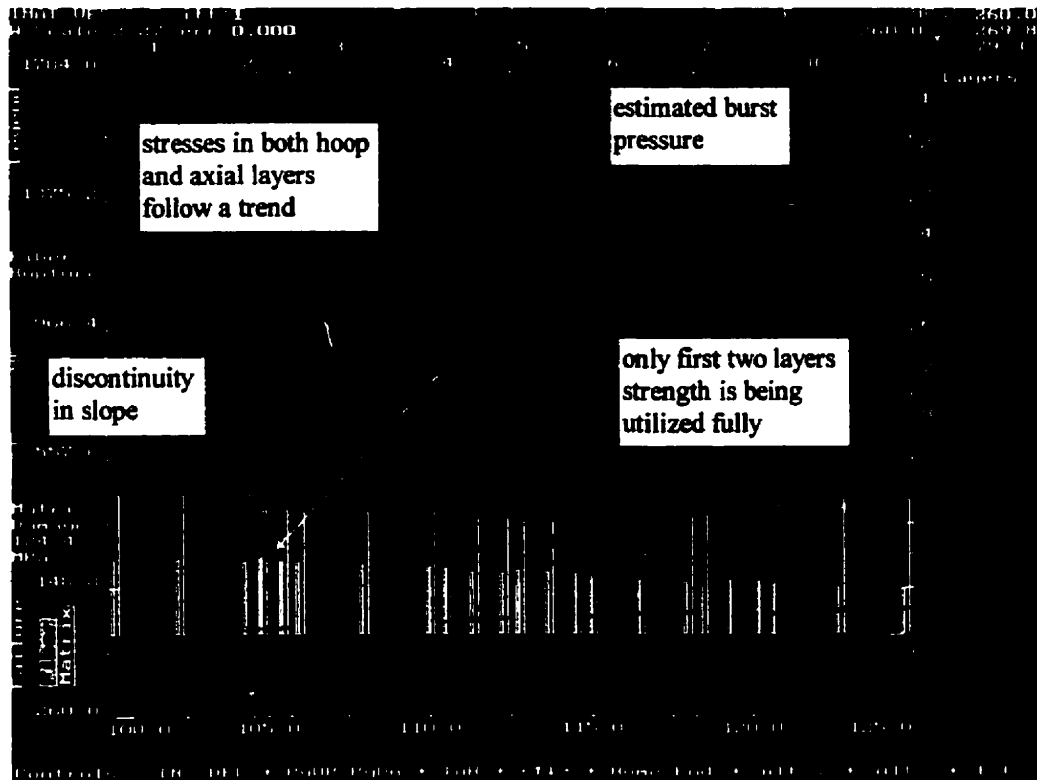
Figure 8.30 An alternate arrangement of mixed helical and hoop windings.
Such arrangements when optimized result in local
maxima for the burst pressure.

This leads one to speculate that a much more optimal solution may lie along the

line of a smooth and continuous variation in the winding angles. Investigating along this

458

line brings forth the lay-up shown in Figure 8.31. Suddenly the pressure capability is vastly

improved and material usage efficiency is about as high as one can get without resorting to
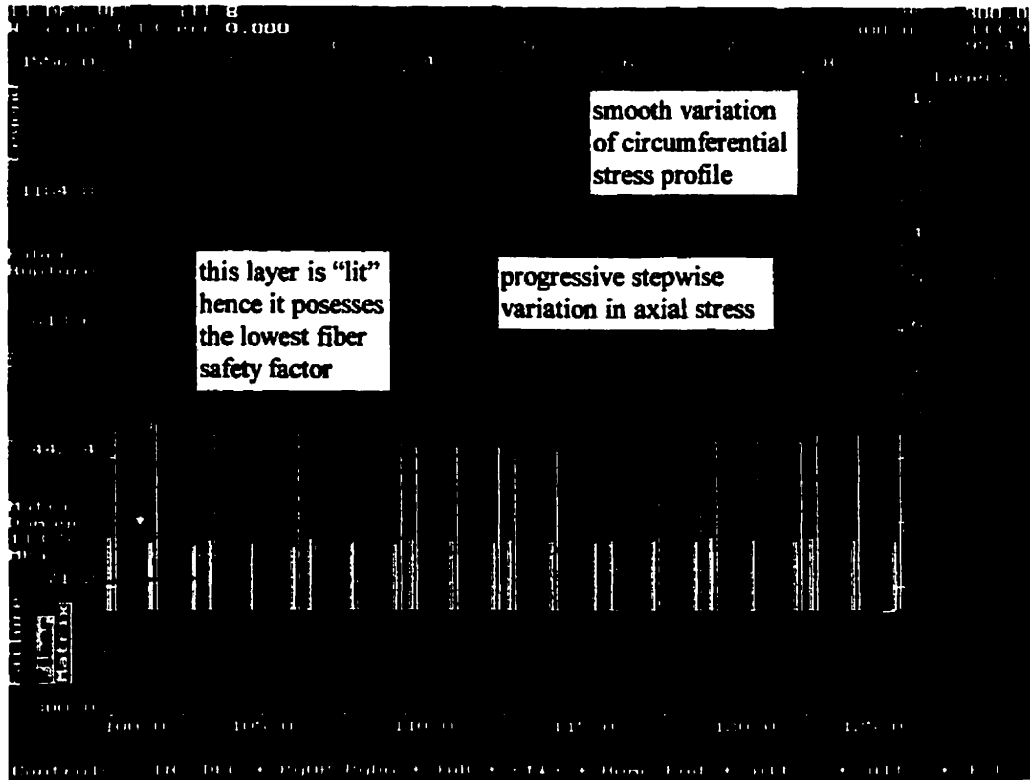
Figure 8.31 Example of an optimized winding angle arrangement following a
progressive variation that leads to continuity in the hoop stress.

an increased number of layers to cut down on the "step size" causing discontinuity. Both

the hoop stress and axial stress follow a smooth trend. Other similar solutions are possible,

where for example with ascending winding angles both the axial and hoop stresses are

varied by incremental steps. Such a situation is depicted in Figure 8.32. For the case

shown there is also a raising of the initiation point for matrix damage (from 124.4 MPa to

152.5 MPa) with some reduction in ultimate pressure capability (down from 334 MPa to 318 MPa). For both cases the fiber strength usage is around 96% indicating that the material throughout the wall is loaded very near to its ultimate capability.
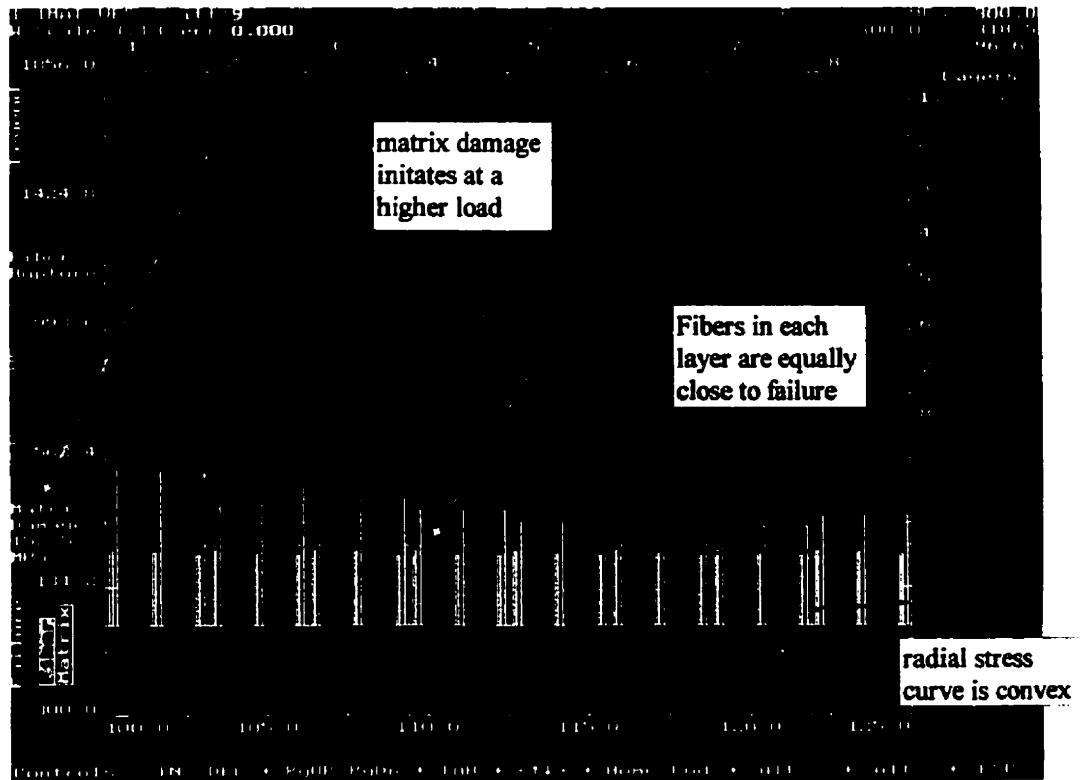
Figure 8.32 Alternate arrangement, single material with ascending winding angles. Strength usage efficiency (E) is very high.

In a manner of reverse analysis one can check whether the predictions of stress distribution arising from the "variable material" solutions employing smooth and continuous alterations in properties (monolithic wall construction) coincides with the optimized discrete layer by layer solution for the wall given above. Figure 8.33, derived from the 6 variable parameter finite difference solution to the same problem clearly shows

this to be the case. The accuracy of the numerical solution stems in part from the close

modeling of the individual layer properties by their power function equivalents as depicted

in Figure 8.34 for the principle reduced compliances β_{ij}. Even though optimal stress

distributions for σ_θ and σ_z in relation to maximizing burst pressure cannot be derived

from the variable properties solution, the back-calculated variation rates required to

achieve optimal burst are of value since they enable easier reproduction or synthesis of

other similar designs, using different materials and dimensions yet based on the same

winding pattern. In addition it should be noted by comparing Figures 8.29 through to

Figure 8.34 that the radial stress σ_r for high efficiency designs may be concave, convex or

stress levels and trends match discrete layer problem

these graphs superpose almost perfectly upon the trends in Figure 8.32

slight convexity of this curve indicates that pressure loads are being transmitted with slight preference to the outside layers
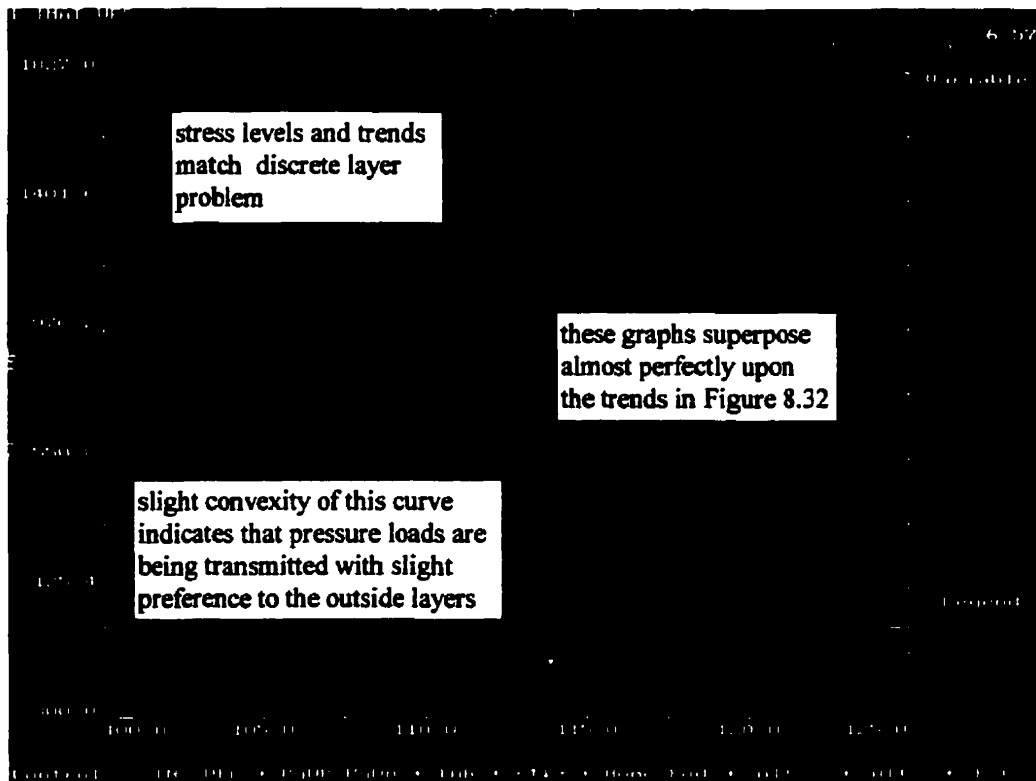
Figure 8.33 Numerical solution for continuous property variation to the
8 layer / single material vessel design of Figure 8.32.

461

straight but always *smooth*. Thus one can speculate that a principle of minimizing the net

discontinuity stresses or stress gradient between layers appears to be operative.
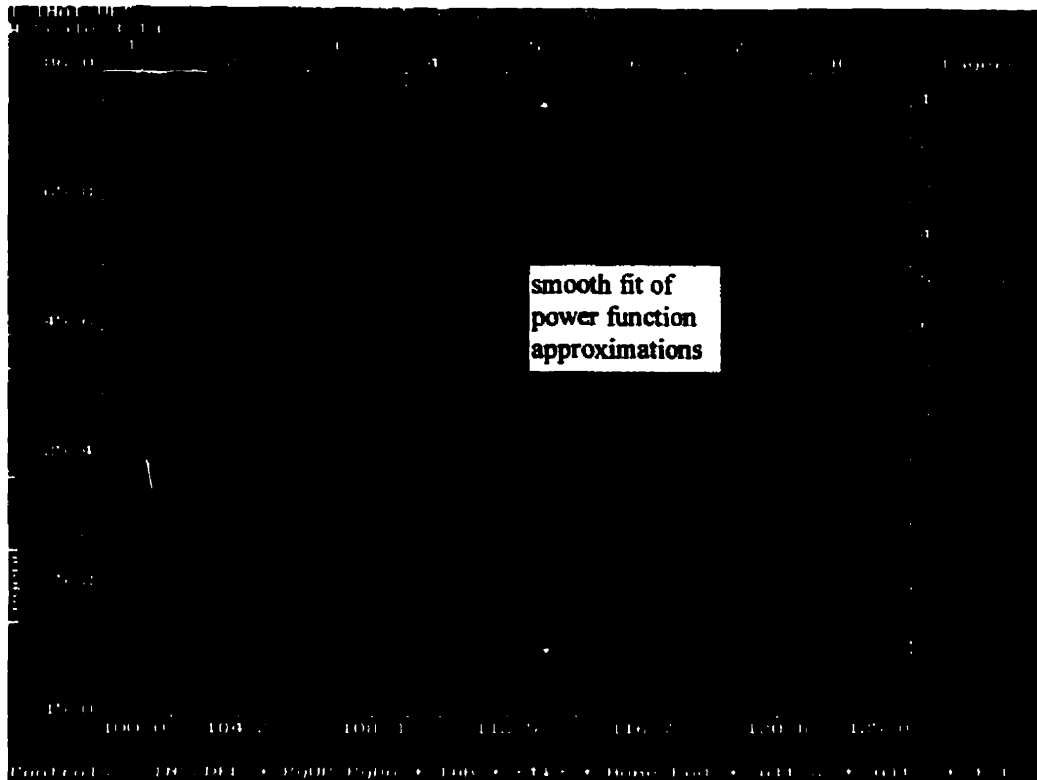
Figure 8.34 Modeling of the layer elastic characteristics by power functions.
Goodness of fit is apparent and contributory to accurate variable
properties solutions.

Let us consider another example, this time using two materials. A situation that

often arises concerns the need for a high containment pressure however the cost of extra

strong fiber grades is prohibiting and it is desirable to minimize such content. Using IM6

as representative of an intermediate cost carbon fiber and T1000 as the fiber representing

the premium material (where the cost factor may range upwards of 4X) it is clear from

Figure 8.35 that a stress distribution can be designed to take advantage of the T1000's

higher strength. Strength usage in both materials is above 95% and burst pressure is

predicted to be approximately 472 MPa (68,450 psi).
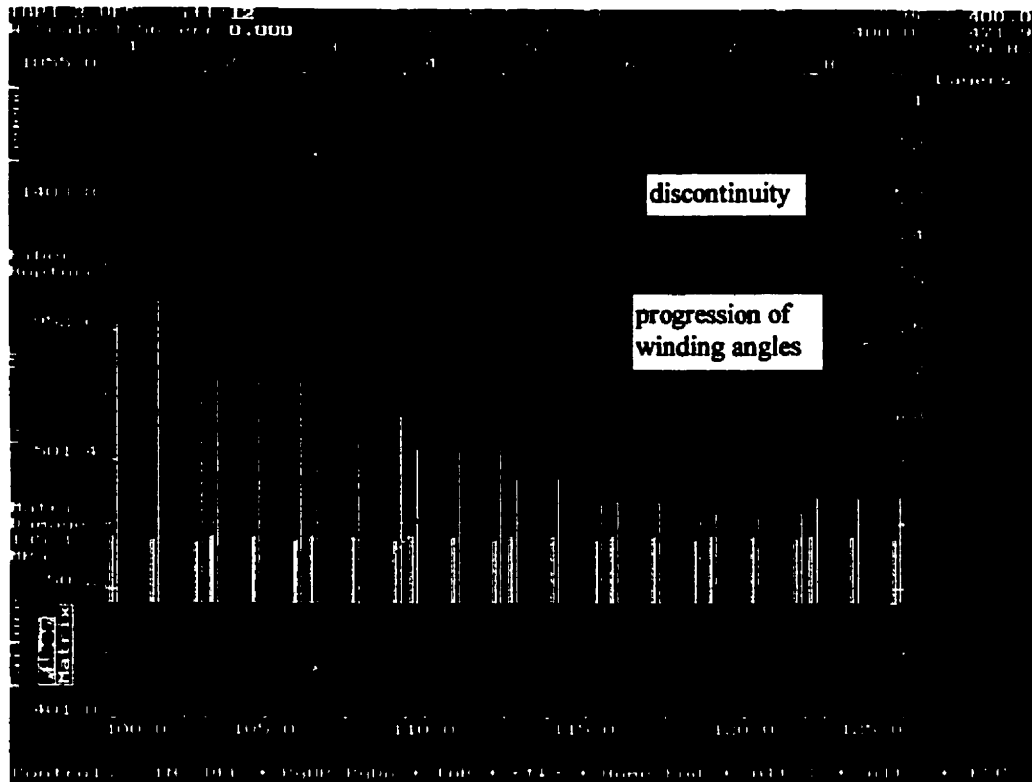
Figure 8.35 Stress distribution in vessel consisting of 2 materials.
T1000 fiber constitutes 25% of the wall thickness,
the balance is lower cost IM6.

However considering the cost factor it is instructive to note that a vessel of

equivalent dimension constituted simply from the lower cost material, when optimized,

would burst at only ≅ 7% (32 MPa) lower pressure. This situation is depicted in Figure

463

8.36. Evidently one must be mindful that use of expensive high strength / high strain material is warranted only when no other method exists to raise the burst pressure for a given wall thickness ratio. The vessel, when constructed entirely of T1000 using exactly the same winding angles at a wall thickness ratio b/a = 1.25, would burst at approximately 552.3 MPa (80,100 psi). This can be verified by calling up file TOP1_T1.VES. The increment in burst pressure using a mixture of 2 materials, when optimized for high fiber usage efficiency, can therefore be considered linearly proportional to the difference between the ultimate pressure capability of the stronger and weaker materials multiplied by the fraction "reinforcement" present. In this case: 439.7 + 0.25(552.3 - 439.7) = 468.9
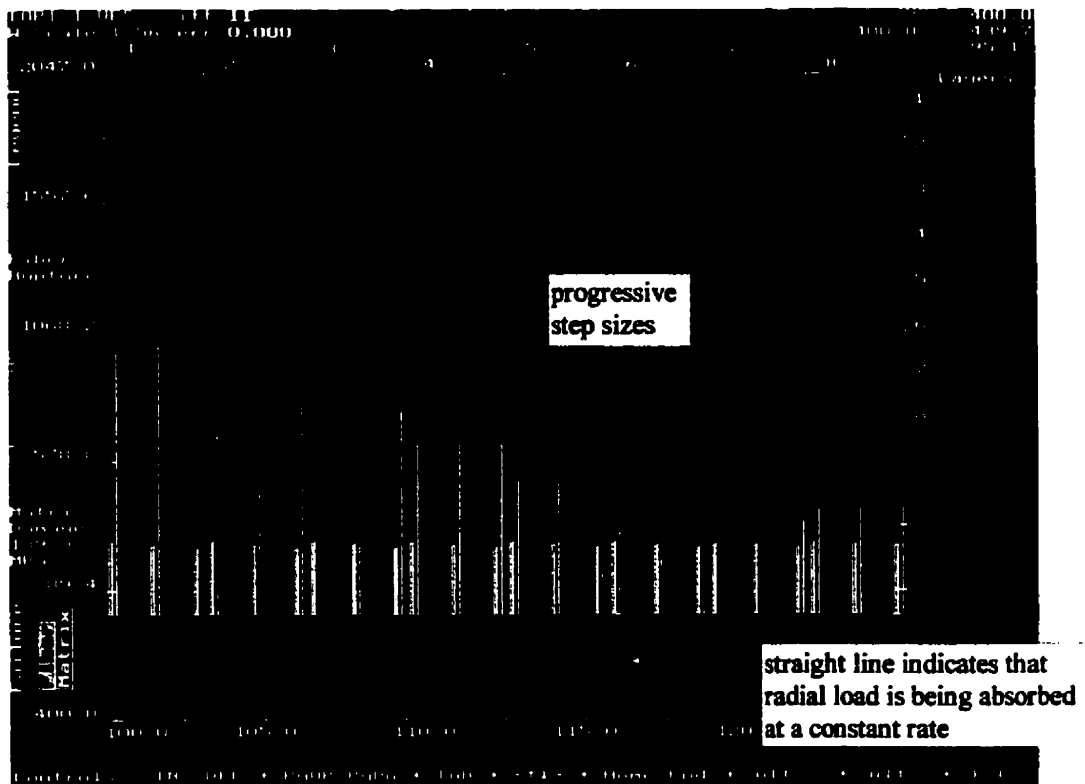
Figure 8.36   Vessel constructed entirely of IM6_SCI material. Burst pressure is lower than configuration shown in Figure 8.35 by a factor proportional to the reinforcement effect provided by the stronger fiber.

$\cong 471.9$ MPa. A parallel equation could be set up relating total material cost to the ultimate pressure capability. Extending this concept under the assumption that laminates can always be designed with a high material usage efficiency (E) one can see that for any given burst pressure and relative thickness ratio (b/a) a balance of different materials might be used to produce the least costly structure (assuming that weaker materials are priced lower).

8.5 Summary

The basic points pertaining to use of the software have been covered. It has been shown how the program can be used to design a stress distribution (or failure distribution), either emanating directly from the variable material elasticity approach or simply by varying the lay-up parameters and watching the failure envelope safety parameter R for fiber or matrix. As a starting point, the concept of designing for constant stress through the wall thickness via the variable elasticity approach is helpful. It permits exploring the action of each material stiffness, these are reviewed in Table 8.2. In practical situations, relatively flat stress distibutions demand that the circumferential compliance β_{22} follow a radial variation rate described by an exponent ranging -1.6 to -2.0 on γ_{22}. Material choice is a powerful means to influence it. The axial stress distribution is strongly governed by α_{13} and α_{23}, these terms being functions dependent mainly on the winding angle. The axial distribution must be looked upon in conjunction with the circumferential stress

465

distribution in the interest of establishing a more level incipient failure level throughout the laminate.

It must have become evident to the reader or user of the program by now that mathematical solutions entailing global stiffness changes according to only a single parameter 'n' have no practical application due to the fact that stress distributions are governed chiefly by the ratio of circumferential to radial stiffness. As a first approximation, radial stiffness can be thought of as an invariant in practical lay-ups since it is matrix dependent. Mathematical formulations which ignore this fact end up giving a very misleading solution. Individual functions can be used to describe the behavior of each elastic constant when the cylinder is modeled as the ideal monolithic continuum. This, when coupled to a numerical solution, results in a satisfactory model describing stress distributions in real discrete lay-ups.

The practical problem however centers on achieving more even *failure distributions* and these are not directly related to the *stress distributions*, rather they are material dependent. A level hoop stress distribution may be used as the starting point for optimization but it must be anticipated that a flat stress distrubution is near impossible to achieve simultaneously in both axial and circumferential directions. The designs get more complicated when multiple materials, each with a different strength, are utilized. In this regard the problem is more easily tackled with a highly interactive visual tool, a feature particular to the "Super Pressure - Vessel Designer" program.

A few simple yet practical examples have been given in relation to obtaining efficient stress distributions for both single and two material vessel walls. The concept of

material strength usage and a proportioning rule to factor cost has been proposed for multi-material lay-ups.

Some review of the history and experimental endeavors related to this work and applications pertaining to the analysis of vessels actually built, both by the author and others, follow in the final chapter.

Chapter 9

Design Considerations, Validation and Contributions to Knowledge

9.0 Design Program History

The history of this project is a rather lengthy one and dates back circa 1984-85 when a laboratory sized filament winding machine was first being considered. The possibility of such an acquisition was based on prior involvement with a large commercial filament-winding operation specializing in vessels and piping for the chemical processing industry, CPF Dualam Inc. Having explored many options, including the design and building of a machine in-house, which had advanced to the drawing board stage, a purchase deal was eventually made and aforementioned plans were dropped in favor of a custom "laboratory sized machine". It represented the second of only two such machines built from then the foremost supplier in the USA, *Maclean Anderson*. This two-axis stepper motor driven machine was controlled by an S-100 bus CP/M based computer system. The equipment had numerous faults and shortcomings, nevertheless with some time and effort many of these were eventually overcome. It was used principally to wind tubes, elliptical cross-sections and finally cylindrical pressure vessels. In its ultimate incarnation, it was fitted with a heat-lamp enclosure and warmed resin bath and a mechanical weight driven fiber tensioning system.

In the context of this work, winding patterns were practiced over wooden mandrels until sufficient experience was gained to overwind a glass-fiber (aluminum lined)
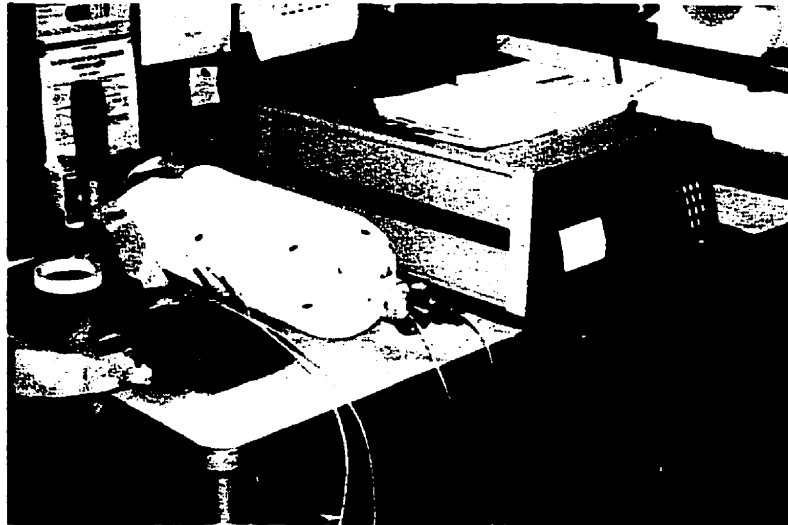
Figure 9.1 Vessel fitted with strain gages connected to data logger. Surface has
been sandblasted for adhesion in preparation for overwinding.

fireman's breathing apparatus with Kevlar 49®. This vessel was then subjected to proof

testing of 845 bars (≈86 MPa) using a liquid nitrogen cylinder filling technique developed

in-house, and operated in a laboratory environment at the 10,000 psi (69 MPa) level for a

number of years. It was fitted with a special neck capable of holding 4 computer peripheral

connectors (serial port DB-9) for easy hook-up to a data acquisition system. During

construction, fourteen strain gages were fitted, divided equally between the glass/Kevlar®

interface and the outer surface, wired with 29 gage (0.011″) enameled magnet wire. A

Fluke® data acquisition system was used to record during test cycles. The filling technique

to achieve the super-pressures was simple, in essence copied from commercial filling

techniques for propane gas bottles. The empty vessel was set onto a scale and a tare

weight was recorded. To this was added the desired fill weight and the balance beam set

accordingly. Liquid nitrogen was pumped in rapidly until the desired

weight was achieved and a sealing plug henceforth set in place with a pneumatic impact wrench. As the cryogenic fluid warmed the pressure rose to a desired equilibrium state, determined in advance with the help of computer generated extrapolations of published thermodynamic tables. The test program was to establish if acceptable limits were being respected with regard to the 10,000 psi operating pressure by going through a secondary proof test and some lower pressure cycles. The vessel was subsequently used in an exploratory study considering the direct injection of hydrogen and / or natural gas into internal combustion engines, underwritten by Bendix Avelex Inc. Some particulars pertaining to the testing are published in an internal report [207][247]. Figures 9.1 through 9.4 record some of this experimentation. The foregoing work did eventually pave the way for a subsequent grant targeted at upgrading the winder to 4-axis servomotor control along with acquisition of an extensive custom software package (Compositrak's: - Operator - File Management - Bottlemaster - Pattern manipulation - Non-linear , etc.) that
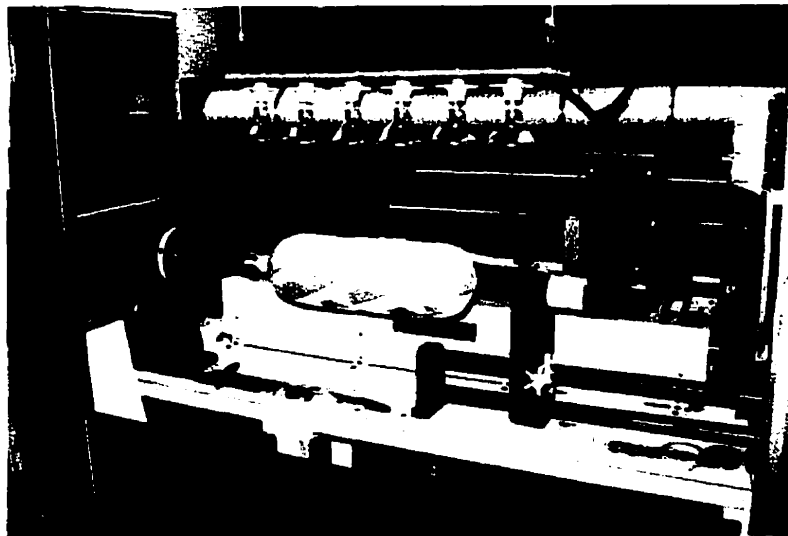
Figure 9.2 S-glass pressure vessel being over-wound with Kevlar 49®.
Stepper motor driven 2-axis winder configuration.

470

Figure 9.3 Frost covered vessel. Baseline strain data being gathered prior to overwinding. Design criteria set forth is partially based on never exceeding the original nominal operating strains even at super-pressures.

can be run on a PC. With these the machine motion paths generated can be uploaded to the winder's disk drive and stored for later execution. The system has enough open architecture to admit user generated motion files from other sources.

The new software was run and also used by others, testing computer generated paths in relation to their own winding projects. A further examination of the fiber trajectories revealed that the "Bottlemaster" software uses an ellipsoidal dome shape to approximate a geodesic profile. Because the software was designed for constructing thin-walled vessels it has no built-in facility for adjusting the winding pattern in a functional relation with the changing dome profiles emmenating from the varying thickness of fiber buildup over the ends.

471

Further it lacks any feature to check for the amount of "slip" (the path is already somewhat non-geodesic to begin with). On the other hand, Compositrack's "Non-linear" routine is very general and can compute slip given a mandrel description but is not set up to generate winding paths for any one particular purpose, but rather designed for winding odd shaped objects.
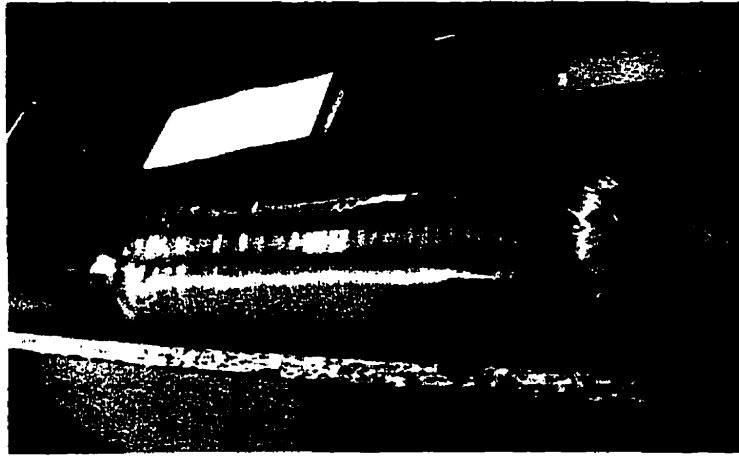
Figure 9.4   Kevlar® 49 overwind near completion. Small support tube at vessel bottom is used to prevent fiber slippage over top of dome and was removed at the end of the winding operation before the resin gelled.

Upon return of the machine it was installed in a new facility complete with a larger fume enclosure. A new insulated and thermostatically controlled convection oven was built (like a muffle), along with a more sophisticated resin impregnation bath complete with closed loop temperature control. Further, a 12 creel tensioning array using a remotely adjustable regulated power supply and individual DC motors acting as torque brakes was designed and fabricated along with an entirely new tailstock assembly running on linear bearings permitting up to 24" diameter by 48" long mandrels (up from the original 14" x

40") to be wound. Figures 9.5 and 9.6 illustrate this later configuration. Also a set of

Haskel® hydro-pneumatic intensifiers (capable of 100,000 psi or 6900 MPa) and a

waterproof, reinforced concrete test-tank was added to the lab facilities.

To this end it was realized that a much more sophisticated analytical approach was

required to generate mandrel shapes and the desired fiber angle at any point, at least on a

single circuit level. Such information can be encapsulated in a file called by "Non-linear"

(TOFRONT) which when combined with other software tools like (TOPATH ,

ADVPATH and MOTION) will generate the required machine movements to control the

system. More direct approaches are available including the generation of Compositrak

source files but details of the system level commands are definitely outside the present

scope and the interested reader is referred to the user manuals [248]. The fundamental

purpose of the work presented in Chapter 3 was to attain the required analytical solutions

to allow generation of mandrel shape and fiber angle data needed for the case when the

lay-up becomes very thick. Interfacing the results presented by these equations to machine

specific language commands represents a further phase of the work, something not yet

complete but hopefully soon to be broached in the future. This will lend support to further

experimental tasks envisioned.

At the conception of this research work it was thought to build and analyze thick

vessels via an experimental program similar to earlier ones carried out by NASA space

programs, air force missile, land-based ballistics or deep-sea submersible oriented efforts

using newer graphite fiber based materials like T-1000, XIM9, UHM and others along

with a later generation of fluropolymer based liners whose potential in concert with
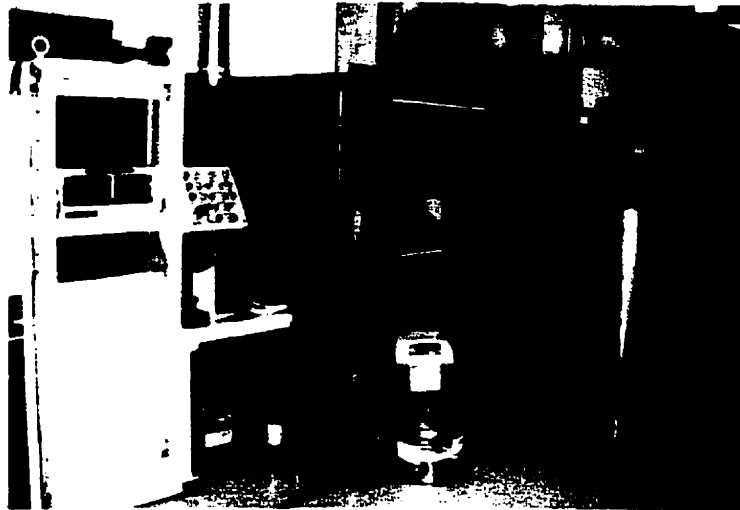
Figure 9.5 4-Axis filament winder in updated configuration. Muffle and
hydro-pneumatic intensifier equipment in background. added controls
for tensioners and heaters located at base of master control panel.

cryogenic filling has never been investigated.

A turning point in emphasis was set in motion with the building and testing of the

hydrogen / natural gas tank for Bendix Avelex. Although (re)designed with a nominal

safety factor of 2.5 and a design proof pressure of 14,700 psi. (1000 bar), the testing

showed that strain levels were higher than anticipated. To ensure staying within acceptable

strain levels a 850 bar (12,500 psi) absolute limit was set, adequate for the promised

minimum (690 bar) 10,000 psi operating pressure and the limited cyclic exposure in the

laboratory. Realizing the inadequacy of current design methods despite the fact that some

of the better predictive efforts then available had been employed it was slowly decided that

embarking on an experimental program might offer no further insight than many of the

more ambitious and well funded programs of earlier times. The real problem entailed

understanding *fundamental* principles governing internal stress distributions and also

having available adequate design tools. Manufacturing techniques and related areas were

steadily being furthered by others since the field had gone commercial, but no one truly

knew enough about governing parameters from the stress analysis point of view to help

make a significant difference to the design philosophy itself. Inspiration came from the

work of Roy and Tsai [91], Foral [43], Gerstle and Moss [15] and many others who made

contributions. From this point forward it was decided to halt further experimental work

and seek first a far more complete theoretical foundation, which lead to the analysis

described in Chapters 4-7. Much of this analytical effort was eventually coded into "Super

Pressure - Vessel Designer" with the aim of creating a tool powerful enough to act as a

basis for future experimental efforts. The programming effort is now in a complete enough

form to demonstrate its application.
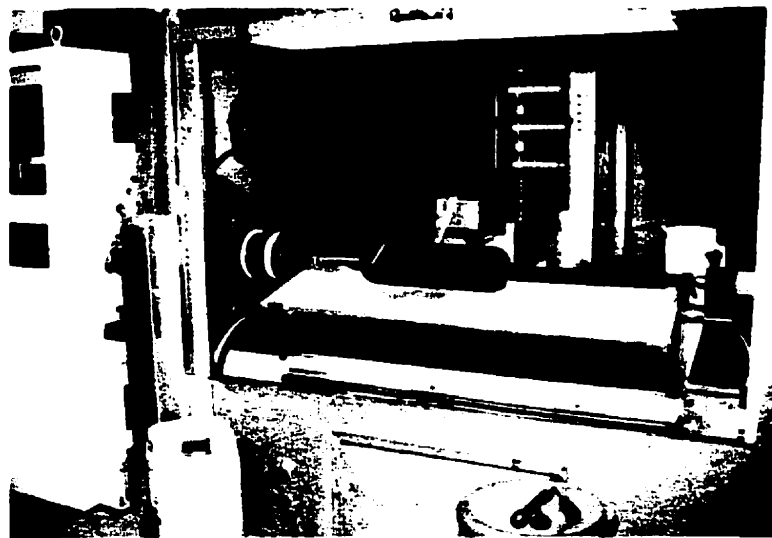
Figure 9.6   Creel holder / tensioner system riding on carriage complete with heated
resin bath and drip-pan / muffle base located inside fume enclosure.

For clarity, work remaining must also be stated. In order of importance, "Super Pressure -Vessel Designer" in its present incarnation still lacks a thermal residual and curing stress analysis, but the basic equations are available [131][249] and should be considered in the future. Also the behavioral effects of an elasto-plastic metallic liner have not yet been incorporated, but this too has successfully been modeled by others, for example [127][130][158] studying thin-walled vessels, and will eventually be adapted to advantage. The full generalized plane strain equations of Chapter 5 (layer by layer rather than ply-pair analysis) have not yet been implemented but do help one understand what is happening from a theoretical perspective and may eventually see themselves written into the code as a final refinement.

The subject of designing spherical vessels has not been addressed in the present work in an effort to limit the scope. It should be noted however that the full equation sets for such analysis have been derived and in fact the variable property solutions brought forth in Chapters 5 and 6 were first derived for the spherical case, preceding the developments put forth here within but are purposely not documented in this write-up in order to retain focus.

The work done is nonetheless sufficient to bring forth better quantified design objectives, and the whole effort has been melded into a package that converts the numbers into graphics for a truly interactive design tool. Many past studies have noted that the potential combination of winding angles, lay-up sequence, materials and individual layer thickness are innumerable. For example a recent study employing heuristic methods and optimization algorithms carried out by Amiouny and Hoa [250] noted that considering the

possible combinations when selecting among 9 distinct winding angles (increments of 10°), for a 50 layer vessel constituted entirely of the same material and equal layer thicknesses, it would require evaluating and ranking 10^{61} different designs. Clearly this number would grow enormously with the addition of further variables. Supposing a very fast computer could solve the entire elasticity equation set in $1/1000^{th}$ second and it had been working on the problem since the beginning of time (about 14 billion years) it would only have solved 4.4×10^{20} cases to date. Obviously, from such a perspective, one faces an intractable problem regardless of the computational power employed.

One strength of the present analysis is that it avoids any brute force approach but rather is governed by a mathematical fundamental, that is coaxing out stiffness variation rates suitable to an objective such as leveling the stresses. This can for instance mean holding the circumferential (primary) stress to a more or less constant value along with ensuring that the axial stress does not go to extremes. There are never any unique solutions and in the design sense one must ultimately look upon the whole as a *strength* problem rather than an exercise in optimizing only the stresses via the material elasticity.

To achieve favorable stress distributions, materials can be selected and parameters such as winding angle, thicknesses and fiber volume fraction adjusted at the designer's discretion via small perturbations to fit the model's "variable property" ideal. The link to strength is via failure criteria and damage modeling. At this point one must then iterate between stress distributions and strength concerns to arrive at a comprehensive design solution. Chapter 8 has brought forth how the program is run and what its capabilities are.

We must now consider the scope of what is (and what is not) within reach presently and then look upon some examples based on vessels that were actually constructed and tested.

9.1 Design Considerations and Limitations.

This work is not intended to be a "cookbook" giving out design parameters and specifications to achieve requirements for any particular vessel performance objective. Rather, the purpose is to advance a more detailed understanding of the factors at play and show how a design tool has been built around this knowledge together with demonstrating its effectiveness at achieving stated objectives. Cookbook solutions in the form of tables giving "optimized" winding angles or similar pretentious results have purposely been avoided for a number of reasons:

First there is little economic motivation to publish pseudo "optimized" designs for the benefit of third parties.

Second, there remain unanswered questions pertaining to the transverse compressive behavior of laminates under extreme pressure and the magnitude of such influence is unknown. (See Figure 7.5) A model is required to predict the elasto-plastic response in this regime and currently none appears available.

Third, neither elasto-plastic liner effects (metal liners) or thermal / cure stress considerations have yet been implemented, both of which can affect the safety due to metal fatigue and or precipitate early matrix damage. It would be improper to state that a design has been optimized without inclusion of such effects.

478

Fourth, good accuracy would entail that a material's characteristic damage parameters as per Table 7.6 be assigned individually upon each layer, rather than taken as a common factor. This too requires a lot more research and experimentation. Although this assumption bears little influence on static burst pressure, it may alter the sequence of damage events leading to failure, and shift a design's proof pressure point. This might then translate into long term cyclic endurance problems if matrix damage exists where none was predicted.

Fifth, failure criteria have long been and will remain contentious issues. Although the one employed in this work has been carefully selected among competitive variants it should not be viewed as the final word on such an unsure topic.

These are not the only shortcomings to vessel design. Much must still be learned in regard to why the manufacturing favors hoop windings strength-wise, to what level and under what conditions. Is the effect sensitive to the material used and can it be predicted analytically? This should in turn be factored into the strength parameters employed in the software. Further, the stress analysis done is purely on the design of a cylindrical cross-section without widening to encompass what happens over the end-domes. Here there exist difficult manufacturing and design challenges to prevent void formation and stress concentrations, especially for thick cylinders. At this point finite element analysis might be brought into the picture to help optimize a design. Doubtless we can find many other topics that need further study. Such considerations will be deferred to Section 9.4.

9.2 Some Comparisons to Experiment

The focus is to gain an understanding on the origins of stress distributions and the building of an analytical tool to model them. Nevertheless limited experimental data is available both from the Bendix Avelex project and from the work of other researchers. This enables one to verify some predictions. Three different data sets comprising a total of 15 thick-walled vessels with burst pressures ranging approximately 30,000 - 60,000 psi (207 - 413 MPa) are examined below.

The test vessel shown in Figures 9.2 - 9.4, overwound in the laboratory, was pressurized to measure strains. This was done both before and after overwinding with Kevlar 49®. The vessel was fitted with 14 strain gages, 8 of which located internal to the structure. Figure 9.7 outlines the basic configuration while the exact gage positions are given in Table 9.2. This vessel, based on a Structural Composite Industries (SCI) model Alt-295 fireman's breathing apparatus, was originally designed to operate at 4500 psi (31 MPa). Construction is S2-glass filament winding over a relatively thick 6061-T6 single piece spun aluminum liner, autofrettaged during proof testing / sizing to operate throughout its full compressive - tensile elastic range. Table 9.1 gives the lay-up sequence and thicknesses and Table 9.2 provides typical strain data at a few different loadings. After overwinding and testing the vessel was put into service, circa 1990, in a laboratory environment at up to ≅ 680 bar (10,000 psi) pressure and utilized as a pressure source in an experimental gaseous fuel injection system. It remained in service for the duration of the project (about 2 years). In 1998 the vessel was slit apart lengthwise for a post-mortem inspection. Figures 9.8 - 9.9 illustrate some additional detail.

The overwinding was done in two stages with an intermediate cure after hoop layer #11. An aluminum filled epoxy was used to fill gaps in the dome region prior to winding the second stage layers. Helical layer #10 was wound approximately 1 inch adjacent to the fill neck in order to prevent excessive thickness build-up in this region. Similarly spaced winding patterns were found in the glass layers at post-mortem.
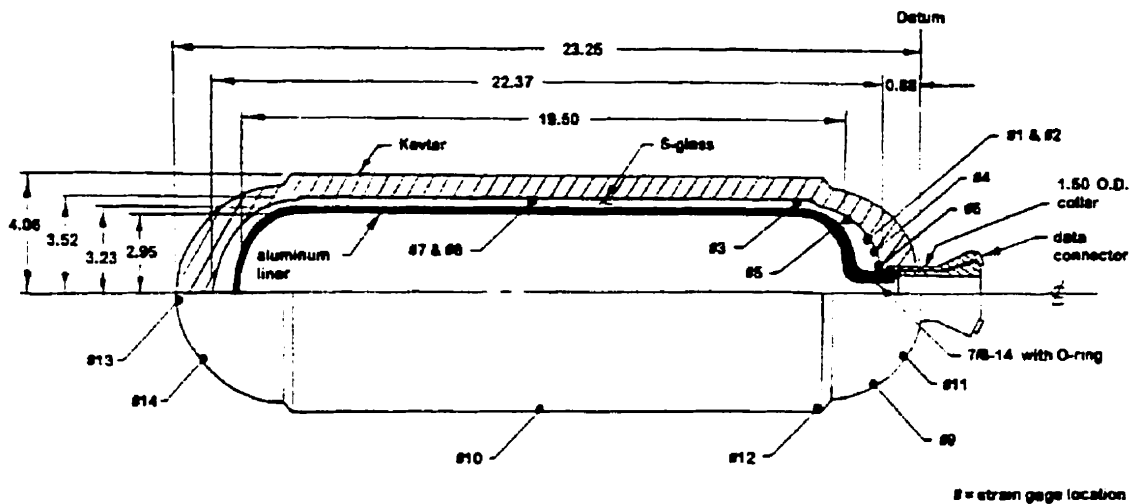
Figure 9.7 Construction detail and stain gage locations
for overwrapped SCI based test vessel.

Strains were measured both during pressurization and depressurization. The cryogenic liquid (nitrogen) cylinder filling technique causes tremendous temperature dips and also strong Joule-Thompson cooling effects via throttling during depressurization. The strain readings were only accurate after attainment of steady state conditions because the gages are temperature sensitive. About one dozen instrumented test cycles up to pressures of ≅ 845 bar (12,425 psi) were run. Only final conditions are listed in the tables.

Instrumentation drift and moisture condensation at the data connector with the vessel caused difficulties however a number of relatively successful runs were achieved using petroleum jelly at the connections to seal out moisture. The best data resulted on the depressurization runs since the cooling effects were much reduced and steady state usually achieved within one hour. Quarter bridge 120 Ω foil gages with a gage factor of approximately 2.0 were used. With 10 volt bridge excitation this translates to about 5×10^{-6} volts / $\mu\varepsilon$. The instrumentation drift, given the data recorder was left running 24 hours a day and laboratory temperature was steady, could be held to about 1 $\mu\varepsilon$ per minute. There appears to be some change in the final strain readings as a result of material relaxation but these levels are difficult to verify since they are on the order of the instrumentation drift.
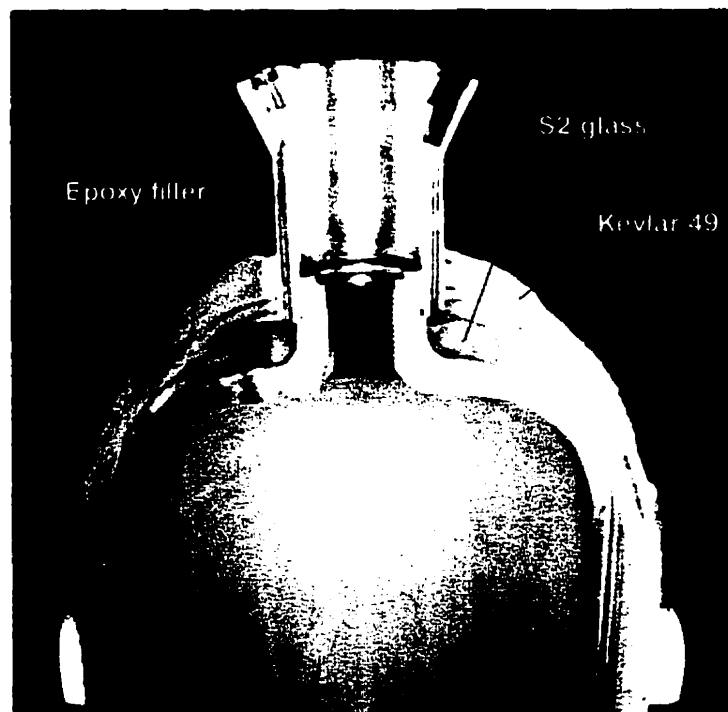
Figure 9.8 Vessel cross-section at fill neck. Glass, Kevlar 49®
and aluminum layers can be distinguished.

Transverse matrix cracking can be seen on a cut cross-section with the naked eye in the hoop layers and also on some portions of the helical layers near the cylinder bottom where the cryogenic fluid impacted. Long interlaminar cracks also exist in this region and are predominant at the interface between the two stages of overwind in the Kevlar 49®. Fiber wrinkling due to insufficient tension and resin rich pockets are prevalent in the outer bands of the dome region, especially near the cylinder bottom. A ¼" diameter pin was inserted at the center of the vessel bottom during winding to prevent fiber bands from sliding off the end. This was removed after the first step of the overwind was cured and filled in with epoxy. During the second step of the overwind an externally held locating pin was used, retracted shortly after winding while the resin was wet, allowing the bands to shift slightly and fill the gap. The same approach appears to have been taken by SCI except that they employed a larger pin (½") and neglected to fill the resulting void. The epoxy filler, voids and some dry spots, are identified in Figures 9.8 and 9.9. Due to the initial winding tension, especially in the hoop layers, resin flowed outwards from the inner layers in the subsequent curing (while rotating). The viscosity became very low while heating under infrared lamps. The majority of this flow dripped off the vessel leaving a high fiber volume fraction but the net effect of the tension appears also to cause an increase in fiber wrinkling on inner layers, probably working to a detriment overall.

Figure 9.9 Test vessel after being slit apart on milling machine. Aluminum liner has been removed. Dry spots and voids can be seen near the vessel ends as indicated.

For analysis an isotropic material with twice the elastic strain range of 6061-T6 aluminum was used to model the innermost layer (liner). Since the vessel as received from the manufacturer was already autofrettaged, and the design objectives were to stay within the compressive - tensile elastic limits of the liner, elastic behavior modeling is expected to be sufficient up until liner yielding. The modeling will deviate from reality beyond the liner yield point whereupon a nearly constant pressure differential will be seen across the liner and further pressure increases will be transferred to and absorbed solely by the composite.

It must be realized that the S2-glass overwind was already substantially stressed when the strain gages were installed due to the autofrettage process, however this only serves to offset the zero point yet not the fundamental linearity of the system.

484

Models of the vessel as received from SCI, (file *sci.ves*), and with the Kevlar 49[®]

overwind *(sci_gr.ves)* were run to compare program predictions with experiment. The

material properties were not tested, however the values used for both S2-glass and Kevlar

49[®] are based on a publication originating from SCI [65]. These material property files

and the laminate properties they are based on, *s2_sci.lam* and *kev_sci.lam* respectively, are

included on the diskette.
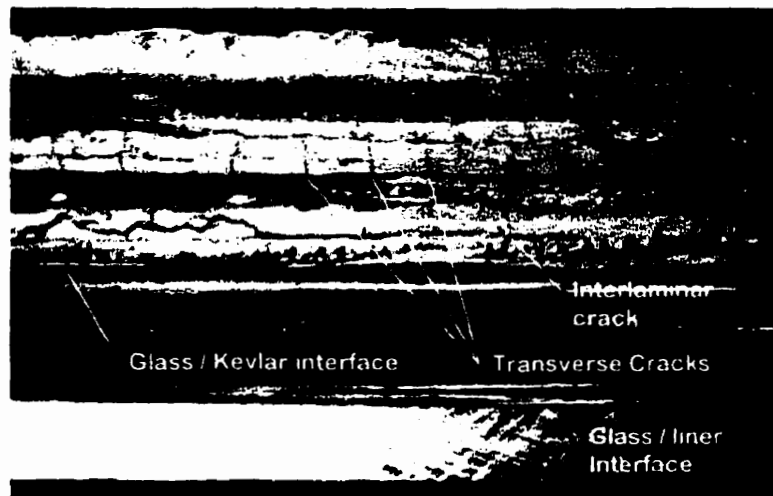
Figure 9.10   Matrix cracking on lower portion of the vessel.
The area worst affected is shown.

Table 9.3 reviews the program predictions in comparison with data gathered from

the vessel. The consistency of the strain gage data is poor and differences of 300 $\mu\varepsilon$

between ascending and descending runs are not uncommon. Often because of

condensation problems and the time periods involved for thermal stability the

discrepancies are much higher. Additionally there were audible cracking sounds,

presumably associated with layer movement and internal redistributions that may have involved some connector vibration in the process. The individual factors were not measurable. For the internal gages, the end-junction location gave a higher strain reading as expected, but for the surface location only the mid-cylinder position (gage #10) gave readings in line with predictions. After cutting the vessel apart it became clear that the end-junction position chosen (gage #12) was past the end of the hoop windings on the inner layers so the data acquired could not be held representative. Strain along the cylinder axis (gage # 7) was not adequately measured since the gage soon broke. Numerous evenly spaced circumferential matrix cracks are visible both in cross-section and on the vessel surface. Figure 9.10 shows this under low power magnification. Gage #7 evidently fell victim to such. The average crack spacing ranges from less than 0.1″ near the bottom to 0.4″ close to the top of the vessel. Because of the peculiar crack spacing it is believed the effect originates from cooling to cryogenic temperatures, the thermal contractions being most pronounced where the cold liquid impinges and vaporizes.

Although the data available is not too consistent and the material values were assumed, program predictions for strains both with the original and overwrapped vessel are within about 10-20% if one discounts a few of the more obviously erroneous strain readings typified by large shifts between the ascending and descending pressurization runs. Data from depressurization runs is graphed in Figure 9.11 while Figure 9.12 shows the anticipated stress distribution as computed from "Super Pressure - Vessel Designer". The Kevlar 49® overwrap sees a higher maximum stress level then the S2-glass and is closer to failure. The strength contribution of the helical layers appears under-utilized. At the

maximum pressures reached under testing, matrix damage initiation was predicted to just have begun occurring. The computed damage onset is @ 83.4 MPa while maximum test conditions were 85.7 MPa. Little if any damage can be ascertained visually on the glass lay-up except for some local whitening adjacent to the fill neck and possibly a few spots in the dome region. The same is true of the Kevlar 49® except for what appear to be cracks of thermal origin. Evidently the resin system used, Ciba Geigy LY556 / HY917 / DY70, became too brittle under cryogenic conditions. The manufacturer claims 4-7% elongation at RT. It should be noted that low temperature curing / high strain resins have found some preference by others. The resin system used did not exhibit the necessary characteristics, whereas the SCI resin is a proprietary formulation and appeared to suffer less from the thermal excursions. Kevlar 49® is a particularly difficult material to achieve good bonding with, transverse tensile values have always been only a fraction (perhaps 1/3) of glass. The Ciba Geigy resin properties were used in the analysis of the glass layers for lack of further information.

Table 9.1 Lamination sequence and layer thicknesses for test vessel

Layer #	Material	± Angle (°)	Thickness (in.)
1	Aluminum 6061-T6	isotropic	0.183
2	S-glass	12	0.063
3	S-glass	90	0.085
4	S-glass	16	0.063
5	S-glass	90	0.056
6	S-glass	12	0.031
7	S-glass	90	0.023
8	Kevlar 49	22	0.069
9	Kevlar 49	90	0.068
10	Kevlar 49	22	0.075
11	Kevlar 49	90	0.075
12	Kevlar 49	25	0.135
13	Kevlar 49	90	0.085

Table 9.2 Gage positions and typical strain readings after depressurization

Gage #	Orientation	Axial Position (in.)	Radial position (in.)	Strain @ 4,879 psi* (µε)	Strain @ 9000 psi* (µε)	Strain @ 12,429 psi* (µε)
At interface between S-glass and Kevlar (between layers #7 & #8)						
1	fiber dir.	2.03	2.91	- 345	- 1560	- 2019
2	transverse	2.03	2.91	+ 117	- 804	- 780
3	fiber dir.	4.13	3.69	- 548	- 2797	- 5755
4	fiber dir.	1.61	2.44	- 624	- 1962	- 2307
5	fiber dir.	2.68	3.41	- 265	- 1570	- 2103
6	fiber dir.	0.96	1.41	- 1002	- 2697	- 3860
7	transverse	11.76	3.56	propagated**	propagated**	propagated**
8	fiber dir.	11.76	3.56	+ 197	- 2305	- 4428
On vessel outer surface (layer #13)						
9	fiber dir.	2.00	3.31	+ 476	- 256	- 859
10	fiber dir.	11.59	4.24	- 541	- 2660	- 5236
11	fiber dir.	1.00	2.50	+ 325	- 529	- 1135
12	fiber dir.	3.62	4.12	+ 100	- 1564	- 3031
13	fiber dir.	23.19	0.00	- 1011	- 2560	- 2895
14	fiber dir.	22.31	2.00	- 689	propagated	- 3025

* delta pressure, depressurization
** gage went open circuit

Table 9.3 Measured strain in test vessel during different pressure cycles and predictions

Pressure change up & down (psi)	Interface @ end-junction hoop strain gage # 3 (µε)	Interface Predicted hoop strain SP-VD (µε)	Interface @ mid-cylinder hoop strain gage # 8 (µε)	Interface @ mid-cylinder axial strain gage # 7 (µε)	Interface Predicted axial strain SP-VD (µε)	Outerlayer @ end-junction hoop strain gage # 12 (µε)	Outerlayer Predicted hoop strain SP-VD (µε)	Outerlayer @ mid-cylinder hoop strain gage # 10 (µε)
Kevlar 49° Overwound Vessel								
- 4152	- 1319	- 1700	- 1233	- 806	- 550	- 989	- 1280	- 1677
- 6908	- 1703	- 2820	- 1147	- 524	- 920	- 936	- 2130	- 1737
- 9000	- 2797	- 3690	- 2305	propagated	- 1200	- 1564	- 2780	- 2660
+ 6912	- 1606	- 2820	- 1167	- 494	- 920	+ 990	+ 2130	- 1838
- 6912	- 2150	- 2820	- 1183	- 465	- 920	- 940	- 2130	- 1720
+ 6014	- 1757	- 2470	- 846	propagated	- 800	+ 679	- 1860	- 1685
- 6005	- 1749	- 2470	- 1088	propagated	- 800	- 657	- 1860	- 1485
+ 12415	- 4874	- 5090	- 4736	propagated	- 1660	+ 3159	- 3840	- 7606
- 12425	- 5756	- 5090	- 4428	propagated	- 1660	- 3033	- 3840	- 5236
Original SCI Vessel								
- 4500**	N/R***	- 3090	- 2719	N/R	- 1080			
- 7500**	- 4756	- 5150	- 4400	- 1739	- 1800			
- 7500**	N/R	- 5150	- 4356	N/R	- 1800			

* strain gage went open circuit
** pressures recorded with mechanical gage
*** not recorded

488
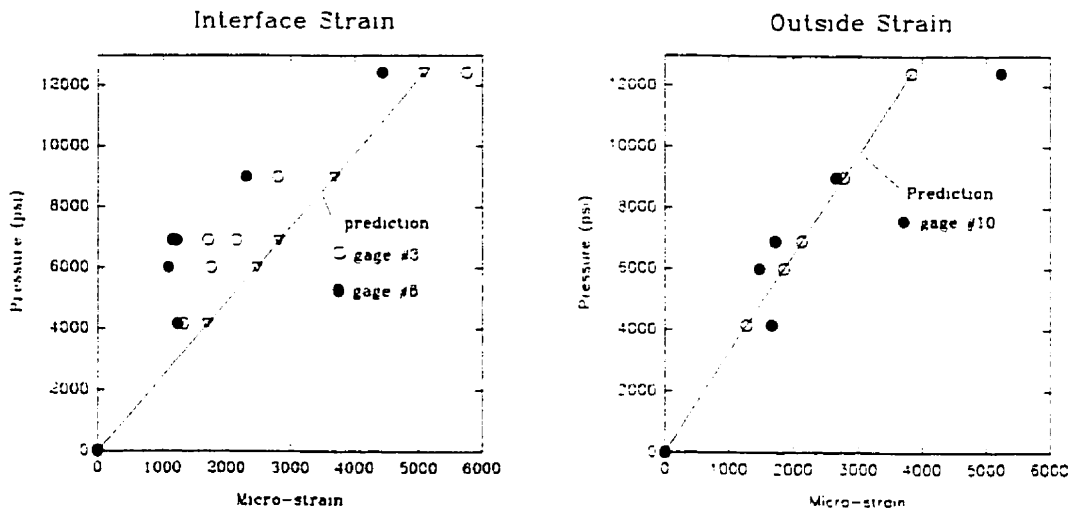
Figure 9.11 Measured strains vs. predictions for depressurization runs.

The 6061-T6 metal liner is expected to remain within its elastic range (± 40 ksi).

(Note: UTS ≅ 45 ksi. @ 17% elongation). Assuming that the autofrettage process

succeeds at establishing a compressive liner stress close to the compressive yield point, the

design proof pressure point would then be set at or near the tensile yield, which would put

the operating pressure point of the aluminum as low as possible in the tensile region

(under normal operation) and thereby establish maximum fatigue life for the liner. The

exterior hoop strain for the overwound vessel at 12,425 psi (85.7 MPa) was seen to

correspond very closely with the strain of the original glass vessel at proof pressure which

is 5/3 x 4500 = 7500 psi (51.7 MPa). This strain value is approximately 0.44%. We also

know that the sizing operation (autofrettage) takes place at 105% - 115% of proof

pressure (yielding the liner) so it would be expected that the liner remains elastic, but just

barely so, on subsequent cycles to proof pressure strain. The program predicts a liner

tensile stress of +39.9 ksi based on a -40 ksi unloaded compressive maximum stress

resulting from autofrettage, quite with expectations. Since the program invokes the Von-

Mises criteria for metal's yielding (whenever a material is identified as being metallic in the

.mat file input, Figure 8.5) the limit elastic behavior is then predicted to be at a liner hoop

stress of ≅ 617 MPa. This represents a total elastic range of ± 44.7 ksi. (± 308 MPa) for

the hoop stress in the liner.
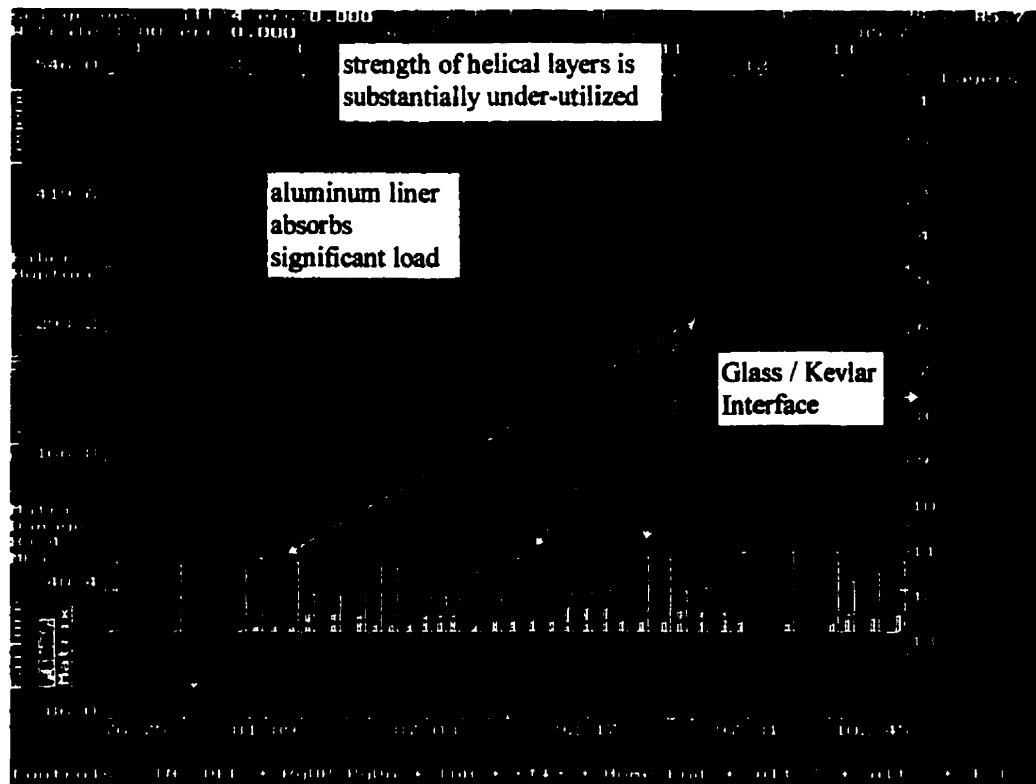
Figure 9.12 Predicted stress distribution in test vessel at 12,425 psi. (85.7 MPa).

Grover and Ayler [45] reported on a series of cylindrical test vessels on behalf of Brunswick Corporation who were under contract from the US Navy in an exploratory study assessing the feasibility of using compressed helium to actuate pneumatic systems aboard air launched tactical missiles. This work was done circa 1980-81. The design goal was to operate at 25,000 psi (172 MPa) and attain a 50,000 psi (345 MPa) burst pressure.

Nineteen vessels were constructed. The first three did not use a stepped boss construction for the liner and failure initiated within the liner, these test results were not published. Materials used were S-2 glass, Kevlar 49® and carbon fiber of undisclosed origin. Judging from the properties listed in their publication, the carbon fiber was likely AS/3501 or similar. The vessels were approximately 3″ inside diameter and filament wound upon a 0.050″ 6061-T6 aluminum liner. This liner was constructed from two impact extrusions which were machined and welded together at the cylinder mid-section. Contributions from the liner appear to have been neglected in the stress analysis performed.

The last 5 vessels in the series had 24 layers to intersperse the plies finely, the final 3 vessels of which employed carbon fiber at and near the outer surface. One of these met the design goal and the others came close, but at the cost of a very thick wall with $(b/a) \cong$ 1.75. The remaining vessels had relative wall thicknesses ranging from 1.35 - 1.62 and employed fewer layers, exhibiting burst pressures between 33,000 - 40,000 psi. None of these employed carbon fiber. Only this later set of results is analyzed below.

After re-creating their designs using "Super Pressure - Vessel Designer" it becomes evident that these vessels exhibit a quite inefficient distribution of the stresses

through the wall with some layers carrying a very high load and others relatively little. The authors used a maximum fiber strain criterion and present figures that plot strain within each layer as a function of the thickness at pressures near the ultimate burst. Their computations are based on a layered plane stress analysis in conjunction with applying Newton's iteration method to solve for the axial strain. In essence the solution should be identical to the (Partial eqns) option explained in Chapter 8, provided all material inputs are identical.

The interesting detail about these experiments is that the figures in the paper also give the actual fiber strain at burst recorded by strain gages placed at each vessel's outer surface. These strains, along with the experimental burst pressures can be compared to predictions. Unfortunately all strain values, along with Grover and Ayler's predictions of fiber limit strains have to be scaled off their figures as no tabular data is provided. Also the layer thicknesses have to be obtained in the same fashion, however the winding angles and their lay-up sequence are given clearly. Some data for the laminate properties are tabulated at the winding angles of concern and one must presume these are the outcome of classical lamination theory. As such, the unidirectional material data of Grover and Alyer was decomposed using the micromechanics features in "Super Pressure-Vessel Designer" and the files (brunswick) *br_s2_gl.lam* and *br_kv_49.lam* were generated. Any missing data for moduli and strength was transferred from the *S-glass.lam* and *Kev_49.lam* files of the micromechanics database shown in Table 8.1. No resin properties were given, so a moderate value (3.6 GPa) was chosen to remain on the conservative side. A volume fraction of 65% was assumed and fiber failure stresses were taken on the basis of the

maximum strain allowables scaled off their figures. Grover and Ayler used slightly higher

allowable fiber strains for the Kevlar 49® hoop windings as opposed to the helical. Since it

is evident from their analysis that the limiting pressure is attributable to the Kevlar 49®

hoop windings, strength data for Kevlar 49® was based on this ultimate strain. A more

refined analysis could have used a separate material with a different strength to

differentiate between helical and hoop layers. It is not too clear whether this enhanced

strength effect is real or basically the outcome of the natural denser fiber compaction that

occurs with hoop windings, (i.e.: higher fiber volume fraction). There evidently appears to

be some intrinsic loss associated with crossed helical lay-ups but this level is

indeterminate.

On the whole, the *.mat* files generated from these inputs were not very different

from *S-glass.mat* and *Kev_49.mat* of the regular database except that the strengths,

Poisson's ratios and principle moduli were matched exactly with Grover and Ayler's

inputs. The vessel files generated are *SN006.ves, SN008.ves, SN009.ves, SN011.ves,*

matching the designations used in [45] and are on the included diskette.

Table 9.4 presents construction details and Table 9.5 some comparative

predictions from Grover and Ayler, "Super Pressure - Vessel Designer" and the

experimental values.

The predicted burst and surface strains for Grover and Ayler's results were

carefully scaled off the figures in their report [45]. Clearly these authors had the advantage

of knowing more precisely the properties of the materials used, nevertheless their

predictions for both surface strain and burst pressures appear less accurate than "Super Pressure -Vessel Designer" output.

Table 9.4 Glass / Kevlar 49[®] vessels in Grover and Ayler experiments [45].

Design serial no.	Lay-up, layers (#) sequence (°)	Total wall thickness (in.)	Relative thickness (b/a)
004, 005, 006	5 glass @ 37 2 glass @ 90 5 Kevlar @ 25 2 glass @ 90 3 Kevlar @ 17 23 Kevlar @ 90	0.54	1.37
007, 008	5 glass @ 37 5 Kevlar @ 25 3 Kevlar @ 17 32 Kevlar @ 90	0.61	1.41
009	5 glass @ 37 8 Kevlar @ 25 2 Kevlar @ 90 4 Kevlar @ 17 38 Kevlar @ 90	0.76	1.51
010, 011	8 glass @ 37 2 glass @ 90 9 Kevlar @ 25 2 glass @ 90 4 Kevlar @ 17 40 Kevlar @ 90	0.94	1.63

Table 9.5 Burst pressure and surface strain predictions compared to experiment.

Design serial no.	Predicted burst (ksi) G&A[*]	Predicted burst (ksi) SP-VD[**]	Exp. failure (ksi)	Surface strain (%) G & A[*]	Surface strain (%) SP-VD[**]	Exp. surface strain (%)
004	41.7	36.5	32.8	1.42	1.21	1.18
005	41.7	36.5	32.9	1.42	1.21	1.18
006	41.7	36.5	33.5	1.42	1.21	1.18
007	43.6	37.0	38.8	1.23	0.95	1.09
008	43.6	37.0	34.4	1.23	0.95	1.09
009	45.5	35.7 / 40.2	40.8	0.97	0.87	0.62
010	60.9	47.7 / 49.0	38.3	1.05	0.77	0.83
011	60.9	47.7 / 49.0	39.8	1.05	0.77	0.83

[*] Grover and Ayler [45]
[**] Super Pressure - Vessel Designer

Additionally predictions of damage onset with the current program ranged from a low of 5,903 psi (SN/006) to a high of 6,918 psi (SN/011) using the non-linear shear option. Discussion of damage is omitted in [45]. The vessel designs designated SN/009, SN/010 & SN/011 were predicted by "Super Pressure -Vessel Designer" to have a non-catastrophic failure of the inner hoop layer at 35.7 and 47.7 ksi respectively. This may in part explain the relatively low experimental burst pressures seen, especially if the maximum strain predictions used in SN/010 & SN/011 for the glass fiber were to be in slight error. The remaining designs were all predicted to initiate failure in the Kevlar 49[®] on the inner surface of the outermost hoop wrap.

Mid-cylinder hoop surface strains were published for 3 of the finely interspersed ply designs using carbon fiber as mentioned earlier. With these, either two gages were separated 180° or three gages at 120°. The notable feature was that the strains differed significantly, ranging as high as 40% difference, more typically 12 - 25%. The authors indicated that low average surface strains and large strain differences indicated possibly defective constructions and were able to provide partial verification with X-rays on at least one such suspect vessel. It is not clear from the report if the surface strains given in Table 9.6 originated from a single gage or if they were averaged from a greater number. A similar large variance in measured surface strains is seen in T. R. Guess's spherical vessels where 8 gages per unit were used to record data. In light of this evidence, the difficulties in obtaining reliable strain readings off the SCI based test vessel could be expected.

Considering the variables involved, it is reassuring that "Super Pressure -Vessel

Designer" on an initial attempt averages within 10% of actual burst pressures and 15% of

surface strains in the set of 8 vessels examined above. Figure 9.13 gives an example of the

computed stress distributions within one of these vessels.
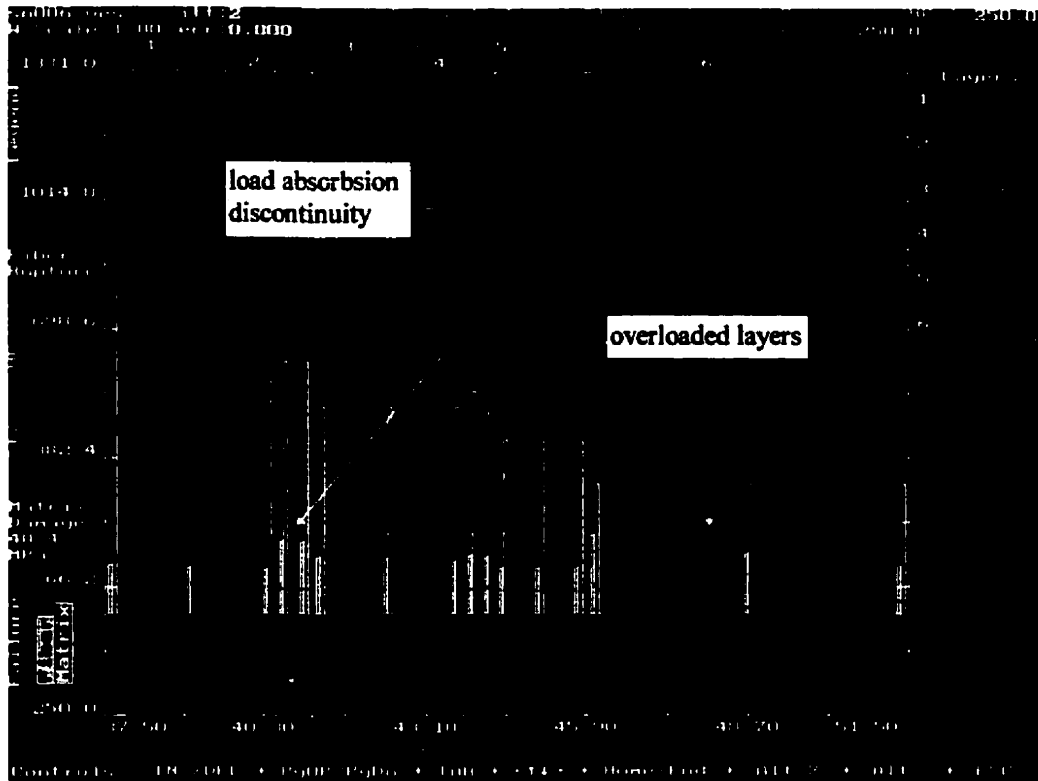
Figure 9.13   Stress distribution in SN/006 vessel of Grover and Ayler.

F.P Gerstle and M. Moss [15] and T.R. Guess [16] were among a group of

researchers operating either out of Sandia National Laboratories (New Mexico). A second

group working in association with Brunswick Corporation (Nebraska) also spent

numerous years developing ultra-high pressure composite vessels. Both these groups

496

concentrated on development work centered around the building of small spheres of approximately 4″ inside diameter, wound on computer controlled spherical winding machines specially built for that purpose. The winding patterns employed were both uniaxial multiangular (polar) and the patented delta axi-symmetric arrangement, which showed some advantages. Details of the theoretical / analytical methods used in the design of these vessels is presented in by F.P. Gerstle [108], T.R. Guess [18], C.E. Knight [126], R.F. Foral [127], R.L. Grover [17]. After more than a decade of effort, Guess [16][18] eventually succeeded in building what are possibly the highest pressure composite vessels ever designed and tested. The record burst pressure attained is 62,500 psi (430 MPa). Within this program there was also an effort to surpass the earlier work of Grover and Ayler at Brunswick [45] who built 50,000 psi (345 MPa) cylindrical vessels which were rather structurally inefficient.

Guess and co-workers developed a method of generating liners by electroforming. A thin aluminum mandrel was used into which a stainless steel fill stem was flush fitted and the assembly slowly rotated while being copper plated to a thickness of 1 mm. Afterwards the aluminum mandrel was etched out with a sodium hydroxide solution leaving a thin copper liner with a metallugically bonded stainless steel fill stem. Finite element analysis was done to perfect the geometry of the fill stem and minimize stress concentrations to very low values.

This same method was later used to form liners for very small cylindrical vessels of 2″ inside diameter by 6.5″ length. The cylindrical liner dome geometry, fill stem and the wind lay-up for these was designed by Hercules Incorporated using finite element analysis.

497

The vessels consisted of a single material (Kevlar 49®) but with many different ± angular layers. Six vessels were constructed, three each with relative thickness ratios (a/b) of 1.35 and 1.51 respectively. The lay-up sequences were identical except that layer thicknesses were scaled up for the later 3 vessels. Vessel construction detail is presented in Figure 9.14. Other parameters are given in Table 9.6 including the burst predictions from the finite element analysis, "Super Pressure - Vessel Designer" and the experiments.
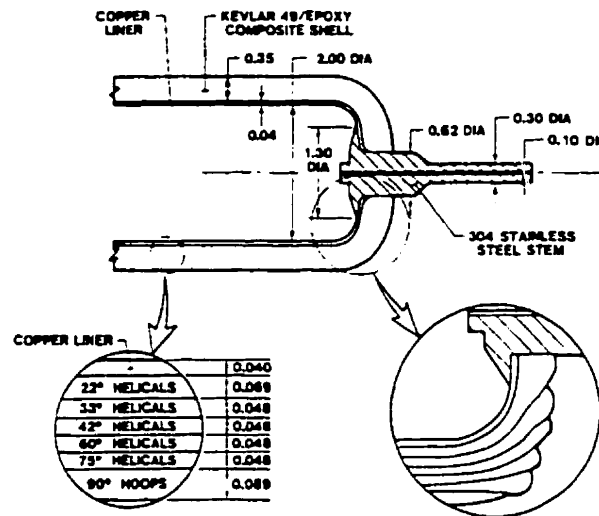
Figure 9.14 Schematic of one end of cylindrical Kevlar 49® / epoxy
pressure vessel. Other end of vessel is identical [16].

The input data for the Kevlar 49® properties used for the finite element analysis was not given however a good idea of the elastic properties being assumed for spherical vessels by the same group of authors can be found in some of their other publications. Gerstle [108] used a matrix stiffness of 450 ksi (3.10 GPa), Grover and Foral [17] indicate 473-478 ksi (3.28 GPa). Estimates for Kevlar 49® strength vary widely. Knight who

Table 9.6 Summary of vessel test data and predictions. Adapted from [16].

Vessel no.	1	2	3	4	5	6
Number of layers at winding angle (±°)	(b/a)=1.35			(b/a)=1.51		
22	7	7	7	10	10	10
33	5	5	5	7	7	7
42	5	5	5	7	7	7
60	5	5	5	7	7	7
75	5	5	5	7	7	7
90	9	9	9	13	13	13
Composite thick. (in)	0.348	0.350	0.355	0.512	0.510	0.517
Fiber volume (%)	77.2	77.7	74.0	74.9	74.6	75.6
Burst Pressure (ksi)						
FEM prediction	50.0	50.0	50.0	55.0	55.0	55.0
SP-VD prediction	47.1	47.1	47.1	59.0	59.0	59.0
Experimental	50.3	48.1	35.0 (leak)	57.0	58.1	56.5

employed statistical failure methods [126] indicates 265 ksi can be expected from a wound

ring test specimen while strand tests would mislead one to believe 370 ksi were possible.

The team at Hercules used a 225 ksi maximum fiber stress criterion to assess failure.

Maximum stress theory is known to be less conservative than maximum strain theory since

the strain calculation includes a radial stress contribution [15][108]. The exact fiber

volume fractions associated with these stress levels is not mentioned explicitly but

averages 65-67% if one examines the data put forth for small spherical Kevlar 49® vessels

by Gerstle and Moss [15] or the test results of Guess [18].

Drawing from the above, inputs chosen for the micromechanics segment of

"Super Pressure - Vessel Designer" code were a tensile strength of 250 ksi (1724 MPa) @

65% fiber volume fraction and a matrix stiffness of 3.1 GPa. These inputs were used in an

effort to closely match the available data. The balance of properties were mainly the

default quantities as presented in Table 7.1 for the generic Kev_49 material. This material

file named *San_Kev.lam* is the one called within *Sand_50k.ves* and *Sand_55k.ves* (on diskette) which define the two constructions given in Table 9.6. Liner contributions are again neglected since the copper layer is very thin and yields at only 25 ksi. Within each group the predictions shown are based on the average fiber volume fraction and the average vessel wall thickness.

One can see that the analytical predictions of "Super Pressure - Vessel Designer" (SP-VD) come very close to both the experimental data and FEM calculations. The high efficiency of these vessel designs is evident in the near uniform fiber failure safety factors seen throughout the wall. These are visible in Figure 9.15 (fiber safety factor "thermometers") and evidenced further by the low (*b/a*) ratio for the given pressure. The results should be contrasted with the efforts of Grover and Ayler shown in Figure 9.13. Evidently the FEM analysis lead the designers at Hercules close to an optimized ascending angular pattern as presented in Chapter 8.

In summary, the tests examined should lend some confidence to the predictions being put forth by the analysis technique devised for thick walled vessel constructions. Certainly there is still much to be learned, particularly in the area of damage development, quantification and modeling of these effects. However static burst predictions and expected strain levels appear to be in line with experimental values. On that basis at least, a considerable step has been taken towards making analytical predictions that will allow the modeling and design of more optimal stress distibutions within a thick composite cylinder.
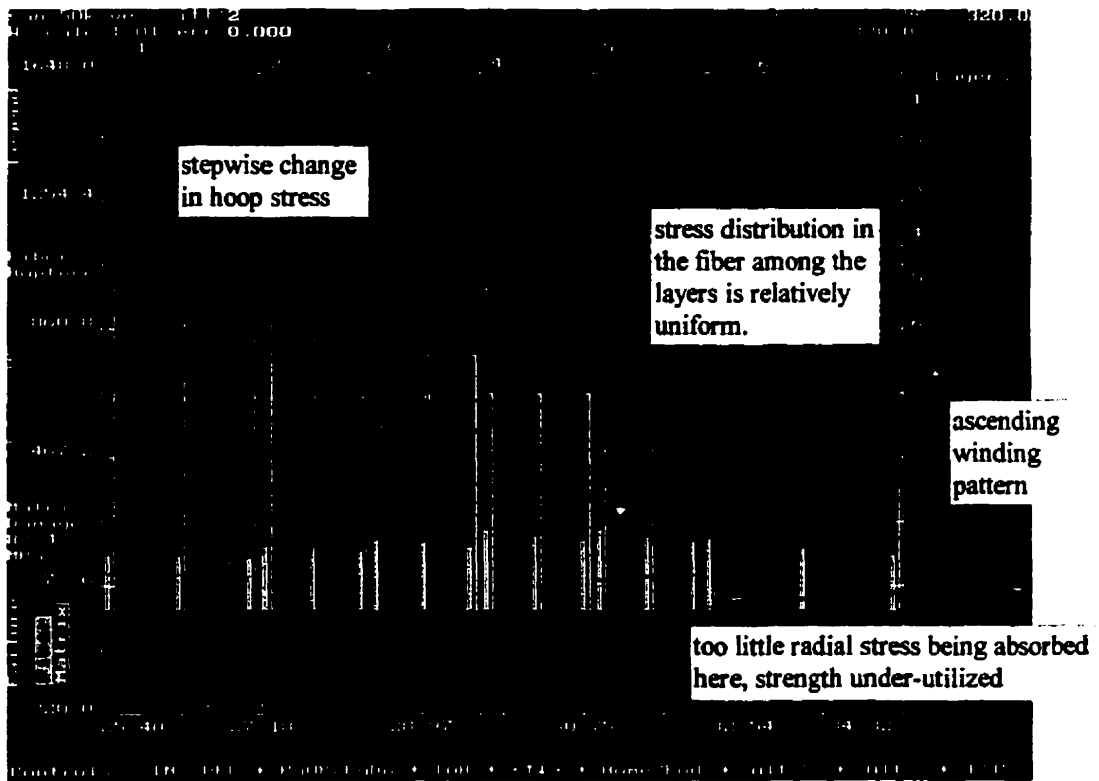
Figure 9.15 Relatively uniform fiber failure level in Sandia Labs /
Hercules Inc. FEM vessel design.

9.3 Contributions to Knowledge

Apart from the self-criticism of Section 9.1 it is also important to point out the

achievements and contributions of the present work and how they push the envelope of

understanding in analysis and design.

1) The elasticity equations are derived in their complete form in Chapter 5. Solution is

presented without resorting to arbitrary elimination of integration constants. This goes

beyond the reknowned work of Roy and Tsai [91] and others, who made mathematically

incorrect assumptions by setting integration constant C_2 in (4.23) to zero. These authors

ended up using a mixture of the plane strain formulations ($\varepsilon_z = 0$) for the stresses σ_r and

σ_θ and then superposing an axial strain ε_z without taking into account how this

superposed axial strain alters the σ_r and σ_θ stress distribution due to Poisson interactions.

The apparent effect of this simplification was seen to be of low significance ($\cong 1\%$) for

lay-ups in pressure vessels, not possibly greater than 10% as inferred by Witherell [74]

who focused on the construction of cannon barrels.

2) The basis for the derivations in Chapter 5 are from Lekhnitskii [88] (originating in part

from St-Venant {1865}, Voigt {1886}, Mitinskii {1936}), who set up the generalized

plane strain problem for one layer but only solved the special circumstances of pure plane-

strain, plane stress, axial force and twisting, each in isolation. These derivations were

extended (Section 5.3 onwards) by including variable elastic properties and working out a

simultaneous solution set for the generalized plane strain problem incorporating both axial

displacement and individual layer twisting effects. A practical subset of this variable

property form accounting for axial extension was then further generalized to

accommodate individual elastic moduli variation rates and solved numerically in Chapter

6. Lekhnitskii [88] (based in part on Plotnikov {1959}, Soós {1963} and Bert {1963})

also presented variable property solutions, but for the pure plane strain case while using a

common variation rate for all elastic properties. Verijenko et al. [166] solved the above

simplified equations for multilayer constructions and made use of the elastic properties of

common composites. However it was shown in Chapter 7, with the help of

micromechanics and details uncovered from studies of a fiber's internal structure, that

such common elastic property variation rates are not admissible for fiber based

composites. The results of Chapter 8 (Figures 8.16 - 8.17 vs. 8.19 - 8.20) indicate that solutions derived under either of these idealizations (plane strain & common elastic property variation rates) are not representative of the stress distributions corresponding to individual elastic property variation rates that approximate real materials (as in Figure 8.22) when the latter are arranged in a graded fashion. The requirement for using the full equations with individual elastic property variation rates, as derived here within, has been established and shown to correspond closely to stress distributions based on discrete approximations thereof. Through these efforts it is now known that any lesser form of the elasticity equations are inadequate for the purpose of designing a specified stress distribution.

3) The present work establishes a clearer approach to solving the generalized plane strain elasticity equation set than used by Witherell [74] who carried out a cumbersome 3 step superposition procedure via computer to combine the plane strain, plane stress and axial force solutions presented by Lekhniskii [88]. The solution given by Hoa and Mannarino [92] where the equation set is solved numerically gives little insight upon what parameters combine to produce the twisting, axial displacement or principle stresses. In this work it is shown clearly how the twisting term arises (equation (5.24)) and detailed under which circumstances twisting and axial extension exists (Section 5.1). The resolution to this problem, involving the solution of simultaneous equations is given in closed form for the variable property form (5.68), and for constant properties (5.97). Neither solution is available elsewhere. The approach to solution is insightful because the differential equation

presented for the variable property form parallels the one later solved in Chapter 6

(equation 6.6) via finite differences for individual property variation rates. Experimenting

with real lay-ups modeled as a continuum leads to identifying the terms that have the most

significance in massaging the stress function to produce a suitable stress distribution. This

is key to designing a discrete lay-up with a more uniform absorption of the load through

its thickness. Understanding and quantifying the relative contribution of each elastic

constant's variation rate (Table 8.1) upon the resulting stress distribution covers new

ground.

4) The Chapter 4 multilayer solution is analogous in concept to the form presented by

Adali et al. [165], except that an equality of the radial displacement at layer interfaces was

used to extract the axial displacement constant rather than employing an equivalence in the

circumferential strain at the interface as in [165]. The utility of the resultant elasticity

equations in this work exceeds that of the aforementioned researchers since they are

embedded in a program that allows multiple materials, layer thicknesses, volume fractions

and winding angles. Rather than being limited to searching for optimal winding angles

given single thickness layers, all of identical material responding to simplistic failure

criteria, the present work reflects reality more closely by using a truly interactive design

tool that models both elastic and damage-range response until rupture. Such software has

not been available until now and is a valuable tool for the generation of further knowledge.

5) Variable elasticity goes beyond techniques employing search algorithms to sift through

the innumerable possibilities for discrete lay-ups as performed for instance by Amiouny

and Hoa [250] or Adali et al. [165]. Because the structure is modeled as continuum one is essentially dealing with a single differential equation shaped by variable parameters rather than a system of equations with innumerable discrete solutions. It has also been noted in Chapter 8 discussions that the stresses are *highly sensitive* to winding angle variations of as little as one degree. This important fact underlines the importance of carefully maintaining these angles during manufacture. By the same token, even relatively simple problems being solved by discrete methods can pose an impossibly large field to search since one should cover all winding angle combinations by small increments, not to mention layer thicknesses, material choice and fiber volume fraction. An incomplete search will result only in extracting local minima. Variable elasticity cannot answer to questions of strength (nor can any discrete elasticity approach do so directly) but it illuminates the elastic properties requisite to achieve a stress distribution. Two factors prescribe the stress distribution in an object: {1} Geometry, {2} Elastic property distribution. Prior to this work only factor {1} coupled with a constant factor {2} had been seriously explored. Understanding, quantifying and solving realistic approximations (numerically) for the influence of the second factor has been a key accomplishment and contribution.

6) Another contributions is having shown, by example, how to arrange winding angles in an ascending or descending sequence to maximize the burst pressures and strength usage efficiency in single material vessels via a minimization in stress discontinuities. In conjunction, having also pointed out that the most efficient thick-walled cylindrical vessels ever designed and built (T.R. Guess) also arrived at a similar pattern indirectly, exploiting the same principle, albeit these designs originated from FEM work. Additionally, on the

same subject, having demonstrated that that the 6 variable properties numerical solution accurately predicts the stress distribution resulting from such a lay-up and that the power functions employed effectively model the resulting variation of principle compliances. The importance of *not* interspersing layers with too high a circumferential stiffness lest they cause an abrupt gradient in the radial stress distribution and thereby isolate remaining layers from sufficient strain to fully utilize their strength has been demonstrated. Lastly, all things being equal, the advantage of using lower strength materials for all but the highest burst pressure requirements has been put into evidence since the pressure increments possible are linear with the material strength but the material cost is not.

7) The modeling of damage development via degradation factors and predicting the sequence of events leading to ultimate or last ply failure has been improved considerably over earlier efforts advanced by Tsai et al. [174][176]. A method of converting from degradation factors to stiffness matrix reductions in 3-D has been developed and shown to adhere to physical expectations (Section 7.5). In contrast to earlier efforts by Tsai et al., the degradation effect is modeled as a variable quantity dependent on the relative loading level above matrix crack initiation, rather than implemented as a step function. The fiber and matrix failure envelopes employed go beyond single quadratic interactive criteria and make good sense on both an intuitive and mathematical level. Luo-You Xu's damage modeling bridges the gap between these envelopes and the "equivalent loading" concept has been extended by applying the matrix safety factor as a measure of the loading state past damage initiation (Chapter 7, equation (7.34) & (7.88)). Further, closed-form micromechanics solutions to the CCA model are employed to get a self-consistent set of

elastic properties for materials in the database. With these factors incorporated into the software, vessels can be optimized for FPF, highest burst pressure or pre-assigned a particular stress distribution. Such an encompassing approach aimed at solving the composite pressure vessel problem has not been seen prior.

8) The analysis and modeling equations presented have been written into code and used to analyze stress distributions in actual vessels. For the cases examined the failure pressure and strain predictions appear to be in line with experimental results, in general predicting the outcome with equal or greater accuracy than the original investigation.

9) A derivation for computing fiber trajectory over geodesic dome enclosures presenting both the slip coefficient and change in fiber stresses over the vessel ends is not available widely and published work emanating from the aerospace industry presents only sketchy outlines [105]. To this end Chapter 3 was written to clarify details and in doing so reduces the need for numerical integrations and other computer stepwise methods commonly used to arrive at suitable fiber trajectories which will not slide over the face of the mandrel. The clarity of method and presentation is contributory to the dissemination of knowledge.

10) A literature survey covering over 260 journal and conference papers, contract reports, standards or book sections reflecting a broad range of issues are discussed throughout Chapters 2 and 7 and to a lesser extent in other sections. Those mentioned specifically are listed in the references; in total nearly 400 publications were consulted. Such an encompassing combination of history, current art, theory and computer methods on the design and analysis of thick walled composite pressure vessels is unique.

9.4 State of the Art, Considerations and Suggestions for Future Work

The methods employed for the design of today's most advanced pressure vessels slated for, or currently in, active service are being further developed, proven and evaluated. Much of this work is now carried out within the Composite Overwrapped Pressure Vessel Program (COPV) of the U.S. Airforce and Missile Systems Center. Wright Laboratories Space Wing, and NASA Headquarters. Methods used by the above organization centers about a pre-processor (COSAP) written in conjunction for use with either COSMOS® or ABACUS® finite element code. It has been utilized to design and analyze carbon fiber based vessels for space flight vehicles, predominantly in the 4,000 - 10,000 psi operating range. The knowledge gained from the current research programs is due to be published in an updated and revised version of Mil Handbook 1522 [60]. Some representative vessel sizes, weights, operating / burst pressures for the above class of aerospace, military and NGV applications are listed in Appendix (A) [257]. These represent today's state of the art composite vessels.

The *detail* design of composite pressure vessels is necessarily a topic for finite element methods since one must deal with geometry details and stress concentrations arising at the cylinder to head juncture and within the liner at transitional sections near the opening. Additionally, the complexity of continually changing fiber angles over the dome profile and the drop-off of plies in this region cannot be treated adequately by any other means. This is where efforts like COSAP and CODSTRAN show their greatest value. The current work with "Super Pressure - Vessel Designer" is not intended to replace finite

element efforts, but only to complement preliminary design by rapidly sifting through a myriad of possibilities in construction and help bring forth the main effects at play and narrow the field.

At various points limitations of the current analysis have already been mentioned with the aim of differentiating factors that are, and those that are not yet being taken into consideration. Basically these can be divided into three groups: {1} Those where the knowledge or mathematical models accounting for the effect in consideration are clear and available but have not yet been introduced into software. {2} Instances where the principle is well known but where further derivations are required to apply the concept in its fullest form. {3} Areas where knowledge is scant and major investigations are needed to uncover the governing parameters.

For the first group it essentially boils down to the expenditure of sufficient time and effort to write the necessary code. An important example of such is the elasto-plastic behavior of the liner. These effects are most important for thin-walled conventional pressure (< 5000 psi) vessels where the liner can be absorbing a significant load. The basic theory and source code can be found in NASA's original (1966) "Computer Program for the Analysis of Filament-Reinforced Metal-Shell Pressure Vessels" [180] or adapted from other researcher's efforts [15][127][128][251].

The second division covers aspects such as thermal and cure stress contractions and matters related to fiber tensioning / resin flow. Equations describing such effects have been developed by a different group of researchers and incorporated into computer models to aid in the manufacturing processes [131][249][252-255]. From a stress analysis point of

509

view, the thermal contraction effects are most significant and effort should be directed at developing a generalized plane strain solution to the problem and incorporating this into the current software. The most compelling reason to complete such an analysis is that these superposed stresses can shift the onset of matrix damage to a much lower level of applied stress. One important determination to be made is whether in the case of cryogenic filling the thermal stress and its distribution can by itself, or in combination with pressure load (a temperature function), cause damage affecting vessel performance. The long term effects of such cycling is an equally important question.

For this second division one can also include investigations as to the effectiveness of the failure criteria chosen and extension of such to a true 3-dimensional form. Moreover, the degradation modeling and parameters describing the shape of the normalized stiffness degradation curves needs far broader investigation. Pinning down the fitting parameters for ± ply groups in isolation and in conjunction with interspersed hoop windings for different materials constitutes a large undertaking, but necessary if we are to come up with more accurate modeling of the degradation process in filament wound structures. Alternately, if some easier to apply fully analytical models were to become available that could be applied to general laminates under combined loadings, then the code might be reformed to substitute this instead.

The third category covers aspects such as exploring the 3-dimensional elasticity exhibited during the through-thickness compaction of thick laminates in the absence of edge effects. Also this must be evaluated in the case where the matrix has already suffered prior damage due to transverse crack development. Little is yet known how laminates

"flow" under such circumstances and to what degree this can be avoided by judicious choice of materials and winding angle sequences. The importance of non-linear behavior in this area must not be underestimated. We have seen that the ratio of radial stiffness to the in plane stiffness is paramount to the stress distributions resulting throughout the wall. A good understanding of this effect and the associated "compaction wave" that likely progresses through the wall under such conditions is key to designing with confidence for containment pressures that exceed the uniaxial compressive failure strength of the matrix. Further investigations are definitely warranted.

References

[1] Wilson, B.A., "Filament Winding - Past, Present and Future", 34th International SAMPE Symposium, 1989, pp. 2429-2439.

[2] Siuta, T., "Final Report: Fiberglass Motor Case Study, Polaris Second Stage End Closure", AD-273964, also Walter Kidde and Company Inc. report # 3642-11, 1962.

[3] Leeds, M.A., "Study of the Use of Preimpregnated Roving With Numerically Controlled Winding Equipment", Rocketdyne report R-3647, California, July, 1962.

[4] Shibley, A.M., Peritt, H.L., "A Survey of Filament Winding: Materials, Design Criteria, Military Applications", Plastics Technical Evaluation Center, Picatinny Arsenal, NJ, 1962.

[5] Sanger, M.J., Mulho, R., Morris, E.E., "Stainless-Steel Lined Glass Filament Wound Tanks for Propellant Storage", Air Force Materials Laboratory, AFML TR-66-264, Also Aerojet General report no. 3243, Dec., 1966.

[6] Sanger, M.J., Molho, R., Howard, W.W., "Exploratory Evaluation of Filament Wound Composites for Tankage of Rocket Oxidizers and Fuels", Air Force Materials Laboratory AFML-TR-381, also Aerojet General Report no. 3078, Jan., 1966.

[7] Sanger, M.J., Reinhart, T.J., "Development of Filament Wound Tankage for Rocket Oxidizers and Fuels", 12th National SAMPE Symposium, section AS-7, 1967.

[8] Morris, E.E., "Glass-Fiber Reinforced Metallic Tanks for Cryogenic Service", 12th National SAMPE Symposium, section AS-4, 1967.

[9] Hoggat, J.T., Workman, L.J., "Liners for Non-metallic Tanks", NASA CR-54868 Final Report, The Boeing Company, Jan., 1966.

[10] Toth, J.M., Barber, J.R., "Structural Properties of Glass-Fiber Filament-Wound Cryogenic Pressure Vessels", Advances in Cryogenic Engineering, Vol. 10, 1965, pp. 134-145.

[11] Toth, J.M., "Barrier Films For Filament Wound Fiberglass Cryogenic Vessels", Advances in Cryogenic Engineering, Vol. 9, 1964, pp. 537-544.

[12] Pope, D.H., "Expulsion Bladders for Cryogenic Liquids", Advances in Cryogenic Engineering, Vol. 10, 1965, pp. 382-392.

[13] Caren, R.P., Coston, R.M., Holms, A.M.C., Dubus, F., "Low-Temperature Tensile, Thermal Contraction, and Gaseous Hydrogen Permeability Data on Hydrogen Vapor Barrier Materials", Advances in Cryogenic Engineering, Vol. 10, 1964, pp. 171-180.

[14] Moris, E.E., Haddock, R.C., "High Pressure, High Performance Filament-Wound Carbon/Epoxy Pressure Tanks With Seamless Aluminium Liners for Expendible Launch Vehicles and Spacecraft", 34th International SAMPE Symposium, 1989, pp. 1545-1555.

[15] Gerstle, F.P., Moss, M., "Thickwalled Spherical Composite Pressure Vessels", Composites in Pressure Vessels and Piping: The Energy Technology Conference, Houston, TX, ASME, Sept., 1977, pp. 69-87.

[16] Guess, T.R., "Thick-Wall Kevlar / Epoxy Presssure Vessels", 29th National SAMPE Symposium, April, 1984, pp. 1007-1021.

[17] Grover, R.L., Foral, R.F., Humphrey, W.D., "Development of Kevlar 49 / Epoxy Pressure Vessels for Ultra High Internal Pressures", 12th National SAMPE Technical Conference, Oct., 1980, pp. 870-881.

[18] Guess, T.R., "Spherical Kevlar 49/Epoxy Vessels with 430 MPa (62KSI) Burst Pressures", Composites Technology Review, Vol. 6, No. 2, 1984, pp. 10-18.

[19] Molho, R., Landes, R.E., "Development of Thick-Wall, Filament-Wound, High Pressure Containers", AD 839480, Air Force Materials Laboratory, Wright Patterson AFB, May, 1968.

[20] Brunswick Corporation, "White Paper, Pressure Vessels", Brunswick-Aarding Composites, The Netherlands, 1992.

[21] Gordon, R., "Composite Pressure Vessels for Gaseous Hydrogen Powered Vehicles", Hydrogen Energy Progress V, 1984, pp. 1225-1236.

[22] Richelieu, R., "SCI Receives Approval for New Carbon Fiber Composite Cylinder Technology", Press Release: www.taylor-wharton.com/12-19-96.htm, 1996.

513

[23] Morris, E.E., "Commercial Filament Wound Pressure Vessels for Military and Aerospace Applications", SAE Technical Paper 811093, 1981.

[24] Weaver, C.S., "Natural Gas Vehicles - A Review of the State of the Art", Gaseous Fuels: Technology, Performance and Emissions, SAE SP-798, (also SAE paper 892133), Sept., 1989, pp. 35-55.

[25] Lawlor, J., "Alternative Fuels Compared", Electric Car, Vol. 1, No. 1, 1994, pp. 64-69.

[26] Lynch, F.E., Egan, G.J., "Near Term Introduction of Clean Hydrogen Vehicles via H2-CH2 Blends", Fourth Canadian Hydrogen Workshop, Toronto, Nov., 1989.

[27] Yamaguchi, J., "NEBUS fuel-cell municipal transit bus", Automotive Engineering International, SAE, Society of Automotive Engineers, Vol. 106, No. 7, 1998, pp. 54-55.

[28] Swain, M.R., Swain, M.N., Adt, R.R., "Considerations in the Design of an Inexpensive Hydrogen-Fueled Engine", SAE paper 881630, Oct., 1988.

[29] Zahr, G.E., Cooper, J.L., "Performance of Aramid Fibers in Filament-Wound Pressure Vessels", Composites '86: Recent Advances in Japan and the United States, K. Kawata et al., Eds., CCM- III, Toyko, 1986, pp. 709-715.

[30] Takagishi, S.K., "Aerospace Technology in NGV Fuel Containers", 38th International SAMPE Symposium, May, 1993, pp. 2050-2054.

[31] Berrisford, R.S., "Advanced Composites in Compressed Gas Applications", 37th International SAMPE Symposium and Exhibition, March, 1992, pp. 34-40.

[32] ASME, "Mandatory Design Rules For Class II Vessels: Section 10; Fiber Reinforced Plastic Pressure Vessels", ASME Boiler and Pressure Vessel Code, July, 1989, pp. 41-75.

[33] USAF, "Standard General Requirements for Safe Design and Operation of Pressurized Missile and Space Systems", Military standard, MIL-STD-1522A (USAF), Nov., 1986.

[34] AGA, "Basic Requirements For Compressed Natural Gas Vehicle (NGV) Fuel Containers", American National Standard, ANSI/AGA NGV2-1992, 1992.

514

[35] DOT, "Transportation Exemption DOT-E-8162", US Department of Transportion. Research and Special Programs Administration, Washington, 1982.

[36] Woerner, R.C., "A Study of Liquid Cylinder Filling Techniques", Advances in Cryogenic Engineering, Vol. 11, 1966, pp. 237-242.

[37] Hoggatt, J.T., "Thin Metal-Lined PRD 49-III Composite Vessels", NASA CR-134555, Jan., 1974.

[38] Hamstad, M.A., Chiao, T.T., Patterson, R.G., "Fatigue Performance of Metal-lined Graphite Epoxy Pressure Vessels", Composites, Nov., 1975, pp. 249-253.

[39] Ecord, G.M., "Composite Pressure Vessels for the Space Shuttle Orbiter", Composites in Pressure Vessels and Piping: Proceedings of the Energy Technology Conference. Houston, Texas, ASME, 1977, pp. 129-140.

[40] Lark, R.F., "Recent Advances in Lightweight Filament-Wound Composite Pressure Vessel Technology", Composites in Pressure Vessels and Piping: The Energy Technology Conference, S.V. Kulkarni and C.H. Zweben, Eds., ASME PVP-PB-021, 1977, pp. 17-49.

[41] Seeley, F.B., Smith, J.O., "Advanced Mechanics of Materials". Second edition (1952), 5th printing, John Wiley & Sons, 1960, pp. 607-635.

[42] Eckold, G.C., "A Design Method for Filament Wound GRF Vessels and Pipework", Composites, Butterworth & Co. Ltd, Vol. 16, No. 1, 1985.

[43] Foral, R.F., "On the Performance of Spherical Composite Pressure Vessels", Developments in Mechanics, Proceedings of the 16th Midwestern Mechanics Conference, S.C. Sinha, P.G. Kirmser and C.L.D. Huang, Eds., Vol. 10, 1979, pp. 25-29.

[44] Gerstle, F.P., Kunz, S.C., "Prediction of Long-Term Failure in Kevlar-49 Composites", Long Term Behavior of Composites, T.K. O' Brian, Ed., ASTM STP 813, 1983, pp. 263-292.

[45] Grover, R.L., Ayler, S., "Development of Thickwalled Composite Pressure Vessels for Ultra High Internal Pressures", 22nd Structural Dynamics and Materials Conference, Atlanta, Georgia, 1981, pp. 341-348.

515

[46] Morris, E.E., Patterson, W.P., Landes, R.E., Gorden, R., "Composite Pressure Vessels for Aerospace and Commercial Applications", Composites in Pressure Vessels and Piping: The Energy Technology Conference, Houston, Texas, ASME, 1977, pp. 89-128.

[47] Tiller, D.B., Newhouse, N.L., Veys, R.B., "Design and Qualification of an All Composite Natural Gas Vehicle Fuel Cylinder", Brunswick Corporation, Lincoln, Nebraska, Product Bulletin No. NGV-001. Sept., 1991.

[48] Gleich, D., "Continuing Report on Kevlar-49 Overwrap Study, Composite Vessel Safety Program", 24th Joint Propulsion Conference, Boston, Ma., paper no. 88-2849, AIAA, July, 1988.

[49] Schmidt, W.W., "Design Assurance of a Leak Failure Mode for Composite Overwrapped Metal Tankage", Mechanical Failure Prevention Group; Proceedings of the 29th Meeting, National Bureau of Standards, R. Sheves and W.A. Willard, Eds., 1979, pp. 198-207.

[50] Chiao, T.T., Wells, J.E., Moore, R.L., Hamstad, M.A., "Stress-Rupture Behavior of Strands of an Organic Fiber / Epoxy Matrix", Composite Materials: Testing and Design, 3rd Conference, ASTM STP 546, March, 1974, pp. 209-224.

[51] Babel, H., Vickers, B., Thomas, D., "Sustained Load Behavior of Graphite Epoxy Metal-Lined Pressure Vessels for Long Life Space Applications", 25th Joint Propulsion Conference, Monterey, California, paper no. 89-2644, AIAA, July, 1989.

[52] Donnet, J.-B., Bansol, R.C., "Precursors for Carbon Fibers", International Fiber Science of Tech. Series: Carbon Fibers, Vol. 3, 1984, pp. 2-7.

[53] Thiokol Corporation, "Conformable and Alternate Fuel Storage Tanks", http://www.thiokol.com/tcr.htm, 1999.

[54] Shibley, A.M., "Filament Winding", Handbook of Composites, G. Lubin, Ed., Van Nostrand Reinhold, 1982, pp. 449-478.

[55] Peters, S.T., Humphrey, W.D., Foral, R.F., "Filament Winding Composite Structure Fabrication", SAMPE publications, Society of the Advancement of Material and Process Engineering, Covina, California, 1991.

[56] Phoenix, S.L., Wu, E.M., "Statistics for the Time Dependent Failure of Kevlar-49 / Epoxy Composites: Micromechanical Modeling and Data Interpretation", Mechanics of Composite Materials, Proceedings of the IUTAM Symposium on Mechanics of Composite Materials, Z. Hashin and C.T. Herakovich, Eds., 1982, pp. 135-162.

[57] Morgan, R.J., Mones, E.T., Steele, J.W., Deutscher, S.B., "The Failure Modes and Durability of Kevlar Composites", 12th National SAMPE Technical Conference, Oct., 1980, pp. 368-379.

[58] Knight, G.K., "Residual Strength of Carbon/Epoxy Pressure Vessels Subjected to Low Velocity Impacts", ANTEC '89, 45th Annual Technical Conference, Society of the Plastics Industry, May, 1989, pp. 1486-1490.

[59] Yener, M., Wolcott, E., "Damage Assessment Analysis of Composite Pressure Vessels Subjected to Random Impact Loading", Journal of Pressure Vessel Technology, Transactions of the ASME, Vol. 111, 1989, pp. 124-129.

[60] Chang, J.B., "COPV Home Page". http://ax.laafb.af.mil/~gowerj/horizontal/copv.html. and discussion with Stanley T. Chiu, (COSAP), 1999.

[61] Pigliacampi, J.J., Riewald, P.G., "Fibrous Reinforcements / Film and Sheet". Modern Plastics Encylopedia, Vol. 6, No. 11, 1989, pp. 230-238 & 692-694.

[62] Humphrey, W.D., "Degradation Data of Kevlar Pressure Vessels". Proceedings of 29th Meeting of the Mechanical Failures Prevention Group, National Bureau of Standards, 1979, pp. 177-197.

[63] Kasen, M.B., "Mechanical and Thermal Properties of Filamentary-Reinforced Structural Composites at Cryogenic Temperatures: Part 1- Glass-Reinforced Composites & Part 2 - Advanced Composites". Cryogenics, Vol. 15, 1975, pp. 327-346 & 701-722.

[64] Walmsley, S., Wilson, J., "HOTOL - A Cryogenic Materials Challenge", Advances in Cryogenic Engineering Materials, A.F. Clark and R.P. Reed, Eds., Vol. 34, 1987, pp. 1-10.

[65] Morris, V.L., "Advanced Composite Structures for Cryogenic Applications", 34th International SAMPE Symposium, 1989, pp. 1867-1876.

[66] Kasen, M.B., "Properties of Filamentary Reinforced Composites at Cryogenic Temperatures", Composite Reliability: ASTM STP 580, 1975, pp. 586-611.

[67] Charpentier, P., Reuille, G., "High Pressure Gas Storage Tanks: A Compromise Between Safety Regulations and Performance", AIAA '85, 21st Joint Propulsion Conference, AIAA paper no. 85-1201, July, 1985.

[68] AGA, "Recommendations for Development of a National Standard for Compressed Natural Gas (CNG) Vehicle Systems, Fuel Dispensing and Bulk Storage Facilities", American Gas Association, Natural Gas Vehicle Committee, May, 1982.

[69] Fawley, N.C., "Report of Severe Abuse Tests Conducted on Composite Reinforced Aluminum CNG (Compressed Natural Gas) Vehicle Fuel Cylinders", SAE, Compressed Natural Gas Conference Proceedings, Paper 831086, 1983.

[70] Knight, C.E., "Residual Stress and Strength Loss in Filament Wound Composites", Composite Materials: Testing and Design, 8th Conference, J.D. Whitcomb, Ed., ASTM STP 972, 1988, pp. 413-422.

[71] Leavesley, P.J., Knight, C.E., "An Analytical Model of Strength Loss in Filament Wound Spherical Pressure Vessels", Journal of Pressure Vessel Technology, Transactions of the ASME, Vol. 109, 1987, pp. 352-356.

[72] Erickson, J.D., Yorgason, J.A., "Graphite Pressure Vessel Dome Reinforcement Design", 32nd International SAMPE Symposium, 1987, pp. 667-684.

[73] Lal, K.M., "Filament Wound Pressure Vessels - Effects of Using Liner Tooling of Low Pressure Vessels for High Pressure Vessels Development", 37th International SAMPE Symposium, March, 1992, pp. 1253-1264.

[74] Witherell, M.D., "A Generalized Plane-Strain Elastic Stress Solution for a Multiorthotropic-Layered Cylinder", AD-A250 487, US Army Armament Research, Development and Engineering Center, Benet Laboratories, Technical Report ARCCB-TR-92013, March, 1992, pp. 1-19.

[75] Wark, K., "Thermodynamics", Fourth Ed., McGraw-Hill, 1983, pp. 137-142.

[76] Vargalfarh, N.B., "Tables on the Thermophysical Properties of Liquids and Gases in Normal and Dissociated States", 2nd Edition, John Wiley and Sons, Chapters 1 & 4, 1975.

[77] Van Wylen, G.J., Sonntag, R.E., "Fundamentals of Classical Thermodynamics", Appendix A, Second edition, John Wiley & Sons, 1978, pp. 703.

[78] "Clean Power Not Enough; Better Efficiency is Key", Hydrogen and Fuel Cell Letter, http://www.mhv.net/~hfcletter, April, 1997.

[79] Dodge, B.F., "Pressure-Volume-Temperature Relationships", Chemical Engineering Themodynamics, McGraw-Hill, 1944, pp. 172-187.

[80] Bikales, N.M., Conrod, J., "Permeability", Encyclopedia of Polymer Science and Technology, Interscience Publishers, John Wiley and Sons Inc., Vol. 9, 1968, pp. 794-806.

[81] Ausimont USA, "HALAR Fluoropolymer Resin Technical Data", Sheet FG-14, Ausimont Fluoropolymers Division, Morristown, NJ, Nov., 1986.

[82] Bringer, R.P., "Chlorotrifluoethylene Polymers", Encyclopedia of Polymer Science and Technology, Vol. 7, 1967, pp. 204-219.

[83] Evans, D., Morgan, J.T., "The Permeability of Composite Materials to Hydrogen and Helium Gas", Advances in Cryogenic Engineering Materials, A.F. Clark and R.P. Reed, Eds., Vol. 34, 1987, pp. 11-16.

[84] Schramm, R.E., Clark, A.F., Reed, R.P., "A Compilation and Evaluation of Mechanical, Thermal, and Electrical Properties of Selected Polymers", National Bureau of Standards, Cryogenic Division, 1973, pp. 9-19 & 335-344.

[85] Penn, L.S., Chiao, T.T., "Chapter 5: Raw Materials", Handbook of Composites, G. Lubin, Ed., Van Nostrand Reinhold, Chapt 5, 1982, pp. 58-88.

[86] Johnson, D.J., "Structure and Properties of Carbon Fibers", Carbon Fiber Filaments and Composites, NATO Advanced Study Institute on Carbon Fibers and Filaments, J.L. Figueiredo et al., Eds., May, 1989, pp. 119-161.

[87] Paterson, I.F., "Preimpregnation Techniques in Filament Winding and Experience in their Operation", Plastics and Polymers, April, 1973, pp. 89-94.

519

[88] Lekhniskii, S.G., "Theory of Elasticity of an Anisotropic Body", (Translated from revised 1977 Russian edition), Mir Publishers, Moscow, 1981.

[89] Lekhnitskii, S.G., Tsai, S.W., Cheron, T., "Anisotropic Plates", (Translated from 2nd Russian edition, 1956), Gordon and Breach Science Publishers, New York, 1968.

[90] Sherrer, R.E., "Filament Wound Cylinders with Axial Symmetric Loads", Journal of Composite Materials, Technomic Publishing Co., Inc., Vol. 1, 1967, pp. 344-355.

[91] Roy, K.A., Tsai, S.W., "Design of Thick Composite Cylinders", Design and Analysis of Composite Material Vessels, Pressure Vessels and Piping Conference, D. Hui and T.J. Kozik, Eds., ASME, Vol. 121, 1987, pp. 75-85.

[92] Hoa, S.V., Mannarino, G., "Twisting of Filament Wound Cylinders under Internal Pressure", Journal of Reinforced Plastics and Composites, Jan., Technomic Publishing Co., Inc., Vol. 8, 1989, pp. 212-231.

[93] Roy, A.K., "Strength Analysis and Design of Multilayered Thick Composite Spherical Pressure Vessels", AD-A236 266, Materials Laboratory, Wright-Patterson AFB, June, 1991.

[94] Roy, A.K., Massard, T.N., "A Design Study of Thick Multilayered Composite Spherical Pressure Vessels", Journal of Reinforced Plastics and Composites, Vol. 2, 1992, pp. 479-493.

[95] Roy, A.K., "Study of Design Parameters of Cylindrical Composite Pressure Vessels", 32nd International SAMPE Symposium, April, 1987, pp. 517-528.

[96] Rogers, T., "Problems for Helically Wound Cylinders", Continuum Theory of the Mechanics of Fibre-Reinforced Composites, Springer Verlag, N.Y, 1984, pp. 147-148.

[97] Whitney, J.M., "On the Use of Shell Theory for Determining Stresses in Composite Cylinders", Journal of Composite Materials, Technomic Publishing Co., Inc., Vol. 5, 1971, pp. 340-353.

[98] Widera, G.E.O., Logan, D.L., "A Shell Theory For Composite Cylindrical Pressure Vessels and Tanks", Pressure vessels Design: Pressure Vessels and Piping Conference, G.E.O. Widera, Ed., ASME, Vol. 57, 1982, pp. 167-179.

[99] Reuter, R.C., "Analysis of Shells Under Internal Presssure", Journal of Composite Materials, Technomic Publishing Co., Inc., Vol. 6, 1972, pp. 94-113.

[100] Lindstrom, D.W., "Series Solution for a Cylindrical Composite Shell Subject to Axisymetric Loadings", PhD. Thesis, University of Ottawa, July, 1990.

[101] Abu-Arja, K.R., Chaudhuri, R.A., "Moderately Thick Angle Ply Cylindrical Shells Under Internal Pressure", Journal of Applied Mechanics, Transactions of the ASME, Vol. 56, 1989, pp. 652-657.

[102] Byon, O., Vinson, J.R., "Stress Analysis of Laminated Thick-Walled Cylindrical Anisotropic Shells", 31st Structural Dynamics and Materials Conference, AIAA paper no. 90-0921, April, 1990.

[103] Vasil'ev, V.V., "Theory of Composite Shells", Mechanics of Composites. I.F. Obraztsov. Ed., Mir Publishers, Moscow, translated from Russian by V.I. Ilyuschenko, 1982, pp. 223-251.

[104] Horgan, C.O., "Saint-Venant End Effects in Composites", Journal of Composite Materials, Technomic Publishing Co., Inc., Vol. 16, 1982, pp. 411-422.

[105] Denost, J.P., "Design of Filament Wound Rocket Cases", NATO Advisory Group for Aerospace Research and Development, AGARD Lecture Series No. 150, April, 1988.

[106] Rogers, C.A., Knight, C.E., Dodge, W.G., "Development of Higher Order Finite Elements to Model Filament Wound Composites", Pressure Vessel Components Design and Analysis: Proceedings of the Pressure Vessels and Piping Conference, New Orleans, 1985, pp. 247-255.

[107] Gleich, D., "Report on Kevlar-49 Composite Presure Vessel Safety Technology Program", JANNAF Propulsion Meeting, San Diego California, Vol. 1, 1985, pp. 321-331.

[108] Gerstle, F.P., "Analysis of Filament Reinforced Spherical Pressure Vessels", Composite Materials: Testing and Design, 3rd conference, ASTM STP 546, March, 1974, pp. 604-631.

[109] Tauchert, T.R., "Optimum Design of a Reinforced Cylindrical Pressure Vessel", Journal of Composite Materials, Technomic Publishing Co., Inc., Vol. 15, 1981, pp. 390-402.

[110] Christensen, R.M., Swanson, S.R.. "Evaluation of a New Failure Criterion for Fibrous Composite Materials", 1988, pp. 63-68.

[111] Christensen, R.M., "Tensor Transformations and Failure Criteria for the Analysis of Fiber Composite Materials", Journal of Composite Materials, Technomic Publishing Co., Inc., Vol. 22, 1988, pp. 874-897.

[112] Christensen, R.M., "Tensor Transformations and Failure Criteria for the Analysis of Fiber Composite Materials Part II: Necessary and Sufficient Conditions for Laminate Failure", Journal of Composite Materials, Technomic Publishing Co., Inc., Vol. 24, 1990, pp. 796-800.

[113] Christensen, R.M., "The Numbers of Elastic Properties and Failure Parameters for Fiber Composites", Journal of Engineering Materials and Technology, Transactions of the ASME, Vol. 120, 1998, pp. 110-113.

[114] Timoshenko, S.P., Goodier, J.N., "Axisymmetric Stress and Deformation in a Solid of Revolution / Two Dimensional Problems in Polar Coordinates", Theory of Elasticity, Second edition, McGraw-Hill Book Co., 1970, pp. 380-432 & 65-149.

[115] Christensen, R.M., "Stress Based Yield / Failure Criteria for Fiber Composites", Int. J. Solids Structures, Elsevier Science Ltd, Vol. 34, No. 5, 1997, pp. 529-543.

[116] Christensen, R.M., "A Critical Evaluation for a Class of Micro-Mechanics Models", Journal of Mechanics and Physics of Solids, Vol. 38, No. 3, 1990, pp. 379-404.

[117] Feng, W.W., "A Failure Criterion for Composite Materials", Journal of Composite Materials, Technomic Publishing Co., Inc., Vol. 25, 1991, pp. 88-100.

[118] Groves, S.E., Sanchez, R.J., Feng, W.W., "Multiaxial Failure Characterization of Composites", ICCM IIIV, 1991, pp. 37-B1 - 37-B15.

[119] Zocher, M.A., Allen, D.H., Groves, S.E., Feng, W.W., "Evaluation of First Ply Failure in a Three-Dimensional Load Space", Journal of Composite Materials, Technomic Publishing Co., Inc., Vol. 29, No. 12, 1995, pp. 1649-1678.

[120] Tennyson, R.C., Wharram, G.E., Elliott, G., "Application of Cubic Strength Failure Criterion to the Failure Analysis of Composite Laminates", Journal of Composite Materials Supplement, Vol. 14, 1980, pp. 28-41.

[121] Jiang, Z., Tennyson, J.C., "Closure of the Cubic Tensor Polynomial Failure Surface", Journal of Composite Materials, Technomic Publishing Co., Inc., Vol. 23, 1989, pp. 208-231.

[122] Wei-xun, F., "On Phenomenological Anisotropic Failure Criteria", Composites Science and Technology, Elsevier Science Publishers, No. 28, 1987, pp. 269-278.

[123] Kallas, N.M., Hahn, T.H., "A Failure Criterion for Composites Under 3-Dimensional State of Stress". 35th International SAMPE Symposium, April, 1990, pp. 674-686.

[124] Guess, T.R., "Biaxial Testing of Composite Cylinders: Experimental-theoretical Comparison", Composites, Butterworth & Co. Ltd, July, 1980, pp. 139-148.

[125] Uemura, M., Fukunaga, H., "Probabilistic Burst Strength of Filament Wound Cylinders Under Internal Pressure", Journal of Composite Materials, Technomic Publishing Co., Inc., Sept., 1981, pp. 462-481.

[126] Knight, C.E., "Analytical Failure Prediction of Spherical Composite Pressure Vessels". Journal of Pressure Vessel Technology, Transactions of the ASME, Vol. 104, 1982, pp. 229-231.

[127] Foral, R.F., "Composite Spherical Pressure Vessels with Hardening Metal Liners", Journal of Pressure Vessel Technology, Transactions of the ASME, Vol. 101, 1979, pp. 200-206.

[128] Chen, P.C.T., "Elastic-Plastic Analysis of a Steel Pressure Vessel Wrapped With Multilayered Composites", AD-A243 420, US Army Armament Research Development and Engineering Center, Benet Laboratories, Dec., 1991.

[129] Chen, P.C.T., "Residual Stresses in a Steel Pressure Vessel Wrapped with Multilayered Composites", AD-A243 429, US Army Armament Research Development and Engineering Center, Benet Laboratories, Dec., 1991.

[130] Moss, M., "Filament Reinforced Cylindrical Pressure Vessels", SAND-77-0403, Sandia Laboratories, 1977.

[131] Roy, A.K., "Influence of Curing Stresses on Mandrel Release of Filament Wound Rings", 35th International SAMPE Symposium, April 2-5, 1990, pp. 1698-1707.

523

[132] Hjellming, L.N., Walker, J.S., "Thermal Curing Cycles for Composite Cylinders with Thick Walls and Thermosetting Resins", Journal of Composite Materials, Technomic Publishing Co., Inc., Vol. 23, 1989, pp. 1048-1065.

[133] Tarnopol'skii, Y.M., Portnov, G.G., Beil', A.I., "Technological Problems in Composite Winding Mechanics", Mechanics of Composites, I.F. Obraztsov, Ed., Mir Publishers Moscow, translated from Russian by V.I. Ilyuschenko, 1982, pp. 186-222.

[134] Lee, S.Y., Springer, G.C., "Filament Winding Cylinders: I- Process Model", Journal of Composite Materials, Technomic Publishing Co., Inc., Vol. 24, 1990, pp. 1270-1303.

[135] Olofsson, K.S., Gudmundson, P., Strombeck Anders, L., "Process Simulation of Wet Filament Winding and Curing of Thick Composite Cylinders", 37th International SAMPE Symposium, March, 1992, pp. 1132-1145.

[136] Spencer, B.E., "Modeling the Filament Winding Process", 34th International SAMPE Symposium, May, 1989, pp. 1556-1570.

[137] Prater, J.L., Hackett, R.M., "Viscoelastic / Damage Modeling of Filament-Wound Cylindrical Pressure Vessels", Composite Materials Testing and Design, 8th Conference, J.D. Whitcomb, Ed., ASTM STP 972, 1988, pp. 401-412.

[138] Efremov, E.D., "A Differential Equation for the Motion of the Winding Point", Tech. of the Textile Industry U.S.S.R., No. 2, 1960, pp. 91-96.

[139] Efremov, E.D., "The Yarn-Winding Parameters on a Cylindrical Bobbin as a Basis for the Design of a Winding Motion", Tech. of the Textile Industry U.S.S.R., No. 6, 1962, pp. 82-92.

[140] Efremov, E.D., "The Movement of the Traverse in Building a Complex Shaped Package", Technology of the Textile Industry U.S.S.R., No. 6, 1966, pp. 70-75.

[141] Efremov, E.D., "The Movement of the Traverse for Given Conditions of Equilibrium for the Yarn in Winding", Tech. of the Textile Industry U.S.S.R., No. 4, 1972, pp. 62-66.

[142] Efremov, E.D., "The Equation Yarn Winding on a Surface of Revolution", Tech. of the Textile Industry U.S.S.R., No. 2, 1965, pp. 76-80.

[143] Vulfson, I.I., "The Optimal Equation of Motion of the Yarn Guide in the Reversing Section", Tech. of the Textile Industry U.S.S.R., No. 6, 1971, pp. 51-55.

[144] Hofeditz, J.D., "Structural Design Considerations for Fibrous Glass Pressure Vessels", Modern Plastics, April, 1964, pp. 127-146.

[145] Denost, J.P., "New Design Concepts for Filament Wound Pressure Vessels with Unequal Polar Openings", AIAA/SAE/ASME 18th Joint Propulsion Conference, Cleveland, Ohio, AIAA-82-1067, June 21-23, 1982.

[146] Wells, G.M., McAnulty, K.F., "Computer Aided Filament Winding Using Non-Geodesic Trajectories", ICCM 6 & ECCM II, Vol. 1, 1987, pp. 1.161-1.173.

[147] Barblat, C., Denizet, P., Massard, T.H., "Design and Filament Winding of Structures by an Incremental Method", 30th National SAMPE Symposium, March, 1985, pp. 1265-1274.

[148] Tezak, K.M., "Countoured/Tapered Composite Reinforcements for High Performance Composite Motor Cases", 32nd International SAMPE Symposium, April, 1987, pp. 1009-1014.

[149] Hady, A.F., Kandil, N., Michauu, D. et al., "Computer Aided Design in Filament Winding of Structures", ICCM 7, Vol. 3, 1989, pp. 352-357.

[150] Hamouda, H., Kang, T.J., El-Shiekh, A., "On the Mechanics of Filament Winding: Part 1- A Generalized Model", 34th International SAMPE Symposium, May, 1989, pp. 1130-1142.

[151] Li, X.L., Lin, D.H., "Non-Geodesic Winding Equations on a General Surface of Revolution", ICCM 6 & ECCM II, Vol. 1, 1987, pp. 1.152-1.160.

[152] Marchetti, M., Cutolo, D., Di Vita, G., "Filament Winding of Composite Structures: Validation of the Manufacturing Process", Proceedings of the 7th International Conference on Composite Materials, ICCM-VII, Guangzhou, China, 1989, pp. 135-140.

[153] Vogt, J.C., Taylor, D.L., "A Workstation for Off-Line Filament Winding Pattern Generation", 34th International SAMPE Symposium, May, 1989, pp. 1538-1543.

[154] Bunakov, V.A., Radovinskii, A.L., "Rationalization of the Shape of Wound Shells of Revolution Composed of High Modulus Material", Polymer Mechanics (Translated from Russian Mekhanika Polimerov), Vol. 11, No. 5, 1976, pp. 704-709.

[155] Bunakov, V.A., Protasov, V.D., "Composite Pressure Vessels", Handbook of Composites, Structure and Design, C.T. Herakovich and Y.M. Tarnopol'skii, Eds., Elsevier Science Publishers, Vol. 2, 1989, pp. 464-530.

[156] Edie, D.D., "Pitch and Mesophase Fibers", Carbon Fiber Filaments and Composites, NATO Advanced Study Institute on Carbon Fibers and Filaments, J.L. Figueiredo et al., Eds., May, 1989, pp. 43-72.

[157] Shoji, Y., Tohru, H., Tomitake, H., "Toraca T1000 Ultra High Strength Carbon Fiber and Its Composite Properties", 32nd SAMPE Symposium, 1987, pp. 928-937.

[158] Darmes, F.J., Landes, R.E., Lambert, J.W. et al., "Computer Program for the Analysis of Filament-Reinforced Metallic Tanks for Cryogenic Service", NASA Lewis Research Center CR-72124, Aerojet General Corp. Von Karmen Center computer code job no. AGC 674, Azusa, California, May, 1966.

[159] Ayres, F. Jr., "Chapter 17: Curvature", Differential and Integral Calculus, second edition, Schaum's Outline Series, McGraw-Hill, 1964, pp. 81-85.

[160] Burden, R.L., Faires, J.D., Reynolds, A.C., "Chapter 10: Boundary Value Problems for Ordinary Differential Equations", Numerical Analysis, second edition, PWS Publishers, 1981, pp. 238-241, 476-480.

[161] Saada, A.S., "Introduction to the Theory of Thin Shells", Elasticity Theory and Applications, Permagon Press, Chapt. 18, 1974, pp. 563-635.

[162] Sechler, E.E., "Strain Conditions", Elasticity in Engineering, John Wiley & Sons, Inc., Chapt. 4, 1952, pp. 40-53.

[163] Hydrospin Inc., "Products and Applications", http://www.hydrospin.com, 1998.

[164] Di Vita, G., Grimaldi, M., Marchetti, M., Moroni, P., "The Filament Winding Manufacturing Technique: Studies on the Determination of the Friction Coefficient and on the Optimization of the Feed Eye Rotation", 35th International SAMPE Technical Conference, Nov., 1990, pp. 972-979.

526

[165] Adali, S., Verijenko, V.E., Tabakov, P.Y., Walker, M., "Optimization of Multilayered Composite Pressure Vessels Using Exact Elasticity Solution", Composites for the Pressure Vessel Industry, ASME, Vol. 302, 1995, pp. 203-212.

[166] Verijenko, V.E., Adali, S., Tabakov, P.Y., "Stress Distribution in Continuously Heterogeneous Thick Laminated Pressure Vessels", Composites for the Pressure Vessel Industry, ASME, Vol. 302, 1995, pp. 163-170.

[167] Polyanin, A.D., Zaitsev, V.F., "Handbook of Exact Solutions for Ordinary Differential Equations", CRC Press, 1995, pp. 145-149.

[168] Hashin, Z., "Analysis of Properties of Fiber Composites With Anisotropic Constituents", Journal of Applied Mechanics, Transactions of the ASME, Vol. 46, 1979, pp. 543-550.

[169] Christensen, R.M., "Mechanics of Composite Materials". John Wiley & Sons, 1979.

[170] Hart-Smith, L.J., "Should Fibrous Composite Failure Modes Be Interacted or Super-Imposed?", Composites. Butterworth-Heinemann Ltd. Vol. 24, No. 1, 1993, pp. 53-55.

[171] Ashton, J.E., Halpin, J.C., Petit, P.H., "Primer on Composite Materials: Analysis. Progress in Materials Science Series", Technomic Publishing Co., Inc., Vol. III, 1969.

[172] Whitney, J.M., Daniel, I.M., Pipes, R.B., "Experimental Mechanics of Fiber Reinforced Composite Materials, Monograph No. 4". Society for Experimental Stress Analysis, 1982.

[173] Jones, R.M., "Mechanics of Composite Materials". McGraw-Hill Book Company, 1969.

[174] Tsai, S.W., Massard, T.N., Susuki,I., "Composite Design". Fourth Edition, Think Composites Inc., Dayton Ohio, 1988.

[175] Tsai, S.W., Hahn, H.T., "Introduction to Composite Materials", Technomic Publishing Co., Inc., 1980.

[176] Tsai, S.W., "Theory of Composite Design", Think Composites Inc., Dayton Ohio, 1992.

527

[177] Tandon, G.P., "Use of Composite Cylinder Model as Representative Volume Element for Unidirectional Fiber Composites", Journal of Composite Materials, Technomic Publishing Co., Inc., Vol. 29, No. 3, 1995, pp. 388-409.

[178] Battley, M., Moltschaniwskyj, G., "Reliability of Stiffness Predictions for Fibre Composites", Proceedings of The Tenth International Conference on Composite Materials, Whistler, B.C., A. Poursartip and K. Street, Eds., The Tenth International Conference on Composite Materials Society, Woodhead Publishing Limited, Vol. IV, 1995, pp. IV-11 - IV-17.

[179] Watt, W., Perov, B.V., "Strong Fibers", Handbook of Composites, Series Editors A. Kelly and Y.N. Rabotnov, Elsevier Science Publishers B.V., Vol. 1, 1985.

[180] Peebles, L.H., Yanovsky, Y.G., Sirota, A.G. et al., "Mechanical Properties of Carbon Fibers". Carbon Fibers, Third Edition, Revised and Expanded. J.-B. Donnet, T.K. Wang, J.C.M. Peng and S. Rebouillat, Eds., Marcel Dekker, Inc., 1995, pp. 311-353.

[181] Kawabata, S., "Measurements of Anisotropic Mechanical Property and Thermal Conductivity of Single Fiber for Several High Performance Fibers", Proceedings of the 4th Japan-US Conference on Composite Materials, Washington D.C., 1988, pp. 253-262.

[182] Smith. R.E.. "Ultrasonic Elastic Constants of Carbon Fibers and Their Composites", Journal of Applied Physics, Vol. 43, No. 6, 1972. pp. 2555-2561.

[183] Dean, G.D., Turner, P.. "The Elastic Properties of Carbon Fibres and Their Composites", Composites, Butterworth & Co. Ltd. Vol. 4. No. 4, 1973, pp. 174-180.

[184] Vong, T.S., Verchery, G., "Optimal Use of Redundant Measurements of Constrained Quantities. Application to Elastic Moduli of Anisotropic Composite Materials", ICCM 3, Paris, France, A.R. Bunsell, C. Bathias et al., Eds., Permagon Press. Vol. 2. 1980, pp. 1783-1795.

[185] Hart-Smith, L.J., "A Re-Examination of the Analysis of In-Plane Matrix Failures in Fibrous Composite Laminates", Composites Science and Technology, Elsevier Science, Vol. 56, 1996, pp. 107-121.

[186] Hart-Smith, L.J., "An Inherent Fallacy in Composite Interaction Failure Curves", Composites, Butterworth-Heinemann Ltd, Vol. 24, No. 6, 1993, pp. 523-524.

[187] Hart-Smith, L.J., "The Truncated Maximum Strain Composite Failure Model", Composites, Butterworth-Heinemann Ltd, Vol. 24, No. 7, 1993, pp. 587-591.

[188] Rowlands, R.E., "Strength (Failure) Theories and their Experimental Correlation", Handbook of Composites - Failure Mechanics of Composites, G.C. Sih and A.M Skudra, Eds., Elsevier Science Publishers B.V., Chapt II, Vol. 3, 1985, pp. 71-77.

[189] Tsai, S.W., Hahn, H.T., "Failure Analysis of Composite Materials", Inelastic Behavior of Composite Materials, The American Society of Mechanical Engineers, Vol. 13, 1975, pp. 73-95.

[190] Christensen, R.M., Zywicz, E., "A Three-Dimensional Constitutive Theory for Fiber Composite Laminated Media", Journal of Applied Mechanics, Transactions of the ASME, Vol. 57, 1990, pp. 948-955.

[191] Swanson, S.R., Christoforou, A.P., Colvin, Jr., G.E., "Biaxial Testing of Fiber Composites Using Tubular Specimens", Experimental Mechanics, 1988, pp. 238-243.

[192] Flaggs, D.L., "Prediction of Tensile Matrix Failure in Composite Laminates", Journal of Composite Materials, Technomic Publishing Co., Inc., Vol. 19, 1985, pp. 29-50.

[193] Choo, V.K.S., Hull, D., "Influence of Radial Compressive Stress Owing to Pressure on the Failure Modes of Composite Tube Specimens", Journal of Composite Materials, Technomic Publishing, Vol. 17, July, 1983, pp. 344-356.

[194] Swanson, S.R., Christoforou, A.P., "Response of Quasi-Isotropic Carbon/Epoxy Laminates to Biaxial Stress", Journal of Composite Materials, Technomic Publishing Co., Inc., Vol. 20, 1986, pp. 457-471.

[195] Hahn, H.T., Erikson, J.B., Tsai, S.W., "Characterization of Matrix/Interface-Controlled Strength of Unidirectional Composites", Fracture of Composite Materials, Proceedings of the Second USA-USSR Symposium, G.C. Sih, V.P. Tamuzs, Eds., Martinus Hijhoff Publishers, March, 1981, pp. 197-214.

[196] Hahn, H.T., Tsai, S.W., "On the Behavior of Composite Laminates After Initial Failures", Journal of Composite Materials, Technomic Publishing Co., Inc., Vol. 8, 1974, pp. 288-305.

[197] Fahmy, A.A., "Stress-Strain Behavior of Kevlar-Epoxy Angle-Ply Laminates under Compression along the Thickness Direction", Proceedings of the International Symposium on Composite Materials and Structures, Beijing, China, 1986, pp. 32-37.

[198] Hashin, Z., "Analysis of Orthogonally Cracked Laminates Under Tension", Journal of Applied Mechanics, Transactions of the ASME, Vol. 54, 1987, pp. 872-879.

[199] Dvorak, G.J., Laws, N., "Analysis of Progressive Matrix Cracking in Composite Laminates - II. First Ply Failure", Journal of Composite Materials, Technomic Publishing Co., Inc., Vol. 21, 1987, pp. 309-329.

[200] Zhang, J., Fan, J., Soutis, C., "Analysis of Mulitple Matrix Cracking in $[\pm 0_m/90_n]_s$ Composite Laminates", Composites, Butterworth-Heinemann Ltd, Vol. 23, No. 5, 1992, pp. 291-298.

[201] Garrett, K.W., Bailey, J.E., "Multiple Transverse Fracture in 90° Cross-Ply Laminates of a Glass Fibre-Reinforced Polyester", Journal of Materials Science, Champman and Hall Ltd, Vol. 12, 1977, pp. 157-168.

[202] Downs, K.S., Hamstad, M.A., "Acoustic Emission from Depressurization to Detect/Evaluate Significance of Impact Damage to Graphite/Epoxy Pressure Vessels", Journal of Composite Materials, Technomic Publishing Co., Inc., Vol. 32, No. 3, 1998, pp. 258-307.

[203] Hamstad, M.A., "Acoustic Emission For Quality Control of Kevlar 49 Filament-Wound Composites", 12th National SAMPE Technical Conference, Oct., 1980, pp. 380-393.

[204] Lee, J.-W., Daniel, I.M., "Progressive Transverse Cracking of Crossply Composite Laminates", Journal of Composite Materials, Technomic Publishing Co., Inc., Vol. 24, 1990, pp. 1225-1243.

[205] Han, Y.M., Hahn, H.T., Croman, R.B., "A Simplified Analysis of Transverse Ply Cracking in Cross-Ply Laminates", Composites Science and Technology, Elsevier Applied Science Publishers Ltd. 1988, pp. 165-177.

[206] Han, Y.M., Hahn, H.T., "Ply Cracking and Property Degradations of Symmetric Balanced Laminates Under General In-Plane Loading", Composites Science and Technology, Elsevier Science Publishers Ltd., Vol. 37, 1989, pp. 377-397.

[207] Carresa, G., Geogantas, A.I., Krepec, T., "Research in the Development of New Concepts for the On-board Storage, Direct Injection and Ignition of Gaseous Fuels in Automotive Internal Combustion Engines", Progress Report No. 1: Model Development, Concordia University CIC - 0027, 1989.

[208] Talreja, R., Yalvac, S., Yats, L.D., Wetters, D.G., "Transverse Cracking and Stiffness Reduction in Cross Ply Laminates of Different Matrix Toughness", Journal of Composite Materials, Technomic Publishing Co., Inc., Vol. 26, No. 11, 1992, pp. 1644-1663.

[209] Flaggs, D.L., Kural, M.H., "Experimental Determination of the In Situ Transverse Lamina Strength in Graphite/Epoxy Laminates", Journal of Composite Materials, Technomic Publishing Co., Inc., Vol. 16, 1982, pp. 103-115.

[210] Takeda, N., Ogihara, S., "In Situ Observation and Probabilistic Prediction of Microscopic Failure Processes in CFRP Cross-Ply Laminates", Composites Science and Technology, Elsevier Science Limited, Vol. 52, 1994, pp. 183-195.

[211] Gudmundson, P., Östlund, S., "First Order Analysis of Stiffness Reduction Due to Matrix Cracking", Journal of Composite Materials, Technomic Publishing Co., Inc., Vol. 26, No. 7, 1992, pp. 1009-1030.

[212] Swanson, S.R., Trask B.C., "Matrix Cracking in Carbon/Epoxy Laminates Under Biaxial Loads", Fracture and Damage-Polymer Matrix Composites, Proceedings of the Fourth Japan-U.S. Conference on Composite Materials, Technomic Publishing Co., Inc., June, 1988, pp. 339-348.

[213] Nuismer, R.J., Tan, S.C., "Constitutive Relations of a Cracked Composite Lamina", Journal of Composite Materials, Technomic Publishing Co., Inc., Vol. 22, 1988, pp. 306-321.

[214] Laws, N., Dvorak, G.J., "Progressive Transverse Cracking in Composite Laminates", Journal of Composite Materials, Technomic Publishing Co., Inc., Vol. 22, 1988, pp. 900-916.

[215] Lee, J.-W., Allen, D.H., Harris, C.E., "Internal State Variable Approach for Predicting Stiffness Reductions in Fibrous Laminated Composites with Matrix Cracks", Journal of Composite Materials, Technomic Publishing Co., Inc., Vol. 23, 1989, pp. 1273-1291.

[216] Hoover, J.W., Kujawski, D., Ellyin, F., "Transverse Cracking of Symmetric and Unsymmetric Glass-Fibre/Epoxy-Resin Laminates", Composites Science and Technology, Elsevier Science Ltd, Vol. 57, 1997, pp. 1513-1525.

[217] Tong, J., Guild, F.J., Ogin, S.L., Smith, P.A., "On Matrix Crack Growth in Quasi-Isotropic Laminates - I. Experimental Investigation", Composites Science and Technology, Elsevier Science Limited, Vol. 57, 1997, pp. 1527-1535.

[218] Caron, J.F., Ehrlacher, A., "Modelling the Kinetics of Transverse Cracking in Composite Laminates", Composites Science and Technology, Elsevier Science Limited, Vol. 57, 1997, pp. 1261-1269.

[219] Groves, S.E., Harris, C.E., Highsmith, A.L., et al., "An Experimental and Analytical Treatment of Matrix Cracking in Cross-Ply Laminates", Experimental Mechanics, March, 1987, pp. 73-79.

[220] Kominar, V., Wagner, H.D., "Some Matrix Failure Peculiarities of Unidirectional Fibre-Reinforced Plastics and Layers in Laminated Composites", Composites, Butterworth-Heinemann Ltd, Vol. 25, No. 1, 1994, pp. 5-10.

[221] Highsmith, A.L., Reifsneider, K.L., "Stiffness Reduction Mechanisms in Composite Laminates", ASTM STP 775, Damage in Composite Materials, 1980, pp. 103-117.

[222] Xu, L.-Y., "On the Law of the Transverse Matrix Crack Growth in Brittle Polymeric Matrix Composite Laminates under Static Loadings". Journal of Composite Materials, Technomic Publishing Co., Inc., Vol. 30, No. 3, 1996. pp. 384-405.

[223] Xu, L.-Y., "Influence of Stacking Sequence on the Transverse Matrix Cracking in Continuous Fiber Crossply Laminates", Journal of Composite Materials, Technomic Publishing Co., Inc., Vol. 29, No. 10, 1995, pp. 1337-1358.

[224] Xu, L.-Y., "Study on the Characteristic Curve of Stiffness Degradation Caused by Transverse Matrix Cracking in Multidirectional Composite Laminates", Journal of Composite Materials, Technomic Publishing Co., Inc., Vol. 30, No. 7, 1996, pp. 820-838.

[225] Xu, L.-Y., Kou, C.-H., "Effect of the Interfacial Interleaf to the Interlaminar Fracture and Intralaminar Fracture of a New BMI Matrix Composites System", Journal of Reinforced Plastics and Composites, Technomic Publishing Co., Inc., Vol. 13, 1994, pp. 509-540.

532

[226] Xu, L.-Y., Kou, C.-H., Yang, B.-X., "An Analogous Investigation on Transverse Cracking in Composite Laminate and Concrete Pavement", Composites, Design. Manufacture, and Application, ICCM/VIII, S.W. Tsai and G.S. Springer, Eds., Section 22-29, 1991, pp. 27-F-1 - 27-F-10.

[227] Xu, L.-Y., "Exploration of Constants Independent of Material and Layup in Transverse Matrix Cracking of Cross-Ply Laminate", Advanced Composites Letters, Woodhead Publishing Ltd, Vol. 2, No. 1, 1993, pp. 25-28.

[228] Zhang, J., Fan, J., Soutis, C., "Analysis of Multiple Matrix Cracking in $[\pm 0_m/90_n]_s$ Composite Laminates, Part 2: Development of Transverse Ply Cracks", Composites, Butterworth-Heinemann Ltd, Vol. 23, No. 5, 1992, pp. 299-304.

[229] Miller, I., Freund, J.E., "Probability and Statistics for Engineers, second edition", Prentice-Hall, Inc., 1977.

[230] Zhu, Y.T., Zong, G., "On the Application of the Statistical Strength Model of Fiber-Reinforced Composites", Journal of Composite Materials, Technomic Publishing Co., Inc., Vol. 27, No. 9, 1993, pp. 944-959.

[231] Zhu, Y., Zhou, B., He, G., Zheng, Z., "A Statistical Theory of Composite Materials Strength", Journal of Composite Materials, Technomic Publishing Co., Inc., Vol. 23, 1989, pp. 280-287.

[232] Smith, P.A., Wood, J.R., "Poisson's Ratio as a Damage Parameter in the Static Tensile Loading of Simple Crossply Laminates", Composites Science and Technology, Elsevier Science Publishers, Vol. 38, 1990, pp. 85-93.

[233] Swanson, S.R., Messick, M., Toombes, G.R., "Comparison of Torsion Tube and Isopescu In-Plane Shear Test Results for a Carbon Fibre-Reinforced Epoxy Composite", Composites, Butterworth & Co. (Publishers) Ltd, Vol. 16, No. 3, 1985, pp. 220-224.

[234] Hong, C.S., Sonn, H.W., "Three-Dimensional Material Characterization of Thick Graphite/Epoxy Composite", Proceedings of the 7th International Conference on Composite Materials, ICCM 7, Permagon Press, Vol. 1, 1989, pp. 254-259.

[235] Kawabata, S., "Measurements of Anisotropic Mechanical Property and Thermal Conductivity of Single Fiber for Several High Performance Fibers", Proceedings of th 4th Japan-US Conference on Composite Materials, Washington D.C., 1988, pp. 253-262.

533

[236] Kriz, R.D., Stinchcomb, W.W., "Elastic Moduli of Transversely Isotropic Graphite Fibers and Their Composites", Experimental Mechanics, Vol. 19, No. 1, 1979, pp. 41-49.

[237] Benzeggagh, M.L., Khellil, K., "Experimental Measurements Methodology for Three-Dimensional Failure Tenseurs", Composite Structures and Materials, S.V. Hoa and R. Gauvin, Eds., Elsevier Applied Science, 1991, pp. 405-411.

[238] Toombes, G.R., Swanson, S.R., Cairns, D.S., "Biaxial Testing of Composite Tubes", Experimental Mechanics, Vol. 25, 1985, pp. 186-192.

[239] Philippidis, T.P., Theocaris, P.S., "The Transverse Poisson's Ratio in Fiber Reinforced Laminae by Means of a Hybrid Experimental Approach", Journal of Composite Materials, Technomic Publishing Co., Inc., Vol. 28, No. 3, 1994, pp. 252-261.

[240] Yuhas, D.E., Dolgin, B.P., Vorres, C.L., et al., "Ultrasonic Methods for Characterization of Interfacial Adhesion in Spectra Composites", Interfaces in Polymer, Ceramic and Metal Matrix Composites, Proceedings of the 2nd International Conference on Interfaces, Ohio, H. Ishida, Ed., Elsevier Science Publishing Co., Inc., 1988, pp. 595-609.

[241] Riewald, P.G., Dhingra, A.K., Chern, T.S., "Recent Advances in Aramid Fiber and Composite Technology", 6th International Conference and 2nd European Conference, ICCM & ECCM, Elsevier Science Publishers B.V., Vol. 5, 1987, pp. 5.362-5.370.

[242] Pindera, M.J., Aboudi, J., "Recent Developments in the Micromechanics of Advanced Composites", Development and Design with Advanced Materials, G.C. Sih, S.V. Hoa and J.T. Pindera, Eds., Elsevier Science Publishers B.V., 1990, pp. 65-77.

[243] Knight, M., "Three-Dimensional Moduli of Graphite Epoxy Composites", Journal of Composite Materials, Technomic Publishing Co., Inc., Vol. 16, 1982, pp. 153-159.

[244] Gerstle, F.P., Reedy, E.D., "On the Application of the Maximum Stress Failure Criterion to Off-Axis and Angle Ply Laminates", Journal of Composite Materials, Technomic Publishing Co., Inc., Vol. 19, 1985, pp. 505-512.

[245] Masters, J.E., Reifsnider, K.L., "An Investigation of Cumulative Damage Development in Quasi-Isotropic Graphite/Epoxy Laminates", Damage in Composite Materials, K.L. Reifsnider, Ed., ASTM STP 775, 1982, pp. 40-62.

[246] Highsmith, A.L., Reifsnider, K.L., "Stiffness-Reduction Mechanisms in Composite Laminates", Damage in Composite Materials, K.L. Reifsnider, Ed., ASTM STP 775, 1982, pp. 103-117.

[247] Geogantas, A.I., Krepec, T., Lisio, C., Rohrauer, G.L., "Research and Development of New Concepts for On-board Storage, Direct Injection and Ignition of Gaseous Fuels in Automotive Internal Combustion Engines", Progress Report No. 2: System Design, Concordia University CIC - 0032, 1990.

[248] McClean Anderson, "Compositrak Manuals", Max4 Maintenance Manual - Filament Winding System, Revision 1.0, Programming/Operator Manual - Filament Winding Control System, User's Guide to the File Management Package, Software Revision 1.10, Bottlemaster - Pattern Software, User's Guide to the Pattern Manipulation Package, Release 1.0, McClean-Anderson, Inc., 1988-1990, .

[249] Kondo, T., Sekine, H., Nakano, K., "Residual Stress Analysis in Forming Process of Filament Wound Thick-Walled CFRP Pipes", Composites for the Pressure Vessel Industry, ASME, Vol. 302, 1995, pp. 195-201.

[250] Amiouny, S.V., Hoa, S.V., "Heuristics for the Design of Thick Composite Cylinders", Computer Methods in Composite Materials VI, Computational Mechanics Publications, 1998, pp. 55-64.

[251] Ladkany, S.G., "Prestressed Circumferentially Reinforced Large Aluminium Composite Pressure Vessels", Pressure vessels Design: Pressure Vessels and Piping Conference, G.E.O. Windera, Ed., ASME, Vol. 57, 1982, pp. 181-190.

[252] Gabrys, C.W., Bakis, C.E., "Simplified Analysis of Residual Stresses in In-Situ Cured Hoop-Wound Rings", Journal of Composite Materials, Technomic Publishing Co., Inc., Vol. 32, No. 13, 1998, pp. 1325-1343.

[253] Kalamkarov, A.L., Drozdov, A.D., "On the Optimal Pretensioning of Cylindrical and Spherical Pressure Vessels", Composites for the Pressure Vessel Industry, ASME, Vol. 302, 1995, pp. 61-67.

[254] Cai, Z., Gutowski, T., Allen, S., "Winding and Consolidation Analysis for Cylindrical Composite Structures", Journal of Composite Materials, Technomic Publishing Co., Inc., Vol. 26, No. 9, 1992, pp. 1374-1399.

[255] Aleong, C., Munro, M., "Effect of Winding Tension and Cure Schedule on Residual Stresses in Radially Thick Fiber Composite Rings", Polymer Engineering and Science, Vol. 31, No. 18, 1991, pp. 1344-1350.

[256] Department of Energy, Ford Motor Co., Program for a New Generation Vehicle (PNGV), "On-board Hydrogen Storage Using Lightweight Pressure Vessels", http://www.ta.doc.gov/pngv/technical/fuelcells.htm, 1999.

[257] Lincoln Composites, "Pressure vessels: Aerospace and Defense, Commercial", http://www.lincolncomposites.com/products/pv_details/ac_missile.html, 1998.

[258] Firth, D., "IANGV Newsletter 49: Cylinder Standard - meeting in Vancouver...", http://www.iangv.org/iangv-a/nl-index.html, October, 1998.

[259] Hill, R., "The Mathematical Theory of Plasticity", Chapter 2: Foundations of the Theory, & Chapter 12: Plastic Anisotropy, Oxford University Press, First edition, 1950, pp. 14-49, 317-340.

[260] Minnetyan, L., Chamis, C.C., Murthy, P.L.N., "Structural Durability of a Composite Pressure Vessel", Journal of Reinforced Plastics and Composites, Technomic Publishing Co., Vol. 11, November, 1992, pp. 1251-1269.

[261] Bury. K.W., "Statistical Models in Applied Science", Chapter 12: The Weibull Model, John Wiley and Sons, 1975, pp. 405-439.

Ultra-high Pressure Composite Vessels with Efficient Stress Distributions

Greg Rohrauer

A thesis

in

The Department

of

Mechanical Engineering

Presented in Partial Fulfillment of the Requirements
for the Degree of Doctor of Philosophy at
Concordia University
Montreal, Quebec, Canada.

June 1999

Volume II
Appendices and Computer Code

Appendix - A

Pressure vessels manufactured by Lincoln Composites (Brunswick Inc.)

Space Pressure Vessels						
Part Number	Minimum Volume (in³)	Diameter x Length (in)	MEOP (psig)	Minimum Burst Pressure (psig)	Maximum Weight (lbs)	Operating Medium
2200148-1	220	5.76 x 14.33	8,500	21,250	5.30	N_2
220130-1	260	5.0 x 18.03	3,750	11,700	3.50	N_2
220147-1	300	5.76 x 17.80	8,500	21,250	6.55	Silane
220135-1	340	6.63 x 14.5	4,000	8,000	4.50	N_2
220063	490	10.43 x 11.02	3,200	7,150	6.00	He, N_2, Air
220088-1	490	10.3 x 11.02	5,000	10,000	5.30	He, N_2, Air
220088-2	490	10.57 x 11.02	5,000	12,500	6.50	He, N_2, Air
220139-1	490	10.3 x 11.02	3,043	7,608	6.60	He, N_2, Air
220069	541	10.66 x 11.82	4,074	8,148	6.80	He, N2
220111	880	13.7 x 12.8	5,075	10,150	19.00	He, N_2, Air
220146-1	900	7.24 x 31.25	8,500	21,250	15.88	H_2, N_2
220144-1	1900	8.3 x 48.6	5,000	10,000	30.00	N_2
220074	2550	18.19 x 19.23	5,000	10,050	33.50	He, N_2, CO_2
220123-1	2650	13.2 x 25.38	4,200	6,300	16.60	He
220098	3010	18.71 x 19.18	4,000	6,000	20.05	He
220121-1	3010	13.02 x 34.5	4,000	6,000	17.05	He, Xenon
220136-1	3370	15.1 x 25.38	4,200	6,300	21.00	He
220134-1	4200	12.5 x 42.98	3,500	5,250	22.14	He, Xenon
220125-1	6000	13.3 x 52.88	4,500	9,000	48.20	He
220086-11	8181	26.13 x 26.31	4,000	6,000	72.50	He
220132-1	11,500	20.0 x 47.60	3,000	6,000	75.00	N_2
220122-1	14,212	20.6 x 56.5	3,726	7,500	90.40	He
220062	18,817	35.77 x 36.86	3,000	12,000	280.00	He
220126-2	31,600	24.0 x 78.44	300	450	43.40	$(NH_2)_2$, N_2O_4

Aircraft and Missile Pressure Vessels

Part Number	Minimum Volume (in^3)	Diameter x Length (in)	MEOP (psig)	Minimum Burst Pressure (psig)	Maximum Weight (lbs)	Operating Medium
220137-1	16	1.77 x 16.06	8,000	22,000	0.78	N$_2$
220133-1	30	2.75 x 10.37	10,000	20,000	0.97	N$_2$
220129-1	67	5.43 x 6.14	2,437	4,874	1.14	H$_2$
220128-1	91	5.79 x 7.65	8,485	16,970	2.27	N$_2$
220120-1	103	5.2 x 9.56	10,000	20,000	2.76	He
220120-2	103	5.25 x 9.71	10,000	24,200	2.98	He
220127-1	104	5.79 x 8.71	9,457	18,914	2.86	He
220060-44	175	5.07 x 17.23	4,200	9,337	7.6	N$_2$
220114-1	198	5.2 x 15.45	10,000	20,000	3.97	He
220060-41	249	5.50 x 19.06	4,000	8,900	7.85	N$_2$
220060-43	261	5.07 x 22.91	4,900	10,900	9.85	N$_2$
220060-42	305	7.12 x 16.31	5,000	11,100	10.98	N$_2$
220119-1	340	6.63 x 14.5	4,000	10,000	4.25	He, N$_2$, Air
220131-1	390	7.06 x 15.5	10,000	20,000	7.25	H$_2$
220007	435	5.01 x 28.78	3,000	7,200	6	N$_2$
220149-1	451	5.25 x 28.99	6,286	18,858	7.8	Air
220063	490	10.43 x 11.02	3,200	7,150	6	He, N$_2$, Air
220043	600	8.24 x 16.96	1,543	3,425	9.4	Air
220083-1	720	8.39 x 20.27	3,500	9,900	9.7	He
220083-2	720	8.63 x 20.27	3,500	14,000	16.76	He
220034	775	8.64 x 21.41	3,250	7,200	16.2	N$_2$
220035	775	8.50 x 21.90	3,080	7,700	9.8	N$_2$
220084	775	8.64 x 21.41	3,250	7,200	16.2	N$_2$
220068	1250	13.66 x 15.8	4,350	10,150	26.75	Air
220151-1	1906	8.52 x 44.30	6,286	18,858	26.8	Air
220140-1	4666	13.90 x 50.00	3,050	9,000	67.3	N$_2$

NGV Fuel Tanks
(thermoplastic liner)

Meets: ANSI/AGA NGV and DOT FMVSS 304 and / or CAN B51

3000 PSI / 207 BAR								
Size (O.D. x Length)		Weight		Water Volume		Gas Capacity	Gasoline Equivalent	
Inches	Millimeters	Lbs.	Kg.	Cu. In.	Liters	SCF**	Gallons***	Liters
13.7" x 35"	348 x 889	60	27.2	3362	55.5	504	4.1	15.5
13.7" x 40"	348 x 1016	68	30.9	3952	64.8	592	4.8	18.1
13.7" x 45"	348 x 1143	76	34.5	4542	74.4	681	5.5	20.8
13.7" x 55"	348 x 1397	93	42.2	5721	93.8	857	6.9	26.2
15.7" x 35"	399 x 889	73	33.1	4413	72.3	661	5.3	20.3
15.7" x 52"	399 x 1321	108	49.0	7089	116.2	1063	8.6	32.5
15.7" x 55"	399 x 1397	114	51.7	7562	123.9	1133	9.1	34.7

3600 PSI / 248 BAR								
Size (O.D. x Length)		Weight		Water Volume		Gas Capacity	Gasoline Equivalent	
Inches	Millimeters	Lbs.	Kg.	Cu. In.	Liters	SCF**	Gallons***	Liters
9.2" x 35"	234 x 889	38	16.8	1431	23.4	244	2.0	7.5
9.2" x 40"	234 x 1016	43	19.1	1666	27.3	284	2.3	8.7
9.2" x 64.5"	234 x 1638	68	30.9	2821	46.2	482	3.9	14.7
13.9" x 35"	353 x 889	65	29.5	3362	55.5	574	4.6	17.5
13.9" x 40"	353 x 1016	75	33.6	3952	64.8	675	5.4	20.6
13.9" x 45"	353 x 1143	84	38.1	4542	74.4	775	6.2	23.7
13.9" x 55"	353 x 1397	102	46.3	5721	93.8	977	7.9	29.8
13.9" x 82.5"	353 x 2095	153	69.4	8964	146.9	1530	12.3	46.7
15.9" x 35"	404 x 889	80	36.3	4413	72.3	753	6.1	23.0
15.9" x 39.5"	404 x 1003	93	42.2	5203	85.3	888	7.2	27.3
15.9" x 49.9"	404 x 1267	111	50.3	6591	108.0	1147	9.3	35.2
15.9" x 52"	404 x 1321	118	53.5	7089	116.2	1210	9.8	37.0
15.9" x 55"	404 x 1397	125	56.7	7562	123.9	1291	10.4	39.4
15.9" x 62"	404 x 1575	141	64.0	8664	142.0	1479	11.9	45.1
15.9" x 71"	404 x 1803	161	73.0	10081	165.2	1721	13.9	52.5
* 15.9" x 120"	404 x 3048	269	122.0	17387	284.9	3023	24.4	88.6
18.4" x 49.7"	467 x 1262	149	67.7	9135	149.7	1559	12.6	47.7
18.4" x 78.5"	467 x 1994	235	106.5	15027	246.3	2613	20.8	78.7
* 18.4" x 120"	467 x 3048	350	158.8	23944	392.4	4096	33.0	124.9

* 2" Valve Port

** Standard Cubic Feet. Natural gas capacity is based on a tank at service pressure filled with gas at a specific gravity of 0.60 and a temperature of 70°F.

*** Based on 124 SCF per equivalent gallon.

Appendix - B

Source Code Listing

```
Program Vessel;
{$F+}

uses
Overlay,Ovrstart,crt,dos,graph,alt_pick,ves_util,fstvideo,
editor,menus,glob_var,plotprop,compmath,GRAedit,failure,
alt_futl,alt_laye;

{$O plotprop}
{$O compmath}
{$O GRAedit}
{$O failure}
{$O menus}
{$O ves_util}
{$O editor}
{$O fstvideo}
{$O glob_var}
{$O dos}
{$O alt_pick}
{$O alt_futl}
{$O alt_laye}

{My overlays are the following (for reference):
-----------------------------------------------------
menus.tpu:
ves_util.tpu:
editor.tpu:
fstvideo.tpu:
glob_var.tpu:
compmath.tpu:
plotprop.tpu:
GRAedit.tpu:
Failure.tpu:
alt_pick.tpu:
alt_futil.tpu:
alt_laye.tpu: }


(*****************************************************)

Procedure Microcalc;

var
keyknown,specialkey,notskip:boolean;
```

```
label
flag2,jumpout2;

begin
  keyknown:=false;

Flag2:
  clrscr;
  mainmenu;
  repeat
  if not keyknown then Inkey(specialkey,ch,'s','o');

  case key of

    AltE:                {Switch to Edit menu}
      begin
      Alt_E;
      goto flag2;
      end;

    AltC:                {Switch to Calculate menu}
      begin
      Alt_C;
      goto flag2;
      end;

    AltL:                {switch to single layer menu}
      begin
      ALT_L;
      goto flag2;
      end;

    ALtU:                {switch to Utility Menu}
      begin
      ALT_U;
      goto flag2;
      end;

     AltX:               {exit and quit program}
      begin
      clrscr;
      goto jumpout2;
      end;
    end; {case}

  If not (Key In [AltE,AltC,ALTL,AltX,AltU,esc]) then
    begin
    GotoXY(58,2);
    textbackground(cyan);
    textcolor(red);
```

```
          beep(600,150);
          Write('Error-Inadmissible Key');
          delay(2000);
          GotoXY(58,2);
          Textbackground(black);
          Write('                        ');
          gotoxy(3,4);
          textcolor(yellow);
          notskip:=true;
          goto flag2;
          end; {main menu selection loop}
     until key = esc;
     jumpout2:
     end;


(******************** MAIN ********************)

Begin
Getscreentype(stype);
curser_off(stype);
currentfile:='Unknown';
backgroundchar:= 255;
FT := 'T';
begincurser := 'S';
lisence;
delay(8000);
{stiffness;}          {below currently only for IDE use}
{stiffinv;}
{thermo;}
mainmenu;
Microcalc;
textcolor(lightgray);  {sets back original DOS video colors}
textbackground(black);
clrscr;
end.
```

```
{$O+,F+}
Unit OvrStart;

(********************************************)

Interface
Uses Overlay;

Implementation

(********************************************)

Begin
OvrInit('ves_9.ovr');
OvrInitEMS;
If OvrResult= OvrNotFound then
  Begin
  Writeln('File vessel.OVR not found.');
  Halt;
  end;
end.
```

.

```
{$L-}
Unit fstvideo;

{$O+,F+}

(**********************************************)

interface

uses crt,dos,glob_var;


Procedure GetScreenType(var stype : char);


Procedure Fastwrite(x,y:byte;
                         S: string;
                         fg,bg:byte);

Procedure Center(y:integer;s:string;fg,
                    bg:integer;stype:char);

Procedure DrawScreen;

Procedure FastBox(x1,y1,x2,y2,fg,bg:byte);

(**********************************************)

implementation

(**********************************************)

Procedure GetScreenType(var stype : char);
Var
  Regs : Registers;
Begin
Regs.AH := $0F;
Intr($10,Regs);
If Regs.AL = 7 then
  stype := 'M'
else
  stype :='C';
end;

(**********************************************)

   Procedure Fastwrite(x,y:byte;
                         S: string;
                         fg,bg:byte);
   var
```

544

```pascal
  w:word;
  i,ColAtr:byte;

Begin
ColAtr:= (bg Shl 4)+fg;    (*create atribute byte*)
w:= ((y-1)*80+(x-1))*2;    (*calculate offset*)

For i:=1 to length(s) do
  begin
  MemW[$B800:w]:=(Colatr Shl 8)+ord(s[i]);
  inc(w,2);
  end;
end;

(********************************************)

Procedure Center(y:integer;s:string;fg,
                 bg:integer;stype:char);

var
  x:integer;

  begin
  x:=40-(length(s) div 2);
  Fastwrite(x,y,s,fg,bg);
  end;

(**********************************************)

Procedure DrawScreen;
  Var
     e: integer;
  Begin
  TextColor(red);
  TextBackground(black);
  ClrScr;
  For e:=2 to 79 do
     Begin
     GotoXY(e,1);Write('-');
     GotoXY(e,25);Write('-');
     GotoXY(e,3);Write('-');
     GotoXY(e,23);Write('-');
        If e<25 Then
        Begin
        GotoXY(1,e);Write('¦');
        GotoXY(80,e);Write('¦');
        End;
     End;
  GotoXY(1,1); Write('+');
  GotoXY(80,1); Write('+');
```

```pascal
     GotoXY(1,25); Write('+');
     GotoXY(1,3); Write('|');
     GotoXY(80,3); Write('|');
     GotoXY(1,23); Write('|');
     GotoXY(80,23); Write('|');
     Fastwrite(80,25,#188,red,black); { allows + without
                                               scrolling }
     TextColor(white);
     GotoXY(25,2);
     Write('Super Pressure - Vessel Designer');
     End;


(************************************************)

Procedure FastBox(x1,y1,x2,y2,fg,bg:byte);
var
  i: byte;
  s:string[1];
begin
Textcolor(fg);
TextBackground(bg);
s:= #205;                         {character that gets written}
for i:=(x1+1) to (x2-1) do
  begin
  fastwrite(i,y1,s,fg,bg);
  Fastwrite(i,y2,s,fg,bg);
  end;
s:= #186;
For i:= (y1+1) to (y2-1) do
  begin
  Fastwrite(x1,i,s,fg,bg);
  Fastwrite(x2,i,s,fg,bg);
  end;
s:= #201;
Fastwrite(x1,y1,s,fg,bg);
s:= #187;
Fastwrite(x2,y1,s,fg,bg);
s:= #200;
Fastwrite(x1,y2,s,fg,bg);
s:= #188;
Fastwrite(x2,y2,s,fg,bg);
end;


(************************************************)

end.{unit}
```

```
{$L-}
Unit Glob_var;
{$O+,F+}


(*********************************************)

interface

const
  np=2;
  mp=3;
  NL=15;        {no. of layers}
  nfe=19;         {no. of finite elements}
Type
  realarray1NL = array[1..NL] of real;
  integerarray16 = array [1..16] of integer;
  IntegerarrayNL = array [1..NL] of integer;
  layerarrayNL =array[1..NL] of string;
  realarrayNL3 = array[1..NL,1..NL,1..NL] of real;
  asciiArray = array[1..18] of string;
  realarrayNLby2by2 = array[1..NL,1..2,1..2] of real;
  realArrayNL = array [0..NL] of real;
  realArrayNL1 =array[0..NL+1] of real;
  realArrayNLbyNL = array[0..NL,0..NL] of real;
  realArray6X6 = array[1..6,1..6] of real;
  realarray16X2 = array[0..16,1..2] of real;
  realarray9X2NL = array[1..9,1..2*NL] of real;
  realarray2NL = array[1..2*NL] of real;
  realarrayNP = array[1..np] of real;
  realarrayMP = array[1..mp] of real;
  realarrayMPbyNP = array[1..mp,1..np] of real;
  Integerarray9 = array[1..9] of integer;
  ary = array[1..5,1..14] of string[26];
  ary1 = array [1..6,1..6] of string[14];
  realarrayNLbyNL2 = array[1..NL,1..NL,1..NL] of real;
  realarrayNLby3 = array[1..nl,1..3] of real;
  stringarray3 = array[1..3] of string[7];
  StringArray5by16 = array[1..5,1..16] of string[20];
  realArrayNLX6X6 = array[1..NL,1..6,1..6] of real;
  realarray4 = array[1..4] of real;
  realarray3 = array[1..3] of real;
  realarray8 = array[1..8] of real;
  realarray2plusN = array[0..nfe+1] of real;
  realarray3NL = array[1..3*NL] of real;
  realarrayNLby2 = array[1..NL,1..2] of real;
  dir_files = array[1..200] of string[13];
  mask_names = array[1..8] of string[5];
  text_files = array[1..3] of text;
  filelines = array[1..282] of string[80];
```

```
      elasticCon = record El,Et,Vl,Vt,Gl,Gt,KK:real;end;
      Econst = array[1..NL] of elasticCon;
      strength = record XT,XC,YT,YC,SS,GL:real;end;
      streng = array[1..NL] of strength;
      approx = record l,m,d,i,j,k,G11,G12,G22,
                        a13,a23,a33:real;end;
      datapoint = record symbol:string;xydata:realarray16X2;end;
      buildup = record Matname,angle,fpercent,
                        thickness:string;end;
      dtapts = array[1..9] of datapoint;
      layermat = array[1..NL] of buildup;
      Keys = (nullkey,f1,f2,f3,f4,f5,f6,f7,f8,f9,f10,
              carriageReturn,tab,shiftTab,bksp,uparrow,
              downArrow,rightArrow,leftArrow,deleteKey,
              insertKey,homeKey,esc,endKey,textKey,
              NumberKey,space,PgUp,PgDn,alts,altx,altc,
              alte,altr,altm,altf,altn,Altd,altb,altv,
              alto,altl,altw,altj,altp,altu,alti);


  {global variables}
     Var
       BeginCurser, EndCurser : char;
       VM,QP,Delta,CV,X1,G,A,C,R,K,Brr,Brf,Bff,
       Si,Vrf,Vfz,Azz,Arz,Afz,Dt:RealarrayNL;
       D:RealarrayNL1;
       SEf,SEm,Sff,SE22:realarray1NL;
       outerlayer:integer;
       xx:integer; {for windows input call}
       Ttotal,FI,InsidePress,OuterPress,ExtForce,
       Wallthick,insideDia,outsideDia: real;
       bfit_store:realarrayNLby3;
       Matrix:realarrayNLbyNL;
       lq,la,lstif:realArrayNLX6X6;
       lb:realArrayNLby2by2;
       failR:realarrayNLby2;
       graphdata:dtapts;
       strg:streng;
       Elconst:Econst;
       graphlabels:layermat;
       plotr,plota:realarray2NL;
       SumC,SumB,ymatrix,Q,CC:realarray6X6;
       cursx,cursy:integer;
       globalK,int_r0,int_z0,int_f0,scalefactor:real;
       holdstr:StringArray5by16;
       vs:word;
       windowlength,maxlength,x,y,backgroundchar:integer;
       ft:char;
       s,currentfile,Ipress,scalef,Filespec:string;
       i,fc:integer;
```

```
        df:dir_files;
        key:keys;
        ch:char;
        stype:char;
        Bfit:approx;
        graphstate:boolean;


(*********************************************)

implementation

end.
```

```
Unit Menus;
{$O+,F+}

(***********************************************)

interface

uses glob_var;

procedure mainmenu;
Procedure Lisence;
procedure editmenu;
procedure utilmenu;
procedure calcmenu;
procedure varplotmenu;
procedure layermenu;
Procedure discretemenu;
procedure inputdesc11(var desc:ary);
procedure inputdesc3(var desc:ary);
procedure inputdesc4(var desc:ary);
Procedure
InputDescTable(ox,oy,nx,ny,wix,sy,sc,wdx,sdi,tabno:integer);
Procedure Rotdesc(var adesc:ary1 ;var qdesc:ary1; var
Amatrix,Qmatrix:realarray6x6);
ProcedureRotDescTable(ox,oy,nx,ny,wix,sy,
                                          sc,wdx,sdi:integer);
Procedure MicroDesc(var Qmatdes,Cmatdes: ary1);
Procedure
OutputDescTable(ox,oy,nx,ny,wix,sy,sc,wdx,sdi:integer;var
                                          Qstor,Cstor:realarray6X6);
Procedure MicroResult;

(***********************************************)

implementation
uses dos,crt,fstvideo,ves_util;

(***********************************************)

Procedure Lisence;

begin
ClrScr;
Drawscreen;
fastbox(20,8,60,13,white,blue);
center(9,'Development & Test Version',green,black,stype);
center(10,'April, 1999',cyan,black,stype);
center(11,'Loaned to S.V. Hoa',green,black,stype);
center(12,'Copywrite 1999 Greg Rohrauer',cyan,black,stype);
end;
```

```
(*****************************************************)

Procedure Mainmenu;

Begin
ClrScr;
Drawscreen;
center(3,' Main Menu ',11,0,stype);
TextColor(yellow);
GotoXY(4,24);
Write('ALT+    Edit files      Calculate      1 Layer
                                  Utilities        eXit');
TextColor(white);
GotoXY(4,24);
Write('ALT+');
GotoXY(12,24);
Write('E');
GotoXY(29,24);
Write('');
GotoXY(28,24);
Write('C');
gotoXY(44,24);
Write('L');
GotoXY(56,24);
Write('U');
GotoXY(73,24);
write('X');
Textbackground(lightblue);
GotoXY(3,4);
TextColor(yellow);
end;


(*****************************************************)

Procedure Utilmenu;

Begin
ClrScr;
Drawscreen;
center(3,' Utility Menu ',11,0,stype);
TextColor(yellow);
GotoXY(4,24);
Write('ALT+        New         Del        Rename
                                  View           eXit');
TextColor(white);
GotoXY(4,24);
Write('ALT+');
GotoXY(15,24);
Write('N');
```

551

```
GotoXY(28,24);
Write('D');
GotoXY(41,24);
Write('R');
GotoXY(56,24);
Write('V');
GotoXY(71,24);
write('X');
Textbackground(lightblue);
GotoXY(3,4);
TextColor(yellow);
end;


(**********************************************)


Procedure editmenu;

Begin
ClrScr;
Drawscreen;
center(3,' File Editor Menu ',11,0,stype);
TextColor(yellow);
GotoXY(3,24);
Write('ALT+      Lam'+char(26)+'Mat        Mat'+char(26)+'Lam
                    Wall      Press      Build      eXit');
TextColor(white);
GotoXY(3,24);
Write('ALT+');
GotoXY(12,24);
Write('L');
GotoXY(25,24);
Write('M');
GotoXY(39,24);
write('W');
GotoXY(49,24);
write('P');
GotoXY(60,24);
write('B');
GotoXY(72,24);
Write('X');
Textbackground(lightblue);
GotoXY(3,4);
TextColor(yellow);
end;


(**********************************************)


Procedure Calcmenu;

Begin
```

```
ClrScr;
Drawscreen;
center(3,' Main Calculate Menu ',11,0,stype);
TextColor(yellow);
GotoXY(4,24);
Write('ALT+      Stiff-Mtx      Vari-wall      Multi-layer
                                Fit-mat      eXit');
TextColor(white);
GotoXY(4,24);
Write('ALT+');
GotoXY(13,24);
Write('S');
GotoXY(28,24);
Write('V');
GotoXY(43,24);
Write('M');
GotoXY(60,24);
write('F');
GotoXY(73,24);
Write('X');
Textbackground(lightblue);
GotoXY(3,4);
TextColor(yellow);
end;


(***********************************************)


Procedure Varplotmenu;

Begin
ClrScr;
Drawscreen;
center(3,' Variable Property Models ',11,0,stype);
TextColor(yellow);
GotoXY(4,24);
Write('ALT+    1V(A-Free)     1V(A-Restrain)     3V(N-Restrain)
                                6V(N-F/C)    eXit ');
TextColor(white);
GotoXY(4,24);
Write('ALT+');
GotoXY(16,24);
Write('F');
GotoXY(30,24);
Write('R');
GotoXY(46,24);
Write('N');
GotoXY(68,24);
Write('C');
GotoXY(74,24);
Write('X');
```

```
Textbackground(lightblue);
GotoXY(3,4);
TextColor(yellow);
end;


(*************************************************)

Procedure LayerMenu;

Begin
ClrScr;
Drawscreen;
center(3,' Layer Calculate Menu ',11,0,stype);
TextColor(yellow);
GotoXY(4,24);
Write('ALT+          Rotate layer          Calculate layer          Load
                                        layer          eXit ');
TextColor(white);
GotoXY(4,24);
Write('ALT+');
GotoXY(14,24);
Write('R');
GotoXY(32,24);
Write('C');
GotoXY(53,24);
Write('L');
GotoXY(70,24);
Write('X');
Textbackground(lightblue);
GotoXY(3,4);
TextColor(yellow);
end;


(*************************************************)

Procedure discretemenu;

Begin
ClrScr;
Drawscreen;
center(3,' Discrete Method Selection Menu ',11,0,stype);
TextColor(yellow);
GotoXY(4,24);
Write('ALT+         Partial eqns          Full eqns     +     Non-
                                        linear Shear       eXit ');
TextColor(white);
GotoXY(4,24);
Write('ALT+');
GotoXY(14,24);
```

```
Write('P');
GotoXY(32,24);
Write('F');
GotoXY(72,24);
GotoXY(50,24);
Write('N');
GotoXY(72,24);
Write('X');
Textbackground(lightblue);
GotoXY(3,4);
TextColor(yellow);
end;


(********************************************)


Procedure InputDesc11(var desc: ary);   {for .lam input file}


begin


desc[1,1]:= 'Modulus E11        (GPa)';
desc[1,2]:= 'Poisson V12       (ratio)';
desc[1,3]:= 'Modulus G12       (ratio)';
desc[1,4]:= '* Modulus E22 *    (GPa)';
desc[1,5]:= '* Poisson V23 *   (ratio)';
desc[1,6]:= '* Modulus G23 *    (GPa)';
desc[1,7]:= '* Modulus K23 *    (GPa)';
desc[1,8]:= 'Matrix Modulus E   (GPa)';
desc[1,9]:= 'Matrix Poisson V (ratio)';
desc[2,1]:= 'L. Tens. Strength  (MPa)';
desc[2,2]:= 'L. Comp. Strength  (MPa)';
desc[2,3]:= 'T. Tens. Strength  (MPa)';
desc[2,4]:= 'T. Comp. Strength  (MPa)';
desc[2,5]:= 'L. Shear Strength  (MPa)';
desc[2,6]:= 'Fiber Vol. Fraction  (%)';
desc[2,7]:= 'Fiber Model <T-iso><iso>';
desc[2,8]:= 'Fit E12 & G12  <Yes><No>';
desc[2,9]:= 'Metal ?        <Yes><No>';


end;


(********************************************)


Procedure InputDesc12(var desc: ary); {fiber properties in
                                               .mat}


begin


desc[1,1]:= 'Fib. Modulus E1     (GPa)';
desc[1,2]:= 'Fib. Poisson V1   (ratio)';
desc[1,3]:= 'Fib. Shear   G1     (GPa)';
```

555

```
desc[1,4]:= '* F. Modulus Et *   (GPa)';
desc[1,5]:= '* F. Poisson Vt * (ratio)';
desc[1,6]:= '* F. Shear   Gt *   (GPa)';
desc[1,7]:= '* F. Modulus Kt *   (GPa)';
desc[1,8]:= 'Matrix Modulus Em   (GPa)';
desc[1,9]:= 'Matrix Poisson Vm (ratio)';
desc[2,1]:= 'L. Tens. Strength   (MPa)';
desc[2,2]:= 'L. Comp. Strength   (MPa)';
desc[2,3]:= 'T. Tens. Strength   (MPa)';
desc[2,4]:= 'T. Comp. Strength   (MPa)';
desc[2,5]:= 'Shear Strength      (MPa)';
desc[2,6]:= 'Fiber Volume Fraction (%)';
desc[2,7]:= 'Fiber Model  <T-iso><iso>';
desc[2,8]:= 'Fit E12 & G12   <Yes><No>';
desc[2,9]:= 'Metal ?         <Yes><No>';

end;


(**************************************************)


Procedure InputDesc3(var desc: ary);

begin

desc[1,1]:= 'Layer';
desc[1,2]:= ' (#)';
desc[2,1]:= '   Material';
desc[2,2]:= '  (filename)';
desc[3,1]:= '    Angle';
desc[3,2]:= '    (+/-)'+char(248);
desc[4,1]:= ' Thickness';
desc[4,2]:= '     (mm)';
desc[5,1]:= ' Fiber Volume';
desc[5,2]:= '  (percent)';
end;


(**************************************************)


Procedure InputDesc1(var desc: ary);

begin

desc[1,1]:= 'Load   (.lds)  input file:';
desc[1,2]:= 'Wall   (.wal)  input file:';
desc[1,3]:= 'Vessel (.ves) output file:';
end;


(**************************************************)
```

```
Procedure InputDesc4(var desc: ary);

begin
desc[1,1]:= 'Inside diameter   (mm)';
desc[1,2]:= 'Wall thickness    (mm)';
desc[1,3]:= 'Internal press. (MPa)';
desc[1,4]:= 'External press. (MPa)';

end;

(*************************************************)

Procedure
InputDescTable(ox,oy,nx,ny,wix,sy,sc,wdx,sdi,tabno:integer);
{ ox = offset x  , starting location
  oy = offset y  , starting location
  nx = number of collums in x direction
  ny = number of rows in y direction
  wix = width of input in x direction
  sy = spacing of rows in y direction
  sc = space between collums
  wdx = width of description in x direction
  sdi = spacing between description and input collum
  tabno = input description table number}

var
  x,y,w,oxx,oyy:integer;
  desc: ary;
  omit: boolean;

begin
oxx:=0;
oyy:=0;
omit:=false;
case tabno of

 1:begin
   inputdesc1(desc);
   end;

 3:begin
   inputdesc3(desc);
   center(oy-3,'Wall Construction',10,0,stype);
   omit:=true;
   end;

 4:begin
   inputdesc4(desc);
   center(oy-3,'Pressures & Dimensions',10,0,stype);
   end;
```

```pascal
    11,12:begin
       inputdesc11(desc);
       center(oy-2,'Lamina Properties',10,0,stype);
       end;

    13:begin
       inputdesc12(desc);
       center(oy-2,'Fiber & Matrix Properties',10,0,stype);
       end;

  end {case};
     for x:=1 to nx do
       begin
       for y:=1 to ny do
         begin
         if x=1 then oyy :=oy;
         if y=1 then oxx :=ox;
           if not omit then
           begin
            textcolor(yellow);
            GotoXY(oxx-wdx-sdi-wix-sc+x*(wdx+
                                wix+sdi+sc),oyy+(y-1)*sy);
            write(desc[x,y]);    {input description}
           end; {if not omit}
           if omit then
           begin
             if (y <= 2) and (x <= 5) then
             begin
              Textcolor(yellow);
              Textbackground(black);
              GotoXY(x*14-8,y+3);
              write(desc[x,y]);    {input description}
             end; {if y less than 2}
           end; {if omit}

       end; {y-loop}
     end;  {x-loop}

       cursx:=ox+wdx+sdi;
       cursy:=oy;
end;    {procedure}

(*****************************************************)


Procedure Rotdesc(var adesc:ary1 ;var qdesc:ary1; var
                                Amatrix,Qmatrix:realarray6x6);

var
```

```
    i,j,lno:integer;

    begin
    lno:=1;
    for i:=1 to 6 do
    for j:=1 to 6 do
        begin
        Amatrix[i,j]:= 0;
        Qmatrix[i,j]:= 0;
        end;

Amatrix[1,1] := la[1,1,1];
Amatrix[1,2] := la[1,1,2];
Amatrix[1,3] := la[1,1,3];
Amatrix[1,4] := la[1,1,4];
Amatrix[2,1] := la[1,1,2];
Amatrix[2,2] := la[1,2,2];
Amatrix[2,3] := la[1,2,3];
Amatrix[2,4] := la[1,2,4];
Amatrix[3,1] := la[1,1,3];
Amatrix[3,2] := la[1,2,3];
Amatrix[3,3] := la[1,3,3];
Amatrix[3,4] := la[1,3,4];
Amatrix[4,1] := la[1,1,4];
Amatrix[4,2] := la[1,2,4];
Amatrix[4,3] := la[1,3,4];
Amatrix[4,4] := la[1,4,4];
Amatrix[5,5] := la[1,5,5];
Amatrix[6,6] := la[1,6,6];
Amatrix[5,6] := la[1,6,5];
Amatrix[6,5] := la[1,6,5];

Qmatrix[1,1] := lq[1,1,1];
Qmatrix[1,2] := lq[1,1,2];
Qmatrix[1,3] := lq[1,1,3];
Qmatrix[1,4] := lq[1,1,4];
Qmatrix[2,1] := lq[1,1,2];
Qmatrix[2,2] := lq[1,2,2];
Qmatrix[2,3] := lq[1,2,3];
Qmatrix[2,4] := lq[1,2,4];
Qmatrix[3,1] := lq[1,1,3];
Qmatrix[3,2] := lq[1,2,3];
Qmatrix[3,3] := lq[1,3,3];
Qmatrix[3,4] := lq[1,3,4];
Qmatrix[4,1] := lq[1,1,4];
Qmatrix[4,2] := lq[1,2,4];
Qmatrix[4,3] := lq[1,3,4];
Qmatrix[4,4] := lq[1,4,4];
Qmatrix[5,5] := lq[1,5,5];
Qmatrix[6,6] := lq[1,6,6];
```

```
Qmatrix[5,6] := lq[1,6,5];
Qmatrix[6,5] := lq[1,6,5];

  adesc[1,1] := 'arr';
  adesc[2,2] := 'a'+char(233)+char(233);
  adesc[3,3] := 'azz';
  adesc[4,4] := 'a'+char(233)+'z';
  adesc[5,5] := 'arz';
  adesc[6,6] := 'ar'+char(233);
  adesc[1,2] := 'a'+char(233)+'r';
  adesc[1,3] := 'azr';
  adesc[2,3] := 'az'+char(233);
  adesc[2,1] := 'ar'+char(233);
  adesc[3,1] := 'arz';
  adesc[3,2] := 'a'+char(233)+'z';

  qdesc[1,1] := 'arr';
  qdesc[2,2] := 'a'+char(233)+char(233);
  qdesc[3,3] := 'azz';
  qdesc[4,4] := 'a'+char(233)+'z';
  qdesc[5,5] := 'arz';
  qdesc[6,6] := 'ar'+char(233);
  qdesc[1,2] := 'a'+char(233)+'r';
  qdesc[1,3] := 'azr';
  qdesc[2,3] := 'az'+char(233);
  qdesc[2,1] := 'ar'+char(233);
  qdesc[3,1] := 'arz';
  qdesc[3,2] := 'a'+char(233)+'z';

  end;


(*******************************************************)

Procedure
RotDescTable(ox,oy,nx,ny,wix,sy,sc,wdx,sdi:integer);

var
  x,y,w,oxx,oyy:integer;
  adesc,qdesc: aryl;
  dum:string;
  transk:real;
  Amatrix,Qmatrix:realarray6X6;
begin
oxx:=0;
oyy:=0;
Rotdesc(adesc,qdesc,Amatrix,Qmatrix);
  for x:=1 to nx do
    for y:=1 to ny do
      begin
      if x=1 then oyy :=oy;
```

560

```
if y=1 then oxx :=ox;

GotoXY(oxx-wdx-sdi-wix-sc+x*(wdx+wix+sdi+sc),
                                        oyy+(y-1)*sy);
Textcolor(blue);
if abs(qmatrix[y,x]) > 1E-10 then
   begin
      if (x=4)and(y<x) or (y=4)and(x<y) or (x+y=11) then
      textbackground(Magenta)
      else
      textbackground(lightgray);
    write(qdesc[x,y]);    {rotated stiffness matrix}
    end
   else
    begin
    textbackground(black);
    write('    ');
   end;                     {if then else}

GotoXY(oxx-wix-sc+x*(sdi+wdx+wix+sc),oyy+(y-1)*sy);
Textbackground(black);
Textcolor(lightcyan);
if abs(qmatrix[y,x]) > 1E-10 then
   begin
   write(qmatrix[y,x]:6:2); {stiffness}   {put qmatrix
                                           when done}

    end
   else
    begin
    write('        ');
   end;                     {if then else}

GotoXY(oxx-wdx-sdi-wix-sc+x*(wdx+wix+sdi+sc),
                                        9+oyy+(y-1)*sy);
Textcolor(blue);
TextBackground(lightgray);
if abs(amatrix[y,x]) > 1E-10 then
   begin
      if (x=4)and(y<x) or (y=4)and(x<y) or (x+y=11) then
      textbackground(Magenta)
      else
      textbackground(lightgray);
    write(adesc[x,y]);    {rotated compliance matrix}
    end
   else
    begin
    textbackground(black);
    write('    ');
   end;                     {if then else}
```

```
            GotoXY(oxx-wix-sc+x*(sdi+wdx+wix+sc),9+oyy+(y-1)*sy);
            Textbackground(black);
            Textcolor(lightcyan);
            if abs(amatrix[y,x]) > 1E-10 then
              begin
              write(1000*amatrix[y,x]:6:2);{compliance}
              end
             else
              begin
              write('            ');
             end;                    {if then else}
            end;                     {for}
            center(5,'
                                                 ',9,0,stype);
            Center(5,'Stiffness Matrix (GPa)',9,0,stype);
            center(14,'
                                                 ',9,0,stype);
            Center(14,'Compliance Matrix (1/TPa)',9,0,stype);
            curser_off(stype);
            transK:=sqrt((la[1,1,1]-
                         sqr(la[1,1,3])/la[1,3,3])/(la[1,2,2]-
                                  sqr(la[1,2,3])/la[1,3,3]));
            str(transk:5:4,dum);
            center(22,'
                                                 ',9,0,stype);
            Center(22,'"Avoidance factor" K is: '+dum,9,0,stype);
            textcolor(blue);
            textbackground(lightgray);
            GotoXY(66,2);
            write(char(241)+'angle plies');
            textbackground(black);
            textcolor(lightcyan);
            Gotoxy(66,4);
            write('r = radial');
            Gotoxy(66,5);
            write(char(233)+' = hoop');
            gotoxy(66,6);
            write('z = axial');
   end;    {procedure}


(********************************************)


Procedure MicroDesc(var Qmatdes,Cmatdes: ary1);
var i,j:integer;

begin
for i:=1 to 6 do
for j:=1 to 6 do
  begin
  Qmatdes[i,j]:= '';
```

```
      Cmatdes[i,j]:= '';    {makes sure that matrix is empty}
    end;

  Qmatdes[1,1]:= 'Arr';
  Qmatdes[2,1]:= 'Ar'+char(233);
  Qmatdes[3,1]:= 'Arz';
  Qmatdes[1,2]:= 'A'+char(233)+'r';
  Qmatdes[2,2]:= 'A'+char(233)+char(233);
  Qmatdes[3,2]:= 'A'+char(233)+'z';
  Qmatdes[1,3]:= 'Azr';
  Qmatdes[2,3]:= 'Az'+char(233);
  Qmatdes[3,3]:= 'Azz';
  Qmatdes[4,4]:= 'A'+char(233)+'z';
  Qmatdes[5,5]:= 'Arz';
  Qmatdes[6,6]:= 'Ar'+char(233);

  Cmatdes[1,1]:= 'arr';
  Cmatdes[2,1]:= 'ar'+char(233);
  Cmatdes[3,1]:= 'arz';
  Cmatdes[1,2]:= 'a'+char(233)+'r';
  Cmatdes[2,2]:= 'a'+char(233)+char(233);
  Cmatdes[3,2]:= 'a'+char(233)+'z';
  Cmatdes[1,3]:= 'azr';
  Cmatdes[2,3]:= 'az'+char(233);
  Cmatdes[3,3]:= 'azz';
  Cmatdes[4,4]:= 'a'+char(233)+'z';
  Cmatdes[5,5]:= 'arz';
  Cmatdes[6,6]:= 'ar'+char(233);

  end;


(*********************************************)

Procedure
OutputDescTable(ox,oy,nx,ny,wix,sy,sc,wdx,sdi:integer;var
Qstor,Cstor:realarray6X6);
{ ox = offset x  , starting location
  oy = offset y  , starting location
  nx = number of collums in x direction
  ny = number of rows in y direction
  wix = width of input in x direction
  sy = spacing of rows in y direction
  sc = space between collums
  wdx = width of description in x direction
  sdi = spacing between description and input collum }

var
  x,y,w,oxx,oyy,i:integer;
  Qmatdes,Cmatdes: ary1;
```

563

```
begin
oxx:=0;
oyy:=0;
microdesc(Qmatdes,Cmatdes);
   for x:=1 to nx do
     for y:=1 to ny do
       begin
       if x=1 then oyy :=oy;
       if y=1 then oxx :=ox;
       GotoXY(oxx-wdx-sdi-wix-sc+x*(wdx+wix+sdi+sc),oyy+(y-
                                                      1)*sy);
       Textcolor(blue);
       Textbackground(lightgray);
         write(Qmatdes[x,y]);      {output description}
       GotoXY(oxx-wix-sc+x*(sdi+wdx+wix+sc),oyy+(y-1)*sy);
       Textbackground(black);
       Textcolor(lightcyan);
       if (x<4) and (y<4) or (x=y) then
         write(Qstor[y,x]:6:2);
       GotoXY(oxx-wdx-sdi-wix-sc+x*(wdx+wix+sdi+sc),9+oyy+(y-
                                                      1)*sy);
       Textbackground(lightgray);
       Textcolor(blue);
         write(Cmatdes[x,y]);
       if (x<4) and (y<4) or (x=y) then
       begin
       GotoXY(oxx-wix-sc+x*(sdi+wdx+wix+sc),9+oyy+(y-1)*sy);
       Textbackground(black);
       Textcolor(lightcyan);
         write(1000*Cstor[y,x]:6:2);
       end;
       end;
       Center(5,'Stiffness Matrix (GPa)',9,0,stype);
       Center(14,'Compliance Matrix (1/TPa)',9,0,stype);
       Curser_off(stype);
       textbackground(black);
       textcolor(lightcyan);
       Gotoxy(66,4);
       write('r = radial');
       Gotoxy(66,5);
       write(char(233)+' = hoop');
       gotoxy(66,6);
       write('z = axial');


end;    {procedure}

(*****************************************************)
```

```
Procedure MicroResult;

var
Qstor,Cstor:realarray6X6;
i,j:integer;
transk: real;
dum:string;

begin
for i:=1 to 6 do
for j:=1 to 6 do
  begin
  Qstor[i,j]:=Q[i,j];
  Cstor[i,j]:=CC[i,j];
end;


Qstor[1,1]:= Q[3,3];
Qstor[3,3]:= Q[1,1];
Qstor[1,2]:= Q[3,2];
Qstor[1,3]:= Q[3,1];
Qstor[2,3]:= Q[2,1];
Qstor[2,1]:= Q[2,3];
Qstor[3,1]:= Q[1,3];
Qstor[3,2]:= Q[1,2];
Qstor[4,4]:= Q[6,6];
Qstor[6,6]:= Q[4,4];


Cstor[1,1]:= CC[3,3];
Cstor[3,3]:= CC[1,1];
Cstor[1,2]:= CC[3,2];
Cstor[1,3]:= CC[3,1];
Cstor[2,3]:= CC[2,1];
Cstor[2,1]:= CC[2,3];
Cstor[3,1]:= CC[1,3];
Cstor[3,2]:= CC[1,2];
Cstor[4,4]:= CC[6,6];
Cstor[6,6]:= CC[4,4];

OutputDescTable(3,7,6,6,7,1,2,3,1,Qstor,Cstor);

Center(22,'"Avoidance factor" K is: 1.0000',9,0,stype);

end;

(**************************************************)

end. {unit}
```

```
Unit Editor;
{$O+,F+}


(**************************************************)

interface

uses glob_var;

Procedure InputEdit(var s: string;
                    var mask:mask_names;
                    new:boolean;
                    sty:integer;
                    var npickf,lpickf,filn:integer;
                    var abandon:boolean;
                    windowlength,
                    maxlength,
                    x,y:integer;
                    FT:char;

   backgroundchar,ox,oy,nx,ny,wix,sy,sc,wdx,sdi:integer);

Procedure
MoveEditWindow(mask:mask_names;new:boolean;ft:char;sty,ox,oy
,nx,ny,wix,sy,sc,wdx,sdi:integer;var notskip,abdon:boolean);

(**************************************************)

implementation

uses dos,crt,fstvideo,ves_util,menus;

(**************************************************)

Procedure InputEdit(var s:string;
                    var mask:mask_names;
                    new:boolean;
                    sty:integer;
                    var npickf,lpickf,filn:integer;
                    var abandon:boolean;
                    windowlength,
                    maxlength,
                    x,y:integer;
                    FT:char;

   backgroundchar,ox,oy,nx,ny,wix,sy,sc,wdx,sdi:integer);

var
   xx,i,j,p,fx,fy,tx,ty: integer;
   ch: char;
```

```pascal
    insertOn,specialkey: boolean;
    offset,fcount: integer;
    tempstr,wfile,filename: String;
    dirf:dir_files;

  label
    flag_out;

(********************************************)

Procedure XY(x,y:integer);           {for multiple lines}
  var
    Xsmall : integer;
  begin
    repeat
      xsmall := x-80;
      if xsmall > 0 then
        begin
          y := y+1;
          x := xsmall;
        end;
    until Xsmall <= 0;
    GotoXY(x,y);
  end;

(*******************************************************)

Procedure Setstring(ox,oy,nx,ny,wix,sy,
                         sc,wdx,sdi:integer);
  var
    i,rx,ry: integer;
  begin
    i:=length(s);  {eliminates trailing bkground char and
                                                     spaces}
    while(s[i]=char(backgroundchar))or(s[i]=char(32)) do
      i:= i-1;
    s[0] := char(i);

    rx:=(x-ox+wix+sc)div(wdx+wix+sc+sdi);
    ry:=(y-oy+sy)div(sy);
    holdstr[rx,ry]:=s;

    curser_small(stype);
  end;

(*******************************************************)

  begin
    offset:=1;
```

567

```
if (x=ox+wdx+sdi) and (y=oy) then   {makes an imported
                                     file immediately visible}
begin
for tx:=1 to nx do
  for ty:= 1 to ny do
  begin
  fx:=x+(tx-1)*(wix+sc+wdx+sdi);
  fy:=y+(ty-1)*sy;
  s:= holdstr[tx,ty];
  tempstr := copy(s,offset,windowlength);
  fastwrite(fx,fy,tempstr,white,black);
  end;
end;

fx:=(x-ox+wix+sc)div(wdx+wix+sc+sdi); {x & y are
          changed by arrow keys, other constants just
                                  provide correct offsets}
fy:=(y-oy+sy)div(sy);
s:=holdstr[fx,fy];

if mask[1] <> 'off' then
begin
  sortdirlist(mask,dirf,fcount);
  displayfiles(filename,filn,sty,npickf,dirf,fcount);
end;

j:= length(s)+1;
for i:=j to maxlength do
  s[i] := char(backgroundchar);
s[0] := char(maxlength);
Tempstr:= copy(s,1,windowlength);

p:=1;
offset:=1;
insertOn:=true;

  repeat
  xx:= x+(p-offset);        {x-position is incremented}
  If (p-offset) = windowlength then
  xx:=xx-1;

  XY(xx,y);

  if insertOn then
    inkey(specialkey,ch,'S','O')
  else
    inKey(specialkey,ch,'B','O');

   If (FT = 'N') then
    begin
```

```
      if (key = textkey) then
        begin
        beep(100,250);
        key := nullkey;
        end
      else if (ch = '-')and((p>1)or(s[1] = '-')) then
        begin
        beep(100,250);
        key:= nullkey;
        end
      else if (ch = '.') then
        begin
        if not((pos('.',s)=0) or (pos('.',s) = p)) then
        begin
        beep(100,250);
        key:=nullkey;
        end
      else if (pos('.',s) = p) then
        delete(s,p,1);
        end;
      end;

  case key of

    numberkey,space,textkey:
      begin
      if (length(s) = Maxlength) then
        begin
        if p= maxlength then
          begin
          delete(s,maxlength,1);
          s:= s+ch;
          {beep(400,50);}
          if p=windowlength+offset then
            offset := offset+1;
          tempstr := copy(s,offset,windowlength);
          fastwrite(x,y,tempstr,white,black);
          end
        else
          begin
          if insertOn then
          begin
          delete(s,maxlength,1);
          insert(ch,s,p);
          if p=windowlength+offset then
            offset := offset+1;
          if p<maxlength then
            p:= p+1;
          tempstr:= copy(s,offset,windowlength);
          fastwrite(x,y,tempstr,white,black);
```

```
          end
       else (* overwrite *)
         begin
         delete(s,p,1);
         insert(ch,s,p);
         if p=windowlength + offset then
           offset := offset+1;
         If p<maxlength then
           p:=p+1;
         Tempstr:= copy(s,offset,windowlength);
         fastwrite(x,y,tempstr,white,black);
         end;
       end;
    end
  else
    begin
    if insertOn then
      begin
      insert(ch,s,p);
      end
    else
      begin
      delete(s,p,1);
      insert(ch,s,p);
      end;
    if p=windowlength+offset then
      offset:=offset+1;
    if p<maxlength then
      p:=p+1;

    Tempstr:= copy(s,offset,windowlength);
    fastwrite(x,y,tempstr,white,black);
    end;
  end;

Bksp:
  begin
  if p>1 then
    begin
    p:= p-1;
    delete(s,p,1);
    s:=s+char(backgroundchar);
    if offset>1 then
      offset:=offset-1;
    tempstr:= copy(s,offset,windowlength);
    fastwrite(x,y,tempstr,white,black);
    ch:= ' ';
    end
  else
    begin
```

570

```
        p:= 1;
        delete(s,p,1);
        s:=s+char(backgroundchar);
        if offset>1 then
          offset:=offset-1;
        tempstr:= copy(s,offset,windowlength);
        fastwrite(x,y,tempstr,white,black);
        beep(100,250);
        ch:=' ';
        end;
     end;

  rightArrow:
    begin
    if p<maxlength then
    begin
    p:=p+1;
    if p=(windowlength+offset) then
      begin
      offset:=offset+1;
      tempstr:= copy(s,offset,windowlength);
      fastwrite(x,y,s,white,black);
      end;
    end
  else
    begin
    beep(400,50);
    p:=maxlength;
    end;
  end;

  leftArrow:
    begin
    if p>1 then
    begin
    p:=p-1;
    if p<offset then
      begin
      offset:=offset-1;
      tempstr:= copy(s,offset,windowlength);
      fastwrite(x,y,s,white,black);
      end;
    end
  else
    begin
    beep(100,250);
    p:=1;
    end;
  end;
```

```
DeleteKey:
  begin
  delete(s,p,1);
  s:=s+char(backgroundchar);
  if ((length(s)+1)-offset) >= windowlength then
    begin
    tempstr :=copy(s,offset,windowlength);
    fastwrite(x,y,tempstr,white,black);
    end
  else
    begin
    tempstr := copy(s,offset,windowlength);
    fastwrite(x,y,tempstr,white,black);
    end;
  end;

InsertKey:

  begin
  fastwrite(x,y,'                  ',white,black);
  s:=filename;
  fastwrite(x,y,s,white,black);
  end;

endkey:
  begin
  if mask[1] <> 'off' then
    begin
    if fcount > 5*(23-sty)+1 then
      begin
        filn:= filn+1;
        if (filn > fcount-5*(23-sty)+1)   then
          filn:=fcount-5*(23-sty)+1;
      end;
      displayfiles(filename,filn,
          sty,npickf,dirf,fcount); {scrolling display}
    end
  else
    goto flag_out;
  end;

homekey:
  begin
  if mask[1] <> 'off' then
    begin
      filn:= filn-1;
      if filn < 1 then filn:=1;
      displayfiles(filename,filn,
          sty,npickf,dirf,fcount);{scrolling display}
    end
```

```
                        else
                          goto flag_out;
                        end;

                   PGDN:
                     begin
                     if mask[1] <> 'off' then
                       begin
                       npickf:= lpickf+1;
                       if npickf > 5*(23-sty) then  npickf:= 5*(23-sty);
                       if npickf > fcount then npickf:= fcount;
                       pickfile(filename,npickf,lpickf,
                                               filn,sty,dirf,fcount);
                       lpickf:=npickf;
                       end
                     else
                       goto flag_out;
                     end;

                   PGUP:
                     begin
                     if mask[1] <> 'off' then
                       begin
                       npickf:= lpickf-1;
                       if npickf < 1 then
                         begin
                         npickf:=1;
                         end;
                       pickfile(filename,npickf,lpickf,
                                               filn,sty,dirf,fcount);
                       lpickf:=npickf;
                       end
                     else
                       goto flag_out;
                     end;

                   else if not(key In [Carriagereturn,upArrow,
                               downArrow,PgDn,PgUp,homekey,endkey,
                               AltM,AltL,AltW,AltD,AltN,AltB,AltP,
                            AltX,nullkey,esc,tab,shifttab]) then
                                               beep(100,250);
                   end;

              until (key In [carriageReturn,tab,shifttab,
                          esc,downarrow,uparrow,
                       AltN,AltM,AltL,AltW,AltX,AltP,AltB,AltD]);
              flag_out:
         curser_small('C');
         if (key=esc) or (key=ALTX) then abandon:= true;
         setstring(ox,oy,nx,ny,wix,sy,sc,wdx,sdi);
```

```
end;

(*********************************************)

Procedure
MoveEditWindow(mask:mask_names;new:boolean;ft:char;sty,ox,
                oy,nx,ny,wix,sy,sc,wdx,sdi:integer;  var
                                     notskip,abdon:boolean);

var
i,j,npickf,lpickf,filn:integer;
p:pathstr;
d:dirstr;
n:namestr;
e:extstr;
dirf:dir_files;
fcount:integer;

label
  jumpout1,flag1;

begin
i:= 1;
npickf:=1;
lpickf:=1;
filn:=1;
Flag1:
  InputEdit(S,mask,new,sty,npickf,lpickf,filn,abdon,
                    windowlength,maxlength,cursx,cursy,ft,
            backgroundchar,ox,oy,nx,ny,wix,sy,sc,wdx,sdi);
  repeat
 case key of

 downarrow:
     begin
     cursy :=cursy+sy;
     if cursy >= oy-sy+ny*sy then cursy:=oy-sy+ny*sy;
     InputEdit(S,mask,new,sty,npickf,lpickf,filn,abdon,
               windowlength,maxlength,cursx,cursy,ft,
               backgroundchar,ox,oy,nx,ny,wix,sy,sc,wdx,sdi);
     end;

 uparrow:
     begin
     cursy :=cursy-sy;
     if cursy < oy then cursy:=oy;
     InputEdit(S,mask,new,sty,npickf,lpickf,filn,abdon,
               windowlength,maxlength,cursx,cursy,ft,
               backgroundchar,ox,oy,nx,ny,wix,sy,sc,wdx,sdi);
     end;
```

```
Tab:
    begin
    cursx := cursx + (wix+sc+wdx+sdi);
    if cursx >= nx*(wdx+sdi+sc+wix)+ox then
                    cursx:= nx*(wdx+sdi+sc+wix)+ox-wix-sc;
    InputEdit(S,mask,new,sty,npickf,lpickf,filn,abdon,
            windowlength,maxlength,cursx,cursy,ft,
            backgroundchar,ox,oy,nx,ny,wix,sy,sc,wdx,sdi);
    end;

ShiftTab:
    begin
    cursx := cursx - (sdi+wdx+sc+wix);
    if cursx < ox+wdx+sdi then cursx:= ox+wdx+sdi;
    InputEdit(S,mask,new,sty,npickf,lpickf,filn,abdon,
            windowlength,maxlength,cursx,cursy,ft,
            backgroundchar,ox,oy,nx,ny,wix,sy,sc,wdx,sdi);
    end;

carriagereturn:
    begin
      notskip:=false;
      goto jumpout1;
    end;

AltL,AltM,AltW,AltP,AltB,AltN,AltD,AltX:
            begin
            notskip:=false;
            Goto Jumpout1;
            end;
end; {case}

until key = esc;
jumpout1:
Gotoxy(3,4);
end;

(*******************************************)

end. {unit}
```

```pascal
Unit Ves_Util;
{$O+,F+}

(*********************************************)

interface

uses glob_var,graph,fstvideo;

(*********************************************)

Procedure DirList(mask_in:string; var Name_list:dir_files;
                  var file_counter: integer);

Procedure Calldir;

Procedure Curser_Off(stype :char);

Procedure Curser_small(stype :char);

Procedure Curser_big(stype :char);

Procedure Beep(Freq,Time:integer);

Procedure Inkey(var functionKey : boolean;
                var ch :char;begincurser, endcurser: char);

Procedure Keypressed(var ch:char; var fk:boolean);

Procedure Deletefile(var success:boolean);

Procedure Renamefile(var success:boolean;var
                     newname:string);

Procedure Savefile;

Procedure getfilepar(extl:mask_names;var fname:string;
                     var qx,qy:integer;new:boolean;
                     var across,abort:boolean);

Procedure displayfiles(var fname:string;var filn,
                       sty,npicf:integer;var dirf:
                           dir_files;var fcount:integer);

Procedure pickfile(var fname:string;var
                   npicf,lpicf,filn,sty:integer;
                   var dirf:dir_files;var fcount:integer);

Procedure SortDirList(var masklist:mask_names;
                      var filelist:dir_files;var count:integer);
```

576

```
Procedure Join(var abandon:boolean);

Procedure Readfile(nx,ny:integer;filename:
                   string;across:boolean);

Procedure getnewfname(var name:string;var success:boolean);

(**********************************************)

implementation

(**********************************************)

uses crt,dos,editor,menus;

(**********************************************)

Procedure DirList(mask_in:string; var Name_list:dir_files;
                  var file_counter: integer);

var
  i:byte;
  regs:registers;
  DTAseg,DTAofs:word;
  Filename:string[20];

begin
fillchar(regs,sizeof(regs),0);
file_counter:=0;

regs.AH:=$2F;
MsDos(regs);
with regs do
  begin
  DTAseg:= ES;
  DTAofs:= BX;
  end;

Fillchar(Regs,Sizeof(regs),0);
Mask_in:= mask_in+#0;
With Regs do
  begin
  AH:= $4E;
  DS:= Seg(mask_in);
  Dx:= Ofs(Mask_in)+1;
  CL:= $00;
  end;

MsDos(regs);
```

577

```
If Regs.AL <> 0 then exit;

i:=1;
  repeat
  Filename[i]:= Chr(mem[DTAseg:DTAofs+29+i]);
  i:= i+1;
  until (Filename[i-1] < #32) or (i>12);

Filename[0]:= Chr(i-1);
File_counter:= 1;
Name_list[file_counter]:= Filename;

  repeat
  FillChar(regs,sizeof(regs),0);
  with regs do
    begin
    AH:= $4F;
    CL:= $00;
    end;
  MsDos(regs);

  If Regs.AL=0 then
    begin
    i:=1;
      repeat
      Filename[i]:= Chr(Mem[DTAseg:DTAofs+29+i]);
      i:= i+1;
      Until (filename[i-1] < #32) or (i>12);

    Inc(file_counter,1);
    Filename[0]:= Chr(i-1);
    Name_list[File_counter]:= Filename;
    end;

  until regs.al <> 0;

end; {procedure}

(*********************************************)

Procedure Curser_Off(Stype :char);
var
  Regs: registers;
  Begin
  With regs do
    begin
    AH :=$01;
    CH :=$20;
    CL :=$20;
```

578

```pascal
      end;
    intr($10,regs);
    end;


  (***************************************************)

  Procedure Curser_small(stype :char);
  var
    regs : Registers;

  Begin
    Case stype of
    'M' :
      Begin
      With Regs do
        begin
        AH := $01;
        CH := $12;
        Cl := $13;
        end;
      end;
     'C' :
      Begin
      With regs do
        begin
        AH := $01;
        CH := 6;
        CL := 7;
        end;
      end;
    end;
    intr($10,regs);
  end;


  (***************************************************)

  Procedure Curser_big(stype :char);
  var
    regs : Registers;

  Begin
    Case stype of
    'M' :
      Begin
      With Regs do
        begin
        AH := $01;
        CH := 0;
        Cl := $13;
        end;
```

579

```
        end;
     'C' :
       Begin
       With regs do
          begin
          AH := $01;
          CH := 0;
          CL := 7;
          end;
       end;
     end;
     intr($10,regs);
end;


(*****************************************)


Procedure Beep(Freq,Time:integer);


begin
   sound(freq);
   delay(time);
   nosound;
end;


(*****************************************)


Procedure Inkey(var functionKey : boolean;
                var ch :char;
                begincurser, endcurser: char);
var
   Col : char;


begin
Col := 'C';

   case begincurser of
   'B' : Curser_big(Col);
   'S' : Curser_small(Col);
   'O' : Curser_off(Col);
   end;

FunctionKey := false;
ch:= readkey;
if (ch = #0) then
   begin
   functionkey :=true;
   ch:= readkey;
   end;

If functionkey then
```

```
case ord(ch) of
  15: key:=shiftTab;
  72: key:=upArrow;
  80: key:=downArrow;
  75: key:=leftArrow;
  77: key:=rightarrow;
  73: key:=PgUp;
  81: key:=PgDn;
  71: key:=HomeKey;
  79: key:=endKey;
  83: key:=deleteKey;
  82: key:=insertKey;
  59: key:=f1;
  60: key:=f2;
  61: key:=f3;
  62: key:=f4;
  63: key:=f5;
  64: key:=f6;
  65: key:=f7;
  66: key:=f8;
  67: key:=f9;
  68: key:=f10;
  23: key:=AltI;
  31: key:=AltS;
  45: key:=AltX;
  46: key:=AltC;
  18: key:=AltE;
  19: key:=AltR;
  50: key:=AltM;
  33: key:=AltF;
  48: key:=AltB;
  47: key:=AltV;
  38: key:=AltL;
  17: key:=AltW;
  36: key:=AltJ;
  25: key:=AltP;
  22: key:=AltU;
  32: key:=AltD;
  49: key:=AltN;
  24: key:=AltO;
  end
else
  case ord(ch) of
  8: key := bksp;
  9: key := tab;
  13: key:= carriagereturn;
  27: key:= esc;
  32: key:= space;
  33..44,47,58..254: Key:=textkey;
  45,46,48..57:  Key:= numberkey;
```

```pascal
      end;

   case endcurser of
   'B' : curser_big(Col);
   'S' : curser_small(Col);
   'O' : curser_off(Col);
   end;
end;


(**************************************************)

Procedure Calldir;

var
   n,r,m,fL,l,lc,u:integer;
   specialkey: boolean;

label flag2;

begin
   flag2:
   textcolor(lightgray);
   textbackground(black);
   GotoXY(57,14);
   write('                              '); {erases previous input
                                                     if program loops}
    for i:= 1 to 7 do
    begin
    gotoxy(4,15+i);
    write('                                                    ');
    end;
   GotoXY(4,14);
   Write('Enter DOS filespec; eg: *.<wal/mat/lam> :');
   textcolor(yellow);
   gotoxy(28,14);
   write('*. wal mat lam');
   textcolor(lightgray);
   Gotoxy(30,14);
   write('<');
   for i:= 0 to 1 do
     begin
     gotoxy(34+i*4,14);
     write('/');
     end;
   gotoxy(46,14);
   readln(filespec);
   curser_off('c');
   if filespec = '' then filespec:='*.*';
   DirList(filespec,df,fc);
    if fc > 35 then
```

582

```
      begin
      gotoxy(35,23);
      write(' PgDn / PgUp ');
      end;

m:=0;
L:= fc div 35;
fL:= fc mod 35;
if L = 0 then u:=fl;
if L <> 0 then u:=35;
   for i:= 0 to u-1 do
      begin
      n:=i div 7;
      r:=i mod 7;
      gotoxy(4+n*15,r+16);
      writeln(df[i+1]);
      end;

   Repeat
   Inkey(specialkey,ch,'s','o');

   case key of

      PgDn: Begin
            m:=m+35;
            u:=m+35;
            if m > 1*35 then m:= 1*35;
            if u > fc then u:= fc;
            for i:= 1 to 7 do
            begin
            gotoxy(4,15+i);
            write('                                        ');
            end;
            for i:= m to u-1 do
               begin
               n:=i div 7;
               r:=i mod 7;
               if n > 4 then
               n:= n mod 5;
               gotoxy(4+n*15,r+16);
               writeln(df[i+1]);
               end;
            end;

      PgUp: begin
            m:= m-35;
            if m < 0 then m:= 0;
            u:= m+35;
            if (u=35) and (l=0) then u:= fl;
            for i:= 1 to 7 do
```

```
                    begin
                    gotoxy(4,15+i);
                    write('                                        ');
                    end;
                    for i:= m to u-1 do
                      begin
                      n:=i div 7;
                      r:=i mod 7;
                      if n > 4 then
                      n:= n mod 5;
                      gotoxy(4+n*15,r+16);
                      writeln(df[i+1]);
                      end;
                    end;
                end;{case}

        if not (key in [F2,AltX,ALtN,AltD,AltE,
                        AltP,AltJ,AltC,AltF,AltL,AltM,
                        AltW,AltU,AltV,AltS,AltR,PgDn,PgUp])
                                    then beep(150,250);
        if key = F2 then goto flag2;
      until key in ([AltX,ALtN,AltD,AltE,AltP,
                        AltJ,AltC,AltF,AltL,AltM,
                            AltW,AltU,AltV,AltS,AltR]);
      curser_small('c');
end;


(*********************************************)

Procedure Keypressed(var ch:char; var fk:boolean);

begin
fk:= false;
ch:= readkey;
if ch = #0 then
  begin
  fk:= true;
  ch:= readkey;
  end;
end;


(*********************************************)

Procedure Deletefile(var success:boolean);
var
fileX:file;
ercd:integer;

begin
{$I-}
```

```pascal
assign(fileX,currentfile);
erase(fileX);
ercd:= IOresult;
if IOresult <> 0 then
  success:= false
else
  success:= true;
{$I+}
end;

(*********************************************)

Procedure Renamefile(var success:boolean;var
newname:string);
var
fileX:file;
npicf,lpicf,filn:integer;
mask:mask_names;
new:boolean;
d:dirstr;
n:namestr;
e,ne:extstr;

begin
fsplit(currentfile,d,n,e);
gotoxy(4,5);
textcolor(white);
write('                                          ');
gotoxy(4,5);
write('Rename as _____('+e+'): ');
textcolor(yellow);
gotoxy(14,5);
write('_____');
cursx:=30;
cursy:=5;
mask[1]:='*.lam';
mask[2]:='*.mat';
mask[3]:='*.wal';
mask[4]:='*.lds';
mask[5]:='*.prs';
mask[6]:='*.ves';
mask[7]:='';
npicf:=1;
lpicf:=1;
filn:=1;
new:=true;
holdstr[1,1]:='';
InputEdit(newname,mask,new,6,npicf,lpicf,filn,success,12,12,
          cursx,cursy,'T',255,cursx,cursy,0,0,0,1,1,0,0);
{$I-}
```

```pascal
curser_off(stype);
assign(fileX,currentfile);
fsplit(newname,d,n,ne);
rename(fileX,n+e);
if IOresult <> 0 then
  success:= false
else
  begin
    success:= true;
    fastwrite(4,5,'['+currentfile+'] has been renamed
                                ['+n+e+']',yellow,red);
    currentfile:=n+e;
    beep(1600,600);
    delay(25000);
  end;
{$I+}
end;


(*************************************************)


Procedure Savefile;
label flag1,flag3;

var
  i,j,IOcode: integer;
  f: Text;
  e:extstr;
  p:pathstr;
  d:dirstr;
  n:namestr;
  qx,qy:integer;
  across:boolean;

begin
 across:=false;   {default=down,ie; collums rather than rows}
 Fsplit(currentfile,d,n,e);
 assign(f,currentfile);
 rewrite(f);

     if (e='.WAL') or (e='.wal') then
       begin
         qx:=5;
         qy:=15;
       across:=true;
       for i:= 1 to qy do
         begin
           fsplit(holdstr[2,i],d,n,e);   {strips extension}
           holdstr[2,i]:=n;
         end;
       end;


                     -
```

```
      if (e='.MAT') or (e='.mat') then
        begin
          qx:=2;
          qy:=9;
        end;
      if (e='.LAM') or (e='.lam') then
        begin
          qx:=2;
          qy:=9;
        end;
      if (e='.LDS') or (e='.lds') then
        begin
          qx:=1;
          qy:=4;
        end;

    if across then
      begin
        for j:= 1 to qy do
        for i:= 1 to qx do
        writeln(f,holdstr[i,j]);
      end
    else
      begin
        for i:= 1 to qx do
        for j:= 1 to qy do
      writeln(f,holdstr[i,j]);
      end;
    close(f);

    flag3:
    end;


(***********************************************)

Procedure Join(var abandon:boolean);

var
f:text_files;
i,j,fc1,fc2,fc3,w,r: integer;
p:string;
nskp:boolean;
mask:mask_names;
d:dirstr;
n:namestr;
e:extstr;

label
flag1,flag2;
```

```
begin
abandon:=false;
nskp:=true;
textcolor(lightgray);
textbackground(black);

holdstr[1,1]:= '';
holdstr[1,2]:= '';
holdstr[1,3]:= '';

for i:=32 to 39 do          {cures curser color bug}
for j:=5 to 7 do
begin
   fastwrite(i,j,#255,white,black);
end;

Inputdesctable(4,5,1,3,8,1,1,26,2,1);
fastwrite(11,5,'(.LDS)',white,black);
fastwrite(11,6,'(.WAL)',white,black);
fastwrite(11,7,'(.VES)',white,black);

mask[1]:='*.LDS';
mask[2]:='*.WAL';
mask[3]:='*.VES';
mask[4]:='';

windowlength:=12;
maxlength:=12;
flag1:
MoveEditwindow(mask,false,'T',9,4,5,1,3,12,1,1,
                                  26,2,nskp,abandon);

if abandon = true then goto flag2;

for i:= 1 to 3 do
begin
fsplit(holdstr[1,i],d,n,e);

if (i = 1) and (e ='.LDS') or (e='.lds') then
  assign(f[i],holdstr[1,i]);
if (i = 2) and (e ='.WAL') or (e='.wal') then
  assign(f[i],holdstr[1,i]);
if (i = 3) and (e ='.VES') or (e='.ves') then
  assign(f[i],holdstr[1,i]);

{$I-}
if i < 3 then
  reset(f[i])
else
  rewrite(f[i]);
```

```
if IOresult <> 0 then
  begin
  gotoxy(4,4);
  write('                                                        ');
  gotoxy(4,4);
  textcolor(lightgray);
  beep(600,100);
  writeln('Filename ['+holdstr[1,i]+']
                                contains bad syntax.');
  textcolor(white);
  gotoxy(14,4);
  writeln(holdstr[1,i]);
  Goto flag1;
  end;
end;
{$I+}
for i:= 1 to 4 do
begin
  readln(f[1],p);
  writeln(f[3],p);
end;
for i:= 1 to N1*5 do
begin
  readln(f[2],p);
  writeln(f[3],p);
end;
close(f[1]);
close(f[2]);
close(f[3]);

gotoxy(4,4);
write('                                                        ');
gotoxy(4,4);
textcolor(lightgray);
Write('File '+holdstr[1,3]+' created');
gotoxy(9,4);
textcolor(white);
write(holdstr[1,3]);
delay(15000);

flag2:
end;


(*******************************************************)

Procedure getfilepar(ext1:mask_names;var fname:string; var
qx,qy:integer;new:boolean;var across,abort:boolean);

var
```

589

```
p:pathstr;
d:dirstr;
n:namestr;
e:extstr;
f: Text;
IOcode,IOext:integer;
fc1,fc2,fc3,fc4,fc5,w,r,npicf,lpicf,filn:integer;
ntskp:boolean;

label flag_abort,flag1;

                begin
                flag1:
                abort:=false;
                textbackground(black);
                textcolor(lightgray);
                GotoXY(4,4);
                If not new then
                begin
                  Writeln('Enter filename or select:');
                  cursx:=30;
                  cursy:=4;
                end;
                If new then
                begin
                  Writeln('Enter filename.
                                        <LAM/MAT/WAL/LDS/VES>:');
                  cursx:=42;
                  cursy:=4;
                  fname:='';
                  gotoxy(18,4);
                  write('.');
                  gotoxy(20,4);
                  write('LAM');
                  gotoxy(24,4);
                  write('MAT');
                  gotoxy(28,4);
                  write('WAL');
                  gotoxy(32,4);
                  write('LDS');
                  gotoxy(36,4);
                  write('VES');
                  gotoxy(42,4);
                  write('                  ');
                                        {erases previous entry}
                end;
                Gotoxy(10,4);
                textcolor(yellow);
                write('filename');
                holdstr[1,1]:='';
```

```
                maxlength:=12;
                windowlength:=12;
                npicf:=1;
                lpicf:=1;
                filn:=1;

    InputEdit(fname,ext1,new,6,npicf,lpicf,filn,abort,12,12,
              cursx,cursy,'T',255,cursx,cursy,0,0,0,1,1,0,0);

       if abort = true then goto flag_abort;

                Fsplit(fname,d,n,e);
                across:=false;
                  if (e='.WAL') or (e='.wal') then
                    begin
                    across:=true;
                    qx:=5;
                    qy:=15;
                    end
                  else if (e='.MAT') or (e='.mat') then
                    begin
                    qx:=2;
                    qy:=9;
                    end
                  else if (e='.LAM') or (e='.lam') then
                    begin
                    qx:=2;
                    qy:=9;
                    end
                  else if (e='.LDS') or (e='.lds') then
                    begin
                    qx:= 1;
                    qy:= 4;
                    end
                  else if (e='.VES') or (e='.ves') then
                    begin
                    qx:= 1;
                    qy:= 3;
                    end
                  else if (copy(e,2,1)='D')or(copy (e,2,1)='d') then
                    begin
                    qx:=80;
                    qy:=15;
                    end
                  else
                  begin
                    fastwrite(4,5,'                                        '
                                                    ,white,black);
                    fastwrite(4,5,'['+e+'] is an improper file
                                        extension',yellow,red);
```

```
            goto flag1;
         end;
         currentfile:=n+e;
flag_abort:
end;


(******************************************************)

Procedure displayfiles(var fname:string;var
filn,sty,npicf:integer;
var dirf:dir_files;var fcount:integer);

var
w,r,uplim,lolimit,rows:integer;

begin
textcolor(lightgray);
rows:=23-sty;
lolimit:=filn;
uplim:=filn+5*(rows)-1;
if fcount < uplim then uplim:= fcount;
for i:= 0 to uplim-lolimit do
  begin
    w:=i div rows;
    r:=i mod rows;
    gotoxy(4+w*15,r+sty);
    writeln('              ');
    gotoxy(4+w*15,r+sty);
    writeln(dirf[lolimit+i]);
  end;

textcolor(white);
w:=(npicf-1) div rows;
r:=(npicf-1) mod rows;
gotoxy(4+w*15,r+sty);
writeln('              ');
gotoxy(4+w*15,r+sty);
writeln(dirf[npicf+filn-1]);
fname:=dirf[npicf+filn-1];

end;


(******************************************************)

Procedure pickfile(var fname:string;var
npicf,lpicf,filn,sty:integer;
var dirf:dir_files;var fcount:integer);

var
lw,lr,w,r,uplim,lolimit,rows:integer;
```

```
begin

rows:=23-sty;
lolimit:=npicf;
uplim:=npicf+5*(rows);
if fcount < uplim then uplim:= fcount;
lw:=(lpicf-1) div rows;
lr:=(lpicf-1) mod rows;
textcolor(lightgray);
gotoxy(4+lw*15,lr+sty);
writeln(dirf[lpicf+filn-1]);

textcolor(white);
w:=(npicf-1) div rows;
r:=(npicf-1) mod rows;
gotoxy(4+w*15,r+sty);
writeln('                  ');
gotoxy(4+w*15,r+sty);
writeln(dirf[npicf+filn-1]);
fname:=dirf[npicf+filn-1];
end;

(**************************************************)

Procedure SortDirList(var masklist:mask_names;
var filelist:dir_files;var count:integer);

var
mask:string;
filenames:dir_files;
i,j,no:integer;

label
flag_end;

begin
count:= 0;
for i:= 1 to 8 do
begin
  mask:=masklist[i];
  if mask = '' then goto flag_end;
  dirlist(mask,filenames,no);
  for j:= 1 to no do
  begin
    count:= count+1;
    filelist[count]:=filenames[j];
  end;
end;
flag_end:
```

```
end;


(*********************************************)

Procedure
Readfile(nx,ny:integer;filename:string;across:boolean);

var
   i,j,IOcode: integer;
   f: Text;
   p:pathstr;
   d:dirstr;
   n:namestr;
   e:extstr;

   begin

      for i:= 1 to 5 do
      for j:= 1 to 15 do
      holdstr[i,j]:='';        {clears edit buffer}
      assign(f,filename);
      reset(f);
      if across then
        begin
        for j:= 1 to ny do
        for i:= 1 to nx do
        readln(f,holdstr[i,j]);
        end
      else
        begin
        for i:= 1 to nx do
        for j:= 1 to ny do
        readln(f,holdstr[i,j]);
      end;
    close(f);

    end;


(*********************************************)

Procedure getnewfname(var name:string;var success:boolean);
                                      {graphical input}
var
ch:char;
funckey:boolean;

label
flag_done,flag_repeat;
```

```
begin
i:= 1;
success:= true;

repeat
   flag_repeat:
   setcolor(white);
   line(32+i*8,19,40+i*8,19);
   ch:=readkey;
   if ch <> #0 then
     Funckey:= false
   else
   begin
     funckey:= true;
     ch:= readkey;
   end;

   if (name = '')and(ch = #13) then {prevents blank filename}
   begin
     beep(600,400);
     goto flag_repeat;
   end;

   if (ch = #13) or (ch = #82) and (length(name) > 0) then
                                           goto flag_done;

{enter or ins}
   if (funckey = true) and (ch = #77) then
     begin
     setcolor(black);                          {right arrow}
     line(32+i*8,19,40+i*8,19);
     i:= i+1;
     if i >= length(name)+1 then i:= length(name)+1;
     goto flag_repeat;
     end;

   if (funckey = true) and (ch = #75) then          .        .
     begin
     setcolor(black);                          {left arrow}
     line(32+i*8,19,40+i*8,19);
     i:= i-1;
     if i <= 1 then i:= 1;
     goto flag_repeat;
     end;

   if (ch = #8) and (funckey = false) then    {backspace}
      begin
        setcolor(black);
        line(32+i*8,19,40+i*8,19);
        i:=i-1;
```

```
            if i < 1 then i:= 1;
              delete(name,i,1);
            end;

        if (ch = #8) or ((funckey = true) and (ch = #83)) then
          begin
            setcolor(black);
            delete(name,i,1);
            line(32+i*8,19,40+i*8,19);              {del key}
          end
        else
          begin
            setcolor(black);                        {insert typed
letter}
            line(32+i*8,19,40+i*8,19);
            insert(ch,name,i);
            i:= i+1;
            if i>= 8 then i:=8;
          end;

        name:=copy(name,1,8);
        bar(40,10,104,19);
        setcolor(white);
        line(32+i*8,19,40+i*8,19);
        outtextxy(40,10,name);

        until (ch = #27) or ((ch = #45) and (funckey = true));
{esc or AltX}

if (ch = #27) or ((ch = #45) and (funckey = true)) then
  success:= false        {operation aborted}
else
  success:= true;
flag_done:
end;

(*********************************************)

end. {unit}
```

```
unit Alt_Pick;
{$O+,F+}


(************************************************)

interface

uses glob_var,dos,crt,graph,compmath,plotprop,ves_util,
     menus,FSTvideo,GraEdit,editor,failure;

procedure Alt_R;
procedure Alt_P;
procedure Alt_C;
procedure Alt_E;
Procedure Alt_D(itter:boolean);


(************************************************)

implementation

(************************************************)

procedure Alt_R;        {calculate - vaRiable options}

var
i,j,AX2,layerno,angl,numb,gra,pk:integer;
update,readkeybd,abrt,dgrad,keyknown,
restnt,specialkey,iterat,rset:boolean;
newmat,wfile,expnt,title:string;
redu,ffail,redSS:realarray1NL;
rad,sig_r,sig_f,sig_z:realarray2plusN;
x_max,x_min,y_max,y_min,exponent:real;
b_fit:realarrayMpbyNp;
nn:integerarray9;
mask:mask_names;

label
flag_end,flag_vplotm,flag_exponent,flag_key;

begin
curser_off(stype);
dgrad:=false;
keyknown:=false;
  for j:=1 to 9 do          {initialization}
    for i:=1 to 5 do
    begin
      holdstr[i,j]:='';
      nn[j]:=0;
    end;
```

```
AX2:= 0;
zerographdata;
update:=false;
readkeybd:= true;
mask[1]:='*.ves';
mask[2]:='';
readvesf(Newmat,mask,redu,ffail,RedSS,outerlayer,layerno,
                         angl,readkeybd,update,dgrad,abrt);
if abrt = true then goto flag_end;
Laminateprop(outerlayer);

flag_vplotm:
varplotmenu;
keyknown:= false;
wfile:= 'file = '+currentfile;
fastwrite(3,2,wfile,red,black);

repeat
if not keyknown then Inkey(specialkey,ch,'s','o');

case key of
(*
  AltL:
    begin
      AX2:= 0;
      two_var('l',rad,sig_r,sig_f,sig_z);
      if graphstate = false then
      begin
        initgraphdriver;
        graphstate:= true;
      end;
      plotvgraphs(rad,Sig_r,Sig_f,Sig_z,x_max,x_min,y_max,
                  y_min,numb);
      plotoutline('Normalized Radius (p)','Stress Mpa',
              'Variable "d-l"',5,5,x_min,x_max,y_min,y_max);
    end;

  AltM:
    begin
      AX2:= 0;
      two_var('m',rad,sig_r,sig_f,sig_z);
      if graphstate = false then
      begin
        initgraphdriver;
        graphstate:= true;
      end;
      plotvgraphs(rad,Sig_r,Sig_f,Sig_z,x_max,x_min,
                  y_max,y_min,numb);
      plotoutline('Normalized Radius (p)','Stress Mpa',
              'Variable "d-m"',5,5,x_min,x_max,y_min,y_max);
```

```
       end;

   AltF:
     begin
       AX2:= 0;
       two_var('f',rad,sig_r,sig_f,sig_z);
       if graphstate = false then
       begin
         initgraphdriver;
         graphstate:= true;
       end;
       plotvgraphs(rad,Sig_r,Sig_f,Sig_z,x_max,x_min,
                   y_max,y_min,numb);
       plotoutline('Normalized Radius (p)','Stress Mpa',
         'Variable "d-m"&"d-1"',5,5,x_min,x_max,y_min,y_max);
     end;
*)

  AltC:           {finite difference itteration on C / editor}
     begin
       AX2:= 0;
       if graphstate = false then
       begin
         initgraphdriver;
         graphstate:= true;
       end;
       iterat:= true;
       alt_d(iterat);
     end;

  AltN:           {finite difference no itteration / editor}
     begin
       AX2:= 0;
       if graphstate = false then
       begin
         initgraphdriver;
         graphstate:= true;
       end;
       iterat:= false;
       alt_d(iterat);
     end;

  AltF,AltR:               {variable property 'n'/ editor}
     begin
     if Key = AltR then
       begin
         restnt:= true;          {C = 0}
         title:='Fixed ends - variation "n"';
       end
     else
```

```pascal
  begin
    restnt:= false;          {C <=> 0}
    title:='Free ends - variation "n"';
  end;
AX2:= 0;

getgraphdata('B');
for gra:= 1 to 3 do
  bestfit(b_fit,pk,gra);
exponent:= bfit_store[3,2];
if graphstate = false then
begin
  initgraphdriver;
  graphstate:= true;
end;

flag_exponent:

statsout(exponent,restnt);
plotvariable(5,5,x_max,x_min,y_max,y_min,exponent);
                                                      {n only}
plotoutline('Radius (mm)','Stress Mpa',
            title,'',5,5,x_min,x_max,y_min,y_max);
setfillstyle(1,black);

flag_key:
Keyknown:=false;
        {graphics submenu for stress when 'n' is variable}
repeat
  if not keyknown then Inkey(specialkey,ch,'s','o');

  case key of

  AltX:                          {calls file directory}
    begin
    for j:= 2 to 6 do          {clean up graph index}
      nn[j]:= 0;
    keyknown:=true;
    closegraph;
    graphstate:= false;
    restorecrtmode;
    AX2:= 1;
    goto flag_vplotm;
  end;

  UpArrow:
    begin
    exponent:= exponent + 0.01;
    bar(596,16,639,24);
    setcolor(2);
```

```
      str(exponent:4:2,expnt);
      outtextxy(596,16,expnt);
      goto flag_key;
      end;

   DownArrow:
     begin
     exponent:= exponent - 0.01;
     bar(596,16,639,24);
     setcolor(2);
     str(exponent:4:2,expnt);
     outtextxy(596,16,expnt);
     goto flag_key;
     end;

   PgUp:
     begin
     exponent:= exponent + 0.1;
     bar(596,16,639,24);
     setcolor(2);
     str(exponent:4:2,expnt);
     outtextxy(596,16,expnt);
     goto flag_key;
     end;

   PgDn:
     begin
     exponent:= exponent - 0.1;
     bar(596,16,639,24);
     setcolor(2);
     str(exponent:4:2,expnt);
     outtextxy(596,16,expnt);
     goto flag_key;
     end;

  HomeKey:
    begin
    exponent:= 0.0;
    bar(596,16,639,24);
    setcolor(3);
    str(exponent:4:2,expnt);
    outtextxy(596,16,expnt);
    goto flag_key;
    end;

  EndKey:
    begin
    exponent:= bfit_store[3,2];
    bar(596,16,639,24);
    setcolor(2);
```

```pascal
                      str(exponent:4:2,expnt);
                      outtextxy(596,16,expnt);
                      goto flag_key;
                      end;

                  InsertKey:
                    begin
                    cleardevice;
                    goto flag_exponent;
                    end;

                  end; {cases graphic editing}

              until (Key = esc) or (key = AltX);
              closegraph;
              restorecrtmode;
              graphstate:=false;
              goto flag_vplotm;

          end; {case of AltF/AltR}

    ALTX:
      begin
      AX2:= AX2+1;
      if (AX2 > 1) or (graphstate = false) then
      begin
        closegraph;
        restorecrtmode;
        graphstate:=false;
        goto flag_end;
      end
      else
      begin
        for j:= 2 to 6 do        {clean up graph index}
          nn[j]:= 0;
        keyknown:=true;
        closegraph;
        graphstate:= false;
        restorecrtmode;
        AX2:=1;
        goto flag_vplotm;
      end;
      end;

    ESC:
     begin
     closegraph;
     calcmenu;
     graphstate:= false;
     currentfile:='Unknown';
```

602

```
      goto flag_end;
      end;

   end; {cases of varplotmenu}

   until (Key = esc) or (Key = AltX);
   closegraph;
   restorecrtmode;
   graphstate:=false;
   goto flag_vplotm;

   flag_end:
   closegraph;
   restorecrtmode;
   graphstate:=false;
   end;


(****************************************************)

procedure Alt_P;    {calculate - plot menu in graphics mode}

var

f:text;
matchoice:dir_files;num,i,sel_mat,topic,param,layerno,angl,
j,X0,X1,spt,errcd,k,h:integer;
nn:integerarray9;
pick:char;switch,update,readkeybd,dgrad,abrt,keyknown,
specialkey,OK:boolean;
description,newmat,tpic,newangle,newperct,newthick,newfile:
string;
redu,ffail,redSS:realarray1NL;
x_max,x_min,y_max,y_min,t:real;
mask:mask_names;

label
flag_end,flag_n,flag_read,flag_dnar,flag_upar,flag_pgdn,
flag_pgup,flag_tab,flag_left,flag_right,flag_exit,flag_save,
flag_del,flag_ins,flag_found;

begin
curser_off(stype);
dgrad:=false;
keyknown:=false;
for j:=1 to 9 do    {initilize holdstr, and graph(s) to plot}
   for i:=1 to 5 do
   begin
     holdstr[i,j]:='';
     nn[j]:= 0;
   end;
```

```
DirList('*.mat',matchoice,num);
          sel_mat:= 0;
          topic:= 1;
          param:= 0;
          layerno:= 1;
          j:= 1;
          h:= 1;
          nn[1]:=1;
          pick:='A';
          switch:= true;
          update:= false;
          description:='Stiff. GPa';
          readkeybd:=true;
          mask[1]:='*.ves';
          mask[2]:='';
          readvesf(Newmat,mask,redu,ffail,redSS,
                    outerlayer,layerno,angl,readkeybd,
                    update,dgrad,abrt);
          if abrt = true then goto flag_end;
          readkeybd:= false;
          initgraphdriver;
          zerographdata;
          flag_n:
          readvesf(Newmat,mask,redu,ffail,
                    redSS,outerlayer,layerno,angl,
                    readkeybd,update,dgrad,abrt);
          if abrt = true then goto flag_end;
          if switch = true then
            begin
              getgraphdata(pick); {comp. or stiffness data}
              laminateprop(outerlayer);
            end;
          plotgraph(nn,j,6,5,x_min,x_max,y_min,y_max);
          plotoutline('Radius (mm)',description,'Variable
                    Properties Approximations','',
                    6,5,x_min,x_max,y_min,y_max);

          if param = 0 then
          begin
            setfillstyle(solidfill,blue);
            str(topic,tpic);
            bar(569-4*length(tpic),24+topic*28,569-
                4*length(tpic)+8*length(tpic),32+topic*28);
            outtextxy(569-4*length(tpic),24+topic*28,tpic);
          end;
          if param = 1 then
          begin
            str(topic,tpic);
            setfillstyle(solidfill,blue);
            bar(585+4*length(tpic),24+topic*28,585+
```

604

```pascal
         4*length(tpic)+8*
         length(graphlabels[topic].angle),
         32+topic*28);
      outtextxy(585+4*length(tpic),24+topic*28,
             graphlabels[topic].angle);
   end;
   if param = 2 then
   begin
      setfillstyle(solidfill,blue);
      str(topic,tpic);
      bar(616,24+topic*28,631,32+topic*28);
      outtextxy(616,24+topic*28,
             copy(graphlabels[topic].fpercent,1,2));
   end;
   if param = 3 then
   begin
      setfillstyle(solidfill,blue);
      str(topic,tpic);
      bar(576,34+topic*28,639,42+topic*28);
      outtextxy(576,34+topic*28,
             graphlabels[topic].matname);
   end;
   if param = 4 then
   begin
      x0:= 59+round(500*(r[topic-1]-x_min)/
                 (x_max-x_min));
      x1:= 59+round(500*(r[topic]-x_min)/
                 (x_max-x_min));
      spt:=round((x1+x0)/2);
      setfillstyle(solidfill,blue);
      str(topic,tpic);
      if odd(topic) then k:=10 else k:=0;
      bar(spt-3,30-k,spt-4+8*
          (length(graphlabels[topic].thickness)
          +length(tpic)),37-k);
      outtextxy(spt-3,30-
             k,graphlabels[topic].thickness);
   end;


flag_read:   {above - xmin,xmax,ymim,ymax, ...
                                    xdiv,ydiv}
   Keyknown:=false;
             {graphics submenu for bestfit curves}
   repeat
   if  not keyknown then
                   Inkey(specialkey,ch,'s','o');
   case key of

   AltX:                        {calls file directory}
     begin
```

```
                    goto flag_end;
                    end;

DownArrow:
     begin
     keyknown:=true;
     flag_DNar:

     if param = 0 then
     begin
        setfillstyle(solidfill,black);
        str(topic,tpic);
        bar(569-4*length(tpic),24+topic*28,
            569-4*length(tpic)+8*length(tpic),
            32+topic*28);
        setcolor(white);
        outtextxy(569-4*length(tpic),24+
                    topic*28,tpic);
        topic:= topic+1;
        if topic > outerlayer then
                                      topic:=outerlayer;
        setfillstyle(solidfill,blue);
        str(topic,tpic);
        bar(569-4*length(tpic),24+topic*28,
            569-4*length(tpic)+8*length(tpic),
            32+topic*28);
        setcolor(white);
        outtextxy(569-4*length(tpic),24+
                    topic*28,tpic);
     end;

     if param = 1 then
     begin
        val(graphlabels[topic].angle,i,errcd);
        str(i-1,newangle);
        graphlabels[topic].angle:=newangle;
        setfillstyle(solidfill,blue);
        str(topic,tpic);
        bar(585+4*length(tpic),24+topic*28,
            585+4*length(tpic)+8*
            length(graphlabels[topic].angle),
            32+topic*28);
        setcolor(white);
        outtextxy(585+4*length(tpic),24+topic*28,
                    graphlabels[topic].angle);
        update:= true;
        switch:=true;
        readkeybd:=false;
     end;
```

606

```
if param = 2 then
begin
   val(graphlabels[topic].fpercent,i,errcd);
   str(i-1,newperct);
   graphlabels[topic].fpercent:=newperct;
   setfillstyle(solidfill,blue);
   str(topic,tpic);
   bar(616,24+topic*28,631,32+topic*28);
   setcolor(white);
   outtextxy(616,24+topic*28,
             copy(graphlabels[topic].fpercent,
             1,2));
   update:= true;
   switch:=true;
   readkeybd:=false;
end;

if param = 3 then
begin
   sel_mat:= sel_mat-1;
   if sel_mat <= 1 then sel_mat:= 1;
   graphlabels[topic].matname:=
                copy(matchoice[sel_mat],1,
                pos('.',matchoice[sel_mat])-1);
   setfillstyle(solidfill,blue);
   str(topic,tpic);
   bar(576,34+topic*28,639,42+topic*28);
   setcolor(white);
   outtextxy(576,34+topic*28,
             graphlabels[topic].matname);
   update:= true;
   readkeybd:= false;
end;

if param = 4 then
begin
   val(graphlabels[topic].thickness,t,errcd);
   t:= t-0.1;
   if t <= 1 then t:= 1;
   str(t:2:1,newthick);
   graphlabels[topic].thickness:= newthick;
   x0:= 59+round(500*(r[topic-1]-
                      x_min)/(x_max-x_min));
   x1:= 59+round(500*(r[topic]-x_min)/
                      (x_max-x_min));
   spt:=round((x1+x0)/2);
   setfillstyle(solidfill,blue);
   str(topic,tpic);
   if odd(topic) then k:=10 else k:=0;
   bar(spt-10+8*length(tpic),30-k,spt-12+8*
```

```
                    (length(graphlabels[topic].thickness)
                     +length(tpic)),37-k);
            setcolor(white);
            outtextxy(spt-10+8*length(tpic),30-k,
                      graphlabels[topic].thickness);
            update:= true;
            readkeybd:= false;
          end;

          repeat
            Inkey(specialkey,ch,'s','o');

            if key = DownArrow then goto flag_DNar;
            if key = UpArrow then goto flag_UPar;
            if key = leftarrow then goto flag_left;
            if key = rightarrow then goto flag_right;
            if key = PgUp then goto flag_pgup;
            if key = PgDn then goto flag_pgdn;
            if key = AltX then goto flag_end;
            if key = Tab then goto flag_tab;
            if key = AltS then goto flag_save;
            if key = Deletekey then
              begin
                nn[j]:= 0;
                switch:=true;
                cleardevice;
                goto flag_n;
              end;
            if key = InsertKey then
              begin
                nn[j]:=j;
                switch:=true;
                cleardevice;
                goto flag_n;
              end;
          until key = esc;
          goto flag_end;
        end;

UpArrow:
  begin
  keyknown:=true;
  flag_UPar:

  if param = 0 then
  begin
    str(topic,tpic);
    setfillstyle(solidfill,black);
    bar(569-4*length(tpic),24+topic*28,
        569-4*length(tpic)+8*length(tpic),
```

```pascal
                32+topic*28);
       setcolor(white);
       outtextxy(569-4*
               length(tpic),24+topic*28,tpic);
       topic:= topic-1;           {layer increment}
       if topic < 1 then topic:= 1;
       setfillstyle(solidfill,blue);
       str(topic,tpic);
       bar(569-4*length(tpic),24+topic*28,
           569-4*length(tpic)+8*
           length(tpic),32+topic*28);
       setcolor(white);
       outtextxy(569-4*length(tpic),
               24+topic*28,tpic);
   end;

   if param = 1 then
   begin
     val(graphlabels[topic].angle,i,errcd);
     str(i+1,newangle);            {angle increment}
     graphlabels[topic].angle:=newangle;
     setfillstyle(solidfill,blue);
     str(topic,tpic);
     bar(585+4*length(tpic),24+topic*28,
         585+4*length(tpic)+8*
         length(graphlabels[topic].angle),
         32+topic*28);
     setcolor(white);
     outtextxy(585+4*length(tpic),24+
             topic*28,graphlabels[topic].angle);
     update:= true;
     switch:=true;
     readkeybd:=false;
   end;

   if param = 2 then
   begin
     val(graphlabels[topic].fpercent,i,errcd);
     str(i+1,newperct);
     graphlabels[topic].fpercent:=newperct;
     setfillstyle(solidfill,blue);
     str(topic,tpic);
     bar(616,24+topic*28,631,32+topic*28);
     setcolor(white);
     outtextxy(616,24+topic*28,
         copy(graphlabels[topic].fpercent,1,2));
     update:= true;
     switch:=true;
     readkeybd:=false;
   end;
```

```
if param = 3 then
begin
  sel_mat:= sel_mat+1;
  if sel_mat >= num then sel_mat:= num;
  graphlabels[topic].matname:=
            copy(matchoice[sel_mat],1,
            pos('.',matchoice[sel_mat])-1);
  setfillstyle(solidfill,blue);
  str(topic,tpic);
  bar(576,34+topic*28,639,42+topic*28);
  setcolor(white);
  outtextxy(576,34+topic*28,
            graphlabels[topic].matname);
  update:= true;
  readkeybd:= false;
end;

if param = 4 then
begin
  val(graphlabels[topic].thickness,t,errcd);
  t:= t+0.1;
  str(t:2:1,newthick);
  graphlabels[topic].thickness:= newthick;
  x0:= 59+round(500*(r[topic-1]-x_min)/
                            (x_max-x_min));
  x1:= 59+round(500*(r[topic]-x_min)/
                            (x_max-x_min));
  spt:=round((x1+x0)/2);
  setfillstyle(solidfill,blue);
  str(topic,tpic);
  if odd(topic) then k:=10 else k:=0;
  bar(spt-10+8*length(tpic),30-k,spt-12+8*
      (length(graphlabels[topic].thickness)
      +length(tpic)),37-k);
  setcolor(white);
  outtextxy(spt-10+8*length(tpic),30-k,
            graphlabels[topic].thickness);
  update:= true;
  readkeybd:= false;
end;

repeat
  Inkey(specialkey,ch,'s','o');

  if key = DownArrow then goto flag_DNar;
  if key = UpArrow then goto flag_UPar;
  if key = leftarrow then goto flag_left;
  if key = rightarrow then goto flag_right;
  if key = PgUp then goto flag_pgup;
```

610

```
          if key = PgDn then goto flag_pgdn;
          if key = AltX then goto flag_end;
          if key = Tab then goto flag_tab;
          if key = AltS then goto flag_save;
          if key = DeleteKey then
            begin
              flag_DEL:
              switch:=true;
              nn[j]:= 0;
              cleardevice;
              goto flag_n;
            end;
          if key = InsertKey then
            begin
              flag_INS:
              switch:=true;
              nn[j]:=j;
              cleardevice;
              goto flag_n;
            end;

      until key = esc;
      goto flag_end;
  end;


PgUp:
    flag_pgup:             {controls which (topic)
                                  parameter to modify}
    begin
    setcolor(black);
      rectangle(44,282+h*14,47,285+h*14);
      j:= j-1;
      h:= h-1;
      if h= 5 then
        h:= h-1;
      if (j > 3) and (pick ='B') then
        begin
          j:=3;
          h:= 3;
        end;
      if j < 1 then j:=1;
      if h < 1 then h:=1;
      setcolor(white);
      rectangle(44,282+h*14,47,285+h*14);
    goto flag_read;
    end;

PgDn:
    flag_pgdn:
    begin
```

611

```
      setcolor(black);
        rectangle(44,282+h*14,47,285+h*14);
        j:= j+1;
        h:= h+1;
        if h = 5 then
          h:=h+1;
        if (j > 3) and (pick ='B') then
          begin
            j:=3;
            h:=3;
          end;
        if j > 9 then j:=9;
        if h > 10 then h:= 10;
        setcolor(white);
        rectangle(44,282+h*14,47,285+h*14);

      goto flag_read;
      end;

LeftArrow:
    begin
    flag_left:

    if param = 0 then
    begin
      setfillstyle(solidfill,black);
      str(topic,tpic);
      bar(569-4*length(tpic),24+topic*28,569-4*
          length(tpic)+8*length(tpic),
          32+topic*28);
      outtextxy(569-4*length(tpic),
                24+topic*28,tpic);
    end;
    if param = 1 then
    begin
      setfillstyle(solidfill,black);
      str(topic,tpic);
      bar(585+4*length(tpic),24+topic*28,
          585+4*length(tpic)+8*
          length(graphlabels[topic].angle),
          32+topic*28);
      setcolor(cyan);
      outtextxy(585+4*length(tpic),24+topic*28,
                graphlabels[topic].angle);
    end;
    if param = 2 then
    begin
      setfillstyle(solidfill,black);
      str(topic,tpic);
      bar(616,24+topic*28,631,32+topic*28);
```

612

```
        setcolor(cyan);
        outtextxy(616,24+topic*28,
            copy(graphlabels[topic].fpercent,1,2));
    end;
    if param = 3 then
    begin
      setfillstyle(solidfill,black);
      str(topic,tpic);
      bar(576,34+topic*28,639,42+topic*28);
      setcolor(cyan);
      outtextxy(576,34+topic*28,
                graphlabels[topic].matname);
    end;
    if param = 4 then
    begin
      x0:= 59+round(500*(r[topic-1]-x_min)/
                                (x_max-x_min));
      x1:= 59+round(500*(r[topic]-x_min)/
                                (x_max-x_min));
      spt:=round((x1+x0)/2);
      setfillstyle(solidfill,black);
      str(topic,tpic);
      if odd(topic) then k:=10 else k:=0;
      bar(spt-10+8*length(tpic),30-k,spt-12+8*
          (length(graphlabels[topic].thickness)
          +length(tpic)),37-k);
      setcolor(cyan);
      outtextxy(spt-10+8*length(tpic),30-k,
                graphlabels[topic].thickness);
    end;

param:= param-1;
if param <= 0 then param:= 0;
setcolor(white);

if param = 0 then
begin
  setfillstyle(solidfill,blue);
  str(topic,tpic);
  bar(569-4*length(tpic),24+topic*28,569-4*
      length(tpic)+8*length(tpic),
      32+topic*28);
  outtextxy(569-4*length(tpic),
            24+topic*28,tpic);
end;

if param = 1 then
begin
  setfillstyle(solidfill,blue);
  str(topic,tpic);
```

```
      bar(585+4*length(tpic),24+topic*28,
          585+4*length(tpic)+8*
          length(graphlabels[topic].angle),
          32+topic*28);
      setcolor(white);
      outtextxy(585+4*length(tpic),24+topic*28,
                graphlabels[topic].angle);
   end;
   if param = 2 then
   begin
      setfillstyle(solidfill,blue);
      str(topic,tpic);
      bar(616,24+topic*28,631,32+topic*28);
      setcolor(white);
      outtextxy(616,24+topic*28,copy
                (graphlabels[topic].fpercent,1,2));
   end;
   if param = 3 then
   begin
      setfillstyle(solidfill,blue);
      str(topic,tpic);
      bar(576,34+topic*28,639,42+topic*28);
      setcolor(white);
      outtextxy(576,34+topic*28,
                graphlabels[topic].matname);
   end;
   if param = 4 then
   begin
      x0:= 59+round(500*(r[topic-1]-x_min)/
                                    (x_max-x_min));
      x1:= 59+round(500*(r[topic]-x_min)/
                                    (x_max-x_min));
      spt:=round((x1+x0)/2);
      setfillstyle(solidfill,blue);
      str(topic,tpic);
      if odd(topic) then k:=10 else k:=0;
      bar(spt-10+8*length(tpic),30-k,spt-12+8*
          (length(graphlabels[topic].thickness)+
          length(tpic)),37-k);
      setcolor(white);
      outtextxy(spt-10+8*length(tpic),30-k,
                graphlabels[topic].thickness);
   end;
   goto flag_read;
   end;

RightArrow:
   begin
   flag_right:
```

```
if param = 0 then
begin
  setfillstyle(solidfill,black);
  str(topic,tpic);
  bar(569-4*length(tpic),24+topic*28,569-4*
      length(tpic)+8*length(tpic),
      32+topic*28);
  outtextxy(569-4*
            length(tpic),24+topic*28,tpic);
end;

if param = 1 then
begin
  setfillstyle(solidfill,black);
  str(topic,tpic);
  bar(585+4*length(tpic),24+topic*28,
      585+4*length(tpic)+8*
      length(graphlabels[topic].angle),
      32+topic*28);
  setcolor(cyan);
  outtextxy(585+4*length(tpic),24+topic*28,
            graphlabels[topic].angle);
end;
if param = 2 then
begin
  setfillstyle(solidfill,black);
  str(topic,tpic);
  bar(616,24+topic*28,631,32+topic*28);
  setcolor(cyan);
  outtextxy(616,24+topic*28,copy
            (graphlabels[topic].fpercent,1,2));
end;
if param = 3 then
begin
  setfillstyle(solidfill,black);
  str(topic,tpic);
  bar(576,34+topic*28,639,42+topic*28);
  setcolor(cyan);
  outtextxy(576,34+topic*28,
            graphlabels[topic].matname);
end;
if param = 4 then
begin
  x0:= 59+round(500*(r[topic-1]-x_min/
                      (x_max-x_min)));
  x1:= 59+round(500*(r[topic]-x_min)/
                      (x_max-x_min)));
  spt:=round((x1+x0)/2);
  setfillstyle(solidfill,black);
  str(topic,tpic);
```

```
         if odd(topic) then k:=10 else k:=0;
         bar(spt-10+8*length(tpic),30-k,spt-12+8*
             (length(graphlabels[topic].thickness)+
             length(tpic)),37-k);
         setcolor(cyan);
         outtextxy(spt-10+8*length(tpic),30-k,
                   graphlabels[topic].thickness);
     end;


     param:= param+1;
     if param >= 4 then param:= 4;
     setcolor(white);

     if param = 1 then
     begin
        setfillstyle(solidfill,blue);
        str(topic,tpic);
        bar(585+4*length(tpic),24+topic*28,
            585+4*length(tpic)+8*
            length(graphlabels[topic].angle),
            32+topic*28);
        setcolor(white);
        outtextxy(585+4*length(tpic),24+topic*28,
                  graphlabels[topic].angle);
     end;
     if param = 2 then
     begin
        setfillstyle(solidfill,blue);
        str(topic,tpic);
        bar(616,24+topic*28,631,32+topic*28);
        setcolor(white);
        outtextxy(616,24+topic*28,copy
                  (graphlabels[topic].fpercent,1,2));
     end;
     if param = 3 then
     begin
        setfillstyle(solidfill,blue);
        str(topic,tpic);
        bar(576,34+topic*28,639,42+topic*28);
        setcolor(white);
        outtextxy(576,34+topic*28,
                  graphlabels[topic].matname);
     end;
     if param = 4 then
     begin
       x0:= 59+round(500*(r[topic-1]-x_min)/
                                (x_max-x_min));
       x1:= 59+round(500*(r[topic]-x_min)/
                                (x_max-x_min));
       spt:=round((x1+x0)/2);
```

616

```
      setfillstyle(solidfill,blue);
      str(topic,tpic);
      if odd(topic) then k:=10 else k:=0;
      bar(spt-10+8*length(tpic),30-k,spt-12+8*
          (length(graphlabels[topic].thickness)+
           length(tpic)),37-k);
      setcolor(white);
      outtextxy(spt-10+8*length(tpic),30-k,
                graphlabels[topic].thickness);
   end;

   goto flag_read;
   end;

InsertKey:
  begin
    goto flag_INS;
  end;

DeleteKey:
  begin
    goto flag_DEL;
  end;

Tab:
  flag_tab:
  begin
    if pick = 'B' then
    begin
      description:= 'Stiff. GPa';
      pick:='A';
      goto flag_found;
    end;
    if pick = 'A' then
    begin
      description:='Comp. 1/TPa';
      pick:='a';
      goto flag_found;
    end;
    if pick = 'a' then
    begin
      description:='R.Comp. 1/TPa';
      pick:='B';
    end;
    flag_found:
    update:=true;
    switch:= true;
    cleardevice;
    goto flag_n;
  end;
```

```
AltS:
  begin
  flag_save:
  setcolor(white);
  setfillstyle(solidfill,black);
  bar(40,19,104,19);
  bar(0,10,39,18);
  setfillstyle(solidfill,blue);
  bar(40,10,104,18);
  newfile:= currentfile;
  delete(newfile,length(newfile)-3,4);
  outtextxy(0,10,'File:'+newfile);
  getnewfname(newfile,OK);
  if OK = false then
    begin
    update:=true;
    switch:= true;
    cleardevice;
    goto flag_n;
    end
  else
    begin
    currentfile:= newfile+'.ves';
    assign(f,currentfile);
    rewrite(f);
    writeln(f,insideDia:5:2);
    writeln(f,wallthick:5:2);
    writeln(f,insidePress:5:2);
    writeln(f,outerPress:5:2);
    for i:= 1 to outerlayer do
      begin
      writeln(f,i); {does layer no}
      writeln(f,graphlabels[i].matname);
      writeln(f,graphlabels[i].angle);
      writeln(f,graphlabels[i].thickness);
      writeln(f,graphlabels[i].fpercent);
      end;
    close(f);
    update:=true;
    switch:= true;
    cleardevice;
    goto flag_n;
    end;
  end;  {altS}
end; {of cases}
until key = esc;


flag_end:
closegraph;
```

```
restorecrtmode;
graphstate:=false;
end;


(********************************************)

procedure Alt_C;     {calculate menu}

var
keyknown,notskip,specialkey,update,readkeybd,dgrad,
full,abrt,axcrs,sucs,NLshear:boolean;
wfile,newmat,p,fpress,newname,extn:string;
redu,ffail,redSS:realarray1NL;
i,layerno,angl:integer;
FilePress:RealarrayNL;
mask:mask_names;

label
flag_end,flag3,flag4,flag_D,flag_6,flag_7,flag_N;

begin
graphstate:=false;
keyknown:=false;

        Flag_7:
        clrscr;
        calcmenu;
        currentfile:='Unknown';
        wfile:= 'file = '+currentfile;
        fastwrite(3,2,wfile,red,black);
        Flag_6:
           repeat
           if not keyknown then
           Inkey(specialkey,ch,'s','o');
           case key of

        AltM:           {vessel interface pressures - discrete
                                           via Roy & Tsai}
              begin
              Repeat
               Flag4:
                discretemenu;
                If not keyknown then
                Inkey(specialkey,ch,'s','o');
                case key of

        AltF:                {vessel interface pressures -
                                        discrete - full}
              begin
              full:=true;
```

619

```
      NLshear:=false;
      if currentfile <> 'Unknown' then
        readkeybd:=false
      else
        readkeybd:=true;
      GraphEditStr(full,readkeybd,NLshear);
      wfile:= 'file = '+currentfile;
      fastwrite(3,2,wfile,red,black);
      goto flag4;
      end;

   AltP:                             {partial equations}
      begin
      full:=false;
      NLshear:= false;
      if currentfile <> 'Unknown' then
        readkeybd:=false
      else
        readkeybd:=true;
      GraphEditStr(full,readkeybd,NLshear);
      wfile:= 'file = '+currentfile;
      fastwrite(3,2,wfile,red,black);
      goto flag4;
      end;

   AltN:                             {nonlinear shear/full}
      begin
      full:=true;
      NLshear:= true;
      if currentfile <> 'Unknown' then
        readkeybd:=false
      else
        readkeybd:=true;
      GraphEditStr(full,readkeybd,NLshear);
      wfile:= 'file = '+currentfile;
      fastwrite(3,2,wfile,red,black);
      goto flag4;
      end;

   AltX,esc:                         {exit to calculate menu}
      begin
      clrscr;
      calcmenu;
      keyknown:=false;
      currentfile:='Unknown';
      goto flag_7;
    end;
end;
If not (Key In [AltX,AltF,AltP,AltN,esc]) then
begin
```

```
GotoXY(58, 2);
textbackground(cyan);
textcolor(red);
beep(600,150);
Write('Error-Inadmissible Key');
delay(2000);
GotoXY(58,2);
Textbackground(black);
Write('                              ');
gotoxy(3,4);
textcolor(yellow);
notskip:=true;
goto flag4;
end; {if}
until key = esc;
notskip:=true;
end; {altV case}

AltS:                    {multilayer laminate properties}
  begin
  update:=false;
  readkeybd:= true;
  mask[1]:='*.VES';
  mask[2]:='';
  readvesf(Newmat,mask,redu,ffail,redSS,
           outerlayer,layerno,angl,readkeybd,
           update,dgrad,abrt);
  if abrt = true then goto flag_7;
  Laminateprop(outerlayer);
  Calcmenu;        {erases previous screen leftovers}
  OutputDescTable(3,7,6,6,7,1,2,3,1,Q,CC);
                                    {displays results}
  fastwrite(64,2,'Laminate Matrix',
           lightgray,black);
  wfile:= 'file = '+currentfile;
  fastwrite(3,2,wfile,lightgray,black);
  Inkey(specialkey,ch,'s','o');
  keyknown:=false; {forces to read again}
  goto flag_7;
  end;

AltV:                              {switch to var plot menu}
  begin
  Alt_R;
  goto flag_7;
  end;

AltF: {Plot of stiff for fitting & graphics editor}
  begin
  Alt_P;
```

621

```
                   goto flag_7;
                   end;

              AltX:                                    {exit to main menu}
                 begin;
                 goto flag_end;
                 end;
              end{case};

              If not (Key In [ALTL,ALTS,AltX,AltM,AltF,ALTV,esc])
                                                                then
              begin
              GotoXY(58, 2);
              textbackground(cyan);
              textcolor(red);
              beep(600,150);
              Write('Error-Inadmissible Key');
              delay(2000);
              GotoXY(58,2);
              Textbackground(black);
              Write('                           ');
              gotoxy(3,4);
              textcolor(yellow);
              notskip:=true;
              goto flag_7;
              end;
              until key = esc;
              notskip:=true;

flag_end:
closegraph;
restorecrtmode;
graphstate:=false;
clrscr;
mainmenu;
keyknown:=false;
currentfile:='Unknown';
end;


(****************************************************)

procedure Alt_E;                    {edit menu}

var
f:text;
keyknown,notskip,specialkey,axcrs,abrt,model,fit,dgrad,
metal:boolean;
p,wfile:string;
qx,qy,wr,sr,i,j:integer;
El,Et,dEt,dGl,Vl,Vt,Gl,Gt,Kt,ffm,Em,Vm,ffs,XT,XC,YT,YC,
```

622

```
SS:real;
ercd:integerarray16;
redu,ffail,Rss:realarray1NL;
mask:mask_names;
d:dirstr;
n:namestr;
e:extstr;

label

flag5,flag_mat,flag_lam,flag_end;

begin

curser_off(stype);
dgrad:=false;
keyknown:=false;
 for j:=1 to 9 do
   for i:=1 to 5 do
   begin
     holdstr[i,j]:='';
   end;

Flag5:
     repeat
     clrscr;
     editmenu;
     curser_off(stype);
     if not keyknown then
     Inkey(specialkey,ch,'s','o');
     case key of

        AltW:                   {edit vessel wall construction}
          begin
          windowlength:=12; {redefine default edit window
                                              size}
          maxlength:=12;
          mask[1]:='*.WAL';
          mask[2]:='';
          fastwrite(3,2,'Ins & Enter',yellow,red);
          fastwrite(61,2,'PgUp:PgDn:Home:End',yellow,red);
          Getfilepar(mask,p,qx,qy,false,axcrs,abrt); {qx,qy =
                                  defines size of file to read}
          if abrt = true then goto flag5;
          Readfile(qx,qy,p,axcrs);          {p=path & filename)}
          clrscr;
          editmenu;
          fastwrite(3,2,'Tab:S-Tab:Ins:Enter',yellow,red);
          fastwrite(61,2,'PgUp:PgDn:Home:End',yellow,red);
          windowlength:=12; {redefine def. edit window size}
```

```
        maxlength:=12;
        mask[1]:='*.mat';
        InputDescTable(5,6,5,15,12,1,0,0,3,3);
        MoveEditWindow(mask,false,'T',21,5,6,5,15,12,
                                    1,0,0,3,notskip,abrt);
        if abrt = true then goto flag5;
        savefile;
        keyknown:=false;                    {forces keyboard read}
        currentfile:='Unknown';
        goto flag5;
        end; {case W}

    AltP:                                   {pressure / loads}
        begin
        mask[1]:='*.LDS';
        Getfilepar(mask,p,qx,qy,false,axcrs,abrt);  {qx,qy =
                            defines size of file to read}
        if abrt = true then goto flag5;
        Readfile(qx,qy,p,axcrs);
        clrscr;
        editmenu;
        wfile:= 'file = '+currentfile;
        fastwrite(3,2,wfile,lightgray,black);
        windowlength:=6;
        maxlength:=6;
        textbackground(black);
        InputdescTable(3,6,1,4,6,1,1,20,2,4);
        mask[1]:='off';
        fastwrite(62,2,'Arrow Keys:Enter',yellow,red);
        MoveEditWindow(mask,false,'N',0,3,6,1,4,6,
                                    1,1,20,2,notskip,abrt);
        if abrt = true then goto flag5;
        savefile;
        keyknown:=false;
        currentfile:='Unknown';
        end; {case P}

    AltB:              {build .ves file}
        begin
        fastwrite(61,2,'PgUp:PgDn:Home:End',yellow,red);
        fastwrite(3,2,'Arrow keys:Ins:Enter',yellow,red);
        join(abrt);
        if abrt = true then goto flag5;
        keyknown:=false;
        currentfile:='Unknown';
        goto flag5;
        end; {case B}

AltL: {input lamina prop., generate & view .mat file}
        begin
```

```
if currentfile='Unknown' then
begin
   mask[1]:='*.LAM';
   mask[2]:='';
   fastwrite(61,2,'PgUp:PgDn:Home:End',yellow,red);
   fastwrite(3,2,'Ins & Enter',yellow,red);
   Getfilepar(mask,p,qx,qy,false,axcrs,abrt);
   if abrt = true then goto flag5;
   Readfile(qx,qy,p,axcrs); {p=path & filename}}
end
else
begin
   Readfile(qx,qy,currentfile,axcrs); {p=path &
                                        filename}}
   goto flag_mat;
end;
clrscr;
editmenu;
fastwrite(3,2,currentfile,lightgray,black);
windowlength:=6;
maxlength:=13;
holdstr[2,8]:='';
holdstr[2,9]:='';
InputDescTable(3,6,2,9,6,2,8,25,2,11);
mask[1]:='off';
fastwrite(61,2,char(24)+char(58)+char(25)+
          ':Tab:Shift-Tab',yellow,red);
MoveEditWindow(mask,false,'T',0,3,6,2,9,6,2,8,
               25,2,notskip,abrt);
if (abrt = true) or (Key = AltX) or (key =
                                   carriagereturn) then
begin
   currentfile:= 'Unknown';
   goto flag5;
end;
savefile;                  {saves .lam and any changes}
if key = carriagereturn then
begin
   currentfile:='Unknown';
   goto flag5;
end;
flag_mat:
 GenerateMatProp(dEt,dGl); {does decomp math &
                         writes fiber prop [.mat] file}
 fsplit(p,d,n,e);
 currentfile:=n+'.MAT';
 Readfile(qx,qy,currentfile,axcrs); {p=path &
                                     filename}}
 clrscr;
 editmenu;
```

```
      fastwrite(3,2,currentfile,lightgray,black);
                              {displays .mat properties}
      windowlength:=6;
      maxlength:=13;
      InputDescTable(3,6,2,9,6,2,8,25,2,13);
      mask[1]:='off';
      fastwrite(61,2,char(24)+char(58)+char(25)+
              ':Tab:Shift-Tab',yellow,red);
      MoveEditWindow(mask,false,'T',0,3,6,2,9,6,2,8,
                  25,2,notskip,abrt);
      if (abrt = true) or (key = AltX) then
      begin
         currentfile:= 'Unknown';
         goto flag5;
      end;
      savefile;    {saves .mat file and any changes made}
      keyknown:=true;
      Goto flag5;
      end;


AltM: {input .mat prop., calculate & view .lam prop.}
      Begin
      if currentfile='Unknown' then
      begin
         mask[1]:='*.MAT';
         mask[2]:='';
         fastwrite(61,2,'PgUp:PgDn:Home:End',yellow,red);
         fastwrite(3,2,'Ins & Enter',yellow,red);
         Getfilepar(mask,p,qx,qy,false,axcrs,abrt);
         if abrt = true then goto flag5;
         Readfile(qx,qy,p,axcrs); {p=path & filename)}
      end
      else
      begin
         Readfile(qx,qy,currentfile,axcrs); {p=path &
                                          filename)}
         goto flag_lam;
      end;
      windowlength:=6;
      maxlength:=13;
      clrscr;
      editmenu;
      fastwrite(3,2,currentfile,lightgray,black);
      InputDescTable(3,6,2,9,6,2,8,25,2,13);
      mask[1]:='off';
      fastwrite(61,2,char(24)+char(58)+char(25)+
              ':Tab:Shift-Tab',yellow,red);
      MoveEditWindow(mask,false,'T',0,3,6,2,9,6,
                  2,8,25,2,notskip,abrt);
      if (abrt = true) or (key = ALTX) then
```

```
    begin
      currentfile:='Unknown';
      goto flag5;
    end;
    savefile;      {saves any changes made to .mat file}
    if key = carriagereturn then
    begin
      currentfile:='Unknown';
      goto flag5;
    end;
flag_lam:
 val(holdstr[1,1],El,ercd[1]);
 val(holdstr[1,2],Vl,ercd[2]);
 val(holdstr[1,3],Gl,ercd[3]);
 val(holdstr[1,4],Et,ercd[4]);
 val(holdstr[1,5],Vt,ercd[5]);
 val(holdstr[1,6],Gt,ercd[6]);
 val(holdstr[1,7],Kt,ercd[7]);
 val(holdstr[1,8],Em,ercd[8]);
 val(holdstr[1,9],Vm,ercd[9]);
 val(holdstr[2,1],XT,ercd[12]);
 val(holdstr[2,2],XC,ercd[13]);
 val(holdstr[2,3],YT,ercd[14]);
 val(holdstr[2,4],YC,ercd[15]);
 val(holdstr[2,5],SS,ercd[16]);
  val(holdstr[2,6],ffm,ercd[10]);
 if (holdstr[2,7]='T-iso')or(holdstr[2,7]=' T-iso')
 or(holdstr[2,7]='t-iso')or(holdstr[2,7]=' t-iso')
                                           then
    Model:=true
 else
    Model:=false;
 if(holdstr[2,8]='Yes') or (holdstr[2,8]= ' Yes')
 or(holdstr[2,8]= '  Yes')or(holdstr[2,8]= '   Yes')
 or(holdstr[2,8]= 'yes')or(holdstr[2,8]= ' yes')
 or(holdstr[2,8]= '  yes')or(holdstr[2,8]= '   yes')
                                           then
    fit:=true
 else
    fit:=false;
 if(holdstr[2,9]= 'Yes')or(holdstr[2,9]= ' Yes')
 or(holdstr[2,9]= '  Yes')or(holdstr[2,9]= '   Yes')
 or(holdstr[2,9]= 'yes')or(holdstr[2,9]= ' yes')
 or(holdstr[2,9]= '  yes')or(holdstr[2,9]= '   yes')
                                           then
    metal:=true
 else
    metal:=false;
 i:= 1;
 calculate_prop(Model,metal,fit,dgrad,i,GL,El,
```

```
                           Et,dEt,Vl,Vt,Gl,dGl,Gt,Kt,ffm,Em,
                           Vm,ffs,redu,ffail,Rss,ercd);

     str(Elconst[1].El:13:10,holdstr[1,1]);
     str(Elconst[1].Vl:13:10,holdstr[1,2]);
     str(Elconst[1].Gl:13:10,holdstr[1,3]);
     str(Elconst[1].Et:13:10,holdstr[1,4]);
     str(Elconst[1].Vt:13:10,holdstr[1,5]);
     str(Elconst[1].Gt:13:10,holdstr[1,6]);
     str(Elconst[1].KK:13:10,holdstr[1,7]);
     str(Em:13:10,holdstr[1,8]);
     str(Vm:13:10,holdstr[1,9]);
     str(XT:7:3,holdstr[2,1]);
     str(XC:7:3,holdstr[2,2]);
     str(YT:7:3,holdstr[2,3]);
     str(YC:7:3,holdstr[2,4]);
     str(SS:7:3,holdstr[2,5]);
     str(ffm:7:3,holdstr[2,6]);
     if model=true then
        holdstr[2,7]:= ' T-iso'
     else
        holdstr[2,7]:= '    iso';
     if fit=true then
        holdstr[2,8]:= '    Yes'
     else
        holdstr[2,8]:= '     No';
     if metal=true then
        holdstr[2,9]:= '    Yes'
     else
        holdstr[2,9]:= '     No';
     clrscr;
     editmenu;
     fsplit(p,d,n,e);
     currentfile:=n+'.LAM';
     fastwrite(3,2,currentfile,lightgray,black);
     InputDescTable(3,6,2,9,6,2,8,25,2,12);   {disp .lam}
     mask[1]:='off';
     fastwrite(61,2,char(24)+char(58)+char(25)+
               ':Tab:Shift-Tab',yellow,red);
     MoveEditWindow(mask,false,'T',0,3,6,2,9,6,
                    2,8,25,2,notskip,abrt);
     if (abrt = true) or (key = AltX)  then
     begin
        currentfile:='Unknown';
        goto flag5;
     end;
     if model=true then
        holdstr[2,7]:= ' T-iso'
     else
        holdstr[2,7]:= '    iso';
```

```
        if fit=true then
          holdstr[2,8]:= '   Yes'
        else
          holdstr[2,8]:= '     No';
        if metal=true then
          holdstr[2,9]:= '   Yes'
        else
          holdstr[2,9]:= '     No';
        savefile;  {saves changes made to .lam or simply
                                        computed values}
        keyknown:=true;
        goto flag5;
        end;  {case M}

  AltX:                   {exit to mainmenu}
        begin
        clrscr;
        mainmenu;
        keyknown:=false;
        currentfile:='Unknown';
        goto flag_end;
        end;

  Carriagereturn:
        begin
        keyknown:=false;{forces to look for next keystroke}
        currentfile:='Unknown';
        goto flag5;
        end;

end;{cases}

    If not (Key In [carriagereturn,AltB,AltL,AltM,
           AltW,AltX,esc]) then
    begin
    GotoXY(58, 2);
    textbackground(cyan);
    textcolor(red);
    beep(600,150);
    Write('Error-Inadmissible Key');
    delay(2000);
    GotoXY(58,2);
    Textbackground(black);
    Write('                          ');
    gotoxy(3,4);
    textcolor(yellow);
    notskip:=true;
    goto flag5;
    end;
    until (key = esc) or (key = altx);
```

```
         notskip:=true;

flag_end:
end;


(*********************************************)

Procedure Alt_D(itter:boolean);    {graphics editor for
                                     finite difference}

var
param,layerno,angl,numb:integer;
variate,keyknown,specialkey:boolean;
Newmat,vexp,Cmult,lab:string;
radius,Sig_r,Sig_z,Sig_f:realarray2plusN;

valu,expn,x_max,x_min,y_max,y_min:real;
stor_l,stor_m,stor_d,stor_i,stor_j,stor_k,stor_G11,stor_G12,
stor_G22,
stor_a13,stor_a23,stor_a33:real;
typ:char;

label
flag_dif,flagX,flag_var;

begin

lab:='B11';
typ:='6';
numb:=1;
param:=2;
variate:= false;
Laminateprop(outerlayer);

flag_var:

finiteD(radius,Sig_r,Sig_f,Sig_z,variate,itter);
plotvgraphs(radius,Sig_r,Sig_f,Sig_z,x_max,x_min,y_max,
            y_min,numb);

if itter = true  then
  plotoutline('Radius (mm)','Stress MPa','All Variable -
Free Axial','',5,5,x_min,x_max,y_min,y_max);
if itter = false then
  plotoutline('Radius (mm)','Stress MPa','All Variable -
              fixed Axial','',5,5,x_min,x_max,y_min,y_max);

if variate = false then
begin
  stor_l:=bfit.l;
```

630

```
      stor_m:=bfit.m;
      stor_d:=bfit.d;
      stor_G11:=bfit.G11;
      stor_G12:=bfit.G12;
      stor_G22:=bfit.G22;
      stor_i:=bfit.i;
      stor_j:=bfit.j;
      stor_k:=bfit.k;
      stor_a13:=bfit.a13;
      stor_a23:=bfit.a23;
      stor_a33:=bfit.a33;

      valu:=bfit.G11;
      expn:=bfit.l;
   end;

   setfillstyle(solidfill,black);
   bar(500,0,639,26);
   setcolor(lightcyan);
   str(1000*valu:4:1,Cmult);
   str(-expn:4:2,vexp);
   settextjustify(righttext,toptext);
   outtextxy(600,18,lab+'='+Cmult+'(p)');
   settextjustify(lefttext,toptext);
   outtextxy(600,12,vexp);

   flag_Dif:
   Keyknown:=false;

   if param = 2 then
   begin
      setfillstyle(solidfill,black);
      str(1000*valu:4:1,Cmult);
      bar(576,18,576-8*length(Cmult),26);
      settextjustify(righttext,toptext);
      setcolor(lightcyan);
      outtextxy(576,18,Cmult);
      setfillstyle(solidfill,black);
      bar(600,12,639,20);
      setfillstyle(solidfill,blue);
      str(-expn:4:2,vexp);
      bar(600,12,600+8*length(vexp),20);
      settextjustify(lefttext,toptext);
      setcolor(white);
      outtextxy(600,12,vexp);
   end;
   if param = 1 then
   begin
      setfillstyle(solidfill,black);
      str(-expn:4:2,vexp);
```

631

```
      bar(600,12,639,20);
      settextjustify(lefttext,toptext);
      setcolor(lightcyan);
      outtextxy(600,12,vexp);
      str(1000*valu:4:1,Cmult);
      setfillstyle(solidfill,blue);
      bar(576,18,576-8*length(Cmult),26);
      settextjustify(righttext,toptext);
      setcolor(white);
      outtextxy(576,18,Cmult);
      settextjustify(lefttext,toptext);
  end;

    repeat
    if not keyknown then Inkey(specialkey,ch,'s','o');

    case key of

    AltX:
      begin
      keyknown:=true;
      goto flagX;
    end;

    UpArrow:
      begin
      variate:=true;
      if param = 2 then
      begin
        expn:= expn - 0.01;
        str(-expn:4:2,vexp);
        setfillstyle(solidfill,blue);
        bar(600,12,600+8*length(vexp),20);
        settextjustify(lefttext,toptext);
        setcolor(white);
        outtextxy(600,12,vexp);

        if numb = 1 then
          begin
            bfit.l:=expn;
            valu:=bfit.G11;
            lab:='B11';
          end;
        if numb = 2 then
          begin
            bfit.m:= expn;
            valu:=bfit.G12;
            lab:='B12';
          end;
        if numb = 3 then
```

```
            begin
               bfit.d:= expn;
               valu:=bfit.G22;
               lab:='B22';
            end;
         if numb = 4 then
            begin
               bfit.i:= expn;
               valu:=bfit.a13;
               lab:='a13';
            end;
         if numb = 5 then
            begin
               bfit.j:= expn;
               valu:=bfit.a23;
               lab:='a23';
            end;
         if numb = 6 then
            begin
               bfit.k:= expn;
               valu:=bfit.a33;
               lab:='a33';
            end;
end;
if param = 1 then
begin
   valu:= valu +0.001;
   str(1000*valu:4:1,Cmult);
   setfillstyle(solidfill,blue);
   bar(576,18,576-8*length(Cmult),26);
   settextjustify(righttext,toptext);
   setcolor(white);
   outtextxy(576,18,Cmult);

   if numb = 1 then
      begin
         expn:=bfit.l;
         bfit.G11:=valu;
         lab:='B11';
      end;
   if numb = 2 then
      begin
         expn:= bfit.m;
         bfit.G12:=valu;
         lab:='B12';
      end;
   if numb = 3 then
      begin
         expn:=bfit.d;
         bfit.G22:=valu;
```

633

```
                  lab:='B22';
              end;
          if numb = 4 then
              begin
                  expn:=bfit.i;
                  bfit.a13:=valu;
                  lab:='a13';
              end;
          if numb = 5 then
              begin
                  expn:=bfit.j;
                  bfit.a23:=valu;
                  lab:='a23';
              end;
          if numb = 6 then
              begin
                  expn:=bfit.k;
                  bfit.a33:=valu;
                  lab:='a33';
              end;
      end;
      goto flag_Dif;
      end;

DownArrow:
    begin
    variate:= true;
    if param = 2 then
    begin
      expn:= expn + 0.01;
      str(-expn:4:2,vexp);
      setfillstyle(solidfill,blue);
      settextjustify(lefttext,toptext);
      bar(600,12,600+8*length(vexp),20);
      setcolor(white);
      outtextxy(600,12,vexp);

      if numb = 1 then
          begin
            bfit.l:=expn;
            valu:=bfit.G11;
            lab:='B11';
          end;
      if numb = 2 then
          begin
            bfit.m:= expn;
            valu:=bfit.G12;
            lab:='B12';
          end;
      if numb = 3 then
```

634

```
      begin
        bfit.d:= expn;
        valu:=bfit.G22;
        lab:='B22';
      end;
   if numb = 4 then
      begin
        bfit.i:= expn;
        valu:=bfit.a13;
        lab:='a13';
      end;
   if numb = 5 then
      begin
        bfit.j:= expn;
        valu:=bfit.a23;
        lab:='a23';
      end;
   if numb = 6 then
      begin
        bfit.k:= expn;
        valu:=bfit.a33;
        lab:='a33';
      end;
end;

if param = 1 then
begin
   valu:= valu -0.001;
   str(1000*valu:4:1,Cmult);
   setfillstyle(solidfill,blue);
   bar(576,18,576-8*length(Cmult),26);
   settextjustify(righttext,toptext);
   setcolor(white);
   outtextxy(576,18,Cmult);

   if numb = 1 then
      begin
        expn:=bfit.l;
        bfit.G11:=valu;
        lab:='B11';
      end;
   if numb = 2 then
      begin
        expn:= bfit.m;
        bfit.G12:=valu;
        lab:='B12';
      end;
   if numb = 3 then
      begin
        expn:=bfit.d;
```

```
                bfit.G22:=valu;
                lab:='B22';
            end;
        if numb = 4 then
            begin
                expn:=bfit.i;
                bfit.a13:=valu;
                lab:='a13';
            end;
        if numb = 5 then
            begin
                expn:=bfit.j;
                bfit.a23:=valu;
                lab:='a23';
            end;
        if numb = 6 then
            begin
                expn:=bfit.k;
                bfit.a33:=valu;
                lab:='a33';
            end;
        end;
    goto flag_Dif;
    end;


LeftArrow:
    begin
    param:= param-1;
    if param <= 1 then
        param:=1;
    if param = 1 then
    begin
        setfillstyle(solidfill,black);
        bar(600,12,639,20);
        settextjustify(lefttext,toptext);
        setcolor(lightcyan);
        str(-expn:4:2,vexp);
        outtextxy(600,12,vexp);
        str(1000*valu:4:1,Cmult);
        setfillstyle(solidfill,blue);
        bar(576,18,576-8*length(Cmult),26);
        settextjustify(righttext,toptext);
        setcolor(white);
        outtextxy(576,18,Cmult);
        settextjustify(lefttext,toptext);
    end;
    goto flag_dif;
    end;
RightArrow:
    begin
```

636

```
         param:= param+1;
         if param >= 2 then
           param:=2;
         if param = 2 then
         begin
            str(1000*valu:4:1,Cmult);
            setfillstyle(solidfill,black);
            bar(576,18,576-8*length(Cmult),26);
            settextjustify(righttext,toptext);
            setcolor(lightcyan);
            outtextxy(576,18,Cmult);
            setfillstyle(solidfill,blue);
            bar(600,12,639,20);
            settextjustify(lefttext,toptext);
            setcolor(white);
            str(-expn:4:2,vexp);
            outtextxy(600,12,vexp);
         end;
         goto flag_dif;
         end;
PgDn:
      begin
      setcolor(black);
      rectangle(583,42+12*numb,585,44+12*numb);
      numb:= numb + 1;
      if numb >= 6 then
         numb:=6;
      setcolor(white);
      rectangle(583,42+12*numb,585,44+12*numb);

         if numb = 1 then
         begin
            valu:=bfit.G11;
            expn:=bfit.l;
            lab:='B11';
         end;
         if numb = 2 then
         begin
            valu:=bfit.G12;
            expn:=bfit.m;
            lab:='B12';
         end;
         if numb = 3 then
         begin
            valu:=bfit.G22;
            expn:=bfit.d;
            lab:='B22';
         end;
         if numb = 4 then
         begin
```

```
            valu:=bfit.a13;
            expn:=bfit.i;
            lab:='a13';
         end;
         if numb = 5 then
         begin
            valu:=bfit.a23;
            expn:=bfit.j;
            lab:='a23';
         end;
         if numb = 6 then
         begin
            valu:=bfit.a33;
            expn:=bfit.k;
            lab:='a33';
         end;

         setfillstyle(solidfill,black);
         bar(500,0,639,26);
         setcolor(lightcyan);
         str(1000*valu:4:1,Cmult);
         str(-expn:4:2,vexp);
         settextjustify(righttext,toptext);
         outtextxy(600,18,lab+'='+Cmult+'(p)');
         settextjustify(lefttext,toptext);
         outtextxy(600,12,vexp);

         goto flag_Dif;
         end;

PgUp:
   begin
   setcolor(black);
   rectangle(583,42+12*numb,585,44+12*numb);
   numb:= numb - 1;
   if numb <= 1 then
      numb:= 1;
   setcolor(white);
   rectangle(583,42+12*numb,585,44+12*numb);

      if numb = 1 then
      begin
         valu:=bfit.G11;
         expn:=bfit.l;
         lab:='B11';
      end;
      if numb = 2 then
      begin
         valu:=bfit.G12;
         expn:=bfit.m;
```

638

```
            lab:='B12';
         end;
      if numb = 3 then
      begin
         valu:=bfit.G22;
         expn:=bfit.d;
         lab:='B22';
      end;
      if numb = 4 then
      begin
         valu:=bfit.a13;
         expn:=bfit.i;
         lab:='a13';
      end;
      if numb = 5 then
      begin
         valu:=bfit.a23;
         expn:=bfit.j;
         lab:='a23';
      end;
      if numb = 6 then
      begin
         valu:=bfit.a33;
         expn:=bfit.k;
         lab:='a33';
      end;

   setfillstyle(solidfill,black);
   bar(500,0,639,26);
   setcolor(lightcyan);
   str(1000*valu:4:1,Cmult);
   str(-expn:4:2,vexp);
   settextjustify(righttext,toptext);
   outtextxy(600,18,lab+'='+Cmult+'(p)');
   settextjustify(lefttext,toptext);
   outtextxy(600,12,vexp);
   goto flag_Dif;
   end;

Insertkey:
   begin
   cleardevice;
   goto flag_var;
   end;
HomeKey:
   begin
   bfit.l:= stor_l;
   bfit.m:= stor_m;
   bfit.d:= stor_d;
   bfit.G11:= stor_G11;
```

```
bfit.G12:= stor_G12;
bfit.G22:= stor_G22;
bfit.i:= stor_i;
bfit.j:= stor_j;
bfit.k:= stor_k;
bfit.a13:= stor_a13;
bfit.a23:= stor_a23;
bfit.a33:= stor_a33;

if numb = 1 then
begin
   valu:=bfit.G11;
   expn:=bfit.l;
   lab:='B11';
end;
if numb = 2 then
begin
   valu:=bfit.G12;
   expn:=bfit.m;
   lab:='B12';
end;
if numb = 3 then
begin
   valu:=bfit.G22;
   expn:=bfit.d;
   lab:='B22';
end;
if numb = 4 then
begin
   valu:=bfit.a13;
   expn:=bfit.i;
   lab:='a13';
end;
if numb = 5 then
begin
   valu:=bfit.a23;
   expn:=bfit.j;
   lab:='a23';
end;
if numb = 6 then
begin
   valu:=bfit.a33;
   expn:=bfit.k;
   lab:='a33';
end;

setfillstyle(solidfill,black);
bar(500,0,639,26);
setcolor(lightcyan);
str(1000*valu:4:1,Cmult);
```

640

```
      str(-expn:4:2,vexp);
      settextjustify(righttext,toptext);
      outtextxy(600,18,lab+'='+Cmult+'(p)');
      settextjustify(lefttext,toptext);
      outtextxy(600,12,vexp);
      goto flag_dif;
      end;

EndKey:

   begin
   if numb = 1 then
   begin
      valu:=stor_G11;
      expn:=stor_l;
      lab:='B11';
   end;
   if numb = 2 then
   begin
      valu:=stor_G12;
      expn:=stor_m;
      lab:='B12';
   end;
   if numb = 3 then
   begin
      valu:=stor_G22;
      expn:=stor_d;
      lab:='B22';
   end;
   if numb = 4 then
   begin
      valu:=stor_a13;
      expn:=stor_i;
      lab:='a13';
   end;
   if numb = 5 then
   begin
      valu:=stor_a23;
      expn:=stor_j;
      lab:='a23';
   end;
   if numb = 6 then
   begin
      valu:=stor_a33;
      expn:=stor_k;
      lab:='a33';
   end;

   setfillstyle(solidfill,black);
   bar(500,0,639,26);
```

```
        setcolor(lightcyan);
        str(1000*valu:4:1,Cmult);
        str(-expn:4:2,vexp);
        settextjustify(righttext,toptext);
        outtextxy(600,18,lab+'='+Cmult+'(p)');
        settextjustify(lefttext,toptext);
        outtextxy(600,12,vexp);
        goto flag_dif;
        end;

   end; {cases}
   until key = esc;

flagX:
end;

(******************************************)

end. {unit}
```

```pascal
unit Alt_Futl;

{$O+,F+}

(*************************************************)

interface

uses glob_var,dos,crt,graph,ves_util,
menus,FSTvideo,editor;

procedure Alt_U;

(*************************************************)

implementation

(*************************************************)

procedure displaycontents(var fline:filelines;var
maxline:integer);

var
keyknown,specialkey:boolean;
i,j,upper:integer;

label
flag_keyin;

begin
keyknown:=false;
j:=0;
gotoxy(3,2);
textbackground(black);
textcolor(lightgray);
write(currentfile+' ');
textbackground(black);
textcolor(white);
window(3,4,79,22);
clrscr;
curser_off(stype);
if maxline < 19 then
  upper:= maxline
else
  upper:= 19;
for i:= 1 to upper do
  writeln(fline[i]);

repeat
if not keyknown then
```

```pascal
      flag_keyin:
      inkey(specialkey,ch,'s','o');

      case key of

      PgDn:
        begin
        j:= j+10;
        if (j+upper) > maxline then
        begin
          j:= maxline-upper;
          beep(1600,600);
          goto flag_keyin;
        end;
        for i:= 1 to upper do
          writeln(fline[i+j]);
        end;

      PgUp:
        begin
        j:= j-10;
        if j < 0 then
        begin
          j:= 0;
          beep(1600,600);
          goto flag_keyin;
        end;
        for i:= 1 to upper do
          writeln(fline[i+j]);
        end;

      Homekey:
        begin
        j:=0;
        for i:= 1 to upper do
          writeln(fline[i+j]);
        end;

      Endkey:
        begin
        j:=maxline-upper;
        for i:= 1 to upper do
          writeln(fline[i+j]);
        end;

      end; {cases}
until (key = esc) or (key = altX);
clrscr;
window(1,1,80,25);
end;
```

```
(*******************************************)

Procedure ALT_U;

var

keyknown,specialkey,axcrs,abrt,sucs:boolean;
mask:mask_names;
p,newname,extn:string;
qx,qy,i,j,maxline:integer;
f:text;
s:string[80];
fline:filelines;

label

flag1,flag_N,flag_D,flag_end,flag_R,jumpout_R;

begin
keyknown:= false;
Flag1:
clrscr;
utilmenu;
repeat
if not keyknown then
   inkey(specialkey,ch,'s','o');

   case key of

   AltR:                  {Rename file}
     begin
     flag_N:
     mask[1]:='*.lam';
     mask[2]:='*.mat';
     mask[3]:='*.wal';
     mask[4]:='*.lds';
     mask[5]:='*.prs';
     mask[6]:='*.ves';
     mask[7]:='';
     fastwrite(3,2,'Ins & Enter',yellow,red);
     fastwrite(61,2,'PgUp:PgDn:Home:End',yellow,red);
     Getfilepar(mask,p,outerlayer,i,true,axcrs,abrt);
     if abrt = true then goto flag1;
     renamefile(sucs,newname);
     if sucs = false then goto flag_N;
     currentfile:=newname;
     goto flag1;
     end;
```

```
AltD:                        {delete file}
   begin
     flag_D:
     mask[1]:='*.lam';
     mask[2]:='*.mat';
     mask[3]:='*.wal';
     mask[4]:='*.lds';
     mask[5]:='*.prs';
     mask[6]:='*.ves';
     mask[7]:='';
     fastwrite(61,2,'PgUp:PgDn:Home:End',yellow,red);
     fastwrite(3,2,'Ins & Enter',yellow,red);
     Getfilepar(mask,p,qx,qy,true,axcrs,abrt);
     if abrt = true then goto flag1;
     deletefile(sucs);
     if sucs = false then goto flag_D;
     gotoxy(4,5);
     textcolor(white);
     textbackground(black);
     write('                ');
     gotoxy(4,5);
     textbackground(red);
     write('File '+currentfile+' Deleted');
     beep(1600,600);
     delay(15000);
     currentfile:='Unknown';
     goto flag1;
   end;

AltN:              {new file}
   begin
     mask[1]:='*.lam';
     mask[2]:='*.mat';
     mask[3]:='*.wal';
     mask[4]:='*.lds';
     mask[5]:='*.prs';
     mask[6]:='';                  {signals exit condition}
     fastwrite(3,2,'Ins & Enter',yellow,red);
     fastwrite(61,2,'PgUp:PgDn:Home:End',yellow,red);
     Getfilepar(mask,p,qx,qy,true,axcrs,abrt);
     if abrt = true then goto flag1;

     for i:= 1 to qx do {makes sure that file saved is
                                           empty}
     for j:= 1 to qy do
     begin
       holdstr[i,j]:= '';
     end;
     savefile;
     textbackground(black);
```

646

```
        textcolor(white);
        gotoxy(4,5);
        write('                                                    ');
        gotoxy(4,5);
        writeln('File '+p+' Created');
        textcolor(yellow);
        gotoxy(9,5);
        writeln(p);
        delay(10000);
        currentfile:='Unknown';            .
        goto flag1;
      end;

  ALTV:
      begin                    {view contents}
      mask[1]:='*.lam';
      mask[2]:='*.mat';
      mask[3]:='*.wal';
      mask[4]:='*.lds';
      mask[5]:='*.prs';
      mask[6]:='*.ves';
      mask[7]:='*.D*';
      mask[8]:='';
      fastwrite(61,2,'PgUp:PgDn:Home:End',yellow,red);
      fastwrite(3,2,'Ins & Enter',yellow,red);
      Getfilepar(mask,p,qx,qy,true,axcrs,abrt);
      if abrt = true then goto flag1;
      assign(f,currentfile);
      reset(f);
      i:= 0;
      while not eof(f) do
        begin
          i:= i+1;
          readln(f,s);
          fline[i]:=s;
          if i > 300 then goto jumpout_R;
        end;
      jumpout_R:
      close(f);
      maxline:=i;
      displaycontents(fline,maxline);
      end;

  AltX:            {exit to main menu}
     begin;
       clrscr;
       mainmenu;
       keyknown:=false;
       currentfile:='Unknown';
       goto flag_end;
```

647

```pascal
          end;
        end{case};

If not (Key In [carriagereturn,AltX,AltD,AltR,
                AltV,ALTN,esc]) then
begin
   GotoXY(58,2);
   textbackground(cyan);
   textcolor(red);
   beep(600,150);
   Write('Error-Inadmissible Key');
   delay(2000);
   GotoXY(58,2);
   Textbackground(black);
   Write('                         ');
   gotoxy(3,4);
   textcolor(yellow);
   goto flag1;
end;
until key = esc;
flag_end:
end;

(***************************************************)

end. {unit}
```

```pascal
unit Alt_Laye;
{$O+,F+}

(*******************************************)

interface

uses glob_var,dos,crt,compmath,ves_util,
     menus,FSTvideo,editor;

procedure Alt_l;

(*******************************************)

implementation

(*******************************************)

procedure Alt_l;        {single layer menu}

var
keyknown,specialkey,dgrad,abrt,readkeybd,update:boolean;
mask:mask_names;
newmat,wfile:string;
redu,ffail,redSS:realarray1NL;
layerno,angl:integer;

label
flag3,flag_7;

begin
keyknown:=false;
Layermenu;
  Repeat
  Flag3:
  If not keyknown then
  Inkey(specialkey,ch,'s','o');
  case key of

  AltC:         {rotate & view file}
    begin
    clrscr;
    layermenu;
    outerlayer:=1;
    dgrad:= false;
    abrt:=false;
    readkeybd:= true;
    mask[1]:='*.mat';
    readvesf(Newmat,mask,redu,ffail,redSS,outerlayer,
             layerno,angl,readkeybd,update,dgrad,abrt);
```

```
        if abrt = true then goto flag3;
        clrscr;
        layermenu;
        wfile:= 'file = '+currentfile;
        fastwrite(3,2,wfile,red,black);
        microresult;     {interchanges index & calls
                                        outputdesctable}
        keyknown:= false;
        goto flag3;
      end;

AltR:           {rotate layer}
   begin
    Rotresult;
    Keyknown:=false;
    goto flag3;
   end;

AltL:           {load as single wall layer}
   begin
    clrscr;
    layermenu;
    wfile:= 'file = '+currentfile;
    fastwrite(3,2,wfile,red,black);
    curser_small('C');
    Lastrstr;
    goto flag3;
   end;

AltX:           {exit to calculate menu}
   begin
    clrscr;
    calcmenu;
    keyknown:=false;
    currentfile:='Unknown';
    goto flag_7;
   end;

end;{single layer case}
If not (Key In [AltX,AltC,AltR]) then
begin
  GotoXY(58, 2);
  textbackground(cyan);
  textcolor(red);
  beep(600,150);
  Write('Error-Inadmissible Key');
  delay(2000);
  GotoXY(58,2);
  Textbackground(black);
  Write('                        ');
```

650

```
          gotoxy(3,4);
          textcolor(yellow);
          goto flag3;
       end; {if}
       until key = esc;
     {notskip:=true; }
   flag_7:
   end;


(*******************************************)

end. {unit}
```

```
unit CompMath;
{$O+,F+}

(*********************************************)

interface

uses glob_var,graph,editor,DOS,crt,ves_util,menus,plotprop,
     failure;

Procedure Ludcmp(var a: realarrayNLbyNL;
                     n: integer;
            var indx: IntegerarrayNL;
                var d: real);

procedure lubksb(var a:  realarrayNLbyNL;
                     n: integer;
            var indx: integerarrayNL;
                var b: RealarrayNL);

procedure mtxinv(lno:integer);

procedure Solvematrix(noeq:integer;var CVx:realarrayNL);

function pow(a,b:real):real;

Procedure GenerateMatProp(var Et,Gl:real);

Procedure Rotate(angle:real; lno:integer);
(*
Procedure computeterms(var vespressures:realarrayNL;var
axialC:real);
 *)
Procedure compute_full(var vespressures:realarrayNL;var
axialC:real;var full:boolean);

Procedure CompStress(intpres:realarrayNL;aConst:real;var
sigmaF,sigmaR,sigmaZ:realarray3NL);

Procedure ReadVesf(var p:string;mask:mask_names;var
redu,ffail,RedSS:realarray1NL;Var outerlayer:integer;
laynumber,z:integer;var
readkey,change,degrade,abort:boolean);

Procedure Laminateprop(TLayers:integer);

Procedure LaStrStr;

Procedure RotResult;
```

```
function Dfac(f,d:real;n:integer):real;

function fac(n:integer):integer;

(*
Procedure Summation(var factor:realarray8;ro:real;last:
integer;typ:char;getfit:boolean);

procedure Two_var(typ:char;var rad,sigma_r,
sigma_f,sigma_z:realarray2plusN);
*)
Procedure Variable_N(var power:real;var restnt:boolean);

procedure statsout(expon:real;var restnt:boolean);

procedure FiniteD(var actrad,sigma_r,sigma_f,sigma_z:
realarray2plusN;variation,itterate:boolean);


(****************************************************)

implementation

(****************************************************)

Procedure Ludcmp(var a:  realarrayNLbyNL;
                       n:  integer;
                 var indx:  IntegerarrayNL;
                    var d:  real);

const
  tiny = 1.0e-20;

var
  k,j,imax,i: integer;
  sum,dum,big:real;
  vv:^realarrayNL;

begin
  new(vv);
  d:= 1.0;
  For i:= 1 to n do begin
    big:= 0.0;
    for j := 1 to n do
      if abs(a[i,j])>big then big:= abs(a[i,j]);
    if big = 0.0 then begin
      writeln('pause in LUDCMP - singular matrix');
      readln
    end;
    vv^[i]:= 1.0/big
```

653

```
      end;
    for j:= 1 to n do begin
      for i:= 1 to j-1 do begin
        sum:=a[i,j];
        for k := 1 to i-1 do
          sum:= sum-a[i,k]*a[k,j];
        a[i,j]:= sum
      end;
      big:= 0.0;
      for i:= j to n do begin
        sum:= a[i,j];
        for k:= 1 to j-1 do
          sum:=sum-a[i,k]*a[k,j];
        a[i,j]:= sum;
        dum:= vv^[i]*abs(sum);
        if dum>= big then begin
          big:= dum;
          imax:=i
        end
      end;
      if j<> imax then begin
        for k:= 1 to n do begin
          dum:= a[imax,k];
          a[imax,k]:= a[j,k];
          a[j,k]:= dum
        end;
        d:= -d;
        vv^[imax] := vv^[j];
      end;
      indx[j] := imax;
      if a[j,j] =0.0 then a[j,j] := tiny;
      if j <> n then begin
        dum:= 1.0/a[j,j];
        for i:= j+1 to n do
          a[i,j]:= a[i,j]*dum
      end
    end;
    dispose(vv);
end;

(*************************************************)

procedure lubksb(var a:  realarrayNLbyNL;
                        n: integer;
                  var indx: integerarrayNL;
                     var b: RealarrayNL);

var
  j,ip,ii,i:integer;
  sum:real;
```

654

```
begin
  ii:= 0;
  for i:= 1 to n do begin
    ip:= indx[i];
    sum:= b[ip];
    b[ip]:= b[i];
    if ii<> 0 then
      for j:= ii to i-1 do
        sum:= sum-a[i,j]*b[j]
    else if sum<> 0.0 then
      ii:= i;
    b[i]:= sum;
  end;
  for i:= n downto 1 do begin
    sum:= b[i];
    for j:= i+ 1 to n do
      sum:= sum-a[i,j]*b[j];
    b[i]:= sum/a[i,i]
  end
end;


(********************************************************)


procedure mtxinv(lno:integer);

var n,i,j:integer;
  d:real;
  indx: integerarrayNL;
  col:RealarrayNL;
  aa: realarrayNLbyNL;

begin

for i:= 1 to 6 do
for j:= 1 to 6 do
  begin
  ymatrix[i,j]:= 0.0;
  aa[i,j]:= 0.0;
  end;

{feed one layer of compliance at a time to local 2D array}

  aa[3,3]:= la[lno,3,3];
  aa[2,2]:= la[lno,2,2];
  aa[1,1]:= la[lno,1,1];
  aa[6,6]:= la[lno,6,6];
  aa[5,5]:= la[lno,5,5];
  aa[4,4]:= la[lno,4,4];
  aa[3,2]:= la[lno,2,3];
```

```
        aa[1,3]:= la[lno,1,3];
        aa[1,4]:= la[lno,1,4];
        aa[1,2]:= la[lno,1,2];
        aa[2,4]:= la[lno,2,4];
        aa[3,4]:= la[lno,3,4];
        aa[6,5]:= la[lno,6,5];
        aa[2,3]:= la[lno,2,3];
        aa[3,1]:= la[lno,1,3];
        aa[4,3]:= la[lno,3,4];
        aa[2,1]:= la[lno,1,2];
        aa[4,2]:= la[lno,2,4];
        aa[4,1]:= la[lno,1,4];
        aa[5,6]:= la[lno,6,5];

    col[1]:=0.0;
    col[2]:=0.0;                    {define collum matrix}
    col[3]:=0.0;
    col[4]:=0.0;
    col[5]:=0.0;
    col[6]:=0.0;

    n:=6;
      ludcmp(aa,n,indx,d);
      for j:= 1 to n do begin
        for i:= 1 to n do col[i] := 0.0;
        col[j] := 1.0;
        lubksb(aa,n,indx,col);
        for i:= 1 to n do ymatrix[i,j]:= col[i]
                    {inverted compliance = stiffness}
      end;
    end;


    (***************************************************)

    procedure Solvematrix(noeq:integer;var CVx:realarrayNL);

    var

    n,i,j: integer;
    d: real;
    indx: integerarrayNL;
    MTX: realarrayNLbyNL;

    begin

    for i:= 1 to NL do
    for j:= 1 to NL do
    Mtx[i,j]:= 0.0;

    for i:= 1 to NL do
```

656

```
      CVx[i]:=0.0;

      for i:= 1 to noeq do
      for j:= 1 to noeq do
      Mtx[i,j]:= Matrix[i,j];

      for i:= 1 to noeq do
      CVx[i]:= CV[i];

      ludcmp(Mtx,noeq,indx,d);
      lubksb(Mtx,noeq,indx,CVx);    {answer returned in CVx}
      end;


   (*******************************************************)


   function pow(a,b:real):real;

   begin
   if a = 0 then
   begin
      pow:=0;
   end
   else if (a<0)and(frac(b)=0)and(odd(trunc(int(b)))=true) then
   begin
      a:= abs(a);
      pow:=-exp(b*ln(a));     {raises -a to power of b for odd b}
   end
   else if (a<b)and(frac(b)=0)and(odd(trunc(int(b)))=false)then
   begin
      a:= abs(a);
      pow:=exp(b*ln(a));      {raises -a to power of b for even b}
   end

   else
      pow:= exp(b*ln(a));   {a to power b - all other cases -
                                        will crash if neg a}
   end;                                 and b not whole number}


   (*******************************************************)

   Procedure GenerateMatProp(var Et,Gl:real);
               {input matrix (2), uni-lamina properties (5/7)}
   var                                      {outputs to .mat}
      fm,Gm,Km:real;
      P,R,Q,H,B1,B2,X,Y,A,B,C,D,BB,CC:real;
      Em,Vm,Kt,Vt,Gt,El,Vl,ff,fs:real;
      Ktf,Elf,Vlf,Glf,Gtf,XT,XC,YT,YC,SS,Vtf,Etf,m:real;
      er1,er2,er3,er4,er5,er6,er7,er8,er9,er10,
      er11,er12,er13,er14,er15,er16:integer;
      f:text;
```

657

```
  e:extstr;
  pa:pathstr;
  dir:dirstr;
  n:namestr;
label
  flag1,flag_metal;

{converts values in .lam file buffer}

begin
val(holdstr[1,1],El,er1);
val(holdstr[1,2],Vl,er2);
val(holdstr[1,3],Gl,er3);
val(holdstr[1,4],Et,er4);
val(holdstr[1,5],Vt,er5);
val(holdstr[1,6],Gt,er6);
val(holdstr[1,7],Kt,er7);
val(holdstr[1,8],Em,er8);
val(holdstr[1,9],Vm,er9);
val(holdstr[2,1],XT,er10);
val(holdstr[2,2],XC,er11);
val(holdstr[2,3],YT,er12);
val(holdstr[2,4],YC,er13);
val(holdstr[2,5],SS,er14);
val(holdstr[2,6],ff,er15);
ff:= ff/100;

{extracts fiber properties from .lam input}

    if holdstr[2,9] = '   Yes' then   {metal case}
      begin
        Elf:=0;
        Vlf:=0;
        Glf:=0;
        Etf:=0;
        Vtf:=0;
        Gtf:=0;
        Ktf:=0;
        goto flag_metal;
      end;

    if Er4 = 0 then
      begin
      if er5 = 0 then
        begin
        {case2}
        Kt:= 1/((2*(1-Vt)/Et)-(4*sqr(Vl)/El));
        Gt:=Et/(2*(1+Vt));
        goto flag1;
        end;
```

```
          if er6 = 0 then
            begin
            {case1}
            Kt:= 1/((4/Et)-(1/Gt)-(4*sqr(Vl)/El));
            goto flag1;
            end;
          if er7 = 0 then
            begin
            {case5}
            Gt:= 1/((4/Et)-(1/Kt)-(4*sqr(Vl)/El));
            goto flag1;
            end;
        end;
      if er5 = 0 then
        begin
        if er6 = 0 then
          begin
          {case3}
          Kt:=1/((2/(Gt*(1+Vt)))-(1/Gt)-(4*sqr(Vl)/El));
          goto flag1;
          end;
        if er7 = 0 then
          begin
          {case6}
          Gt:=(Kt*(1-Vt))/((1-Vt)*(4*Kt*sqr(Vl)/El)-Vt+1);
          goto flag1;
          end;
        end;
      if er6 = 0 then
        begin
        if er7 = 0 then
          begin
          {case4 - direct application}
          goto flag1;
          end;
        end;

flag1:
    if (er1<>0) or (er2<>0) or (er3<>0) or (er8<>0) or
               (er9<>0)or (er15<>0)    then    halt;
    fm:=1-ff;
    Gm:=Em/(2*(1+Vm));
    Km:=Gm/(1-2*Vm);    {plane strain bulk modulus of matrix}
    Q:=(Km*fm)+ff*(Gm+Km);
    P:=(Gm*fm)+ff*(Km+Gm);
    Ktf:=(Km*Gm*fm-P*Kt)/(Kt*fm-Q);            {Plane strain
                                        fiber transverse mod.}
    R:=(ff*fm*((1/Km)-(1/Ktf)))/((fm/Ktf)+(ff/Km)+(1/Gm));
    Vlf:=(Vl-Vm*fm+Vm*R)/(ff+R);    {long fiber poisson ratio}
    H:=(4*sqr(Vlf-Vm)*ff*fm)/((fm/Ktf)+(ff/Km)+(1/Gm));
```

```
            Elf:=(E1-Em*fm-H)/ff;             {Fiber tension long. mod.}
            Glf:=((G1*Gm*(1+ff))-Gm*Gm*fm)/(Gm+ff*Gm-G1*fm);
                                               {Fiber shear long. mod.}
            B1:= 1/(3-4*Vm);
            B2:= 1/(3-4*Vlf);
            X:=((1+B1)*ff)/((Gt/Gm)-1);
            Y:=3*B1*B1*fm*fm;
            A:=X*B2-X*ff*ff*ff*B2+ff*B2-ff*ff*ff*ff*B2+ff*B2*Y;
            B:=X*ff*ff*ff*B1+X+ff*ff*ff*ff*B1+ff+ff*Y;
            C:=B2-ff*ff*ff*B2;
            D:=ff*ff*ff*B1+1;
            BB:=(B1*C+A+D-B)/(C-A);
            CC:=(B1*D+B)/(C-A);
            Gtf:=((-BB+sqrt(BB*BB-4*CC))/2)*Gm;

            m:= 1+(4*ktf*sqr(Vlf)/Elf);
            Etf:=(4*Ktf*Gtf)/(Ktf+m*Gtf);
            Vtf:=(Ktf-m*Gtf)/(Ktf+m*Gtf);

            flag_metal:

            Fsplit(currentfile,dir,n,e);
            assign(f,n+'.MAT');
            rewrite(f);  {16 values put into file buffer to gen .mat}
            writeln(f,Elf:13:10);
            writeln(f,Vlf:13:10);
            writeln(f,Glf:13:10);
            writeln(f,Etf:13:10);
            writeln(f,Vtf:13:10);
            writeln(f,Gtf:13:10);
            writeln(f,Ktf:13:10);
            writeln(f,Em:13:10);
            writeln(f,Vm:13:10);
            writeln(f,XT:13:10);
            writeln(f,XC:13:10);
            writeln(f,YT:13:10);
            writeln(f,YC:13:10);
            writeln(f,SS:13:10);
            writeln(f,ff*100:13:10);           {modulus ff}
            writeln(f,holdstr[2,7]);
            writeln(f,holdstr[2,8]);
            writeln(f,holdstr[2,9]);
            close(f);

      end;{procedure}


(*****************************************************)


Procedure Rotate(angle:real; lno:integer);
                                   {layer number}
```

660

```
var
  z,d: real;            { the equations apply to compliances }
  n,i,j,l:integer;
  indx: integerarrayNL;
  col:RealarrayNL;
  aa: realarrayNLbyNL;

{ the equations below are for 1 lamina off-axis }
{ for (+/- angle) layers, equations are the same
        except 16,26,36,45 components cancel out}

  begin
  z:=angle*pi/180;    {equations below require radians input}
  if lno = 1 then    {initialize first time around only}
    begin
      for i:=1 to NL do
      for j:=1 to 6 do   {note: rectangular system, rotation
                                          about z-axis}

      for l:=1 to 6 do
      begin

      la[i,j,l]:=0;
      lq[i,j,l]:=0;
      if (j<=2) and (l<=2) then
      lb[i,j,l]:=0;
      end;
    end;
    {uni-lamina compliance, store for failure surfaces use}

  lstif[lno,1,1]:=Q[1,1];
  lstif[lno,2,2]:=Q[2,2];
  lstif[lno,3,3]:=Q[3,3];
  lstif[lno,6,6]:=Q[6,6];
  lstif[lno,1,2]:=Q[1,2];
  lstif[lno,1,3]:=Q[1,3];
  lstif[lno,2,3]:=Q[2,3];
  lstif[lno,2,1]:=Q[1,2];
  lstif[lno,3,1]:=Q[1,3];
  lstif[lno,3,2]:=Q[2,3];
  lstif[lno,4,4]:=Q[4,4];
  lstif[lno,5,5]:=Q[5,5];


{global coordinate stiffness}
{rot stiff equations for +/- angle plies in 3D - cyl. coor}

{22}
lQ[lno,2,2]:=Q[1,1]*sqr(sqr(sin(z)))+(2*Q[1,2]+4*Q[6,6])*sqr
            (sin(z))*sqr(cos(z))+Q[2,2]*sqr(sqr(cos(z)));
```

```
{11}
lQ[lno,3,3]:=Q[1,1]*sqr(sqr(cos(z)))+(2*Q[1,2]+4*Q[6,6])*sqr
              (sin(z))*sqr(cos(z))+Q[2,2]*sqr(sqr(sin(z)));
{21}
lQ[lno,2,3]:=(Q[1,1]+Q[2,2]-4*Q[6,6])*sqr(sin(z))*sqr
         (cos(z))+(sqr(sqr(cos(z)))+sqr(sqr(sin(z))))*Q[1,2];
{66}
lQ[lno,4,4]:=(Q[1,1]+Q[2,2]-2*Q[1,2])*sqr(sin(z))*
             sqr(cos(z))+Q[6,6]*sqr(sqr(cos(z))-sqr(sin(z)));
{44}    lQ[lno,6,6]:=Q[4,4]*sqr(cos(z))+Q[5,5]*sqr(sin(z));
{55}    lQ[lno,5,5]:=Q[4,4]*sqr(sin(z))+Q[5,5]*sqr(cos(z));
{31}    lQ[lno,1,3]:=Q[1,3]*sqr(cos(z))+Q[2,3]*sqr(sin(z));
{32}    lQ[lno,1,2]:=Q[1,3]*sqr(sin(z))+Q[2,3]*sqr(cos(z));
{33}    lQ[lno,1,1]:=Q[3,3];
        lQ[lno,3,2]:=lQ[lno,2,3];
        lQ[lno,3,1]:=lQ[lno,1,3];
        lQ[lno,2,1]:=lQ[lno,1,2];

        for i:= 1 to 6 do
        for j:= 1 to 6 do
        aa[i,j]:= 0.0;

        aa[3,3]:= lq[lno,3,3];
        aa[2,2]:= lq[lno,2,2];
        aa[1,1]:= lq[lno,1,1];
        aa[6,6]:= lq[lno,6,6];
        aa[5,5]:= lq[lno,5,5];
        aa[4,4]:= lq[lno,4,4];
        aa[3,2]:= lq[lno,2,3];
        aa[1,3]:= lq[lno,1,3];
        aa[1,4]:= lq[lno,1,4];
        aa[1,2]:= lq[lno,1,2];
        aa[2,4]:= lq[lno,2,4];
        aa[3,4]:= lq[lno,3,4];
        aa[6,5]:= lq[lno,6,5];
        aa[2,3]:= lq[lno,2,3];
        aa[3,1]:= lq[lno,1,3];
        aa[4,3]:= lq[lno,3,4];
        aa[2,1]:= lq[lno,1,2];
        aa[4,2]:= lq[lno,2,4];
        aa[4,1]:= lq[lno,1,4];
        aa[5,6]:= lq[lno,6,5];

  n:= 6;
  ludcmp(aa,n,indx,d);
  for j:= 1 to n do begin
    for i:= 1 to n do col[i] := 0.0;
    col[j] := 1.0;
    lubksb(aa,n,indx,col);
    for i:= 1 to n do la[lno,i,j]:= col[i]
```

662

```
                              {inverted stiffness = compliance}
     end;

{la = compliance each +/-layer, global coordinates}
{above -redefined directions for cylinder: axis = z;
thickness = r;
circumferential = f; (theta)
fiber angle is measured away from cylinder axis. Polar type
windings are near 0 degrees, circumferential windings are
approximately 90 degrees.

     cyl.   rect.

     r(1)  = z(3)
     z(3)  = x(1)
     f(2)  = y(2)

note: cylindrical system, rotation about r, (from z to f)
gives less cylindrical compliance with increasing angle,
"la" represents layer compliance, "lq" stiffness, "lb"
equivalent stiffness}

Brr[lno]:= la[lno,1,1]-sqr(la[lno,1,3])/la[lno,3,3];
  {Brr, through-thickness direction}
Brf[lno]:= la[lno,1,2]-la[lno,1,3]*la[lno,2,3]/la[lno,3,3];
  {Brf, through-principle direction}
Bff[lno]:= la[lno,2,2]-sqr(la[lno,2,3])/la[lno,3,3];
  {Bff, principle fiber direction}
Vrf[lno]:= la[lno,1,3]/la[lno,3,3];
  {Vrf, poisson's ratio, out-of-plane}
Vfz[lno]:= la[lno,2,3]/la[lno,3,3];
  {Vfz, poisson's ratio, in-plane}

Azz[lno]:=la[lno,3,3];  {Azz compliance - cylinder axis}
Arz[lno]:=la[lno,1,3];  {Arz compliance - thickness to axis}
Afz[lno]:=la[lno,2,3];  {Afz compliance - circum. to axis}

K[lno]:= sqrt(Brr[lno]/Bff[lno]);

lb[lno,1,1]:= la[lno,1,1]-sqr(la[lno,1,3])/la[lno,3,3];
  {Brr, through-thickness direction}
lb[lno,1,2]:= la[lno,1,2]-la[lno,1,3]*la[lno,2,3]/
  la[lno,3,3];
  {Brf, through-principle direction}
lb[lno,2,2]:= la[lno,2,2]-sqr(la[lno,2,3])/la[lno,3,3];
  {Bff, principle fiber direction}
  end;

(*************************************************)
```

663

```
{solves the discrete multilayer cylinder interface
pressures}
(*
Procedure computeterms(var vespressures:realarrayNL;var
axialC:real);

var
location:string;
term1,term2,term3,term4,term5,term6,
term7,term22,term44:real;
i,j,l:integer;
sumdelta,sumintf:real;
NorLoadAbsorb:RealarrayNL;

begin
sumdelta:=0;
sumintf:=0;
for i:= 0 to NL do     {init., flanks edges of matrix with 0}
begin
Xl[i]:=0;
D[i]:=0;
Delta[i]:=0;
G[i]:=0;
A[i]:=0;
d[i]:=0;
CV[i]:=0;
VM[i]:=0;
QP[i]:=0;
VesPressures[i]:=0;
end;

for i:= 0 to NL do
for j:= 0 to NL do               {initializes with zeros}

Matrix[i,j]:= 0;

QP[0]:= InsidePress;
QP[outerlayer]:= OuterPress;

FI:= (InsidePress-OuterPress)*sqr(R[0]);   {constant axial
                                     pressure load, newtons}

for l:= 1 to outerlayer do
begin

term1:= -1/((Azz[l])*(1-pow(C[l],2*K[l])));
term2:= (Arz[l]+K[l]*Afz[l])*R[l]*pow(C[l],K[l]+1);
term3:= (R[l]-pow(C[l],K[l])*R[l-1])/(K[l]+1);
term4:= (Arz[l]-K[l]*Afz[l])*R[l-1];
term5:= (R[l]*pow(C[l],K[l])-R[l-1])/(1-K[l]);
```

```
D[l]:=  term1*((term2*term3)-(term4*term5));

term22:= (Arz[l]+K[l]*Afz[l])*R[l];
term44:= (Arz[l]-K[l]*Afz[l])*(R[l])*pow(C[l],K[l]);

X1[l]:=  term1*((-term22*term3)+(term44*term5));

A[l]:= -pow(C[l],K[l])*(2*Bff[l]*K[l])/(1-pow(C[l],2*K[l]));
                                                      {alpha}


Delta[l]:= ((sqr(R[l])-sqr(R[l-1]))/(0.001*Azz[l]));
                                        {convert to MPa-1, r=mm}
end;


for l:= 1 to outerlayer do
Sumdelta:= Sumdelta+Delta[l];


for l:= 1 to outerlayer-1 do
begin

CV[l]:= ((Vfz[l+1]-Vfz[l])*R[l]*FI)/sumDelta;        {Constant
                                                       vector}


term6:= ((1+pow(C[l],2*K[l]))*(K[l]*Bff[l])/(1-
pow(C[l],2*K[l])))+Brf[l];
term7:= ((1+pow(C[l+1],2*K[l+1]))*(K[l+1]*Bff[l+1])/
        (1-pow(C[l+1],2*K[l+1])))-Brf[l+1];
G[l]:=  term6+term7;                                 {gamma}

VM[l]:= 2*R[l]*(Vfz[l+1]-Vfz[l])/sumDelta;
end;

for i:= 1 to outerlayer-1 do        { collums }
for j:= 0 to outerlayer do          { rows }
  Matrix[i,j]:= VM[i]*(D[j+1]+X1[j]);

for i:= 1 to outerlayer-1 do        { collums }
for j:= 0 to outerlayer do          { rows }
begin
  if i=j then
      Matrix[i,j]:= Matrix[i,j] - R[i]*G[i];
  if 1+j=i then
      Matrix[i,j]:= Matrix[i,j] - R[j]*A[i];
  if i+1=j then
      Matrix[i,j]:= Matrix[i,j] - R[j]*A[j];
end;

for i:= 1 to outerlayer-1 do
begin
```

```
CV[i]:= CV[i]-(QP[0]*Matrix[i,0]+QP[outerlayer]*
        Matrix[i,outerlayer]);
end;

solvematrix(outerlayer-1,vesPressures);
                            {number of equations to be solved}
VesPressures[0]:=insidepress;
VesPressures[outerlayer]:=outerpress;

for i:= 1 to outerlayer do
   sumintf:= sumintf + (D[i]*vespressures[i-1]+
                         X1[i]*vespressures[i]);
axialC:= (FI-2*sumintf)/sumDelta;

end; {procedure}

*)

(********************************************************)

Procedure compute_full(var vespressures:realarrayNL;var
                       axialC:real;var full:boolean);

var
location:string;
term1,term2,term3,term4,term5,term6,term7,
term22,term44:real;
i,j,l:integer;
sumdelta,sumintf,Y31,Y32,Y33,Y41,Y42,Y43:real;
NorLoadAbsorb,W1,W2,W3,W4,Y1,Y2,Y3,Y4,YY:RealarrayNL;

begin
sumdelta:=0;
sumintf:=0;
for i:= 0 to NL do    {initialize, flanks edges of matrix
                                              with 0}
begin
X1[i]:=0;
D[i]:=0;
Delta[i]:=0;
G[i]:=0;
A[i]:=0;
d[i]:=0;
CV[i]:=0;
VM[i]:=0;
QP[i]:=0;
Si[i]:=0;
W1[i]:=0;
W2[i]:=0;
W3[i]:=0;
```

```
W4[i]:=0;
Y1[i]:=0;
Y2[i]:=0;
Y3[i]:=0;
Y4[i]:=0;
VesPressures[i]:=0;
end;

for i:= 0 to NL do
for j:= 0 to NL do            {initializes with zeros}

Matrix[i,j]:= 0;

QP[0]:= InsidePress;
QP[outerlayer]:= OuterPress;

FI:= (InsidePress-OuterPress)*sqr(R[0]);
                        {constant axial pressure load, newtons}

for l:= 1 to outerlayer do
begin

term1:= -1/((Azz[l])*(1-pow(C[l],2*K[l])));
term2:= (Arz[l]+K[l]*Afz[l])*R[l]*pow(C[l],K[l]+1);
term3:= (R[l]-pow(C[l],K[l])*R[l-1])/(K[l]+1);
term4:= (Arz[l]-K[l]*Afz[l])*R[l-1];
term5:= (R[l]*pow(C[l],K[l])-R[l-1])/(1-K[l]);

D[l]:=  term1*((term2*term3)-(term4*term5));

term22:= (Arz[l]+K[l]*Afz[l])*R[l];
term44:= (Arz[l]-K[l]*Afz[l])*(R[l])*pow(C[l],K[l]);

X1[l]:=  term1*((-term22*term3)+(term44*term5));

A[l]:= -pow(C[l],K[l])*0.001*(2*Bff[l]*K[l])/
        (1-pow(C[l],2*K[l]));    {alpha - needs MPa-1 units}

Si[l]:=(Arz[l]-Afz[l])/(0.001*Azz[l]*(Bff[l]-Brr[l]));
                                        {units MPa-1}

W1[l]:=((sqr(R[l])-sqr(R[l-1]))/(0.001*2*Azz[l]));
                            {convert to MPa-1, r=mm}

W2[l]:=(Si[l]*(Arz[l]+Afz[l])*(sqr(R[l])-
                        sqr(R[l-1])))/(2*Azz[l]);

W3[l]:=(Si[l]*(Arz[l]+K[l]*Afz[l])*
   (1-pow(C[l],K[l]+1))*R[l]*(R[l]-R[l-1]*pow(C[l],K[l])))/
   (Azz[l]*(1-pow(C[l],2*K[l]))*(K[l]+1));
```

```
W4[1]:=(Si[1]*(Arz[1]-K[1]*Afz[1])*(1-pow(C[1],
    K[1]-1))*R[1]*pow(C[1],K[1]+1)*(R[1]-R[1-1]*pow(C[1],
    -K[1])))/(Azz[1]*(1-pow(C[1],2*K[1]))*(1-K[1]));

  if full = true then
    Delta[1]:=W1[1]-W2[1]+W3[1]+W4[1]
  else
    Delta[1]:=W1[1];
end;

for 1:= 1 to outerlayer do
Sumdelta:= Sumdelta+Delta[1];

for 1:= 1 to outerlayer-1 do
begin

Y1[1]:=(Vfz[1+1]-Vfz[1])*R[1];

Y2[1]:=((Si[1+1]*(Brf[1+1]+Bff[1+1]))-
        (Si[1]*(Brf[1]+Bff[1])))*R[1]*0.001;
                                {units MPa-1 for both B's and Si}

Y31:=(0.001*Si[1+1]*R[1+1])/(1-pow(C[1+1],2*K[1+1]));
                                {Convert B's to MPa-1}
Y32:=(Brf[1+1]+K[1+1]*Bff[1+1])*pow(R[1]/R[1+1],K[1+1])*
      (pow(C[1+1],K[1+1]+1)-1);
Y33:=(-Brf[1+1]+K[1+1]*Bff[1+1])*(pow(C[1+1],K[1+1]+1)-
      pow(C[1+1],2*K[1+1]))*pow(R[1+1]/R[1],K[1+1]);
Y3[1]:=Y31*(Y32+Y33);
Y41:=(0.001*Si[1]*R[1])/(1-pow(C[1],2*K[1]));
                                {Convert B's to MPa-1}
Y42:=(Brf[1]+K[1]*Bff[1])*(pow(C[1],K[1]+1)-1);
Y43:=(-Brf[1]+K[1]*Bff[1])*(pow(C[1],K[1]+1)-
      pow(C[1],2*K[1]));
Y4[1]:=-Y41*(Y42+Y43);

  if full = true then
    YY[1]:=Y1[1]+Y2[1]+Y3[1]+Y4[1]
  else
    YY[1]:=Y1[1];

CV[1]:= (YY[1]*FI)/(2*sumDelta);      {Constant vector}

term6:= ((1+pow(C[1],2*K[1]))*(K[1]*Bff[1])/
        (1-pow(C[1],2*K[1])))+Brf[1];
term7:= ((1+pow(C[1+1],2*K[1+1]))*(K[1+1]*Bff[1+1])/
        (1-pow(C[1+1],2*K[1+1])))-Brf[1+1];
G[1]:=  0.001*(term6+term7);      {gamma - needs MPa-1 units}
```

```
VM[l]:= (2*YY[l])/(2*sumDelta);
end;

for i:= 1 to outerlayer-1 do                          { collums }
for j:= 0 to outerlayer do                            { rows   }
Matrix[i,j]:= VM[i]*(D[j+1]+X1[j]);

for i:= 1 to outerlayer-1 do                          { collums }
for j:= 0 to outerlayer do                            { rows   }
begin
   if i=j then
      Matrix[i,j]:= Matrix[i,j] - R[i]*G[i];
   if i+j=i then
      Matrix[i,j]:= Matrix[i,j] - R[j]*A[i];
   if i+1=j then
      Matrix[i,j]:= Matrix[i,j] - R[j]*A[j];
end;

for i:= 1 to outerlayer-1 do
begin
   CV[i]:= CV[i]-(QP[0]*Matrix[i,0]+
           QP[outerlayer]*Matrix[i,outerlayer]);
end;

solvematrix(outerlayer-1,vesPressures);

for i:= 1 to outerlayer-1 do                          {number of equations to be solved}
VesPressures[0]:=insidepress;
VesPressures[outerlayer]:=outerpress;

for i:= 1 to outerlayer do
   sumintf:= sumintf + (D[i]*vespressures[i-1]+
             X1[i]*vespressures[i]);
axialC:=(FI-2*sumintf)/(2*sumDelta);

end; {procedure}

(*********************************************************
**************************************************)

Procedure CompStress(intpres:realarrayNL;aConst:real;var
sigmaF,sigmaR,sigmaZ:realarray3NL);

type
realarray3 = array [1..3] of real;

var
i,j:integer;
ro,fact1,fact2,fact3,fact4,fact5,fact6,fact7,
fact8,denom:real;
rr:realarray3;
```

```
begin

for i:= 1 to outerlayer do
begin
rr[1]:=r[i-1]/r[i];      {inner}
rr[2]:=(rr[1]+1)/2;      {middle}
rr[3]:=1;                {outer}
  for j:= 1 to 3 do
  begin
    denom:=1-pow(c[i],2*k[i]);

    fact1:=(pow(rr[j],k[i]-1)*(intpres[i-1]*
            pow(c[i],k[i]+1)-intpres[i]))/denom;
    fact2:=(pow(rr[j],-k[i]-1)*(intpres[i]*pow(c[i],k[i]-1)-
            intpres[i-1])*pow(c[i],1+k[i]))/denom;
    fact3:=(pow(rr[j],k[i]-1)*(1-pow(c[i],k[i]+1)))/denom;
    fact4:=(pow(rr[j],-k[i]-1)*pow(c[i],k[i]+1)*
            (1-pow(c[i],k[i]-1)))/denom;

    sigmaR[3*(i-1)+j]:=fact1+fact2+(Aconst*Si[i]*
                       (1-fact3-fact4));

    fact5:=(k[i]*pow(rr[j],k[i]-1)*(intpres[i-1]*
            pow(c[i],k[i]+1)-intpres[i]))/denom;
    fact6:=(k[i]*pow(rr[j],-k[i]-1)*
            (intpres[i]*pow(c[i],k[i]-1)-intpres[i-1])*
            pow(c[i],1+k[i]))/denom;
    fact7:=k[i]*fact3;
    fact8:=k[i]*fact4;

    sigmaF[3*(i-1)+j]:=fact5-fact6+(Aconst*Si[i]*
                       1-fact7+fact8));

    sigmaZ[3*(i-1)+j]:=aConst/(0.001*Azz[i])+
                       (-Arz[i]*sigmaR[3*(i-1)+j]-
                       Afz[i]*sigmaF[3*(i-1)+j])/(Azz[i]);
  end;

end; {layer loop}
end; {procedure}


(********************************************)

  Procedure ReadVesf(var p:string;mask:mask_names;var
                     redu,ffail,RedSS:realarray1NL;Var
                     outerlayer:integer;
                     laynumber,z:integer;var
                     readkey,change,degrade,abort:boolean);
```

670

```pascal
label flag1,flag2,flag3,flag4,flag5;

var
  writeautoscale:boolean;
  i,j,IOcode,layno,w,sr,sty,npicf,lpicf,filn:integer;
  matfile:string;
  f,mf: text;
  lds:layerarrayNL;
  Mdata:asciiarray;
  matvalue:RealArrayNLbyNL;
  errcd:integerarray16;
  Layerno,angle,thick,perfib:string;
  pr,od,id,fr:real;
  dpf,XT,XC,YT,YC,SS,ff,fm,Gm,vm,Em,Ef,Et,dEt,vf,vt,kf,km,
  Gf,dGl,GL,ppf:real;
  ktf,Etf,vtf,Gtf: real;
  DTS: realarrayNL;
  T_iso,fit,metal,notskip:boolean;
  d:dirstr;
  n:namestr;
  e:extstr;

  begin
  sty:=6;
  notskip:=false;
      if readkey = true then
      begin
        flag1:
        abort:=false;
        textbackground(black);
        textcolor(lightgray);
        GotoXY(4,4);
        Writeln('Enter filename <'+copy(mask[1],2,5)+'> :');
        Gotoxy(10,4);
        textcolor(yellow);
        write('filename');
        p:= '';
        gotoxy(28,4);
        write('                ');
        holdstr[1,1]:='';
        npicf:=1;
        lpicf:=1;
        filn:=1;
        mask[2]:='';
        maxlength:=12;
        windowlength:=12;
        cursx:=28;
        cursy:=4;
        moveEditwindow(mask,false,ft,6,28,4,1,1,12,
                        1,0,0,0,notskip,abort);
```

```
      if abort = true then goto flag4;
      fsplit(holdstr[1,1],d,n,e);
   {$I-}
      assign(f,n+e);
      currentfile:=n+e;
      reset(f);
      if currentfile='' then goto flag1;
   {$I+}
      IOcode:= IOresult;
      if IOcode <> 0 then
        begin
        gotoxy(4,5);
        write('                                    ');
        gotoxy(4,5);
        textcolor(white);
        beep(600,100);
        write('Filename ['+n+e+'] contains bad syntax or
               cannot be found');
        textcolor(yellow);
        gotoxy(14,5);
        write(n+e);
        Goto flag1;
        end;
      end
   else
      assign(f,currentfile);
      writeautoscale:=false;
      if (e = '.MAT') or (e = '.mat') then  goto flag2;
for i:= 0 to NL do
   begin
      R[i]:=0;     {initialization}
      DT[i]:=0;
      DTS[i]:=0;
      C[i]:=0;
      K[i]:=0;
      Afz[i]:=0;
      Arz[i]:=0;
      Azz[i]:=0;
      Brr[i]:=0;
      Brf[i]:=0;
      Bff[i]:=0;
      Vrf[i]:=0;
      Vfz[i]:=0;
   end;

reset(f);
for i:= 1 to 4 do   {read loads information}
   readln(f,lds[i]);
               {store vessel load parameters in this array}
```

672

```
Ttotal:=0;
flag5:
for i:= 1 to NL do   {reads data on the NL(constant)
                                      , i= layer no}
   begin
      readln(f, layerNo);        {first entry}
      readln(f, MatFile);        {second entry}
      readln(f, angle);          {3 rd entry}
      readln(f, thick);          {4 th entry}
      readln(f, perfib);         {fiber percent}

      if  (change = true) and (readkey = false) then
      begin
        Matfile:=graphlabels[i].matname;
        angle:=graphlabels[i].angle;
        thick:= graphlabels[i].thickness;
        perfib:= graphlabels[i].fpercent;
        lds[3]:=Ipress;
      end;

      outerlayer:=i;
      if layerNo = '' then
        begin           {counter for total number of layers}
          outerlayer:=i-1;
          goto flag3; {exit criteria}
        end;

      val(layerno,Layno,errcd[1]);
      val(angle,Z,errcd[2]);        {angle is refer to as Z}
      val(thick,Dt[Layno],errcd[3]); {stores thick-global}
      val(perfib,ppf,errcd[4]); {prescribed percent fiber}
      val(lds[1],InsideDia,errcd[5]);   {inside diameter}
      val(lds[2],wallthick,errcd[6]);     {Wall thickness}
      val(lds[3],InsidePress,errcd[7]);
      val(lds[4],OuterPress,errcd[8]);
      outsidedia:=InsideDia+2*wallthick;  {define out dia}

   assign(mf,matfile+'.mat');
                   { next step... dig out fiber info }
   reset(mf);
       flag2:      {used for single layer menu selection}
       if (mask[1] = '*.mat') or (mask[1] = '*.MAT') then
       begin
         assign(mf,n+e);
         reset(mf);
       end;
   for j:= 1 to 18 do
     readln(mf, Mdata[j]);
   close(mf);
             { convert data to numeric representation}
```

```
      val(Mdata[1],Ef,errcd[1]);
      val(Mdata[2],Vf,errcd[2]);
      val(Mdata[3],Gf,errcd[3]);
      val(Mdata[4],Et,errcd[4]);
      val(Mdata[5],Vt,errcd[5]);
      val(Mdata[6],Gtf,errcd[6]);
      val(Mdata[7],Ktf,errcd[7]);
      val(Mdata[8],Em,errcd[8]);
      val(Mdata[9],Vm,errcd[9]);
      val(Mdata[10],XT,errcd[10]);   {default percent fiber}
      val(Mdata[11],XC,errcd[11]);
      val(Mdata[12],YT,errcd[12]);
      val(Mdata[13],YC,errcd[13]);
      val(Mdata[14],SS,errcd[14]);
      val(Mdata[15],dpf,errcd[15]);

      T_iso:= false;
      If (Mdata[16] = 'T-iso')or(Mdata[16] =
                          ' T-iso')or(Mdata[16] = ' T-iso')
      then  T_iso:= true;
      If (mask[1] = '*.mat') or (mask[1] = '*.MAT') then
      begin
        ppf:=dpf;
        i:= 1;
        layno:=1;
      end;

      if (mask[1]='*.ves')or(mask[1]='*.VES') then
        fit:= false;

      if (Mdata[18]='   Yes')or(Mdata[18]='  Yes') or
         (Mdata[18]=' Yes')or(Mdata[18]='Yes')or
         (Mdata[18]= '   yes')or(Mdata[18]='  yes')or
         (Mdata[18]=' yes')or(Mdata[18]='yes') then
        metal:= true
      else
        metal:= false;
calculate_prop(T_iso,metal,fit,degrade,i,GL,Ef,Et,
               dEt,Vf,Vt,Gf,dGl,Gtf,Ktf,ppf,Em,Vm,dpf,
               redu,ffail,RedSS,errcd);

{micromechanics strength equations}

if metal = false then
  strg[layno].XT:=XT*(ppf/dpf)
else
  strg[layno].XT:=XT;
strg[layno].XC:=XC;
strg[layno].YT:=YT;
strg[layno].YC:=YC;
```

```
              strg[layno].SS:=SS;
              strg[layno].GL:=GL;

              if (mask[1] = '*.mat') or (mask[1] = '*.MAT') then
                goto flag4;   {one layer not rotated}
              rotate(Z,layno);
               {stores all results in global array lq & la[Lno,i,j]}

              graphlabels[layno].angle:=angle;
              graphlabels[layno].Matname:=matfile;
              graphlabels[layno].fpercent:=perfib;
              graphlabels[layno].thickness:=thick;
                  end; {i loop for layers}
flag3:
              close(f);

              Ttotal:=0;
                for i:= 1 to outerlayer do
                Ttotal:=Ttotal+DT[i];
              if mask[1] = '*.wal' then goto flag4;
                                      {skips to end of procedure}
              scalefactor:= Ttotal/wallthick;
              str(1/scalefactor:4:2,scalef);
                  for i:= 1 to NL do
                    DTS[i]:= Dt[i]/scalefactor;
                               {scaled thickness, id & od given}
                    writeautoscale:=true;
              for i:= 1 to NL do
                begin
                  R[0]:=insideDia/2;
                  R[i]:=R[i-1]+DTS[i];
                  if R[i] = R[i-1] then R[i]:=0;
                                              {wall radii - global}
                end;
              if lds[2] = '' then              {od is blank}
              begin
                writeautoscale:=false;
                R[0]:=InsideDia/2;              {inside radius}
                for i:= 1 to NL do
                    begin
                    R[i]:=R[i-1]+Dt[i];        {layer radius}
                      if R[i] = R[i-1] then R[i]:=0;
                    end;
                    end;
              if lds[1] = '' then              {id is blank}
              begin
                writeautoscale:=false;
                R[outerlayer]:=OutsideDia/2;
                for i:= outerlayer downto 1 do
                    R[i-1]:=R[i]-Dt[i];
```

```
                end;
                for i:=1 to outerlayer do
                C[i]:= R[i-1]/R[i];
                        {relative wall radii,each layer - global}

                    if (writeautoscale = true) and (change = true)
                        and (readkey = false) then
                    begin
                        setcolor(lightgray);
                        outtextxy(0,10,'W-Scale:'+scalef);
                    end;
            flag4:
        end; {procedure}


(*********************************************************)


Procedure Laminateprop(TLayers:integer);
                            {Tlayers = total number of layers}

{computes smeared stiffness / compliance of whole laminate}
{Net compliance is net stiffness matrix inverted}

var
    n,i,j,k:integer;
    d:real;
    indx: integerarrayNL;
    col:RealarrayNL;
    NetC,NetQ: realarray6X6;
    aa: realArrayNLbyNL;

begin   {procedure}

for i:= 0 to NL do
for j:= 0 to NL do
    begin
        aa[i,j]:= 0.0;
    end;
for i:= 1 to 6 do
for j:= 1 to 6 do
    begin
    ymatrix[i,j]:= 0.0;
    NetQ[i,j]:= 0.0;        {initialize matrix}
    NetC[i,j]:= 0.0;
    SumC[i,j]:= 0.0;
    SumB[i,j]:= 0.0;
    end;
    for k:= 1 to Tlayers do
        for i:= 1 to 6 do
        for j:= 1 to 6 do
        Lq[k,j,i]:= Lq[k,i,j];                  {symmetric counterpart}
```

```
    for k:= 1 to Tlayers do
      for i:= 1 to 6 do
      for j:= 1 to 6 do
      begin
        NetQ[i,j]:=NetQ[i,j] + (Dt[k]/Ttotal)*Lq[k,i,j];
        SumC[i,j]:=SumC[i,j] + (Dt[k]/Ttotal)*La[k,i,j];
        if (i<=2) and (j<=2) then
          SumB[i,j]:=SumB[i,j] + (Dt[k]/Ttotal)*Lb[k,i,j];
      end;
                                    {gets orthotropic part of matrix}
    for i:= 1 to 3 do               {and makes local copy}
    for j:= 1 to 3 do
      aa[i,j]:= NetQ[i,j];
    for i:= 4 to 6 do
      aa[i,i]:= NetQ[i,i];


            {following gets inverse of matrix}
            {NetC is the result, aa gets destroyed in process}
n:=6;

col[1]:=0.0;
col[2]:=0.0;                        {define collum matrix}
col[3]:=0.0;
col[4]:=0.0;
col[5]:=0.0;
col[6]:=0.0;
  ludcmp(aa,n,indx,d);
  for j:= 1 to n do begin
    for i:= 1 to n do col[i] := 0.0;
    col[j] := 1.0;
    lubksb(aa,n,indx,col);
    for i:= 1 to n do NetC[i,j]:= col[i]
  end;
  for i:= 1 to 6 do
  for j:= 1 to 6 do
    begin
    Q[i,j]:=NetQ[i,j];              {assigns computed values
to a matrix}
    CC[i,j]:=NetC[i,j];            {read by OutputDescTable}
    end;
end; {procedure}


(***********************************************)

Procedure LaStrStr;
      {computes stress and strain of a layer}
var
  c,b,a,p,q,deltar,Cc,Si,kk,D,F1,F2,F3,F4,T1,T2,T3,T4,T5,T6,
  Dout,Din:real;
  sigmaF,sigmaR,sigmaZ,dispU,epsif,ro:realarray3;
```

677

```
      Sig_theta,epsilon_f,displacement,Sig_radial,
      sigma_zz:stringarray3;
      i:integer;
      numberk:string[7];

begin
textcolor(yellow);
textbackground(black);
textcolor(lightgray);
gotoxy(4,4);
write('Outside diameter (mm): ');
textcolor(yellow);
gotoxy(12,4);
write('diameter');
gotoxy(26,4);
read(Dout);
textcolor(lightgray);
gotoxy(4,6);
write('Inside diameter (mm): ');
textcolor(yellow);
gotoxy(11,6);
write('diameter');
gotoxy(25,6);
read(Din);
Textcolor(lightgray);
gotoxy(4,8);
write('Internal pressure (MPa): ');
textcolor(yellow);
gotoxy(13,8);
write('pressure');
gotoxy(28,8);
read(p);
gotoxy(4,10);
Textcolor(lightgray);
write('External pressure (MPa): ');
textcolor(yellow);
gotoxy(13,10);
write('pressure');
gotoxy(28,10);
read(q);
c:= Din/Dout;
b:=Dout/2; {outside radius}
a:=Din/2;

Si:=(Arz[1]-Afz[1])/(0.001*Azz[1]*(Bff[1]-Brr[1]));
kk:=K[1];
D:=1-pow(c,2*kk);
F1:=(p*pow(c,kk+1)-q)/D;
F2:=(q*pow(c,kk-1)-p)*pow(c,kk+1)/D;
F3:=(1-pow(c,kk+1))/D;
```

```
F4:=(1-pow(c,kk-1))*pow(c,kk+1)/D;
T1:=(sqr(b)-sqr(a))/(2*0.001*Azz[1]);
T2:=Si*(Arz[1]+Afz[1])*(sqr(b)-sqr(a))/(2*Azz[1]);
T3:=(b*(b-
pow(c,kk)*a)*(Arz[1]+kk*Afz[1])*F1)/(Azz[1]*(kk+1));
T4:=(b*(b-pow(c,-kk)*a)*(Arz[1]-kk*Afz[1])*F2)/
     (Azz[1]*(1-kk));
T5:=(Si*b*(b-pow(c,kk)*a)*(-Arz[1]-
     kk*Afz[1])*F3)/(Azz[1]*(kk+1));
T6:=(Si*b*(b-pow(c,-kk)*a)*
     (-Arz[1]+kk*Afz[1])*F4)/(Azz[1]*(1-kk));
CC:=((P-Q)*(Sqr(a)/2)+T3+T4)/(T1-T2-T5-T6);

for i:= 1 to 3 do
begin
   ro[i]:=(a+((b-a)/2)*(i-1))/b;
   Sigmar[i]:=F1*pow(ro[i],kk-1)+F2*pow(ro[i],
             -kk-1)+Si*CC*(1-F3*pow(ro[i],kk-1)-
             F4*pow(ro[i],-kk-1));
   Sigmaf[i]:=F1*kk*pow(ro[i],kk-1)-F2*kk*pow(ro[i],
             -kk-1)+Si*CC*(1-F3*kk*pow(ro[i],kk-
             1)+F4*kk*pow(ro[i],-kk-1));
   sigmaz[i]:=(CC/(0.001*Azz[1]))-
             ((Arz[1]*Sigmar[i]+Afz[1]*sigmaf[i])/Azz[1]);
   epsif[i]:=(0.001*Brf[1]*Sigmar[i]+0.001*Bff[1]*Sigmaf[i]+
             (Afz[1]*CC/Azz[1]));
   dispu[i]:=ro[i]*b*epsif[i];
end;

Textcolor(lightgray);
for i:= 1 to 3 do
begin
str(sigmaf[i]:7:5,Sig_theta[i]);
str(100*epsif[i]:6:4,epsilon_f[i]);
str(dispu[i]:7:5,displacement[i]);
str(sigmar[i]:7:5,sig_radial[i]);
str(sigmaz[i]:7:5,sigma_zz[i]);
end;
gotoxy(4,12);
textcolor(white);
write('Parameter                        Inside        Middle
      Outside');
gotoxy(4,14);
write('Sigma ('+#233+') MPa:');
gotoxy(32,14);
textcolor(lightgray);
write(Sig_theta[1]+'        '+Sig_theta[2]+'
      '+Sig_theta[3]);
gotoxy(4,16);
textcolor(white);
```

```
write('Sigma (r)   MPa:');
gotoxy(32,16);
textcolor(lightgray);
write(sig_radial[1]+'        '+Sig_radial[2]+'
      '+Sig_radial[3]);
gotoxy(4,18);
textcolor(white);
write('Sigma (z)   MPa:');
gotoxy(32,18);
textcolor(lightgray);
write(sigma_zz[1]+'        '+Sigma_zz[2]+'
      '+Sigma_zz[3]);
gotoxy(4,20);
textcolor(white);
write('Radial Disp. (mm):');
gotoxy(32,20);
textcolor(lightgray);
write(displacement[1]+'        '+displacement[2]+'
      '+displacement[3]);
gotoxy(4,22);
textcolor(white);
write('Hoop strain (%):');
gotoxy(32,22);
textcolor(lightgray);
write(epsilon_f[1]+'        '+epsilon_f[2]+'
      '+epsilon_f[3]);
str(k[1]:7:5,numberk);
gotoxy(40,7);
textcolor(white);
write('"Avoidance factor" K:');
textcolor(lightgray);
gotoxy(62,7);
write(numberk);
curser_off(stype);
end;

(*******************************************************)

Procedure RotResult;

var
  z:real;
  i,j,cd,npicf:integer;
  Qprt,Cprt:realarray6X6;
  dumk,ang:string;
  abdn:boolean;
  mask:mask_names;

label
  flag_abrt;
```

```
begin
curser_small(stype);
Textcolor(yellow);
        { purely for reason of setting curser color...TP bug}
Textbackground(black);
gotoxy(45,4);
write('          ');
Gotoxy(4,4);
textcolor(lightgray);
write('Enter desired rotation angle in degrees: ');
gotoxy(36,4);
textcolor(lightgreen);
write('degrees');
textcolor(yellow);
gotoxy(45,4);
abdn:=false;
holdstr[1,1]:='';
mask[1]:='off';
npicf:=1;
inputedit(ang,mask,false,0,npicf,npicf,npicf,abdn,3,3,45,4,
          'N',255,45,4,0,0,0,1,1,0,0);
if abdn=true then
  begin
  gotoxy(4,4);
  write('                                      ');
  curser_Off(stype);
  goto flag_abrt;
  end;
val(ang,z,cd);
Rotate(z,1);    {does the math}
for i:= 1 to 6 do
for j:= 1 to 6 do
begin
  Qprt[i,j]:=Lq[1,i,j];
  Cprt[i,j]:=La[1,i,j];
end;
outputdesctable(3,7,6,6,7,1,2,3,1,Qprt,Cprt);
                                    {displays results}
str(K[1]:5:4,dumk);
gotoxy(25,22);
write('                                      ');
gotoxy(25,22);
textcolor(lightblue);
write('"Avoidance factor" K is: '+dumk);

flag_abrt:
end;


(********************************************)
```

```
function Dfac(f,d:real;n:integer):real;

var
iDfac:real;
label
flag_0;

begin
if n = 0 then
begin
  Dfac:= 1;
  goto flag_0;
end;
iDfac:=1;
for i:= 1 to n do
begin
  iDfac:= iDfac * (i*f+d);
end;
Dfac:=iDfac;
flag_0:
end;

(*************************************************)

function fac(n:integer):integer;

var
ifac:integer;

begin
ifac:=1;
for i:= 1 to n do
ifac:= ifac*i;

Fac:= ifac;
end;

(*************************************************)

(*
Procedure Summation(varfactor:realarray8;ro:real;last:
integer;typ:char;getfit:boolean);

var

G11,G12,G22,a13,a23,a33,f,g,AA,BB,l,m,d,i,j,k,C1,C2,DD,b,
AposD,AnegD,BposD,BnegD,AdposD,AdnegD,BdposD,BdnegD,
AddposD,AddnegD,BddposD,BddnegD,fact1,fact2,fact3,fact4,
ii,jj,kk,ll,mm,f1s,f2s,f3s,f4s,f2ds,f1ds,f3ds,f4ds:real;
```

```
    b_fit:realarrayMPbyNp;
    pic,grNo,lastL,n:integer;

    begin

    if getfit = true then
    begin
      getgraphdata('B');

      grNo:= 1;
      bestfit(b_fit,pic,grNo,lastL);
      bfit.l:=-b_fit[pic,2];
      bfit.G11:=b_fit[pic,1]/1000;

      grNo:= 2;
      bestfit(b_fit,pic,grNo,lastL);
      bfit.m:=-b_fit[pic,2];
      bfit.G12:=b_fit[pic,1]/1000;

      grNo:= 3;
      bestfit(b_fit,pic,grNo,lastL);
      bfit.d:=-b_fit[pic,2];
      bfit.G22:=b_fit[pic,1]/1000;

      getgraphdata('a');

      grNo:= 8;
      bestfit(b_fit,pic,grNo,lastL);
      bfit.i:=-b_fit[pic,2];
      bfit.a13:=b_fit[pic,1]/1000;   {actually alpha values}

      grNo:= 9;
      bestfit(b_fit,pic,grNo,lastL);
      bfit.j:=-b_fit[pic,2];
      bfit.a23:=b_fit[pic,1]/1000;

      grNo:=4;
      bestfit(b_fit,pic,grNo,lastL);
      bfit.k:=-b_fit[pic,2];
      bfit.a33:=b_fit[pic,1]/1000;
    end;

    G11:=bfit.G11;
    G12:=bfit.G12;
    G22:=bfit.G22;
    a13:=bfit.a13;
    a23:=bfit.a23;
    a33:=bfit.a33;
    i:=bfit.i;
    j:=bfit.j;
```

```
k:=bfit.k;
l:=bfit.l;
m:=bfit.m;
d:=bfit.d;
f:=d-1;
g:=d-m;
b:=1;
AA:= G11/(G22*pow(b,2-f));
BB:= m*G12/(G22*pow(b,2-g));
DD:= (d+b-1)/b;

if typ = 'm' then
  AA:= 0;
if typ = 'l' then
  BB:= 0;

f1s:=0;
f2s:=0;
f3s:=0;
f4s:=0;
f1ds:=0;
f2ds:=0;
f3ds:=0;
f4ds:=0;

for n:= 0 to last do
begin

{sigma-r terms}

f1s:= f1s + (n*f+d)*pow(ro,n*f+d-2)*
      pow(AA,n)/(dfac(f,d,n)*pow(f,n)*fac(n));
f2s:= f2s + (n*f)*pow(ro,n*f-2)*pow(AA,n)/
      (dfac(f,-d,n)*pow(f,n)*fac(n));
f3s:= f3s + (n*g+d)*pow(ro,n*g+d-2)*
      pow(BB,n)/(dfac(g,d,n)*pow(g,n)*fac(n));
f4s:= f4s + (n*g)*pow(ro,n*g-2)*pow(BB,n)/
      (dfac(g,-d,n)*pow(g,n)*fac(n));

{sigma-f terms}

f1ds:=f1ds + (n*f+d)*(n*f+d-1)*pow(ro,n*f+d-2)*
      pow(AA,n)/(dfac(f,d,n)*pow(f,n)*fac(n));
f2ds:=f2ds + (n*f)*(n*f-1)*pow(ro,n*f-2)*pow(AA,n)/
      (dfac(f,-d,n)*pow(f,n)*fac(n));
f3ds:=f3ds + (n*g+d)*(n*g+d-1)*pow(ro,n*g+d-2)*
      pow(BB,n)/(dfac(g,d,n)*pow(g,n)*fac(n));
f4ds:=f4ds + (n*g)*(n*g-1)*pow(ro,n*g-2)*pow(BB,n)/
      (dfac(g,-d,n)*pow(g,n)*fac(n));
end;
```

```
factor[1]:=  fls+f3s;
factor[2]:=  f2s+f4s;
factor[3]:=  flds+f3ds;
factor[4]:=  f2ds+f4ds;
factor[5]:= -(a13/a33)*pow(ro,-i+k);
factor[6]:= -(a23/a33)*pow(ro,-j+k);

end; *)

(*******************************************)

(*
procedure Two_var(typ:char;var
rad,sigma_r,sigma_f,sigma_z:realarray2plusN);

var
P,Q,a,b,C1,C2,ro,factor3a,factor3b,factor4a,factor4b,
C1s,C2s,factor1a,factor1b,factor2a,factor2b:real;
i,terms:integer;
grp:realarray8;
getfit:boolean;

begin

P:= insidePress;     {GPa}
Q:= outerPress;
terms:=10;
a:=insideDia/Outsidedia;
b:=1;
getfit:=true;

summation(grp,a,terms,typ,getfit);
getfit:= false;

factor3a:=grp[3];
factor4a:=grp[4];

factor1a:=grp[1];
factor2a:=grp[2];

summation(grp,b,terms,typ,getfit);

factor3b:=grp[3];
factor4b:=grp[4];

factor1b:=grp[1];
factor2b:=grp[2];
```

```
C1s:=(-P*factor2b+Q*factor2a)/((factor1a*factor2b)-
      (factor1b*factor2a));
C2s:=(-Q*factor1a+P*factor1b)/((factor1a*factor2b)-
      (factor1b*factor2a));

ro:= a;
for i:= 0 to NL do
begin
   summation(grp,ro,terms,typ,getfit);

   sigma_r[i]:=C1s*grp[1]+C2s*grp[2];
   sigma_f[i]:=C1s*grp[3]+C2s*grp[4];
   sigma_z[i]:=sigma_r[i]*grp[5]+sigma_f[i]*grp[6];
   rad[i]:=ro;
   ro:= ro+((b-a)/NL);

end;


end;
*)


(******************************************)

Procedure Variable_N(var power:real;var restnt:boolean);

var
n,G11,G12,G22,A13,A23,A33,a,b,c,Gn,s,t,M,L,E,ro,f1,f2,f3,f4,
P,G,Q,Sigma_r,Sigma_f,Sigma_z,C1,C2,C3,C4,C5,C6,rr,dr,
direct_r,direct_f,indirect_f,indirect_r,direct_z,indirect_z,
rinc,rdim:real;

begin
P:= InsidePress;
Q:= Outerpress;
G11:=bfit_store[1,1]/1000;      {to get proper units of GPa-1}
G12:=bfit_store[2,1]/1000;
G22:=bfit_store[3,1]/1000;
A13:=la[outerlayer,1,3];    {based on outer layer compliance}
A23:=la[outerlayer,2,3];
A33:=la[outerlayer,3,3];
n:=-power;
b:=1.0;
a:=r[0]/r[outerlayer];
c:=a/b;
Gn:=(n*G12+G11)/G22;
s:=(n+sqrt(sqr(n)+4*Gn))/2;
t:=(n-sqrt(sqr(n)+4*Gn))/2;
G:=(A13-A23)/(G22*A33*0.001);    {units of MPa-1}
M:=G/(1+n-Gn);
L:=((P-Q)*sqr(a))/2;
```

```
f1:=(-c*pow(a,n)+pow(c,t)*pow(b,n))/(pow(c,s)-pow(c,t));;
f2:=(c*pow(a,n)-pow(c,s)*pow(b,n))/(pow(c,s)-pow(c,t));;
f3:=(-P*c+Q*pow(c,t))/(pow(c,s)-pow(c,t));
f4:=(-Q*pow(c,s)+P*c)/(pow(c,s)-pow(c,t));
C1:=pow(b,n+2)*(1-pow(c,n+2))/(A33*0.001*(n+2));
                                  {units of MPa-1}
C2:=pow(b,n+2)*M*((A13+(n+1)*A23)*
     (1-pow(c,n+2))/((n+2)*A33));
C3:=sqr(b)*M*(1-pow(c,s+1))*(A13+s*A23)*f1/(A33*(s+1));
C4:=sqr(b)*M*(1-pow(c,t+1))*(A13+t*A23)*f2/(A33*(t+1));
C5:=((A13+t*A23)*(1-pow(c,t+1))*sqr(b))*f4/(A33*(t+1));
C6:=((A13+s*A23)*(1-pow(c,s+1))*sqr(b))*f3/(A33*(s+1));
E:=(L+C5+C6)/(C1-C2-C3-C4);
if restnt = true then
   E:=0;
rr:=c;
dr:=(b-a)/16;
rinc:=wallthick/16;
rdim:=insideDia/2;
for i:= 0 to 16 do
begin
   ro:=rr/b;
   direct_r:=(pow(ro,s-1)*f3)+(pow(ro,t-1)*f4);
   indirect_r:=E*M*(pow(rr,n)+pow(ro,s-1)*f1+pow(ro,t-1)*f2);
   Sigma_r:= direct_r + indirect_r;
   direct_f:=(s*pow(ro,s-1)*f3)+(t*pow(ro,t-1)*f4);
   indirect_f:=E*M*((n+1)*pow(rr,n)+s*
                pow(ro,s-1)*f1+t*pow(ro,t-1)*f2);
   Sigma_f:= direct_f + indirect_f;
   indirect_z:=-(A13*Sigma_r + A23*Sigma_f)/A33;
   direct_z:= (E*pow(rr,n))/(0.001*A33);
   Sigma_z:=direct_z + indirect_z;
   graphdata[1].xydata[i,2]:=Sigma_r;
   graphdata[2].xydata[i,2]:=Sigma_f;
   graphdata[3].xydata[i,2]:=Sigma_z;
   graphdata[4].xydata[i,2]:=indirect_r;
   graphdata[5].xydata[i,2]:=indirect_f;
   graphdata[6].xydata[i,2]:=indirect_z;
   graphdata[1].xydata[i,1]:=rdim;
   graphdata[3].xydata[i,1]:=rdim;
   graphdata[2].xydata[i,1]:=rdim;
   graphdata[4].xydata[i,1]:=rdim;
   graphdata[5].xydata[i,1]:=rdim;
   graphdata[6].xydata[i,1]:=rdim;
   graphdata[7].xydata[i,1]:=rdim;
   rr:=rr+dr;
   rdim:=rdim+rinc;
end;

graphdata[1].symbol:=char(229)+'rr';
```

```
graphdata[2].symbol:=char(229)+char(233)+char(233);
graphdata[3].symbol:=char(229)+'zz';
(* graphdata[4].symbol:=char(27)+char(229)+'r'+char(26);
graphdata[5].symbol:=char(27)+char(229)+char(233)+char(26);
graphdata[6].symbol:=char(27)+char(229)+'z'+char(26);
graphdata[7].symbol:=(' '+char(232)+' ');
*)
end;


(*****************************************************)

procedure statsout(expon:real;var restnt:boolean);

var
ra_f,ra_z,ra_r,rint_f,rint_z,rint_r:string;
ratio_f,ratio_z,ratio_r,int_f,int_z,int_r:real;

begin
int_f:=0;
int_r:=0;
int_z:=0;
variable_n(expon,restnt);
ratio_f:=(graphdata[2].xydata[16,2]-
          graphdata[2].xydata[0,2])/
          (0.5*(graphdata[2].xydata[16,2]
          +graphdata[2].xydata[0,2]));
ratio_z:=(graphdata[3].xydata[16,2]-
          graphdata[3].xydata[0,2])/
          (0.5*(graphdata[3].xydata[16,2]+
          graphdata[3].xydata[0,2]));
ratio_r:=(0.5*(graphdata[1].xydata[0,2]-
          graphdata[1].xydata[16,2])
          -graphdata[1].xydata[8,2])/
          ((graphdata[1].xydata[16,2]-
          graphdata[1].xydata[0,2])/2);
for i:= 0 to 16 do
(* begin
  int_f:= int_f+ graphdata[2].xydata[i,2];
  int_z:= int_z+ graphdata[3].xydata[i,2];
  int_r:= int_r+ graphdata[1].xydata[i,2];
end;
if expon = 0 then
  begin
  int_f0:= int_f;
  int_z0:= int_z;
  int_r0:= int_r;
  end;           not needed for 3 principal stresses only *)

setfillstyle(1,black);
setcolor(white);
```

```
outtextxy(573,50,'Stress');
outtextxy(569,62,'ratio %');

str(100*ratio_r:4:1,ra_r);
setcolor(cyan);
outtextxy(569,86,char(229)+'rr');
setcolor (lightgray);
bar(599,86,639,94);
outtextxy(599,86,ra_r);

str(100*ratio_f:4:1,ra_f);
setcolor(green);
outtextxy(569,100,char(229)+char(233)+char(233));
setcolor(lightgray);
bar(599,100,639,108);
outtextxy(599,100,ra_f);

str(100*ratio_z:4:1,ra_z);
setcolor(red);
outtextxy(569,114,char(229)+'zz');
setcolor(lightgray);
bar(599,114,639,120);
outtextxy(599,114,ra_z);

(*      {not needed for plotting only principal stresses}
setcolor(white);
outtextxy(569,140,char(127)+' stress');
outtextxy(569,152,'Integral');

setcolor(cyan);
outtextxy(569,176,char(229)+'rr');
setcolor(lightgray);
str(100*int_f/int_f0:3:1,rint_r);
bar(599,176,639,184);
outtextxy(599,176,rint_r);

setcolor(green);
outtextxy(569,190,char(229)+char(233)+char(233));
setcolor(lightgray);
str(100*int_z/int_z0:3:1,rint_f);
bar(599,190,639,198);
outtextxy(599,190,rint_f);

setcolor(red);
outtextxy(569,204,char(229)+'zz');
setcolor(lightgray);
str(100*int_r/int_r0:3:1,rint_z);
bar(599,204,639,212);
outtextxy(599,204,rint_z);
*)
```

689

```pascal
end;

(*****************************************************)

Function FA(r:real):real;

begin

FA:=(bfit.d-1)/r;
end;

(*****************************************************)

Function FB(r:real):real;

var
a,b,f,g,va:real;

begin

a:=bfit.G11/bfit.G22;
b:=bfit.m*bfit.G12/bfit.G22;
f:=bfit.d - bfit.l;
g:=bfit.d - bfit.m;
va:=(a*pow(r,f)+b*pow(r,g))/sqr(r);
FB:=va;
end;

(*****************************************************)

Function FCC(r:real):real;

var
u,i,v,h:real;

begin

u:=bfit.a13/(bfit.a33*0.001*bfit.G22);
v:=(1 - bfit.j + bfit.k)*bfit.a23/(Bfit.a33*0.001*Bfit.G22);
h:=bfit.d - bfit.i + bfit.k - 1;
i:=bfit.d - bfit.j + bfit.k - 1;
FCC:=(u*pow(r,h)-v*pow(r,i));
end;

(*****************************************************)

Function phi_1(r:real):real;

begin
phi_1:=(bfit.a13/bfit.a33)*pow(r,-bfit.i+bfit.k+1);
```

```
end;

(**********************************************)

Function phi_2(r:real):real;

begin
phi_2:=(bfit.a23/bfit.a33)*pow(r,-bfit.j+bfit.k+1);
end;

(**********************************************)

Procedure FiniteD(var
actrad,sigma_r,sigma_f,sigma_z:realarray2plusN;variation,itt
erate:boolean);

type realarrayN = array[1..nfe] of real;

var         .

b_fit:realarrayMPbyNp;
pic,grNo,itt,n:integer;
a,b,c,d,u,l,z:realarrayN;
w,rad:realarray2plusN;
h,r,cc,newcc,diff,aa,bb,P,Q,phi_a,phi_b,constZ,pois_1,
pois_2,sum_1,sum_2,integral,multip,tol:real;
num:string;

label
flag1;

begin

if variation = false then        {reads data only first time}
begin
  getgraphdata('3');

  grNo:= 1;
  bestfit(b_fit,pic,grNo);
  bfit.l:=-b_fit[pic,2];
  bfit.G11:=b_fit[pic,1]/1000;     {gives data in GPa-1}

  grNo:= 2;
  bestfit(b_fit,pic,grNo);
  bfit.m:=-b_fit[pic,2];
  bfit.G12:=b_fit[pic,1]/1000;

  grNo:= 3;
  bestfit(b_fit,pic,grNo);
  bfit.d:=-b_fit[pic,2];
```

```
   bfit.G22:=b_fit[pic,1]/1000;

   getgraphdata('a');

   grNo:= 8;
   bestfit(b_fit,pic,grNo);
   bfit.i:=-b_fit[pic,2];
   bfit.a13:=b_fit[pic,1]/1000;   {actually alpha values}

   grNo:= 9;
   bestfit(b_fit,pic,grNo);
   bfit.j:=-b_fit[pic,2];
   bfit.a23:=b_fit[pic,1]/1000;

   grNo:=4;
   bestfit(b_fit,pic,grNo);
   bfit.k:=-b_fit[pic,2];
   bfit.a33:=b_fit[pic,1]/1000;
end;
(*
bfit.a33:=0.03803;
bfit.a23:=-0.04224;
bfit.a13:=0.001948;
bfit.G22:=0.00906;
bfit.G12:=-0.00377;
           {test case values for error checking using gtank1}
bfit.G11:=0.13048;
bfit.i:=2.066;
bfit.j:=2.066;
bfit.k:=2.066;
bfit.l:=2.066;
bfit.m:=2.066;
bfit.d:=2.066;
*)
P:=-insidepress;
Q:=-outerpress;
aa:=insideDia/outsideDia;
bb:=1;

tol:=0.000001;
cc:=0;
n:=nfe;

for itt:= 1 to 50 do
begin

   phi_a:= P*aa;
   phi_b:= Q*bb;

   h:=(bb-aa)/(n+1);
```

```
r:=aa+h;
   a[1]:=2+sqr(h)*FB(r);
   b[1]:=-1+(FA(r)*(h/2));
   d[1]:=cc*(-sqr(h)*FCC(r))+(1+(h/2)*FA(r))*Phi_a;

for i:= 2 to n-1 do
begin
   r:=aa+(i*h);
   a[i]:=2+sqr(h)*FB(r);
   b[i]:=-1+(FA(r)*(h/2));
   c[i]:=-1-((h/2)*FA(r));
   d[i]:=cc*(-sqr(h)*FCC(r));
   end;

r:=bb-h;
   a[n]:=2+sqr(h)*FB(r);
   c[n]:=-1-((h/2)*FA(r));
   d[n]:=cc*(-sqr(h)*FCC(r))+(1-(h/2)*FA(r))*Phi_b;


l[1]:=a[1];
u[1]:= b[1]/a[1];

for i:= 2 to n-1 do
begin
   l[i]:= a[i]-c[i]*u[i-1];
   u[i]:= b[i]/l[i];
end;

l[n]:=a[n]-c[n]*u[n-1];
z[1]:=d[1]/l[1];

for i:= 2 to n do
   z[i]:= (d[i]-c[i]*z[i-1])/l[i];

w[0]:=phi_a;
w[n+1]:=phi_b;
w[n]:= z[n];

for i:= n-1 downto 1 do
w[i]:= z[i]-u[i]*w[i+1];

for i:= 0 to n+1 do
   begin
   rad[i]:=aa+i*h;
   sigma_r[i]:=(1/rad[i])*w[i];
   actrad[i]:=(insideDia/2)+i*(wallthick/(n+1));
   end;
for i:= 1 to n do
sigma_f[i]:=(w[i+1]-w[i-1])/(2*h);
```

```
sigma_f[0]:=(1/(2*h))*(-3*w[0]+4*w[1]-w[2]);

sigma_f[n+1]:=(1/(2*h))*(w[n-1]-4*w[n]+3*w[n+1]);

if itterate = false then goto flag1;

sum_1:= 0;
sum_2:= 0;

for i:= 0 to n do
  begin
  sum_1:= sum_1 + (h/2)*(phi_1(rad[i])*sigma_r[i]+
          phi_1(rad[i+1])*sigma_r[i+1]);
   sum_2:= sum_2 + (h/2)*(phi_2(rad[i])*sigma_f[i]+
          phi_2(rad[i+1])*sigma_f[i+1]);

   end;
  integral:= sum_1 + sum_2;
  multip:= 0.001*bfit.a33*(bfit.k+2)/
          (pow(bb,bfit.k+2)-pow(aa,bfit.k+2));{units MPa-1}
  newcc:=multip*(0.5*(-P+Q)*sqr(aa)+integral);
  diff:=abs(newcc-cc);
  if diff < tol then goto flag1;
  cc:=newcc;
end; {itteration loop}

if itt = 50 then
begin
str(itt,num);
writeln('No convergence after' +num+ 'itterations');
end;
flag1:

for i:= 0 to n+1 do
begin
  constZ:= (cc/(0.001*bfit.a33))*pow(rad[i],bfit.k);
  pois_1:= (phi_1(rad[i])*sigma_r[i]/rad[i]);
  pois_2:= (phi_2(rad[i])*sigma_f[i]/rad[i]);
  sigma_z[i]:=constZ - pois_1 - pois_2;
end;

end;

(*********************************************************)

end.
```

```
unit Failure;
{$O+,F+}


(***********************************************)

interface
uses Glob_var;

procedure Tsai_wu(var Acon:real;var stressR,stressF,
                  stressZ,SafetyFPF,SafetyL:realarray3NL);

procedure Calculate_prop(var T_iso,metal,fit,degrd:
                         boolean;var lno:integer;var
                         Gl,Ef,Et,dEt,Ef,Vt,Gf,dGl,
                         Gtf,Kf,ffm,Em,Vm,ffs:real;var
                         redu,ffail,Rss:realarray1NL;
                         var errcd:integerarray16);

Procedure Feng(var ACon:real;var StressR,StressF,StressZ,
               Mfail,Ffail:realarray3NL);

procedure Christensen(var ACon:real;var StressR,StressF,
                      StressZ,sig_1,sig_2,sig_3,sig_4,Rm,Rf,
                      ef,ez,e1,e2,e3,e4:realarray3NL;var
                      Redu,Rff:realarray1NL;
                      var degr,first:boolean);

procedure XUdegrad(var Rmatrix,Ffail,e66,
                   e22,e11:realarray3NL;var degrade,first,
                   rupture,NLshear,skip:boolean;
                   varlastE2,Req,Rff,Rss,LastRs,eci,
                   ec6,eff,ecs,Layfail,Layfiberf:
                   realarray1NL;var count:integer;var
                   indxD,IndexS,Dmat,Dhigh,Pprof:real);

procedure stiffness;
procedure stiffinv;
procedure thermo;


(***********************************************)

implementation

(***********************************************)

function pow(a,b:real):real;
begin
  if b = 0 then
    pow:=1
  else if a = 0 then
```

```pascal
      pow:=0
    else
      pow:= exp(b*ln(a));
end;


(***************************************************)


function tanh(a:real):real;
begin
    if a < -20 then
      tanh:=-1.0
    else
      tanh:=(exp(a)-exp(-a))/(exp(a)+exp(-a));
end;


(***************************************************)


procedure Calculate_prop(var T_iso,metal,fit,degrd:
                           boolean;var lno:integer;
                           var Gl,Ef,Et,dEt,Vf,Vt,Gf,dGl,
                           Gtf,Kf,ffm,Em,Vm,ffs:real;var
                           redu,ffail,Rss:realarray1NL;
                           var errcd:integerarray16);
       {Synthesizes laminate properties}

var
Gm,Km,ff,fm,df,dfm,kk,vtt:real;
N,L,Gt,m,GtX:real;     {composite characteristics-calculated}
El,vl,Gld,Gth,Gtl:real;
                  {values used in transversely isotropic case}
gama,alpha,betam,betaf,row,storEm,storEf,storVm,
erE,erG:real;
code,i,j: integer;
PDgrad:real;

label
    flag1,flag_metal;

begin
If metal = true then
    begin                   {case for metal}
      El:=Em;
      vl:=Vm;
      Gl:=Em/(2*(1+Vm));
      Gt:=Gl;
      KK:=Gt/(1-(2*Vm));
      ffm:=0.0;
      ffs:=0.0;
      goto Flag_metal;
    end;
```

```
storEm:= Em;
storVm:= Vm;
storEf:= Ef;

   if errcd[4]=0 then
     begin
     if errcd[5]=0 then
       begin
       Kf:=1/((2*(1-Vt)/Et)-(4*sqr(Vf)/Ef));
       goto flag1;
       end;
     if errcd[6]=0 then
       begin
       Kf:= 1/((4/Et)-(1/Gtf)-(4*sqr(Vf)/Ef));
       goto flag1;
       end;
     if errcd[7]=0 then
       begin
       Gtf:= 1/((4/Et)-(1/Kf)-(4*sqr(Vf)/Ef));
       goto flag1;
       end;
     end;
   if errcd[5]=0 then
     begin
     if errcd[6]=0 then
       begin
       Kf:= 1/((2/(Gtf*(1+Vt)))-(1/Gtf)-(4*sqr(Vf)/Ef));
       goto flag1;
       end;
     if errcd[7]=0 then
       begin
       Gtf:= (Kf*(1-Vt))/(((1-Vt)*4*Kf*sqr(Vf)/Ef)-Vt+1);
       goto flag1;
       end;
     end;
   if errcd[6]=0 then
     begin
     if errcd[7]=0 then
       begin
       goto flag1;    {equations apply directly}
       end;
     end;

   flag1:

   Gm:= Em/(2*(1+Vm));
   km:= Gm/(1-2*Vm);              {plane strain bulk modulus};
   ff:= ffm/100;                  {prescribed fiber fraction}
   fm:= 1-ff;
```

```pascal
        df:= ffs/100;                    {default fraction-strength}
        dfm:= 1-df;

   If not T_iso then                {isotropic fibers case}
      if (errcd[1]=0)and(errcd[2]=0)and
         (errcd[8]=0)and(errcd[9]=0) then
        begin
          Gf:=Ef/(2*(1+Vf));
          Gtf:=Gf;
          Kf:=Gf/(1-(2*Vf));
        end;

      if T_iso then
        if (errcd[1]<>0)or(errcd[2]<>0)or
           errcd[3]<>0)or(errcd[8]<>0)or(errcd[9]<>0) then
           halt;

   KK:= Km+(ff/((1/(Kf-Km))+(fm/(Km+Gm))));
   El:= Em*fm+Ef*ff+((4*sqr(vf-vm)*fm*ff)/
        ((fm/kf)+(ff/km)+(1/Gm)));
   vl:= vm*fm+vf*ff+(((vf-vm)*((1/km)-(1/kf))*fm*ff)/
        ((fm/kf)+(ff/km)+(1/Gm)));
   Gl:= Gm+(ff/((1/(Gf-Gm))+fm/(2*Gm)));
   Gld:= Gm+(df/((1/(Gf-Gm))+dfm/(2*Gm)));
                              {shear modulus with def.fiber fract}

   gama:= Gtf/Gm;
   betaf:= 1/(3-4*vf);
   betam:= 1/(3-4*vm);
   row:= (gama+betam)/(gama-1);
   alpha:= (betam-gama*betaf)/(1+gama*betaf);

   Gth:= Gm*(1+(((1+betam)*ff)/
        (row-ff*(1+((3*sqr(betam*fm))/
        (alpha*ff*ff*ff+1))))));
   Gt:=Gth;
  {if (Gf > Gm) then Gt:= Gth;
   Gtl:= Gm*(1+(((1+betam)*ff)/
        (row-ff*(1+((3*sqr(betam*fm))/
        (alpha*ff*ff*ff-betam))))));
   if  (Gf < Gm) then Gt:= Gtl;}

{note:bounds assigned are generally the upper
                            value unless metallic type matrix}

Flag_metal:

   N:= El+4*KK*vl*vl;
   L:= 2*KK*vl;
   Et:= 4/((1/Gt)+(1/kk)+(4*vl*vl/El));
```

698

```
m:= 1+4*KK*vl*vl/El;
vtt:= (KK-(m*Gt))/(KK+(m*Gt));

if fit=true then
begin
  erE:=(dEt-Et)/dEt;
  erG:=(dGl-Gl)/dGl;
  if (abs(erE+erG))>0.001 then
    begin
    Em:=(Em*(erE+erG)/2)+Em;
    goto flagl;
    end;
end;

for i:= 1 to 6 do
for j:= 1 to 6 do
begin
CC[i,j]  := 0;
Q[i,j]  := 0;
end;

Elconst[lno].El:= El;
Elconst[lno].Et:= Et;
Elconst[lno].vl:= vl;
Elconst[lno].vt:= vtt;
Elconst[lno].Gl:= Gl;
Elconst[lno].Gt:= Gt;
Elconst[lno].kk:= kk;

{compliance terms of unidirectional lamina}

CC[1,1]:= 1/El;
CC[1,2]:= -vl/El;
CC[1,3]:= -vl/El;
CC[2,1]:= -vl/El;
CC[2,2]:= 1/Et;
CC[2,3]:= -vtt/Et;
CC[3,1]:= -vl/El;
CC[3,2]:= -vtt/Et;
CC[3,3]:= 1/Et;
CC[4,4]:= 1/Gt;
CC[5,5]:= 1/Gl;
CC[6,6]:= 1/Gl;

Q[1,1]:= N;
Q[1,2]:= L;         {stiffness terms of unidirectional lamina}
Q[1,3]:= L;                    {using engineering shear strain}
Q[2,1]:= L;
Q[2,2]:= kk+Gt;
Q[2,3]:= kk-Gt;
```

```
        Q[3,1]:= L;
        Q[3,2]:= kk-Gt;
        Q[3,3]:= kk+Gt;
        Q[4,4]:= Gt;
        Q[5,5]:= Gl;
        Q[6,6]:= Gl;

        {microcracked matrix reduction}

    if (degrd = true) and ((redu[lno]<1) or (Rss[lno] > 1)) then
      begin
        {curve fit factor for moduli reduction}
        PDGrad:=0.265+1.02*redu[lno]-0.295*sqr(redu[lno]);
        Q[1,2]:= Q[1,2]*PDGrad;
        Q[2,2]:= Q[2,2]*redu[lno];
        Q[2,3]:= Q[2,3]*PDGrad;
        Q[2,1]:= Q[1,2];
        Q[3,2]:= Q[2,3];
        Q[4,4]:= Q[2,2]-Q[2,3];
        Q[6,6]:= Q[6,6]*PDgrad/Rss[lno];
                            {nonlinear in-plane shear correction}
      end;
                              {broken fibers in layer reduction}
    if (degrd = true) and (ffail[lno]<1) then
      begin
        Q[1,1]:= Q[2,2]*ffail[lno]*1.1; {fiber factor}
        Q[1,3]:= Q[1,3]*ffail[lno]*0.5;
        Q[3,1]:= Q[1,3];
      end;


end; {procedure}


(*************************************************)


procedure Tsai_wu(var Acon:real;var stressR,stressF,
                  stressZ,SafetyFPF,SafetyL:realarray3NL);

var
i,j,l,errcd,layer:integer;
sig_1,sig_2,sig_3,sig_4,XT,XC,YT,YC,SS,angl,
Frr,Fzz,Fss,Fr,Fz,Frz,Frf,ro,zeta,e1,e2,e3,e4,ef,ez,
factA,FactB,SafetyMtx:realarray3NL;
safFPF,safMtx:realarray1NL;
mult,root:real;

begin

for i:=1 to outerlayer do
begin
  val(graphlabels[i].angle,angl[i*3-2],errcd);
```

700

```
    val(graphlabels[i].angle,angl[i*3-1],errcd);
    val(graphlabels[i].angle,angl[i*3],errcd);

    XT[i*3-2]:=strg[i].XT;
    XT[i*3-1]:=strg[i].XT;
    XT[i*3]:=strg[i].XT;
    XC[i*3-2]:=strg[i].XC;
    XC[i*3-1]:=strg[i].XC;
    XC[i*3]:=strg[i].XC;
    YT[i*3-2]:=strg[i].YT;
    YT[i*3-1]:=strg[i].YT;
    YT[i*3]:=strg[i].YT;
    YC[i*3-2]:=strg[i].YC;
    YC[i*3-1]:=strg[i].YC;
    YC[i*3]:=strg[i].YC;
    SS[i*3-2]:=strg[i].SS;
    SS[i*3-1]:=strg[i].SS;
    SS[i*3]:=strg[i].SS;
end;

for i:= 1 to 3*outerlayer do
begin
  l:=trunc((i+2)/3);
  angl[i]:=angl[i]*pi/180;
  e3[i]:=0.001*lb[l,1,1]*stressR[i]+0.001*lb[l,1,2]*
          stressF[i]+(la[l,1,3]/la[l,3,3])*Acon;
  ef[i]:=0.001*lb[l,1,2]*stressR[i]+0.001*lb[l,2,2]*
          stressF[i]+(la[l,2,3]/la[l,3,3])*Acon;
  ez[i]:=Acon;
                    {strains in local fiber coordinates}

  e1[i]:=sqr(cos(angl[i]))*ez[i]+sqr(sin(angl[i]))*ef[i];
  e2[i]:=sqr(sin(angl[i]))*ez[i]+sqr(cos(angl[i]))*ef[i];
  e4[i]:=2*(-sin(angl[i])*cos(angl[i])*ez[i]+sin(angl[i])*
          cos(angl[i])*ef[i]);

                    {local strains to local stresses}

  sig_1[i]:=1000*(e1[i]*lstif[1,1,1]+e2[i]*
          lstif[1,1,2]+e3[i]*lstif[1,1,3]);
  sig_2[i]:=1000*(e1[i]*lstif[1,2,1]+e2[i]*
          lstif[1,2,2]+e3[i]*lstif[1,2,3]);
  sig_3[i]:=1000*(e1[i]*lstif[1,3,1]+e2[i]*
          lstif[1,3,2]+e3[i]*lstif[1,3,3]);
  sig_4[i]:=1000*e4[i]*lstif[1,6,6];

  Frr[i]:= 1/(YT[i]*YC[i]);
  Fzz[i]:= 1/(XT[i]*XC[i]);
  Fss[i]:=1/sqr(SS[i]);
  Fr[i]:=(1/YT[i])-(1/YC[i]);
```

```
      Fz[i]:=(1/XT[i])-(1/XC[i]);
      Frz[i]:=-0.5*sqrt(Frr[i]*Fzz[i]);
      Frf[i]:=-0.5*Frr[i];

      ro[i]:=(Frr[i]*(sqr(sig_3[i])+sqr(sig_2[i])))+
             2*(Frf[i]*sig_3[i]*sig_2[i])+
             2*(Frz[i]*(sig_3[i]+sig_2[i])*
             sig_1[i])+Fzz[i]*sqr(sig_1[i])+
             Fss[i]*sqr(sig_4[i]);
      zeta[i]:=Fr[i]*(sig_3[i]+sig_2[i])+Fz[i]*sig_1[i];

      safetyFPF[i]:=-(zeta[i]/(2*ro[i]))+
                     sqrt((sqr(zeta[i]/(2*ro[i])))+(1/ro[i]));
      safetyL[i]:=1000;

      factA[i]:= Frr[i]*sqr(sig_2[i])+Fss[i]*sqr(sig_4[i]);
      factB[i]:= Fr[i]*sig_2[i];
      mult:=1/(2*factA[i]);
      root:=sqrt(sqr(factB[i])+4*FactA[i]);
      safetyMtx[i]:=mult*(-factB[i]+root);
end;

for l:= 1 to outerlayer do
  begin
    SafFPF[l]:= 9999;
    safMTX[l]:= 9999;
  end;
for i:= 1 to 3*outerlayer do
begin
l:=trunc((i+2)/3);
if safetyFPF[i] < safFPF[l] then
  safFPF[l]:= safetyFPF[i];
                    {find fail ini for each layer, matrix}
if safetyMtx[i] < safMtx[l] then
  safMtx[l]:= safetyMtx[i];
                    {find fail ini for each layer, matrix}
end;

end;{procedure}


(**************************************************)

Procedure Feng(var ACon:real;var
               StressR,StressF,StressZ,Mfail,
               Ffail:realarray3NL);
var

i,j,l,errcd:integer;
E11,E22,G12,V12,V21,V23,e1t,e1c,e2t,e2c,es,A,B,AA,BB,
A1,A11,A2,A22,A4,A5,A55,P1,P2,fact,F1,F2,F3,F4,F5,
```

```
F6,J1,J2,J4,J5:real;
XT,XC,YT,YC,SS,ez,ef,e3,e1,e2,e4,angl:realarray3NL;
safM,safF,SafE1,SafE2,SafE4:realarray1Nl;

begin
for i:= 1 to outerlayer do
begin
  val(graphlabels[i].angle,angl[i*3-2],errcd);
  val(graphlabels[i].angle,angl[i*3-1],errcd);
  val(graphlabels[i].angle,angl[i*3],errcd);
  XT[i*3-2]:=strg[i].XT;
  XT[i*3-1]:=strg[i].XT;
  XT[i*3]:=strg[i].XT;
  XC[i*3-2]:=strg[i].XC;
  XC[i*3-1]:=strg[i].XC;
  XC[i*3]:=strg[i].XC;
  YT[i*3-2]:=strg[i].YT;
  YT[i*3-1]:=strg[i].YT;
  YT[i*3]:=strg[i].YT;
  YC[i*3-2]:=strg[i].YC;
  YC[i*3-1]:=strg[i].YC;
  YC[i*3]:=strg[i].YC;
  SS[i*3-2]:=strg[i].SS;
  SS[i*3-1]:=strg[i].SS;
  SS[i*3]:=strg[i].SS;

  SafE1[i]:= 999;
  SafE2[i]:= 999;
  SafE4[i]:= 999;
end;

for i := 1 to 3*outerlayer do
                        {strains in global coordinates}
begin
  l:=trunc((i+2)/3);
  angl[i]:=angl[i]*pi/180;
  e3[i]:=0.001*lb[l,1,1]*stressR[i]+0.001*lb[l,1,2]*
          stressF[i]+(la[l,1,3]/la[l,3,3])*Acon;
  ef[i]:=0.001*lb[l,1,2]*stressR[i]+0.001*lb[l,2,2]*
          stressF[i]+(la[l,2,3]/la[l,3,3])*Acon;
  ez[i]:=Acon;
                        {strains in local fiber coordinates}

  e1[i]:=sqr(cos(angl[i]))*ez[i]+sqr(sin(angl[i]))*ef[i];
  e2[i]:=sqr(sin(angl[i]))*ez[i]+sqr(cos(angl[i]))*ef[i];
  e4[i]:=2*(-sin(angl[i])*cos(angl[i])*ez[i]+sin(angl[i])*
          cos(angl[i])*ef[i]);
                        {engineering shear strain}

  J1:= e1[i]+e2[i]+e3[i];
```

```
J2:= 0.16666666*(sqr(e1[i]-e2[i])+sqr(e2[i]-e3[i])+
     sqr(e3[i]-e1[i]))+sqr(e4[i]);
J4:= sqr(e4[i]);
J5:= e1[i];

E11:=Elconst[1].E1*1000;                              {strain limits}
E22:=Elconst[1].Et*1000;
G12:=Elconst[1].G1*1000;
V12:=Elconst[1].v1;
V23:=Elconst[1].vt;
V21:=(E22/E11)*V12;

elt:=XT[i]/E11;
elc:=-XC[i]/E11;
e2t:=YT[i]/E22;
e2c:=-YC[i]/E22;
es:=SS[i]/G12;

1:=trunc((i+2)/3);
if (elt/el[i]) < safE1[1] then
safE1[1]:= elt/el[i];
                        {find simple max strain for each layer, fiber}
if (e2t/e2[i]) < SafE2[1] then
safE2[1]:= e2t/e2[i];
                        {find simple max strain for each layer, matrix}
if (es/e4[i]) < SafE4[1] then
safE4[1]:= es/e4[i];
                        {find simple max strain for each layer, matrix}

A55:=-1/(elt*elc);
A5:= (1/elt)+(1/elc);
A2:=1/sqr(es/2);                  {tensorial shear strain}

P1:=1-V21-V23;
P2:=sqr(1+v21)+sqr(v21-v23)+sqr(1+v23);
fact:=(A2/6)*(P2);
F1:=e2t*P1;
F2:=sqr(e2t)*sqr(P1);
F3:=1-(fact*sqr(e2t));
F4:=e2c*P1;
F5:=sqr(e2c)*sqr(P1);
F6:=1-(fact*sqr(e2c));
A1:=((F3*F5)-(F6*F2))/((F1*F5)-(F4*F2));
A11:=((F1*F6)-(F4*F3))/((F1*F5)-(F4*F2));

A:= A55*sqr(J5);
B:= (A5*J5)+(A2*J4);
AA:= A11*sqr(J1);
BB:= (A1*J1)+(A2*J2);
```

```pascal
    Mfail[i]:=  (-BB/(2*AA))+sqrt(sqr(BB/(2*AA))+(1/AA));
    Ffail[i]:=  (-B/(2*A))+sqrt(sqr(B/(2*A))+(1/A));
end;
for l:= 1 to outerlayer do
begin
   SafM[l]:= 999;
   SafF[l]:= 999;
end;
for i:= 1 to 3*outerlayer do
begin
l:=trunc((i+2)/3);
if Mfail[i] < safM[l] then
   safM[l]:= Mfail[i]; {find fail ini for each layer, matrix}
if Ffail[i] < safF[l] then
   safF[l]:= Ffail[i]; {find fail ini for each layer, matrix}
end;

end;


(*******************************************************)

procedure Christensen(var ACon:real;var StressR,
                      StressF,StressZ,sig_1,sig_2,sig_3,
                      sig_4,Rm,Rf,ef,ez,e1,e2,e3,e4:
                      realarray3NL;var Redu,Rff:
                      realarray1NL;var degr,first:boolean);
var
errcd:integer;
XT,XC,YT,YC,SS,angl,k1,k2,a1,a2,b1,
Am,Bm,Cm,Af,Bf,Cf:realarray3NL;
i,j,l:integer;
SafSS,SafS1,SafS2:realarray1NL;
metal:boolean;
discrimF,discrimM:real;

label
flag_metal;

begin

for i:= 1 to outerlayer do
begin

   val(graphlabels[i].angle,angl[i*3-2],errcd);
   val(graphlabels[i].angle,angl[i*3-1],errcd);
   val(graphlabels[i].angle,angl[i*3],errcd);

   XT[i*3-2]:=strg[i].XT;
   XT[i*3-1]:=strg[i].XT;
   XT[i*3]:=strg[i].XT;
```

```
XC[i*3-2]:=strg[i].XC;
XC[i*3-1]:=strg[i].XC;
XC[i*3]:=strg[i].XC;
YT[i*3-2]:=strg[i].YT;
YT[i*3-1]:=strg[i].YT;
YT[i*3]:=strg[i].YT;
YC[i*3-2]:=strg[i].YC;
YC[i*3-1]:=strg[i].YC;
YC[i*3]:=strg[i].YC;
SS[i*3-2]:=strg[i].SS;
SS[i*3-1]:=strg[i].SS;
SS[i*3]:=strg[i].SS;

Safss[i]:= 999;
Safs1[i]:= 999;
Safs2[i]:= 999;
end;

for i := 1 to 3*outerlayer do              {strains in global coordinates}

begin
if XT[i]<>YT[i] then metal:=false else metal:=true;
  1:=trunc((i+2)/3);
  angl[i]:=angl[i]*pi/180;
  e3[i]:=0.001*lb[1,1,1]*stressR[i]+0.001*lb[1,1,2]*
         stressF[i]+(la[1,1,3]/la[1,3,3])*Acon;
  ef[i]:=0.001*lb[1,1,2]*stressR[i]+0.001*lb[1,2,2]*
         stressF[i]+(la[1,2,3]/la[1,3,3])*Acon;
  ez[i]:=Acon;                             {strains in local fiber coordinates}

  e1[i]:=sqr(cos(angl[i]))*ez[i]+sqr(sin(angl[i]))*ef[i];
  e2[i]:=sqr(sin(angl[i]))*ez[i]+sqr(cos(angl[i]))*ef[i];
  e4[i]:=2*(-sin(angl[i])*cos(angl[i])*
         ez[i]+sin(angl[i])*cos(angl[i])*ef[i]);
                                           {local strains to local stresses}

sig_1[i]:=1000*(e1[i]*lstif[1,1,1]+e2[i]*lstif[1,1,2]+
          e3[i]*lstif[1,1,3]);
sig_2[i]:=1000*(e1[i]*lstif[1,2,1]+e2[i]*lstif[1,2,2]+
          e3[i]*lstif[1,2,3]);
sig_3[i]:=1000*(e1[i]*lstif[1,3,1]+e2[i]*lstif[1,3,2]+
          e3[i]*lstif[1,3,3]);
sig_4[i]:=1000*e4[i]*lstif[1,6,6];
if e4[i] = 0.0 then
   sig_4[i]:=1.0E-6;                       {prevents division by zero}

if (XT[i]/sig_1[i]) < Safs1[1] then
safs1[1]:= XT[i]/sig_1[i];
```

```pascal
                 {find simple max stress for each layer, fiber}
if (YT[i]/sig_2[i]) < SafS2[l] then
   safS2[l]:= YT[i]/sig_2[i];
              {find simple max stress for each layer, matrix}
if (SS[i]/sig_4[i]) < SafSS[l] then
   safSS[l]:= SS[i]/sig_4[i];
              {find simple max stress for each layer, matrix}

   k1[i]:=YC[i]/2;
   a1[i]:=0.5*((YC[i]/YT[i])-1);
   b1[i]:=sqr(YC[i]/(2*SS[i]));
   k2[i]:=XT[i]/2;
   a2[i]:=0.5*((XT[i]/XC[i])-1);

   Am[i]:=b1[i]*sqr(sig_4[i])+(1+2*a1[i])*
          (0.25*sqr(sig_2[i]-Sig_3[i]));
   Bm[i]:=a1[i]*k1[i]*(sig_2[i]+Sig_3[i]);
   Cm[i]:=-sqr(k1[i]);
   Af[i]:=(0.25*(1+2*a2[i])*sqr(sig_1[i]))-(0.25*
          sqr(1+a2[i])*sig_1[i]*(sig_2[i]+sig_3[i]));
   Bf[i]:=-a2[i]*k2[i]*sig_1[i];
   Cf[i]:=-sqr(k2[i]);
                            {Christensen criteria}

   if (metal = true) and (l=1) then
   begin                        {Von Mises theory}
      Rf[i]:=1E9;
      Rm[i]:=XT[i]/(sqrt((sqr(sig_1[i]-sig_2[i])+
             sqr(sig_2[i]-sig_3[i])+sqr(sig_3[i]-
             sig_3[i]))/2)));
      if Rm[i] < 1 then Rm[i]:=1;
                           {constant plastic strength};
      goto flag_metal;
   end;
   if Rff[l] < 1 then
      Rf[i]:=Rff[l]
              {sets damaged material pseudo safety factor}
   else
      begin
        discrimF:=sqr(Bf[i])-4*Af[i]*Cf[i];
        if discrimF < 0.000 then
          discrimF := 0.000;
        Rf[i]:= (-Bf[i]+sqrt(discrimF))/(2*Af[i]);
      end;

   discrimM:=sqr(Bm[i])-4*Am[i]*Cm[i];
      if discrimM < 0.000 then
        discrimM := 0.000;
   Rm[i]:= (-Bm[i]+sqrt(discrimM))/(2*Am[i]);
```

```pascal
          if (Rf[i]<1) or (Rm[i]<1) then degr:= true;
          flag_metal:

end; {each layer}

end;  {procedure}

(*********************************************)

procedure XUdegrad(var Rmatrix,Ffail,e66,e22,
                   ell:realarray3NL;var degrade,first,
                   rupture,NLshear,skip:boolean;
                   var lastE2,Req,Rff,Rss,LastRs,eci,
                   ec6,eff,ecs,Layfail,Layfiberf:
                   realarray1NL;var count:integer;var
                   indxD,indexS,Dmat,Dhigh,Pprof:real);
var
i,l:integer;
e6,e2,e1,eeq,Deq,e2t:realarray1NL;
Ovstr,cw,ck,xpon,DE,fac0,fac1,tt,B,C,p,f,M,eta,
Rbroken,Rftotal,Rmtotal,discrim,err,ers:real;

label
flag_end,Flag_99;

begin

{cw:=0.744;    (* alternate set *)
ck:=3.09;}

cw:=0.952;
ck:=1.17;

DE:=0.15;

for i:= 1 to NL do
begin
  Layfail[i]:=999;
  Layfiberf[i]:=999;
  eeq[i]:=0;
  e2[i]:=0;
  e1[i]:=0;
  e6[i]:=0;
  Rss[i]:=1;
end;

  for i:= 1 to 3*outerlayer do
  begin
    l:=trunc((i+2)/3);
    if e66[i] >  e6[l] then
```

```
                              {find largest shear strain  in each layer}
         e6[1]:= e66[i];
       if Rmatrix[i] < Layfail[1] then
         begin
           Layfail[1]:= Rmatrix[i];
                           {find fail ini for each layer, matrix}
           e2[1]:= e22[i];
         end;
       if Ffail[i] < Layfiberf[1] then
         begin
           Layfiberf[1]:= Ffail[i];
                            {find fail ini each layer, fiber}
           el[1]:= ell[i];
         end;
                       {store crack init based on no degradation}
       if first = true then
       begin
           ec6[1]:= e6[1]*layfail[1];
           eci[1]:= e2[1]*Layfail[1];
           eff[1]:= el[1]*Layfiberf[1];
           ecs[1]:=3*eci[1];              {estimate for saturation}
           lastE2[1]:=1;                  {starter value only}
           lastRs[1]:=1;
         end;
     end;


first:= false;
indxD:= 0;

if degrade=true then               {max itteration exit}
   begin
     count:= count+1;
     if count > 29 then
     begin
         degrade:=false;             {forces a graphical output}
         goto flag_end;
     end;
   end;


for i:= 1 to outerlayer do
begin

   if layfail[i] < 1 then          {matrix is cracked}
   begin
     e2t[i]:=(0.5*Layfail[i]+0.5*lastE2[i]);    {test value}
       lastE2[i]:=e2t[i];               {store for next iteration}
       err:=abs(Layfail[i]-lastE2[i]);
       if err < 0.001 then               {convergence criteria}
         indxD:=indxD+0
       else
```

```
        indxD:=indxD+err;
    fac0:=(9-sqr(1/e2t[i]))/(sqr(1/e2t[i])-1);
    if fac0<0 then        {if strained past saturation level}
        fac0:= 0;
    eeq[i]:=(1/3)*sqrt(fac0);
    xpon:=-pow((eeq[i]/cw),ck);

    if xpon < -15 then
        Deq[i]:= 3E-7
    else
        Deq[i]:=exp(xpon);

    facl:=(ln(DE))/(2*Deq[i]);

    Req[i]:=(1-((1/facl)*tanh(facl)));
    degrade:= true;                          {matrix intact}
    end                                      {update estimate}
    else
        Req[i]:=1;

end;

Rbroken:=1-((2/ln(DE))*tanh(0.5*ln(DE)));
for i:= 1 to outerlayer do
                        {fiber is fractured via christensen}
begin
    if layfiberf[i] < 1 then
        begin
        Rff[i]:=Rbroken;
        Req[i]:=Rbroken;
                {matrix must also have failed when fiber goes}
        degrade:=true;
        end
    else
        Rff[i]:= 1;
end;

indexS:= 0;

if NLshear = true then
begin
    for i:= 1 to outerlayer do          {nonlinear shear correction}
        begin
        if layfail[i] > 1 then      {use only before damage starts}
            begin
            Rss[i]:=0.5*(lastRs[i]+sqrt(1+sqr((1000*strg[i].GL*
                e6[i])/strg[i].ss)));
            ers:= abs((Rss[i]-lastRs[i])/Rss[i];
            if (ers > 0.01)   then
                begin
```

```
                 indexS:= indexS+ers;
                 degrade:=true;
              end
              else
                 indexS:=indexS+0;
              lastRs[i]:=Rss[i];                {store for next iteration}
              end
          else                    {shear correction when damage has begun}
              begin

Rss[i]:=sqrt(1+sqr((1000*strg[i].GL*ec6[i])/strg[i].ss));

{Rss[i]:=0.5*(lastRs[i]+sqrt(1+sqr((1000*strg[i].GL*ec6[i])/
          strg[i].ss)));}
              ers:= abs((Rss[i]-lastRs[i])/Rss[i]);
              if (ers > 0.01)  then
              begin
                 indexS:= indexS+ers;
                 degrade:=true;
              end
              else
                 indexS:=indexS+0;
              lastRs[i]:=Rss[i];                {store for next iteration}
           end; {if layfail}
       end;  {i loop}
end; {if nonlinear shear}

If NLshear = false then
 ers:= 0.000;

RFtotal:=0;
RmTotal:=0;
for i:= 1 to outerlayer do
begin
   RFtotal:= Rff[i]+RFtotal;
   Rmtotal:= Req[i]+Rmtotal;
end;

if (RFtotal=outerlayer)and(Rmtotal=outerlayer)and(indexS=0)
                                                    then
begin
   degrade:= false;                    {system is completely linear}
   err:=0;
   goto flag_end;
end;

discrim:= RFtotal/Rbroken;                     {all fibers broken}
if (abs(discrim-outerlayer))<0.01 then
begin
   rupture:= true;
```

```
        goto flag_end;
    end;

    if (indxD = 0) and (degrade = true) and (indexS = 0) then
    begin
        degrade:= false;
        {normal exit when degraded matrix & shear = converged}
        goto flag_end;
    end;

flag_end:

    for i:= 1 to 3*outerlayer do
    begin
        l:=trunc((i+2)/3);
        if Req[l] < 1.0 then
        Rmatrix[i]:= Req[l];
        If Rff[l] < 1.0 then
        Ffail[i]:= Rff[l];
    end;

    Dmat:=9999;
    if Pprof < insidepress then
    begin
        for i:= 1 to outerlayer do
        begin
        if (Layfail[i] < 1) or (Layfiberf[i] < 1) then
                                {a damaged layer exists}
        begin
            if Dhigh = 999 then
                {case when first iteration is already in damage}
            begin
                Dmat:= 999;
                goto flag_99;
            end
            else
            begin
                Skip:=true;
                {otherwise exit and use Dhigh from previous}
                goto flag_99;
            end;
        end;
    end; {if Pprof}

    if skip = false then
        {won't execute if previous iteration had matrix failure}
    begin
        for i:= 1 to outerlayer do
        begin
```

712

```
if Layfail[i] < Dmat then          {find lowest safety factor}
  Dmat:= Layfail[i];
if LayfiberF[i] < Dmat  then
  Dmat:= Layfiberf[i];

Dhigh:= Dmat*insidepress;          {stores value for next round}
end; { i loop}
end;  {if skip}

flag_99:
end;


(*************************************************)

Procedure stiffness;

var
fact,E1,E2,E3,V12,V13,V23,V21,V31,V32,D,
C11,C22,C33,C12,C13,C23:real;

begin

fact:=0.25;
E1:=136.47;
E2:=11.84*0.25;
E3:=8.933;
V21:=0.021274*0.63;
V13:=0.325;
V23:=0.479*0.51;
V12:=V21*(E1/E2);
V31:=V13*(E3/E1);
V32:=V23*(E3/E2);

D:=(1-(V12*V21)-(V23*V32)-(V31*V13)-
   (2*V21*V32*V13))/(E1*E2*E3);
C11:=(1-(V23*V32))/(E2*E3*D);
C22:=(1-(V13*V31))/(E1*E3*D);
C33:=(1-(V12*V21))/(E1*E2*D);
C12:=(V21+(V31*V23))/(E2*E3*D);
C13:=(V31+(V21*V32))/(E2*E3*D);
C23:=(V32+(V12*V31))/(E1*E3*D);

end;


(********************************************)

procedure stiffinv;

var
```

```
factf,fact12,fact23,C11,C22,C33,C12,C13,C21,C23,C31,C32,E11,
E22,E33,V12,V21,V13,V31,V23,V32:real;

begin
factf:=0.50;
fact12:=0.50;
fact23:=0.50;
C11:=9.350*0.25*1.1;
C22:=9.35*0.250;
C33:=9.35;
C12:=3.88*fact12;
C13:=3.88*factf;
C21:=3.88*fact12;
C23:=4.03*fact23;
C31:=3.88*factf;
C32:=4.03*fact23;

E11:=C11+((C12*(C23*C31-C21*C33))+(C13*(C32*C21-C31*C22)))/
        (C22*C33-C23*C32);
E22:=C22+((C21*(C13*C32-C12*C33))+(C23*(C13*C31-C32*C11)))/
        (C33*C11-C31*C13);
E33:=C33+((C31*(C12*C23-C13*C22))+(C32*(C21*C13-C23*C11)))/
        (C11*C22-C12*C21);
V12:=(C21*C33-C23*C31)/(C22*C33-C32*C23);
V21:=(C12*C33-C13*C32)/(C11*C33-C13*C31);
V13:=(C31*C22-C32*C21)/(C22*C33-C23*C32);
V31:=(C13*C22-C12*C23)/(C11*C22-C12*C21);
V23:=(C32*C11-C13*C31)/(C33*C11-C31*C13);
V32:=(C23*C11-C21*C13)/(C22*C11-C21*C12);

end;

(***********************************************)

procedure Thermo;

var
R,T,v,B0,A0,C0,a,alpha,c,gamma,b,T1,T2,f1,f2,f3,
T3,T4,T5,P1,P2,Psi1,Psi2,Psi3,aa,bb,
PC,TC,AAA,BBB,e,ATM:real;

begin

{methane- Bennedit-Webb-Rubin}

R:=0.08314;
T:=330;
v:= 0.002345*16.043*1.545;
a:= 0.050;
A0:= 1.8791;
```

```
b:= 0.003380;
B0:= 0.0426;
c:= 2.578E3;
C0:=2.286E4;
alpha:=1.244E-4;
gamma:=0.006;

T1:= R*T/v;
T2:= (B0*R*T-A0-C0/sqr(T))*(1/sqr(v));
T3:= (b*R*T-a)/pow(v,3);
T4:= (a*alpha)/pow(v,6);
T5:= (c/(pow(v,3)*sqr(T)))*(1+gamma/sqr(v))*
     exp(-gamma/sqr(v));
P1:= T1+T2+T3+T4+T5;
psi1:=P1*14.5034;

{hydrogen Redlich Kwong}

PC:=13.0; {bar}
TC:=33.3; {K}
v:=0.0141*2.018*1.04;

aa:=0.4275*Sqr(R)*Pow(TC,2.5)/PC;
bb:=0.0667*R*TC/PC;

P2:= ((R*T)/(v-bb))-(aa/(sqrt(T)*v*(v+bb)));
Psi2:=P2*14.5034;

{hydrogen Beattie-Bridgeman eq using Deming & Shupe}

R:=0.08206;
AAA:=0.12404*(1-0.05618/v);
BBB:=0.01750*(1+0.01968/v);
e:=2.0E-4/(v*pow(T,3));
f1:=(R*T*(1-e)/sqr(v));
f2:=(v+BBB);
f3:=-AAA/sqr(v);
ATM:= f1*f2+f3;
psi3:=ATM*14.696;

end;

(********************************)

end.
```

```
unit GraEdit;
{$O+,F+}

interface

(****************************************************)

uses glob_var,graph,crt,ves_util,menus,plotprop,
     compmath,failure,DOS;

procedure GEdit(var topic,param,sel_mat:integer;var
                exit,update,full,nlshear:boolean;
                var Mred,Fred,Sred,MS,FS:realarray1NL;var
                Firstdam,proof:real;var filenum:integer;
                var sigr,sigf,sigz,sig1,sig2,sig3,sig6,
                ef,ez,e1,e2,e3,e6:realarray3NL;
                var rupt,rset:boolean);

procedure GraphEditStr(var full,readkeybd,NLshear:boolean);

procedure filedata(var Mred,Fred,Sred,MS,FS:
                realarray1NL;firstdam,proof:real;
                var nfileno:integer;var
                sigr,sigf,sigz,sig1,sig2,sig3,sig6,ef,ez,
                e1,e2,e3,e6:realarray3NL;var
                rupt,print,full,nlshear:boolean);

(****************************************************)

implementation

(****************************************************)


procedure GraphEditStr(var full,readkeybd,NLshear:boolean);
     {editor for discrete wall Vessel}

var
sigf,sigr,sigz,sig1,sig2,sig3,sig6,Msaf,Fsaf,ef,ez,e1,e2,e3,
e6,e21,e11:realarray3NL;
FilePress:RealarrayNL;
update,exit,sw,degrd,burst,
once,abrt,first,rupt,skip,rset:boolean;
axialcon,x_max,x_min,y_max,y_min,error,esh,
Pprof,Mdam,Dhi:real;
Newmat,cnt,err,ers,Ptop,Pin,title2:string;
layerno,angl,topic,param,sel_mat,i,count,Tlen,
filenumber:integer;
E2last,redu,Rfib,ReSS,LstRs,ECRI,EC6,ECSAT,EFF,
MSL,FSL:realarray1NL;
```

```
      mask:mask_names;

      label
      flag_readf,flag_end,flag_burst,flag_reset;

      begin
      rset:=false;
      flag_reset:
      zerographdata;
      skip:=false;
      abrt:= false;
      exit:=false;
      update:=false;
      degrd:=false;
      first:=true;
      once:= false;
      rupt:=false;
      topic:=1;
      param:=0;
      Pprof:=0;
      sel_mat:=0;
      count:=0;
      filenumber:=0;
      Mdam:=999;
      Dhi:=999;

      if full = true then
         title2:='Full Equation Set'
      else
         title2:='Partial Equation Set';
      if NLshear = true then
         title2:= 'NL shear / Full Equations';

      for i:= 1 to NL do
      begin
         Rfib[i]:=1;   {initaliize}
         Redu[i]:=1;
         ReSS[i]:=1;
         LstRs[i]:=1;
      end;

      flag_readf:
      mask[1]:='*.VES';
      mask[2]:='';
      readvesf(Newmat,mask,redu,Rfib,ReSS,outerlayer,layerno,angl,
      readkeybd,update,degrd,abrt);
      if abrt = true then goto flag_end;
      Laminateprop(outerlayer);
      if graphstate = false then
          initgraphdriver;
```

```
compute_full(filepress,axialCon,Full);
                        {passes back interface pressures}

compstress(filepress,axialCon,sigf,sigr,sigz);

{Tsai_Wu(axialcon,sigr,sigf,sigz,Msaf,Fsaf);}

{Feng(axialCon,sigr,sigf,sigz,Msaf,Fsaf);}

Christensen(axialCon,sigr,sigf,sigz,sig1,sig2,sig3,sig6,
            Msaf,Fsaf,ef,ez,e1,e2,e3,e6,redu,
            Rfib,degrd,first);
if ((Pprof <= insidepress) and (rupt = false)) then
  XUdegrad(Msaf,Fsaf,e6,e2,e1,degrd,first,rupt,NLshear,skip,
            E2last,Redu,Rfib,ReSS,LstRs,ECRI,EC6,EFF,ECSAT,
            MSL,FSL,count,error,esh,Mdam,Dhi,Pprof);
cleardevice;
setcolor(lightgray);
outtextXY(0,10,'W-Scale:'+scalef);
str(count,cnt);
str(error:4:3,err);
str(esh:4:3,ers);
setfillstyle(solidfill,red);
setcolor(white);
bar(136,0,137+(8*length(cnt)),7);
outtextXY(106,0,'itt:'+cnt);
bar(136,10,138+(8*length(err)),17);
outtextXY(106,10,'err:'+err);
If Nlshear = true then
  begin
  bar(184,0,186+(8*length(ers)),7);
  outtextXY(154,0,'ers:'+ers);
  end;

plotLstress(sigr,sigf,sigz,Msaf,Fsaf,x_max,x_min,
            y_max,y_min,Dhi,rupt,Redu,Rfib);

plotoutline('Radius (mm)','Stress MPa','Discrete
            Layer Stresses',Title2,5,5,x_min,x_max,
            y_min,y_max);

if ((rupt = true) and (once = false)) then
  begin
    readkeybd:= false;
    once:= true;
          {executes only once on rupture to update stresses}
    count:= count+1;
    goto flag_readf;
  end;
```

718

```
if (degrd=true)and(Pprof<insidepress)and(once = false) then
                                  {iteration for rising press}
   begin
     readkeybd:= false;
     goto flag_readf;
   end;

if (insidepress > Pprof) and (rupt = false) then
   Pprof:= insidepress;   {record peak}
str(Pprof:3:1,Ptop);
str(insidepress:3:1,Pin);
setcolor(cyan);
outtextxy(480,10,'Proof:');
if Pprof<=Dhi then
   setcolor(white)
else
   setcolor(yellow);
outtextxy(528,10,Ptop);
setcolor(white);
if rupt = true then
begin
   setcolor(white);
   setfillstyle(solidfill,blue);
   Tlen:=8*(length(Ptop)+Length(Pin));
   bar(309-round((88+Tlen)/2),10,309+round((88+Tlen)/2),18);
   outtextxy(309-round((88+Tlen)/2),11,Ptop+' <Burst< '+Pin);
end;
GEdit(topic,param,sel_mat,exit,update,full,nlshear,
       redu,Rfib,ReSS,MSL,FSL,Dhi,Pprof,filenumber,
       sigr,sigf,sigz,sig1,sig2,sig3,sig6,ef,
       ez,e1,e2,e3,e6,rupt,rset);
count:=0;
if exit = true then goto flag_end;
if rset = true then
begin
   readkeybd:=false;
   degrd:=false;
   rset:=false;
             {switch back to default condition for next run}
   goto flag_reset;
end;
readkeybd:=false;
degrd:= true;
goto flag_readf;

flag_end:
end;

(*******************************************************)
```

719

```pascal
procedure formfeed(var print:boolean;var count:integer;
increment:integer);
var
ff:text;

begin

count:= count+increment;
   if (count >= 60) and (print = true) then
     begin
       assign(ff,'LPT1');
       rewrite(ff);
       write(ff,#12);    {form feed}
       close(ff);
       count:= increment;
     end;
end;


(******************************************************)

procedure filedata(var Mred,Fred,Sred,MS,FS:
                     realarray1NL;firstdam,proof:real;
                     var nfileno:integer;var
                     sigr,sigf,sigz,sig1,sig2,sig3,sig6,ef,ez,
                     e1,e2,e3,e6:realarray3NL;var
                     rupt,print,full,nlshear:boolean);

var
exten,newfile,pres,PPr,fd,thic,id,title:string;
F:text;
count,i:integer;

label
flag_end;

begin
if full=true then
   title:='Full Equations'
else
   title:='Partial Equations';
if nlshear = true then
   title:='NL Shear / Full equations';

count:= 0;
newfile:= currentfile;
Delete(newfile,length(newfile)-3,4);       {remove file ext}
str(nfileno,exten);
{$I-}
if print = true then
   assign(F,'LPT1')
```

```
      else
        begin
          assign(F,newfile+'.D'+exten);
          setfillstyle(solidfill,red);
          setcolor(white);
          bar(0,0,96,8);
          outtextxy(0,0,newfile+'.D'+exten);
          beep(1600,1600);
          delay(15000);
          setfillstyle(solidfill,black);
          bar(0,0,96,8);
          textcolor(lightgray);
          outtextxy(0,0,currentfile);
        end;
  rewrite(F);

  writeln(F,'                    Super Pressure - Vessel Designer');
  if IOresult <> 0 then
      begin
          setfillstyle(solidfill,red);
          setcolor(white);
          bar(0,0,96,8);
          outtextxy(0,0,'LPT1: Error!');
          beep(600,1600);
          delay(15000);
          setfillstyle(solidfill,black);
          bar(0,0,96,8);
          textcolor(lightgray);
          outtextxy(0,0,currentfile);
          goto flag_end;
      end;
  {$I+}
  writeln(F);
  Writeln(F);
  writeln(F,'Vessel Filename: '+currentfile);
  writeln(F,'Calculation Method: '+title);
  writeln(F,'Current Pressure (MPa): ',insidepress:3:1);
  writeln(F,'Proof Pressure (MPa): ',Proof:3:1);
  writeln(F,'First Damage (MPa): ',firstdam:3:1);
  writeln(F,'Rupture: ',rupt);
  writeln(F,'Wall Thickness (mm): ',Wallthick:3:1);
  writeln(F,'Inside Diameter (mm): ',insidedia:3:1);
  writeln(F,'Wall Scaling Factor: ',(wallthick/Ttotal):4:3);
  writeln(F);
  formfeed(print,count,17+outerlayer);
  writeln(F,'Lay  ','Material  ','Thick  ','Angle  ',' Fiber
      ','Matrix  ','Fiber   ','Matrix ','Fiber    ','Shear');
  writeln(F,'No.  ','  Name     ',' (mm)   ','(+/-)   ','Percent
      ','Safety  ','Safety  ','Degrad. ','Degrad. ','Red.');
  writeln(F);
```

```
for i:= 1 to outerlayer do
begin
  write(F,i:2,'    ');
  write(F,graphlabels[i].matname:8,'   ');
  write(F,graphlabels[i].thickness:3,'     ');
  write(F,graphlabels[i].angle:4,'     ');
  write(F,graphlabels[i].fpercent:4,'   ');
  if Fred[i] < 1.0 then
    write(F,Fred[i]:6:3,'  '){if fiber is broken, so is mtx}
  else
    write(F,MS[i]:6:3,'  ');
  write(F,FS[i]:6:3,'  ');
  write(F,Mred[i]:6:3,'  ');
  write(F,Fred[i]:6:3,'  ');
  writeln(F,(1/Sred[i]):6:3);
end;
formfeed(print,count,4+outerlayer);
writeln(F);
writeln(F,'Layer         Sigma (r)                  Sigma
        ('+#233+')                 Sigma (z)');
writeln(F,'no.  inside   mid.  outer    inside    mid.  outer
        inside    mid.   outer');
writeln(F);
for i:= 1 to outerlayer do
begin
  write(F,i,'    ');
  write(F,sigr[3*(i-1)+1]:6:1,'  ');
  write(F,sigr[3*(i-1)+2]:6:1,'  ');
  write(F,sigr[3*(i-1)+3]:6:1,'   ');
  write(F,sigf[3*(i-1)+1]:6:1,'  ');
  write(F,sigf[3*(i-1)+2]:6:1,'  ');
  write(F,sigf[3*(i-1)+3]:6:1,'   ');
  write(F,sigz[3*(i-1)+1]:6:1,'  ');
  write(F,sigz[3*(i-1)+2]:6:1,'  ');
  writeln(F,sigz[3*(i-1)+3]:6:1);
end;
formfeed(print,count,4+outerlayer);
writeln(F,'');
writeln(F,'Layer      Epsilon (r) %              Epsilon
        ('+#233+') %              Epsilon (z) %');
writeln(F,'no.  inside   mid.  outer    inside    mid.  outer
        inside    mid.   outer');
writeln(F);
for i:= 1 to outerlayer do
begin
  write(F,i,'    ');
  write(F,100*e3[3*(i-1)+1]:6:3,'   ');
  write(F,100*e3[3*(i-1)+2]:6:3,'   ');
  write(F,100*e3[3*(i-1)+3]:6:3,'    ');
  write(F,100*ef[3*(i-1)+1]:6:3,'   ');
```

722

```
      write(F,100*ef[3*(i-1)+2]:6:3,'   ');
      write(F,100*ef[3*(i-1)+3]:6:3,'    ');
      write(F,100*ez[3*(i-1)+1]:6:3,'   ');
      write(F,100*ez[3*(i-1)+2]:6:3,'   ');
      writeln(F,100*ez[3*(i-1)+3]:6:3);
   end;
   formfeed(print,count,4+outerlayer);
   writeln(F,'');
   writeln(F,'Layer                Sigma (1)                     Sigma
            (2)');
   writeln(F,' no.      inside    mid.    outer     inside    mid.
            outer');
   writeln(F);
   for i:= 1 to outerlayer do
   begin
      write(F,i:2,'          ');
      write(F,sig1[3*(i-1)+1]:6:1,'   ');
      write(F,sig1[3*(i-1)+2]:6:1,'   ');
      write(F,sig1[3*(i-1)+3]:6:1,'    ');
      write(F,sig2[3*(i-1)+1]:6:1,'   ');
      write(F,sig2[3*(i-1)+2]:6:1,'   ');
      write(F,sig2[3*(i-1)+3]:6:1,'    ');
      writeln(F);
   end;
   formfeed(print,count,4+outerlayer);
   writeln(F,'');
   writeln(F,'Layer                Sigma (3)                     Sigma
            (6)');
   writeln(F,' no.      inside    mid.    outer     inside    mid.
            outer');
   writeln(F);
   for i:= 1 to outerlayer do
   begin
      write(F,i:2,'          ');
      write(F,sig3[3*(i-1)+1]:6:1,'   ');
      write(F,sig3[3*(i-1)+2]:6:1,'   ');
      write(F,sig3[3*(i-1)+3]:6:1,'    ');
      write(F,sig6[3*(i-1)+1]:6:1,'   ');
      write(F,sig6[3*(i-1)+2]:6:1,'   ');
      write(F,sig6[3*(i-1)+3]:6:1,'    ');
      writeln(F);
   end;
   formfeed(print,count,4+outerlayer);
   writeln(F,'');
   writeln(F,'');
   writeln(F,'Layer                Epsilon (1) %                 Epsilon (2)
            %');
   writeln(F,' no.      inside    mid.    outer     inside    mid.
            outer');
   writeln(F);
```

723

```
for i:= 1 to outerlayer do
begin
   write(F,i:2,'         ');
   write(F,100*e1[3*(i-1)+1]:6:3,'  ');
   write(F,100*e1[3*(i-1)+2]:6:3,'  ');
   write(F,100*e1[3*(i-1)+3]:6:3,'   ');
   write(F,100*e2[3*(i-1)+1]:6:3,'  ');
   write(F,100*e2[3*(i-1)+2]:6:3,'  ');
   write(F,100*e2[3*(i-1)+3]:6:3,'   ');
   writeln(F);
end;
formfeed(print,count,4+outerlayer);
writeln(f);
writeln(F,'Layer          Epsilon (3) %          Epsilon (6)
        %');
writeln(F,' no.      inside    mid.    outer    inside    mid.
        outer');
writeln(F);
for i:= 1 to outerlayer do
begin
   write(F,i:2,'         ');
   write(F,100*e3[3*(i-1)+1]:6:3,'  ');
   write(F,100*e3[3*(i-1)+2]:6:3,'  ');
   write(F,100*e3[3*(i-1)+3]:6:3,'   ');
   write(F,100*e6[3*(i-1)+1]:6:3,'  ');
   write(F,100*e6[3*(i-1)+2]:6:3,'  ');
   write(F,100*e6[3*(i-1)+3]:6:3,'   ');
   writeln(F);
end;
writeln(F,'');
for i:= 1 to outerlayer do
begin
   formfeed(print,count,9);
   writeln(F,'Local Stiffness Matrix [Cij] (MPa), Layer:
        ',i);
   writeln(F,'');
   writeln(F,Lstif[i,1,1]:6:2,'  ',Lstif[i,1,2]:6:2,'
        ',Lstif[i,1,3]:6:2);
   writeln(F,Lstif[i,2,1]:6:2,'  ',Lstif[i,2,2]:6:2,'
        ',Lstif[i,2,3]:6:2);
   writeln(F,Lstif[i,3,1]:6:2,'  ',Lstif[i,3,2]:6:2,'
        ',Lstif[i,3,3]:6:2);
   writeln(F,'                          ',Lstif[i,4,4]:6:2);
   writeln(F,'
        ',Lstif[i,5,5]:6:2);
   writeln(F,'
        ',Lstif[i,6,6]:6:2);
   writeln(F,'');
end;
if print = true then
```

724

```
      writeln(f,#12);        {form feed}
close(F);
flag_end:
end;


(*****************************************************)

procedure GEdit(var topic,param,sel_mat:integer;var
                exit,update,full,nlshear:boolean;
                var Mred,Fred,Sred,MS,FS:realarraylNL;var
                Firstdam,proof:real;var filenum:integer;
                var sigr,sigf,sigz,sigl,sig2,sig3,
                sig6,ef,ez,el,e2,e3,e6:realarray3NL;
                var rupt,rset:boolean);

var
Keyknown,specialkey,OK,print:boolean;
num,layerno,j,x0,x1,spt,errcd,i:integer;
matchoice:dir_files;
tpic,newangle,newperct,newthick,description,
newfile,oldfile,oldangle,oldthick:string;
pick:char;
f:text;
n,thick:real;
rt:realarrayNL;

label
flag_end,flag_DNar,flag_UPar,flag_left,flag_right,flag_save,
flag_read,flag_INS,flag_PgUp,flag_PgDn,flag_endkey,flag_home
key,
flag_return,flag_restart,flag_del,flag_AltI,flag_tab;

begin                        {graphics editor for discrete Vessel}
DirList('*.mat',matchoice,num);

Keyknown:=false;

outtextxy(580,39,'Layers');
flag_restart:
for i:= 1 to outerlayer do
begin
  val(graphlabels[i].thickness,n,errcd);
  str(n:3:1,graphlabels[i].thickness);
  setcolor(cyan);
  str(i,tpic);
  if odd(i) then j:=10 else j:=0;
  Outtextxy(569-4*length(tpic),24+i*28,tpic+':
             '+char(241)+graphlabels[i].angle+char(248));
  Outtextxy(616,24+i*28,copy(graphlabels[i].fpercent,
             1,2)+char(37));
```

```
   Outtextxy(576,34+i*28,graphlabels[i].matname);
   setcolor(white);
   Outtextxy(569-4*length(tpic),24+i*28,tpic+':');
   setcolor(cyan);
   X1:= 59+round(500*(r[i]-r[0])/(r[outerlayer]-r[0]));
   X0:= 59+round(500*(r[i-1]-r[0])/(r[outerlayer]-r[0]));
   Outtextxy(round((x1+x0)/2)-10+8*length(tpic),
             30-j,graphlabels[i].thickness);
   Setcolor(white);
   Outtextxy(round((x1+x0)/2)-18,30-j,tpic+':');
   Line(x0,40,x0,46);
end;

setfillstyle(solidfill,black);
bar(600,0,639,7);
setcolor(white);
setfillstyle(solidfill,blue);
str(InsidePress:1:1,Ipress);
bar(600,0,600+(8*length(Ipress)),7);
outtextxy(600,0,Ipress);

str(topic,tpic);
if param = 0 then
begin
   setfillstyle(solidfill,blue);
   str(topic,tpic);
   bar(569-4*length(tpic),24+topic*28,569-4*
       length(tpic)+8*length(tpic),32+topic*28);
   outtextxy(569-4*length(tpic),24+topic*28,tpic);
end;
if param = 1 then
begin
   setfillstyle(solidfill,blue);
   bar(585+4*length(tpic),24+topic*28,585+4*length(tpic)+8*
       length(graphlabels[topic].angle),32+topic*28);
   outtextxy(585+4*length(tpic),24+topic*28,
             graphlabels[topic].angle);
end;
if param = 2 then
begin
   setfillstyle(solidfill,blue);
   bar(616,24+topic*28,631,32+topic*28);
   outtextxy(616,24+topic*28,
             copy(graphlabels[topic].fpercent,1,2));
end;
if param = 3 then
begin
   setfillstyle(solidfill,blue);
   bar(576,34+topic*28,639,42+topic*28);
   outtextxy(576,34+topic*28,graphlabels[topic].matname);
```

```
end;
if param = 4 then
begin
  x0:= 59+round(500*(r[topic-1]-r[0])/(r[outerlayer]-r[0]));
  x1:= 59+round(500*(r[topic]-r[0])/(r[outerlayer]-r[0]));
  spt:=round((x1+x0)/2);
  setfillstyle(solidfill,blue);
  if odd(topic) then j:=10 else j:=0;
  bar(spt-10+8*length(tpic),30-j,spt-12+8*(length
      (graphlabels[topic].thickness)+length(tpic)),37-j);
  outtextxy(spt-10+8*length(tpic),
            30-j,graphlabels[topic].thickness);
end;


flag_read:

repeat
if  not keyknown then Inkey(specialkey,ch,'s','o');
case key of

AltX:
  begin
    goto flag_end;
  end;

DownArrow:
  begin
  flag_DNar:

  if param = 0 then
  begin
    setfillstyle(solidfill,black);
    str(topic,tpic);
    bar(569-4*length(tpic),24+topic*28,
        569-4*length(tpic)+8*length(tpic),32+topic*28);
    setcolor(white);
    outtextxy(569-4*length(tpic),24+topic*28,tpic);
    topic:= topic+1;
    if topic > outerlayer then topic:=outerlayer;
    setfillstyle(solidfill,blue);
    str(topic,tpic);
    bar(569-4*length(tpic),24+topic*28,
        569-4*length(tpic)+8*length(tpic),32+topic*28);
    setcolor(white);
    outtextxy(569-4*length(tpic),24+topic*28,tpic);
  end;

  if param = 1 then
  begin
    val(graphlabels[topic].angle,i,errcd);
```

```
      str(i,oldangle);
      i:= i-1;
      if i < 1 then i:=1;
      str(i,newangle);
      graphlabels[topic].angle:=newangle;
      setfillstyle(solidfill,black);
      bar(585+4*length(tpic),24+topic*28,585+4*length(tpic)+
          8*length(oldangle),32+topic*28);
      setfillstyle(solidfill,blue);
      bar(585+4*length(tpic),24+topic*28,585+4*length(tpic)+
          8*length(newangle),32+topic*28);
      setcolor(white);
      outtextxy(585+4*length(tpic),24+topic*28,newangle);
      update:= true;
  end;

  if param = 2 then
  begin

    val(copy(graphlabels[topic].fpercent,1,2),i,errcd);
    i:= i-1;
    if i < 1 then i:=1;
    str(i,newperct);
    graphlabels[topic].fpercent:=newperct;
    setfillstyle(solidfill,blue);
    bar(616,24+topic*28,631,32+topic*28);
    setcolor(white);
    outtextxy(616,24+topic*28,copy(newperct,1,2));
    update:= true;
  end;

  if param = 3 then
  begin
    sel_mat:= sel_mat-1;
    if sel_mat <= 1 then sel_mat:= 1;
    graphlabels[topic].matname:=copy(matchoice[sel_mat],1,
                               pos('.',matchoice[sel_mat])-1);
    setfillstyle(solidfill,blue);
    bar(576,34+topic*28,639,42+topic*28);
    setcolor(white);
    outtextxy(576,34+topic*28,graphlabels[topic].matname);
    update:= true;
  end;

  if param = 4 then
  begin
    val(graphlabels[topic].thickness,n,errcd);
    oldthick:=graphlabels[topic].thickness;
    n:= n-0.1;
    if n <= 0.1 then n:= 0.1;
```

```
          str(n:3:1,newthick);
          graphlabels[topic].thickness:= newthick;
          x0:= 59+round(500*(r[topic-1]-r[0])/
               (r[outerlayer]-r[0]));
          x1:= 59+round(500*(r[topic]-r[0])/(r[outerlayer]-r[0]));
          spt:=round((x1+x0)/2);
          if odd(topic) then j:=10 else j:=0;
          setfillstyle(solidfill,black);
          bar(spt-10+8*length(tpic),30-j,
               spt-12+8*(length(oldthick)+length(tpic)),37-j);
          setfillstyle(solidfill,blue);
          bar(spt-10+8*length(tpic),30-j,
               spt-12+8*(length(newthick)+length(tpic)),37-j);
          setcolor(white);
          outtextxy(spt-10+8*length(tpic),30-j,newthick);
          update:= true;
        end;

      repeat
         Inkey(specialkey,ch,'s','o');

         if key = DownArrow then goto flag_DNar;
         if key = UpArrow then goto flag_UPar;
         if key = leftarrow then goto flag_left;
         if key = rightarrow then goto flag_right;
         if key.= AltS then goto flag_save;
         if key = PgUp then goto flag_PgUp;
         if key = PgDn then goto flag_PgDn;
         if key = homekey then goto flag_homekey;
         if key = endkey then goto flag_endkey;
         if key = insertkey then goto flag_ins;
         if key = deletekey then goto flag_del;
         if key = AltI then goto flag_AltI;
         if key = TAB then goto flag_tab;

         if key = carriagereturn then
            goto flag_return;

      until (key = esc) or (key = AltX);
      goto flag_end;
   end; {downarrow}

UpArrow:
   begin
   flag_UPar:

   if param = 0 then
   begin
      setfillstyle(solidfill,black);
      str(topic,tpic);
```

```
        bar(569-4*length(tpic),24+topic*28,
            569-4*length(tpic)+8*length(tpic),32+topic*28);
        setcolor(white);
        outtextxy(569-4*length(tpic),24+topic*28,tpic);
        topic:= topic-1;                        {layer increment}
        if topic < 1 then topic:= 1;
        setfillstyle(solidfill,blue);
        str(topic,tpic);
        bar(569-4*length(tpic),24+topic*28,
            569-4*length(tpic)+8*length(tpic),32+topic*28);
        setcolor(white);
        outtextxy(569-4*length(tpic),24+topic*28,tpic);
    end;

    if param = 1 then
    begin
        val(graphlabels[topic].angle,i,errcd);
        str(i,oldangle);
        i:= i+1;                                {angle increment}
        if i > 90 then i:=90;
        str(i,newangle);
        graphlabels[topic].angle:=newangle;
        setfillstyle(solidfill,black);
        bar(585+4*length(tpic),24+topic*28,585+4*length(tpic)+
            8*length(oldangle),32+topic*28);
        setfillstyle(solidfill,blue);
        bar(585+4*length(tpic),24+topic*28,585+4*length(tpic)+
            8*length(newangle),32+topic*28);
        setcolor(white);
        outtextxy(585+4*length(tpic),24+topic*28,newangle);
        update:= true;
    end;

    if param = 2 then
    begin
        val(copy(graphlabels[topic].fpercent,1,2),i,errcd);
        i:= i+1;
        if i > 78 then i:= 78;
        str(i,newperct);
        graphlabels[topic].fpercent:=newperct;
        setfillstyle(solidfill,blue);
        bar(616,24+topic*28,631,32+topic*28);
        setcolor(white);
        outtextxy(616,24+topic*28,copy(newperct,1,2));
        update:= true;
    end;

    if param = 3 then
    begin
        sel_mat:= sel_mat+1;
```

730

```
    if sel_mat >= num then sel_mat:= num;
    graphlabels[topic].matname:=copy(matchoice[sel_mat],
                         1,pos('.',matchoice[sel_mat])-1);
    setfillstyle(solidfill,blue);
    bar(576,34+topic*28,639,42+topic*28);
    setcolor(white);
    outtextxy(576,34+topic*28,graphlabels[topic].matname);
    update:= true;
  end;

  if param = 4 then
  begin
    val(graphlabels[topic].thickness,n,errcd);
    n:= n+0.1;
    str(n:3:1,newthick);
    graphlabels[topic].thickness:= newthick;
    x0:= 59+round(500*(r[topic-1]-r[0])/
         (r[outerlayer]-r[0]));
    x1:= 59+round(500*(r[topic]-r[0])/(r[outerlayer]-r[0]));
    spt:=round((x1+x0)/2);
    setfillstyle(solidfill,blue);
    if odd(topic) then j:=10 else j:=0;
    bar(spt-10+8*length(tpic),30-j,
        spt-12+8*(length(newthick)+length(tpic)),37-j);
    setcolor(white);
    outtextxy(spt-10+8*length(tpic),30-j,newthick);
    update:= true;
  end;

  repeat
    Inkey(specialkey,ch,'s','o');

    if key = DownArrow then goto flag_DNar;
    if key = UpArrow then goto flag_UPar;
    if key = leftarrow then goto flag_left;
    if key = rightarrow then goto flag_right;
    if key = AltS then goto flag_save;
    if key = PgUp then goto flag_PgUp;
    if key = PgDn then goto flag_PgDn;
    if key = homekey then goto flag_homekey;
    if key = endkey then goto flag_endkey;
    if key = insertkey then goto flag_ins;
    if key = deletekey then goto flag_del;
    if key = AltI then goto flag_altI;
    if key = TAB then goto flag_tab;

    if key = carriagereturn then
      begin
        goto flag_return;
      end;
```

```
       until (key = esc) or (key=AltX);
       goto flag_end;
end; {uparrow}

LeftArrow:
   begin
   flag_left:

   if param = 0 then
   begin
      setfillstyle(solidfill,black);
      str(topic,tpic);
      bar(569-4*length(tpic),24+topic*28,
          569-4*length(tpic)+8*length(tpic),32+topic*28);
      outtextxy(569-4*length(tpic),24+topic*28,tpic);
   end;
   if param = 1 then
   begin
      setfillstyle(solidfill,black);
      str(topic,tpic);
      bar(585+4*length(tpic),24+topic*28,585+4*length(tpic)+
          8*length(graphlabels[topic].angle),32+topic*28);
      setcolor(cyan);
      outtextxy(585+4*length(tpic),24+topic*28,
                graphlabels[topic].angle);
   end;
   if param = 2 then
   begin
      setfillstyle(solidfill,black);
      bar(616,24+topic*28,631,32+topic*28);
      setcolor(cyan);
      outtextxy(616,24+topic*28,
      copy(graphlabels[topic].fpercent,1,2));
   end;
   if param = 3 then
   begin
      setfillstyle(solidfill,black);
      bar(576,34+topic*28,639,42+topic*28);
      setcolor(cyan);
      outtextxy(576,34+topic*28,graphlabels[topic].matname);
   end;
   if param = 4 then
   begin
      x0:= 59+round(500*(r[topic-1]-r[0])/
           (r[outerlayer]-r[0]));
      x1:= 59+round(500*(r[topic]-r[0])/(r[outerlayer]-r[0]));
      spt:=round((x1+x0)/2);
      setfillstyle(solidfill,black);
      if odd(topic) then j:=10 else j:=0;
```

732

```
      bar(spt-10+8*length(tpic),30-j,spt-12+8*(length
          (graphlabels[topic].thickness)+length(tpic)),37-j);
      setcolor(cyan);
      outtextxy(spt-10+8*length(tpic),30-j,
                graphlabels[topic].thickness);
   end;

   param:= param-1;
   if param <= 0 then param:= 0;
   setcolor(white);

   if param = 0 then
   begin
      setfillstyle(solidfill,blue);
      str(topic,tpic);
      bar(569-4*length(tpic),24+topic*28,
          569-4*length(tpic)+8*length(tpic),32+topic*28);
      outtextxy(569-4*length(tpic),24+topic*28,tpic);
   end;

   if param = 1 then
   begin
      setfillstyle(solidfill,blue);
      str(topic,tpic);
      bar(585+4*length(tpic),24+topic*28,585+4*length(tpic)+
          8*length(graphlabels[topic].angle),32+topic*28);
      setcolor(white);
      outtextxy(585+4*length(tpic),24+topic*28,
                graphlabels[topic].angle);
   end;
   if param = 2 then
   begin
      setfillstyle(solidfill,blue);
      bar(616,24+topic*28,631,32+topic*28);
      setcolor(white);
      outtextxy(616,24+topic*28,
                copy(graphlabels[topic].fpercent,1,2));
   end;
   if param = 3 then
   begin
      setfillstyle(solidfill,blue);
      bar(576,34+topic*28,639,42+topic*28);
      setcolor(white);
      outtextxy(576,34+topic*28,graphlabels[topic].matname);
   end;
   if param = 4 then
   begin
      x0:=59+round(500*(r[topic-1]-r[0])/
          (r[outerlayer]-r[0]));
      x1:=59+round(500*(r[topic]-r[0])/(r[outerlayer]-r[0]));
```

733

```
        spt:=round(((x1+x0)/2);
        setfillstyle(solidfill,blue);
        if odd(topic) then j:=10 else j:=0;
        bar(spt-10+8*length(tpic),30-j,spt-12+8*(length
            (graphlabels[topic].thickness)+length(tpic)),37-j);
        setcolor(white);
        outtextxy(spt-10+8*length(tpic),
            30-j,graphlabels[topic].thickness);
    end;
    goto flag_read;
    end;      {leftarrow}

RightArrow:
   begin
   flag_right:

   if param = 0 then
   begin
      setfillstyle(solidfill,black);
      str(topic,tpic);
      bar(569-4*length(tpic),24+topic*28,
          569-4*length(tpic)+8*length(tpic),32+topic*28);
      outtextxy(569-4*length(tpic),24+topic*28,tpic);
   end;

   if param = 1 then
   begin
      setfillstyle(solidfill,black);
      str(topic,tpic);
      bar(585+4*length(tpic),24+topic*28,585+4*length(tpic)+
          8*length(graphlabels[topic].angle),32+topic*28);
      setcolor(cyan);
      outtextxy(585+4*length(tpic),24+topic*28,
          graphlabels[topic].angle);
   end;
   if param = 2 then
   begin
      setfillstyle(solidfill,black);
      bar(616,24+topic*28,631,32+topic*28);
      setcolor(cyan);
      outtextxy(616,24+topic*28,copy
          (graphlabels[topic].fpercent,1,2));
   end;
   if param = 3 then
   begin
      setfillstyle(solidfill,black);
      bar(576,34+topic*28,639,42+topic*28);
      setcolor(cyan);
      outtextxy(576,34+topic*28,graphlabels[topic].matname);
   end;
```

734

```
if param = 4 then
begin
  x0:= 59+round(500*(r[topic-1]-r[0])/
       (r[outerlayer]-r[0]));
  x1:= 59+round(500*(r[topic]-r[0])/(r[outerlayer]-r[0]));
  spt:=round((x1+x0)/2);
  setfillstyle(solidfill,black);
  if odd(topic) then j:=10 else j:=0;
  bar(spt-10+8*length(tpic),30-j,spt-12+8*(length
      (graphlabels[topic].thickness)+length(tpic)),37-j);
  setcolor(cyan);
  outtextxy(spt-10+8*length(tpic),30-j,
            graphlabels[topic].thickness);
end;

param:= param+1;
if param >= 4 then param:= 4;
setcolor(white);

if param = 1 then
begin
  setfillstyle(solidfill,blue);
  str(topic,tpic);
  bar(585+4*length(tpic),24+topic*28,585+4*length(tpic)+
      8*length(graphlabels[topic].angle),32+topic*28);
  setcolor(white);
  outtextxy(585+4*length(tpic),24+topic*28,
            graphlabels[topic].angle);
end;
if param = 2 then
begin
  setfillstyle(solidfill,blue);
  bar(616,24+topic*28,631,32+topic*28);
  setcolor(white);
  outtextxy(616,24+topic*28,
            copy(graphlabels[topic].fpercent,1,2));
end;
if param = 3 then
begin
  setfillstyle(solidfill,blue);
  bar(576,34+topic*28,639,42+topic*28);
  setcolor(white);
  outtextxy(576,34+topic*28,graphlabels[topic].matname);
end;
if param = 4 then
begin
  x0:=59+round(500*(r[topic-1]-r[0])/
       (r[outerlayer]-r[0]));
  x1:=59+round(500*(r[topic]-r[0])/(r[outerlayer]-r[0]));
  spt:=round((x1+x0)/2);
```

735

```pascal
      setfillstyle(solidfill,blue);
      if odd(topic) then j:=10 else j:=0;
      bar(spt-10+8*length(tpic),30-j,spt-12+8*(length
          (graphlabels[topic].thickness)+length(tpic)),37-j);
      setcolor(white);
      outtextxy(spt-10+8*length(tpic),30-j,
                graphlabels[topic].thickness);
    end;

  goto flag_read;
end; {rightarrow}

PgUp:
  begin
  flag_PgUp:
  InsidePress:= InsidePress+0.10;
  setfillstyle(solidfill,black);
  bar(600,0,639,8);
  setcolor(white);
  setfillstyle(solidfill,blue);
  str(InsidePress:1:1,Ipress);
  bar(600,0,600+(8*length(Ipress)),8);
  outtextxy(600,0,Ipress);
  update:=true;
  goto flag_read;
  end;

Homekey:
  begin
  flag_homekey:
  InsidePress:= InsidePress+1.0;
  setfillstyle(solidfill,black);
  bar(600,0,639,8);
  setcolor(white);
  setfillstyle(solidfill,blue);
  str(InsidePress:1:1,Ipress);
  bar(600,0,600+(8*length(Ipress)),8);
  outtextxy(600,0,Ipress);
  update:=true;
  goto flag_read;
  end;

PgDn:
  begin
  flag_PgDn:
  InsidePress:= InsidePress-0.1;
  if InsidePress < 1 then InsidePress:= 1;
  setfillstyle(solidfill,black);
  bar(600,0,639,8);
  setcolor(white);
```

```
      setfillstyle(solidfill,blue);
      str(InsidePress:1:1,Ipress);
      bar(600,0,600+(8*length(Ipress)),8);
      outtextxy(600,0,Ipress);
      update:=true;
      goto flag_read;
      end;

endkey:
   begin
   flag_endkey:
   InsidePress:= InsidePress-1.0;
   if InsidePress < 1 then InsidePress:= 1;
   setfillstyle(solidfill,black);
   bar(600,0,639,8);
   setcolor(white);
   setfillstyle(solidfill,blue);
   str(InsidePress:1:1,Ipress);
   bar(600,0,600+(8*length(Ipress)),8);
   outtextxy(600,0,Ipress);
   update:=true;
   goto flag_read;
   end;

Insertkey:
   flag_ins:
   begin
   if outerlayer < 15 then
   begin
      for i:= outerlayer+1 downto topic+1 do
      begin
         graphlabels[i].matname:=graphlabels[i-1].matname;
         graphlabels[i].fpercent:=graphlabels[i-1].fpercent;
         graphlabels[i].thickness:=graphlabels[i-1].thickness;
         graphlabels[i].angle:=graphlabels[i-1].angle;
      end;
      graphlabels[topic].matname:=copy(matchoice[1],1,
                                   pos('.',matchoice[1])-1);
      graphlabels[topic].fpercent:='60';
      graphlabels[topic].thickness:='1.0';
      graphlabels[topic].angle:='55';
      for i:= 0 to outerlayer do
         r[i]:=(r[i]-insideDia/2)*scalefactor;
      for i:= outerlayer+1 downto topic+1 do
         r[i]:= r[i-1]+1;
      r[topic]:=r[topic-1]+1;
      scalefactor:=((wallthick*scalefactor)+1)/wallthick;
      str(1/scalefactor:4:2,scalef);
      for i:= 0 to outerlayer+1 do
         r[i]:=r[i]/scalefactor+insideDia/2;
```

```
        setfillstyle(solidfill,black);
        bar(0,18,58,26);
        bar(59,18,639,38);
        bar(560,48,639,469);
        outerlayer:= outerlayer+1;
        assign(f,currentfile);
        rewrite(f);
        writeln(f,insideDia:5:2);
        writeln(f,wallthick:5:2);
        writeln(f,insidePress:5:2);
        writeln(f,outerPress:5:2);
        for i:= 1 to outerlayer do
        begin
          writeln(f,i); {does layer no}
          writeln(f,graphlabels[i].matname);
          writeln(f,graphlabels[i].angle);
          writeln(f,graphlabels[i].thickness);
          writeln(f,graphlabels[i].fpercent);
          end;
        close(f);
        update:=true;
        goto flag_restart;
     end;   {if topic < 15}
     end;   {case}

AltI:
   flag_altI:
   begin
     if outerlayer < 15 then
   begin
     for i:= outerlayer+1 downto topic+2 do
     begin
       graphlabels[i].matname:=graphlabels[i-1].matname;
       graphlabels[i].fpercent:=graphlabels[i-1].fpercent;
       graphlabels[i].thickness:=graphlabels[i-1].thickness;
       graphlabels[i].angle:=graphlabels[i-1].angle;
     end;
     graphlabels[topic+1].matname:=copy(matchoice[1],1,
                              pos('.',matchoice[1])-1);
     graphlabels[topic+1].fpercent:='60';
     graphlabels[topic+1].thickness:='1.0';
     graphlabels[topic+1].angle:='55';
     for i:= 0 to outerlayer do
       r[i]:=(r[i]-insideDia/2)*scalefactor;
     for i:= outerlayer+1 downto topic+2 do
       r[i]:= r[i-1]+1;
     r[topic+1]:=r[topic]+1;      {new layer}
     scalefactor:=((wallthick*scalefactor)+1)/wallthick;
     str(1/scalefactor:4:2,scalef);
     for i:= 0 to outerlayer+1 do
```

738

```
      r[i]:=r[i]/scalefactor+insideDia/2;
    setfillstyle(solidfill,black);
    bar(0,18,58,26);
    bar(59,18,639,38);
    bar(560,48,639,469);
    outerlayer:= outerlayer+1;
    topic:= topic+1;
    assign(f,currentfile);
    rewrite(f);
    writeln(f,insideDia:5:2);
    writeln(f,wallthick:5:2);
    writeln(f,insidePress:5:2);
    writeln(f,outerPress:5:2);
    for i:= 1 to outerlayer do
    begin
       writeln(f,i); {does layer no}
       writeln(f,graphlabels[i].matname);
       writeln(f,graphlabels[i].angle);
       writeln(f,graphlabels[i].thickness);
       writeln(f,graphlabels[i].fpercent);
       end;
    close(f);
    update:=true;
    goto flag_restart;
  end;  {if topic < 15}
  end;


Deletekey:
  flag_del:
  begin
  if outerlayer > 1 then
  begin
    thick:=0;
    for i:= topic to outerlayer-1 do
    begin
       graphlabels[i].matname:=graphlabels[i+1].matname;
       graphlabels[i].fpercent:=graphlabels[i+1].fpercent;
       graphlabels[i].thickness:=graphlabels[i+1].thickness;
       graphlabels[i].angle:=graphlabels[i+1].angle;
    end;
    for i:= 1 to outerlayer do
       r[i]:=(r[i]-r[0])*scalefactor;
    for i:= 2 to outerlayer do
       rt[i]:=r[i]-r[i-1];
    rt[1]:=r[1];
    for i:= topic to outerlayer-1 do
       rt[i]:= rt[i+1];
    for i:= 1 to outerlayer-1 do
       begin
          thick:= thick+rt[i];
```

739

```
            r[i]:=r[0]+thick;
          end;
       scalefactor:=thick/wallthick;
       str(1/scalefactor:4:2,scalef);
       for i:= 1 to outerlayer-1 do
          r[i]:=((r[i]-r[0])/scalefactor)+r[0];
       setfillstyle(solidfill,black);
       bar(0,18,58,26);
       bar(59,18,639,38);
       bar(560,48,639,469);
       outerlayer:= outerlayer-1;
       if outerlayer < 1 then outerlayer:=1;
       topic:= topic-1;
       if topic < 1 then topic:= 1;
       assign(f,currentfile);
       rewrite(f);
       writeln(f,insideDia:5:2);
       writeln(f,wallthick:5:2);
       writeln(f,insidePress:5:2);
       writeln(f,outerPress:5:2);
       for i:= 1 to outerlayer do
       begin
          writeln(f,i); {does layer no}
          writeln(f,graphlabels[i].matname);
          writeln(f,graphlabels[i].angle);
          writeln(f,graphlabels[i].thickness);
          writeln(f,graphlabels[i].fpercent);
          end;
       close(f);
       update:=true;
       goto flag_restart;
     end;  {if topic > 1}
     end;  {case}

Carriagereturn:
   begin
     goto flag_return;
   end;

ALTF:     {write to file}
   begin
   print:=false;
   filenum:= filenum+1;
   filedata(Mred,Fred,Sred,MS,FS,Firstdam,proof,filenum,
            sigr,sigf,sigz,sig1,sig2,sig3,sig6,ef,ez,el,
            e2,e3,e6,rupt,print,full,nlshear);
   end;

ALTP:     {print}
   begin
```

```
           print:=true;
           filenum:= filenum+1;
           filedata(Mred,Fred,Sred,MS,FS,Firstdam,proof,filenum,
                   sigr,sigf,sigz,sig1,sig2,sig3,sig6,ef,ez,e1,
                   e2,e3,e6,rupt,print,full,nlshear);
           end;


    TAB:       {restart}
           begin
           flag_tab:
           rset:=true;
           goto flag_return;
           end;


    AltS:
           begin
           flag_save:
           setcolor(white);
           setfillstyle(solidfill,black);
           bar(40,19,104,19);
           bar(0,10,39,18);
           setfillstyle(solidfill,blue);
           bar(40,10,104,18);
           newfile:= currentfile;
           Delete(newfile,length(newfile)-3,4);       {remove file ext}
           outtextxy(0,10,'File:'+newfile);
           getnewfname(newfile,OK);
           if OK = false then
             begin
             update:=true;    {operation aborted}
             cleardevice;
             goto flag_end;
             end
           else
             begin
             oldfile:= currentfile;    {buffer}
             currentfile:= newfile;
             {$I-}
             assign(f,newfile+'.ves');
             rewrite(f);
             errcd:= IOresult;
             if errcd <> 0 then
             begin
               beep(800,2000);
               setcolor(red);
               setfillstyle(solidfill,black);
               bar(0,0,104,8);
               outtextxy(0,0,'Error');
               delay(15000);
               bar(0,0,104,8);
```

```
         setcolor(lightgray);
         outtextxy(0,0,oldfile+'.ves');
         currentfile:=newfile+'.ves';
         goto flag_save;
      end;
      {$I+}
      writeln(f,insideDia:5:2);
      writeln(f,wallthick:5:2);
      writeln(f,insidePress:5:2);
      writeln(f,outerPress:5:2);
      for i:= 1 to outerlayer do
      begin
        writeln(f,i); {does layer no}
        writeln(f,graphlabels[i].matname);
        writeln(f,graphlabels[i].angle);
        writeln(f,graphlabels[i].thickness);
        writeln(f,graphlabels[i].fpercent);
        end;
      close(f);
      setcolor(red);
      setfillstyle(solidfill,black);
      bar(0,0,104,8);
      bar(0,10,104,19);
      setcolor(lightgray);
      outtextxy(0,0,newfile+'.VES');
      outtextxy(0,10,'W-Scale:'+scalef);
      currentfile:=newfile+'.VES';
      beep(1600,600);
      delay(15000);
      update:=true;
      goto flag_read;
      end;
   end;  {altS}
end; {of cases}

until (key = esc) or (key = AltX);
flag_end:
exit:=true;
closegraph;
graphstate:=false;
restorecrtmode;
flag_return:
end;

(************************************************)

end.
```

```pascal
unit PlotProp;
{$O+,F+}

interface

(*********************************************)

uses glob_var,graph,crt;

procedure initgraphdriver;

function SRS(var pr:realarrayNP):real;

procedure amoeba(var p: realarrayMPbyNP; var yy:
                 RealArrayMP;ndim:integer;
                 ftol:real; var nfunc,pick: integer);

procedure getgraphdata(graphtype:char);

Procedure zerographdata;

procedure Plotgraph(ngraph:integerarray9;marker,xdiv,ydiv:
                    integer;var xmin,xmax,ymin,ymax:real);
     {ngraph = graphnumber(s) to plot, marker = edit point}

Procedure plotoutline(xlabel,ylabel,Title,title2:string;
                xdiv,ydiv:integer;xmin,xmax,ymin,ymax:real);

Procedure bestfit(var b_fit:realarrayMPbyNP;
                var pk,n:integer);

procedure plotvariable(xdiv,ydiv:integer; var
                  xMX,xMN,yMX,yMN,power:real);

procedure plotvgraphs(r,sig_r,sig_f,sig_z:realarray2plusN;
                    var xmx,xmn,ymx,ymn:real;nn:integer);

procedure PlotLStress(var sig_r,sig_f,sig_z,Msaf,
                 Fsaf:realarray3NL;var xmx,xmn,ymx,ymn,
                 Dhi:real;var rupt:boolean;
                 var MSL,FSL:realarray1NL);

(*********************************************)

implementation

(*********************************************)

procedure initgraphdriver;
```


743

```pascal
var
grdriver,grmode,errcode:integer;

begin

grDriver:= Detect;
  initGraph(grDriver,grMode,'\TP');
  errCode:=GraphResult;
if errcode <> grOk then
  begin
    gotoxy(4,6);
    Writeln('Graphics error: ',GraphErrorMsg(ErrCode));
    delay(4000);
    exit;
  end;
graphstate:=true;
end;

(**************************************************)

function pow(a,b:real):real;

begin
pow:=exp(b*ln(a));
end;

(**************************************************)

function SRS(var pr:realarrayNP):real;

var
sum,c:real;

begin
sum:=0;
  for i:= 1 to 2*outerlayer do
  begin
  c:=plota[i]-pr[1]*pow(plotr[i]/plotr[2*outerlayer],pr[2]);
  sum:= sum + sqr(c);
  end;
srs:= sum;
end;

(**************************************************)

procedure amoeba(var p:realarrayMPbyNP;var yy:
                 RealArrayMP;ndim:integer;ftol:real;
                 var nfunc,pick:integer);

label flag1;
```

```
const
  nfuncmax = 5000;
  alpha = 1.0;
  beta = 0.5;
  gamma = 2.0;

var
  mpts,j,inhi,ilo,ihi,i:integer;
  ytry,ysave,sum,rtol:real;
  psum:^realarrayNP;


(*********************************************)

Function amotry(var p:realarrayMPbyNP;
               var yy: realarrayMP;
               var sum:realarrayNP;
               ndim,ihi:integer;
               var nfunct:integer;
               fac:real):real;
var
  j: integer;
  fac1,fac2,ytry:real;
  ptry:^realarrayNP;

begin
  new(ptry);
  fac1:= (1.0-fac)/ndim;
  fac2:= fac1-fac;
  for j:= 1 to ndim do
    ptry^[j]:= sum[j]*fac1-p[ihi,j]*fac2;
  ytry:= srs(ptry^);
  nfunc:= nfunc+1;
  if ytry < yy[ihi] then begin
    yy[ihi]:= ytry;
    for j:= 1 to ndim do begin
      sum[j]:= sum[j]+ptry^[j]-p[ihi,j];
      p[ihi,j]:= ptry^[j];
    end
  end;
  amotry:= ytry;
  dispose(ptry)
end;

(*********************************************)

begin {procedure}
  new(psum);
  mpts:= ndim+1;
  nfunc:=0;
```

```
for j:= 1 to ndim do begin
  sum:= 0.0;
  for i:= 1 to mpts do
    sum:= sum+p[i,j];
  psum^[j]:= sum
end;
while true do begin
ilo:=1;
if yy[1] > yy[2] then begin
  ihi:= 1;
  inhi:= 2
end
else begin
  ihi:= 2;
  inhi:= 1
end;
for i:= 1 to mpts do begin
    if yy[i] < yy[ilo] then ilo := i;
    if yy[i] > yy[ihi] then begin
      inhi:= ihi;
      ihi:=i
    end
    else if yy[i] > yy[inhi] then
      if i<> ihi then inhi := i
end;
rtol:= 2.0*abs(yy[ihi]-yy[ilo])/
      (abs(yy[ihi])+abs(yy[ilo]));
if rtol < ftol then goto flag1;
if nfunc >= nfuncmax then begin
  writeln('pause in Amoeba - too many iterations');
  readln
end;
ytry:= amotry(p,yy,psum^,ndim,ihi,nfunc,-alpha);
if ytry <= yy[ilo] then
  ytry:= amotry(p,yy,psum^,ndim,ihi,nfunc,gamma)
  else if ytry >= yy[inhi] then begin
    ysave:= yy[ihi];
    ytry:= amotry(p,yy,psum^,ndim,ihi,nfunc,beta);
    if ytry >=ysave then begin
      for i:= 1 to mpts do
        if i<> ilo then begin
          for j:= 1 to ndim do begin
            psum^[j]:= 0.5*(p[i,j]+p[ilo,j]);
            p[i,j]:= psum^[j]
          end;
          yy[i]:= SRS(psum^)
        end;
    nfunc:=nfunc+ndim;
    for j:= 1 to ndim do begin
      sum:= 0.0;
```

746

```
            for i:= 1 to mpts do
               sum:= sum+p[i,j];
            psum^[j]:= sum
          end
        end
      end
   end;
flag1:
pick:= ilo;
   dispose(psum)
end;   {procedure}


(********************************************)

procedure getgraphdata(graphtype:char);

var
i,j,k,g:integer;
m,n:string[1];
thickness:real;

label
flag_q12,flag_q23,flag_q66,flag_q11,flag_q22,flag_q13,
flag11,flag22,flag23,flag13,flag66,flag12;

begin
case graphtype of

'A':       {stiffnesses}

begin                                              {A11}
g:= 0;

   g:=g+1;              {graph index}
   thickness:=0;              {reset thickness}
   for k:= 1 to NL do
   begin
   if lq[k,1,1] = 0 then goto flag_q11;  {no more layers}
      graphdata[g].symbol:='A'+'11';
      graphdata[g].xydata[k,2]:= lq[k,1,1];
                              {stiffness value along x-axis}
      thickness:=thickness + Dt[k];
      graphdata[g].xydata[k,1]:= thickness;
   end; {layer loop}
   flag_q11:
                                                   {A12}
   g:=g+1;              {graph index}
   thickness:=0;              {reset thickness}
   for k:= 1 to NL do
   begin
```

```
if lq[k,1,2] = 0 then goto flag_q12;   {no more layers}
   graphdata[g].symbol:='A'+'12';
   graphdata[g].xydata[k,2]:= lq[k,1,2];
                            {stiffness value along x-axis}
   thickness:=thickness + Dt[k];
   graphdata[g].xydata[k,1]:= thickness;
end; {layer loop}
flag_q12:
                                              {A22}
g:=g+1;              {graph index}
thickness:=0;              {reset thickness}
for k:= 1 to NL do
begin
if lq[k,2,2] = 0 then goto flag_q22;   {no more layers}
   graphdata[g].symbol:='A'+'22';
   graphdata[g].xydata[k,2]:= lq[k,2,2];
                            {stiffness value along x-axis}
   thickness:=thickness + Dt[k];
   graphdata[g].xydata[k,1]:= thickness;
end; {layer loop}
flag_q22:

for i:= 3 to 6 do                       {A33 ..A66}
begin
g:=g+1;              {graph index}
thickness:=0;        {reset thickness}
for k:= 1 to NL do   {layer index}
begin
if lq[k,i,i] = 0 then goto flag_q66;   {no more layers}
   str(i,m);
   str(i,n);
   graphdata[g].symbol:='A'+m+n;
   graphdata[g].xydata[k,2]:= lq[k,i,i];
                                {stiffness value along x-axis}
   thickness:=thickness + Dt[k];
   graphdata[g].xydata[k,1]:= thickness;
flag_q66:
end; {layer loop}
end;   {i loop}
                                              {A13}
g:=g+1;              {graph index}
thickness:=0;              {reset thickness}
for k:= 1 to NL do
begin
if lq[k,1,3] = 0 then goto flag_q13;   {no more layers}
   graphdata[g].symbol:='A'+'13';
   graphdata[g].xydata[k,2]:=lq[k,1,3];
                            {stiffness value along x-axis}
   thickness:=thickness + Dt[k];
   graphdata[g].xydata[k,1]:= thickness;
```

748

```
end; {layer loop}
flag_q13:

g:=g+1;                {graph index}
thickness:=0;          {reset thickness}
for k:=1 to NL do                                {A23}
begin
if lq[k,2,3] = 0 then goto flag_q23;   {no more layers}
  graphdata[g].symbol:='A23';
  graphdata[g].xydata[k,2]:= lq[k,2,3];
                              {stiffness value along x-axis}
  thickness:=thickness + Dt[k];      {increment thickness}
  graphdata[g].xydata[k,1]:= thickness;
end; {layer loop}
flag_q23:

end; {first case}


'a':

begin
g:= 0;
  g:= g+1;             {graph index}            {a11}
  thickness:=0;        {reset thickness}
  for k:= 1 to NL do  {layer index}
  begin
  if lq[k,1,1] = 0 then goto flag11;  {no more layers}
    graphdata[g].symbol:='a11';
    graphdata[g].xydata[k,2]:=1000*la[k,1,1];
                              {stiffness value along x-axis}
    thickness:=thickness + Dt[k];
    graphdata[g].xydata[k,1]:= thickness;
  flag11:
  end; {layer loop}
                                                {a12}
g:=g+1;                {graph index}
  thickness:=0;        {reset thickness}
  for k:= 1 to NL do  {layer index}
  begin
  if lq[k,1,2] = 0 then goto flag12;  {no more layers}
    graphdata[g].symbol:='a12';
    graphdata[g].xydata[k,2]:=1000*la[k,1,2];
                              {stiffness value along x-axis}
    thickness:=thickness + Dt[k];
    graphdata[g].xydata[k,1]:= thickness;
  flag12:
  end; {layer loop}
                                                {a22}
g:=g+1;                {graph index}
  thickness:=0;        {reset thickness}
```

```
for k:= 1 to NL do  {layer index}
begin
if lq[k,2,2] = 0 then goto flag22;  {no more layers}
   graphdata[g].symbol:='a22';
   graphdata[g].xydata[k,2]:=1000*la[k,2,2];
                                {stiffness value along x-axis}
   thickness:=thickness + Dt[k];
   graphdata[g].xydata[k,1]:= thickness;
flag22:
end; {layer loop}

for i:= 3 to 6 do                               {a33 ..a66}
begin
g:=g+1;                {graph index}
thickness:=0;          {reset thickness}
for k:= 1 to NL do  {layer index}
begin
if lq[k,i,i] = 0 then goto flag66;  {no more layers}
   str(i,m);
   str(i,n);
   graphdata[g].symbol:='a'+m+n;
   graphdata[g].xydata[k,2]:=1000*la[k,i,i];
                                {stiffness value along x-axis}
   thickness:=thickness + Dt[k];
   graphdata[g].xydata[k,1]:= thickness;

flag66:
end; {layer loop}
end;  {i loop}


                                                {a13}
g:=g+1;                {graph index}
thickness:=0;          {reset thickness}
for k:= 1 to NL do  {layer index}
begin
if lq[k,1,3] = 0 then goto flag13;  {no more layers}
   graphdata[g].symbol:='a13';
   graphdata[g].xydata[k,2]:=1000*la[k,1,3];
                        {stiffness value along x-axis}
   thickness:=thickness + Dt[k];
   graphdata[g].xydata[k,1]:= thickness;
flag13:
end; {layer loop}

g:=g+1;                {graph index}
thickness:=0;          {reset thickness}
for k:=1 to NL do                               {a23}
begin
 if lq[k,2,3] = 0 then goto flag23;  {no more layers}
   graphdata[g].symbol:='a23';
```

```pascal
      graphdata[g].xydata[k,2]:=1000*la[k,2,3];
                                  {stiffness value along x-axis}
      thickness:=thickness + Dt[k];       {increment thickness}
      graphdata[g].xydata[k,1]:= thickness;
    end;  {layer loop}
    flag23:

  end; {second case}

'B':         {compliances}
  begin
  g:=0;
  for i:= 1 to 2 do                              {B11 ..B33}
  for j:= 1 to 2 do
  if i<=j then
    begin
    g:=g+1;                 {graph index}
    thickness:=0;          {reset thickness}
    for k:= 1 to NL do  {layer index}
      begin
      str(i,m);
      str(j,n);
      graphdata[g].symbol:='B'+m+n;
      graphdata[g].xydata[k,2]:=1000*lb[k,i,j];
                              {stiffness value along x-axis}
      thickness:=thickness + Dt[k];
      graphdata[g].xydata[k,1]:= thickness;
      end; {layer loop}
    end;  {i,j loop}
  end; {3rd case}
end;  {all cases}
end; {procedure}


(*****************************************************)


Procedure zerographdata;

var
i,j,k:integer;

begin
  for k:= 1 to 9 do                    {space for 9 graphs}
      graphdata[k].symbol := '';
    for k:= 1 to 9 do
    for i:= 0 to NL do       {0th layer is for plot origin}
    for j:= 1 to 2 do
    graphdata[k].xydata[i,j]:=0;
end;


(*************************************)
```

```
Procedure bestfit(var b_fit:realarrayMPbyNP;var
                  pk,n:integer);

var                      {n=graph# to fit curve to}

result:realarrayMP;
init:realarrayNP;
iter,i,j:integer;

label
flag3,flag_end;

begin
flag3:
for i:= 1 to outerlayer do
                  (set up variables for optimization routine)

    begin
    j:= 2*i;
    plotr[j-1]:=r[i-1]{           {r[0] = inside dia}
    plotr[j]:=r[i];
    plota[j-1]:=graphdata[n].xydata[i,2];
    plota[j]:=graphdata[n].xydata[i,2];
    end;

if outerlayer = 1 then
begin
    Bfit_store[n,1]:=plota[1];
    b_fit[1,1]:=plota[1];
    Bfit_store[n,2]:=0.0;
    b_fit[1,2]:=0.0;
    pk:=1;
    goto flag_end;
end;

b_fit[1,1]:= 10.0;         {initial guesses, 3 vectors}
b_fit[1,2]:= 5.0;
b_fit[2,1]:= 20.0;
b_fit[2,2]:= 3.0;
b_fit[3,1]:= 10.0;
b_fit[3,2]:= -1.0;
init[1]:=10;
init[2]:=5.0;
result[1]:=srs(init);     {SRS = sum of residuals squared}
init[1]:=20.0;            {results from initial guesses}
init[2]:=3.0;
result[2]:=srs(init);
init[1]:=10.0;
init[2]:=-1.0;
result[3]:=srs(init);
```

752

```
amoeba(b_fit,result,2,1E-5,iter,pk);
                    {pk = index for lowest srs of 3 choices}
  bfit_Store[n,1]:=b_fit[pk,1];
              {result = y value, 2 = number of parameters}
  bfit_Store[n,2]:=b_fit[pk,2];
              {1E5 = tolerance ,b-fit = required variables}
  bfit_Store[n,3]:=iter;
flag_end:
end;

(*********************************************)

procedure plotvariable(xdiv,ydiv:integer;var
                        xMX,xMN,yMX,yMN,power:real);
                        {one variable property - n}
type
realarray9XNL = array[1..9,0..NL] of real;

var
xvaluemin,xvaluemax,yvaluemin,yvaluemax,xstep,ystep:real;
plotv:realarray9XNL;
i,n,MaxX,MaxY,x0point,y0point,x1point,y1point,
yorigin:integer;
alph,pwr:string;

begin
xvaluemin:=9E30;
yvaluemin:=9E30;
xvaluemax:=-9E30;
yvaluemax:=-9E30;
MaxX:=GetMaxX;
MaxY:=GetMaxY;

for n:= 1 to 3 do    {may go up to 7}
  for i:= 0 to 16 do          {extract max and min values}
    begin
    if
      graphdata[n].xydata[i,1] > xvaluemax then
      xvaluemax:=graphdata[n].xydata[i,1];
    if
      graphdata[n].xydata[i,2] > yvaluemax then
      yvaluemax:= graphdata[n].xydata[i,2];
    if
      graphdata[n].xydata[i,1] < xvaluemin then
      xvaluemin:= graphdata[n].xydata[i,1];
    if
      graphdata[n].xydata[i,2] < yvaluemin then
      yvaluemin:= graphdata[n].xydata[i,2];
    end;   {for lastlayer loop}
```

753

```
ystep:=((yvaluemax-yvaluemin)/ydiv);
xstep:=((xvaluemax-xvaluemin)/xdiv);
ymn:=yvaluemin;
if frac(ymn) <> 0 then
  ymn:=int(yvaluemin)-1;
xmn:=xvaluemin;
xmx:=xvaluemax;
ymx:=yvaluemax;
if frac(ymx) > 0 then
  ymx:= int(ymx)+1;
setcolor(green);
str(bfit_store[3,1]:3:2,alph);
settextjustify(righttext,toptext);
settextstyle(0,0,1);
outtextxy(596,20,'B22='+alph+'(p)');
settextjustify(lefttext,toptext);
str(power:4:2,pwr);
outtextxy(596,16,pwr);
setcolor(white);
outtextxy(584,334,'Legend');
Setlinestyle(0,0,1);
setcolor(white);
line(59,439-round(400*(-ymn)/(ymx-ymn)),559,
      439-round(400*(-ymn)/(ymx-ymn)));

for n:= 1 to 3 do    {may go up to 7}
begin

  if n = 1 then
    setcolor(cyan);
  if n = 2 then
    setcolor(green);
  if n = 3 then
    setcolor(red);
  if n = 4 then
    setcolor(cyan);
  if n = 5 then
    setcolor(green);
  if n = 6 then
    setcolor(red);
  if n = 7 then
    setcolor(magenta);
  if n > 3 then
    begin
    Outtextxy(592,334+n*14,graphdata[n].symbol);
    Setlinestyle(1,0,1)
    end
  else
    begin
    Outtextxy(596,334+n*14,graphdata[n].symbol);
```

```pascal
        Setlinestyle(0,0,1);
        end;
      for i:= 1 to 16 do   {plots variable property}
      begin
        y0point:=439-round(400*(graphdata[n].xydata[i-1,2]-ymn)/
                 (ymx-ymn));
        y1point:=439-round(400*(graphdata[n].xydata[i,2]-ymn)/
                 (ymx-ymn));
        x0point:=59+round(500*((graphdata[n].xydata[i-1,1])-xmn)
                 /(xmx-xmn));
        x1point:=59+round(500*((graphdata[n].xydata[i,1])-xmn)/
                 (xmx-xmn));
        Line(x0point,y0point,x1point,y1point);
      end; {for i}
  end; {for n}

  setlinestyle(0,0,1);
  end; {procedure}


(*********************************************************)


procedure plotvgraphs(r,sig_r,sig_f,sig_z:realarray2plusN;
                      var xmx,xmn,ymx,ymn:real;nn:integer);

var
y0point,x0point,y1point,x1point,yorigin,n:integer;
lab,valu,expon:string;

begin
ymn:=9E30;
ymx:=-9E30;
n:= nfe;

   for i:= 0 to n+1 do              {extract max and min values}
     begin
     if sig_z[i] > ymx then
       ymx:= sig_z[i];
     if sig_f[i] > ymx then
       ymx:= sig_f[i];
     if sig_r[i] > ymx then
       ymx:= Sig_r[i];
     if sig_r[i] < ymn then
       ymn:= sig_r[i];
     if sig_f[i] < ymn then
       ymn:= Sig_f[i];
     if sig_z[i] < ymn then
       ymn:= Sig_z[i];
     end;
xmn:= r[0];
xmx:= r[n+1];
```

755

```
if frac(ymn) <> 0 then
 ymn:=int(ymn)-1;
if frac(ymx) > 0 then
  ymx:= int(ymx)+1;

Outtextxy(580,364,'Legend');
if ymn < 0 then
    begin
      yorigin:=439-round(400*(-ymn/(ymx-ymn)));
      setcolor(white);
      setlinestyle(0,0,1);
      Line(59,yorigin,559,yorigin);
    end;
setcolor(green);
for i:= 1 to n+1 do  {plots sig-f}
  begin
    y0point:=439-round(400*(sig_f[i-1]-ymn)/(ymx-ymn));
    y1point:=439-round(400*(sig_f[i]-ymn)/(ymx-ymn));
    x0point:=59+round(500*(r[i-1]-xmn)/(xmx-xmn));
    x1point:=59+round(500*(r[i]-xmn)/(xmx-xmn));
    Line(x0point,y0point,x1point,y1point);
  end;
outtextxy(596,376,char(229)+char(233));
setcolor(cyan);
for i:= 1 to n+1 do  {plots sig-r}
  begin
    y0point:=439-round(400*(sig_r[i-1]-ymn)/(ymx-ymn));
    y1point:=439-round(400*(sig_r[i]-ymn)/(ymx-ymn));
    x0point:=59+round(500*(r[i-1]-xmn)/(xmx-xmn));
    x1point:=59+round(500*(r[i]-xmn)/(xmx-xmn));
    Line(x0point,y0point,x1point,y1point);
  end;
outtextxy(596,388,char(229)+'r');
setcolor(red);
for i:= 1 to n+1 do  {plots sig-z}
  begin
    y0point:=439-round(400*(sig_z[i-1]-ymn)/(ymx-ymn));
    y1point:=439-round(400*(sig_z[i]-ymn)/(ymx-ymn));
    x0point:=59+round(500*(r[i-1]-xmn)/(xmx-xmn));
    x1point:=59+round(500*(r[i]-xmn)/(xmx-xmn));
    Line(x0point,y0point,x1point,y1point);
  end;
outtextxy(596,400,char(229)+'z');

setcolor(white);
outtextxy(570,40,'Variable');
setcolor(lightcyan);
setcolor(cyan);
outtextxy(590,52,'B11');
```

```pascal
outtextxy(590,64,'B12');
outtextxy(590,76,'B22');
outtextxy(590,88,'a13');
outtextxy(590,100,'a23');
outtextxy(590,112,'a33');
setcolor(white);
rectangle(583,42+12*nn,585,44+12*nn);

end;


(**********************************************)

procedure PlotLStress(var sig_r,sig_f,sig_z,Msaf,Fsaf:
                        realarray3NL;var xmx,xmn,ymx,ymn,Dhi:
                        real;var rupt:boolean;var MSL,
                        FSL:realarray1NL);

var
y0point,x0point,y1point,x1point,x2point,y2point,
yorigin:integer;
n,i,j,l,leftpt,midpt,rightpt,htFL,htML,plthtFL,plthtML,htFM,
htMM,plthtFM,plthtMM,htFR,htMR,plthtFR,plthtMR:integer;
pdm,Pin:string;

begin
ymn:=9E30;
ymx:=-9E30;
n:=3*outerlayer;

   for i:= 1 to n do            {extract max and min values}
     begin
     if sig_z[i] > ymx then
       ymx:= sig_z[i];
     if sig_f[i] > ymx then
       ymx:= sig_f[i];
     if sig_r[i] > ymx then
       ymx:= Sig_r[i];
     if sig_r[i] < ymn then
       ymn:= sig_r[i];
     if sig_f[i] < ymn then
       ymn:= Sig_f[i];
     if sig_z[i] < ymn then
       ymn:= Sig_z[i];
     end;

str(Dhi:3:1,pdm);
str(insidepress:3:1,Pin);

xmn:= r[0];
xmx:= r[outerlayer];
```

```
if frac(ymn) <> 0 then
 ymn:=int(ymn)-1;
if frac(ymx) > 0 then
   ymx:= int(ymx)+1;
settextstyle(0,1,1);
Outtextxy(8,48,'Legend');
settextstyle(0,0,1);
if ymn < 0 then
    begin
       yorigin:=439-round(400*(-ymn/(ymx-ymn)));
       setcolor(white);
       setlinestyle(0,0,1);
       Line(59,yorigin,559,yorigin); {horizontal zero line}
    end;
setlinestyle(1,0,1);
for i:= 1 to outerlayer-1 do
begin
  x2point:=59+round(500*(r[i]-xmn)/(xmx-xmn));
                                   {vertical dotted line}
  line(x2point,39,x2point,439);
end;

setcolor(yellow);
line(59,Yorigin-50,559,yorigin-50); {safety factor = 1 line}
line(59,Yorigin-227,559,yorigin-227);{full degradation line}

setlinestyle(0,0,1);
OuttextXY(0,306,'Matrix');
outtextXY(0,316,'Damage:');
outtextXY(0,150,'Fiber');
outtextXY(0,160,'Rupture');
outtextXY(0,326,Pdm);
outtextXY(0,336,'MPa');
setfillstyle(solidfill, cyan);
bar3D(17,419,28,377,0,topoff);
setfillstyle(solidfill, magenta);
bar3D(28,419,39,369,0,topoff);
setcolor(black);
setTextstyle(0,1,1);
outtextxy(27,378,'Fiber');
setcolor(white);
outtextxy(38,370,'Matrix');
outtextxy(8,365,'Failure');
setTextstyle(0,0,1);
setcolor(cyan);
OuttextXY(480,0,'Pressure (MPa):'+Pin);

for i:=1 to 3*outerlayer do
                  {to stay within integer range for round}
```

```
begin
if FSaf[i]<0.01 then
 FSaf[i]:=0.01;
if MSaf[i]<0.01 then
 Msaf[i]:=0.01;
end;

for i:= 1 to 3*outerlayer do
begin
l:=trunc((i+2)/3);
if MSL[l] < 1 then
  Msaf[i]:=MSL[l];
end;

for i:= 1 to outerlayer do
begin

  leftpt:= 59+round(500*(r[i-1]-xmn)/(xmx-xmn))+2;
  rightpt:=59+round(500*(r[i]-xmn)/(xmx-xmn))-2;
  midpt:=59+round(500*(((r[i-1]+r[i])/2)-xmn)/(xmx-xmn));

  htFL:= round(50*(1/FSaf[3*(i-1)+1]));
  htFM:= round(50*(1/FSaf[3*(i-1)+2]));
              {plots inverse of eq stiffness when damaged}
  htFR:= round(50*(1/FSaf[3*(i-1)+3]));

  htML:= round(50*(1/MSaf[3*(i-1)+1]));
  htMM:= round(50*(1/MSaf[3*(i-1)+2]));
  htMR:= round(50*(1/MSaf[3*(i-1)+3]));

  plthtFL:=yorigin-htFL;
     if plthtFL<40 then plthtFL:=40;
  plthtFM:=yorigin-htFM;
     if plthtFM<40 then plthtFM:=40;
  plthtFR:=yorigin-htFR;
     if plthtFR<40 then plthtFR:=40;
  plthtML:=yorigin-htML;
     if plthtML<40 then plthtML:=40;
  plthtMM:=yorigin-htMM;
     if plthtMM<40 then plthtMM:=40;
  plthtMR:=yorigin-htMR;
       if plthtMR<40 then plthtMR:=40;

  setcolor(yellow);
  if FSL[i] < 1 then
     setfillstyle(solidfill,lightcyan)
  else
     setfillstyle(solidfill,cyan);
  if ((rightpt-leftpt)>3) and ((rightpt-leftpt)<=12) then
       bar3D(midpt-3,Yorigin,Midpt,plthtFM,0,topoff);
```

759

```
        if ((rightpt-leftpt)>12) and ((rightpt-leftpt)<=20) then
          begin
            bar3D(leftpt,Yorigin,leftpt+3,plthtFL,0,topoff);
            bar3D(rightpt-6,Yorigin,rightpt-3,plthtFR,0,topoff);
          end;
        if (rightpt-leftpt)> 20 then
          begin
            bar3D(leftpt,Yorigin,leftpt+3,plthtFL,0,topoff);
            bar3D(midpt-3,Yorigin,Midpt,plthtFM,0,topoff);
            bar3D(rightpt-6,Yorigin,rightpt-3,plthtFR,0,topoff);
          end;
        if MSL[i] < 1 then
          setfillstyle(solidfill,lightmagenta)
        else
          setfillstyle(solidfill,magenta);
          if ((rightpt-leftpt)>3) and ((rightpt-leftpt)<=12) then
            bar3D(midpt,Yorigin,Midpt+3,plthtMM,0,topoff);
          if ((rightpt-leftpt)>12) and ((rightpt-leftpt)<=20) then
            begin
              bar3D(leftpt+3,Yorigin,leftpt+6,plthtML,0,topoff);
              bar3D(rightpt-3,Yorigin,rightpt,plthtMR,0,topoff);
            end;
        if (rightpt-leftpt) >20 then
          begin
            bar3D(leftpt+3,Yorigin,leftpt+6,plthtML,0,topoff);
            bar3D(midpt,Yorigin,Midpt+3,plthtMM,0,topoff);
            bar3D(rightpt-3,Yorigin,rightpt,plthtMR,0,topoff);
          end;
  end;
setcolor(green);
for j:= 1 to outerlayer do  {plots sig-f}
  begin
    i:=3*j;
    y0point:=439-round(400*(sig_f[i-2]-ymn)/(ymx-ymn));
    y1point:=439-round(400*(sig_f[i-1]-ymn)/(ymx-ymn));
    y2point:=439-round(400*(sig_f[i]-ymn)/(ymx-ymn));
    x0point:=59+round(500*(r[j-1]-xmn)/(xmx-xmn));
    x1point:=59+round(500*((r[j-1]+r[j])/2-xmn)/(xmx-xmn));
    x2point:=59+round(500*(r[j]-xmn)/(xmx-xmn));
    Line(x0point,y0point,x1point,y1point);
    Line(x1point,y1point,x2point,y2point);
  end;
outtextxy(20,60,char(229)+char(233));
setcolor(cyan);
for j:= 1 to outerlayer do  {plots sig-r}
  begin
    i:=3*j;
    y0point:=439-round(400*(sig_r[i-2]-ymn)/(ymx-ymn));
    y1point:=439-round(400*(sig_r[i-1]-ymn)/(ymx-ymn));
    y2point:=439-round(400*(sig_r[i]-ymn)/(ymx-ymn));
```

```pascal
        x0point:=59+round(500*(r[j-1]-xmn)/(xmx-xmn));
        x1point:=59+round(500*((r[j-1]+r[j])/2-xmn)/(xmx-xmn));
        x2point:=59+round(500*(r[j]-xmn)/(xmx-xmn));
        Line(x0point,y0point,x1point,y1point);
        Line(x1point,y1point,x2point,y2point);
      end;
  outtextxy(20,70,char(229)+'r');
  setcolor(red);
  for j:= 1 to outerlayer do  {plots sig-z}
    begin
      i:=3*j;
      y0point:=439-round(400*(sig_z[i-2]-ymn)/(ymx-ymn));
      y1point:=439-round(400*(sig_z[i-1]-ymn)/(ymx-ymn));
      y2point:=439-round(400*(sig_z[i]-ymn)/(ymx-ymn));
      x0point:=59+round(500*(r[j-1]-xmn)/(xmx-xmn));
      x1point:=59+round(500*((r[j-1]+r[j])/2-xmn)/(xmx-xmn));
      x2point:=59+round(500*(r[j]-xmn)/(xmx-xmn));
      Line(x0point,y0point,x1point,y1point);
      Line(x1point,y1point,x2point,y2point);
    end;
  outtextxy(20,80,char(229)+'z');

  end;


  (*********************************************************)

  procedure Plotgraph(ngraph:integerarray9;marker,
                     xdiv,ydiv:integer;var xmin,xmax,ymin,
                     ymax:real);
      {ngraph = graphnumber(s) to plot, marker = edit point}

  type
  realarray9XNL = array[1..9,0..NL] of real;

  var
  MaxX,MaxY,x1point,y1point,x0point,y0point,xpoint,lastgraph,
  i,j,k,n,code1,code2,errcd:integer;
  graphlabel,number,strip0,strip1,strip2,avgstif,alph,pwr,itt,
  thickness:string;
  XvalueMax,YvalueMax,YvalueMin,XvalueMin,xstep,ystep,ln_a,
  power,rr,drr,t:real;
  a_bestf:realarrayNL;
  plotv:realarray9XNL;
  b_fit:realarrayMPbyNP;
  pk,yorigin,sk,up:integer;

  label
  flag1,flag2;

  begin {procedure}
```

```
xvaluemin:=9E30;
yvaluemin:=9E30;
xvaluemax:=-9E30;
yvaluemax:=-9E30;
MaxX:=GetMaxX;
MaxY:=GetMaxY;
sk:=0;
if graphdata[1].symbol = 'B11' then
lastgraph:=3  {3 = B11,B12,B22}
else
lastgraph:=9;
for k:= 1 to lastgraph do
begin
  setcolor(k+1);
  if k >= 5 then sk:=14;              {skips one space}
  if k > 6 then  setcolor(k+2);
    Outtextxy(17,280+k*14+sk,graphdata[k].symbol)
end;

for k:= 1 to lastgraph do
begin
  n:=ngraph[k];
  if n <> 0 then
    begin
      bestfit(b_fit,pk,n);
      drr:= (r[outerlayer]-r[0])/NL;
            {var coeff: alpha=b_fit[pk,1], n=b_fit[pk,2]}
      for i:= 0 to NL do
      begin
        rr:=(r[0]+drr*i)/r[outerlayer];
        plotv[n,i]:=b_fit[pk,1]*pow(rr,b_fit[pk,2]);
                            {variable properties plot}
      end;
    end;   {if n}
end; {do}

for k:=1 to lastgraph do
begin
n:=ngraph[k];
if ngraph[k] <> 0 then
  begin
    for i:= 1 to outerlayer do  {extract max and min values}
      begin
      if
        graphdata[n].xydata[i,1] > xvaluemax then
        xvaluemax:=graphdata[n].xydata[i,1];
      if
        graphdata[n].xydata[i,2] > yvaluemax then
        yvaluemax:= graphdata[n].xydata[i,2];
      if
```

762

```
        graphdata[n].xydata[i,1] < xvaluemin then
        xvaluemin:= graphdata[n].xydata[i,1];
      if
        graphdata[n].xydata[i,2] < yvaluemin then
        yvaluemin:= graphdata[n].xydata[i,2];
      end;  {for lastlayer loop}
    for i:= 0 to NL do
      begin
      if
        plotv[n,i] > yvaluemax then
        yvaluemax:= plotv[n,i];
      if
        plotv[n,i] < yvaluemin then
        yvaluemin:= plotv[n,i];
      end; {for NL loop}
    end; {if <> 0}
end;

for k:= 1 to lastgraph do    {major loop}
begin
  n:=ngraph[k];
  if ngraph[k] = 0 then goto flag2;
                               {skip this particular graph}
    ystep:=((yvaluemax-yvaluemin)/ydiv);
    xstep:=((r[outerlayer]-r[0])/xdiv);
    strip0:=copy(graphdata[n].symbol,1,1);
    if strip0 = 'A' then          {for stifnesses}
      ymin:=0
    else
      ymin:=int(yvaluemin)-1;     {for compliances}
    xmin:=int(r[0]);
    xmax:=r[outerlayer];
    ymax:=yvaluemax;
    if frac(ymax) > 0 then
      ymax:= int(ymax)+1;

    graphlabel:= graphdata[n].symbol;
                        {if less than 9 graphs jump out}
    if graphlabel = '' then goto flag1;
    strip1:=copy(graphlabel,2,1);
                        {extracts 2nd and 3rd index in label}
    strip2:=copy(graphlabel,3,1);
    strip0:=copy(graphlabel,1,1);
              {gets 1st index, stiffness or compliance}
    val(strip1,code1,i);      {disects graphlabel}
    val(strip2,code2,i);
    setcolor(white);
    Outtextxy(580,30,'Layers');
    settextstyle(0,1,1);
    Outtextxy(8,334,'Legend');
```

```
settextstyle(0,0,1);
if ymin < 0 then
begin
   yorigin:=439-round(400*(-ymin/(ymax-ymin)));
   setcolor(white);
   setlinestyle(0,0,1);
   Line(59,yorigin,MaxX-80,yorigin);
end;
setcolor(n+1);
if n > 6 then setcolor(n+2);
   for i:=1 to outerlayer do
    begin
    y1point:=439-round(400*(graphdata[n].xydata[i,2]-
            ymin)/(ymax-ymin));
    x1point:=59+round(500*(r[i]-xmin)/(xmax-xmin));
    y0point:=439-round(400*(graphdata[n].xydata[i-1,2]-
            ymin)/(ymax-ymin));
    if y0point > 439 then
       {prevents starting below the axis when ymin > 0}
      y0point:=439;
    x0point:=59+round(500*(r[i-1]-xmin)/(xmax-xmin));
    if strip0 = 'A'  then
      qpoint:=439-round(400*(q[code1,code2]-ymin)/
             (ymax-ymin));
             {strip0 decides on type of graph}
    if strip0 = 'B' then
      qpoint:=439-round(400*(1000*sumB[code1,code2]-
             ymin)/(ymax-ymin));
    if strip0 = 'a' then
      qpoint:=439-round(400*(1000*sumC[code1,code2]-
             ymin)/(ymax-ymin));
    Line(x0point,y1point,x1point,y1point);
                                       {vertical increment}
    Line(x0point,y0point,x0point,y1point);
                                       {horizontal increment}
     setcolor(cyan);
     str(i,number);
     Outtextxy(569-4*length(number),24+i*28,
             number+':'+char(241)+
             graphlabels[i].angle+char(248));
     Outtextxy(616,24+i*28,copy
             (graphlabels[i].fpercent,1,2)+char(37));
     Outtextxy(576,34+i*28,graph labels[i].matname);
     setcolor(white);
     Outtextxy(569-4*length(number),
             24+i*28,number+':');
     setcolor(cyan);
     if odd(i) then up:=10 else up:=0;
     val(graphlabels[i].thickness,t,errcd);
     str(t:2:1,thickness);
```

```
        graphlabels[i].thickness:=thickness;
        Outtextxy(round(((xlpoint+x0point)/2)-10+
                8*length(number),30-up,thickness);
        Setcolor(white);
        Outtextxy(round(((xlpoint+x0point)/2)-18,
                30-up,number+':');
        Line(x0point,40,x0point,46);
        setlinestyle(1,0,1);
        Line(xlpoint,40,xlpoint,439);
        setlinestyle(0,0,1);
        setcolor(n+1);
        if n > 6 then setcolor(n+2);
    end; {for i loop}
  for i:= 1 to NL do   {plots variable property}
  begin
     y0point:=439-round(400*(plotv[n,i-1]-ymin)/
              (ymax-ymin));
     ylpoint:=439-round(400*(plotv[n,i]-ymin)/
              (ymax-ymin));
     x0point:=59+round(500*((r[0]+drr*(i-1))-xmin)/
              (xmax-xmin));
     xlpoint:=59+round(500*((r[0]+drr*i)-xmin)/
              (xmax-xmin));
     Line(x0point,y0point,xlpoint,ylpoint);
  end;
  if strip0 = 'A' then
     str(q[code1,code2]:4:1,avgstif);
                                      {stiffness case}
  if strip0 = 'B' then
     str(1000*SumB[code1,code2]:4:1,avgstif);
                                      {eq stiffness case}
  if strip0 = 'a' then
     str(1000*SumC[code1,code2]:4:1,avgstif);
                                      {compliance case}
  Line(59,qpoint,67,qpoint);
  outtextxy(70,qpoint-4,avgstif);

  if k > 5 then
     sk:=14
  else
      sk:=0;                          {k = graph number}
  rectangle(15,278+k*14+sk,42,288+k*14+sk);

  if k = marker then
  begin {outputs properties equation for selected graph}
     str(bfit_store[n,1]:3:2,alph);
     str(bfit_store[n,2]:3:2,pwr);
     str(bfit_store[n,3]:3:0,itt);
     settextjustify(righttext,toptext);
     outtextxy(596,4,graphdata[marker].symbol+
```

765

```pascal
                        '='+alph+'(p)');
          settextjustify(lefttext,toptext);
          out textxy(596,0,pwr);
         { outtextxy(596,20,itt); }
                        {just to check algorithm efficiency}
      end;

    flag2:
    end; {major loop}

    setcolor(white);
    if marker > 5 then
      sk:=14
    else
      sk:=0;
    rectangle(44,282+marker*14+sk,47,285+marker*14+sk);

flag1:
end;  {procedure}


(*******************************************************)


Procedure plotoutline(xlabel,ylabel,Title,Title2:
                      string;xdiv,ydiv:integer;
                      xmin,xmax,ymin,ymax:real);
var

MaxX,MaxY,graphno,i,j,nw,rhs: integer;
Keyknown,specialkey:boolean;
n:string;
xticpix,yticpix:real;
xstep,ystep:real;

label
flag2;

begin
      setcolor(white);
      MaxX:=GetMaxX;
      MaxY:=GetMaxY;
      Line(59,39,MaxX-80,39);
      Line(59,39,59,MaxY-40);
      Line(59,MaxY-40,MaxX-80,MaxY-40);
      Line(MaxX-80,39,MaxX-80,MaxY-40);
      xstep:=((xmax-xmin)/xdiv);
      ystep:=((ymax-ymin)/ydiv);
      xticpix:=(500/xdiv);
      yticpix:=(400/ydiv);
      for i:= 0 to xdiv do
        begin
```

```
          str(xmin:4:1,n);
          if i = xdiv then
            rhs:=20
          else if
          i = 0 then
            rhs:=-20
          else rhs:=0;
          OutTextXY(round(39+i*Xticpix)-rhs,443,n);

Line(trunc(59+i*xticpix),439,trunc(59+i*xticpix),431);
          if ((59+i*xticpix)-xticpix/2) > 59 then
          Line(round((59+i*xticpix)-xticpix/2),
              439,round((59+i*xticpix)-xticpix/2),435);
          xmin:=xmin+xstep;
          end;

      for i:= 0 to ydiv do
        begin
        nw:=0;
        Str(ymin:4:1,n);
        nw:=textwidth(n);
        if nw > 55 then nw:=55;
        OutTextXY(55-nw,round(431-i*Yticpix),n);
                                              {axis numeral}
        Line(59,trunc(439-i*yticpix),67,
            trunc(439-i*yticpix));            {ticks}
        Line(MaxX-88,trunc(439-i*yticpix),maxX-80,
            trunc(439-i*yticpix));
        if ((439-i*yticpix)+yticpix/2) < 439 then
          begin
          Line(59,round((439-i*yticpix)+yticpix/2),
              63,round((439-i*yticpix)+yticpix/2));
          Line(MaxX-84,round((439-i*yticpix)+yticpix/2),
              MaxX-80,round((439-i*yticpix)+yticpix/2));
          end;
        ymin:=ymin+ystep;
        end;

      setcolor(lightgray);
      outtextxy(0,0,currentfile);
      Setcolor(Yellow);
      OutTextxy(464,470,'Alt-X    Alt-S   ESC');
      Setcolor(white);
      OutTextxy(444,470,'+         +        +');
      setcolor(yellow);
      Outtextxy(90,470,'INS/DEL   PgUP/PgDn');
      Outtextxy(266,470,'TAB    '+char(27)+
              char(24)+char(25)+char(26)+'    Home End');
      Setcolor(white);
```

```pascal
      Outtextxy(2,470,'Controls =      /      +      /      +
                +      ÷      /');
      Setcolor(lightgreen);
      SetTextStyle(0,1,1);
      i:= textwidth(ylabel);
      OutTextXY(8,240-round((i)/2),ylabel);
      SetTextStyle(0,0,1);
      i:= textwidth(xlabel);
      OutTextXY(310-round((i)/2),458,xlabel);
      i:= textwidth(title);
      j:= textwidth(title2);
      OutTextXY(330-round((i)/2),0,title);
      OutTextXY(330-round((j)/2),10,title2);
      setcolor(white);
Graphdefaults;
end; {procedure}


(*****************************************************)

end. {unit}
```

NOTE TO USERS

The diskette is not included in this original manuscript. It is available for consultation at the author's graduate school library.

This reproduction is the best copy available.

UMI